MONITORING CONCRETE PERFORMANCE UNDER SIMULATED AND NATURAL CHLORIDE ENVIRONMENTS

By

Jaehwan Kim BSc MSc

Submitted for the degree of Doctor of Philosophy

School of Energy, Geoscience, Infrastructure and Society

Institute for Infrastructure and Environment

Heriot-Watt University

April 2018

ABSTRACT

Deterioration of reinforced concrete structures caused by chloride-induced corrosion is well-known in the construction industry, but it is still difficult to evaluate the performance of the structures due to various exposure conditions and characteristics of concrete, especially containing supplementary cementitious materials (SCMs). In this study, comprehensive assessments of both chloride transport and corrosion initiation/propagation were, therefore, performed to study the performance of concrete subjected to a chloride environment. Chloride transport in concrete was assessed using the migration/diffusion coefficient, porosity/degree of saturation and electrical resistance/resistivity. The electrical resistivity of the concrete was used as a single 'performance' factor. In addition to chloride transport, the condition of steel embedded in concrete was monitored using electrochemical methods. The electrical resistance/resistivity of concrete was monitored over a period of 382 days and then analysed using a normalisation technique to identify the chloride transport and corrosion process. In addition, the condition of concrete slabs (18 years old) retrieved from the Dornoch Firth marine exposure site (representing XS3 environmental exposure class) were evaluated using the same procedures conducted in the laboratory. In monitoring the electrical resistance/resistivity, the activation energy was calculated to reflect the environmental conditions, in this instance diurnal and annual temperature variation. Finally, for time to corrosion initiation, the ClinConc model was combined with two new environmental factors and during corrosion propagation, the polarisation resistance was estimated using a fitting method.

DEDICATION

To my beloved wife and son

Hye Jung and Doyun

To my parents

Chang Sun, Kim and Hyang In, Jwa

For their endless love, support and encouragement

ACKNOWLEDGEMENTS

Most of all, I would like to thank Prof. W. John McCarter for his patience, valuable comments and guidance for the last 4 years. I would like to thank Dr. Gerard Starrs and Dr Benny Suryanto for their support. The help of the Technical staff in the experimental work is also gratefully acknowledged.

I would like to express my gratitude to my parents-in-law Kibal, Ryu and Ok Nam, Lee for their unfailing moral support. I am also thankful for heart-warming kindness from the family of my brother-in-law: Chung Seok, Yu and Yunhee, Park.

Finally, I am indebted to my father, Chang Sun Kim, my mother, Hyang In, Jwa and my younger sister, Min Kyeong, Kim for their unseen support throughout this entire journey. I have been inspired and encouraged by the belief of my wife, Hye Jung, Yu and my son, Doyun, Kim, who made this thesis possible.

DECLARATION STATEMENT

TABLE OF CONTENTS

LIST OF FIGURES

LIST OF TABLES

LIST OF ABBREVIATIONS

Latin letter

AC	Alternating current
CP	Corrosion potential
CPE	Constant element phase
CSE	Copper-copper(II) sulfate electrode
CTL	Chloride threshold level
DC	Direct current
EDP	Equivalent durability performance
EIS	Electrochemical impedance spectroscopy
FA	Fly ash
GDP	Gross domestic product
GGBS	Ground granulated blast-furnace slag
GP	Galvanostatic pulse polarisation
LPR	Linear polarisation resistance
LS	Steel with long exposed area
MC	Macrocell current
ML	Mass loss
OCP	Open circuit potential
PC	Portland cement
PDP	Potentiodynamic polarisation
pH	Potential of hydrogen
PT	Potentiostatic polarisation
RH	Relative humidity
SCE	Saturated calomel electrode
SCM(s)	Supplementary cementitious material(s)
SS	Steel with small exposed area
TEP	Tefel extrapolation
W/D	Wet/dry cyclic regime
w/b	Water to binder ratio
VI	Visual inspection

Index

a	Anode
app	Apparent
c	Cathode
cl	Chloride
corr	Corrosion
conc	Concrete
dry	Dry condition of sample
hyd	Hydration
pit	Pitting corrosion
pore	Pore solution
sat	Saturated condition of sample
vsat	Vacuum saturated condition of sample
w	Distilled water
0	Original or initial in general

LIST OF SYMBOLS

Symbol	unit	Description and definitions
Latin letters		
A	m^2 or cm^2	Area
a		Constant in general
B	mV	Stern-Geary constant
b		Constant in general
C		Chloride concentration
C_b	%, by weight of binder	Bound chloride concentration
C_{dl}	F	Double layer capacitance
C_f	%, by weight of binder	Free chloride concentration
C_p	F	Capacitance
C_s	%, by weight of binder	Surface chloride concentration
C_t	%, by weight of binder	Total chloride concentration
c		Constant in general
D_d	m^2/s	Diffusion coefficient
D_m	m^2/s	Migration coefficient
d		Constant in general
E	mV or V	Electrical potential
E_a	kJ/mol	Activation energy
F		Formation factor
F	J/(V·mol)	Faraday constant (=96,487 J/(V·mol))
f	Hz	Frequency
f_c	MPa	Compressive strength
I	mA or A	Current
i	mA/m^2	Current density
J		Flux
L	mm or m	Length
M	kg/m^3	Unit mass
M	g/mol	Atomic weight
m	g or kg	Mass
N		Normalised value
n		Archie's exponent
R	Ω	Electrical resistance
R	J/(K·mol)	Gas constant
R_p	$Ω/m^2$	Polarisation resistance
S_r	%	Degree of saturation
T	K or ℃	Temperature
t	sec or days	Time
V	µm/year	Corrosion velocity
V	cm^3	Volume
Z	Ω	Impedance
z		Absolute value of ion valence

Greek Letter

β	mV/dec	Tafel slope
δ	g/cm^3	Density
Ø	%	Porosity
ξ		Tortuosity
ρ	Ω·m	Electrical resistivity
σ	S/m	Electrical conductivity
τ	sec	Time constant

LIST OF PUBLICATIONS

Publications

1. Kim, J., McCarter, W.J., Suryanto, B., Nanukuttan, S., Basheer, P.A.M. and Chrisp, T.M., 2016. Chloride ingress into marine exposed concrete: A comparison of empirical- and physically- based models. *Cement and Concrete Composites*, 72 (September), 133-143.

In preparation

1. Kim, J., McCarter, W.J., Suryanto, B., Monitoring electrical resistance of concrete subjected to a simulated chloride environment.
2. Kim, J., McCarter, W.J., Suryanto, B., Performance assessment of 18 years-old concrete exposed to XS3 environment.
3. Kim, J., McCarter, W.J., Suryanto, B., Evaluating performance of concrete using electrical resistivity.

CHAPTER 1
INTRODUCTION

1.1 Background

Even though the alkaline environment provided by concrete forms a passive layer on steel surfaces, corrosion of steel is unavoidable in concrete structures. Among common factors contributing to the deterioration of concrete structures (see figure 1.1), corrosion accounts for 38% (Tilly, 2005), and this deterioration results in considerable economic loss both indirectly and directly. According to a survey conducted by Nwaubani and Katsanos (2014), the annual corrosion costs are estimated to be in the range of 2 – 6.2% of gross domestic product (GDP) for many developed countries, including the US, Canada, Japan, Australia, and the UK. The indirect cost of corrosion, for instance traffic congestion, delays in product transport, and wear and tear on automobiles, is conservatively estimated to be at least as much as direct costs (Koch *et al.*, 2002).

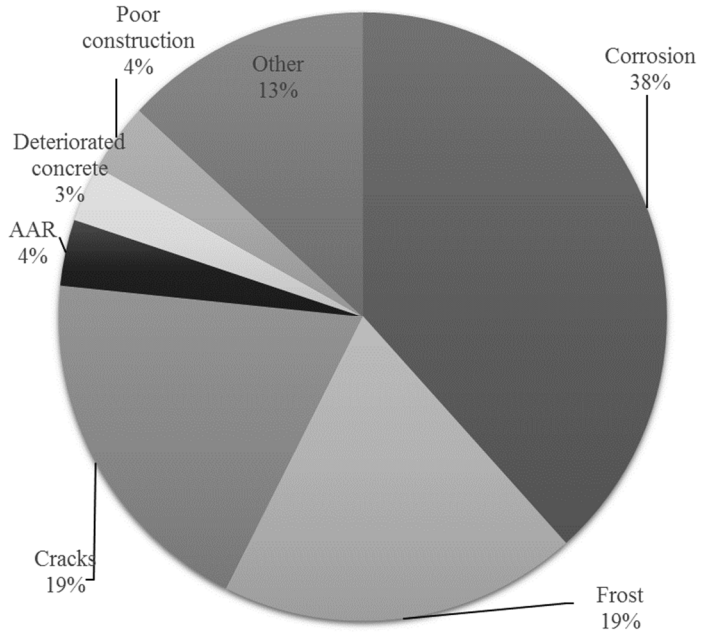

Figure 1.1 Primary factors affecting the durability of concrete structures (Tilly, 2005).

Chloride-induced corrosion is considered to be the most important deterioration mechanism in reinforced concrete structures and many cases for deteriorated reinforced concrete by chloride-induced corrosion have been reported. For example, the Tay bridge in Scotland, UK; the Midland Links motorway viaducts in England, UK; the Ynys-y-Gwas bridge in Wales, UK; a 45-year old concrete located over the Pittwater Estuary in

Tasmania, Australia; Ponte Moesa bridge in Switzerland, and the Nile channel bridge and Mid-bay bridge in Florida, USA were diagnosed with chloride-induced corrosion of steel in the structures caused by de-icing salt or seawater (Wood, 1997; Angst *et al.*, 2012; Christodoulou *et al.*, 2014; Powers *et al.*, 2004). A wide range of studies on this topic have been undertaken around the world, ranging from design methods to material properties.

It is apparent that developments in materials and testing and monitoring techniques are contributing to advancing our knowledge of durability and performance of concrete structures. To this end, the concept of a performance-based approach is generally accepted as the best way forward in terms of the specification of concrete (Alexander and Thomas, 2015; RILEM TC 230-PSC, 2016). A performance-based approach is central to improved durability of concrete structures and is beneficial for both engineers and owners. However, it is necessary to establish a testing methodology to assess concrete durability and performance using such an approach. In addition, tests performed on concrete in the laboratory should be representative of the behaviour of concrete exposed to field conditions. Finally, the developments of reliable models are required to reflect ambient environmental conditions as the latter are crucial in deterioration processes in concrete. This leads to an improved understanding of the durability/performance evaluation of concrete structures exposed to aggressive environments, especially chloride environments. Thus, these must be considered in the development of a performance-based approach.

1.2 Objectives

This study aims to investigate methods of durability/performance evaluation associated with a performance-based approach. The thrust has been to examine the application of the electrical properties of concrete as a performance factor to evaluate the service life of concrete structures subjected to chloride environments using both laboratory and field data.

The study is divided into three parts:

(i) establishing the relationship between the electrical properties of concrete and a range of parameters related to chloride transport;

(ii) monitoring the electrochemical properties at the steel and concrete interface caused by chloride ingress or chloride-induced corrosion; and,

(iii) monitoring electrical resistance of concrete using embedded electrodes.

Chloride transport parameters including degree of saturation and diffusion coefficient are highly correlated with electrical properties of concrete as electrical conduction through concrete occurs via the pore fluid in the continuous pore network. In this study, corrosion activity at the steel and concrete interface was detected using non-destructive methods based on electrochemical theory. The parameters used are generally representative of chloride-induced corrosion of steel in concrete. Electrical properties were measured from embedded electrodes and analysed, including influencing factors to which the property is sensitive. In addition, the experimental results were used to update a physical model with due consideration to environmental factors. Furthermore, the influence of binder type and water/binder (w/b) on electrical properties was also investigated.

In summary, the following investigative programme was carried out.

(a) Transport parameters:

(1) evaluate the degree of saturation and porosity of concrete subjected to wet/dry cycles;

(2) evaluate the diffusion/migration coefficient of concrete with type of binder and w/b; and,

(3) evaluate the electrical properties of samples prior to the above measurements to establish the relationship between electrical properties and other related parameters.

(b) Corrosion parameters:

(1) evaluate the corrosion rate of steel with type of binder and w/b using electrochemical measurements;

(2) estimate the B constant for calculation of corrosion rate using Tafel's slope with binder types and w/b;

(3) compare the corrosion rate/behaviour of steel using qualitative/quantitative methods and destructive/non-destructive methods; and,

(4) evaluate the behaviour of corrosion propagation of steel with time.

(c) Monitoring electrical properties of concrete:

(1) evaluate factors influencing the electrical properties of concrete, e.g. moisture content and temperature;

(2) monitor the electrical properties of concrete with chloride ingress and corrosion propagation; and,

(3) establish a method for monitoring the electrical properties of concrete subjected to chloride ingress.

(d) Prediction of service life of concrete:

(1) update the existing ClinConc model for chloride transport using field/lab-environmental factors;

(2) propose a corrosion model using a simple empirical equation; and,

(3) determine the activation energy to reflect an exposure condition.

1.3 Outline of thesis

The thesis presents a literature review, experimental design and execution, modelling, and verification of chloride ingress and subsequent corrosion of reinforcement steel into concrete.

Chapters 2 and 3 review the existing work on deterioration of concrete structures by chloride-induced corrosion. Application to the 'real world' is a challenge, while the theoretical background is now well established. It is necessary to bridge the gap between laboratory studies and 'real world' structures. In this respect, Chapter 2 considers chloride diffusion and chloride-induced corrosion, including a range of relevant variables. Current design codes are also reviewed, allowing for the development of a performance-based approach. Chapter 3 reviews a number of experimental and modelling techniques which provide the development of an integrated 'performance' factor and refinement of the current models.

Chapter 4 presents the experimental programme comprising three parts, including chloride transport, steel corrosion, and electrical resistance monitoring. This chapter introduces the overall framework in terms of experimental work, including sample fabrication, exposure conditions and materials.

Chapter 5 reports the results obtained from the laboratory study related to chloride transport. The investigation includes chloride migration/diffusion, electrical properties (resistivity) and moisture content of unsaturated concrete. Performance factors specified in current codes and the literature are evaluated with electrical resistivity.

Chapter 6 reports the results obtained from the laboratory study related to steel corrosion. A number of corrosion techniques are employed to evaluate the corrosion rate. The required parameters are investigated to detect and evaluate chloride-induced corrosion.

Chapter 7 evaluates a monitoring system using the electrical resistance of concrete subjected to a chloride environment. The chapter introduces the methodology to analyse data on the electrical resistance of concrete exposed to a chloride solution. From the results, a change in electrical resistance of concrete is also explained with chloride transport and the chloride-induced corrosion behaviour of steel

Chapter 8 evaluates the parameters used in the previous chapters with data obtained from field samples. Based on the results from the field samples, environmental factors are introduced to update the existing model for chloride transport. For the corrosion model, a simplified empirical equation is suggested using the polarisation resistance with time instead of the corrosion rate with time. Furthermore, to analyse the electrical resistivity of field samples, the chapter presents a correction factor for ambient environments in the field (activation energy).

Finally, Chapter 9 draws conclusions from the above studies, highlighting several findings and proposing a number of recommendations for further research. It further describes the continuation of several the experiments presents in this thesis.

Figure 1.2 provides a diagrammatic representation of the thesis.

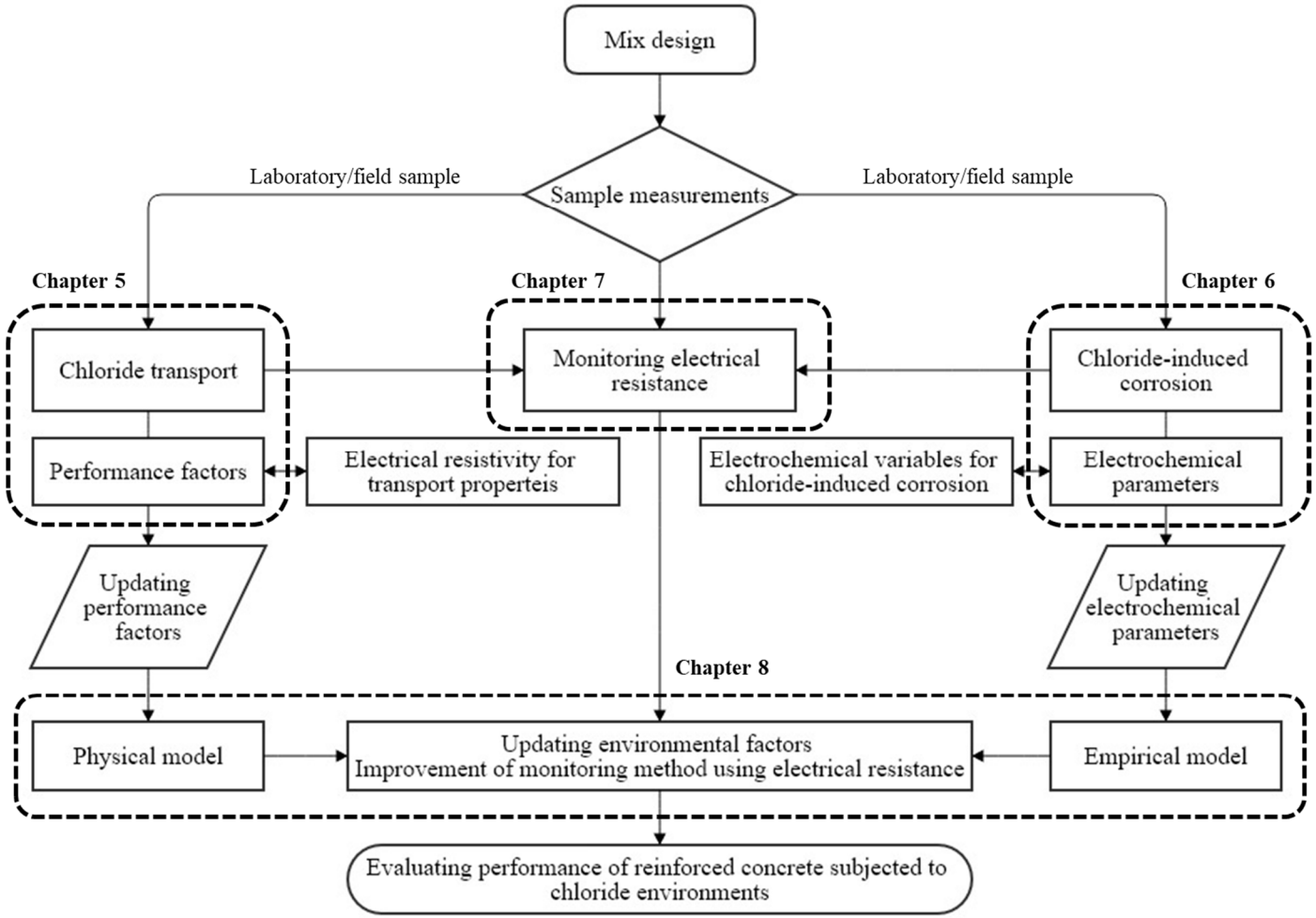

Figure 1.2 Flow chart of the research programme.

CHAPTER 2
REVIEW OF CHLORIDE-INDUCED CORROSION OF STEEL IN CONCRETE

2.1 Introduction

In marine/highway structures, corrosion caused by chloride ingress is the main concern regarding the durability of reinforced concrete. In addition, it is still a challenge to evaluate/predict the service life of these structures due to the inhomogeneity of concrete, environmental exposure conditions and unstandardized methods for analysis. Furthermore, although new materials with high performance are rapidly being developed, their application is limited in practice due to lack of knowledge about their long-term behaviour.

To address these limitations, specifying the durability of concrete is changing from a 'deemed to safety approach' to a 'performance-based approach'. In other words, the limitations can be flexibly managed using a performance-based approach which is based on experimental data on the properties of concrete instead of on an empirical relationship. Performance factors and numerical models are being vigorously developed, but there is currently a lack of field application.

This chapter presents an outline of the process of chloride-induced corrosion in reinforced concrete, detailing the causes and mechanisms concerning chloride transport and corrosion of steel in concrete. Current trends in specification are also described.

2.2 Overview of concrete durability

Concrete is an excellent material for durability/performance, but the deterioration of concrete structures is also unavoidable, primarily due to the presence of (ferrous) steel reinforcement. Deterioration processes include chloride attack, carbonation, sulphate attack, and freeze/thaw damage. To control the durability of concrete subjected to aggressive environments, two strategies are available: (i) avoidance and (ii) optimisation of material performance (Altmann and Mechtcherine, 2013; Alexander and Nganga, 2016). The former entails preventing deterioration directly, such as by coating the steel

with an impervious material, whilst the latter consists of enduring/resisting deterioration within the service life, for example by using supplementary cementitious materials (SCMs) and/or increasing cover depth (a performance-based approach). A performance-based approach thus involves explicitly evaluating material properties with performance factors obtained from performance tests and simulating the performance of structures from deterioration models. The results from the models are also supported by data from performance tests, combined with exposure conditions.

Although BS EN 206 (British Standards Institution, 2014) still defines a prescriptive design method for durability, Section 5.3.3 of this code allows for performance-related methods and defines concrete on the basis of an equivalent durability procedure (EDP); further detail on the EDP is presented in PD CEN/TR 16563 (British Standards Institution, 2013a). To fully implement the concept of a performance-based approach, the following are considered crucial:

(i) Long-term experience with local materials and practices, and detailed knowledge of the local environment;

(ii) Test methods based on approved and proven tests that are representative of actual conditions and have approved performance criteria; and,

(iii) Analytical models that have been calibrated against test-data representative of actual conditions in practice.

Regarding each condition above, long-term monitoring of the target structure relates to (i); evaluation of concrete performance using well-established tests such as the migration test (Nordtest, 1999) relates to (ii); and updating the parameters used in predictive models considering ‘real situation’ relates to (iii).

2.2.1 Changing trend for durability evaluation

The trend for controlling the durability of concrete appears to be moving towards the performance-based approach and away from the prescriptive method (British Standards Institution, 2013a, 2014). The prescriptive method stipulates limiting parameters such as minimum binder content, type of binder, cover depth, exposure class and maximum w/b. Concrete is then deemed to satisfy the durability requirement during the intended service life of the structure. However, as these limiting values are strongly dependent on previous

experience (Alexander and Thomas, 2015), this approach cannot cope with the rapid development of materials. The durability of concrete, which is defined as the ability to resist aggressive agents in a given environment during the service life, cannot be covered by a simple mix of parameters and a wide range of exposure conditions.

In a performance-based approach, predictive models are helpful as concrete structures can be readily simulated using various environmental scenarios, but the simulated results should be corroborated by both performance tests and field conditions (Polder and De Rooij, 2005; Val and Trapper, 2008; Baroghel-Bouny *et al.*, 2014). A performance test is essentially used to evaluate 'potential ability' and 'quality control'. The test provides information on performance of a candidate mix, leading to the selection of a mix for the target structure based on pre-qualification. The test on the supplied concrete is also carried out with samples replicated in laboratory or extracted from a 'real structure' for the purpose of quality control. Both cases are primarily aimed at assessing the as-built quality of the structure with equivalent durability procedures (British Standards Institution, 2013a).

Although the durability indicators based on performance tests and predictive models have developed rapidly, the move to the specifications for concrete durability in terms of a performance-based approach is slow due to risk in practical use. Specifications are currently close to a 'hybrid method', including exposure class, prescriptive values and the values from performance tests (Kessy *et al.*, 2015). In addition, avoidance methods, such as coated steel and surface treatments, are also recommended in the specifications, but there are no quantitative results for this method (Japan Society of Civil Engineers, 2010a; Li *et al.*, 2008; ACI Committee 318, 2014; British Standards Institution, 2014). The characteristics of the specifications used in several countries are investigated and presented in table 2.1 and table 2.2. Note that the part related to chloride-induced corrosion is only summarized in these tables. As shown in table 2.1, a sub-category for chloride environments impinging on concrete structures is described within different codes. Overall, this sub-category consists of two or three zones and the tidal/splash zone is considered to be the most vulnerable. Interestingly, the local peculiarities of each country are reflected in their codes. For example, in the case of China, a sub-category with temperature is included due to the country's large geographic area with a varied climate. Canada considers a deterioration process combining chloride attack with freeze-thawing and has the highest severity regarding chloride attack among the codes listed in the table. Japan is an island country, and hence airborne chlorides are intimately categorised with regions and distance from coast.

Table 2.2, on the other hand, presents the limiting values for different countries: the w/b is around 0.4 in most codes, which is typical for high resistance of concrete to chloride ingress. As shown in figure 2.1, the required cover-depth and compressive strength are varied in the codes. It appears that local differences in materials and environments are applied and it may be difficult to design/estimate durability of concrete structures with only prescriptive values. Different test methods are suggested as a performance-based approach, but these tests are mainly related to chloride transport and are accelerated methods. Various indicators have been used with different interpretations.

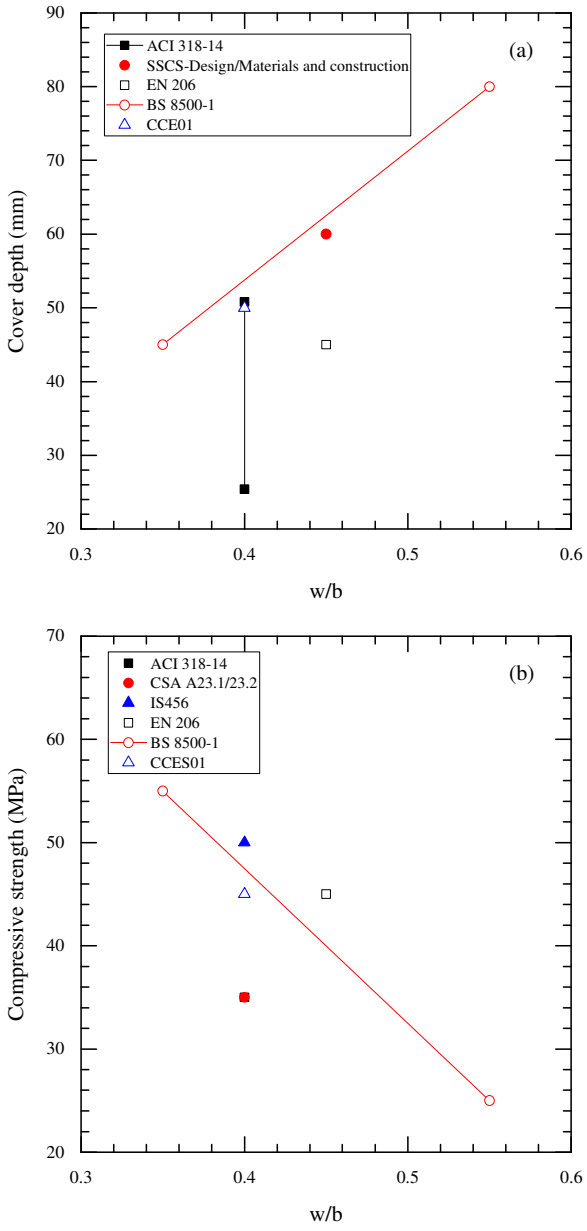

Figure 2.1 Limiting values specified in codes for mix design of concrete using common cements subjected to XS3 environment, (a) cover-depth, and (b) compressive strength.

Table 2.1 Exposure environments for concrete structures subjected to chloride environments classified in the codes

Code (year)	Exposure class	Sub-classes	Description	Sub-classes adjusted to EN 206	Nation	Reference
ACI 318-14 (2014)	Corrosion protection of reinforcement	C2	Concrete exposed to moisture and an external source of chloride from deicing chemicals, salt, brackish water, seawater, or spray from these sources	XS1,2,3 XD1,2,3	USA	ACI Committee 318 (2014)
CSA A23.1/23.2 (2009)	Chloride	C-XL	Structurally reinforced concrete exposed to chlorides or other severe environments with or without freezing-and- thawing conditions, with higher durability performance expectations than the C-1, A-1, or S-1 classes	+	Canada	Kessy *et al.*(2015)
		C-1	Structurally reinforced concrete exposed to chlorides with or without freezing-and-thawing conditions. Examples: bridge decks, parking decks and ramps, portions of marine structures located within the tidal and splash zones, concrete exposed to seawater spray, and salt water pools	XS3/XD3		
		C-3	Continuously submerged concrete exposed to chlorides but not to freezing and thawing. Examples: underwater portions of marine structures.	XS2/XD2		
AS 3600 (2001)	Sea water	B-2	Coastal (up to 1 km from coastline excluding tidal and splash zone)	XS1	Australia	Kulkarni (2009), Kessy *et al.*(2015)
		B-2	Permanently submerged	XS2		
		C	In tidal and splash zone	XS3		
	Chlorides	B-1	Near-coastal (1–50 km from coastline) any climatic zone	XD1		
IS456 (2000)	Chlorides	Moderate	Concrete surfaces sheltered from saturated salt air in coastal area	XD1	India	Kulkarni (2009)
		Severe	Concrete completely immersed sea water; concrete exposed to coastal environment	XS2, XS1		
		Very severe	Concrete surfaces exposed to sea water spray	XS3		
		Extreme	Surface of members in tidal zone, members in direct contact with liquid/solid aggressive chemicals	XS3/XD3		
EN 206 (2014)	Sea water	XS1	Exposed to airborne salt but not in direct contact with sea water	XS1	Europe	British Standards Institution (2014)
		XS2	Permanently submerged	XS2		
		XS3	Tidal, splash and spray zones	XS3		
	Chlorides other than sea water	XD1	Concrete structures exposed to airborne chlorides Parts of structures exposed to slightly chloride conditions	XD1		
		XD2	Reinforced concrete surfaces totally immersed in water containing chloride	XD2		
		XD3	Parts of bridges exposed to spray containing chlorides, e.g. pavements and car park slabs	XD3		

(continued)

CCES01 (2004)	Marine	C	Bridge pier permanently in sea water, 1–1.5 m under lowest water level (Immersion seawater)	XS2	China	Li *et al.* (2008)
		D	Members situated at 100–300 m from the coast line or 15 m above the sea level (Slight air borne salt)	XS1		
		E	Members exposed to the tidal and splash zones of sea water, or within 1.5 m under the lowest water level in a mild climate (yearly average temperature <20 °C) (Tidal and splash zones in mild climate)	XS3		
		F	Members exposed to the tidal and splash zones of sea water, or within 1.5 m under the lowest water level in a hot climate (yearly average temperature near or above 20 °C) (Tidal and splash zones in hot climate)	XS3		
	Chlorides other than sea water	C	Slight deicing frog Immersion in chloride water Water with low chloride content and drying–wetting cycles	XD1,2		
		D	Deicing salt spray Water with medium chloride content and drying–wetting cycles	XD3		
		E	Direct contact with deicing salt solution Heavy spray of deicing salt Water with high chloride content and drying–wetting cycle	XD3		
SSCS-Design (2010)	Reinforcement corrosion	Corrosive	Environment of marine structures submerged in seawater In comparison to the normal environment, environment with more frequent cyclic drying and wetting, and underground environment below the level of underground water containing especially corrosive (or detrimental) substances, which may cause harmful corrosion of reinforcement.	XS2/XD3	Japan	Japan Society of Civil Engineers (2010a)
		Severely corrosive	Environment of marine structures subjected to tides, splash, or exposed to severe ocean winds etc. Environment in which reinforcement is subjected to detrimental influences considerably	XS3/XD3		
SANS 10100-2 (2014)	Marine	Very severe	All exposed surfaces of structures within 30 km from the sea	XS1,XS2,XS3	South Africa	Smith (2016)

Table 2.2 Limiting values for concrete structures subjected to marine environments classified in the codes corresponding to XS3 in adjusted subclasses

Code	Limiting values with prescriptive approach					Limiting values with performance-based approach			Nation	References
	Min. Cover depth (mm)	Max. w/b	Min. binder content (kg/m^3)	Min. f_c (MPa)	Additions	Test	Limiting value (days)	Max. chloride content (% by wt. cem.)		
ACI 318-14 (2014)	25.4 – 50. 8*	0.4	+	35	+	ASTM C 1202	+	0.15**	USA	ACI Committee 318 (2014)
CSA A23.1/23.2 (2009)	+	0.4	+	35	Air content/ curing type	ASTM C 1202	< 1500 *C* (56 d) (with no single value > 1750 *C*)	+	Canada	Kessy *et al.*(2015)
AS 3600 (2001)	40***		470	>50	>32 at 7 day	+	+	+	Australia	Kulkarni (2009)
IS456 (2000)	75	0.4	360	50	+	+	+	+	India	Kulkarni (2009)
EN 206 (2014)	45	0.45	340	45	+	NT build 492	$\leq 5\times10^{-12}$ m^2/s (97 d)	0.40	Germany	British Standards Institution (2013, 2014)
						Resistivity	< 10 kΩ·cm		Italia	
						NT build 492	+ (28 – 364 d)		The Netherlands	
						NT build 443	+ (31 d)			
						NT build 492	+ (28 d)		Portugal	
						LNEC E 393	+ (28 d)			
						NP 12390-3	+ (28 d)			
						Resistivity	+ (28 d)		Spain	

(continued)

BS 8500-1 (2016)	45-80	0.35-0.55	320-380	25-55	+	+	+	0.30	British	British Standards Institution (2016)
CCES01 (2004)	50	0.4	340	45	+	NT Build 355	$\leq 6\times10^{-12}$ m^2/s	+	China	Li *et al.* (2008)
SSCS-Design/Materials and constructions (2010)	60	0.45#	330	+	Surface chloride content## (13 kg/m^3)	JSCE 571 (migration test)	+	1.2 kg/m^3	Japan	Japan Society of Civil Engineers (2010a, 2010b)
						JSCE 572 (Immersion test)	+			
SANS 10100-2 (2014)	65	+	+	50	+	+	+	+	South Africa	Smith (2016)
Note	*Reinforcement size is considered for determination of cover depth **Water soluble chloride content (% by weight of cement) ***Cover depth is adjustable and is determined by strength # Diffusion coefficient is estimated with equation C.5.2.25/26 in Standards specifications for concrete structures – 2007 'Design' ## Cover depth is estimated with surface chloride content and diffusion coefficient using Fick's 2nd law									

2.2.2 Performance factors

Performance factors (or durability indicators) are typical parameters used for describing performance-based concepts. They reflect concrete characteristics with 'physical, chemical and electro-chemical parameters in the view of engineers' and should thereby fulfil efficiency and accuracy at the same time (Alexander and Thomas, 2015). In addition, the factors become important when short-term data in laboratory are correlated with long-term data in the field (Alexander *et al.*, 2008). To date, various parameters, strongly related to the deterioration mechanism of concrete, have been employed and have evaluated durability of concrete both directly and indirectly. Among them, parameters related to chloride-induced corrosion are discussed below.

As a physical parameter, compressive strength, as a performance factor, is conventional for a prescriptive approach but is more closely related to a mechanical property than a material property of concrete. In other words, the compressive strength from well-controlled laboratory samples cannot be fully representative of the characteristics of cover concrete directly exposed to aggressive environments. In addition, the compressive strength at 28-days is useful to confirm a rapid quality control, but could detract from the durability of concrete. However, it is still the preferred factor for engineers due to the rapid and reliable acquisition of data and the indirect reference by using the maximum water-to-cement ratio. Porosity is also an important factor, as deterioration of concrete occurs by the movement of aggressive agents through an inter-connected pore network. Thus, this parameter is quantified using the oven-dry method or mercury intrusion porosimetry.

Diffusivity is expressed by the migration coefficient and diffusion coefficient for chloride transport in concrete. Diffusion occurs due to concentration gradients established within a medium, but migration is generated by a difference in electrical potential. Although diffusivity is sensitive to various factors including age, environmental condition and type of binder, this is a determining factor to describe an initiation phase in chloride-induced corrosion of concrete. Meanwhile, electrical resistivity is one of the electro-chemical parameters and is informative regarding durability of concrete. In addition, its measurement is easy and low cost. The electrical resistivity of concrete involves information on all parameters including diffusivity (Van Noort *et al.*, 2016), the condition

of pores (Li *et al.*, 2016) and strength (Ferreira and Jalali, 2010); it also indicates that unexpected errors in the result can be involved in a poorly controlled condition.

As typical electrochemical parameters in corrosion, corrosion potential and corrosion current density are introduced. Both parameters indicate the condition of steel but they differ in that a qualitative method is used for corrosion potential while a quantitative method is used for corrosion current density. Table 2.3 and table 2.4 present the criteria for the severity of corrosion of steel in concrete for both parameters. As shown in these tables, the criteria for corrosion of steel are expressed with a range of values instead of a single value, as these parameters are affected by a range of factors.

Table 2.3 Ranges of corrosion current density values (RILEM TC 154-EMC, 2004)

i_{corr} (mA/m^2)	V_{corr} (μm/year)	Corrosion level
≤1.0	≤1.0	Negligible
1.0 to 5.0	1.0 to 5.0	Low
5.0 to 10.0	5.0 to 10.0	Moderate
> 10.0	> 10.0	High

Table 2.4 Corrosion condition related with half-cell potential measurement (ASTM International, 2015)

Open circuit potential (OCP) values		Corrosion conditions
(mV vs SCE)	(mV vs CSE)	
-425	< -500	Severe corrosion
<-275	<-350	High (<90% risk of corrosion)
-125 to -275	-350 to -200	Intermediate corrosion risk
> -125	>-200	Low (10% risk of corrosion)

Performance factors (or durability indicators) are valuable to describe the performance of concrete directly or indirectly and are used with the following methods (Baroghel-Bouny *et al.*, 2014):

(i) Estimation of 'potential' durability of concrete within defined criteria;

(ii) Reference values in the practical codes as a performance-based concept; and,

(iii) Input values for physical- and chemical-based models.

Any parameter related to the performance of concrete can be a performance factor. Regarding the latter, a number of parameters related to concrete performance have been proposed/developed, but data are significantly scattered due to various conditions, including experimental set-up and environmental conditions. Therefore, it is necessary to integrate a number of indicators with minimum indicators. By doing so, the scatter in the data is expected to decrease to some extent.

2.3 Chloride transport

Chlorides dissolved in the pore solution move through the inter-connected pore system. As a result, transport rate is affected by the pore structure and the interaction between chlorides and cement hydrates. Considering that aggregates have a low permeability in concrete, the transport properties of cement paste are controlled by w/b, binder content. The type of binder is a leading factor to determine the transport properties of concrete.

Various driving forces in concrete result in different transport mechanisms including diffusion by concentration gradient, absorption by moisture gradient, permeability by pressure gradient, migration in electrical field and wick-action by a combination of water absorption and water vapour diffusion. Although diffusion and absorption generally coexist in concrete due to unsaturated conditions, the absorption range controlled by a low moisture content is relatively small, especially in a marine environment, and thus diffusion becomes the dominant mechanism for chloride transport.

The following section discusses the basic mechanisms and laws governing chloride diffusion, influencing factors and measurements.

2.3.1 Mass transport and flow in concrete transport systems

Ions in an ideal solution are governed by the Nernst-Planck equation based on mass conservation:

$$J_i = -D_i \frac{\partial C_i}{\partial x} - vC_i \frac{\partial \mathrm{E}}{\partial x} + C_i u \tag{2.1}$$

where J_i is the flux of ith ion, D_i is the diffusion coefficient of ith ion, C_i is the concentration of ith ion, v is the ion mobility, E is the electrical potential and u is the average mass velocity.

According to equation (2.1), ion movement is determined by diffusion, migration and convection and thus the equation extends Fick's law. Considering that diffusion of chlorides is the main mechanism and the spatial distribution, i.e. non-steady state condition, is given, the Nernst-Planck equation can be simplified as Fick's second law as follows:

$$\frac{\partial C}{\partial t} = D_d \frac{\partial^2 C}{\partial x^2} \tag{2.2}$$

where C is the chloride concentration, x is the transport distance of chlorides and D_d is the chloride diffusion coefficient.

Chloride transport can be accelerated using an applied electrical field. This principle is frequently applied to concrete so as to reduce time to evaluate the quality of concrete or to initiate corrosion. Considering that the convection term in equation (2.1) is neglected, i.e. ion mobility is controlled by the diffusion coefficient by the Nernst-Einstein relation, migration-diffusion of chloride in non-steady state conditions is equated as follows (Tang, 1996a):

$$v = D_m \frac{zF}{RT} \tag{2.3}$$

$$J = -D_m \left(\frac{\partial C_f}{\partial x} - \frac{zF}{RT} C_f \frac{\partial \mathrm{E}}{\partial x} \right) \tag{2.4}$$

where D_m is the chloride migration coefficient, $\frac{\partial C_f}{\partial x}$ is the concentration gradient of free chloride (C_f), z is the absolute value of ion valence (1 for the chloride ion), T is the solution temperature (K), R is the gas constant (8.314 J/(K·mol)), and F is the Faraday constant (96,487 J/(V·mol)).

In steady-state conditions, equation (2.4) can be simplified as given in equation (2.5) below, because the flux is constant irrespective of time and space provided that a constant chloride exists through the bulk solution. Hence, the equation only represents the migration process,

$$J = -D_m \frac{zF}{RT} C_f \frac{\partial \mathrm{E}}{\partial x} \tag{2.5}$$

In general, chloride transport is described by the above equations; however, the governing equation for modelling or analysis is determined by the main transport mechanism and concrete condition. The description of chloride transport in concrete is not straightforward due to various influencing factors. In the process of transport through inter-connected liquid-filled pores, a portion of chlorides reacts with the cement matrix either physically or chemically. In the following section, the factors influencing transport processes are discussed.

2.3.2 *Influencing factors*

Effect of pore structure

As concrete is a porous material, dissolved aggressive agents move through the (connected) pore system which can eventually lead to deterioration. Consequently, the pore structure is a main factor in determining the rate of deterioration. In concrete, there are two general types of pores: meso- and micro-pores. The meso-pores are visible including entrained and occluded air voids. The entrained air voids are around 0.1 mm in diameter evenly distributed throughout the cement paste and in some cases they are deliberately formed. On the other hand, entrapped air voids up to several millimetres in diameter are formed by improper compacting procedures. The voids are considered to have an insignificant influence on transport because they have less connectivity (Glass and Buenfeld, 2000a).

Capillary pores, gel pores, and the interfacial-transition zone could be included at the micro-scale. These pores are, typically, distributed in cement pastes. Capillary pores, up to a few microns, provide the main path for chloride transport into concrete. They are randomly distributed with an inter-connected system (Neville, 2011). The size of capillary pores decreases with the process of hydration. The gel pores, up to 2 or 3 nm in nominal diameter, are much smaller than the capillary pores. These pores comprise 28% of total volume in the gel. The interfacial-transition zone between cement paste and aggregates can be observed and has high porosity due to the wall effect. There are two opposing effects within the interfacial-transition zone: one is to restrict the movement of aggressive ions due to its isolated formation, and the other is that the ions percolate into the inner concrete rapidly when the amount of aggregate increases.

Transport rate is dominated by the connectivity or tortuosity of the pore network, which is affected by a number of factors including environmental conditions and material properties. For example, the hydration process reduces the transport rate of chlorides as the inter-connected capillary pores are isolated by the development of the gel. For dried concrete, ionic movement is also limited due to the loss of pore-fluid connectivity in the concrete.

Effect of chloride binding

Chlorides are present in concrete as two types: bound chloride and free chloride. In the process of transport in concrete, some chlorides are bound by hydration products either physically or chemically, while the remaining chlorides, termed free chloride, move inward. Free chlorides lead to steel corrosion by destroying the passive layer on the steel surface. For this reason, chloride binding is important in the evaluation of concrete durability in the case of chloride attack.

Chlorides present in pore water react with tri-calcium aluminate, denoted by C_3A ($3CaO \cdot Al_2O_3$), or tetra-calcium almuminoferrite, denoted by C_4AF ($4CaO \cdot Al_2O_3 \cdot Fe_2O_3$), to form Fridel's salt ($C_3A \cdot CaCl_2 \cdot 10H_2O$) or its analogue ($C_3F \cdot CaCl_2 \cdot 10H_2O$) (Hirao *et al.*, 2005). Binding is also established with the adsorption to calcium silicate, denoted by C-S-H. Adsorption is described by ionic exchange between chlorides in the pore solution and hydroxides from C-S-H, which takes place in the electrical double-layer at the C-S-H/pore solution interface or by inserting chlorides into C-S-H interlayer spaces (Florea and Brouwers, 2012). Chloride binding capacity by physical binding is 20% of that by chemical binding; however, the mass of C-S-H is much higher than monosulface hydrate (AFm: $C_3A \cdot CaSO_4 \cdot 12H_2O$), which is the main hydrate in chemical binding. Hence, it is assumed that physical binding is predominant compared to chemical binding (Hirao *et al.*, 2005), particularly, for binders with larger quantity of CaO-SiO_2 elements.

Chloride binding affects transport process by a refinement of pore structure and a decrease of free chloride in the pore-water. When chloride was present in concrete, the density of C-S-H increased and total porosity decreased (Midgley and Illston, 1984; Suryavanshi *et al.*, 1995) and the formation of Fridel's salt decreased the pore space via the pore blocking effect (Andrade *et al.*, 2011). The concentration relation between bound chlorides and free chlorides at a given temperature is the chloride binding isotherm, of which there are

three types: linear, Langmuir and Freundlich isotherm. Tuutti (1982) proposed the linear binding isotherm as follows:

$$C_b = \mathrm{a} \cdot C_f \tag{2.6}$$

where C_b is the concentration of bound chloride, C_f is the concentration of free chlorides, and a is a constant.

Arya et al. (1990) modified the linear relation by adding the intercepts of the bound or total chloride axis. The relation has sometimes been found in field-exposed samples, which has been attributed to the leaching of hydroxides (Sandberg, 1999). However, a non-linear relationship between bound and free chlorides has been generally accepted. Both Langmuir and Freundlich isotherms are typical for describing the non-linear relationship as shown in equations (2.7) and (2.8), respectively. Tang and Nilsson (1993) found that the Langmuir and the Freundlich isotherms are suitable at a range of chloride concentration < 0.05 mol and > 0.05 mol, respectively. The authors suggested that the adsorption process in a high chloride concentration is more complex than monolayer adsorption. It is notable that the Freundlich isotherm can cover chlorides dissolved in seawater and is simpler in mathematical calculations. In addition to chloride concentration, chloride binding is also sensitive to cementitious materials and hydration products (Song *et al.*, 2008b).

(a) Langmuir isotherm:

$$C_b = \frac{\mathrm{a} \cdot C_f}{1 + \mathrm{b} \cdot C_f} \tag{2.7}$$

(b) Freundlich isotherm:

$$C_b = \mathrm{c} \cdot C_f^{\mathrm{d}} \tag{2.8}$$

where a and b are Langmuir's parameters, and c and d are Freundlich's parameters, which vary with binder content and the binder and pore solution compositions.

Effect of concrete mix

Both pore structure and chloride binding are influenced by factors such as type of binder and w/b. Aggregate itself is regarded as an impermeable material, and thus the transport

through aggregate is negligible due to low permeability. Although it has been reported that transport rate is influenced by aggregate distribution and aggregate-to-cement-paste-volume ratio (Oh *et al.*, 2002; Andrade *et al.*, 2011), the characteristic of cement paste (e.g. the connected capillary pores in the cement matrix) is more crucial in determining the transport rate.

According to previous studies (Leng *et al.*, 2000; Yu and Ye, 2013; Bostanci *et al.*, 2016), SCMs are advantageous as they form a finer/disconnected pore network to create denser concrete due to the pozzolanic reaction. Moreover, it has also been reported that for concrete using SCMs, pore structures are refined by the particle size distributing in the range 10 to 100 nm (Hussain and Rasheeduzafar, 1994). Concretes using SCMs bind more chlorides than ordinary Portland cement (PC) concrete because cement pastes containing ground granulated blast-furnace slag (GGBS) and fly ash (FA) are favourable to form C_3A or C_4AF by chemical composition in cementitious materials (Luo *et al.*, 2003; Thomas *et al.*, 2012; Song *et al.*, 2008a). In addition, large amounts of C-S-H formed in concrete using SCMs are helpful to bind chlorides due to the large surface area of C-S-H available for adsorption (Hirao *et al.*, 2005; Tang and Nilsson, 1993).

It is well known that concrete with a high w/b has a low resistance to chloride transport due to a high (connected) porosity, but for chloride transport it is of interest that w/b is linked with cement content. First, it has been observed that the surface chloride content decreases with an increase in w/b at a given cement content; this is because a thick skin layer of concrete with a high w/b enhances dielectric activity between hydroxyl ions in concrete skin and chloride ions in the external source, and thus the repulsive force between these ions prevents the accumulation of chlorides in the concrete surface (Song *et al.*, 2008a). Blended concrete shows higher surface chloride contents than PC concrete because of its higher binding capacity. The build-up of chloride on the concrete surface can result from the binding effect, which increases the content of total chloride on the concrete surface (Tang and Nilsson, 2000; Glass and Buenfeld, 2000b). In addition, the binding effect is dependent on the concentration of chloride; thereby, the binding capacity increases with an increase in the ingress depth of chloride into concrete (Glass and Buenfeld, 2000b).

Effect of degree of saturation

The moisture condition of concrete is decisive in determining transport properties and it varies depending on environmental conditions such as temperature, exposure duration/location and relative humidity. Ionic diffusion takes place through the liquid phase in the inter-connected pore system; hence, the degree of saturation is one of the main influences on transport properties. It is also accepted that unsaturated concrete, (i.e. concrete above the mid-tide/splash zone in a marine environment) is more vulnerable to chloride-induced corrosion than saturated concrete, (i.e. concrete below the mid-tide level) (British Standards Institution, 2016), due to absorption of chloride and high availability of oxygen for the corrosion process. Hence, the degree of saturation should be considered when evaluating the chloride transport.

For unsaturated concrete, both diffusion and absorption have been simultaneously considered as chloride transport mechanisms in many studies (Nilsson, 2000; Sleiman *et al.*, 2009; Kumar, 2010; Baroghel-Bouny *et al.*, 2014). Chloride profiles in unsaturated concretes sometimes show that the chloride contents are decreased in the surface concrete, which is attributed to moisture transport during wet/dry cycles (see figure 2.2). However, in addition to moisture transport, various reasons for this shape have been presented, including (i) the skin effect or wall effect, (ii) the dielectric reaction between the concrete surface and chloride environment, (iii) the washing-out effect, (iv) leaching, and (v) carbonation. Moreover, the convective zone ($< 3.99 \pm 1.05$ mm in marine structures, (Gao *et al.*, 2017)) formed in concrete subjected to chloride environments is relatively small compared to the cover depth, and thus diffusion is only considered as a transport mechanism during the regression analysis with experimental data, as shown figure 2.2.

In addition, Tang (2003) reported that capillary pores were almost saturated in the submerged zone while degree of capillary saturations was ~80% in the splash zone, irrespective of depth from the surface of the concrete subjected to a marine environment. Chloride ingress was severe, with the following order: submerged > splash > atmospheric zone (Tang, 2003). It seems reasonable that diffusion is taken as the main transport mechanism, but the difference in the transport rate should be considered with unsaturated concrete. When only diffusion is considered, it has been reported that the diffusion coefficient becomes smaller with a decrease in the degree of saturation (Yokozeki *et al.*, 2003; Kumar, 2010; Nilsson, 2000; Nanukuttan *et al.*, 2008). As shown in figure 2.3, it is noteworthy that the diffusion coefficient is dramatically decreased when degree of

saturation reduces. In summary, considering chloride ingress and the relation between the degree of saturation and the diffusion coefficient, the durability of concrete structures subjected to chloride environments, in particular marine environments, is estimated only using diffusion at degree of saturation larger than 20 %.

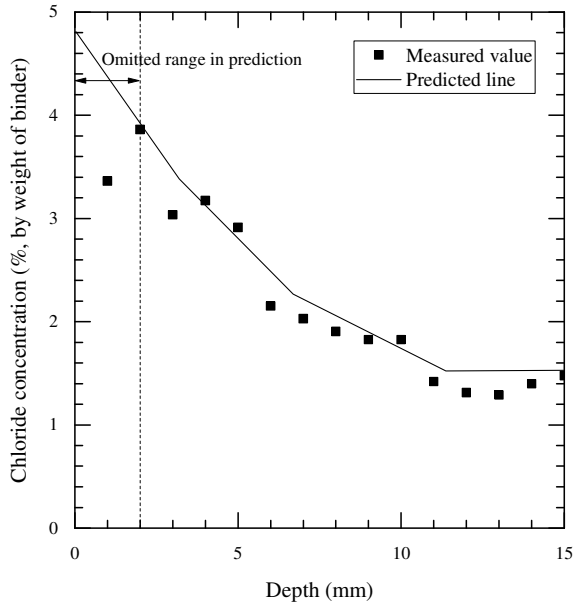

Figure 2.2 A modified example of the prediction of chloride profile in unsaturated concrete (Song *et al.*, 2008a) modified by the author.

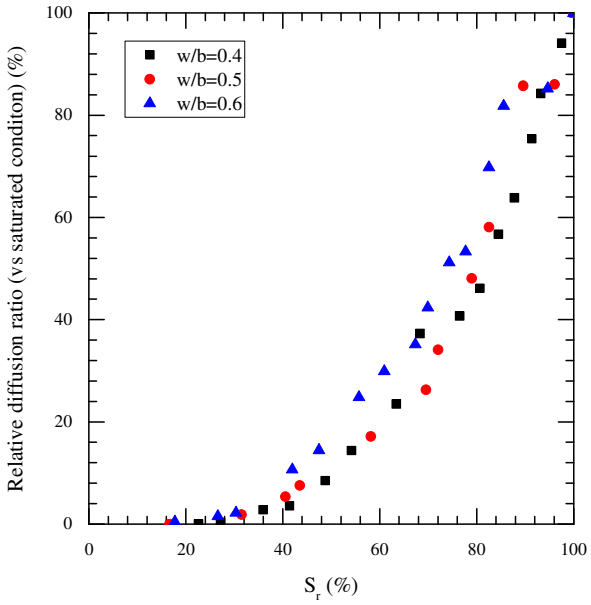

Figure 2.3 Relative diffusion rate with saturation degree of PC concrete (Kumar, 2010) replotted by the author.

2.4 Chloride-induced corrosion of steel

The concrete cover protects the reinforcing steel from the ambient environment. A low permeability slows down the ingress of aggressive agents and the high alkalinity of the pore solution provides a stable oxide layer on the steel surface. However, in the case of the corrosion of steel in concrete subjected to chloride environments, attention has mainly been paid to the presence of chloride, which triggers the local destruction of the passive layer.

In Tuutti's model (1982), the service life of a concrete structure is divided into two stages: (i) corrosion initiation and (ii) corrosion propagation. The corrosion initiation stage relates to chloride ingress through the cover-zone concrete before destroying the passive film, while the corrosion propagation stage describes the active condition for corrosion after the chloride content at the steel depth exceeds the threshold level. For chloride-induced corrosion, to estimate the service life of concrete, the corrosion propagation stage is considered in addition to the initiation of corrosion corresponding to chloride transport. Meanwhile, the limit of the serviceability, which refers to user comfort, aesthetic aspects and functionality, is defined as the limit that indicates whether the performance of the concrete structure is acceptable or not according to Vrouwenvelder and Schießl (1999). As shown in figure 2.4, the limit states to define the service life of a concrete structure include (i) depassivation of steel in the reinforced concrete structure exposed to a chloride environment corresponding to the end of the corrosion initiation stage in Tuutti's model; (ii) the acceptable crack width by chloride-induced corrosion, which is limited to 0.3 mm; (iii) the loss of performance of the concrete structures by spalling of concrete and section loss of steel which cause a fatal accident; and (iv) excessive deflection and collapse.

The following section reviews chloride-induced corrosion including the depassivation process and influencing factors. In addition, the critical chloride threshold level for corrosion resistance is also investigated.

2.4.1 *Corrosion mechanism*

Corrosion requires both oxygen and water, and metallic corrosion involves redox reactions occurring simultaneously. Corrosion depends on environmental conditions, i.e. acid and neutral/alkaline conditions, as follows.

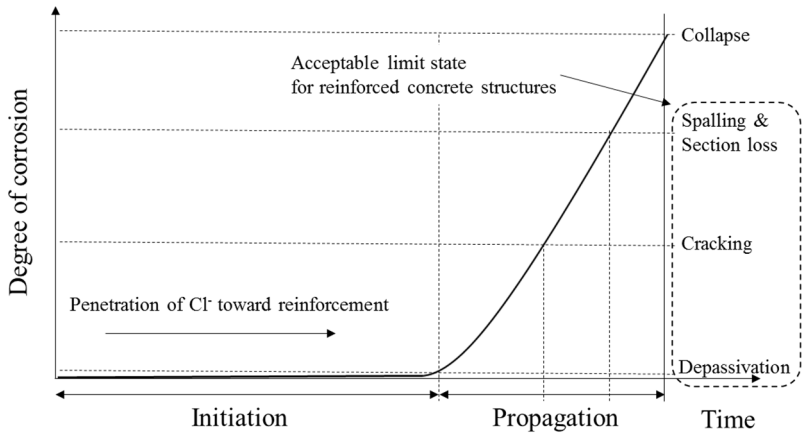

Figure 2.4 The service life of reinforced concrete structures and possible limit states.

In acidic conditions,

$$Fe + 2H^{+} \rightarrow Fe^{2+} + H_{2(g)} \tag{2.9}$$

In neutral/alkaline conditions,

$$4Fe + 6H_2O + 3O_2 \rightarrow 4Fe(OH)_3\downarrow \tag{2.10}$$

$$2Fe(OH)_3 \rightarrow Fe_2O_3 + 3H_2O \tag{2.11}$$

Steel corrosion in concrete is described as an electrochemical process consisting of two half-cell reactions including oxidation in the anodic area and reduction in the cathodic area. In a highly alkaline environment, such as concrete with a pH in the range 12.5–13.5, steel is protected by a thin oxide layer, called a passive layer. Once chlorides dissolved in the pore solution reach the steel surface, the passive film is locally destroyed by adsorption of Cl^-, and then chloride-induced corrosion is triggered. In addition, corrosion accelerates as Cl^- also competes with OH^- for adsorption on the steel surface. This corrosion can occur even in an alkaline environment such as concrete when chloride content exceeds the threshold level. After depassivation, the electrons from the iron move through the metal to the cathode, and the cathodic reaction is affected by the pH of the pore solution and the potential at the steel surface. An electric circuit is formed by an ionic exchange current through the electrolyte to maintain electro-neutrality between oxidation in the anode and reduction in the cathode. Thereby, the corrosion rate is controlled by one dominate factor in an electrochemical cell consisting of the anode in

steel (R_a resistance and I_a current in the anode), the cathode in steel (R_c resistance and I_c current in the cathode), steel itself (R_m resistance and I_m current in steel), and concrete (R_{conc} concrete resistance and I_{conc} current through concrete), as shown in figure 2.5. Therefore, the performance or the durability of the reinforced concrete structure is lost by corrosion, which leads to cracking, spalling, and a reduced cross-section area of reinforcement.

The anodic reaction and chloride effect in concrete can be summarised as follows:

$$2NaCl \text{ or } CaCl_2 \rightarrow 2Na^+ \text{ or } Ca^{2+} + 2Cl^- \text{ (dissolution of chloride)} \quad (2.12)$$

$$Fe \rightarrow Fe^{2+} + 2e^- \text{ (dissolution of iron)} \quad (2.13)$$

$$Fe^{2+} + 2(OH)^- \rightarrow Fe(OH)_2 \text{ (precipitation of rust)} \quad (2.14)$$

$$2Fe(OH)_2 + H_2O + O_2 \rightarrow 2Fe(OH)_3 \text{ (oxidation of rust)} \quad (2.15)$$

$$Fe^{2+} + 2\,Cl^- \rightarrow FeCl_2 \text{ (precipitation of green rust)} \quad (2.16)$$

$$4FeCl_2 + O_2 + 6H_2O \rightarrow 4FeOOH + 8HCl \text{ (oxidation of green rust)} \quad (2.17)$$

The cathodic reaction in concrete is:

$$O_2 + 2H_2O + 4e^- \rightarrow 4(OH)^- \text{ (hydrolysis)} \quad (2.18)$$

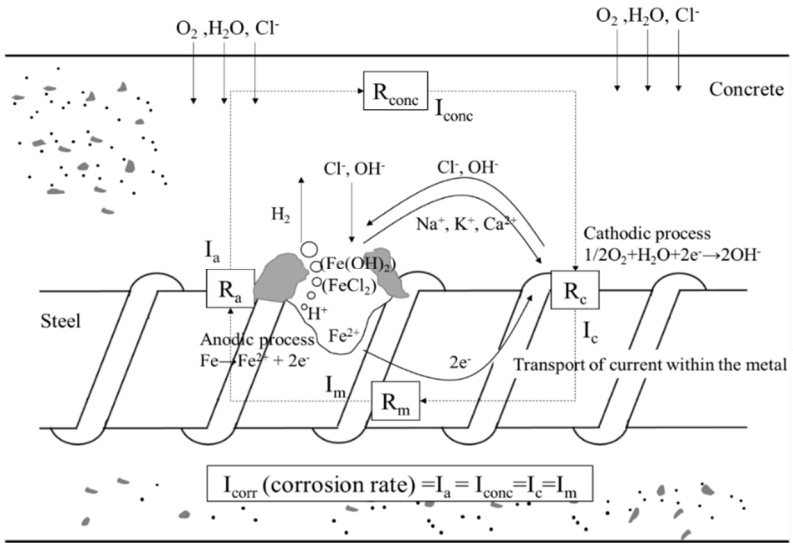

Figure 2.5 Schematics for chloride-induced corrosion of steel in concrete.

The types of corrosion, including uniform corrosion and pitting corrosion, are determined by the spatial distribution of the anode and cathode on the steel surface or the resistivity of concrete. Uniform corrosion (microcell corrosion) is distributed in the overall steel surface and is generally detected in reinforced concrete degraded by carbonation. Pitting corrosion (macrocell corrosion) occurs in small areas of steel surface but is more severe by cross-section loss of the reinforcing steel and is detected in chloride-contaminated reinforced concrete.

In theory, under localised (or pitting) corrosion, a significant difference between the electrical potential of the anode and the cathode exists. However, it is difficult to measure the potentials in a pure anode and a pure cathode, which are important to model corrosion propagation in practice as the measured potential is affected by concrete resistivity, cover depth, oxygen availability and anode-to-cathode area ratio (Pour-Ghaz *et al.*, 2009). In addition, the potential in the cathode is also decreased by the lowered potential in the anode caused by corrosion and the range influencing the potential in the cathode, called a correlation length, is up to 2 m from the anode (Keßler *et al.*, 2014; Ji *et al.*, 2013). Hence, measured potential using the half-cell potential technique was sometimes shown as a corrosion potential gradient between anode and cathode in pitting corrosion (Keßler *et al.*, 2014; Liam *et al.*, 1992), and it is recommended that corrosion evaluation is carried out with the gradient instead of an absolute value (RILEM TC 154-EMC, 2003). Although various detection methods for corrosion have been suggested, the measured corrosion values remain scattered, including corrosion potential and corrosion rate. The corrosion process is also sensitive to the exposure environment as the process is controlled by oxygen and moisture availability in addition to chloride concentration. The following sections review the influencing factors and measurement techniques affecting the corrosion process.

2.4.2 *Chloride threshold level*

Chloride threshold level (CTL) is defined differently from two standpoints: (i) the scientific view and (ii) the engineering view (Angst *et al.*, 2009). In the former, the CTL is a tolerated chloride level for depassivation, while in the latter the CTL is considered to be the accumulated chloride content up to ‘the acceptable deterioration’. The CTL based on the engineering view is pragmatic, but the criterion for the degree of deterioration is ambiguous, leading to a high scatter in the CTL. In the scientific view, although the

criterion is clear, the value is significantly underestimated considering the effect of corrosion on the structure.

Regarding the representation of CTL, total chloride concentration (by weight of binder or concrete) is generally preferred among various expressions including $[Cl^-]/[OH^-]$ and free chloride concentration (by weight of binder or concrete). The $[Cl^-]/[OH^-]$ indicates the inhibitive effect of hydroxide ions dissolved in pore solution. However, alkaline minerals (e.g. precipitated calcium hydroxide) of the cement matrix on the steel surface also buffer the reduction of pH in the pore solution. The bound chlorides significantly decrease in a high pH (> 12.6) and a low pH, and this expression thus does not consider the dependence of chloride binding capacity on hydroxide ion concentration (Ann and Song, 2007). On the other hand, the representation of CTL using free chloride concentration (by weight of binder or concrete) may ignore the release of bound chloride caused by acidification during pit growth and a buffering effect, i.e. resisting a pH drop, by hydration products such as calcium hydroxide, while total chloride concentration (by weight of binder or concrete) is easy to measure and reflects corrosion risk of bound chloride and hydration products. Thus, the CTL with total chloride concentration (by weight of binder or concrete) is reasonable, but it is still highly scattered due to a number of factors affecting it simultaneously (Angst *et al.*, 2009).

According to Angst et al. (2009) and Bertolini and Redaelli (2009), factors influencing the CTL are well-established and include (i) the steel-concrete interface, (ii) the electrochemical potential of steel, (iii) the surface condition of the steel, (iv) the hydroxide content, (v) the moisture content of concrete, (vi) the oxygen availability at the steel surface, (vii) the concrete temperature, (viii) the mix components, (ix) the electrical resistivity of concrete, (x) the source of chlorides, and (xi) the expression of chloride concentration. The CTLs obtained from several papers (Glass and Buenfeld, 1997; Alonso *et al.*, 2002; Angst *et al.*, 2009) are presented in table 2.5, and only summarised for concrete. The values are distributed in the range of 0.1–2.7% (total chloride concentration by weight of binder). As mentioned above, a dominating factor cannot be identified to affect the CTL. In addition, no standard method exists for estimating the CTL and detecting depassivation; instead, different researchers have used a number of methods.

Table 2.5 Published CTL values obtained from concrete

Authors	Year	CTL (%, total chloride)	Detection method	Exposure condition	Cited in
Gouda	1970	0.75, 1, 2	GP	+	Alonso et al. (2002)
Page	1991	2.5	CP	+	
Arup	1996	1.7-2.7	PP	+	
Stratfull	1975	0.2-1.4	CP	Field	Angst et al. (2009)
Vassie	1984	0.25-1.5	CP	Field	
Hope and lp	1987	0.1-0.19	LPR, EIS, VI, ML	W/D	
Thomas	1996	0.2-0.65, 0.7	ML	Field	
Sandberg	1998	0.4-1.5	CP	Field	
Zimmermann	2000	0.2-0.4	MC	Field	
Fluge	2001	0.72	VI	Field	
Morris et al	2004	0.4-1.3	LPR, CP	Field	
Kaesche	1959	0.32	GDP, VI	Sub	
Baumel	1959	0.57-1.09	PDP, VI	Sub	
Gouda and Halaka	1970	0.45, 0.15	GP	+	
Locke and Siman	1980	0.4-0.8	LPR	Air	
Schies and Raupach	1990	0.48-2.02	MC	+	
Lambert, page et al	1991	1.5-2.5	LPR, CP, ML	+	
Schiessl and Breit	1996	0.5-1.5	MC	Air	
Oh et al	2003	0.68-0.97	CP, VI	95% RH	
Morris et al	2004	0.4-1.3	LPR, CP	Sub/Air	
Nygaard and Geiker	2005	0.52-0.75	PT	+	
Mannera et al.	2008	0.6-2.0	LPR, CP	Air	Glass and Buenfeld (1997)
Henriken	1993	0.3-0.7	+	Field	
Treadway et al	1989	0.32-1.96	ML	Field	
Bamforth and Chapman-Andrews	1994	0.4	+	Field	
Tuutti	1993	0.5-1.4	+	+	
Lukas	1985	1.8-2.2	+	Field	

* GP: galvanostatic pulse polarisation, CP: corrosion potential, PT: potentiostatic polarisation, LPR: linear polarisation resistance, EIS: electrochemical impedance spectroscopy, VI: visual inspection, ML: mass loss, MC: macrocell current, GDP: galvanodynamic polarisation, PDP: potentiodynamic polarisation, W/D: wet/dry cyclic regime

2.4.3 *Influencing factors of steel corrosion*

The corrosion process involves electrical phenomena combined with chemical reaction. Electrical potentials, which are required for ionic dissolution at the anodic site and reduction reaction at the cathodic site, can be represented by the Nernst equations:

$$\mathrm{E_a} = \mathrm{E_a^0} - \frac{RT}{z(=1)F} ln \frac{[\mathrm{Fe^{2+}}]}{[Fe]} \tag{2.19}$$

$$\mathrm{E_c} = \mathrm{E_c^0} - \frac{RT}{z(=4)F} ln \frac{[\mathrm{H_2O}]^2[\mathrm{O_2}]}{[\mathrm{OH^-}]^4} \tag{2.20}$$

where $\mathrm{E_a}$ and $\mathrm{E_c}$ are the electrode potential for oxidation at the anode and cathode, respectively (V); $\mathrm{E_a^0}$ and $\mathrm{E_c^0}$ are the standard electrode potential of steel at the anode and cathode, respectively (V); $[\mathrm{Fe}]$ is the activity of an Fe molecule in the steel bar (=1); $[\mathrm{Fe^{2+}}]$ is the concentration of Fe^{2+} in the electrolyte (mol/l); $[\mathrm{OH^-}]$is the concentration of OH^- in the electrolyte (mol/l) ($\log[\mathrm{OH^-}] = pH - 14$); $[\mathrm{O_2}]$ is the concentration of oxygen (mol/l); $[\mathrm{H_2O}]$ is the amount of capillary water (l/m^3); z is the absolute value of ion valence; T is the solution temperature (K); R is the gas constant (8.314 J/(K·mol)); and F is the Faraday constant (96,487 J/(V·mol)).

The difference of electrical potential in the corrosion cell triggers the electromotive force, leading to corrosion current flowing through the electrolyte from anode to cathode. From the above equations and figure 2.5, it is evident that the corrosion process is affected by the following factors:

(i) the availability of oxygen and water;

(ii) the concentration of Fe^{2+}; and,

(iii) the pH of the pore solution in the vicinity of steel.

In addition, the corrosion process is also influenced by external sources such as temperature, aggressive agents, and the concrete resistivity in the region of the corrosion activity. Poubaix (or the equilibrium potential/pH) and Evans diagrams are useful in explaining the corrosion process from depassivation to propagation. The two diagrams

depict the effects of the influencing factors on the corrosion process. In general, steel embedded in concrete is protected by the formation of a passive film including alkaline hydrates, i.e. a calcium hydroxide layer and oxide film. The oxide film such as magnetite, denoted by Fe_3O_4, is formed in a high-pH environment, which reacts with aggressive ions (i.e. chlorides), as shown in figure 2.6, and thus retards direct dissolution of the steel. On the other hand, the inhibitive effect of calcium hydroxide on corrosion is evident by maintaining a high pH of the pore solution, but the formation of the layer appears to be irregular (Glass *et al.*, 2001) and thus the inhibitive effect is randomly distributed along the bar. Before the depassivation process, the role of oxygen and moisture is negligible as steel dissolution is very low.

However, once chloride reaches the steel depth, the depassivation process is immediately triggered and the anodic reaction proceeds rapidly, as shown in figure 2.7 (a) in the Evans diagram. After depassivation, the corrosion rate is controlled by factors other than chlorides (Angst *et al.*, 2011a). For the cathodic reaction, availability of oxygen is crucial, and thus the corrosion rate in saturated concrete is reduced compared to the unsaturated concrete, as shown in figure 2.7 (b). Conversely, a low moisture-content in concrete increases its electrical resistivity, leading to prevention of corrosion cell formation. It has been reported that the critical degree of water saturation to accelerate corrosion is ~ 70 – 80% (Ožbolt *et al.*, 2011). Anodic dissolution is, on the other hand, affected by type of steel (Freire *et al.*, 2011), as it is well known that noble materials such as stainless-steel show high resistance to corrosion. Moreover, corrosion propagation is controlled by the concrete itself. SCMs produce a disconnected pore network (hence, high electrical resistivity), so ionic movement between the anode and cathode is reduced. However, the pH of the pore solution in SCM concrete is lowered in comparison to that in PC concrete. A lower pH results in an increase in corrosion rate as well as rapid depassivation. These two competing effects make the corrosion resistance of SCMs controversial.

It has been reported that chloride content in the tidal/splash zone is lower than in the submerged zone (Tang, 2003), but it is accepted concrete in the tidal/splash zone is prone to the most severe deterioration. It can be deduced that chloride content at the steel depth is not the only factor to determine service life of a structure, although higher chloride content increases the possibility of corrosion. In addition, it should be noted that the CTL in the laboratory is lower than that found in the field.

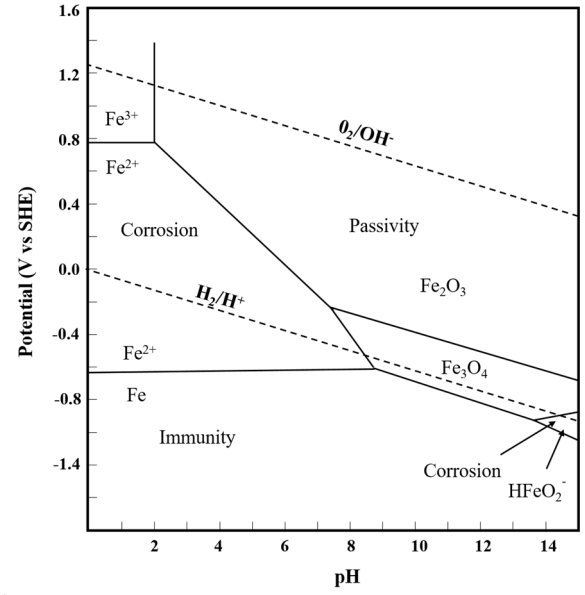

Figure 2.6 Pourbaix diagram for iron showing the most stable products at a given pH and potential (Roberge, 2008).

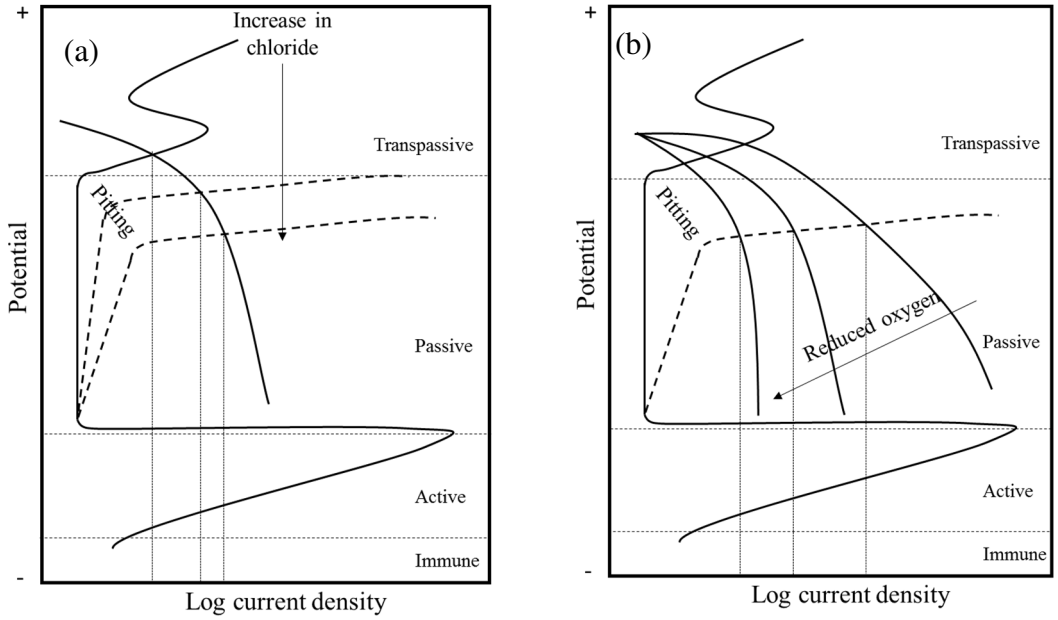

Figure 2.7 Schematics for Evans diagram (a) with an increase in chlorides and (b) with a decrease in oxygen availability.

2.5 Electrical resistivity

The electrical resistivity of concrete has recently come to be of importance, as this parameter is closely related to transport properties as well as corrosion rate. It has become attractive to use electrical resistivity as a candidate 'performance' factor. Essentially,

electrical resistance is measured in a non-destructive manner and the electrical resistivity is calculated. Resistivity is a geometrically independent parameter and for a prismatic sample is given by:

$$\rho = \mathrm{R}\frac{A}{L} \tag{2.21}$$

where ρ is the electrical resistivity (Ω·m), R is the electrical resistance (Ω), A is the area contact with electrode (m^2) and L is the length between two electrodes (m). The resistivity, however, is sensitive to a number of influencing factors which must be considered. The next section critically reviews these influencing factors.

2.5.1 *Factors influencing resistivity measurements*

Pore solution in concrete

The pore solution within the cementitious binder comprises Na^+, Ca^{2+}, K^+, SO_4^{2-}, OH^- and Cl^-, and its resistivity varies depending on the SCMs and degree of hydration. To account for the effect of the pore solution, the formation factor, F, is introduced as follows:

$$\mathrm{F} = \frac{\rho_{bulk}}{\rho_p} \tag{2.22}$$

where ρ_{bulk} is the bulk resistivity of the concrete (Ω·m) and ρ_p is the pore solution resistivity (Ω·m).

Provided that an accurate resistivity of the pore solution is determined, it should be relatively easy to estimate the transport property or corrosion process. However, it is another challenge to measure the resistivity of the pore solution in concrete, and pore-fluid extraction technique is not practical. The model based on the empirical equation can be used (Snyder *et al.*, 2003). In this study, the resistivity of the pore solution is estimated using the model provided by National Institute of Standards and Technology (NIST, USA) (Bentz, 2007), in which the resistivity is calculated with the oxide composition of the binder and degree of hydration.

Environment

Concrete structures are influenced by their ambient environment (e.g. exposure conditions, wetting/drying action and temperature), which changes the moisture-state of concrete cover-zone. The changing moisture state alters the resistivity of the concrete, which decreases with increasing degree of saturation. The changing degree of saturation also affects ionic transport in concrete. Figure 2.8 shows the relationship between the electrical resistivity and the diffusivity in concrete (Sengul, 2014). Moreover, the temperature to which concrete is exposed also influences the resistivity of concrete. It is well known that the resistivity decreases with an increase in temperature. In this respect, Polder (2001) states that the electrical resistivity for saturated and for dry concrete is changed by 3% and 5% for each degree of absolute temperature change, respectively. An activation energy approach using an Arrhenius relationship can be used to standardise measurements to a reference temperature (McCarter *et al.*, 2012).

The movement of chlorides into concrete influences its resistivity due to the reduction in resistivity of the pore solution. However, it should be mentioned that the binding process of chloride in concrete could refine the pore structure, leading to an increase in the bulk resistivity of concrete due to a restricted electrical path. In summary, the factors influencing resistivity mentioned above should be considered to evaluate the transport properties or the corrosion process using this parameter.

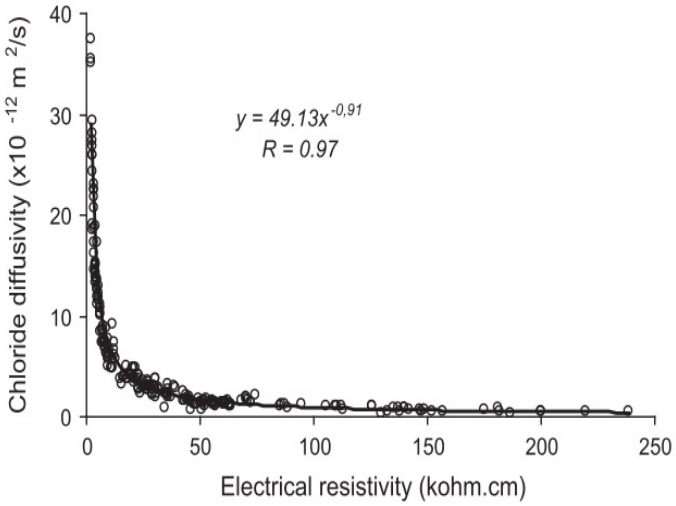

Figure 2.8 The relationship between electrical resistivity and diffusivity (Sengul, 2014).

Hydration

In concrete, chemical reactions continuously occur and subsequently lead to a refined pore structure. Moreover, it has been reported that the electrical resistivity increases with the hydration process (McCarter *et al.*, 2013a). This trend is clearer for SCM concrete. The effect of hydration on the electrical resistivity is not negligible for analysis, and it is difficult to extract a change of electrical resistivity by hydration from the measured resistivity of concrete, especially exposed to a chloride environment at an early age. For example, the presence of chlorides in the pore solution generally leads to a decrease in the electrical resistivity, while the electrical resistivity increases with both hydration and chloride binding. Theses phenomena occur at the same time. In addition, the latent hydration for SCM concrete requires a longer measurement period to minimise the hydration effect on the electrical resistivity. Consequently, significantly limited data are available for concrete, in particular subjected to a chloride environment, considering the hydration effect.

2.5.2 Representation of electrical resistivity

Resistivity (equation (2.21)) is independent of the volume of the sample, whereas resistance depends upon the size and shape of sample. To account for different geometrical arrangements of electrodes, calibration of the electrode system may be required using computational modelling or an experiment (Angst *et al.*, 2011c; McCarter *et al.*, 2012). Meanwhile, although the absolute comparison with the values obtained from experiments is not established, the normalisation method is useful (McCarter *et al.*, 2001):

$$N_{\rho \text{ or } R} = \frac{\rho_t}{\rho_0} = \frac{\mathrm{R_t}}{\mathrm{R_0}} \tag{2.23}$$

where $N_{\rho \text{ or } R}$ is the normalised resistivity or resistance, ρ_t and R_t are the electrical resistivity (Ω·m) or resistance (Ω) at time t, and ρ_0 and R_0 are resistivity (Ω·m)/resistance (Ω) measured at that respective electrode position taken at a datum point in time.

This expression can minimise the effect of influencing factors on the electrical resistivity, and especially the effect of the pore solution. However, the expression represents a

relative value rather than an absolute value; thereby, the result is only useful for the description of a trend and not for quantification.

2.6 Summary

This chapter reviews the mechanisms and influencing factors in terms of deterioration of reinforced concrete caused by chloride-induced corrosion. In literature, it was found that a wide range of influencing factors influences on chloride transport and chloride-induced corrosion of steel in reinforced concretes and due to these, there are scatters in data such as CTL and diffusion coefficient. Especially, environmental factors such as degree of saturation and temperature are not readily simulated in the laboratory to represent the field concrete; thereby field study is also required to reflect these conditions properly.

Although evaluating performance of concrete is increasingly emphasized, specification, especially in UK, only specifies a prescriptive method. This is because a dearth of information on the relationship between values obtained from performance factors and those from the field. In addition, it is generally accepted that chloride transport rate is a performance factor to reinforced concrete subjected to chloride environments according to specifications, but the representations or testing methods for evaluation of chloride transport are various; thereby it is inevitable to show the scatters in data. To overcome this limitation, a representative parameter to describe performance of reinforced concrete subjected to chloride environments is required. In this study, electrical resistivity as a representative parameter was chosen as the resistivity is highly correlated to both chloride transport rate and corrosion rate of steel which are main factors to describe deterioration of reinforced concrete in chloride environments.

The following chapter reviews the methodology to evaluate the performance of reinforced concrete subjected to chloride environments.

CHAPTER 3
A METHODOLOGICAL REVIEW OF CHLORIDE-INDUCED CORROSION OF STEEL IN CONCRETE

3.1 Introduction

The premature deterioration of reinforced concrete structures leads to a significant drain on resources in terms of repair and maintenance. To date, various test methods and modelling have been suggested to estimate the service life of concrete structures, but it is still difficult to accurately evaluate this because influencing factors, including differences in techniques, differences in analysis, and differences in exposed environments, result in errors.

This chapter presents a methodological review of chloride transport in chloride-induced corrosion, measurements and existing predictive models. A range of electrochemical techniques, visual observation, mass loss, and predictive models relating to corrosion propagation are also summarised for chloride-induced corrosion propagation. In addition, the chapter reviews the electrical resistance measurement as a non-destructive method, which includes chloride transport and steel corrosion.

3.2 Measurement for chloride transport in concrete

According to Tuutti's model, chloride transport processes are important during the initiation phase of chloride-induced corrosion. Various methods have been developed to evaluate the chloride transport properties of concrete and this review focuses on those that are widely used. Electrical resistance measurements for evaluating pore structure are also reviewed. Figure 3.1 presents techniques that are classified with the test conditions, including type of parameters measured and test set-up. The sub-categories are explained in the following sections.

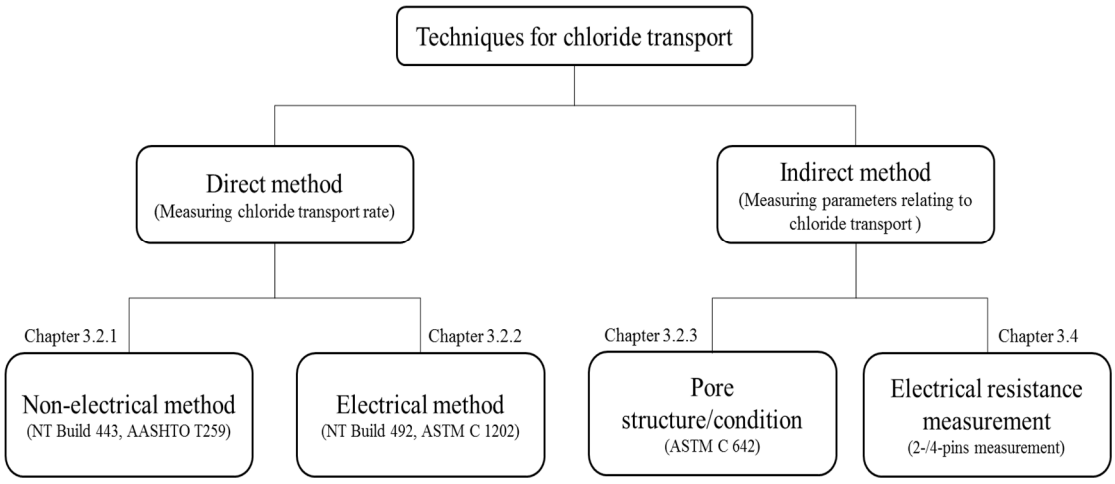

Figure 3.1 Classification of techniques for chloride transport

3.2.1 *Non-electrical methods*

Diffusion tests are based on the principle that chloride transport occurs due to a concentration gradient. The result is expressed with a chloride profile, i.e. the chloride content with respect to the penetration depth, and then the diffusion coefficient and surface chloride content are estimated from the chloride profile using regression analysis and error function based on Fick's law.

Two tests are specified in the codes: AASHTO T259 (Stanish *et al.*, 1997), called the ponding test, and NT Build 443 (Nordtest, 1995), called the bulk diffusion test. In the ponding test as shown in figure 3.2 (a), sorption and wick-action are considered in addition to diffusion as the sample is dried for 28-days prior to the measurement. Furthermore, one side of the sample is exposed to a 50% RH environment during the test. Although all possible transport mechanisms that can be found in a structure are described, the behaviour of chloride transport is exaggerated compared to the real behaviour (Stanish *et al.*, 1997). The bulk diffusion test as shown in figure 3.2 (b), on the other hand, measures chloride transport by establishing a concentration gradient across the sample. A chloride solution (2.8 mol NaCl) is applied to the sample for $\geq$ 35 days, and this solution is higher than the chloride content (3% NaCl) in the ponding test for 90 days.

Recently, all immersion, inversion and ponding tests in BS EN 12390-11 (British Standards Institution, 2015a) have been prescribed as a diffusion test; the 3% NaCl solution and 90-day test duration are also suggested. These tests describe a behaviour of chloride transport similar to that in a structure, but they can be both time-consuming and

laborious. Hence, it may be better to use the tests to obtain an input value for modelling and not evaluating the quality of concrete.

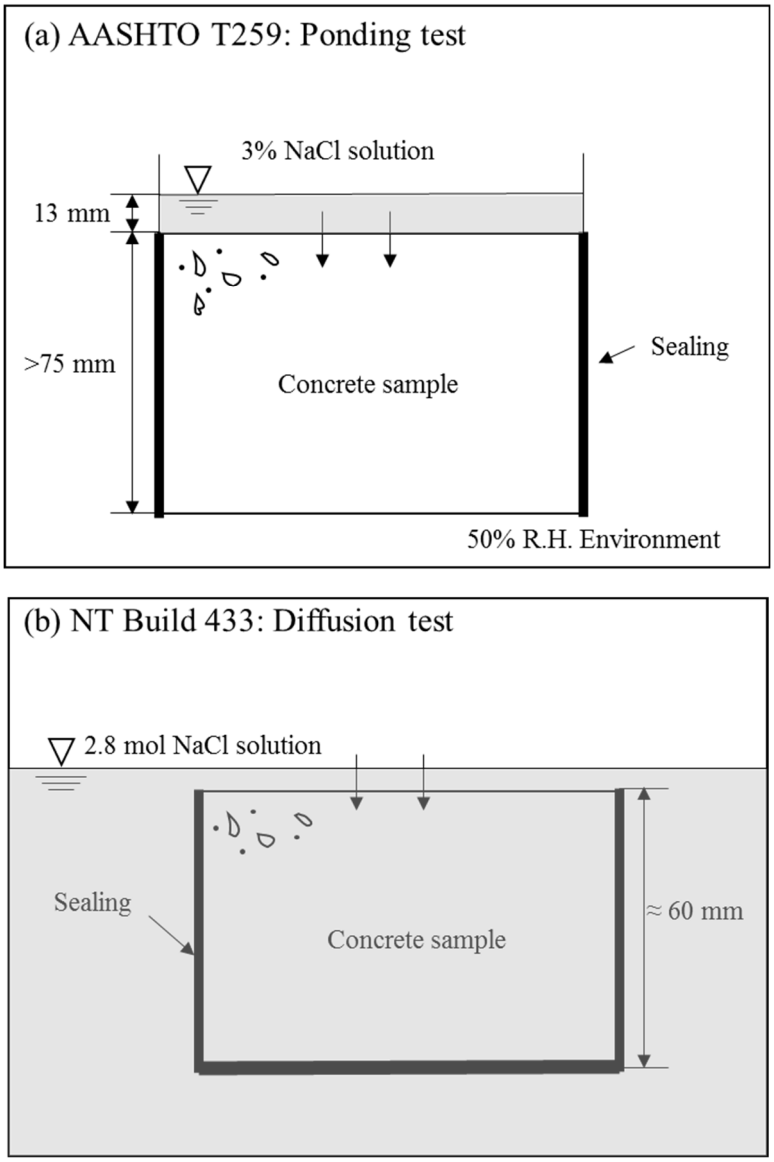

Figure 3.2 Test set-ups for (a) AASHTO T259 and (b) NT Build 443

3.2.2 *Electrical method*

The migration test accelerates chloride ingress using an electrical field and is suitable to evaluate concrete quality in the laboratory and to obtain an input parameter for predictive modelling. Migration testing is attractive in determining the chloride transport property of concrete, although the application of an electrical field is still controversial (Spiesz and Brouwers, 2012). Migration testing is subdivided into several types depending on whether

chlorides pass through the sample or not, namely non-steady state and steady state of concrete, and depends on applied voltage and duration.

ASTM C1202 *'Electrical indication of concrete's ability to resist chloride ion penetration'* (ASTM International, 2012) is a typical migration test used as a performance factor in North America. The test measures a total passed charge through the sample, Φ 100 × 50 mm with an applied potential difference of 60 V between two electrolytes during a period of 6 hours. The solutions filled in the cells are 3.0% NaCl as the catholyte and 0.3 mol NaOH as the anolyte, respectively. The chloride permeability of concrete is rated as shown in Table 3.1. However, this test has been criticised due to (i) the joule heating effect by applying a high voltage, and (ii) the current measurement related to the chemical composition of the pore solution in addition to chlorides.

Table 3.1 Chloride ion penetrability based on charge passed (ASTM International, 2012)

Charge passed (coulombs)	Chloride ion penetrability
>4,000	High
2,000 to 4,000	Moderate
1,000 to 2,000	Low
100 to 1,000	Very low
<100	Negligible

NT Build 492 is an update of ASTM C 1202 using a lower applied voltage and an increase in the amount of catholyte (Nordtest, 1999). In addition, the applied voltage and measurement time are adjustable with an initial current measured at 30 V. 10% NaCl solution and 0.3 mol NaOH are filled in the cathodic compartment and the anodic compartment, respectively. The migration coefficient is calculated based on the penetration depth using a colorimetric method. This test is widely used in Europe as a performance factor, although the simplified equation used for estimating the migration coefficient has been criticised (Spiesz *et al.*, 2012)

Another test is the multiregime test (Castellote *et al.*, 2001; Andrade *et al.*, 2011), where the migration cell is similar to the cell used in ASTM C1202, but the applied voltage is 12 V. Distilled water is used as the anolyte and a 1 mol NaCl solution is filled in the cathodic compartment. The conductivity of the solution in the anodic compartment is

measured, and the steady state and the non-steady state migration coefficients are calculated. The required time for chloride break-through is longer than in the other discussed tests. Monitoring the solution in a downstream cell is also laborious.

3.2.3 *Porosity/degree of saturation*

Porosity and degree of saturation are important parameters in chloride transport, reflecting both concrete properties and environmental conditions. The test for porosity is well documented and the degree of saturation, S_r, can be estimated from an additional measurement. The porosity, φ , is given as

$$\emptyset\ (\%) = \frac{\frac{1}{\delta_{solvent}}(m_{sat} - m_{dry})}{V_{sample}} \times 100 \tag{3.1}$$

$$S_r\ (\%) = \frac{m_{sample} - m_{dry}}{m_{sat} - m_{dry}} \times 100 \tag{3.2}$$

where $\delta_{solvent}$ is the density of the saturating medium (g/cm^3), m_{sample} is the mass of the sample (g), V_{sample} is the volume of the sample (cm^3) and m_{sat} and m_{dry} are the mass of the sample in saturated and dried conditions (g), respectively.

According to ASTM C642 (ASTM International, 2013), it is recommended that a sample be oven-dried at ~110 ± 5ºC for no less than 24 hours to achieve a dried weight. The temperature for drying has been criticised as it can lead to the formation of micro-cracks. However, this micro-cracking can be minimised by conducting the drying phase at a lower temperature of 50 ± 5ºC (Gallé 2001). The solvents for saturation are different with the specifications, corresponding to 1,1,1-trichlorethane in BS 1881-124 or water in ASTM C642 (British Standards Institution, 2015b; ASTM International, 2013). The degree of saturation is estimated using the original weight of the sample before the treatment process. Although it is difficult to directly estimate the transport rate with porosity and degree of saturation, they are essential in chloride transport in the modelling and estimation of quality of concrete.

3.3 Measurements for steel corrosion

Corrosion and corrosion rate measurement are important in the management of structures. The following presents inherent limitations and basic principles of corrosion monitoring to obtain reliable interpretation of data. Moreover, basic information on commonly used corrosion techniques is also provided.

3.3.1 Half-cell potential measurement

Metals have a natural potential which occurs by a reaction with the surrounding environment. The potential is measured with respect to a standard reference electrode, such as a copper-copper sulphate electrode (CSE), a saturated calomel electrode (SCE), or a silver-silver chloride electrode, as shown in figure 3.3. This technique is specified in ASTM C876, in which corrosion is indicated by the probability of corrosion, as given in table 3.2 (ASTM International, 2015). The key requirement for the measurement is to maintain sufficient moisture in the concrete for the formation of an electrical circuit, and the measured potential changes less than ± 20 mV within a 5-minute period. Although this technique is practical and widely used in the field, the measurement is sensitive to various factors including concrete resistivity, type of binder, moisture content and temperature. The use of the potential gradient is recommended in corrosion detection instead of the absolute value specified in ASTM C876 (RILEM TC 154-EMC, 2003). This technique is qualitative and is appropriate as an auxiliary method.

3.3.2 Macrocell current

The macrocell technique measures the current between separate metals (corroding anode and cathode) in a corrosion cell. For reinforced concrete, the steel exposed to the corrosive environment is the anode and the steel with a low possibility of corrosion (or a noble material such as stainless-steel, graphite, or titanium) is the cathode.

The macrocell current, also called the galvanic current, indicates the initiation of corrosion with a sudden increase, but the quantification of the corrosion rate using this technique is questionable. As the measured current represents the whole steel condition, the technique is inappropriate to evaluate localised or pitting corrosion. Moreover, the macrocell current is dependent on the distance between the two electrodes (Elsener, 2002)

as it is influenced by the electrical resistance of concrete. As this technique is non-destructive, it is useful to monitor macrocell current for corrosion of steel with time (Raupach, 1996; Elsener, 2002).

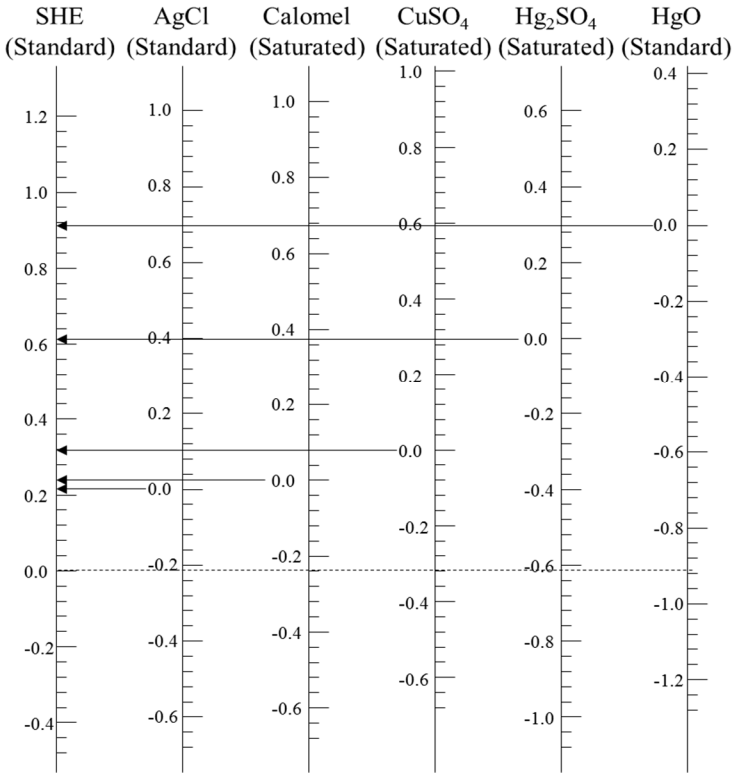

Figure 3.3 Graphical scheme to compare the potentials of the most commonly used reference electrodes (Roberge, 2008)

Table 3.2 Probability of corrosion (ASTM International, 2015)

Potential (mV vs CSE)	Potential (mV vs Calomel electrode)	Probability of corrosion
> -200	> -126	Low (<10 %)
-200 to -350	-126 to -276	Intermediate
< -350	< -276	High (>90 %)

3.3.3 Polarisation resistance

The polarisation resistance technique is an important method in estimating the corrosion rate in concrete structures. The basic principle is to measure a change in electrical potential or current of the steel due to an electrical perturbation using a counter electrode.

This technique is attractive due to the relation between the measured polarisation resistance and the corrosion rate. The corrosion rate is estimated by dividing the constant potential (the B value in mV) by the polarisation resistance, R_p through the Stern-Geary equation (Stern and Geary, 1957),

$$I_{corr} = \frac{B}{R_p} \tag{3.3}$$

where I_{corr} is the corrosion current (mA).

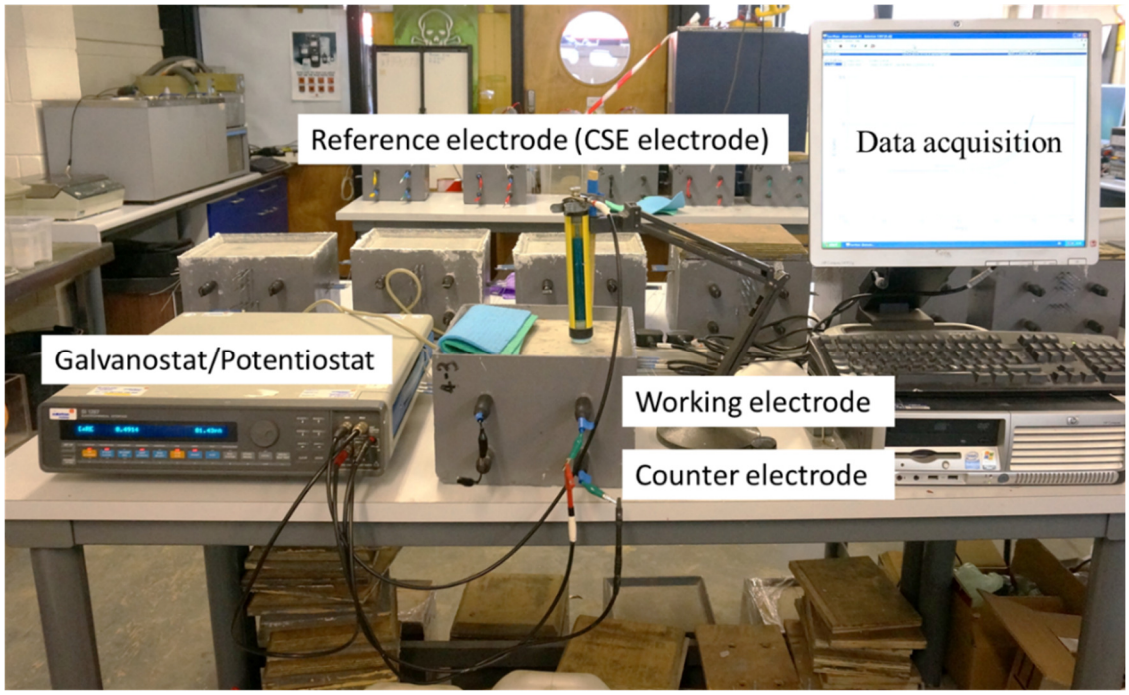

Figure 3.4 Set-up for polarisation resistance measurement

The B value is empirically set as 26 mV for the active state and 52 mV for the passive state or is determined by Tafel curve extrapolation. The value is distributed widely depending on concrete conditions, as shown in Table 3.3. The B value calculated with Tafel constants, β_a for the anodic branch (mV/dec) and β_c for the cathodic branch (mV/dec) in Tafel curve (E vs. log I) is given by:

$$B = \frac{\beta_a \beta_c}{2.3\,(\beta_a + \beta_c)} \tag{3.4}$$

Table 3.3 Variation in reported *B* value for active steel

B (mV)	Method	Sample types	Reference
21 - 37	Experiment	Simulated pore solution	Garcés *et al.* (2005)
2.2 – 37.1	Experiments /simulation	Concrete	Michel *et al.* (2016)
8 - 17	Simulation	Concrete	Song (2000)
63 - 86	Experiment	Concrete	Chang *et al* (2008a)
4 - 43	Experiment	Simulated pore solution and mortar	Vedalakshmi *et al.* (2009a)
19 – 26.8	Experiment	Sea water	Zou *et al.* (2011)

For concrete structures, the ohmic resistance should be considered when using the polarisation resistance technique. Even though a wetted concrete is assumed to be a highly conductive material (electrolyte) between the working electrode and counter electrode, the electrical resistance of concrete, called ohmic drop, is considerably higher than the electrical resistance of pore solution. Hence, the corrosion current is underestimated when the concrete resistance is neglected. In addition, it is unclear that the polarised area of steel is defined in large structures using a small counter electrode (Andrade and Alonso, 2001). If the steel is passive, the applied current spreads (e.g. 50 cm) from the application point; thereby, the true polarised area is wider than the assumed polarised area. Conversely, in the active state, especially in pitting corrosion, the current applied from the counter electrode is drained towards the small corrosion spot on the steel. The polarised area, which is assumed to be the area of the counter electrode, is larger than the true polarised area. Thus, the calculated corrosion rate is under- or overestimated using the assumed polarised area. From an empirical relationship (González *et al.*, 1995), the corrosion rate for pitting corrosion is 8 – 10 times higher than the corrosion rate measured using the polarisation technique. Although the auxiliary electrode, called the guard-ring system, is used to confine the polarised area, a dispersion or confinement effect for the polarisation is not fully resolved (Nygaard *et al.*, 2009).

To estimate the corrosion rate using polarisation techniques, the polarisation resistance needs to be measured. Depending on the electrical source or the method for applying a perturbation to the steel, various techniques are suggested, such as the potentiodynamic

technique using a voltage sweep, the potentiostatic technique using a constant voltage, the galvanostatic technique using a constant current, the galvanodynamic technique using a current sweep and electrochemical impedance spectroscopy using an AC voltage sweep.

The potentiodynamic technique can be divided into several branches depending on the voltage sweep range, with or without a reverse scan. The linear polarisation resistance technique (LPR) is the most general method due to its simple interpretation and rapid response. The measurement is performed within a small voltage sweep in the range of ± 30 mV at the corrosion potential. The low scan rate, which is <10 mV/min (RILEM TC 154-EMC, 2004), is generally set to allow the maintenance of the reaction equilibrium. In this potential range, the relation between the applied potential and the corresponding current is linear (Figure 3.5(a)), and thus the polarisation resistance is calculated using Ohm's law,

$$R_p = \frac{\Delta E}{\Delta I} \tag{3.5}$$

where $R_p$is the polarisation resistance (Ω), ΔE is the change in voltage (mV), and ΔI is the change in current (mA).

The Tafel extrapolation technique (TEP), or cyclic potentiodynamic technique, is similar to LPR, but a wide voltage range is swept. The range is from -200 to +1,000 mV with respect to the corrosion potential. Due to the large sweep range, a rapid scan rate is generally set at 60–120 mV/min. However, a high scan rate can induce unbalanced reaction, leading to a distorted result to estimate corrosion rate. In addition, the large perturbation leads to a disturbance of the corrosion environment of steel, and this technique could thus be considered destructive. However, it is necessary to determine the B value as given in equation (3.4). The cyclic potentiodynamic technique is useful to determine corrosion behaviour using reverse scan and repeated sweeps. Figure 3.5 (b) describes the pitting corrosion state of steel using this technique. As can be seen, the pitting potential (E_{pit}) and the protection or re-passivation potential (E_{pro}) are observed from the curve. If E_{pro} is more positive than E_{pit}, there is no pitting tendency, but if E_{pro} is more negative than E_{pit}, pitting could happen. Neither technique can directly measure an ohmic drop, but most commercial equipment provides an ohmic compensation function.

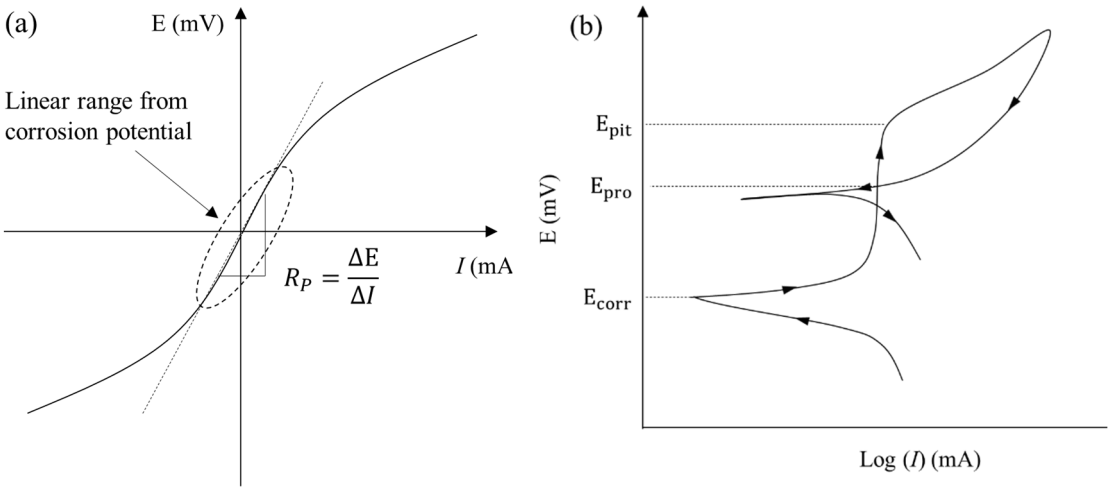

Figure 3.5 (a) Linear polarisation curve and (b) cyclic polarisation curve

Galvanostatic pulse technique (GP) is preferred in the field. The basic principle is to apply a constant current (10–100 μA) to the steel. This suddenly increases the voltage from the corrosion potential within a very short time. The sudden increase is considered to be an 'ohmic drop'. The interpretation is based on the equivalent electrical circuit, which can reflect a non-linear relationship between the applied current and the corresponding voltage. This technique also requires a very short time (less than 10s) to achieve a result. However, there is no criterion to set an applied current in the specification, and thus caution is required when applying this technique because a large perturbation is induced by an applied current.

The pontentiostatic technique (PT) is a reverse method of the GP technique. A constant voltage is applied to the steel until a constant current is achieved. The static current is determined as the corrosion current. However, the require time to achieve the constant current can be long. As a consequence, this technique is not preferred, although in the present study it is applied to estimate the B value. The interpretation process for calculating the B value is addressed in Section 6.3.4 in detail.

3.3.4 *Electrochemical impedance spectroscopy*

The electrochemical impedance spectroscopy (EIS) technique is elaborate compared to the techniques described above. Using a wide range of frequency (0.1 mHz – 100 kHz), EIS provides all electrical characteristics of the interface, as well as a simple faradic and non-faradic component. In addition, using an alternating current to perturb the steel

electrode makes it possible to minimise disturbance to the concrete/steel system. The measured impedance is expressed with a complex form consisting of a real part (resistance) and an imaginary part (reactive), as follows:

$$Z(\omega) = Z'(\omega) - iZ''(\omega) \tag{3.6}$$

where ω is the angular frequency ($\omega = 2\pi f$, f is frequency (Hz)), $Z'(\omega)$ is the real part, $Z''(\omega)$ is the imaginary part, and $i = \sqrt{-1}$.

There are two types of representation of EIS data: the Nyquist format and the Bode format (Barsoukov and Macdonald, 2005).

(i) Nyquist format: The real part ($Z'(\omega)$) and the imaginary part ($Z''(\omega)$) are expressed on the x-axis and the y-axis, respectively (figure 3.6). The impedance can be represented with a vector length ($|Z(\omega)|$) and the angle between this vector and the x-axis. This representation cannot express the frequency directly.

(ii) Bode format: Both the modulus impedance and phase shift on the y-axis are plotted with respect to the frequency on the x-axis (figure 3.7). The Bode format explicitly shows frequency information, unlike the Nyquist format.

The EIS technique does have limitations. To investigate the interface or condition of steel in concrete, a very low frequency is required, which is time-consuming. In the presence of concrete, the passive layer on the steel and localised corrosion, the response can be ambiguous, leading to difficulty in the interpretation. In general, an equivalent electrical circuit are used to analyse EIS data; circuits suggested by researchers are shown in figure 3.8 and table 3.4. It is worth noting that all circuits are able to fit any impedance data, but physical meaning regarding elements used in the circuit are variable even if the same elements are employed in the different circuits. In addition, the transmission line model, which is a complex circuit, provides better fitting and mechanistic characters for the corrosion process, e.g. pitting corrosion, diffusion processes and presence of passive film (Kranc and Sagüés, 1992; Chen and Orazem, 2015), but its application is not straightforward for engineers. The following review excludes the transmission line model.

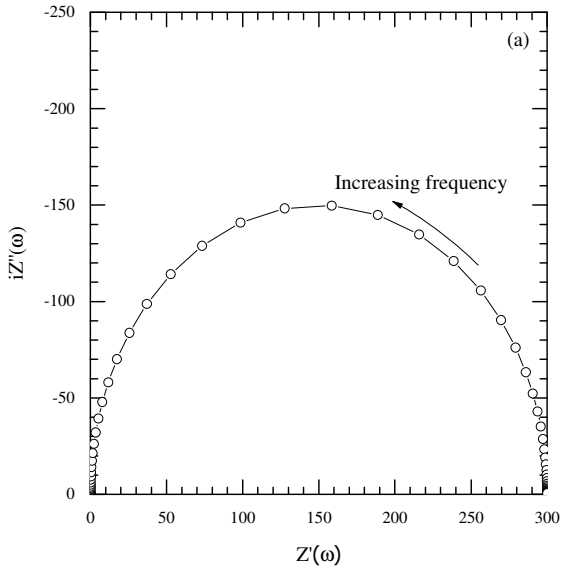

Figure 3.6 Nyquist format for data presentation

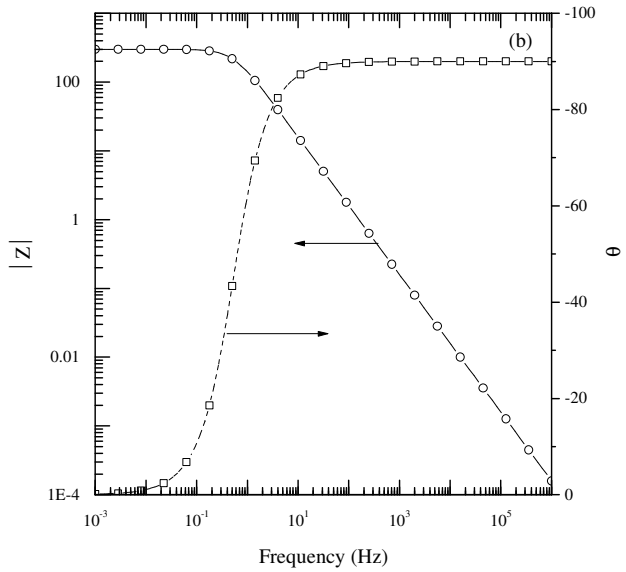

Figure 3.7 Bode format for data presentation

In most electrical equivalent circuits to analyse the steel/concrete interface, the response of bulk concrete (R_c) is simplified with a single resistor, as shown in figure 3.8, for which the high frequency limit is set as an origin even though capacitances exist at high frequencies in addition to resistances. It may be concluded that an error in analysis is involved depending on the high frequency limit to determine the concrete resistance. Moreover, a charge transfer resistance (R_{ct}) in conjunction with a constant phase element (CPE_{dl}) for the double-layer are used to represent the steel-concrete interface.

To describe the presence of the low frequency tail (<0.01 Hz) representing the diffusion control of oxygen in the vicinity of the steel surface in the Nyquist plot, a Warburg impedance in series with the charge transfer resistance is introduced, which extracts the

Faradic process in the interface (Circuits A-2, B-2 and B-3). This phenomenon can explain why it is difficult for traditional DC measurements to achieve the steady-state in a prolonged period of time. However, when a Warburg impedance is introduced, it is uncertain whether fitting is correct or not as this tail cannot always be observed, even at low frequency (Montemor *et al.*, 2000).

The elements (R_{if} and CPE_{if}) representing the response in the intermediate frequency range are introduced in the circuits (all circuits B and C), but the physical meaning is varied. For example, the response for the intermediate frequency in R-CPE series circuits (Circuit B) is described by the effect on the interfacial layer between mortar and steel (Pereira *et al.*, 2015), dielectric properties of concrete (Choi *et al.*, 2006) and the effect of a surface film on steel (Park *et al.*, 2005). Meanwhile, hierarchical R-CPE series circuits (Circuit C) are used to describe the response at the intermediate frequencies. This response is considered with redox transformation on the steel (Morozov *et al.*, 2013; Bautista *et al.*, 2015) but according to Dhouibi *et al.* (2002), the response in the circuit (Circuit C-3) is separated into hydration products formed in cement pores around the steel surface (R_{cif} and CPE_{cif}) and redox transformation (R_{if} and CPE_{if}).

In a steel/concrete system, depressed semi-circles are plotted due to the non-ideal behaviour of capacitance (i.e. the decrease in capacitance with increasing frequency), which is represented by a pseudo-capacitance or constant phase element (CPE). This is explained by the uneven surface of steel and the heterogeneous nature of concrete (Feliu *et al.*, 1998); however, there is no consensus on a detailed description of its physical origin. Nonetheless, the CPE element is useful as a flexible parameter to improve curve fitting to impedance spectra (Jorcin *et al.*, 2006), as shown in the following equation.

$$Z''_{CPE}(\omega) = \frac{1}{C_{p0}(i\omega)^{a}} \tag{3.7}$$

where $i = \sqrt{-1}$, C_0 is a coefficient and a is the exponent ($0 < a < 1$); if a =1, the circuit is an ideal capacitor (C_{p0}).

Clearly, an impedance spectrum in a Nyquist plot consists of a concrete response and a steel response, approximating two semi-circles. The electrical circuits are expanded to describe additional semi-circles or tails with a combination of resistor and capacitor or CPE, or a Warburg element. However, the roles of some elements used in the circuit are still unclear, so that it is necessary to define each of them.

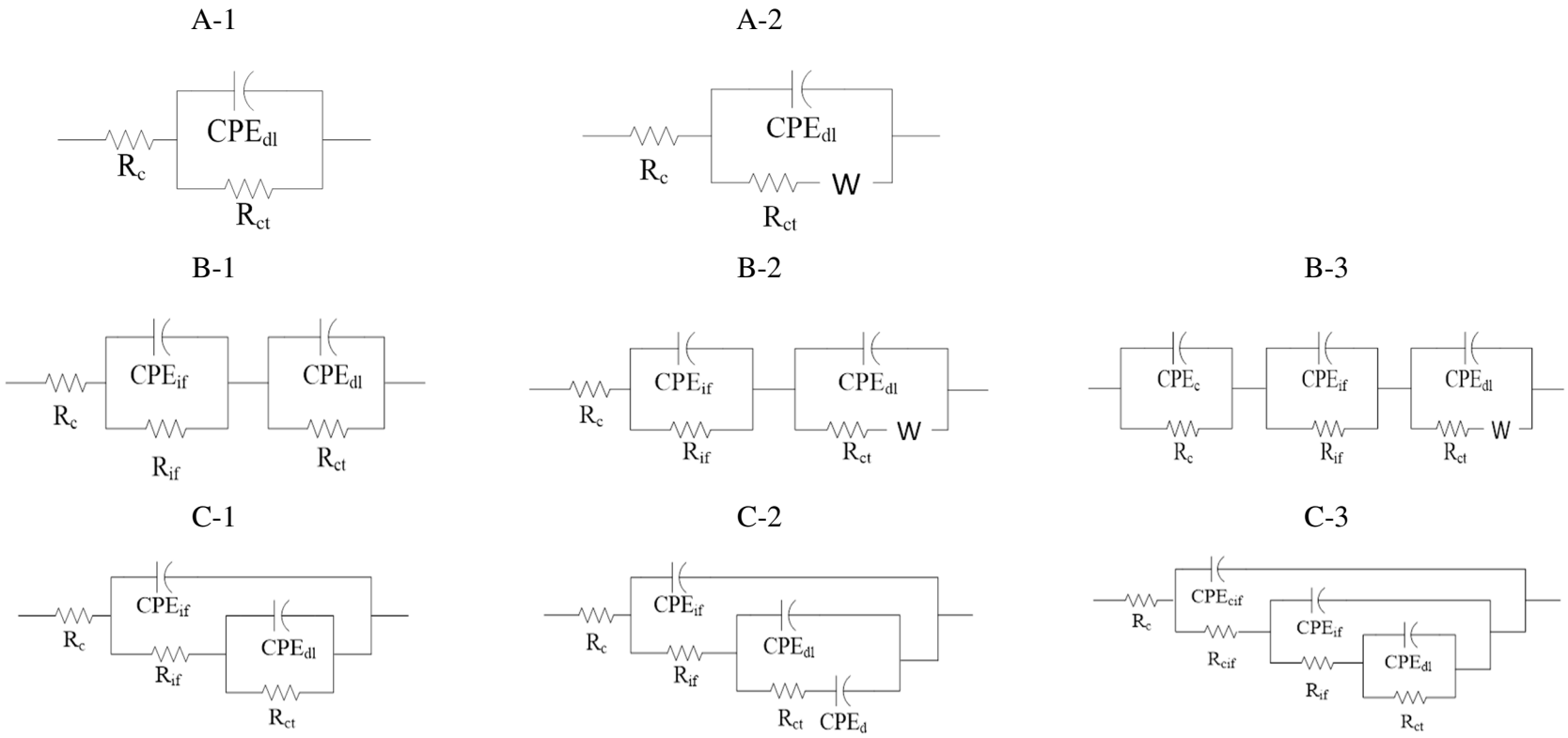

Figure 3.8 Equivalent electrical circuits for analysis of steel corrosion in concrete/mortar (refer to table 3.4).

Table 3.4 Experimental set-up details for using EIS measurement

Electrical equivalent circuit in figure 3.8	Sample type	Location	Exposure condition	Counter electrode type	Steel condition	Reference electrode	Reference
A-1	Concrete	Lab	Immersion (3.5% NaCl)	Graphite (Ex)	Passive	SCE	Choi *et al.* (2006)
A-2	Concrete	Field	Atmospheric zone	Elastomer (Ex)	Passive/ active	Activated titanium rod	Pech-Canul and Castro (2002)
	Mortar	Lab	Pre-mixed (3% $CaCl_2$)	N.I.	Passive/ active	N.I	Feliu *et al.* (1998)
B-1	Concrete	Lab	Immersion (3.5% NaCl)	Graphite (Ex)	Active	SCE	Choi *et al.* (2006)
	Concrete	Lab	Immersion (3.5% NaCl)	Graphite (In)	Passive/ active	CSE	Park *et al.* (2005)
B-2	Concrete	Lab	Partial or full immersion (3% NaCl)	Steel (In)	Passive/ active	SCE	Montemor *et al.* (2000)
B-3	Mortar	Lab	Wet/dry cycle (3% NaCl)	Stainless steel (Ex)	Passive/ active	SCE	Pereira *et al.* (2015)
C-1	Mortar	Lab	Immersion (sea water) and premixed (0.1, 1.0 and 3.6% Cl^-)	Graphite (Ex)	Passive/ active	SCE	Deus *et al.* (2014)
	Mortar	Lab	Immersion (3.5% NaCl) and premixed (3% $CaCl_2$)	Copper cylinder (Ex)	Passive/ active	SCE	Bautista *et al.* (2015)
C-2	Mortar	Lab	Partial immersion (3% NaCl)	Titanium (Ex)	Passive/ active	SCE	Morozov *et al.* (2013)
C-3	Concrete	Lab	Immersion (3% NaCl)	Stainless steel (Ex)	Passive/ active	SCE	Dhouibi *et al.* (2002)

* Ex: external counter electrode, In: embedded counter electrode in sample, ** N.I. No information, *** SCE: standard calomel electrode, CSE: copper copper-sulphate electrode.

3.3.5 Commercial equipment

Non-destructive methods for detecting and quantifying corrosion in concrete structures are attractive. To date, commercial instruments for on-site investigation are available but the measured values vary depending on the electrochemical techniques and control methods for applied current (referred to as confinement techniques). Therefore, results are still ambiguous when on-site investigation is carried out.

Typical commercial instruments include GECOR 6 and GalvaPulse. Both instruments measure a potential shift using the galvanostatic technique, but for the GECOR 6 the result is analysed using a linear relationship between polarisation potential and current, while for the GalvaPulse this is done with exponential curve fitting using a simple Randle circuit. In addition to their analysis method, their current confinement methods are also different. The potential difference of steel between different locations is kept constant as an initial value, i.e. the potential difference before applying current, for both instruments. However, while applying current to the guard-ring is constant over the measurement for the GalvaPulse, an increase in current is applied for the GECOR 6.

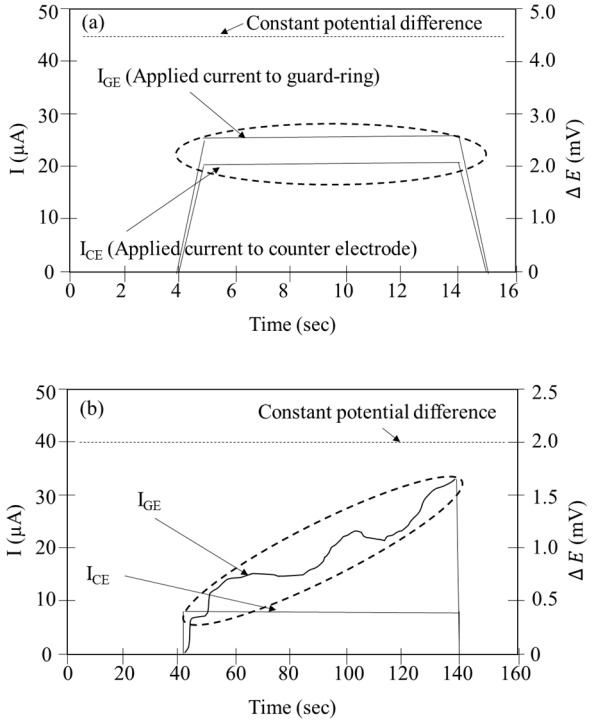

Figure 3.9 Examples of current confinement method using (a) GalvaPulse and (b) GECOR 6 (Nygaard *et al.*, 2009) modified by the author (ΔE potential difference in the steel at different locations for controlling the guard-ring)

Nygaard et al. (2009) investigated the corrosion rate of steel in concrete using these two commercial instruments. For the passive state, corrosion rates were overestimated because the predefined polarisation lengths were smaller than the real polarised lengths. Changes of electrical potential in steel caused by polarisation, corresponding to +176 mV for the GECOR 6 and +76 mV for the GalvaPulse, were large, leading to a violation in linearity between current and potential and a destructive environment at the concrete-steel interface. In contrast, the measured corrosion rates were underestimated due to self-confinement behaviour, which resulted in a smaller polarisation length compared to the predefined length. The authors concluded that correction factors must be determined to evaluate the corrosion rate correctly.

3.3.6 *Mass loss*

The corrosion rate of steel is directly determined by the mass loss method. ASTM G1 (ASTM International, 2011) suggests a wide range of solutions to clean corrosion products from the steel surface, although a suspension based on hydrochloric acid is generally used to clean corroded steel in concrete. Mass change is calculated using mass difference between steel before corrosion and cleaned steel after corrosion,

$$m_{loss} = \left(m_0 - m_f\right) - m_{bl} \tag{3.8}$$

where m_{loss} is the mass loss of steel by corrosion products (g), m_0 is the initial mass of steel before corrosion (g), m_f is the mass of steel after cleaning corrosion products (g), and m_{bl} is the mass loss for the cleaning process (g).

The average corrosion rate is then determined using Faraday's law as follows:

$$i = \frac{m_{loss} zF}{tMA_{exp}} \times 1000 \tag{3.9}$$

where i is the average corrosion rate (mA/m^2), F is Faraday's constant (= *96,487 C/mol*), t is the duration of the test (s), M is the atomic mass of material $(Fe \approx 55.85 g/mol)$, A_{exp} is the exposure area of steel contributing to the corrosion process (m^2), and z is the number of electrons transferred in the corrosion process $(= 2 : Fe \rightarrow Fe^{2+} + 2e^-)$.

With time, the corrosion rate obtained from the mass loss method is an average value, while electrochemical measurements obtain the instantaneous corrosion rate. To compare the two values, it is necessary to integrate the instantaneous corrosion rate with test time.

3.4 Measurements for electrical resistivity of concrete

The electrical resistivity of concrete is measured using at least two electrodes. This property gives an indirect assessment of the permeation properties and is being vigorously researched as a factor to measure performance and durability of concrete. The basic principle is to measure both current and voltage-drop, and then calculate the resistance using Ohm's law. The resistivity is obtained by multiplying the cell geometrical factor, which will depend on the electrode arrangement.

This technique uses current sources that can be either alternating current (AC) or direct current (DC). A two- or four-electrode configuration can be used, with electrodes being embedded and/or externally applied. The AC technique (within a frequency range of 50 – 1,000 Hz) is preferred to the DC technique to minimise the polarisation of electrode (McCarter *et al.*, 2015). Intimate contact between electrodes and concrete can be achieved by embedding electrodes within the concrete, while the geometrical factor for external electrodes can be easily estimated to calculate the electrical resistivity. Two- and four-electrode methods are typical (see Figure 3.10). The voltage is applied and then the current is measured for the sample between two electrodes, while four electrodes are positioned equidistantly. The AC current is injected through the outer two electrodes, and then the inner two electrodes measure the voltage drop. This technique is known as the Wenner method. The resistivity of concrete is obtained using the following equation for the Wenner method:

$$\rho_{app} = 2\pi a \mathrm{R} \tag{3.10}$$

where $\rho_{app}$is the apparent resistivity of the concrete ($\Omega \cdot m$), a is the electrode spacing (m), and R is the resistance (Ω).

The Wenner method was developed in soil science, but is now widely used in civil engineering. It has been confirmed that the formula is applicable to concrete, although the assumptions for equation (3.10) are not completely satisfied in concrete: (i) electrodes are not point-shaped, (ii) the concrete volume is not semi-infinite, and (iii) the domain

has inhomogeneous resistivity (Angst and Elsener, 2014). It is apparent that the resistivity measurement is useful to estimate transport properties in concrete, but it has also been reported that the value is sensitive to various factors such as the degree of contact between the electrode and the concrete, the contact solution, and the influence of the concrete surface itself (Lataste, 2010).

Nevertheless, the Wenner method is attractive for both on-site and laboratory measurements as it is inexpensive and relatively easy to use. The error level, related to the measurement process itself or to material variability, is also acceptable: for example, the tolerance in the field is approximately ± 20% (Polder, 2001). This is because of limitations relating to moisture, chloride and temperature variations, and it is difficult to control all factors when investigating a change of the resistivity. However, this technique is widely used to investigate the performance and durability of concrete structures in terms of assessing the risk of corrosion (Basheer *et al.*, 2002; Polder and Peelen, 2002), the moisture/ionic ingress (Gjørv *et al.*, 1977; Streicher and Alexander, 1995; McCarter *et al.*, 2005) and the cracking in concrete (Lataste *et al.*, 2003).

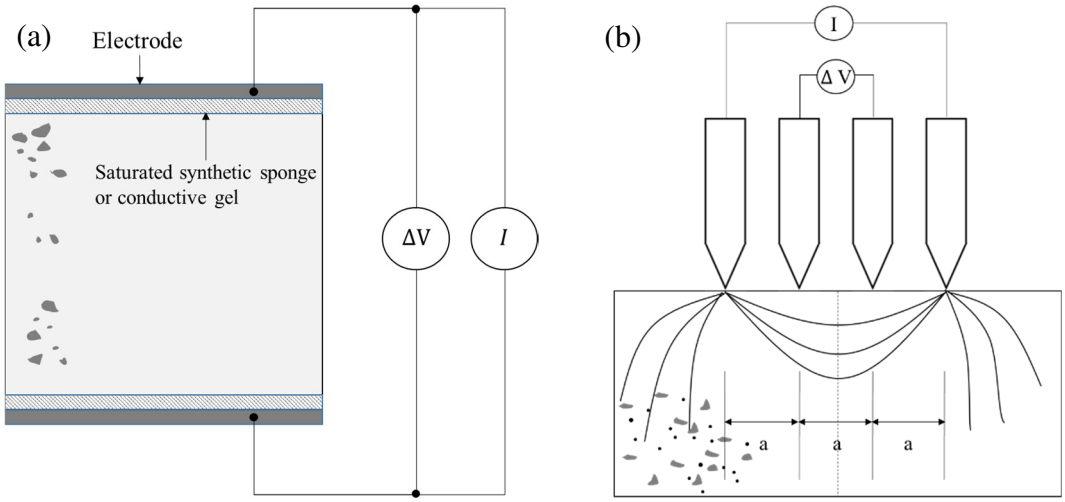

Figure 3.10 Set-up for (a) two-electrode and (b) four-electrode method (the Wenner method).

3.5 Overview of predictive models

Various predictive models have been developed to estimate the service life of concrete structures. These models are useful to simulate a range of situations without the need for long-term experiments and monitoring, especially regarding the corrosion of steel in

concrete. However, deterioration processes of concrete structures in the field are complex hence a simple model that only considers a single reaction, or a constant environment, can lead to an erroneous result. It is necessary to update predictive models to take into account additional factors (e.g. exposure conditions, material property and workmanship during construction) that influence the deterioration of concrete. This section reviews the main models identified in the literature.

3.5.1 *Transport models*

Transport models predict the chloride distribution in concrete structures subjected to chloride environments and, based on the CTL, the service life can be evaluated. The models are divided into empirical models and analytical models. The Fickian model is an empirical model and is widely used. The input parameters for this model are obtained empirically, and the process can therefore be laborious. On the other hand, an analytical model contains multiple variables within concrete, such as temperature, chemical reactions, moisture distribution and ionic movement. With an increase in knowledge, both types of model have been significantly refined but still need to be improved due to their inherent limitations. For an empirical model, a wide range of results are required to verify the proposed parameters, whereas in analytical models, the quantifiable input data from the target structure are limited as the models are developed from a scientific background.

Fickian model

The Fickian model is robust because of its convenience in use and calculation. The model can describe the transport behaviour in concrete using Crank's solution, referred to as the error function solution (erf), to Fick's second law (Crank, 1975) (see equations (3.11) and (3.12)). The chloride distribution in concrete can be estimated provided that (i) the concrete structure is infinite, (ii) the diffusion coefficient and surface chloride content are constant, (iii) the penetration behaviour is one-dimensional, and (iv) interactions with other ions and with the electrical double-layer are ignored. In this model, the input parameters to determine the time to corrosion initiation include the diffusion coefficient, cover depth, the initial chloride concentration at the concrete surface, and the CTL.

$$\frac{\partial C_t}{\partial t} = D_{app} \frac{\partial^2 C_t}{\partial x^2} \tag{3.11}$$

$$C_t(x,t) = (C_s - C_0)\left(1 - erf\left(\frac{x}{2\sqrt{D_{app}t}}\right)\right) \quad (3.12)$$

where C_t is the total chloride concentration (free and bound chloride) at the exposure time, t (sec), at depth x (m) from the surface; D_{app} is the apparent diffusion coefficient (m^2/s); C_s is the equilibrium chloride concentration on the concrete surface; and C_0 is the initial chloride concentration of the concrete before the exposure to the chloride environment.

There are, however, some limitations when applying the Fickian model to real structures to evaluate their service life. This is because the input parameters involve a number of uncertainties: (i) the diffusion coefficient is time-dependent, which decreases with increasing time resulting from the hydration process (Pack *et al.*, 2010); (ii) it is incorrect to assume that the surface chloride content is constant, as the chlorides build-up at the surface of concrete with time (Ann *et al.*, 2009); (iii) the transport behaviour within the concrete skin layer is different compared to that of the inner concrete (Andrade *et al.*, 1997); and (iv) the error function model is only valid to describe the diffusion phenomenon (Saetta *et al.*, 1993).

To overcome these limitations, numerous studies have introduced the concept of age-factors for the chloride diffusion coefficient and surface chloride concentration to consider the time-dependent properties of concrete, as shown in Table 3.5. It is noteworthy that the input data cannot be generalised without considering environmental conditions. In other words, the values obtained from a particular test, such as the diffusion coefficient and surface chloride content, are only valid for the target structure as the values contain environmental conditions corresponding to that structure.

Flux-based models

Flux-based models, referred to as physical models, are based on scientific theory. Their accuracy for prediction is superior to that of empirical models. However, the large amount of input data (e.g. initial amount of cement hydrates, chemical composition of pore solution and chloride binding) is not easily available and must be quantified through tests. In addition, the models cannot be easily modified or updated as the coding using the finite element method or finite difference method is complex.

Table 3.5 Aging functions used in erf solution to Fick's equation

Surface chloride concentration, C_s	Apparent diffusion coefficient ,D_{app}	Reference
C_o (constant)	$D_{app}(t) = \frac{D_{ref}}{1-a}\left(\frac{t_{ref}}{t}\right)^{\mathrm{a}}$	Mangat and Molloy (1994)
C_o (constant)	$D_{app}(t) = D_{ref}\left(\frac{t_{ref}}{t}\right)^{\mathrm{a}}$	Maage *et al.* (1996), Bamforth (1999)
C_o (constant)	$D_{app}(t) = \frac{D_{ref}}{(1-\mathrm{a})} t_{ref}^{\mathrm{a}}\left(\frac{t^{1-\mathrm{a}} - t_I^{1-\mathrm{a}}}{t - t_I}\right)$	Stanish and Thomas (2003)
$C_o(1\text{-}e^{-\mathrm{b}t})$	D_{app} (constant)	Kassir and Ghosn (2002)
$\frac{C_o t}{C_o\sqrt{t}}$	D_{app} (constant)	Amey *et al.* (1998)
$C_o t^{\mathrm{b}}$	$D_{app}(t) = D_{ref}\left(\frac{t_{ref}}{t}\right)^{\mathrm{a}}$	Costa and Appleton (1999)
$C_o[1\text{-}e^{-\mathrm{b}(t-t_{ref})}]$	$D_{app}(t) = \frac{D_{ref}}{(1-\mathrm{a})}\left[\left(\frac{t_{ref}}{t}\right)^{\mathrm{a}} - \frac{t_{ref}}{t}\right]$	Maheswaran and Sanjayan (2004)
$C_o\sqrt{t} + \mathrm{c}$	$D_{app} = \frac{D_{ref}}{1-m}\left[\left(1+\frac{t_I}{t_E}\right)^{1-a} - \left(\frac{t_I}{t_E}\right)^{1-a}\right]\left(\frac{t_{ref}}{t_E}\right)^{a} t_E$	Petcherdchoo (2013)
$C_o[ln(\mathrm{d}t+1)] + \mathrm{c}$	$D_{app}(t) = \frac{D_{ref}}{(1-a)}\left(\frac{t_{ref}}{t}\right)^{a}$	Pack *et al.* (2010)

Note: C_o, a, b, c, and d are regression values; t_{ref} the reference time; D_{ref} the diffusion coefficient at time t_{ref}; t_I the time at the first exposure to chlorides; t_E the time of exposure to chlorides; and *t* is the age of the concrete (i.e. $t = t_I + t_R$).

Physical models have a governing differential equation that is solved instead of a closed-form equation such as the Crank equation. As noted above, additional equations are required as different phenomena, including moisture distribution, chloride binding and temperature distribution, are included with respect to a micro-structural environment. For chloride transport, the typical governing equation is Fick's law or the Nernst-Einstein relation as given in equations (3.13) and (3.14) and the mass-balance equation is solved using equation (3.15) (Tang, 1996a; Samson and Marchand, 2007).

$$J = D\frac{dC_t}{dx} \tag{3.13}$$

$$J = -\left(D\nabla C_t + zD\left(\frac{F}{RT}\nabla E\right)C_t + DC_t\nabla \ln a - C_t u\right) \quad (3.14)$$

$$\frac{\partial(C_f + C_b)}{\partial t} = -\nabla \mathrm{J} \quad (3.15)$$

In the above equations, J is the flux of total chloride ion, D is the diffusion coefficient, C_t is the total chloride concentration, z is the charge number for the diffusing ion (Cl^- = 1), F is Faraday's constant, R is the gas constant (8.314 *J/(K·mol)*), T is temperature (K), E is the electrostatic potential, a is the chemical activity coefficient, u is the average velocity of the fluid under the capillary suction, C_f is the free chloride concentration, and C_b is the bound chloride concentration.

The transport property is significantly affected by various parameters including moisture distribution, material properties and temperature, hence the relation between the parameters and diffusion in unsaturated concrete is normally expressed by equation (3.16) (Xi and Bažant, 1999). The functions in terms of each variables are arranged in the Appendix A.1.

$$D = f_1\left(\frac{w}{b}, t_0\right) f_2(g_i) f_3(H) f_4(T) f_5\left(C_f\right) \quad (3.16)$$

where t_0 is the curing time (days), *w/b* is the water-to-cement ratio, g_i is the volume fraction of aggregate in concrete, and H is the humidity.

In addition, only the free chlorides move in concrete transport, and it is necessary to consider the bound chlorides involved in either the chemical reaction or physical adsorption. The relation between bound and free chlorides is equated with the Langmuir or Freundlich binding isotherm shown in equation (2.8) and (2.9), respectively. According to Tang and Nilsson (1993), constants for both binding isotherms irrespective of w/b are suggested as a = 5.41 and b = 0.013 in the Langmuir binding isotherm and c = 101.14 and d = 0.38 in the Freundlich binding isotherm. The temperature in the concrete influences the propagation of ions and the moisture distribution. The relation with temperature is also expressed through the Arrhenius relationship. Table 3.6 summarises the main transport models.

Table 3.6 Summary for typical transport models (Tang, 2005)

Type	Model's name	Governing equation	Main input parameters	Characteristics
Empirical model	DuraCrete	Fick's 2nd law (Erfc function)	Time dependent diffusion coefficient Constant surface chloride content	• Using correction factors to reflect the field condition • Simple method
	HETEK	Fick's 2nd law (Mejlbro-Poulsen function)	Time dependent diffusion coefficient Time dependent surface chloride content	• Estimating all parameters from mix compositions and environmental conditions • Being sensitive with quality of measurement
	LIFE 365	Fick's 2nd law (Numerical solution)	Time dependent diffusion coefficient Time dependent surface chloride content	• Considers the effect of temperature on diffusion coefficient • Considers environmental conditions • User friendly interface
Physical model	ClinConc	Fick's 1st law	Migration coefficient at 6 months Mix compositions	• Considering chloride binding, the effect of temperature variations and alkali leaching • Only treating cases with saturated concrete exposed in submerged conditions
	STADIUM	Nernst-Planck flux equation	A number of input parameters including various types for transport rate, environmental conditions and chloride binding isotherm	• Being available to describe complex chloride transport behaviour • Difficulty in practical application due to a lot of input data

3.5.2 *Corrosion models*

Corrosion models predict the corrosion rate of steel in concrete subjected to aggressive environments. The loss of steel cross-section, or the volume expansion of corrosion products on the steel surface, is directly related to failure (end of service life) of concrete structures. The corrosion model is of interest in evaluating the residual service life or in the practical management of the structure.

In a similar fashion to the transport models, there are two types of corrosion models: empirical and analytical. In the empirical models, the solution establishes the relation between corrosion rate and factors influencing the corrosion process based on laboratory testing. The calculation process is relatively simple, but the result becomes less accurate when conditions, e.g. steel type, types of aggressive agent, concrete material properties etc., are different compared to conditions proposed in the model. In addition, the applicability is low as laboratory testing is carried out using accelerated methods including pre-mixed chloride during casting or wet/dry cycles to reduce time to corrosion initiation.

Analytical models have also been developed to improve knowledge of the corrosion behaviour of steel in concrete. As these models are based on electrochemical theory, Laplace's equation for electric potential or Ohm's law based on an equivalent circuit is used as the governing equation. Non-linear boundary conditions are applied on the steel surface using the Stern-Geary polarisation equation (Stern and Geary, 1957) or the Butler-Volmer kinetics equation (Pour-Ghaz, 2007). While the theoretical background used in the models enhances their accuracy, their openness is significantly limited to the users. Moreover, multiple corrosion processes within complex geometries require a large amount of computation; hence, these models are more appropriate for comprehensive academic research than for practical use.

The Stern-Geary polarisation equation is given by,

$$\mathrm{E_a} = \mathrm{E_a^0} + \beta_a log \frac{i_a}{i_{0a}} \tag{3.17}$$

$$\mathrm{E_c} = \mathrm{E_c^0} + \beta_c log \frac{i_c}{i_{0c}} - \frac{2.303RT}{z_c F} log \frac{i_L}{i_L - i_c} \tag{3.18}$$

and the Butler-Volmer kinetics equation is given by,

$$i_a = i_{0a} e^{\left(\frac{E_a^0 - E_{corr}}{\beta_a}\right)} \tag{3.19}$$

$$i_c = i_{0c} e^{\left(\frac{E_{corr} - E_c^0}{\beta_c}\right)} \tag{3.20}$$

where E_a and E_c are the anodic and cathodic potentials (V), z_c is the number of electrons involved in the cathodic reaction, R is the universal gas constant (8.314 J/(mol·K)), F is Faraday's constant (96,487 C/mol), T is temperature (K), i_L is the limiting current density (A/m^2), i_a and i_c are the anodic and cathodic current densities (A/m^2), β_a and β_c are the anodic and cathodic Tafel slopes (V/dec), i_{0a} and i_{0c} are the anodic and cathodic exchange current densities (A/m^2), E_{corr} is the corrosion potential (V), and E_a^0 and E_c^0 are the equilibrium potential for anodic and cathodic reactions (V).

Table 3.7 summarises typical empirical corrosion models. This review has shown that modelling the corrosion process in concrete is difficult due to unpredictable factors such as steel conditions, concrete properties and environmental conditions. In addition, obtaining corrosion results through the experiments is time-consuming to establish the empirical relation.

3.6 Summary

This chapter presents a methodological review including measurements and predictive models related to chloride transport in concrete and chloride induced corrosion, respectively. To date, a number of well-established methods and predictive models have been developed. However, most methods are destructive and laborious for chloride transport and there is no standardized method for corrosion test. Alternatively, electrical resistance measurement is non-destructive and easy, but this method is still close to a qualitative method; thereby it is necessary to made relation between traditional method and resistance method to improve the applicability of the electrical resistance measurement. Finally, to reflect the environmental conditions located in the reinforced concrete, it is necessary to add the parameters in predictive models. Therefore, the applicability of the models is improved.

Table 3.7 Summary for empirical corrosion models

Equation	Detection of corrosion	Source of corrosion	Characteristics		Reference
			Advantage	Disadvantage	
$i_{corr} = \frac{k_{corr}}{\rho}$	LPR* Mass loss	C+	• simple • using resistivity as a durability indicator	• no consideration in size effect • no consideration in environmental factors	Alonso *et al.* (1988)
$i_{corr} = i_0 e^{-Ct}$	HP** LPR	Cl++	• simple	• no consideration in influencing factors including environment conditions and material properties • accelerated corrosion method using admixed chlorides	Yalcyn and Ergun (1996)
$\log I = 0.171 + 0.823 logSD$	HP EN***	Cl	• simple • the relation between half-cell potential and corrosion rate	• the ambiguous relation between half-cell potential and corrosion rate due to sensitivity of measurement • no practical method (electrochemical noise technique)	Katwan *et al.* (1996)
$i_{corr} = 102.47 + 10.09\ln(1.69\ Cl) - 39038.96\ (T^{-1}) - 0.0015R_c + 290.91t^{-0.215}$	LPR	Cl	• considering environmental conditions and simple	• accelerated corrosion method using admixed chlorides	Liu and Weyers (1998)
$i_{corr} = \frac{k_{corr}}{\rho(t)} F_{cl} F_{Galv} F_{oxide} F_{O_2}$ $\rho(t) = \rho_0 f_e f_t \left(\frac{t}{t_0}\right)^n$	N.I.****	Cl	• considering influencing factors • aging effect on concrete resistivity	• no information on the relation of influencing factors	DuraCrete (1998)
$i_{corr} = \left(\frac{37.8(1-\frac{w}{b})^{-1.64}}{C}\right) \alpha t_P^{\beta}$	N.I.	N.I.	• considering material properties	• limited application only by considering oxygen availability • considering high corrosion rate at start of corrosion propagation	Vu *et al.* (2005)

* LPR = linear polarisation resistance technique, ** HP = half-cell potential technique, *** EN = electrochemical noise technique,
**** N.I. = no information , + C = carbonation, ++ Cl = Chloride

CHAPTER 4
EXPERIMENTAL PROGRAMME

4.1 Introduction

A number of studies have investigated chloride-induced corrosion of steel in concrete structures, but a gap still remains between field studies and laboratory studies due to (i) a lack of long-term data, (ii) different environmental conditions, and, (iii) various test methods. To reduce this gap, mix proportions and materials used in the laboratory samples in the present study were similar to those in the samples installed in the field (the Dornoch Firth in northern Scotland). A range of test methods were carried out including (i) compressive strength test, (ii) migration/diffusion test, (iii) porosity/degree of saturation test, (iv) polarisation resistance, (v) half-cell potential, (vi) macrocell current technique, (vii) mass loss of steel measurement, and (viii) visual observation of the corrosion activity on the surface of the steel.

From laboratory test using accelerated methods by reducing cover-depth and a wet/dry cyclic exposure regime, supporting information was obtained about chloride-induced corrosion. The following sections describe the experimental programme, from sample fabrication to experimental set-up.

4.2 Materials and concrete mix preparation in laboratory

Three binders comprising ordinary Portland cement (PC), CEM I 52.5N to BS EN 197-1 (British Standards Institution, 2015c), fly ash (FA) conforming to BS EN 450-1 (British Standards Institution, 2012a), and ground granulated blast-furnace slag (GGBS) conforming to BS EN 15167-1 (British Standards Institution, 2006) were used to prepare concrete samples.

The coarse and matching fine aggregates were crushed granite. The coarse aggregate was 4/20 mm grade while the fine aggregate was ≤4 mm. Prior to casting, the aggregate was conditioned to a saturated surface condition to avoid absorption of the mixing water. A slump test was carried out to ensure the consistency of the mix. Workability of all concrete mixes was designated as S3 specified in BS 8500-1 (British Standards

Institution, 2016). For the low water-to-binder ratio (w/b=0.4), the slump test was performed to adjust the optimised dosage of superplasticizer before the main mixing. A mid-range, water reducer/plasticizer (SikaPlast 15RM) conforming to BS EN 934-2 (British Standards Institution, 2012b) was used throughout.

Experimental work was undertaken on six concrete mixes consisting of high/low w/b (w/b = 0.4 and 0.6) and SCM such as GGBS and FA; 40% GGBS denoted by CEM III/A, and 30% FA denoted by CEM II/B-V, respectively, based on BS EN 197-1 (British Standards Institution, 2015c). The concrete mixes with low w/b were similar to the concrete used at the Dornoch field site, whereas concrete mix for high w/b were designed conforming to XD1 environmental exposure class with an intended service life of at least 50 years ($> 35 + \Delta c$ mm cover depth) or at least 100 years ($> 50 + \Delta c$ mm cover depth) (corrosion induced by chloride other than seawater, e.g. de-icing salt) in BS 8500-1 (British Standards Institution, 2016).

Concrete samples were mixed in accordance with BS 1881-125 (British Standards Institution, 2013b) using a concrete pan mixer (0.1 m^3 capacity); an additional mixing time of 2 minutes was used for low w/b concrete. To achieve uniformity, all samples for each mix were fabricated from the same batch. Three replicates per type of experiment were fabricated for each mix. The chemical compositions of binders and mix design details used in this study are presented in table 4.1 and table 4.2. Sample specifications are described in the following section.

4.3 Sample specifications

The samples cast comprised (i) 100 mm cubes cast in steel moulds for electrical resistivity measurement and compressive strength test, (ii) cylinders (Ø 100 × 300 mm) for the migration test (NT Build 492) and resistivity measurements using a PVC mould, and (iii) 250 × 250 × 152 mm slabs with a 18-mm dyke to facilitate a wet/dry cycle regime using the plywood. A total of three samples were cast for each sample type. Slabs were used for chloride profiling, resistivity measurement, resistance measurement using stainless-steel pin electrodes, and corrosion measurements. The sample used in this study is shown in figure 4.1.

Prior to casting, all moulds were cleaned and oiled with *Sika Release Mould Formwork Release Agent* to facilitate the demoulding process and to prevent mixing water loss by the plywood during casting/curing. All samples were filled in two layers, each layer compacted using a vibrating table.

Table 4.1 Chemical compositions and fineness for binder type

% by weight	SiO_2	Al_2O_3	Fe_2O_3	CaO	MgO	TiO_2	P_2O_5	SO_3	K_2O	Na_2O	Fineness (% retained on 45µm)
CEM I (PC)	20.68	4.83	3.17	63.95	2.53	+	+	2.80	0.54	0.08	+
FA	51.00	27.40	4.60	3.40	1.40	1.60	0.30	0.70	1.00	0.20	< 29.8
GGBS	33.27	13.38	0.56	41.21	8.49	0.9	+	0.62	0.5	0.33	< 7.8

Notes: All values except the fineness were taken from the technical specification provided by the suppliers, + not determined,

Table 4.2 Concrete mixes used in the experimental programme (Laboratory samples)

Mix designation	w/b	Water (kg/m^3)	Total binder (kg/m^3)	CEM I (kg/m^3)	GGBS (kg/m^3)	FA (kg/m^3)	Coarse agg. (kg/m^3)	Fine agg. (kg/m^3)	Plast (kg/m^3)	Slump (mm)
CEM I (PC)	0.4	184	460	460	+	+	1012	650	1.84	140
	0.6	180	300	300	+	+	1101	707	+	110
CEM III/A (GGBS/40)	0.4	180	450	270	180	+	1016	652	1.35	100
	0.6	180	300	180	120	+	1096	704	+	110
CEM II/B-V (FA/30)	0.4	212	530	370	+	160	890	571	1.59	130
	0.6	180	300	210	+	90	1078	692	+	100

Note: * w/b=water/binder ratio; Coarse agg.=Coarse aggregate and Fine agg.=Fine aggregate; and Plast=Plasticizer

(a) Cuboidal sample

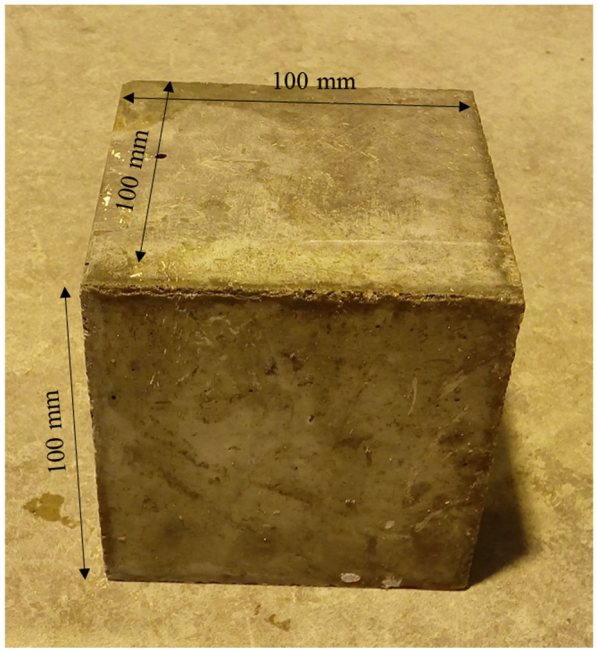

(b) Cylinder sample

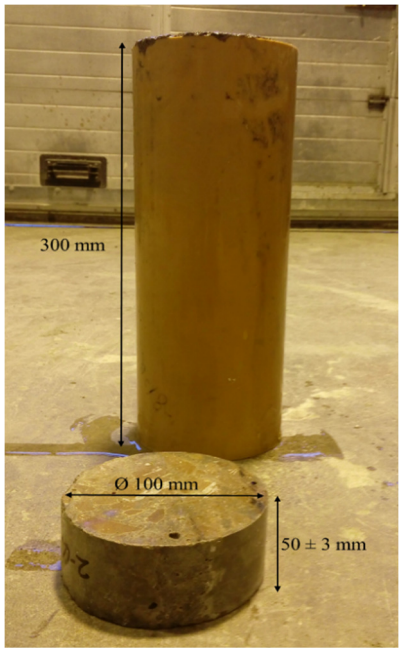

(c) Slab sample

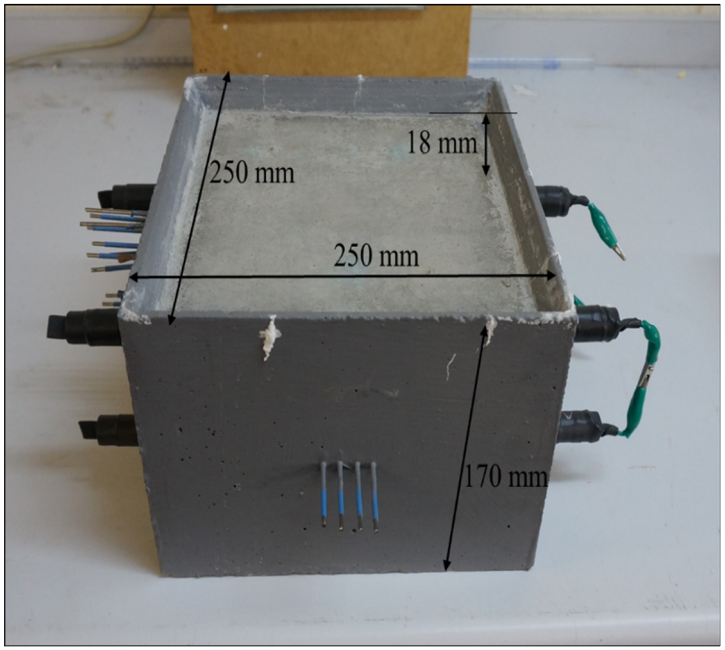

Figure 4.1 (a) Cubic sample for compressive strength and electrical resistivity test, (b) cylinder sample for migration test (NT build 492) and electrical resistivity test and (c) slab sample used for monitoring corrosion parameters and electrical resistance

For corrosion measurements and electrical resistance monitoring, each of the three slabs contained four mild steel bars (Ø 16 × 350 mm), seven pairs of stainless-steel (316 L Marine grade) pins (Ø 2.4 × 110 mm), and one thermistor positioned at the steel depth (25 mm from exposure surface) to correct concrete resistance for temperature fluctuations (see figure 4.2). For chloride profiling and degree of saturation/porosity, one plain slab was additionally cast per mix with a dyke.

Figure 4.2 shows a schematic diagram for slabs containing mild steel bars for corrosion monitoring and stainless-steel pin electrodes for electrical resistance measurement. Photographs of the mould with steel and stainless steel electrode, and concrete slab samples are presented in Appendix B.1.

The details concerning the mild steel bars and stainless-steel pin electrodes are as follows.

(1) Mild steel for corrosion measurements

(i) General treatments

Prior to casting, all steels were degreased with acetone and weighed. The exposed area was limited using heat-shrink sleeving. Electrical connection to the steel was made using a copper wire. The wire consisting of a crocodile clip attached at one end of all mild steels and then both ends of the mild steel were wrapped with heat-shrink sleeving to prevent corrosion.

After demoulding, the protruding ends of the steels were again sealed with heat-shrink sleeving. Prior to sealing the protruding ends of the steels were sandblasted to remove any blemishes, e.g. cement paste and corrosion products formed on the steels during casting and curing.

(ii) Two steel bars at 25 mm from the exposure surface (acting as working electrodes)

One steel bar had 150 mm of length of exposed area accounting for 75.40 cm^2, denoted by LS (steel with long exposed area). The other had two 50 mm lengths of exposed area accounting for 50.27 cm^2, denoted by SS (steel with small exposed area) (see the Appendix B1.2 and figure 4.3). The centre of the SS with 50 mm of length was insulated to position stainless-steel pin electrodes for measuring concrete resistance, and one thermistor for measuring temperature.

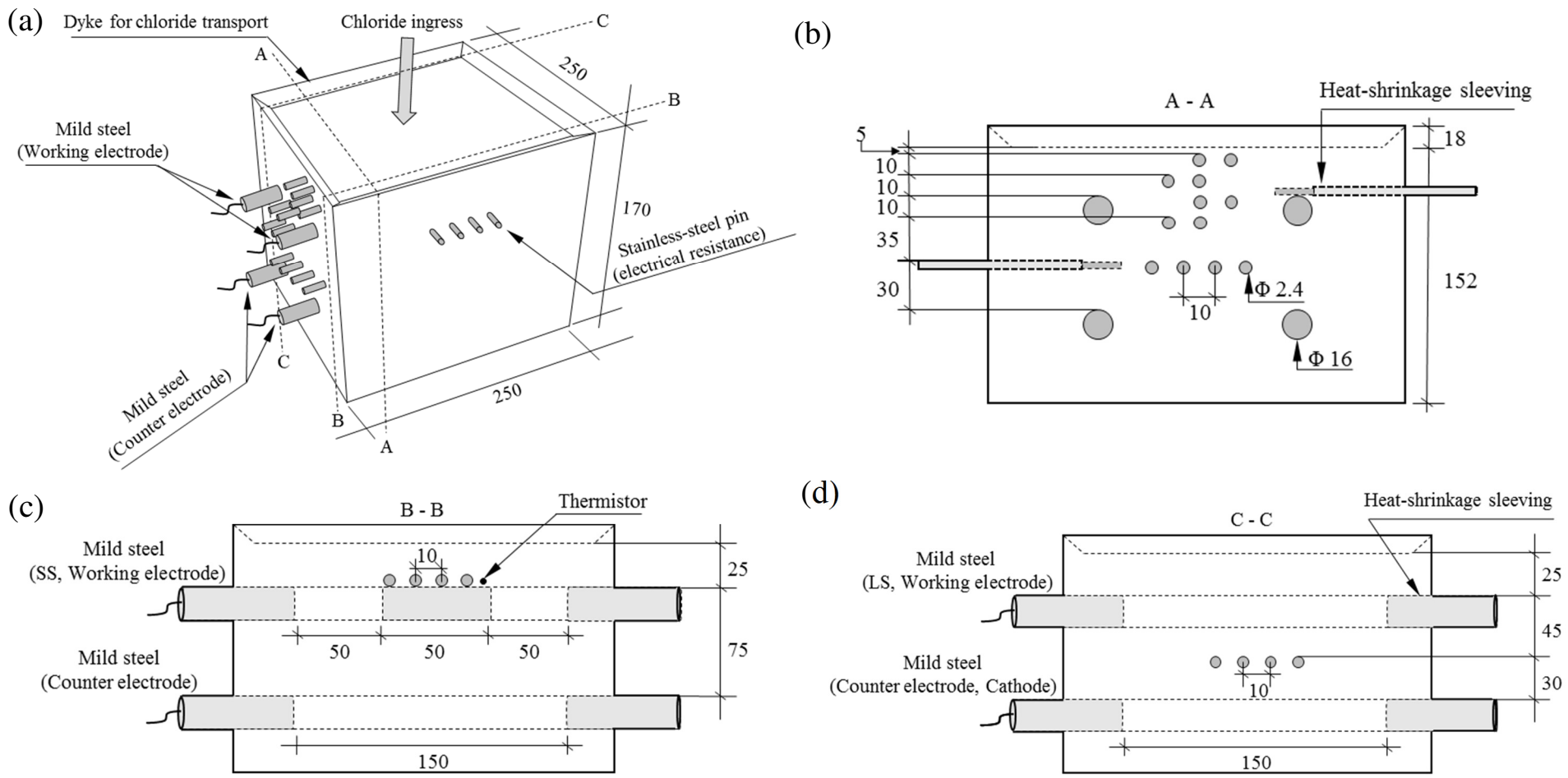

Figure 4.2 Schematics of concrete slab (dimensions in mm): (a) isometric (b) end elevation, A-A, (c) end elevation, B-B and (d) end elevation, C-C; SS (steel having small exposed area), LS (steel having large exposed area).

(iii) Two steels at 100 mm cover depth, positioned in parallel to each working electrode (acting as counter electrodes)

Both steels at this depth had 150mm of length of exposed area and were used as a counter electrode when corrosion tests were performed in a three-electrode arrangement, i.e. working electrode, counter electrode and reference electrode. In addition, the counter electrodes located under the LS (the working electrode) played a role as a cathode and was thereby always connected with the LS for increasing cathode area, except during measurements.

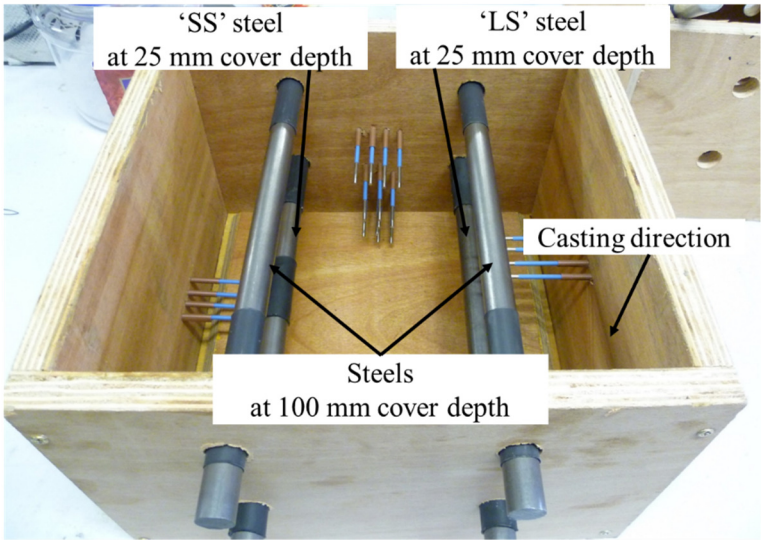

(a)

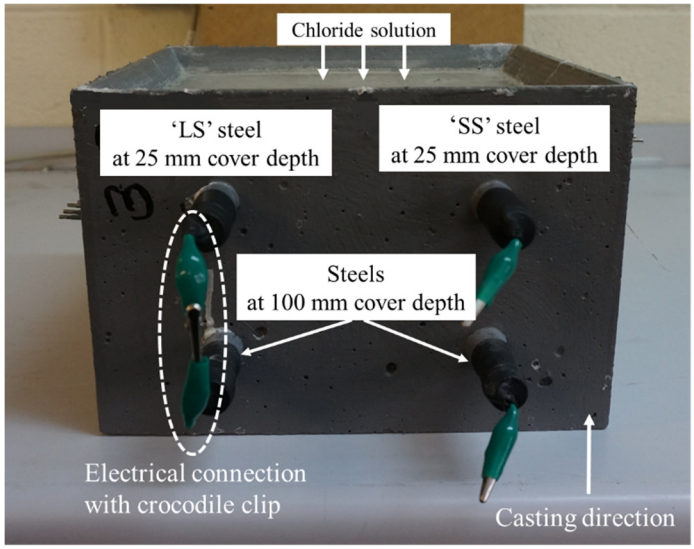

(b)

Figure 4.3 Steel configuration in slab (a) before casting and (b) after demoulding

(2) Stainless-steel pin electrodes used for concrete resistance monitoring

(i) General treatments

For stainless-steel pin electrodes, seven sets of electrodes were installed at discrete positions within the concrete slab sample, and consisted of two arrangements: two-pin electrode and four-pin electrode (see figure 4.4). All electrodes were sleeved with a heat-shrink sleeving to expose their 20-mm tip. Each electrode pair had a centre-to-centre spacing of 10 mm and the exposure length was set to the same size with nominal maximum aggregate to minimise an error caused by aggregate trapped between electrodes. To account for the influence of temperature, a thermistor was embedded at the steel depth.

(ii) Two-pin electrode arrangement for monitoring the electrical resistance

In this configuration, a pair of two-pin electrodes was mounted at four discrete positions – 5, 15, 25, and 35 mm – within the surface region of the slab (figure 4.4 (a)). These electrodes monitored local resistances due to (a) chloride movement, (b) a change of moisture condition, and (c) a change of pore structure.

(iii) Four-pin electrode arrangement for monitoring the electrical resistance

A four-pin electrode arrangement was mounted at three positions, including 25 mm and 70 mm cover depth installed on different sides, respectively. At 25-mm cover depth, a four-pin electrode was positioned on the sleeved part of the steel (i.e. on the centre of the SS), which prevented interference of the electrical field by steel during the measurement (figure 4.4 (b)). Two sets of four-pin electrodes were mounted on the other sides. One electrode was positioned between two mild steel bars (i.e. between the LS [the working electrode] and the counter electrode) at 70 mm of cover depth on one side (figure 4.4(c)), while the other one was placed on the other side containing two-pin electrodes (figure 4.4(d)). The electrodes aimed to monitor the resistance caused by the corrosion process as well as the chloride and hydration process. In addition, to monitor a change in electrical resistance caused by hydration, two-pin electrode which is centrally positioned in four-pin electrode arrangement at 70 mm cover depth (figure 4.4 (a)) was used.

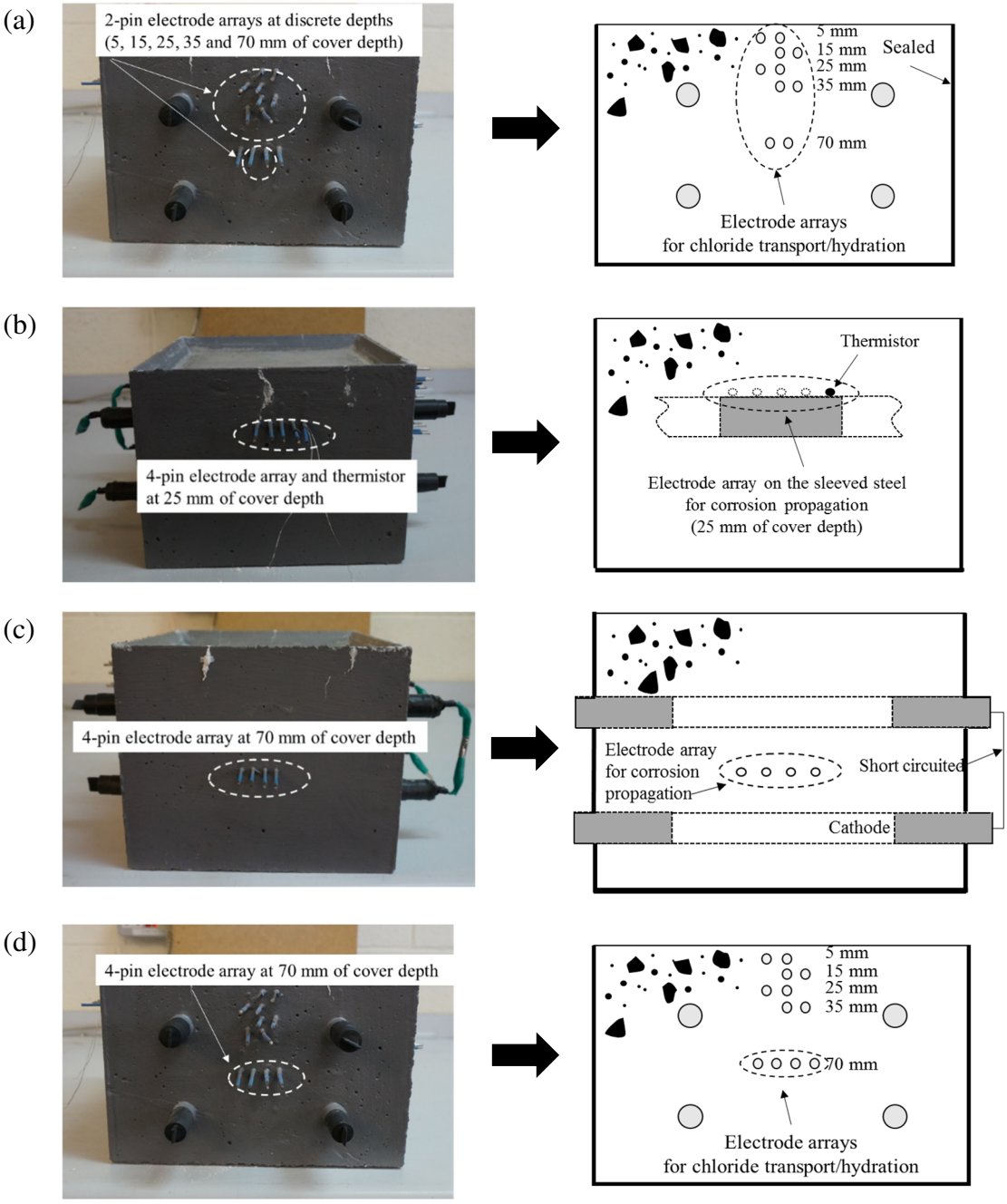

Figure 4.4 Arrangement of electrodes for monitoring electrical resistance of concrete subjected to chloride attack; (a) electrode arrays for chloride transport, and (b), (c) and (d) electrode arrays for corrosion propagation

4.4 Curing and exposure regime

After casting, all samples were covered with a heavy-duty polythene sheet to prevent evaporation of water from the concrete surface. The cube samples were de-moulded after 24 hours and then stored in a curing tank at 20 ± 1ºC until required times for measurements (compressive strength and bulk resistivity). The cylinder samples (Ø 100

× 300 mm) for the migration test were cured in the same curing tank without de-moulding to minimise leaching of hydrates and to simulate taking cores in a real structure.

The slab samples were kept in the mould and wrapped with polythene for seven days. After de-moulding, all faces of the sample, except for the face with the dyke, were double-coated with an epoxy-based paint. To minimise moisture loss during air curing, the samples were again wrapped with polythene and then further cured for 28 days at 20 ± 3 ºC, so no moisture was lost during curing.

A cyclic wet/dry regime was used in the laboratory to accelerate chloride-induced corrosion in concrete. Although other accelerated methods, such as the impressed current method (Austin *et al.*, 2004), pre-mixed chloride method (Martinez *et al.*, 2015; Michel *et al.*, 2013; Manera *et al.*, 2008) and simulated pore solution method (Sánchez-Moreno *et al.*, 2009; Ghods *et al.*, 2010; Chen and Orazem, 2015) are relatively common due to the short time they require, the method used in this study is more realistic to simulate the effects of chloride on steel and concrete. The exposure solution comprised sodium chloride (NaCl) dissolved in distilled water at 20 ± 3ºC to give a concentration of 19.6 g/l Cl^- (0.55 mol). This concentration is representative of the chloride content in the North Sea (McCarter *et al.*, 2008). Prior to starting wet/dry cycles, slabs were saturated for 7 days with distilled water. The samples were consequently contaminated by chloride solution from 42 days of concrete age using a dyke formed in the concrete surface. During the drying period, the chloride solution was removed from the surface and then the surface was exposed to a controlled laboratory environment (20 ± 3ºC and 50 ± 2% RH). The cyclic wet/dry regime, especially the drying period, was sequentially adjusted to prevent rapid ingress of chloride caused by the absorption effect. The regime increased from a weekly to a bi-weekly regime, i.e. 2 days drying and 5 days wetting for the first month, 5 days drying and 2 days wetting for the second month, and 8 days drying and 6 days wetting for the remaining period. The drying period increased step-wise, as the rate of chloride transport by cyclic drying is faster than by pure diffusion.

4.5 Sample preparation

For chloride profiling, the degree of saturation test and the migration test, samples were additionally prepared from concretes prior to measurements. The plain slab (250 × 250 × 152 mm slab with a 18-mm dyke, without stainless-steel pin electrodes and mild steel) was split into thin slices in sequence for the degree of saturation test and profiling. To minimise

the change of chloride distribution and moisture distribution within the concrete, all cutting was carried out with a diamond saw (3.5 mm thickness) without water. As seen in Figure 4.5, a layer was first extracted for the degree of saturation test at the end of the final wet cycle (382 days), and then the remaining part was sealed with a polythene except for the working surface (the side with a dyke). At the end of the final dry cycle (390 days), two slices were extracted from the remaining part, one (50 × 250 × 152 mm) for the degree of saturation test and the other (100 × 250 × 152 mm) for chloride profiling.

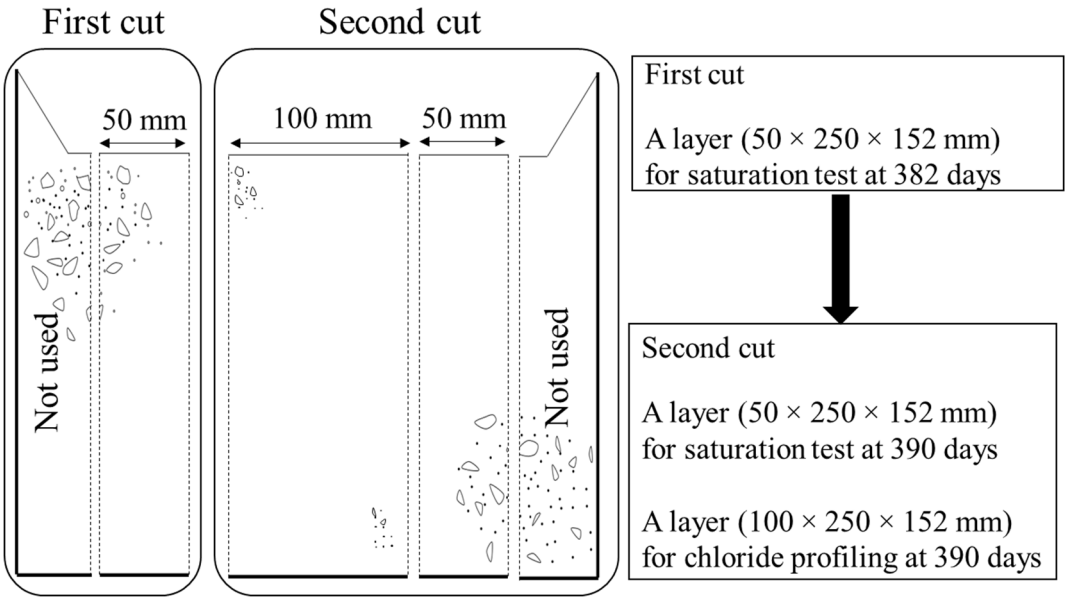

Figure 4.5 Cutting the plain slab for chloride profiling and the saturation test

To prepare samples for the degree of saturation test, the slice (50 × 250 × 152 mm) was sectioned to obtain five cubes (50 × 50 × 20 mm) from the concrete surface up to 100 mm of depth (see figure 4.6). The experimental procedures following cutting are described in Chapter 5.2.2. Meanwhile, for chloride profiling, powders were obtained from the slice (100 × 250 × 152 mm) using a hammer-drilling machine at 390 days. The investigated depth for all concretes was 0-32 mm using a 4-mm diameter drill bit except for CEM I (w/b=0.6) concrete, where the depth increment was a 8-mm diameter drill bit due to larger contamination of chloride. The lateral parts of the slice for collecting powder were drilled parallel to the concrete surface. Several holes (approximately 6–8 holes at each depth) were drilled up to 30 mm depth and taken to be representative of bulk concrete powder, as shown in figure 4.7. The powder was sieved with a 125 μm sieve and at least 10 g of powder was collected at every depth.

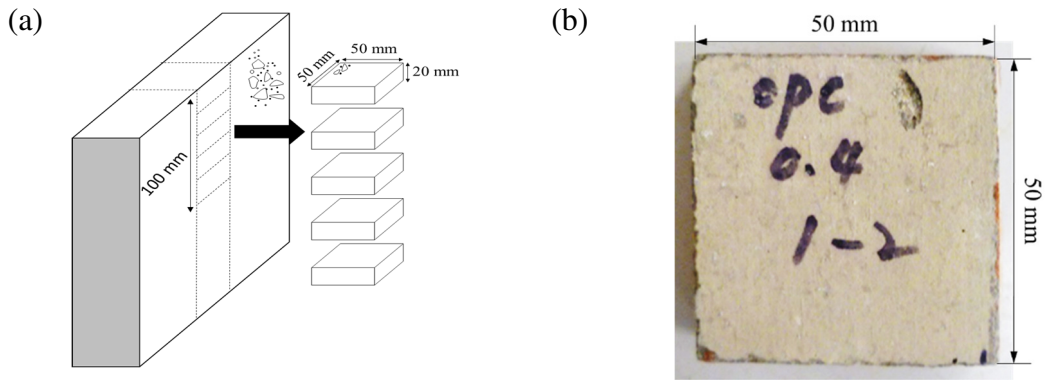

Figure 4.6 (a) Cutting process from the sectioned slice and (b) a sample for the degree of saturation test

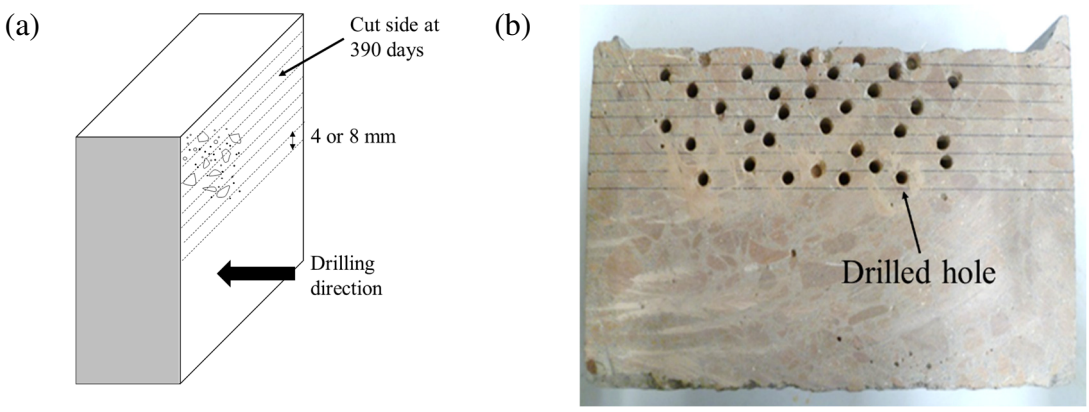

Figure 4.7 (a) Drilling process from the sectioned slice and (b) a drilled sample for collecting powder

For samples using the migration test/electrical resistivity measurement, the cylinder (Ø 100 × 300 mm) was sectioned using a water-cooled diamond saw to extract slices (Ø 100 × 50 ± 3 mm) from the central portion of the cylinder. Three replicates were subsequently obtained from one cylinder, as shown in figure 4.8.

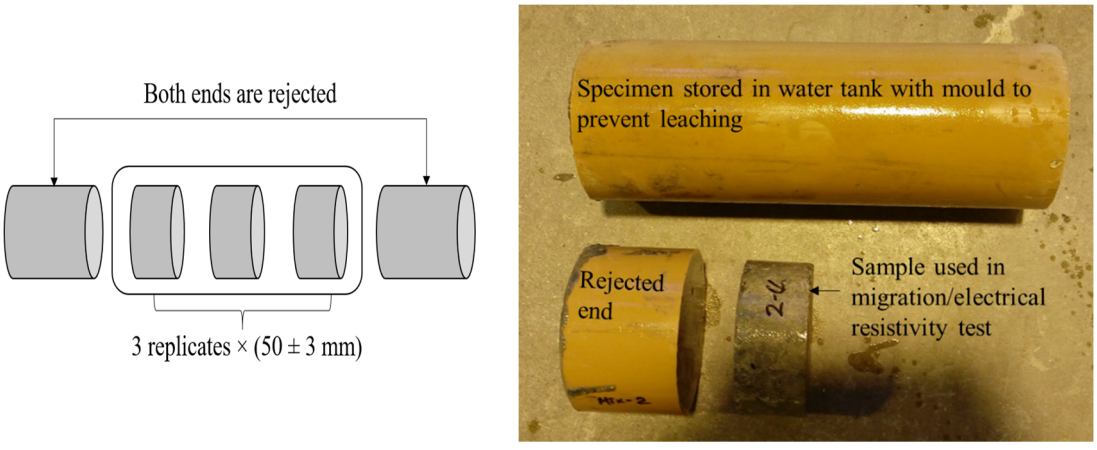

Figure 4.8 Sample cutting for migration/electrical resistivity test

4.6 Marine exposure conditions and samples in field

For field study, the concrete slabs used in this study were installed at Dornoch Firth marine exposure site in Scotland in 1998 to investigate the response of cover concrete exposed to a marine environment. Three concrete mixes were used to cast concrete slabs. A total of six samples per mix were positioned as follows: above the high-water level in the atmospheric spray zone; just below the water-level and below the mid-tide level. These levels are classified as XS1, XS3, and XS2, respectively, specified in BS EN 206 (2014). The slabs were secured in galvanised steel frames. The samples were 300 × 300 × 200 (thick) mm and contained two Ø 16 mm mild steel rebars with 50mm cover depth. Electrical connections were made to measure the steel condition using electrochemical methods. Except for one surface exposed to the marine environment, all sides were coated with epoxy resin to ensure one-dimensional movement of water/moisture. Pairs of stainless-steel pin electrodes were installed at discrete distances from the exposed surface: 5, 10, 15, 20, 30, 40, and 50 mm. Four thermistors were positioned at 10, 20, 30, and 40 mm to monitor temperature. Colour-coded cables for the electrodes, rebars and thermistors were taken into a watertight glass-reinforced plastic box placed in the face opposite to the working face; a 37-pin, multi-pole female D connector was used to terminate all wires. In the XS2 and XS3 exposure conditions, three samples (one from each mix) were hard-wired to a control-box facility to interrogate/monitor the samples remotely.

In this study, samples exposed to XS3 environment were chosen (see figure 4.9) as concrete is the most vulnerable to deterioration by chlorides in this zone (British Standards Institution, 2016). Three samples, one in each mix, were retrieved and double-sealed with polythene film to avoid moisture loss during transportation. A series of experiments and sampling was conducted in the laboratory within one week from the date of removal from the site. The mix proportion presents in table 4.3. Note that to distinguish between field samples and laboratory samples, the notation used for the field samples are PC, GGBS/40 and FA/30 corresponding to CEM I, CEM III/A and CEM II/B-V, respectively in this study.

Table 4.3 Mix design used in field samples (McCarter *et al.*, 2012)

Mix designation	CEM I (kg/m^3)	GGBS (kg/m^3)	FA (kg/m^3)	Coarse aggregate		Fine aggregate (kg/m^3)	WR* (l/m^3)	w/b
				20 mm (kg/m^3)	10 mm (kg/m^3)			
CEM I (PC)	460	+	+	700	350	700	1.84	0.4
CEM III/A (GGBS/40)	270	180	+	700	375	745	3.60	0.44
CEM II/B-V (FA/30)	370	+	160	695	345	635	2.65	0.39

*WR water reducer

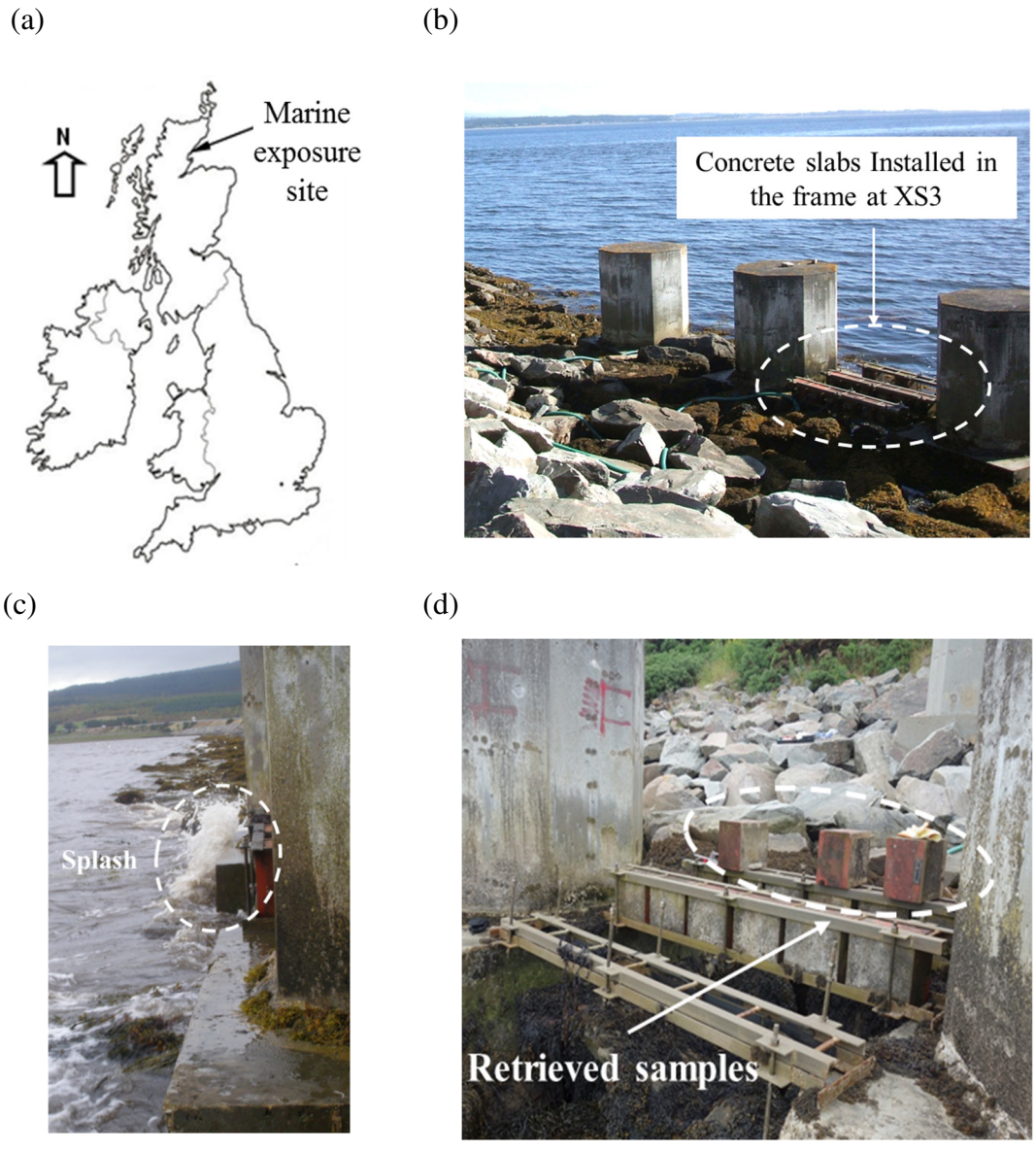

Figure 4.9 (a) Location of marine exposure site, (b) position of frames installed in XS3 environment, (c) breaking waves during the period of rising tide, and (d) retrieved samples positioned in the frame.

4.7 Summary

Chloride-induced corrosion of reinforcement can be divided into two stage, before and after corrosion initiation. In turn, different methods were applied depending on the condition of the concrete. In general, the period before time to onset of corrosion is referred to as the initiation period, where tests were related to chloride transport within concrete, while corrosion propagation indicates the process after corrosion has initiated, which was evaluated with the amount of corrosion (or corrosion rate) on the surface of the steel. Therefore, both parameters related to corrosion and chloride transport were evaluated with time. Due to the on-going hydration process, especially in concrete containing SCMs, it was necessary to monitor continuously instead of one-off measurement. Monitoring electrical resistance of concrete using stainless steel electrodes with different depths was also carried out to evaluate chloride ingress and corrosion behaviour of steel in concrete subjected to chloride environments.

In order to reflect exposure condition in the field, 18-years old samples exposed to marine environment (XS3) was retrieved from field site in Dornoch Firth and then the tests, which were used in the laboratory samples, were performed. Parameters such as the diffusion/migration coefficient, porosity, degree of saturation and polarisation resistance are used in modelling, together with mix design and are discussed in Chapter 8. Table 4.4 presents the overall experimental programme comprising sample type and test details; the experimental procedures are described in the corresponding sections. The relationship between durability assessment and required parameters are presented in table 4.5.

Table 4.4 Overall frameworks for experimental programme

Chapter	Classification	Sample		Measurement		
		Types (Replicate)	Dimension (mm)	Test	Type	Time (days)
5	Material /environmental properties	Concrete (3)	100 × 100 × 100	Compressive strength Resistivity	D ND	28, 90, 180, 365
		Concrete (1)	50 × 50 × 20	Porosity/saturation degree Resistivity	D ND	382, 390
	Transport	Concrete (3)	Ø 100 × 50	Migration Resistivity	D ND	180, 270, 365
		Concrete (1)	100 × 250 × 152	Chloride profile	D	390
6	Corrosion	Concrete (3)	250 × 250 × 152	Half-cell potential Macrocell current	ND/NQ	42 – 382 (Every end of wet/dry cycle)
				Linear polarisation Galvanostatic pulse Potentiostatic	ND/Q	186 – 382 (Every end of wet cycle)
				Electrochemical impedance spectroscopy	ND/Q	Specific dates**
				Tafel extrapolation	ND/Q	382
				Mass loss	D/Q	382 (for corroded samples)
7	Electrical resistance monitoring	Concrete (3)	250 × 250 × 152	Two-pin electrodes for chloride transport	ND	42 – 382 (Every end of wet/dry cycle)
				Four-pin electrodes for corrosion process	ND	

Table 4.4 (continued)

8	Environmental properties	Concrete (1)	50 × 50 × 20	Porosity/saturation degree Resistivity	D ND	18 years
	Transport	Concrete (1)	100 × 300 × 200	Chloride profile	D	
	Corrosion	Concrete (1)	300 × 300 × 200	Half-cell potential	ND/NQ	
				Linear polarisation Galvanostatic pulse Potentiostatic	ND/Q	
				Electrochemical impedance spectroscopy	ND/Q	
				Tafel extrapolation	ND/Q	
	Electrical resistance monitoring	Concrete (1)	300 × 300 × 200	Two-pin electrodes for chloride transport	ND	

* D destructive method, ND non-destructive method, Q Quantitative method, NQ Qualitative method

** CEM I (w/b=0.4): 186, 270 and 382 days, CEM I (w/b=0.6): 186, 228 and 382 days, CEM III/A (w/b=0.4): 186, 228 and 382 days, CEM III/A (w/b=0.6): 186, 270 and 382 days, CEM II/B-V (w/b=0.4): 186, 228 and 382 days and CEM II/B-V (w/b=0.6): 186, 228 and 382 days

Table 4.5 Summary of research related to performance-based approach

Requirements	Phases in service life	Types	Main parameters	Description
Test methods	Initiation	Transport rate	Diffusion/migration coefficient	• Investigate the relation between migration and diffusion coefficients
		Chloride binding	Binding isotherm	• Review the binding isotherm from literature review
		Electrical resistivity	Resistivity	• Investigate the relation between migration coefficient and electrical resistivity of concrete • Monitor concrete resistivity with chloride transport
	Propagation	Electrical parameters	Corrosion potential, Macrocell current, Polarisation resistance	• Investigate time to corrosion initiation and development of corrosion rate with time • Compare the corrosion values with various electrochemical tests
		Tafel's constant	B constant	• Investigate B values for calculation of corrosion rate using Tafel's method and simple monitoring techniques including potentiostatic tests
		Electrical resistivity	Resistivity	• Monitor concrete resistivity after corrosion initiation • Investigate the relation between corrosion process and concrete resistivity
Environmental conditions	Initiation	Physical properties	Degree of saturation	• Investigate the relation between electrical resistivity of concrete and saturation degree and then establish the relation using Arch's law
	Propagation	Physical properties	Oxygen availability	• Investigate cathodic branch in Tafel slope
			Chloride content	• Investigate the effect of Tafel constant on chlorides
Models	Initiation	Physical model	Migration coefficient	• Estimate chloride profile using ClinCon model with migration coefficients • Update environmental factors corresponding to XS3 area with comparison between estimated chloride profile and that from the field samples • Determine chloride threshold level with updated chloride profiles and corrosion rates
	Propagation	Empirical model	Polarisation resistance	• Estimate corrosion rate with time • Establish an empirical relation of polarisation resistance with time

CHAPTER 5
CHLORIDE TRANSPORT AND PERFORMANCE FACTORS

5.1 Introduction

Ideally, a performance factor should quantify those concrete properties related to deterioration, leading to an improved understanding of concrete durability. There has been a growing interest in such factors as they are essential in a performance-based approach. Essentially, factors should be easy to apply and reliable as well as being appropriate for the particular deterioration mechanism(s) for the structure, and their numerical values should also be satisfied with suitable performance limiting values (Andrade *et al.*, 2013).

Chloride-induced corrosion in structures is described by Tuutti's model comprising the initiation and propagation phases. During the initiation phase, chlorides move into concrete from an external source, such as sea-water or de-icing salt due to concentration gradient. In this phase, the degree of saturation of the pore system and the chemical composition of the pore solution are important as chlorides penetrate the pore solution. After depassivation (the propagation phase), the corrosion process is controlled by electrochemical parameters on the steel surface including oxygen availability, moisture content and concrete resistivity. These properties must be included in a performance-based test for the target structure. The electrical resistivity of concrete is a powerful candidate as a performance factor, as this parameter is easily and rapidly evaluated. In addition, resistivity quantifies a number of variables including environmental conditions and concrete properties and it is believed that this single parameter could be developed as a viable, performance factor, especially in chloride transport.

This section analyses performance factors related to chloride transport, including the compressive strength, migration/diffusion coefficient, electrical resistivity, degree of saturation and porosity. These parameters are then correlated with the electrical resistivity of concrete. The measured values are also applied to a predictive model as input parameters in this study (Chapter 8). Experiments were carried out on laboratory samples; the details of the experimental set-up and test samples are described in Chapter 4.

5.2 Experimental

A range of experiments were conducted to assess the transport properties of concrete, including migration/diffusion tests, electrical resistivity test and degree of saturation test; compressive strength and porosity tests were also measured. This section outlines the experimental procedures used to measure the aforementioned parameters.

5.2.1 *Compressive strength*

Compressive strength tests were undertaken in accordance with BS EN 12390-3 (British Standards Institution, 2009). The samples were cured in a water bath at 20 ± 2ºC until the test date, and three replicates per mix were measured at 28, 90, 180, and 365 days. An average of three replicate measurements is presented as strength value for test age of 28, 90, 180, and 365 days.

5.2.2 *Porosity/saturation degree*

At the end of final wet/dry cycle, small cubes of concrete (ca. 50 × 50 × 20 mm) described in Section 4.5 (figure 4.6) were swan to a depth of 100 mm from the concrete surface to estimate the degree of saturation and porosity. For each depth, only one replicate was obtained.

After cutting, the weight and electrical resistance of the samples were immediately measured before loss of moisture to the surrounding environment which was at 20 ± 3ºC and 50 ± 2% RH; samples were then dried in an oven at 50 ± 2ºC. The low drying temperature prevented any potential change in microstructure due to micro-cracking and the difference in weight change per each measurement was marginal for the different drying temperature (Streicher and Alexander, 1995; Otieno *et al.*, 2014). Saturation was carried out using distilled water in a vacuum chamber. A pressure of 30 mbar was maintained for 4 hours and then the sample was placed in the chamber until weighing. To determine the equilibrium condition at each stage, the mass of each sample was periodically measured using a scale of ± 0.01 g accuracy. The equilibrium was assumed to be achieved when the following criterion was satisfied:

$$\left|\frac{m(t_i) - m(t_{i+1})}{m(t_{i+1})}\right| \times 100 \leq 0.1(\%) \quad (5.1)$$

where $m(t_i)$ is the mass (g) measured at time t_i and $m(t_{i+1})$ is the mass (g) measured after time t_{i+1}.

The degree of saturation and porosity were then calculated as follows:

$$S_r\ (\%) = \frac{m_o - m_{dry}}{m_{vsat} - m_{dry}} \times 100 \quad (5.2)$$

$$\emptyset\ (\%) = \frac{\frac{1}{\delta_w}(m_{vsat} - m_{dry})}{V_{sample}} \times 100 \quad (5.3)$$

where S_r is degree of saturation (%), m_o is the original sample mass (g), m_{dry} is the dried sample mass (g), m_{vsat} is the vacuum saturated sample mass (g), $\emptyset$ is porosity (%), δ_w is the density of distilled water (=1 g/cm^3), and V_{sample} is the sample volume (cm^3).

5.2.3 *Chloride profiling*

A chloride profile was established by plotting the total chloride content versus depth. A non-linear curve fitting method was then used to determine the diffusion coefficient from the chloride profile.

To simplify the chloride analysis, Chloride QuanTab® strips (manufactured by HACH) were used. To measure the chloride concentration, the concrete dust in a 100 ml glass beaker was weighed using a scale with an accuracy of ± 0.001 g. The chloride in the powder sample was dissolved in a diluted nitric acid solution of 50 ml (~ 2 mol HNO_3) at 80 ± 2ºC for 4–5 minutes. The suspension was neutralised with $Na(OH)_2$, maintaining a pH of 6-8 in a suspension, as Chloride QuanTab® strips are only valid in a neutral solution. The neutralised suspension was then allowed to cool to room temperature and filtered. The chloride content was measured with a Chloride QuanTab® strip with ppm unit. Although various representations have been suggested for chloride content in concrete, total chloride concentration (by weight of binder or concrete) is a typical representation (Glass and Buenfeld, 1997). This is because total chlorides participate in the corrosion process (Glass *et al.*, 2000) and the measurement is convenient compared

to other methods. In this method, the measured chloride concentration is converted into total chloride concentration (by weight of binder) using the following equation assuming uniform distributions of cement and chloride at the sampling depth (Song *et al.*, 2008a):

$$C_t(\%) = \frac{V_{solution} \times C_{dissolution}}{m_{dust} \times \frac{\mathrm{M}_{binder}}{\mathrm{M}_{concrete}}} \times 100 \tag{5.4}$$

where C_t is the total chloride content by mass of cement (%), $V_{solution}$ is the suspension volume (l), $C_{dissolution}$ is the chloride content dissolved in the suspension (g/l), m_{dust} is the mass of concrete dust (g), M_{binder} is the unit mass for binder (kg/m^3), and $\mathrm{M}_{concrete}$ is the unit mass for concrete (kg/m^3).

The apparent chloride diffusion coefficient was determined by fitting the error function solution to Fick's second law for non-steady state diffusion in a semi-infinite medium. A curve was fitted to the chloride profile with a surface chloride content and a diffusion coefficient using the Newton-Rapshon method in the Mathcad® program. Due to the erratic behaviour at the outermost layer, two methods were simultaneously carried out: (i) fitting with all points and (ii) fitting with points omitting the first point. Figure 5.1 illustrates an example of the determination of the diffusion coefficient and surface chloride concentration using curve fitting. The background chloride concentration, i.e. pre-existing chloride concentration in mix ingredients, was neglected in analysing the chloride profiles because there was only a very low amount of chloride.

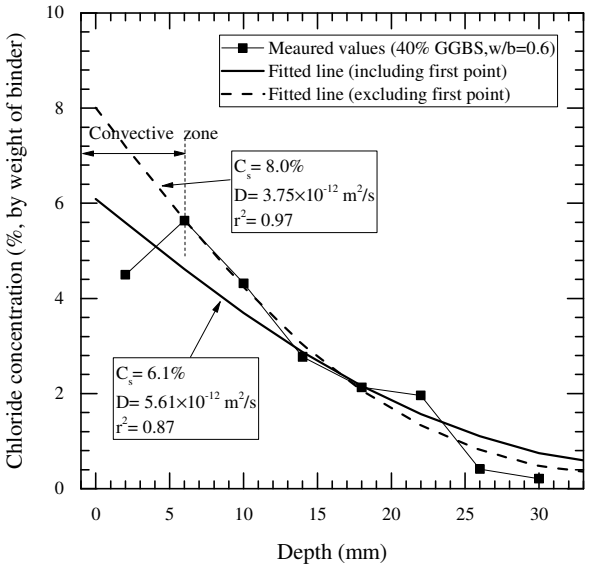

Figure 5.1 Examples of curve fitting from the chloride profile data.

5.2.4 *Migration test*

Accelerated chloride migration testing was carried out using the NT Build 492 method (Nordtest, 1999), which is widely used in Europe. The measurements using the sample (Ø 100 × 50 ± 3 mm) were performed at 180, 270, and 365 days to minimise the hydration effect of SCMs. The samples were vacuum-saturated under a pressure of 30 mbar for 24 hours in a desiccator containing saturated $Ca(OH)_2$ solution (4 g/l). After saturation, the electrical resistivity was measured using the end-to-end electrode configuration with two stainless-steel plates. The details of resistivity measurement are described in Section 5.2.5.

Test procedures for the migration test conformed to the NT Build specification except for measurement time and voltage. For all samples, the applied voltage was fixed at 30 V and the measurement time was increased except for the CEM I (w/b = 0.6) concrete, in which the applied voltage was 20 V due to the rapid ingress of chlorides. This method is similar to the original version proposed by Tang (1996b) to minimise the effect of voltage on the chloride transport rate and is still controversial (Spiesz and Brouwers, 2012).

After completing the migration test, chloride penetration depth was measured using a colorimetric method with 0.1 mol $AgNO_3$ solution. The migration coefficient was then calculated using the following equation (Nordtest, 1999):

$$D_m = \frac{0.0239(273+T)}{(\mathrm{E}-2)t}\left(x_d - 0.0238\sqrt{\frac{(273+T)L \times x_d}{\mathrm{E}-2}}\right) \tag{5.5}$$

where T is temperature of the NaOH solution (ºC), E is the applied voltage (V), x_d is the average chloride penetration depth (mm) and L is the sample thickness (mm).

5.2.5 *Electrical resistivity of concrete*

To establish the relation between performance factors and electrical resistivity, electrical resistance of concrete was measured using a HP 4263B LCR meter. The measurements were performed on concrete samples used for the compressive strength test, the migration test and porosity/degree of saturation. For the compressive strength test, the electrical resistance of the concrete samples (100 mm cube) was measured before the test, while for

the migration test samples (Ø 100 × 50 ± 3 mm) the electrical measurement was performed between saturating and migration test. For samples measuring porosity/degree of saturation (ca. 50 × 50 × 20 mm), the measurements were carried out at each equilibrium state and original condition, respectively.

The end-to-end measurement method was carried out at a frequency of 1 kHz and signal amplitude of 350 mV, which minimised electrode polarisation effects (McCarter and Brousseau, 1990). Before measurements, sample surfaces were dried with a synthetic sponge. To achieve intimate contact, synthetic sponges (2 mm thickness) were placed between the electrodes and the concrete, and a mass of 2 kg was placed on the upper electrode to ensure uniform contact. The synthetic sponge was soaked in saturated $Ca(OH)_2$ solution and squeezed until no water dripped to reduce any surface conduction effects (Newlands *et al.*, 2007). The overall testing arrangement is shown in figure 5.2.

The averaged resistivity for three replicates per mix is expressed in this study. The resistivity (or reciprocal conductivity) of bulk concrete was calculated as

$$\rho = \frac{A}{L}\mathrm{R} = \frac{1}{\sigma} \tag{5.6}$$

where ρ is the resistivity (Ω·m), σ is the conductivity (S/m), A is the cross-sectional area (m^2), L is the sample thickness (m), and R is the resistance (Ω).

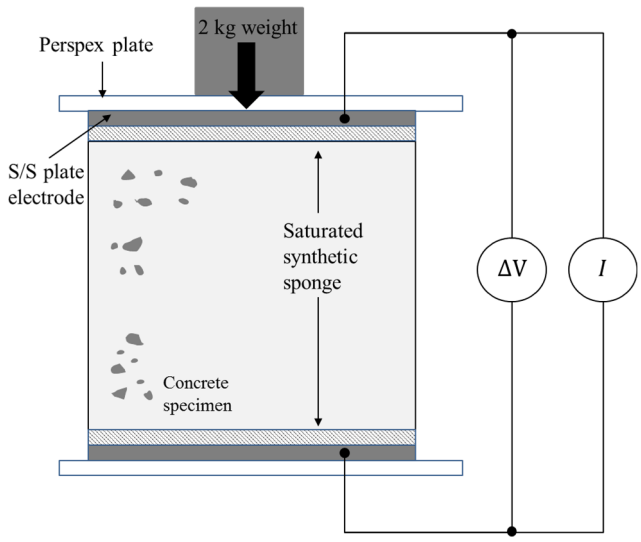

Figure 5.2 Schematic of testing arrangement for end-to-end electrical resistance measurements

5.3 Results and discussion

5.3.1 *Development of compressive strength*

Compressive strength is used in durability design as part of code requirements, although it is considered that this parameter cannot fully reflect the durability properties of concrete (Alexander *et al.*, 2008). However, according to PD/CEN 16563 (British Standards Institution, 2013a), where compressive strength is specified as part of the durability provision, this parameter is considered to be the reference parameter in the quality control of concrete. It is accepted that compressive strength is essential at the ultimate limit state.

Compressive strength at 28 days is generally used in the design stage but data beyond 28 days are required to describe the durability and performance (or serviceability) of concrete. Strength development is ongoing due to continuous hydration but slows down after 28 days. The use of pozzolanic materials or latent hydraulic binders such as FA and GGBS lead to a slower development in compressive strength (Ann *et al.*, 2008), but continuous refinement of microstructure over a longer time scale.

The development of strength for the concretes is presented in figure 5.3. The values are average values for three replicates per mix, with the error bars being ± one standard deviation. The overall trend is that compressive strength increased with time irrespective of the type of binder. Even though the compressive strength of SCMs concretes at 28-days were lower than that of CEM I concrete, the strength development from 28 – 365 days for the CEM III/A concrete (46% for w/b=0.4 and 35% for w/b=0.6) and CEM II/B-V concrete (69% for w/b=0.4 and 81% for w/b=0.6) was higher than those for the CEM I concrete (44% for w/b=0.4 and 30% for w/b=0.6) due to pozzolanic reaction (Ann *et al.* 2008). The continuous increase in the strength for SCM concretes is a characteristic of this type of concrete. An insoluble and dense calcium silicate hydrate gel is formed in the cement matrix resulting from the reaction of siliceous oxide in SCMs with calcium hydroxide in the pore solution of the binder. The SCMs subsequently lead to refinement of pore structure and an increase in binding capacity of chloride in concrete (Yuan *et al.*, 2009). Compressive strength at 365 days was ranked as CEM I (w/b=0.4) > CEM II/B-V (w/b=0.4) > CEM III/A (w/b=0.4) > CEM I (w/b=0.6) > CEM III/A (w/b=0.6) > CEM II/B-V (w/b=0.6) concrete. Considering the compressive strength as a performance factor, it would be reasonable to consider development of compressive strength for SCM concrete instead of compressive strength at 28 days.

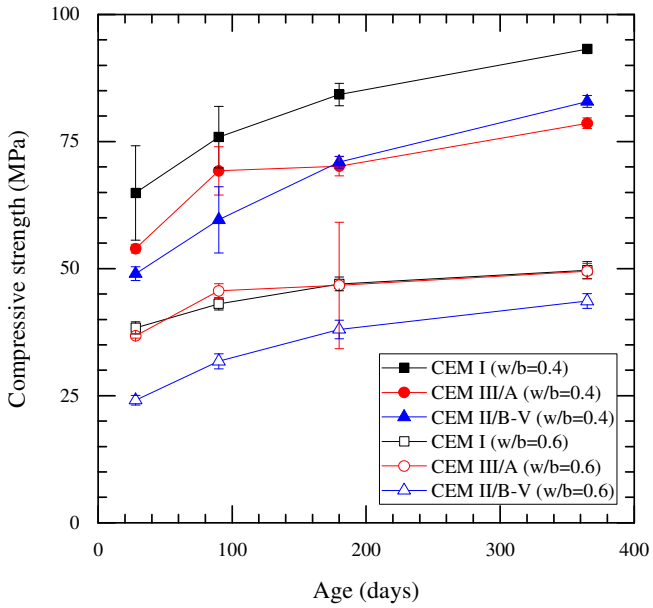

Figure 5.3 Development of compressive strength.

Compressive strength is considerably affected by concrete mix design, and the prediction of compressive strength within the mix design is still valuable. Abram's equation (equation (5.7)) is first proposed to predict compressive strength depending on the w/b (Abd elaty, 2014) and is then developed further considering SCMs. Another type is the power equation, which is a general form in concrete technology (Abd elaty, 2014) (equation (5.8)). The equations are described below:

$$f_c = \mathrm{a} \cdot \mathrm{b}^{-x}, x = \frac{w}{c + kf + s} \tag{5.7}$$

$$f_c = \mathrm{c} \cdot x^{-\mathrm{d}} \tag{5.8}$$

where f_c is the compressive strength (MPa), x is w/b, c is CEM I content (kg/m^3), f is FA content (kg/m^3), s is GGBS content (kg/m^3), k is the efficiency factor and a, b, c, and d are empirically determined parameters.

Both equations are only available to estimate the compressive strength at a certain age (usually 28 days) so that it is necessary to introduce an additional factor to explain time dependency. It is notable that durability/performance of concrete is correlated with time dependency of compressive strength rather than compressive strength at 28 days, as the continuous hydration for SCMs results in the development of compressive strength as well as durability/performance. The development of compressive strength in concrete,

which follows a logarithmic form with time (Abd elaty, 2014), is related to clinker minerals in the cement paste,

$$f_{c,t} = \mathrm{a} \cdot ln(t) + \mathrm{b} \tag{5.9}$$

where a is a constant for strength gain, b is a constant for strength grade and *t* is age (days).

Recently, constants have been determined based on comprehensive data on compressive strength using the fitting method, and they can be estimated using the following equations (Abd elaty, 2014). It was confirmed that development of compressive strength is attributed to the hydration of clinker minerals,

$$\mathrm{a} = 1.4035 \ln(\mathrm{b}) + 2.9956 \tag{5.10}$$

$$\mathrm{b} = 0.005\left(f_{c,28}\right)^{2.20} \tag{5.11}$$

Whether the long-term strength can be estimated accurately for concrete using SCMs is questionable due to the limitation of the logarithmic form, which shows an asymptotic behaviour with time instead of a continuous increase, and due to the lack of long-term data. However, the suggested equation is useful to estimate compressive strength with time in the view of a performance-based concept, although only compressive strength at 28 days is required in the code. Thus, it is necessary to secure additional data for long-term strength of concrete using SCMs to refine the model.

To estimate the time dependency in the compressive strength of concrete, figure 5.4 compares measured values and estimated values in this study using equation (5.9) (see Appendix D.1). The solid line indicates the line of equality. Although the difference increased by up to 20% in the high strength range from ~70 MPa, the estimated value was significantly close to the measured values. However, a latent hydration effect in the SCMs was not fully reflected in the empirical equation. Therefore, it was necessary to collect additional data on compressive strength of concrete using SCMs.

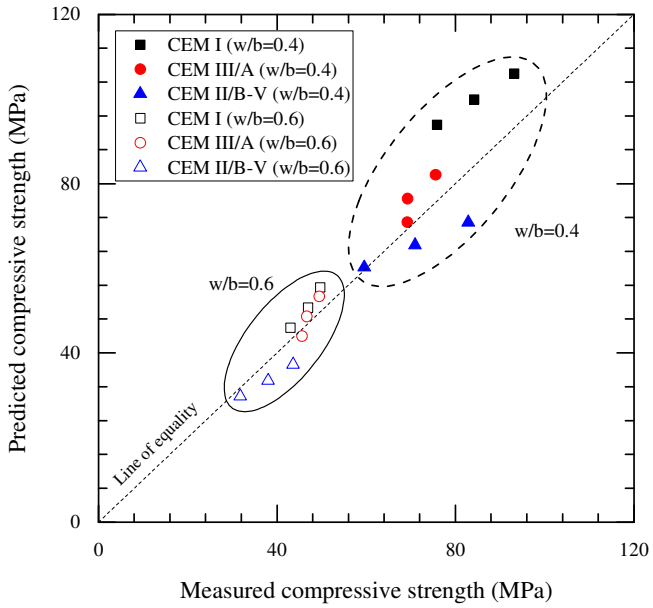

Figure 5.4 Comparison between measured and predicted values for compressive strength at different ages and different binders (expect for values at 28 days).

5.3.2 *Pore conditions in unsaturated concrete*

Concrete is a porous material and durability is determined by the pore structure. Currently, it is believed that two transport mechanisms, diffusion and absorption, co-exist in unsaturated concrete, i.e. concrete subjected to a wet/dry cyclic regime or the tidal zone in marine environments. Therefore, two mechanisms are simultaneously reflected to model the transport behaviour in unsaturated concrete. However, to introduce these two mechanisms in modelling is complex as there is no reference to distinguish between the diffusion and absorption rates in unsaturated concrete (Nilsson, 2000). For example, to trigger absorption, data on the degree of saturation of concrete have rarely been investigated. Alternatively, one transport mechanism, generally diffusion, is mainly considered for simplification of the calculation, but is still debated by researchers (Marchand and Samson, 2009). Therefore, it is necessary to investigate the degree of saturation and porosity in addition to direct measurement of transport rate.

It is generally agreed that the more porous the concrete, the less resistant it is to chloride ingress; thus, porosity can be used as a performance factor. In the present study, the porosity of concrete was evaluated (refer to Chapter 4) at different depths and is tabulated in table 5.1. Firstly, porosity at 390 days was ranked as CEM I (w/b=0.4) < CEM III/A (w/b=0.4) < CEM I (w/b=0.6) < CEM III/A (w/b=0.6) < CEM II/B-V (w/b=0.6) < CEM II/B-V (w/b=0.6) concrete. It is evident that concrete with a low w/b is dense except for CEM

II/B-V concrete. For the latter, the difference in porosity is marginal with changing w/b. Furthermore, CEM III/A (11.47% for w/b=0.4 and 12.44% for w/b=0.6) and CEM II/B-V (13.81% for w/b-0.4 and 13.91% for w/b=0.6) concretes show higher porosity compared to CEM I concrete (10.0% for w/b=0.4 and 12.3% for w/b=0.6). These trends are more prominent for the low w/b. This may be caused by the large portion of micro-pores due to the fine particles of SCMs. On the other hand, porosities at 10-mm depth for each mix are lower than at other depths regardless of type of binder and w/b. One possible reason is pore densification caused by carbonation, but in this study, carbonation was not observed as shown in figure 5.5. It can be seen that the formation of Fridel's salt by chloride binding or denser C-S-H morphology by Cl^- reduces porosity in this region (Suryavanshi *et al.*, 1995).

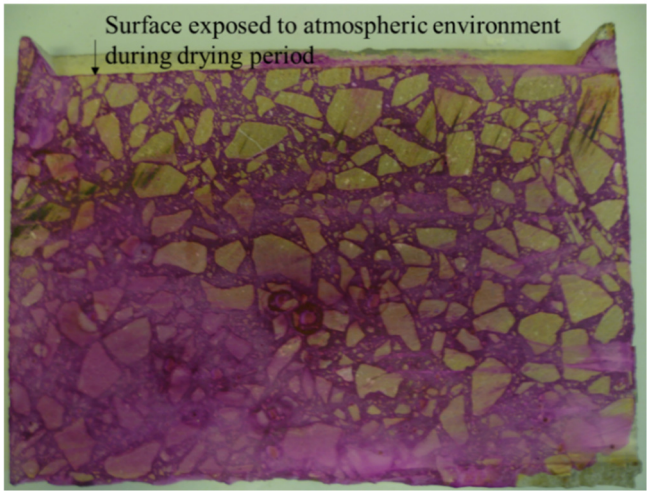

Figure 5.5 Colour change with phenolphthalein indicator (CEM I, w/b=0.4).

Table 5.1 shows that porosity is significantly affected by w/b, and furthermore that SCMs lead to higher porosity for low w/b. This result is in contrast to the results of the chloride profiling/migration test in this study and the previous study on SCMs (Bamforth *et al.*, 1997). The pore network of concrete containing SCMs is more disconnected; thereby the concrete has high resistance to chloride transport. Therefore, it should be noted that porosity itself cannot be fully explained with resistance to chloride transport in concrete. This is because pore tortuosity, connectivity, and pore size also affect ionic transport.

The degree of saturation (S_r) is also an important factor in determining the main transport mechanism. S_r was evaluated (refer to Chapter 4) with depth and is shown in Figure 5.6. S_r values are similar at each depth except for the surface layer (0-20 mm) regardless of the wet/dry process. It is worth noting that S_r decreases with depth, especially for CEM III/A concrete. In addition, concretes with low w/b have a lower S_r.

Table 5.1 Average porosity (%) with depth at 382 and 390 days.

Depth (mm)	w/b=0.4			w/b=0.6		
	CEM I	CEM III/A	CEM II/B-V	CEM I	CEM III/A	CEM II/B-V
10	8.1	10.4	13.2	10.9	11.7	12.4
30	10.3	11.6	13.7	11.8	12.8	13.8
50	10.5	11.9	13.6	12.7	12.4	14.1
70	10.6	11.9	13.6	12.7	11.9	14.3
90	10.5	11.6	15.0	13.5	13.4	15.0
Average	10.0	11.5	13.8	12.3	12.4	13.9

Based on the results, self-desiccation is significantly influenced with w/b and type of binder (Li *et al.*, 2014), especially in CEM III/A concrete, leading to a reduced amount of pore solution. Continuous hydration within disconnected pore network is beneficial to resist chloride transport due to lower moisture content as well as refined pore network. In other words, in the region beneath the convective zone, chloride resistance is controlled by w/b and type of binder, which also determines the degree of saturation.

As shown in figure 5.6, for the convective zone, i.e. the surface ~ 20 mm, it is evident that concrete is virtually saturated (> 90% saturation) after the wetting phase (382 days), while S_r values range from 75 to 93% after 8 days of drying (390 days) under room temperature and relative humidity of 20 ± 2ºC and 50 ± 2% RH. This shows that the drying process is slower than expected. On the other hand, the outermost layer in the CEM II/B-V concrete, especially with a high w/b, is vulnerable to drying compared to other concretes, however, beneath this layer, S_r values for CEM II/B-V concretes are higher than for other concretes. From both results, it can be deduced that higher porosity makes the outmost layer of CEM II/B-V concrete vulnerable to drying, but other influencing factors, e.g. small pore size, tortuosity and the presence of disconnected pores, prevent further drying in CEM II/B-V concrete.

As noted above, the degree of saturation is significant in determining the main mechanism of chloride transport in concrete. Although absorption may occur in concrete as the outer layer is affected by the wet/drying process, in the field, the convective zone is limited (Gao *et al.*, 2017). In this section, convective zones were observed in the surface 0-20 mm for all concretes; however, this zone may be overestimated due to the thickness of the sample. This is discussed in Chapter 7. In addition, at depths > 20 mm, concretes were unsaturated, and S_r values were stable, irrespective of wet/dry process. Thus, a low S_r value could result

in a low diffusion due to a low portion of pore solution. Consequently, chloride transport in concrete structures subjected to a wet/drying cyclic regime, especially in the tidal zone of marine structures, is primarily controlled by diffusion. It is possible that the pure diffusion rate in unsaturated conditions is lower than in the fully saturated condition.

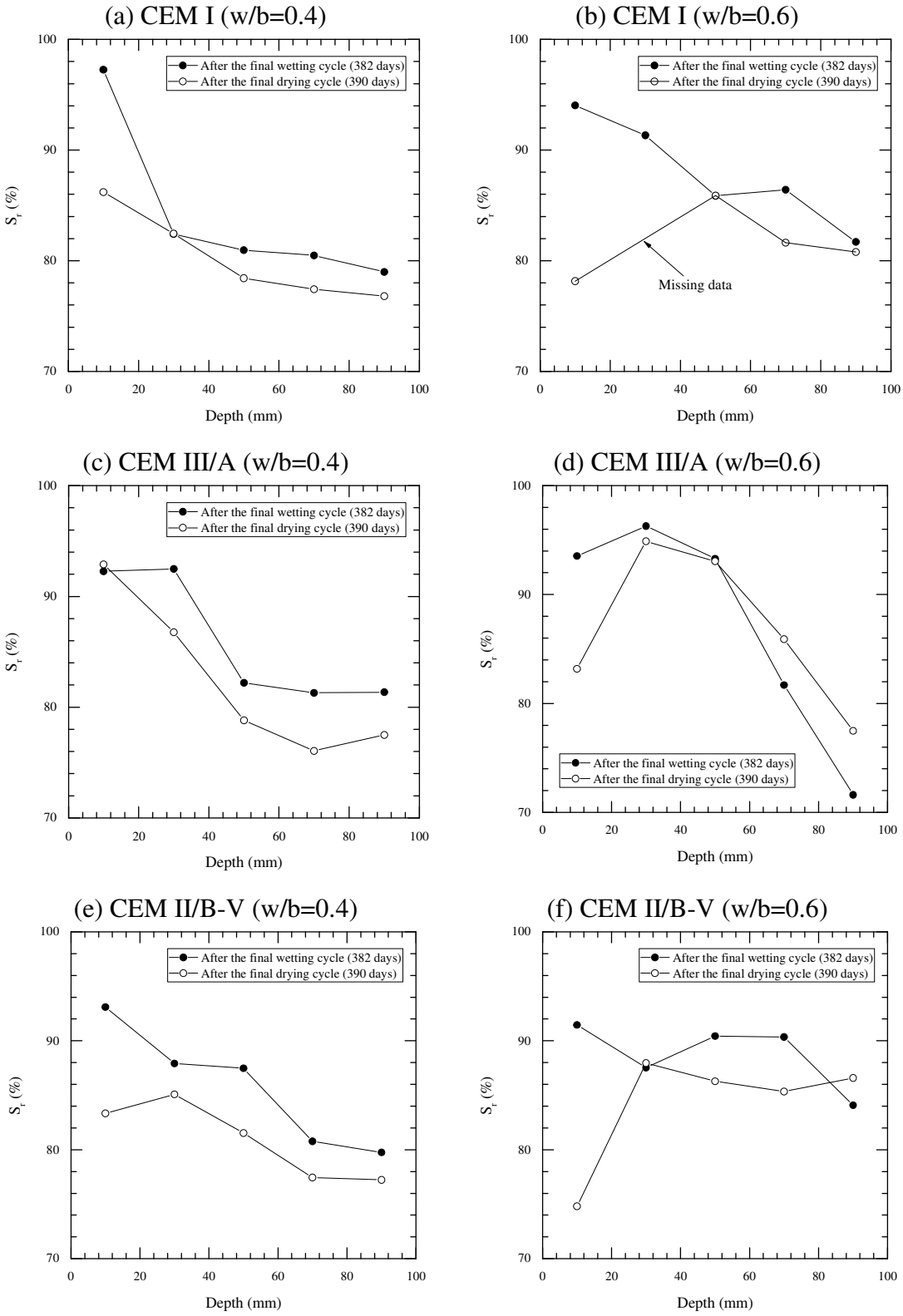

Figure 5.6 Degree of saturation profiles for the concrete mixes.

5.3.3 *Diffusion/Migration coefficient*

As diffusivity in concrete is directly related to performance and durability, empirically determined values are applied to predictive models. Different methods in the literatures are employed to determine diffusion/migration coefficients (Stanish *et al.*, 1997). The diffusion coefficient is obtained from field or laboratory samples by curve fitting with the 'erf' function solution, and the migration coefficient is obtained using the NT Build 492 method, which is widely used in European countries (British Standards Institution, 2014).

The age of the concrete specified in studies for the migration/diffusion coefficient is relatively short. For example, 28 days is used in the LIFE 365 model (Ehlen, 2014) and Duracrete model (Altmann *et al.*, 2012), and 180 days in the ClinConc model (Tang, 2008). For immersion testing, the salt solution is maintained for 90 days in AASHTO T259 (Stanish *et al.*, 1997) and 35-120 days in NT Build 443 (Nordtest, 1995). An aging factor that reflects both hydration and binding effects may be employed to the diffusion coefficient in the evaluation of the long-term durability of concrete, especially for SCMs. Combined effects on the aging factor subsequently lead to higher scatter in the results.

The aging factors also vary across studies. For example, the values from exposure trials and structures have been reported to be 0.3 for CEM I concrete, 0.62 for CEM III/A concrete, and 0.7 for CEM II/B-V concrete (Bamforth *et al.*, 1997), while the values for CEM I and CEM II/B-V concretes have been reported as -0.03 and 1.0, respectively (Andrade *et al.*, 2011). The sensitivity of the aging factor to the diffusion coefficient is shown in figure 5.7, where it can be observed that the diffusion coefficient is significantly affected by the aging factor. When the aging factor is increased from 0.4 to 0.8, the diffusion coefficient at 100-years exposure time decreases 6.3 times. Hence, misinterpretation of the aging factor results in an error in evaluating the service life of concrete structures. To reduce the error, it is desirable to eliminate this factor or to retain a large amount of data to evaluate the factor.

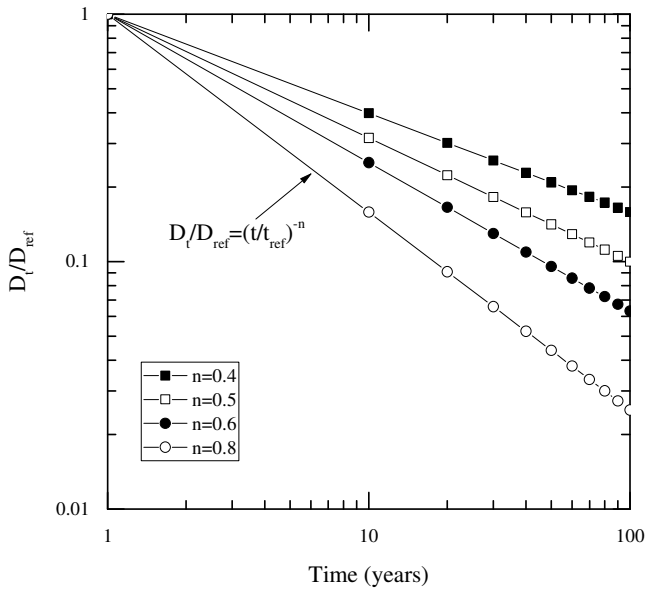

Figure 5.7 Effect of exponent n on the decrease ratio of the diffusion coefficient with time (D_t diffusion coefficient at time, t, and D_{ref} diffusion coefficient at time, t_{ref} [=1 year]).

Diffusion coefficients obtained from field investigations are valuable, as environmental exposure conditions are quantified in addition to concrete properties. However, diffusion coefficients obtained from field data are not always comparable to diffusion coefficients obtained from laboratory testing, as exposure condition influences the diffusion coefficient. In other words, it is necessary to reduce the discrepancy between the field and the laboratory data to improve the accuracy of the predictive model.

To use the diffusion/migration coefficient correctly with a performance-based approach, two limitations must be considered: (i) the hydration effect, and (ii) the difference between the field and the laboratory conditions in the transport rate. To overcome these limitations, it is necessary to determine the migration and diffusion coefficients of both laboratory and field samples through long-term exposure. The migration coefficient is widely used to predict chloride transport in concrete, especially in the Duracrete model, the ClinConc model. In addition, this coefficient is also used to evaluate the resistance to chloride penetration specified in the European codes as the basis of a performance-based approach. In this study, the migration coefficients from NT Build 492 were adopted for the ClinConc model to estimate chloride transport.

The changes in migration coefficient with time are presented in figure 5.8. Mean values are plotted with the error bar representing ± one standard deviation. As expected, the coefficients of concrete containing SCMs are much lower than those of CEM I concrete,

irrespective of w/b and exposure time. In addition, the w/b considerably influences chloride transport. Migration coefficients for concretes with the low w/b (w/b=0.4) are 2–3 times lower than those for concretes with the high w/b (w/b=0.6) irrespective of type of binder. On the other hand, CEM I concrete show 3.1–6.7 times higher migration coefficients at 365 days compared to CEM III/A and CEM II/B-V concretes. It is clear that SCMs are significantly beneficial to the resistance of chloride transport due to the refinement of their pore structures by fineness of cementitious materials and the continuous hydration effect. In general, the migration coefficients for all concretes show a continuous decrease with time. For example, the decrease between 180 and 365 days is 60% for CEM II/B-V concretes with both w/b=0.4 and 0.6; 40-45% for CEM III/A concretes with both w/b=0.4 and 0.6; and 30% for CEM I concrete with w/b=0.4. In contrast, CEM I (w/b=0.6) concrete shows only a 2% reduction during this period. Migration coefficient at 365 days was ranked as CEM II/B-V (w/b=0.4) < CEM III/A (w/b=0.4) < CEM II/B-V (w/b=0.6) < CEM III/A (w/b=0.6) < CEM I (w/b=0.4) < CEM I (w/b=0.6) concrete.

Although the developments of the migration coefficient of concrete using SCMs are advantageous with respect to durability, it is evident that this phenomenon makes the computational model difficult. For example, the ClinConc model uses a migration coefficient at 6 months to estimate chloride profile. The main assumption in this model is that the migration coefficient is stable at that age, and the aging effect, i.e. a reduction in chloride transport, is considered only caused by chloride binding (Tang, 2008). Thereby, when migration coefficients at 6 months are used to estimate chloride profiles for SCM concrete, it is possible that the predicted values are overestimated without consideration of aging factors. Moreover, provided that the aging factor of SCM concrete exposed to a long-term chloride environment (i.e. a field site) is used, the predicted value may be underestimated. This is because the aging factor contains both the binding effect and the hydration effect.

Clearly, the migration coefficient becomes an increasingly important parameter for the predictive model of chloride transport, as well as a performance factor. However, as shown in the result for concretes, and particularly those using SCMs, there are limitations to determining durability with the migration coefficient at an early age, normally 28 days, and in finding the intrinsic diffusion coefficient considering only the hydration effect. Therefore, it is necessary to find the aging factor or long-term data for the migration coefficient to improve the accuracy of the model.

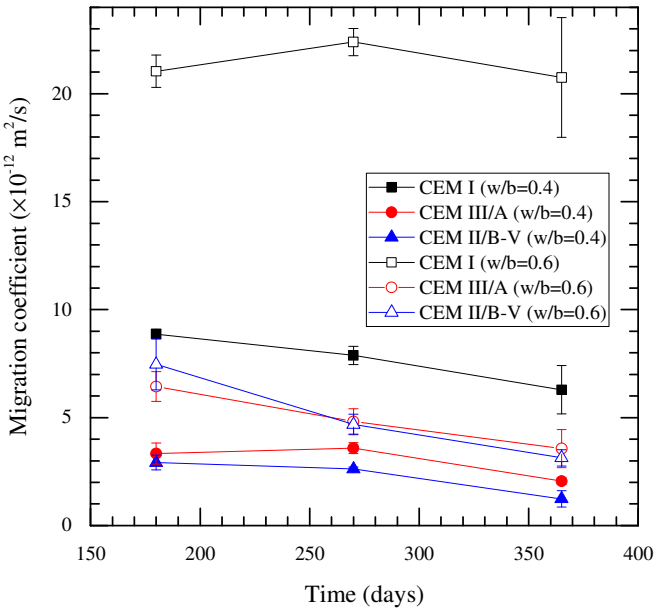

Figure 5.8 Development of migration coefficients with time.

Chloride profiling describes a 'real' chloride distribution in concrete compared to the migration test, but is laborious and time-consuming. Chloride profiling only gives the 'time-averaged' diffusion coefficient, which is not instantaneous; thus, use of the estimated diffusion coefficient is limited in the predictive model. In addition, it is difficult to determine whether the measured diffusion coefficient in the laboratory can be representative of field concrete, as chloride transport behaviour is sensitive to exposure conditions.

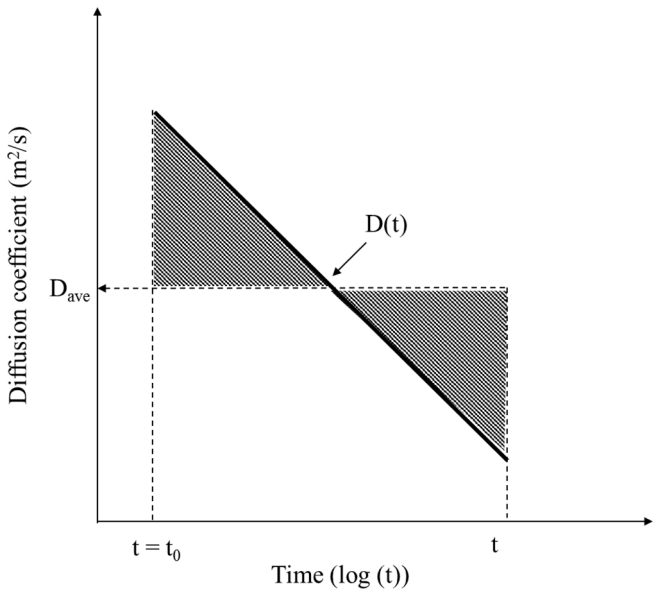

Figure 5.9 Time-averaged diffusion coefficient at time t from chloride profiling.

$$D_{ave} = \frac{1}{t - t_0} \int_{t_0}^{t} D(t)dt \quad (5.12)$$

where D_{ave} is the time-averaged diffusion coefficient obtained from chloride profiling at time t, and t_0 is the time of first exposure to chlorides.

The diffusion coefficients obtained from chloride profiling in the laboratory are useful to upgrade the transport model. The existing models for chloride transport focus on chloride movement in saturated concrete, but concretes in accelerated laboratory testing or the field are generally in an unsaturated condition. Therefore, the new parameters, or the new model, should be developed to reflect these conditions. In this study, chloride profiling was performed with concrete subjected to a wet/dry cyclic regime in the laboratory. Based on the results, environmental factors are evaluated to add to the existing model (the ClinConc). This is described in Chapter 8. The diffusion coefficient and chloride transport resistance of concrete are discussed using chloride profiles in this Chapter.

Figure 5.10 presents the chloride profiles for CEM I, CEM III/A, and CEM II/B-V concretes with different w/b subjected to a wet/dry cyclic regime at 390 days. It can be observed that concretes with a low w/b have a higher resistance to chloride transport. At steel depth, chloride concentrations for concrete at the high w/b (w/b = 0.6) are 3.4% for CEM I concrete, 0.8% for CEM III/A concrete, and 1.04 % for CEM II/B-V concrete, all of which are higher than the 0.3% in BS 8500-1 (British Standards Institution, 2016) and 0.4% in BS EN 206 (British Standards Institution, 2014) as CTL. However, corrosion was only detected for CEM I (w/b = 0.6) concrete. Details of the corrosion behaviour are discussed in Chapter 6. All concretes with w/b = 0.4 have a low chloride concentration (less than 0.4% by weight of binder) at the steel depth, but determination of the CTL is still controversial. In particular, the CTLs for CEM II/B-V concrete show evidently contrasting results to those of Thomas and Matthews (2004), however, in this study, SCMs show a high resistance to corrosion initiation as well as chloride transport. On the other hand, at the point nearest to the exposure surface, an erratic behaviour of CEM II/B-V (w/b = 0.4/0.6) and CEM III/A (w/b = 0.6) concretes was observed, which is attributed to the wet/dry cyclic regime or the wash-out effect (Song *et al.*, 2008a; Nilsson, 2000) in figure 5.10.

At the time of sampling, the specimen was in a dry condition and the behaviour was more apparent in concretes with w/b = 0.6. From the results, it can be deduced that the convective zone is less than 6 mm considering an erratic behaviour is contributed to

absorption. Hence, absorption is another transport mechanism in these concretes in addition to diffusion, but the boundary between diffusion and absorption cannot be quantified in this study.

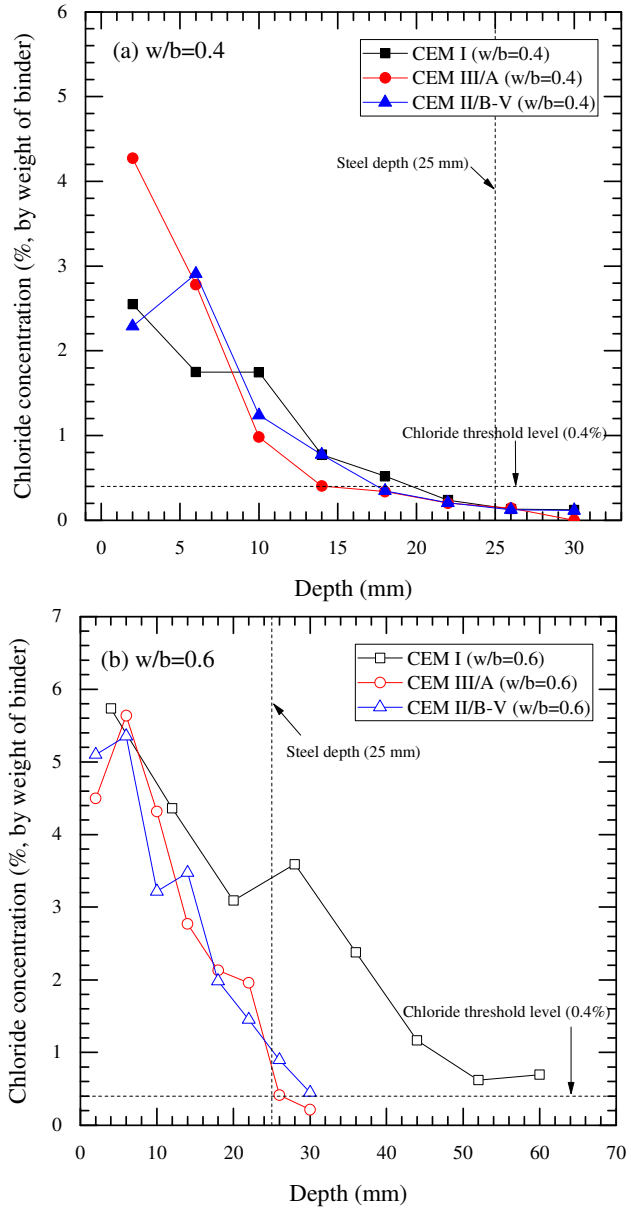

Figure 5.10 Chloride profiles at 390 days.

As the coefficients of determination, denoted r^2 (see Appendix C1.4), for curve fitting excluding the first point were higher than those including the first point, and as the erratic behaviour at the first point led to an error, the diffusion coefficient and surface chloride content were evaluated with chloride profiles excluding the first point. Diffusion is considered as the main transport mechanism. The diffusion coefficient and surface chloride concentration are presented in table 5.2. Surface chloride concentrations for concretes containing SCMs were higher than for CEM I concretes, irrespective of w/b.

This is because an increase in total chloride concentration at the exposure surface is attributed to high chloride binding for SCM concretes or the porous surface region of these concretes (Song *et al.*, 2008a). Meanwhile, diffusion coefficients show an opposite compared to surface chloride concentration, and are in the following order; CEM III/A (w/b=0.4) < CEM II/B-V (w/b=0.4) < CEM I (w/b=0.4) < CEM III/A (w/b=0.6) < CEM II/B-V (w/b=0.6) < CEM I (w/b=0.6) concrete. It is also notable that the largest increase for both the surface chloride concentration and the diffusion coefficient were shown in CEM I concrete with an increase in w/b. It seems that the accumulating chloride concentration at the concrete surface, and the transport rate of chloride in concrete, are affected by exposure conditions, such as a wet/drying cyclic regime as well as chloride binding, as CEM I (w/b=0.6) concrete was vulnerable to resistance to chloride transport in a wet/dry condition due to a rapid drying.

Table 5.2 Surface chloride concentration and diffusion coefficient obtained from chloride profiles at 390 days

Binder	w/b	C_s* (%, by weight of binder)	D_d** ($\times 10^{-12}$ m^2/s)	r^2
CEM I	0.4	2.91	2.81	0.93
	0.6	5.89	22.0	0.94
CEM III/A	0.4	6.74	0.77	0.98
	0.6	8.00	3.75	0.87
CEM II/B-V	0.4	5.60	1.19	0.98
	0.6	7.01	4.36	0.94

*C_s surface chloride concentration, **D_d diffusion coefficient

Figure 5.11 presents the comparison between the migration and diffusion coefficients measured in this study. The migration coefficients at 365 days are similar to the diffusion coefficients at 390 days assuming that a change in diffusion coefficient is marginal within 25 days, while the migration coefficients at 180 days are significantly higher than the diffusion coefficients at 390 days. It was also observed that the migration coefficient is proportional to the diffusion coefficient (Tang, 1996b, 2001). Thus, migration coefficients at 28 days or 6 months are sometimes used as an input parameter in computational models to predict chloride transport. However, caution should be taken to directly replace the diffusion coefficient by the migration coefficient for the chloride transport model, and especially for the 'erf' model. In addition, the concretes used in this study were subjected to a wet/dry cyclic regime, which will cause an increase in transport rate, especially for concretes with a high w/b, due to the drying phase (refer to table 5.2). In summary,

migration coefficients for CEM II/B-V concretes are lower than those for other concretes, but diffusion coefficients for these concretes are marginally higher than those for CEM III/A concretes. This indicates that the slow hydration process by pozzolanic reaction increases chloride transport rate and high chloride binding reduce the rate. Therefore, it is necessary to clearly establish the relation between the hydration process/chloride binding and chloride transport for concrete, and especially SCM concrete.

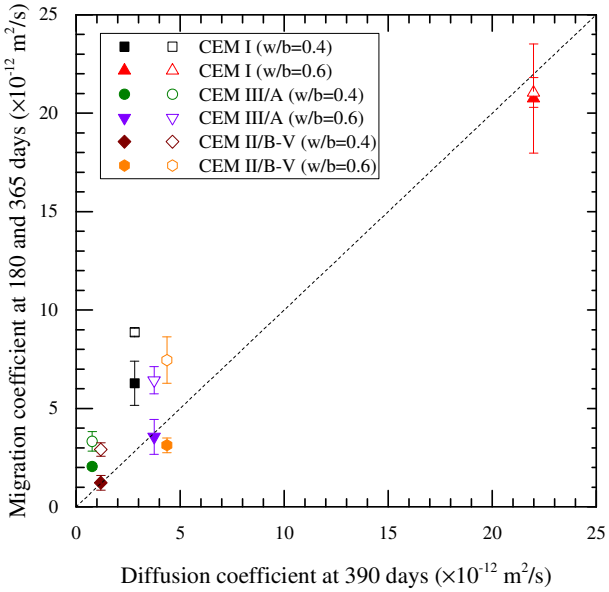

Figure 5.11 Relation between the migration coefficient at 365 (closed markers) and 180 (open markers) days and the diffusion coefficient at 390 days.

5.3.4 *Electrical resistivity of concrete*

The electrical resistivity of concrete, as a non-destructive method, is useful to describe chloride-induced corrosion as it is strongly related to the corrosion rate in concrete as well as chloride transport (Polder, 2001). However, although electrical resistivity is advantageous, interpretation of results can be difficult. The result is affected by several factors including chemical composition of the pore solution, geometrical constrains, concrete inhomogeneity, presence of steel and temperature (Kurumisawa and Nawa, 2016). As in Polder (2001), Newlands *et al.*(2007) and McCarter *et al.* (2015), the resistivity of bulk concrete is generally measured by applying AC current using a frequency response analyser or LCR meter. The frequency with which to determine bulk resistance varies depending on the researcher, ranging from 50 Hz to 1 kHz (McCarter *et al.*, 2015). It has been reported that the measured resistances of the same concrete can differ by up to ~ 3 times, depending on experimental set-up and conditions (Newlands *et*

al., 2007). To minimise the effects on the resistivity of concrete, the measurement should be carried out under the same condition. In addition, for concrete structures subjected to chloride environments, it is specified in most codes that concretes exposed to XS3/XD3 are vulnerable to chloride-induced corrosion due to the high availability of oxygen and the rapid ingress of chloride from the wet/drying cycle. As a consequence, these concretes are likely to be sensitive to the resistivity of concrete as they are unsaturated (Chrisp *et al.*, 2002; Polder and Peelen, 2002). From the literature review, it is evident that the degree of saturation significantly affects the transport rate and transport mechanism.

In this section, electrical resistivity is estimated with time and degree of saturation. The resistivity is closely related to the durability of concrete, especially in the chloride transport. As a result, the measured values are correlated with the performance factors such as the migration coefficient and compressive strength. The relation between degree of saturation and resistivity is also presented. Prior to the compressive strength tests and migration tests, the electrical resistance was measured using the end-to-end resistance method described in figure 5.2, and the resistivity was calculated using equation (5.6).

Figure 5.12 presents the electrical resistivity of the samples (100 mm cube) used in the compressive strength test. The resistivity of CEM I concretes was lower than that of SCM concretes irrespective of w/b except at 28-days. At 28-days, the electrical resistivity of the CEM II/B-V (w/b = 0.4 and 0.6) concretes was 62.9 Ω·m and 65.4 Ω·m, respectively, which are lower than that of the CEM I (w/b = 0.4) concrete (75.8 Ω·m). However, trend was reversed after ~ 37 days. This is due to the densification of the pore structure by pozzolanic reaction in the intervening period, although the resistivity of the pore solution will also influence concrete resistivity. It can be observed that the development of the resistivity of concrete is different depending on type of binder. The resistivity for CEM I concretes was almost stable throughout the duration of the testing period, unlike SCM concretes. The rate of increase in resistivity for the CEM III/A (w/b = 0.6) concrete was reduced after ~ 90 days, whereas the resistivity of CEM II/B-V (w/b = 0.4 and 0.6) and CEM III/A (w/b = 0.4) concretes continuously increased with time. All concretes with w/b = 0.6 had lower resistivity than those concretes with w/b = 0.4 from 28 days and 90 days. An increase rate in resistivity of CEM II/B-V concrete with a low w/b was higher than with a high w/b. According to McCarter *et al.* (2015), in terms of the resistance to corrosion, concrete can be classified as follows: at 365 days CEM III/A and CEM II/B-V concretes have a very high range of corrosion resistance, CEM I (w/b = 0.4) concrete has a high range, and CEM I (w/b = 0.6) concrete has a low/moderate range.

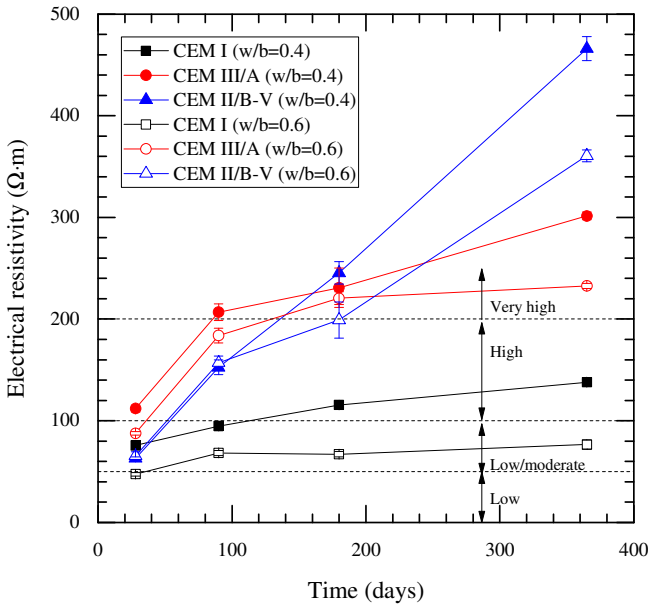

Figure 5.12 Development of electrical resistivity for samples (100 × 100 × 100 mm) used in the compressive strength test.

Figure 5.13 shows the resistivity of concrete (Ø 100 × 50 ± 3 mm) used in the migration tests. Similar trends were observed with those samples used for compressive strength testing. The CEM II/B-V (w/b = 0.4) concretes showed the highest resistivity, followed by CEM III/A (w/b = 0.4) concrete. At 365 days, the resistivity of CEM II/B-V (w/b = 0.6) concrete was still lower than CEM III/A (w/b = 0.4). The vacuum saturating using $Ca(OH)_2$ results in a large drop in the electrical resistivity. The increase in resistivity over the test period was apparent for CEM II/B-V and CEM III/A (w/b = 0.4) concretes, while other concretes showed only a marginal increase.

It is notable that the electrical resistivity of the samples for the migration test is slightly lower than that of samples for the compressive strength test. According to Newlands *et al.* (2007), lower resistivity is attributed to the vacuum saturation process with a saturated calcium hydroxide solution ($Ca(OH)_2$). To confirm the effect of the saturation process on electrical resistivity, the electrical measurements before and after vacuum saturation were carried out for 3 samples (Ø 100 × 50 ± 3 mm) per a mix at 365 days. The results are shown in figure 5.14. The reduction in electrical resistivity was ~ 9.0 – 22.8%, but it was observed that the points diverged from the line of equality with increasing concrete resistivity. The rate was higher than that in Spiesz and Brouwers' (2012) study (6.0 – 14.2%), which used mortar. It is noteworthy that concrete with higher electrical resistivity showed a larger reduction. It is possible that parts of connected micro-pores are partly or totally unsaturated

in the normal condition, especially in concrete with a low w/b, but that a high pressure leads to these pores filling with the solution.

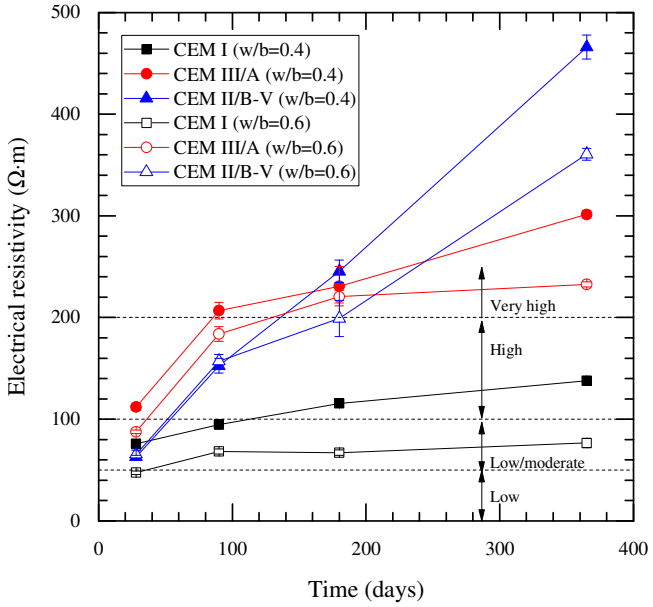

Figure 5.13 Development of electrical resistivity for samples (Ø 100 × 50 ± 3 mm) used in the NT Build 492 test.

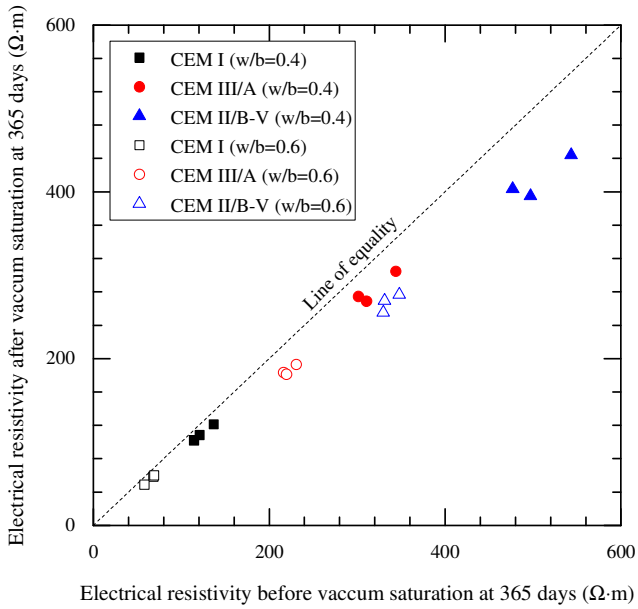

Figure 5.14 Comparison between electrical resistivity of migration test samples before and after vacuum saturation with saturated $Ca(OH)_2$ solution.

Considering that the development of resistivity is related to pore structure, durability, and performance, the concretes can be ranked as follows: CEM II/B-V (w/b=0.4) > CEM III/A (w/b=0.4) > CEM II/B-V (w/b=0.6) > CEM III/A (w/b=0.6) > CEM I (w/b=0.4) >

CEM I (w/b=0.6). This order is in line with the result of migration testing. It can be deduced that electrical property is closely related to migration behaviour in concrete.

In addition to electrical resistivity regarding chloride transport, the relation between moisture content and electrical resistivity was also investigated, as concrete is generally in an unsaturated condition. This section considers the electrical resistivity in terms of concrete (50 × 50 × 20 mm) subjected to a wet/dry cyclic regime, which was also used in the degree of saturation test (Section 5.2.2 and 5.3.2).

The electrical resistivity of concrete versus depth profile is shown in figure 5.15 (as an example), and all profiles are presented in the Appendix C.2. Because sampling time was short, including cutting, and measuring electrical resistance and weighing, and sampling was carried out at 382 and 390 days, the chloride movement and hydration effect on the electrical resistance are negligible. The difference in resistivity between drying and wetting profiles was only evident within 20 mm of cover depth for all concretes. Considering that the convective zone was only a few millimetres, from the results on chloride profiling, the zone obtained from the electrical resistivity was overestimated due to the large sampling size (20 mm thickness). However, the resistivity was observed to be stable at deeper levels, which indicates that the moisture distribution remained unchanged. Hence, it is reasonable to assume that diffusion was the main chloride transport mechanism for the samples used in this study.

To describe the drying effect at the exposure surface, figure 5.16 shows an increased rate of electrical resistivity in the dry phase (at 390 days) compared to the wet phase (at 382 days) at 10 mm cover depth (a nominal cover depth). The electrical resistivity increased during the drying phase, and this trend was especially observed in concretes with a high w/b. The reason for the large increase in electrical resistivity of the concrete is the more (connected) porous concrete. It is notable that the resistivity of the CEM II/B-V concrete increased more than that of the CEM III/A concrete. From the result, it can be deduced that CEM II/B-V concretes at the concrete surface may be more susceptible as they contain more free chloride.

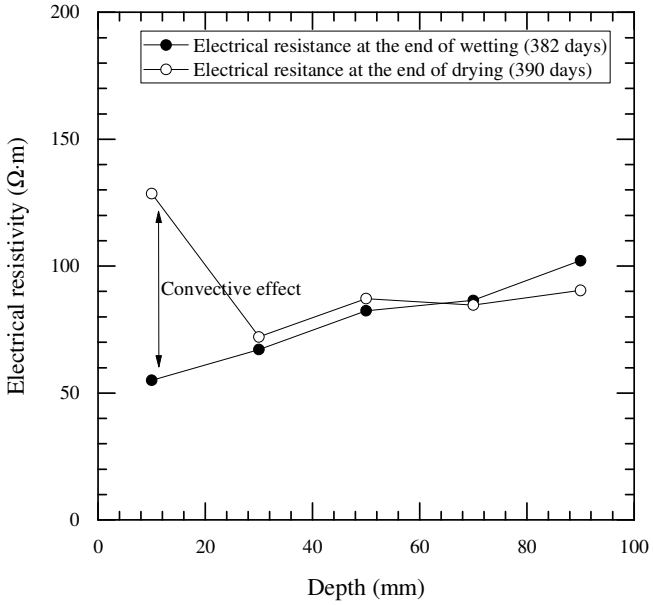

Figure 5.15 Example of resistivity profiles at the end of a wet/dry cycle (CEM I concrete, w/b=0.6).

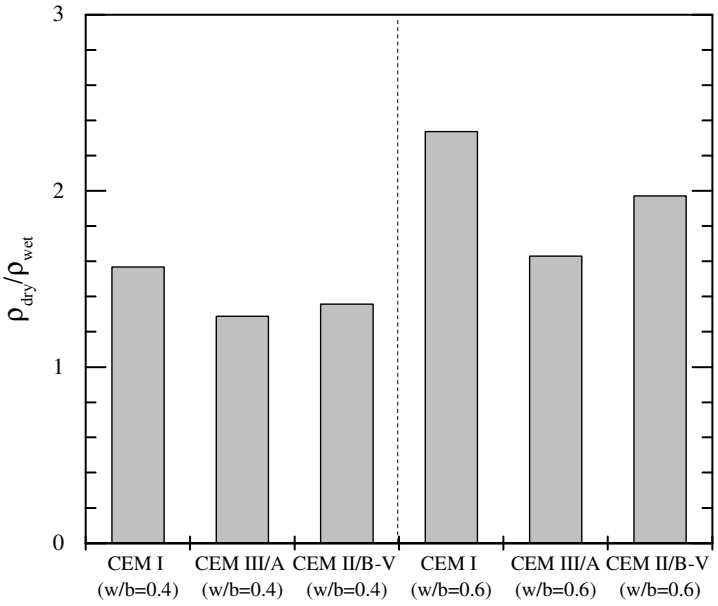

Figure 5.16 An increase ratio of electrical resistivity with a dry phase at 10 mm cover depth (ρ_{dry} electrical resistivity at the end of final drying phase [390 days] and ρ_{wet} electrical resistivity at the end of final wetting phase [382 days]).

5.3.5 *Relation between compressive strength and electrical resistivity*

Compressive strength is still used in practice as a factor to evaluate the durability of concrete structures. To estimate compressive strength, the sample must be crushed in a

compressive machine. As the test is destructive, engineers have increasingly studied electrical resistivity as a non-destructive method to predict strength (Ferreira and Jalali, 2010; Lübeck *et al.*, 2012).

The developments of resistivity and compressive strength with time display a similar trend: an asymptotic curve due to hydration processes. Thus, the relation between compressive strength and resistivity has been observed as a linear correlation. There are two ways of to describe this relation (Ferreira and Jalali, 2010):

(i) an empirical model with a regression method; and,

(ii) a theoretical model describing the hydration process.

In the empirical model, time or w/b is used as a variable, as shown in equations (5.13) and (5.14). The equation used depends on the variables,

$$y = \frac{t}{\mathrm{a}t + \mathrm{b}} \tag{5.13}$$

$$y = \frac{\mathrm{c}}{\mathrm{d}^{w/b}} \tag{5.14}$$

where y is the compressive strength or resistivity; w/b is the water-to-binder ratio; t is time; and a, b, c, and d are constants.

Meanwhile, a theoretical model considers the nucleation and the growth of cementitious materials, and adjusts to the prediction of strength development. The physical meaning for constants reduces the errors in the fitting process, but it is difficult to determine the maximum values,

$$y = y_{max}\left(1 - e^{-at^b}\right) \tag{5.15}$$

where y is the compressive strength or electrical resistivity; a is the growth rate dependent on temperature; b is the dominant morphology of the formation process; and y_{max} is the maximum compressive strength or electrical resistivity when $t \to \infty$.

From the previous studies (Ferreira and Jalali, 2010; Lübeck *et al.*, 2012), these equations were used to predict the relation between the compressive strength and resistivity at 28

days. Each fitting was performed to obtain constants and the models were then verified, but the investigated periods up to 91 days were short for estimating the values of SCM concretes.

The electrical resistivity of concrete (or its reciprocal of conductivity) is influenced by the resistivity of the pore solution as well as the pore network. Other influencing factors include type of binder, degree of hydration, and mix design (Snyder *et al.*, 2003). The development of resistivity can be grouped by type of binder, while the effect of hydration degree on the resistivity of the pore solution is relatively negligible after ~ 28 days (Bu and Weiss, 2014). The compressive strength is related to pore structure and mineral phases instead of pore-fluid chemistry. However, when the relation between compressive strength and electrical resistivity is established, the effect of the pore solution should be eliminated, which can be expressed in the following format (McCarter *et al.*, 2000):

$$N_\rho = \frac{\rho_{conc,t}}{\rho_{pore\_28}} \tag{5.16}$$

where N_ρ is the normalised resistivity; ρ_{conc} is the resistivity of concrete (Ω·m) at time, t; and ρ_{pore_28} is the resistivity of the pore solution at 28 days (Ω·m).

Prior to evaluating the relationship between performance factors and electrical resistivity, electrical resistivity of pore solution depending on binder types was estimate. Figure 5.17 shows pore solution resistivity with time using the NIST model (http://ciks.cbt.nist.gov/ poresolncalc.html) (Snyder *et al.*, 2003; Bentz, 2007). In this model, the degree of hydration and mix proportions are required as input parameters. To estimate the degree of hydration at 28 days, the power's law based on the effective w/b was used (see Appendix A.2) (Tang, 1996a). CEM III/A and CEM II/B-V are assumed to be equivalent to 60% of cement (0.6) and 40% of cement (0.4), respectively, according to BS EN 206 (British Standards Institution, 2014). The chemical composition of binders and mix proportions are described in table 4.1 and table 4.2, respectively. It is evident that the pore solution resistivity is different for each binder type, but a change in the resistivity of the pore solution caused by the hydration process is marginal.

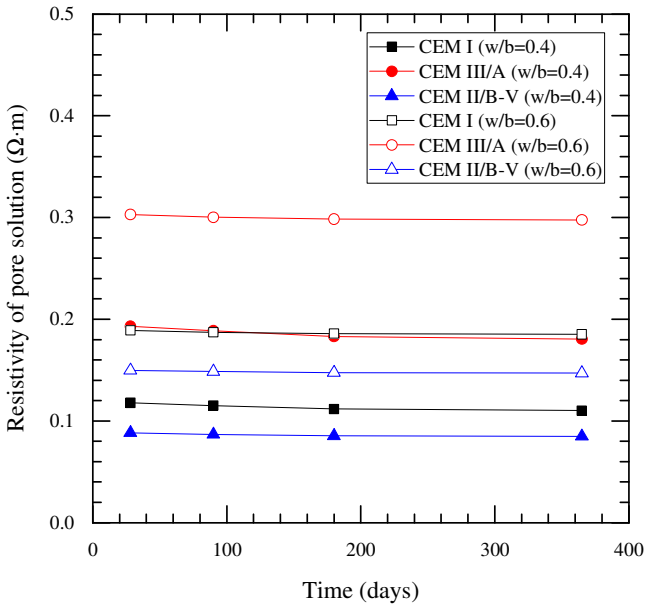

Figure 5.17 Estimated resistivity of pore solution with time and binder types using NIST model.

In this chapter, the main aim is to establish relations between electrical resistivity and performance factors, thus justifying electrical resistivity as a main performance factor. To this end, the relation between electrical resistivity and compressive strength is first described in figure 5.18. The resistivity of pore solution was considered as the resistivity obtained from NIST model (refer to figure 5.17). It can be observed that a linear relationship exists between compressive strength and normalised resistivity with type of binder. However, for CEM III/A and CEM II/B-V concretes, the coefficients of determination (r^2) are low: 0.93 for CEM III/A and 0.73 for CEM II/B-V. The possible reasons for the scatter in the data are that (i) the estimation of the resistivity of the pore solution is less accurate in the process of calculation, (ii) in addition to pore structure, hydration products produced in concrete using SCMs influence compressive strength, and (iii) electrical measurements themselves contain error during the process. Regarding (i), the degree of hydration is estimated based on CEM I concrete although effective factors (k-factor) are introduced. The compressive strength is related to hydration products in addition to pore structure, but the electrical resistance is determined by the connected pore path through the pore network with the pore solution chemistry forming an electrical medium. Electrical measurements cannot directly detect specific hydration products that can help in the development of compressive strength. In this respect, compressive strength is less related to the durability of concrete assuming that aggressive ions for deterioration of concrete, especially chlorides, move through the connected porosity. Although chemical or physical reactions occur between hydration products and aggressive ions, to

the best of the author's knowledge, the relation between the compressive strength and the reactions can be ambiguous. Finally, the tolerance range for electrical measurements is approximately 20%, thereby leading to the scatter in the data (Polder, 2001).

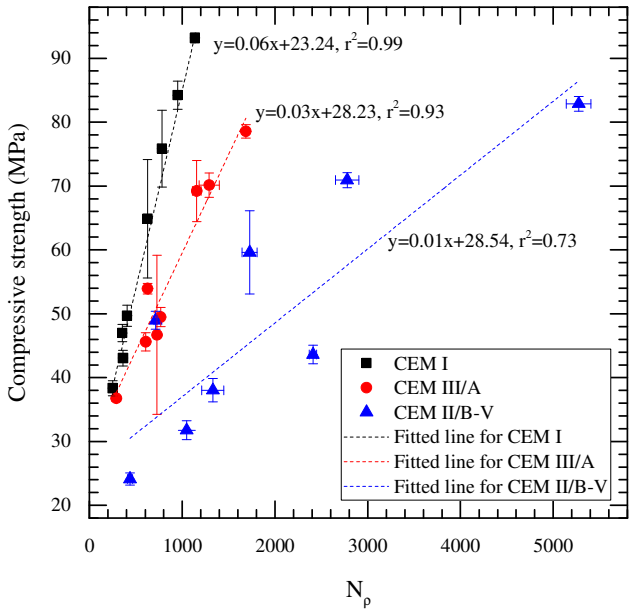

Figure 5.18 The relation between normalised resistivity and compressive strength with binder type.

5.3.6 *Relation between transport properties and electrical resistivity*

To assess the transport properties of concrete, different techniques are used to evaluate a parameter. These techniques can be laborious and destructive. On the other hand, the electrical resistance measurement is practical due to its ease of measurement and its link with pore structures. However, its values tend to be qualitative. To improve the applicability of electrical resistance or resistivity, it is necessary to establish a direct relationship with transport properties. In this section, the relationship between transport properties (e.g. degree of saturation and migration coefficient) and electrical resistivity are established from the experimental results.

For porous materials, Archie's law is employed to express the relationship between electrical resistivity and degree of saturation (Archie, 1942), but the interpretability of the conductivity of fully saturated porous materials using the following equation is debatable.

$$\frac{\rho_{sat}}{\rho_t} = {S_r}^n \tag{5.17}$$

where $\rho_t$is the measured electrical resistivity for the unsaturated condition, ρ_{sat} is the electrical resistivity for the saturated condition, S_r is the saturation degree, and n is Archie's exponent

To improve the discrepancy between the experimental and predicted data, percolation theory is incorporated into the equation. Percolation theory focuses on geometrical or physical properties of materials. For cementitious materials, percolation through capillary pores has been reported by McCarter and Garvin (1989). Based on the percolation theory, the model is extended to describe the electrical conductivity, σ (the reciprocal of resistivity), of a composite material composed of different phases (Li *et al.*, 2016),

$$S_r\left[\frac{\sigma_0^{1/m}-\sigma_t^{1/m}}{\sigma_0^{1/m}+\left(\frac{1-S_c}{S_c}\right)\sigma_t^{1/m}}\right]+(1-S_r)\left[\frac{\sigma_a^{\frac{1}{m}}-\sigma_t^{\frac{1}{m}}}{\sigma_a^{\frac{1}{m}}+\left(\frac{1-S_c}{S_c}\right)\sigma_t^{\frac{1}{m}}}\right]=0 \qquad (5.18)$$

where S_c is the threshold or critical saturation degree for pore solution percolation in the microstructure of the material, and σ_a is the conductivity of the air phase.

As $\sigma_a \approx 0$, the equation above can be simplified as follows:

$$\frac{\rho_0}{\rho_t}=\frac{\sigma_t}{\sigma_0}=\left(\frac{S_r-S_c}{1-S_c}\right)^m \qquad (5.19)$$

In the equation above, the degree of saturation, S_r, in Archie's law is replaced by the degree of the saturation based on the percolation theory. Although the modified Archie law explains the relation between electrical resistivity and degree of saturation for porous material, it is difficult to define the critical saturation degree, i.e. S_c. As the range for S_r is narrow in this study, Archie's law (equation (5.17)) is used to establish the relation. Figure 5.19 presents the relative electrical resistivity with S_r. The outliners indicated by 'open' markers on the figure have been removed from the fitting. In addition, the values for the fully saturated condition are fixed to improve the fitting result.

As shown in figure 5.19, the ratio of resistivity between the saturated condition and measured (unsaturated) condition generally decreases with degree of saturation. It can be observed that Archie's exponents depend on w/b and type of binder. The estimated exponents are presented in table 5.3. For w/b = 0.4, the exponents for CEM I, CEM III/A and CEM II/B-V concretes are 1.61, 2.16, and 5.16, respectively, while for CEM III/A

and CEM II/B-V concretes with w/b=0.6 they are 3.48 and 6.91. The exponents imply that CEM II/B-V concrete is the most sensitive to a change in resistivity with moisture content, while resistivity change for CEM I concrete is insensitive to degree of saturation. However, to explain the relationship, the number of samples per mix is too small and the measured range is narrow. Moreover, w/b is also an important factor to determine the electrical resistivity. Concrete with a high w/b is sensitive to a change in the electrical resistivity as moisture can be retained/lost due to more porous materials. For CEM I (w/b=0.6) concrete, the relation is not displayed as it was irregular due to the chloride contamination of the concrete. This erratic behaviour, which is displayed as 'open' markers in both figures, were also observed in other concretes. The markers correspond to surface layers (0-20 mm cover depth) in the samples. This may be because the presence in the sample of crystallised chlorides, which are not bound chlorides, further reduced the resistivity of the sample during the saturation process.

Table 5.3 Archie's exponent with binder

Binder	w/b	Archie's exponent
CEM I	0.4	1.61
	0.6	+
CEM III/A	0.4	2.16
	0.6	3.48
CEM II/B-V	0.4	5.61
	0.6	6.91

* + not determined

The most important parameter for chloride transport is the chloride transport rate, i.e. the diffusion coefficient or sorptivity. However, its measurement is considerably time-consuming and destructive, although accelerated methods have been developed. Among the accelerated methods, NT Build 492 is widely used to determine an input value in predictive models or to evaluate the durability of samples as a performance factor. As shown in figure 5.20, Tang (1996a) expected that after the NT Build 492 test, the chloride penetration front within the sample would be sharp, called a *'tsunami shape'*. The measured chloride profiles, however, were non-linear curves (S-shaped curves) (Andrade *et al.*, 1999; Spiesz and Brouwers, 2013). Tang (1996a) hypothesized that the possible reasons for these S-shaped curves are pore distribution and the movement of other ions. In other words, although the chloride profile obtained from NT Build 492 is not

completely in line with that based on the background theory, NT Build 492 is still attractive as the migration coefficient can be readily calculated from this method. Meanwhile, it is increasingly attractive to use non-invasive methods. Among these methods, the electrical resistance method is the most relevant because ionic ingress through concrete coincides with the electrical conduction path, but it is difficult to obtain the migration coefficient with the electrical resistivity directly.

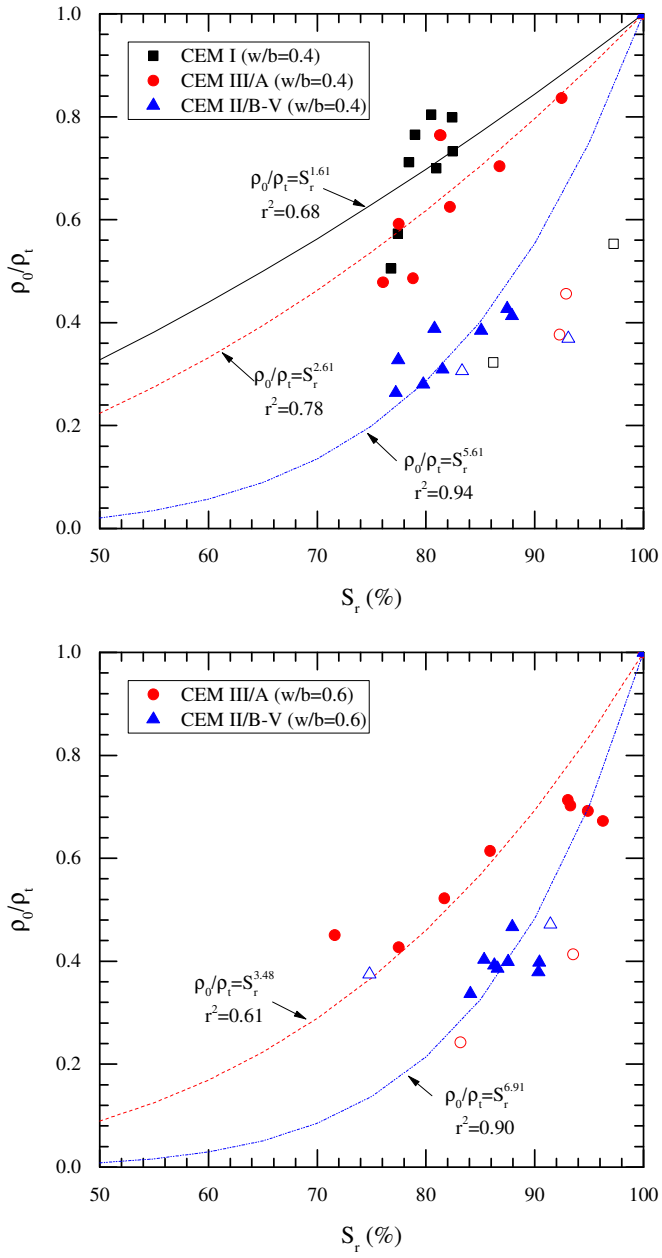

Figure 5.19 Relation between saturation degree and resistivity with binder type (a) w/b=0.4 and (b) w/b=0.6 (outliners [open markers] are removed from fitting equations).

Studies have been conducted to determine the relationship between the electrical resistivity and transport rate (Sengul, 2014; Lim *et al.*, 2016; Van Noort *et al.*, 2016), but so far, the relations have been obtained empirically. This means that a number of

experiments have to be carried out to establish the relation and constants in empirical equations have no physical meanings. Therefore, in the present study, the relationship between the migration coefficient and the electrical resistivity is investigated using a simplified Nernst-Planck equation.

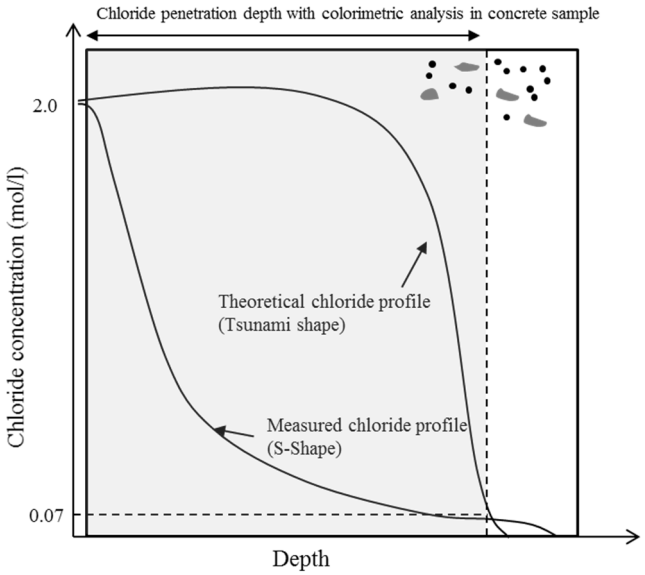

Figure 5.20 Schematic diagram for chloride distribution in samples after migration test (Tang, 1996a).

The diffusion flux of ions in a porous material is expressed by the Nernst-Planck equation (Kurumisawa and Nawa, 2016):

$$J_i = D_{eff}\frac{\partial C_i}{\partial x} + \frac{z_i F}{RT} D_{eff} C_i \frac{\partial E}{\partial x} \tag{5.20}$$

where J_i is the flux of an ion species, D_{eff} is the effective diffusion coefficient, C_i is the concentration of an ion species, z_i is the valence number of an ion species, R is the gas constant, F is Faraday's constant, E is the electrical field and x is the position of the medium.

Provided that no concentration gradient within a porous medium and an external potential is large enough, the above equation can be simplified as follows:

$$J_i = \frac{z_i F}{RT} D_{eff} C_i \frac{\partial \varphi}{\partial x} \tag{5.21}$$

Flux is converted into the current density, and then substituting the current density with the electrical resistivity gives the following relation:

$$\frac{1}{\rho} = D_{eff}\frac{z_i^2 F^2 C_i}{RT} = D_{eff} \cdot \mathrm{a} \cdot C_i \qquad (5.22)$$

where ρ is the bulk electrical resistivity and 'a' is a constant ($=\frac{z_i^2 F^2}{RT}$).

Based on equation (5.22), it is apparent that the migration coefficient is correlated with electrical resistivity. Moreover, previous studies (Sengul and Gjørv, 2009; Van Noort *et al.*, 2016) have reported that the electrical resistivity is correlated to the migration coefficient. Namely, high electrical resistivity of concrete indicates high resistance to chloride transport. To improve the applicability of the electrical resistivity of concrete to determine the transport rate, the physical parameter, C_i, in equation (5.22) must be evaluated.

The relationship between the electrical resistivity and migration coefficient is established based on the above equations, as described in Figure 5.21. Note that the resistivity (equation (5.22)) was estimated with the samples (Ø 100 × 50 ± 3 mm) used in the migration test after $Ca(OH)_2$ saturation. The outliner indicated by an 'open' marker on this figure has been omitted from the fitting. Based on equation (5.22), the constant (C_i) obtained in this study indicates the chloride concentration in a porous medium; is 0.356 mol/l of chloride was uniformly distributed in the sample. In a study by Streicher and Alexander (1995), a concrete sample was pre-saturated with 5 mol/l of chloride solution to apply equation (5.22), which is valid in steady-state processes. The migration coefficient obtained from NT Build 492, on the other hand, is determined in non-steady state conditions, so the assumptions shown in figure 5.22 are required to calculate the migration coefficient using equation (5.22), as follows: (i) the average chloride concentration in the sample applied to NT Build 492 over the chloride contaminated depth is equal to 0.356 mol/l (see figure 5.21), therefore the migration coefficient measured in NT Build 492 is equal to the migration coefficient obtained from a sample saturated with 0.356 mol/l of chloride, and (ii) the chloride binding is ignored. However, this study was only carried out for the migration test and the electrical resistance measurement. To verify the suggestion regarding the relationship between migration coefficient and electrical resistivity (equation (5.22), it would be

necessary to conduct experiments for chloride profiling of the sample (Ø 100 × 50 ± 3 mm) directly after the migration test, and then to calculate the average value for chloride concentration within the chloride contaminated area.

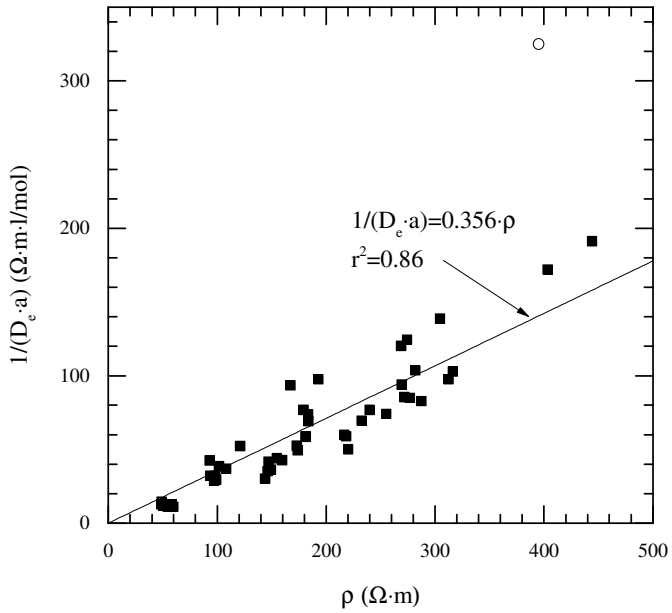

Figure 5.21 Relation between the migration coefficient and bulk electrical resistivity irrespective of binder types and w/b.

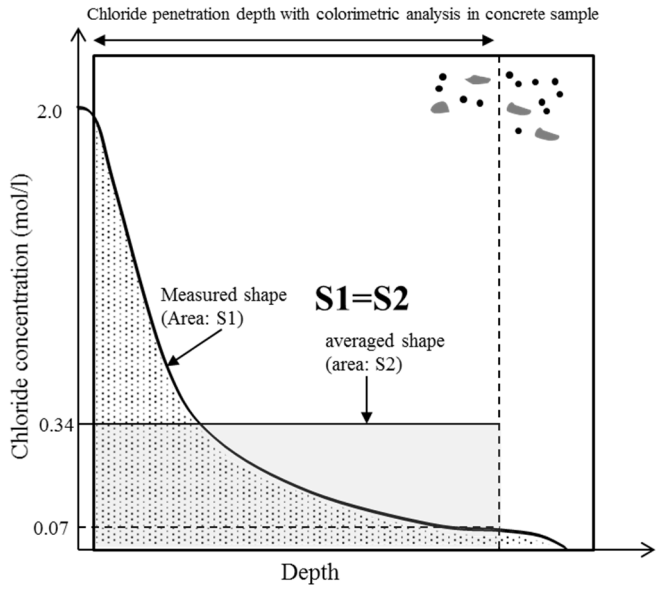

Figure 5.22 Schematic diagram for assumption of chloride distribution in terms of the suggested parameter (C_i) after the migration test in this study.

5.4 Summary

This section investigated performance factors (compressive strength, transport rate, degree of saturation, and porosity) regarding chloride transport, and then correlated them with the electrical resistivity. The general findings are summarised below.

- The performance factors investigated in this study are ranked in table 5.4 except for degree of saturation. It was confirmed that w/b and type of binder are crucial to improve the durability/performance of concrete. Compressive strength and porosity are more influenced by w/b, while diffusion/migration coefficients and resistivity are influenced by type of binder.

- Diffusion/migration coefficients are less related to compressive strength and porosity. Therefore, care is required to explain transport property with only compressive strength or porosity. The ranking order of the migration coefficients is similar to that of the resistivity, as the pore network is determinant for the parameters.

Table 5.4 Ranking order with performance factors

w/b	Binder	Durability indicators				
		$f_{c,365}$	$Ø$	D_d	D_m	ρ
0.4	CEM I	1	1	3	5	5
	CEM III/A	3	2	1	2	4
	CEM II/B-V	2	5	2	1	1
0.6	CEM I	4	3	6	6	6
	CEM III/A	5	4	4	4	3
	CEM II/B-V	6	6	5	3	2

$f_{c,365}$ = compressive strength at 365 days, D_d=diffusion coefficient at 390 days, D_m=migration coefficient at 365 days, $Ø$=porosity at 390 days, and ρ=resistivity at 365 days; rank order: 1 → 6 (good → bad)

- All samples subjected to a wet/dry cyclic regime were in an unsaturated condition even though the degrees of saturation of the sample were measured after the wetting phase. Except for the surface layer, the degrees of saturation were stable across depths, but the degree of saturation varied with type of

binder. It was observed that the surface layer in CEM II/B-V concrete was the most sensitive to the drying effect.

- The transport rate decreased with time irrespective of type of binder. The diffusion coefficients were linearly related to the migration coefficient. However, caution must be taken to ensure that the latter is directly used in the transport model using the 'erf' function.

- The electrical resistivity was closely related to performance factors. The compressive strength first had a linear relation with the electrical resistivity, but it was necessary to reduce the scatters in the results by estimating the degree of hydration and the resistivity of the pore solution. On the other hand, the relationship between the migration coefficient and the electrical resistivity was established from the fitting, and the constant (0.356 mol/l) was suggested. The constant is useful for calculating the migration coefficient with electrical resistivity, but additional investigation is required to verify the constant.

- According to the result for the diffusion coefficient, CEM III/A concretes have higher resistance to chloride transport than CEM II/B-V concretes. Therefore, it can be deduced that CEM II/B-V concrete is beneficial to prevent chloride transport based on the result of migration coefficient, but CEM III/A concrete is more efficient to improve the chloride resistance of concrete as a replacement as the hydration process in CEM III/A concrete is relatively helpful in forming a dense pore structure earlier than in CEM II/B-V concrete.

CHAPTER 6
CHLORIDE-INDUCED CORROSION OF STEEL WITH PERFORMANCE OF CONCRETE

6.1 Introduction

The corrosion of steel in reinforced concrete, from the initiation to the propagation phase, has been extensively investigated and a number of models regarding the corrosion propagation have also been developed (see Section 3.5.2). Most models require electrochemical parameters to estimate the development of corrosion, and these are generally determined from laboratory tests in which variables such as environmental conditions and material properties are well-controlled. To achieve corrosion within a short time period, accelerated methods are employed, such as wet/dry cyclic regimes (Polder and Peelen, 2002; Vedalakshmi *et al.*, 2009b; Angst *et al.*, 2011b; Pereira *et al.*, 2015), application of current to the steel (Austin *et al.*, 2004) and pre-mixed chloride in the concrete (Elsener, 2002; Videm, 2007; Nygaard *et al.*, 2009; Martinez *et al.*, 2015). However, corrosion parameters obtained from controlled or accelerated conditions could be inappropriate in estimating the corrosion behaviour of field structures. For example, the B value, i.e. the Stern-Geary constant, is, essentially, required to determine the corrosion rate of steel in an electrochemical measurement. This can be estimated with Tafel's constants (equation (3.4)) or an empirical value, corresponding to 26 mV for the active state and 52 mV for passive state of steel. However, the value can vary depending on the concrete or steel condition, which is affected by environmental conditions from literatures. In this regard, it has been reported that Tafel's constants are distributed within a wide range. Therefore, determining the B value without considering concrete or environmental conditions leads to misinterpretation of data or an unreliable prediction of the residual life of the concrete structure.

In this section, a range of electrochemical techniques are applied to laboratory samples to estimate corrosion rate and determine whether corrosion occurred. Furthermore, the B values for the laboratory samples are estimated and compared using the Tafel extrapolation technique and a simple monitoring technique using the potentiostatic method. Based on the results, the chapter then discusses the methodology and quantification for corrosion products.

6.2 Experimental

The samples used in this study are described in Chapter 4. The following corrosion measurements were carried out: the half-cell potential, macrocell current, linear polarisation, Tafel extrapolation, potentiostatic, galvanostatic pulse and electrochemical impedance spectroscopy. To secure depolarisation time, the time-gap between measurements was more than 10 minutes for recovering the corrosion potential. The experimental set-up for each measurement is described below.

Comprehensive corrosion tests were conducted for two steels with different exposure areas per sample, as mentioned in Section 4.3. Detailed schedules are presented for each test (table 4.3) with monitoring data up to 382 days. In the case of those samples in which corrosion was detected on the steel, the steel was retrieved from the concrete after 382 days. Visual observation and mass loss tests were then undertaken. All measurements were performed for each mix in one day.

6.2.1 *Half-cell potential*

For the half-cell potential measurement, a copper-copper sulphate electrode (CSE) (model 8-A manufactured by Farwest corrosion control) was used as a reference electrode. The measurement for two steel bars at 25 mm cover depth was carried out at the end of both wetting and drying phases, from 42 days up to 382 days. At the end of the dry phase, a synthetic sponge saturated with 19.8 g/l NaCl solution was placed on the surface of the sample for 10 minutes before the measurement to obtain electrical connectivity between the working electrodes and the reference electrode. The potential reading between two electrodes was performed with a high impedance multi-meter (1705 True RMS programmable multi-meter) (see figure 6.1).

6.2.2 *Macrocell current*

The current flowing between the steel bar at 25 mm and 100 mm cover depth was monitored at the end of every wetting and drying phase by measuring the potential drop across a resistor (R=10 kΩ) using a high impedance multi-meter as shown in figure 6.2. To avoid the sudden drop in the potential, the measurements were carried out 5 minutes after connection with the resistor. For electrically connected steels with a large exposure

area, more than 10 minutes were given to depolarise. To calculate the macrocell current density, the unmasked area of steel embedded in concrete is considered as the exposure steel area. The following equation based on Ohms's law is used:

$$i_{macro} = \frac{\Delta E}{R \times A_{exp}} \tag{6.1}$$

where i_{macro} is the macrocell current density (mA/cm^2), ΔE is the potential drop between two steels (V), R is the resistor (=10 kΩ), and A is the exposure area of steel (cm^2).

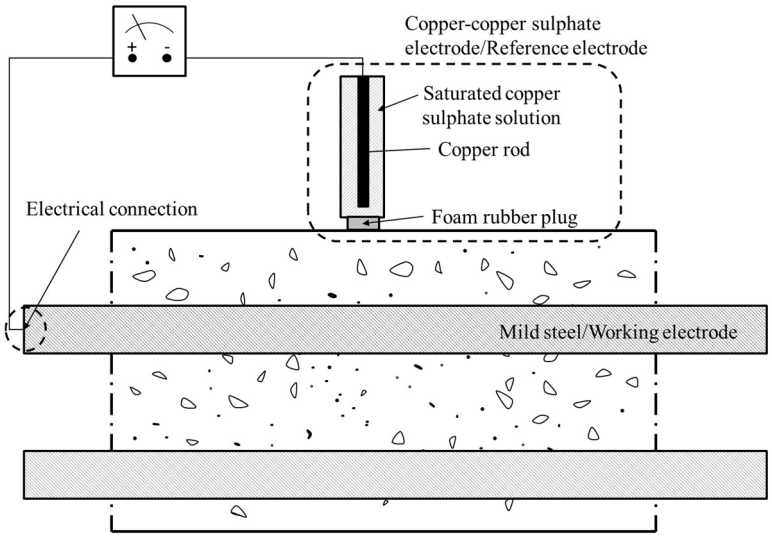

Figure 6.1 Half-cell potential technique.

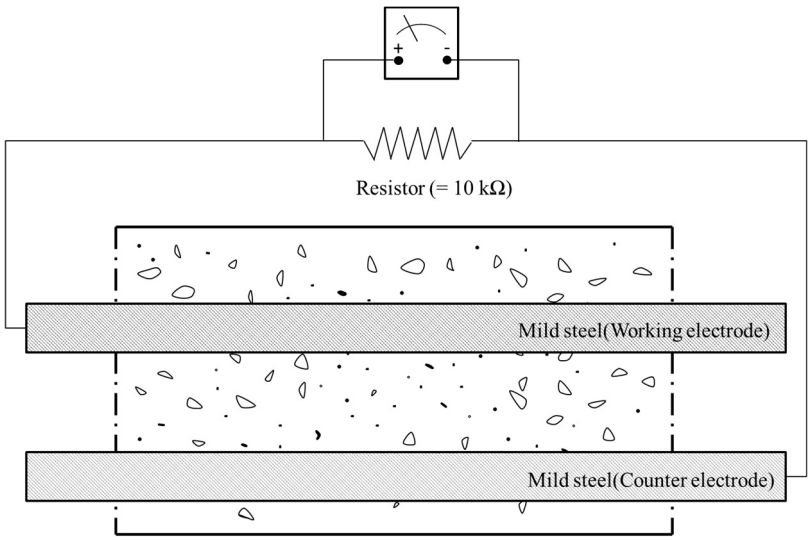

Figure 6.2 Macrocell current technique.

6.2.3 *DC polarisation techniques*

DC polarisation techniques are widely used to estimate a corrosion rate for concrete structures as shown in figure 6.3. A three-electrode configuration is traditionally employed, comprising a reference electrode, a working electrode and a counter electrode. In this study, the reference electrode was a CSE and the steels at 25 and 100 mm of cover depth were used as the working electrode and the counter electrode, respectively. The measurements were carried out in both galvanostat and potentiostat modes using a Solartron 1287 Electrochemical Interface. CorrWare ® software was used to control all techniques in sequence, and the measured data were automatically recorded. The linear polarisation technique, galvanostatic pulse technique, potentiostatic technique, and Tafel extrapolation technique were employed. Before using the polarisation techniques, the corrosion potential, i.e. open-circuit potential (OCP), was determined when the potential changed by less than 10 mV/s. The DC polarisation techniques were used to evaluate the B value and the polarisation resistance, R_p.

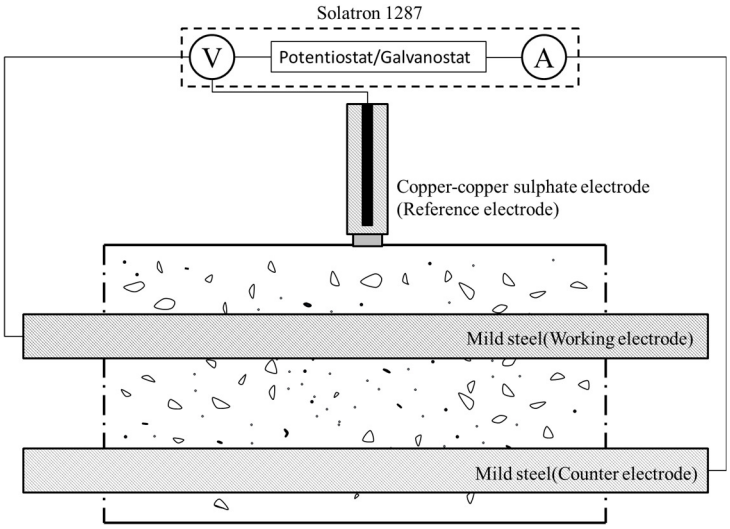

Figure 6.3 DC polarisation technique.

Two types of potentiodynamic polarisation techniques were used in this study. The first test applied small potential perturbations (± 10 mV at the corrosion potential) to the working electrode, referred to as the linear polarisation resistance technique (LPR). The scan rate was 0.1 mV/s and the ohmic resistance to estimate the corrosion rate was considered with the value obtained from the galvanostatic pulse technique (GP). The polarisation resistance from the measured data was calculated in Matlab using a manual

coding program. To avoid an initial surge charge effect, i.e. a sudden increase in the current once the potential is perturbed (Kouřil *et al.*, 2006; Chang *et al.*, 2008b), only data corresponding to ± 5 mV at the corrosion potential were analysed, as shown in Figure 6.4. The initial surface charge occurred due to the capacitive property of steel; thereby, the potential was shifted slightly to the cathodic direction when the current was 0. However, during the LPR measurement, the potential at the current (= 0 μA) was theoretically equal to the corrosion potential (Chang *et al.*, 2008b). Nevertheless, the effect is not considered in this study because the shift was small.

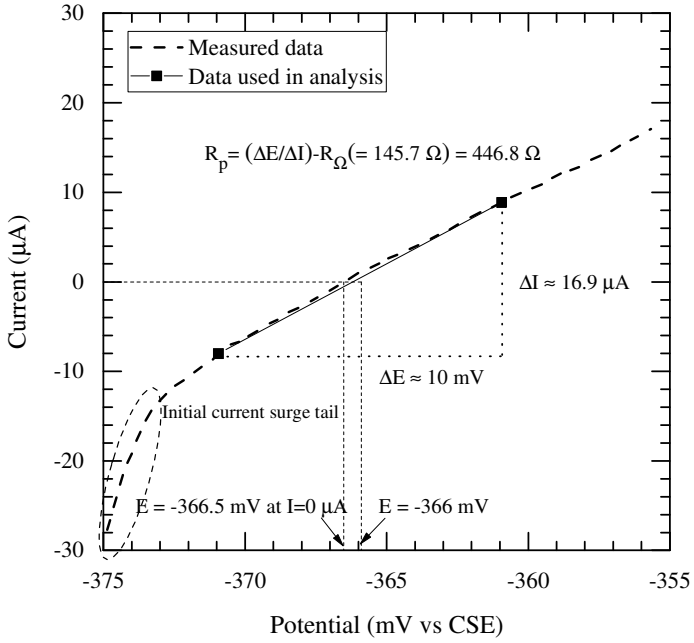

Figure 6.4 Calculating the polarisation resistance from the linear polarisation curve.

The Tafel extrapolation technique (TEP) was also used to obtain the B value to calculate the corrosion rate. This technique uses a large potential perturbation (- 200 mV to + 1,000 mV at corrosion potential), which may lead to a destruction of the interface between concrete and steel. To minimise damage at the interface between steel and concrete, a one-off measurement was carried out at the end of the entire measurement and reverse scanning was also employed. The sweep range was set from - 300 mV to + 600 mV at the corrosion potential, and a low scan rate was used (10 mV/min) (RILEM TC 154-EMC 2004). As shown in figure 6.5, a curve fitting using a commercial program (CView Version 3.5a.) was carried out for data corresponding to ± 200 mV at the corrosion potential. The Tafel constants obtained from the fitting were used to calculate a *B* value using equation (3.4).

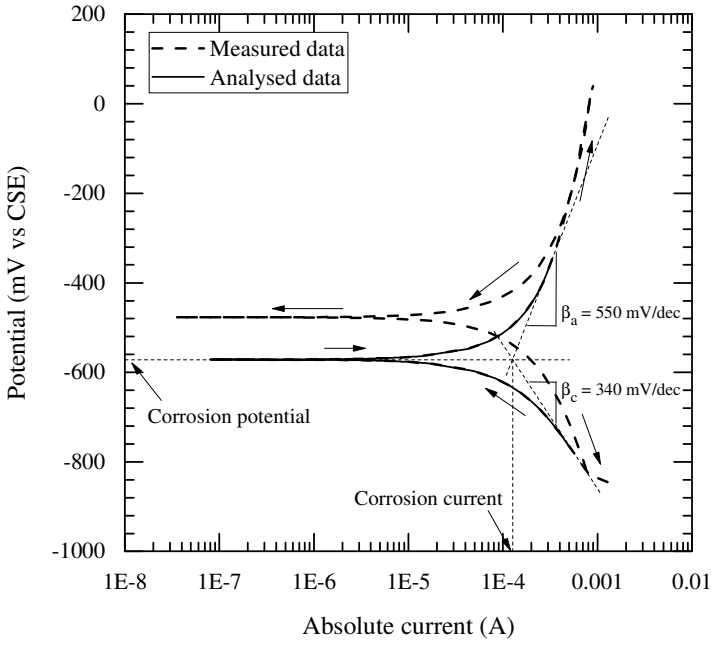

Figure 6.5 Evaluation of the Tafel slope in a potentiodynamic polarisation test including reverse scan.

For the galvanostatic pulse technique (GP), a constant current was applied to the working electrode and the change in potential with the applied current was measured. The applied current was fixed at 25 μA irrespective of the steel condition, unlike in previous studies (Birbilis *et al.*, 2004; González *et al.*, 2004; Elsener, 2005), and the duration was 10s. From the result, polarisation resistance and ohmic resistance were estimated using a modified Randle circuit with equation (6.2) as shown in Figure 6.6. For the fitting purpose, an exponential analysis to calculate the polarisation/ohmic resistances was carried out using Matlab software.

$$\mathrm{E}_t(t) = I_{in}R_\Omega + I_{in}R_p\left[1 - \mathrm{e}^{-\left(\frac{t}{\tau}\right)^n}\right] \tag{6.2}$$

where $\mathrm{E}_t(t)$ is the potential of steel with measuring time t; I_{in} is the applied current; R_p is the polarisation resistance; R_Ω is the ohmic resistance; τ is the time constant (=R_pC_{dl}); n is the non-ideality exponent (0<n ≤1); and C_{dl} is the double layer capacitance.

Finally, the potentiostatic technique (PT) was used to calculate the B value as well as the polarisation resistance (Poursaee, 2010). The constant voltage, i.e. 10 mV at corrosion potential, was applied to the anodic direction for 100s. To minimise 'destruction' of the

corrosion environment, the applied potential was deliberately injected at the corrosion potential for 100s.

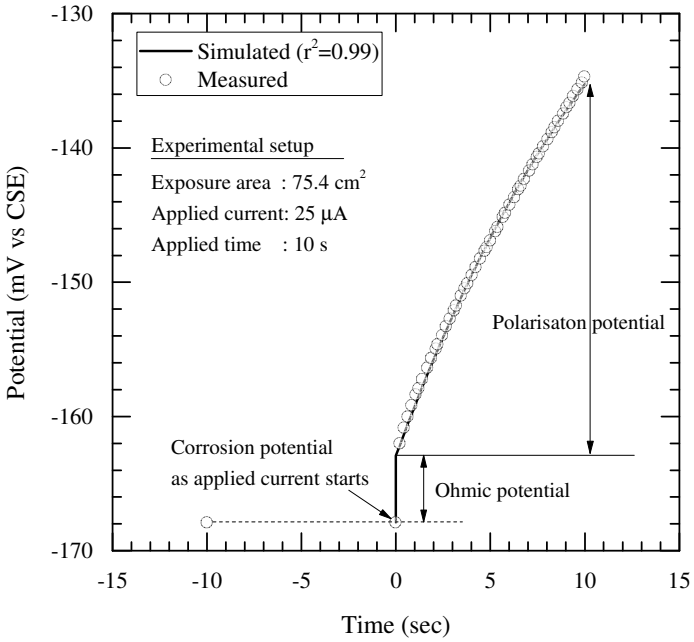

Figure 6.6 Calculating the polarisation resistance using the GP.

Analysis of the polarisation resistance was conducted with data on anodic potential pulse. In this analysis, the following equation for ohmic resistance and corrected polarisation resistance was used; it is also based on a modified Randle circuit (Feliu *et al.*, 1986).

$$I_t(t) = \frac{E_{in}}{R_\Omega(R_\Omega + R_p)}\left[R_\Omega + R_p e^{\left(\frac{-t}{\frac{C_{dl}R_pR_\Omega}{R_\Omega+R_p}}\right)}\right] \tag{6.3}$$

where $I_t(t)$ is the current of steel with measuring time t, E_{in} is the applied potential, R_p is the polarisation resistance, R_Ω is the ohmic resistance and C_{dl} is the double layer capacitance.

In addition to the fitting process as shown in figure 6.7, the total charge in the polarisation process was calculated using the integration with respect to the total applied time. The details on the calculation of the B value are described in Section 6.3.4.

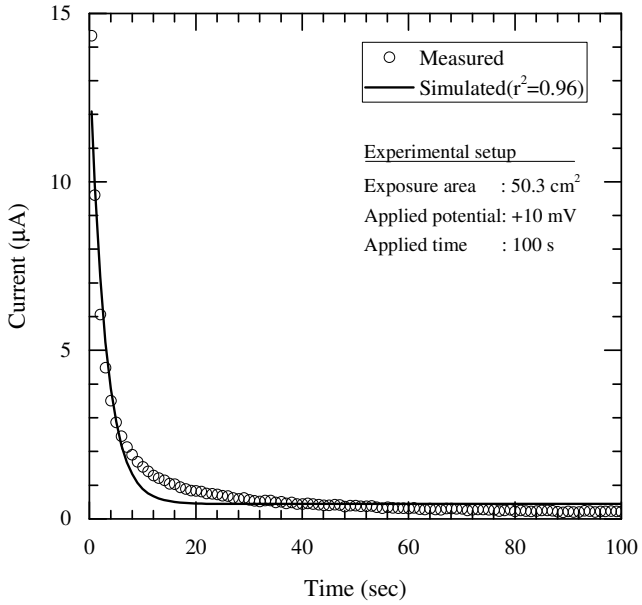

Figure 6.7 Calculating the polarisation resistance using the PT.

6.2.4 *Electrochemical impedance spectroscopy*

Electrochemical impedance spectroscopy (EIS) is possibly the most powerful method to determine corrosion behaviour. Over the last few decades, a considerable number of studies have used it to investigate the corrosion of steel. However, this technique is still challenging due to the ambiguous interpretation of steel corrosion in concrete, although the ohmic resistance and polarisation resistance can be obtained using a simple electrical circuit. A wide frequency range is used in this measurement and to provide information on the interface behaviour between concrete and steel. In addition, in contrast to DC polarisation techniques, this technique is appropriate for corrosion monitoring in laboratory conditions as the working electrode is perturbed with an alternating current (AC).

In this study, the electrochemical impedance of steel embedded in concrete was measured using a Solartron 1260A Impedance/Gain-phase Analyzer in conjunction with a Solartron Analytical 1287 Electrochemical Interface. The sinusoidal wave of 10 mV r.m.s. at corrosion potential was applied over a frequency range of 5 mHz–100 kHz using a logarithmic sweep with 10 frequency points per decade. The corrosion potential was within <10 mV/min. Curve fitting was performed with ZView® (Scribener Associates Inc.). The equivalent electrical circuit used in this study is shown in figure 6.8 and consisted of an interfacial effect, concrete resistance, and polarisation resistance. To improve fitting of the depressed semi-circle for the Nyquist plot, constant phase elements (CPE) were employed instead of capacitance elements.

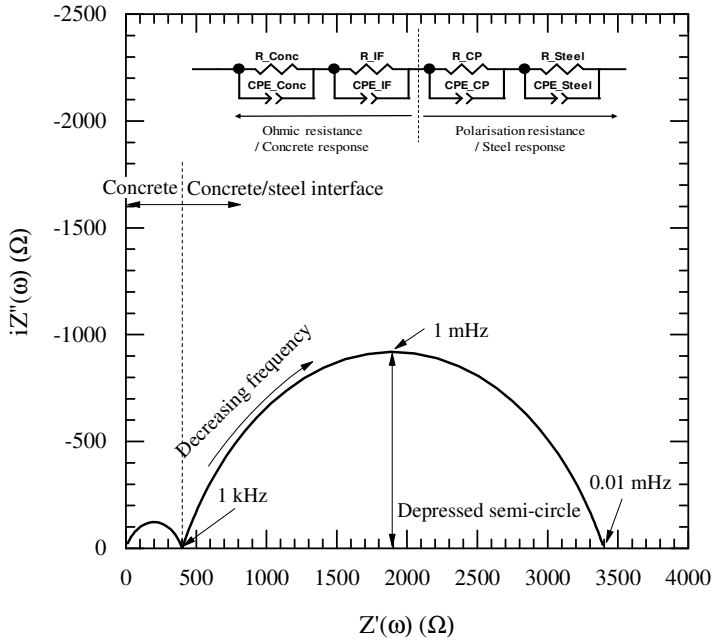

Figure 6.8 Simulation of electrochemical spectra of steel in concrete; R_Conc and R_IF=400 Ω, CPE_Conc and CPE_IF=1×10^{-9} $Fs^{-0.3}$ for concrete and R_CP and R_Steel =3000 Ω and CEP_CP and CEP_Steel=0.01 $Fs^{-0.3}$ for steel and equivalent electrical circuit (insert).

6.2.5 *Mass loss and visual inspection*

Mass loss is useful to determine the rate of corrosion, but it is not practical for site application as rust on the steel surface is directly eliminated. In this study, the mass loss method was only used for samples (CEM I concrete, w/b = 0.6) containing corroded steels. After 382 days, the steel bars were retrieved from the concrete samples. They were then immersed in 500 ml of 60% hydrochloric acid for 20 minutes and the steel was subsequently cleaned with distilled water. The mass of the cleaned steel was measured with a scale of ± 0.01 g accuracy after approximately 1 hour of drying. The mass loss was calculated with steel weights before casting and after cleaning. To reduce errors caused by the cleaning procedure (i.e. to estimate a background loss), the procedure described above was also used with non-corroded steel. From the three non-corroded steels, the average background loss was determined. After a mass loss measurement, the characteristics of the pit corrosion on the steel surface were recorded and the maximum pit depths were quantified using a digital microscope at low magnification, combined with computer-based image analysis (Portable Capture Pro software provided by Veho). Before capturing pit depth, the part of the steel containing maximum pit depth was cut to

obtain a cross-section. The pit depths were then estimated with the captured image using the software.

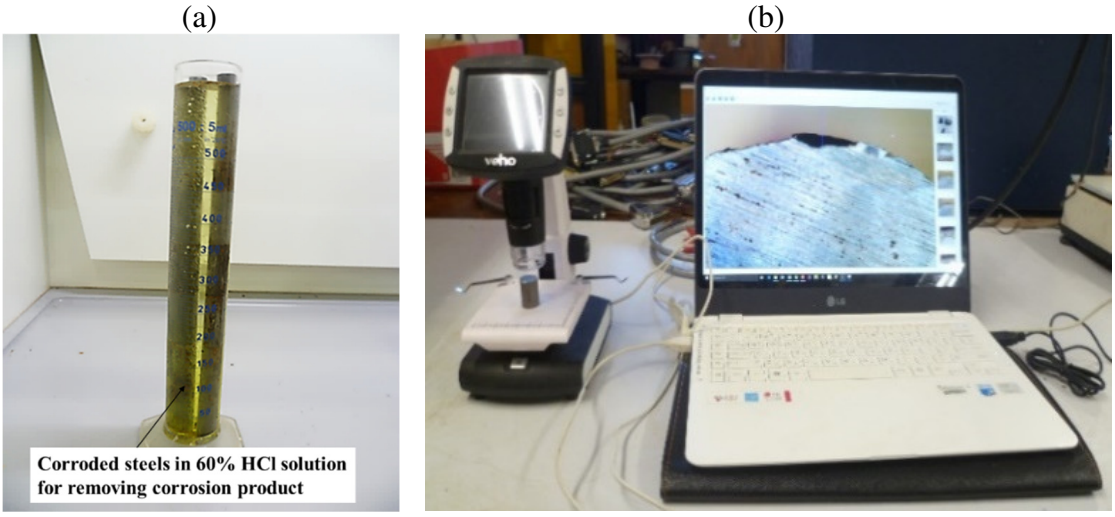

Figure 6.9 (a) Corroded steel immersed in hydrochloric acid solution for mass loss test and (b) pit depth estimation using digital microscope

6.3 Results and discussion

6.3.1 *Corrosion potential with time*

It should first be noted that the notation used for the steel samples in this Chapter are denoted as follows:

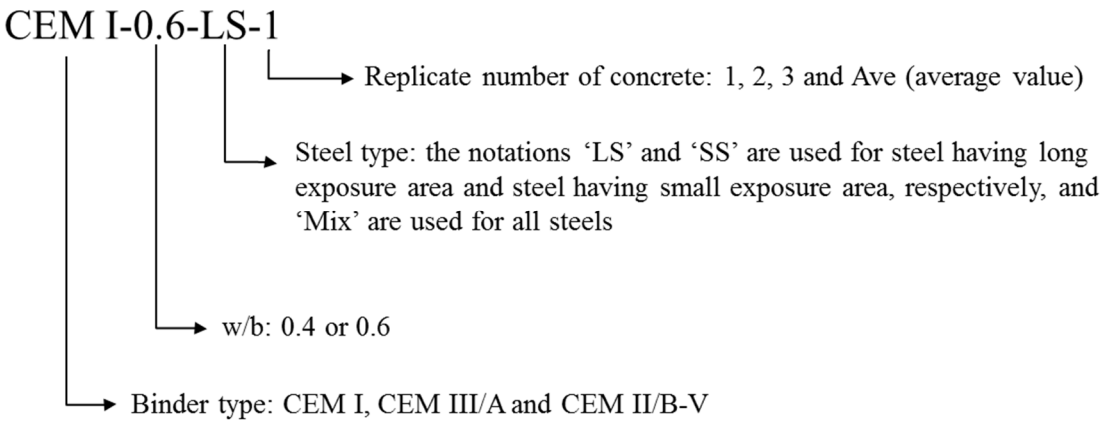

Figure 6.10 Sample notation used in the presentation of experimental results.

The half-cell potential results (monitoring the change from the passive to the active state of steel in CEM I (w/b = 0.6) concrete are shown in figure 6.11. In this study, corrosion

on the steel was only detected in CEM I (w/b = 0.6) concretes. After immersion in the chloride solution, a sharp decrease in the potential was evident for all samples, resulting from an increase in the electrical conductivity of the concrete by contamination of the chloride solution (Elsener, 2002). In the passive state, the fluctuations of corrosion potentials were observed with a wet/dry cyclic regime before reaching a corrosion threshold potential, -350 mV, according to ASTM C 876 (ASTM International, 2015). It seems that the corrosion potential is sensitive to exposure conditions in addition to the condition of the steel itself. After an initial decrease, corrosion potentials slowly increased during the passive period, which may indicate the enhancement of corrosion resistance with a growth of the passive layer (Angst *et al.*, 2011c) or may also indicate chloride binding. However, the explanation for the growth of the passive layer with a continuous increase in the potential is unclear with only corrosion potentials. Section 6.3.3 further discusses this.

The corrosion behaviour of steel in concrete detected by corrosion potential is divided into three types: (i) a sharp decrease in corrosion potential, (ii) a relatively gradual decrease in corrosion potential ranging between -250 mV and -350 mV, and (iii) a decrease in corrosion potential followed by a repassivation period (Angst *et al.*, 2011c). This behaviour was also observed in the present study, as shown in figure 6.11. The time to initiation varied between 171 days and 317 days even though the steels were in the same sample and/or the same mix design. This implies that local effects, such as localized conditions of steel and concrete significantly influence the depassivation process in addition to environmental conditions including chloride content, oxygen availability and moisture content. In addition, corrosion potentials were observed to continuously decrease with time after depassivation. The experimental conditions, i.e. wet/dry cyclic regime, which provided sufficient oxygen and moisture, appear to contribute to the acceleration of the corrosion process. Based on the results, the trends for corrosion can be explained using the half-cell potential monitoring technique, although this technique is limited to quantifying a critical corrosion rate (Reou and Ann, 2009).

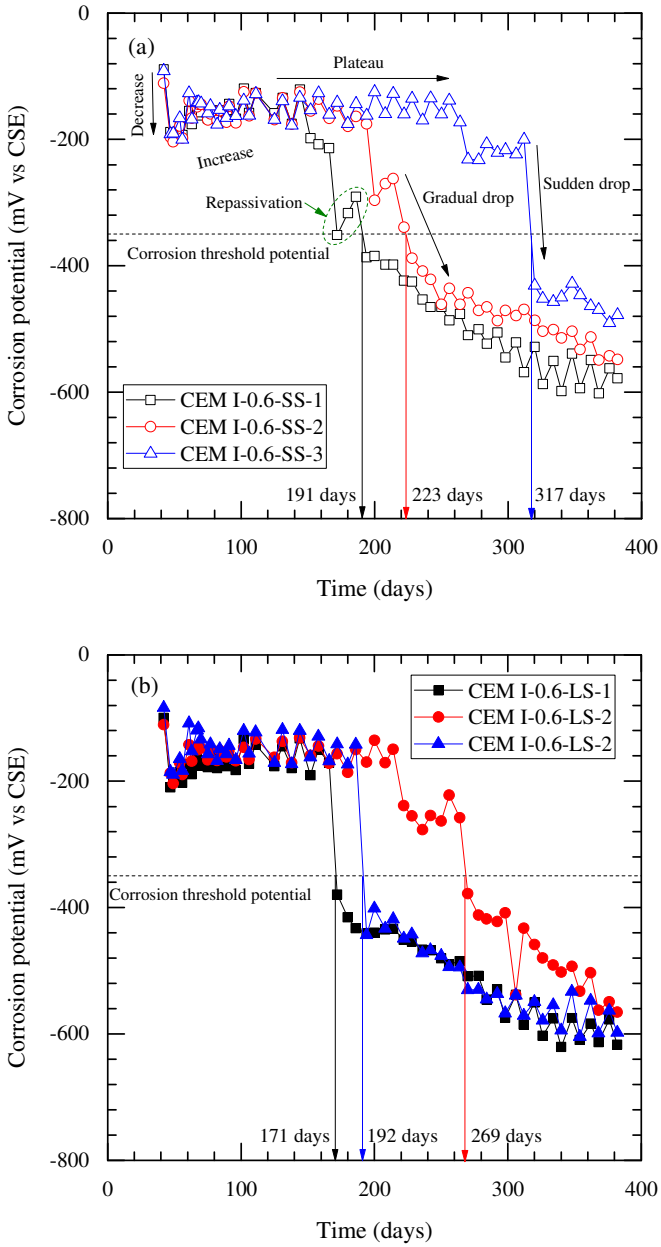

Figure 6.11 Corrosion potential monitoring from 42 days for (a) steel with small exposure area, and (b) steel with large exposure area at 25 mm cover depth in CEM I (w/b=0.6) concrete.

Figure 6.12 shows the distribution of the corrosion potential of steel in concrete (apart from CEM I concrete, w/b = 0.6). These steels were passivated during the whole experimental period, with the averaged value indicated and the minimum and maximum value corresponding to 42 days and 382 days, respectively. The boxes represent ± one standard deviation. In the passive condition, corrosion potentials were generally similar, regardless of w/b and type of binder. It was shown that corrosion potentials in concretes with a low w/b were more positive compared to in concretes with a high w/b. This is because concrete is more (electrically) conductive at the high w/b, leading to lower corrosion potential.

Moreover, it was observed that corrosion potentials moved to the positive direction with time. As mentioned above, this trend, i.e. an increase of potential with time, may be related to the growth of the passive layer due to oxygen availability or related to pore blocking due to chloride binding. Although the fluctuation in corrosion potential for CEM I (w/b = 0.4) concrete was the most severe, the most positive value in corrosion potential was observed in this concrete. Provided that an increase in corrosion potential is only related to a growth of the passive layer, it should be possible to have a high CTL for CEM I (w/b = 0.4) concrete. However, this could not be confirmed in the present study and the literature shows that the CTL is still controversial. Therefore, it seems that an increase in the corrosion potential, particularly for CEM I (w/b=0.4) concrete, also relates to the lower moisture content caused by the hydration process or a chemical reaction, such as the formation of Fridel's salt.

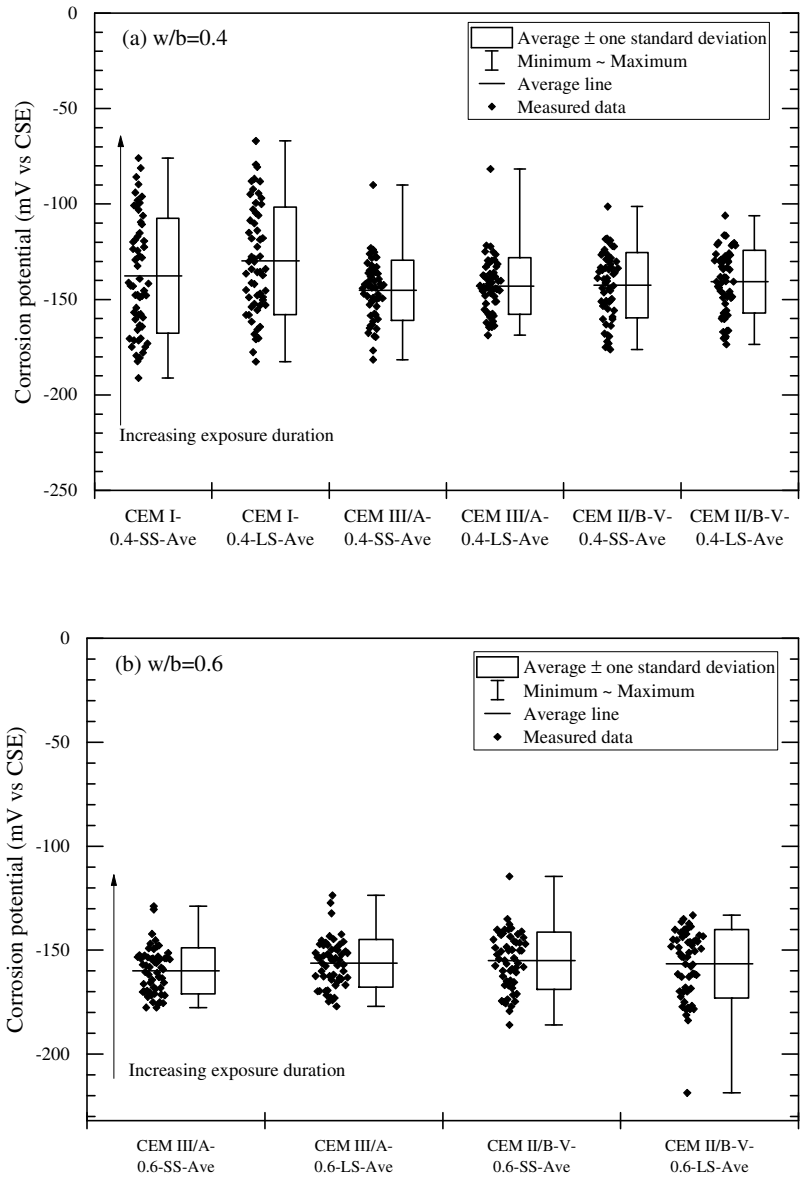

Figure 6.12 Corrosion potential of passivated steel over the period 42-382 days for concretes (a) (w/b=0.4) and (b) (w/b=0.6).

6.3.2 *Macrocell current with time*

It is relatively easy to detect corrosion using macrocell current measurement as, after depassivation, the corrosion potential changes leading to an abrupt increase in macrocell current. This technique is well-established in ASTM G109 (ASTM International, 2007) as a standard method; however, its use is questionable for the quantification of the corrosion rate (Reou and Ann, 2009). Hence, in this study, only corrosion trends are described using the technique.

Before depassivation, the macrocell currents were stable. In other words, a short-circuit, i.e. 0 mA/m^2, seemed to be established between the counter and working electrodes because the same type of steel was used as the counter electrode. As the counter electrodes were located at 100 mm of cover depth, macrocell current values were sometimes in the cathodic direction (Vedalakshmi *et al.*, 2008; Xu *et al.*, 2016). Based on the results, the corrosion potential of steel located with a deeper cover depth was more negative than that of steel in a cover depth close to the surface of concrete, although the difference in the value was marginal. Similar to corrosion potential, macrocell currents changed dramatically after depassivation, as shown in figure 6.13. It was observed that the current increased up to 130 nA/cm^2 due to a change in condition of the working electrode. After an abrupt increase, the current continuously increased with time. The results are closely in line with those of half-cell potential monitoring. In addition, after depassivation, a fluctuation in the current was evident. This indicates that the propagation of corrosion is affected by environmental conditions such as degree of saturation and temperature, as the condition of counter electrode was still stable. It is notable that the macrocell current for CEM I-0.6-LS-3 was abnormal after 334 days, as shown in Figure 6.13 (b). The current suddenly dropped at that time. This implies that the counter electrode was also corroding, but the chloride-induced corrosion of steel at 100 mm depth was negligible for the following reasons:

(i) there was a low chloride content at 100 mm of cover depth based on chloride profiling; and,

(ii) there was no corrosion detected at the other counter electrodes in the same sample or the other samples.

The possible explanation for the abnormal behaviour is the presence of internal cracking caused by the corrosion products of the working electrode. The internal crack leads to

acceleration of chloride ingress partly to the counter electrode, initiating corrosion of the counter electrode. During the corrosion propagation period, cracking is the main concern; it results in accelerating deterioration of the concrete structure. However, considering that the crack pattern is highly random and the time period between the corrosion initiation and the observation of visual cracking on the concrete surface is short (approximately 135 days in this study), it is reasonable to assume that the service life of a concrete structure is determined at the initiation of corrosion.

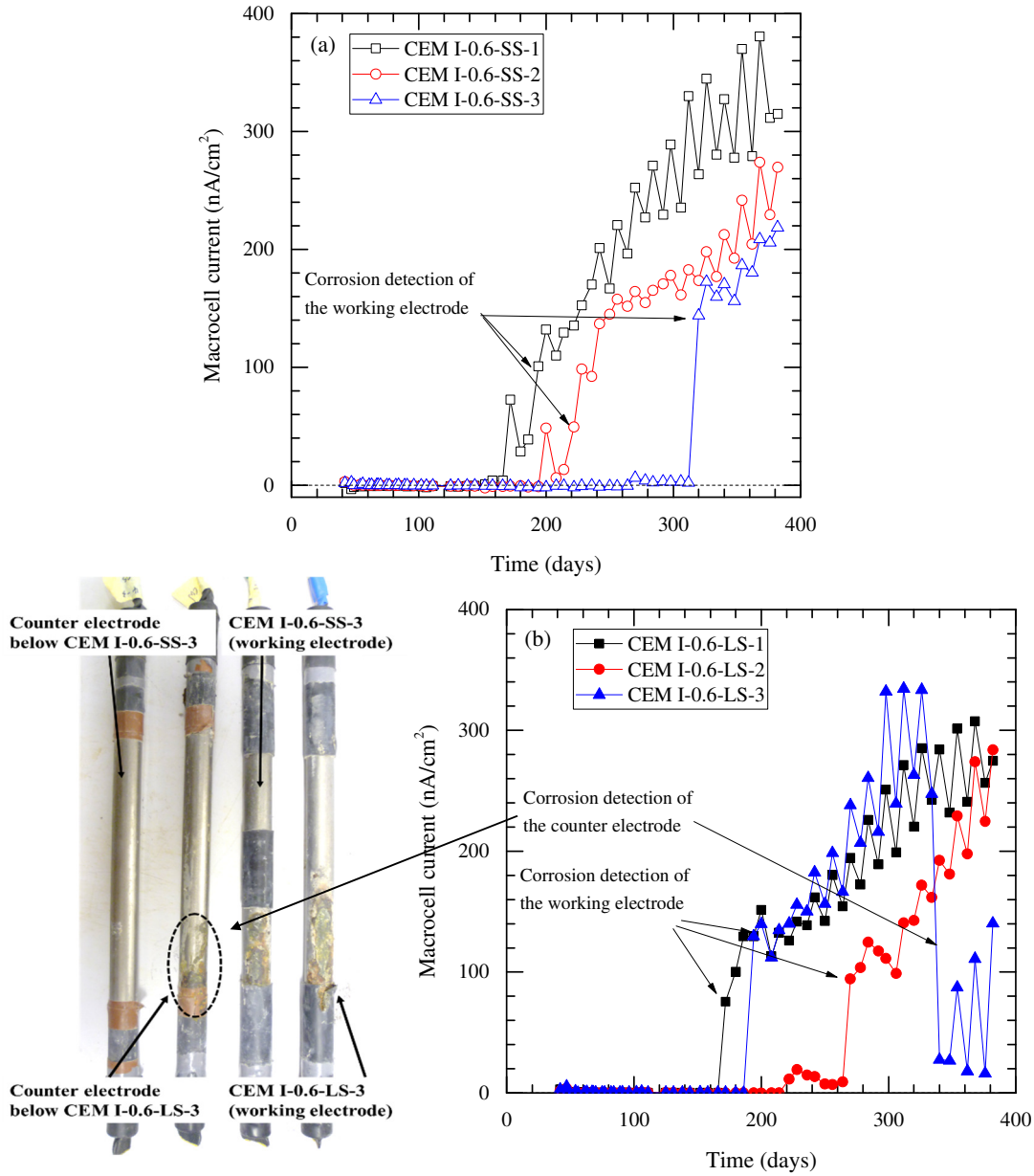

Figure 6.13 Macrocell current monitoring with time, steel with (a) short exposure area and (b) large exposure area.

For passivated steel, except for steel in CEM I (w/b=0.6) concrete (see figure 6.13), shown in figure 6.14, the macrocell current is close to 0 nA/cm^2, regardless of mix and

type of steel. During the passivated condition of the steel, macrocell current between anodic and cathodic regions is negligible. Although this technique is also a qualitative method, it is beneficial in the detection of corrosion.

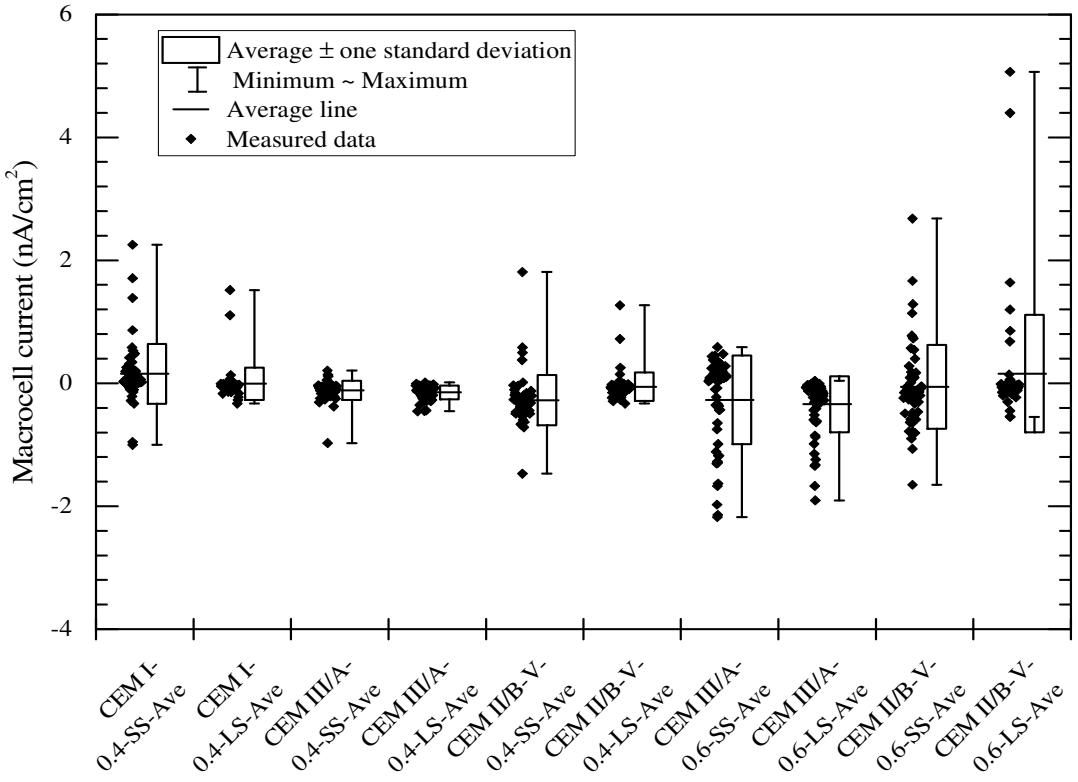

Figure 6.14 Macrocell current distribution of steel in concrete.

6.3.3 *Parameters for electrochemical techniques*

This section presents the parameters obtained from the electrochemical techniques. These parameters are useful to determine the corrosion rate and the corrosion behaviour of the steel.

Ohmic resistance

Ohmic resistance, i.e. electrical resistance of the concrete, is an important parameter to determine corrosion rate. In general, a highly conductive material is present between the counter electrode and working electrode in the electrochemical set-up for uniform polarisation; thus, the resistance for a conductive material, i.e. electrolyte, is negligible. For a saturated concrete, the ohmic resistance has sometimes been neglected assuming that a saturated condition leads to a lower resistance of concrete. However, polarisation

resistance of steel in concrete can be highly overestimated, especially steel embedded in the high electrical resistance of SCM concretes, without considering ohmic resistance.

Equipment can compensate for ohmic resistance automatically, and polarisation resistance can therefore be measured directly. However, to understand the role of concrete in the corrosion process, and find differences in ohmic resistance using polarisation techniques, the measurements were carried out without a function for ohmic resistance compensation involved in the equipment (Solartron 1287 Electrochemical Interface) in this study. Ohmic resistances were measured for the GP, PT, and EIS techniques. The analysis methods are described in Section 6.2.

Figure 6.15 shows the ohmic resistances for the three types of binders. The resistances of CEM II/B-V concrete were the highest, ranging from 3.9 to 9.3 $\Omega \cdot m^2$ at 382 days, and the resistances of CEM I concrete were the lowest, ranging from 0.9 to 3.6 $\Omega \cdot m^2$ at 382 days. For CEM I concrete, ohmic resistances were stable or slightly decreased, while ohmic resistances of CEM III/A and CEM II/B-V concrete continuously increased due to the latent hydration process and pozzolanic reaction. The pozzolanic reaction in the CEM II/B-V concrete resulted in a high electrical resistance of concrete, leading to more disconnected pore structure which retarded the chloride ingress into the concrete. It is also evident that concretes with a high w/b had lower ohmic resistance compared to concrete with a low w/b, resulting from a more porous material at the high w/b.

Depending on the technique employed, ohmic resistances are different. The differences between the GP technique and the EIS technique are < 10%, whereas the ohmic resistance for the PT technique is ~ 52.1% higher than that yielded from the other techniques. It seems that the ohmic resistance in the PT technique involves a double layer effect on the steel surface, and the total current increment may result in charging the steel as well as ohmic resistance, once a constant voltage is applied to the steel. It is necessary to further investigate this effect.

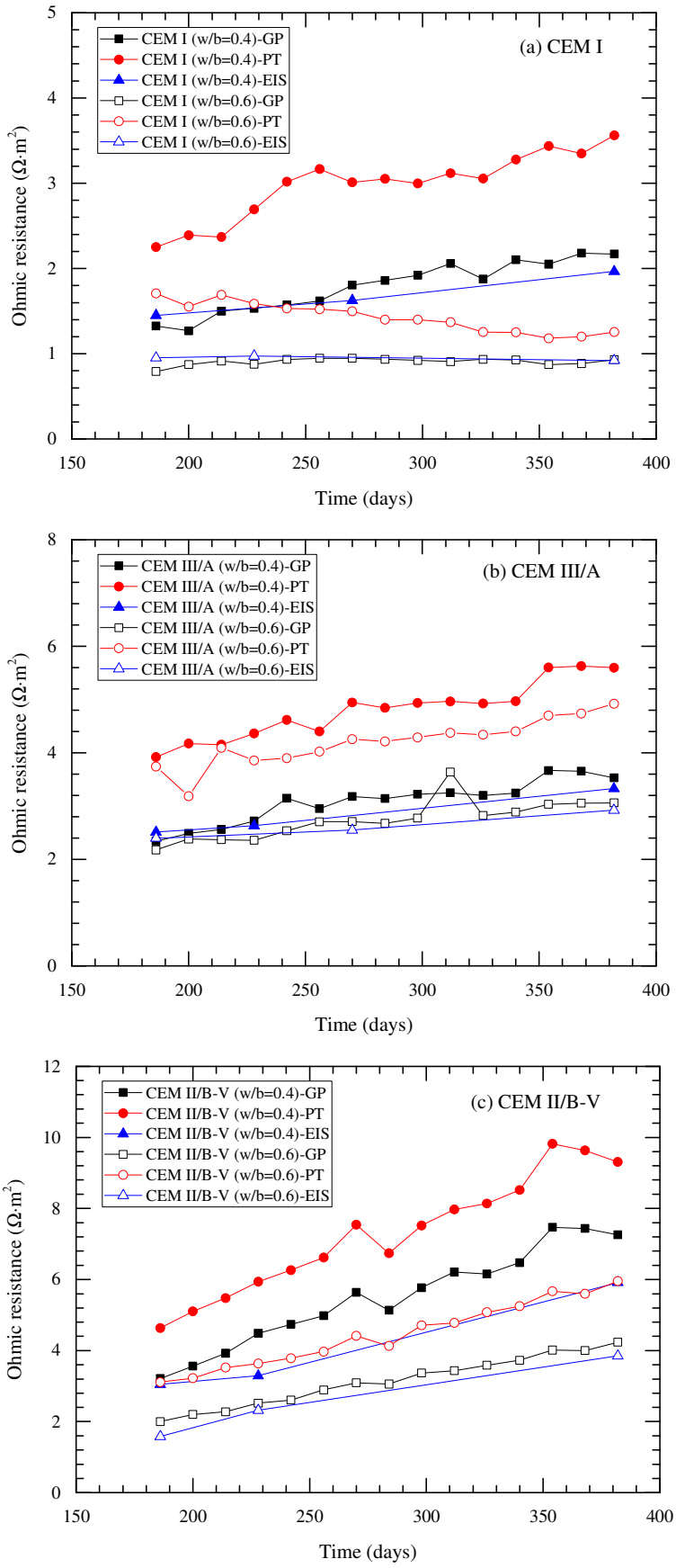

Figure 6.15 Ohmic resistance with time for (a) CEM I, (b) CEM III/A, and (c) CEM II/B-V concrete.

Polarisation resistance, R_p

Polarisation resistance is directly related to corrosion rate and is essential when determining corrosion rate based on Ohm's law. In this study, polarisation resistances were measured using different techniques; in addition, the ohmic resistances in the linear polarisation resistance technique was used with those obtained from the GP technique.

In this study, polarisation resistances for the passive state of steel are described with different techniques and mix designs. It is possible to neglect corrosion rate in the passive state of steel due to the high polarisation resistance compared to that in the active state. The values in the passive state range from 75 to 163 $\Omega \cdot m^2$, although the values depend on type of binder. In addition, it was observed that polarisation resistance in CEM I concrete (w/b = 0.4) was the highest, which coincides with this concrete having the most positive value for corrosion potential in Section 6.3.1. The formation of the passive layer is favourable in CEM I concrete (w/b = 0.4) due to the high availability of oxygen, and thereby the CTL in CEM I concrete (w/b = 0.4) may be the highest. However, as previously mentioned, the results cannot be confirmed in this study.

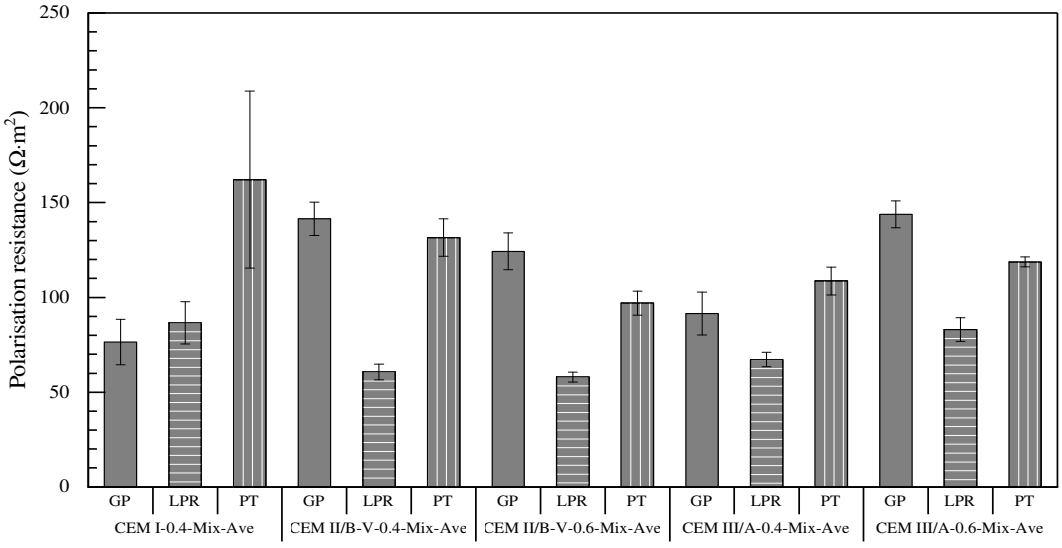

Figure 6.16 Polarisation resistance of passivated steel with mix design.

In the EIS technique, the polarisation resistance in the low frequency range (5 mHz – 1 kHz in this study), corresponding to the diameter of the semi-circular arc, could not be analysed in the passive state due to the straight line formed in this region (see figure 6.17). Various reasons have been suggested for this response, including (i) the

diffusion process of ions caused by the passive layer (Bisquert and Compte, 2001) and (ii) the part of a very large semi-circle, i.e. size effect (Dhouibi *et al.*, 2002). However, the presence of the line remains unclear. Therefore, this study omits the polarisation resistance in the passive state using EIS due to the 'infinite' values obtained.

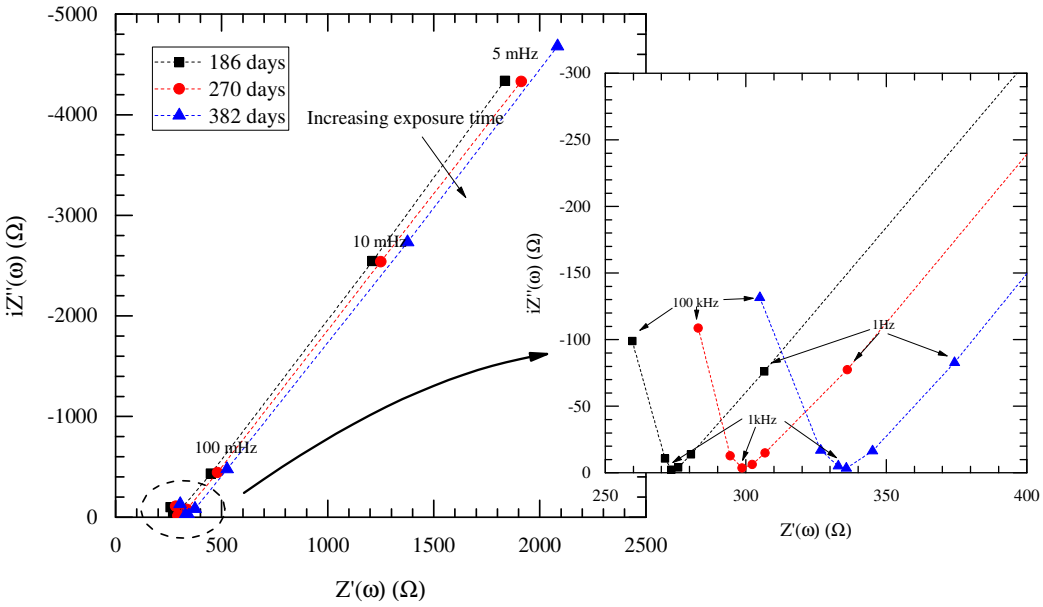

Figure 6.17 Nyquist plot for passivated steel embedded in concrete with time (CEM I concrete, w/b=0.4).

For CEM I (w/b = 0.6) concrete, changes in polarisation resistance were observed from the passive to the active state. After depassivation, polarisation resistances for all samples of CEM I (w/b = 0.6) dramatically decreased, irrespective of the technique used. There was a hundredfold drop from the polarisation resistance in the passive state to that in the active state. As shown in figure 6.18 and figure 6.19, the polarisation resistances were variable depending on technique, but the differences were reduced once the condition of steel changed from the passive (40 – 57%) to the active state (14 – 43%). It appears that the reduced scatter with the techniques resulted in reaching a steady-state for corroded steel in transient and the polarisation process rapidly ended in the active state. In addition, for the half-cell potential and macrocell current measurement, corrosion potentials and macrocell currents consistently increased or decreased, whereas polarisation resistances for all samples were generally stable after depassivation. To this end, it is difficult to determine corrosion rate using the half-cell potential or macrocell current only, and a lower corrosion potential does not necessarily indicate a higher corrosion rate. Finally, considering polarisation resistance for evaluating corrosion of steel, the GP technique is the most effective due to its rapid response (< 10s).

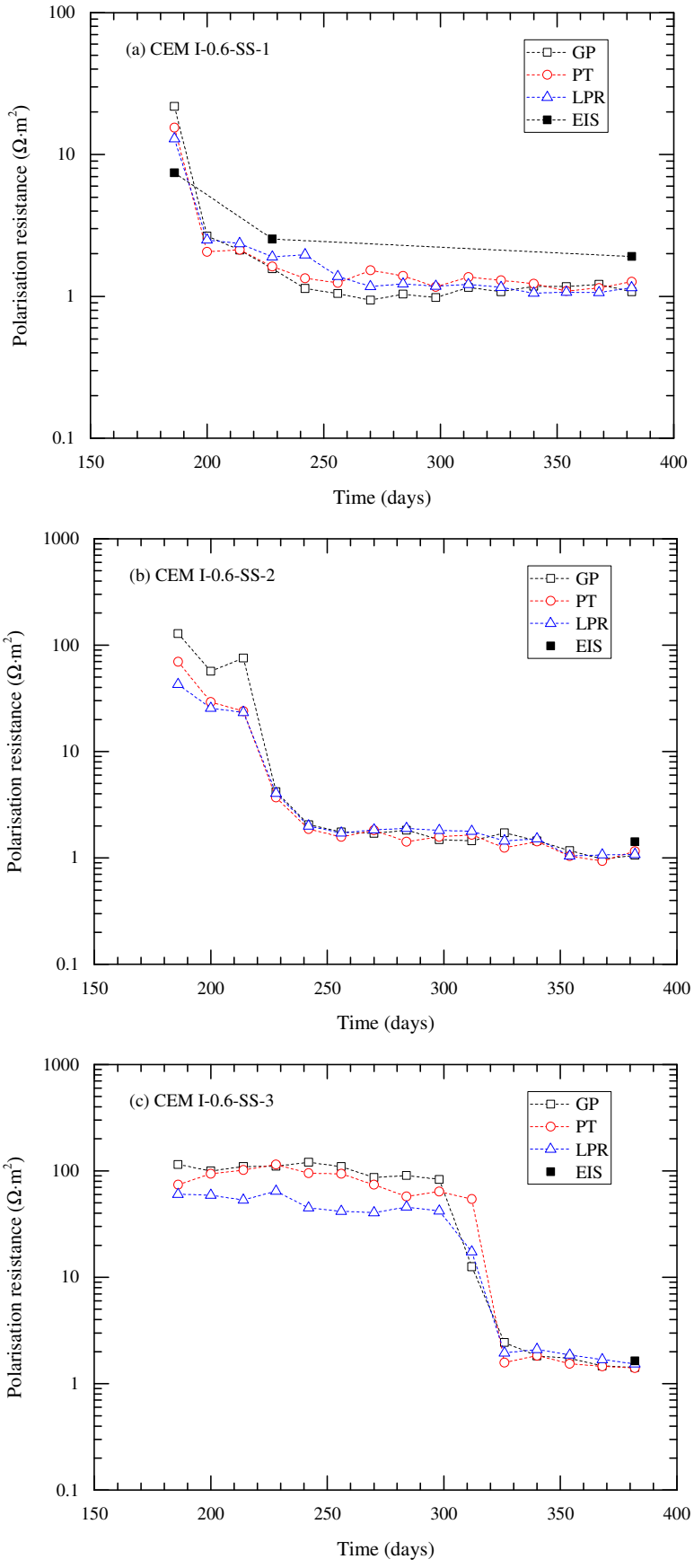

Figure 6.18 Polarisation resistance of steel having a small exposure area in CEM I (w/b = 0.6) concrete with time.

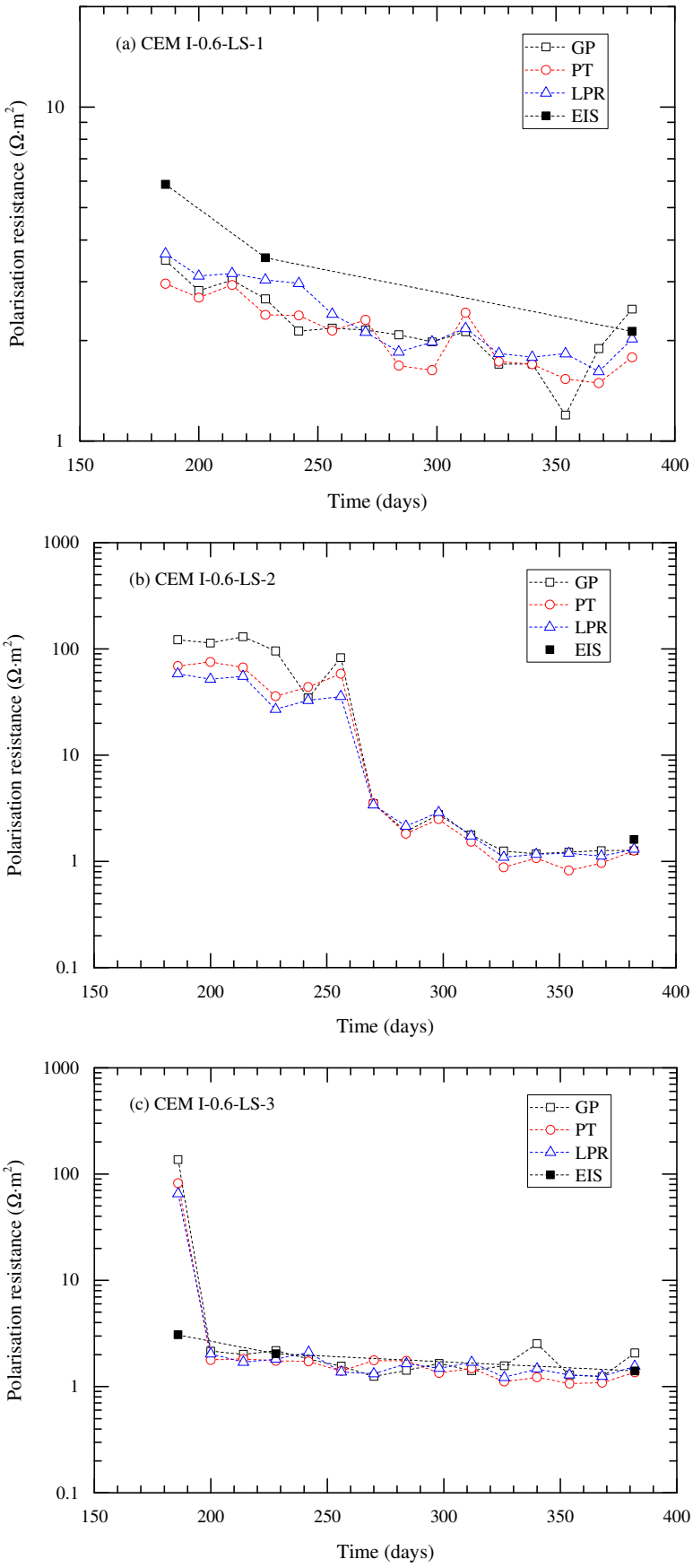

Figure 6.19 Polarisation resistance of steel having a large exposure area in CEM I (w/b = 0.6) concrete with time.

Capacitance

In this study, the capacitance obtained from the GP technique is a measure of the steel condition itself. A high capacitance could support a porous surface of the steel, as an increase in polarisable length on the steel surface provides more electric charge (Freire *et al.*, 2011). Corrosion, therefore, results in an increase in capacitance, as the dense passive layer becomes porous during depassivation process (see figure 6.20). Figure 6.21 presents the capacitance of passivated steel. For passivated steel, the capacitance decreased with time, regardless of the concrete mix, from 7% for CEM II/B-V (w/b=0.4) concrete to 30% for CEM III/A (w/b = 0.4) concrete. After a rapid passivation during the early stages (Sánchez *et al.*, 2007), the passive layer on the steel surface seemed to be enhanced because there was enough oxygen availability. Irrespective of w/b, the highest capacitance was observed for the CEM II/B-V concrete, corresponding to 2.73 F/m^2 for CEM II/B-V (w/b = 0.4) concrete and 2.78 F/m^2 for CEM II/B-V (w/b = 0.6) concrete at 382 days, while CEM I concretes had the lowest capacitance, corresponding to 1.38 F/m^2 for CEM I (w/b=0.4) concrete. Although the thickness of the passive layer could not be determined, it would appear that the passive layer on the steel in the CEM II/B-V concrete was more porous. Montemor et al. (1998) reported that the passive layer of steel in CEM II/B-V concrete is thicker and porous due to alkali ions, although the mechanism behind this is still unclear. The porous structure is partly susceptible to corrosion due to the presence of the thin layer (Ghods *et al.*, 2013), but it would be beneficial in retarding the propagation of corrosion since a myriad of pit corrosion leads to relatively uniform corrosion.

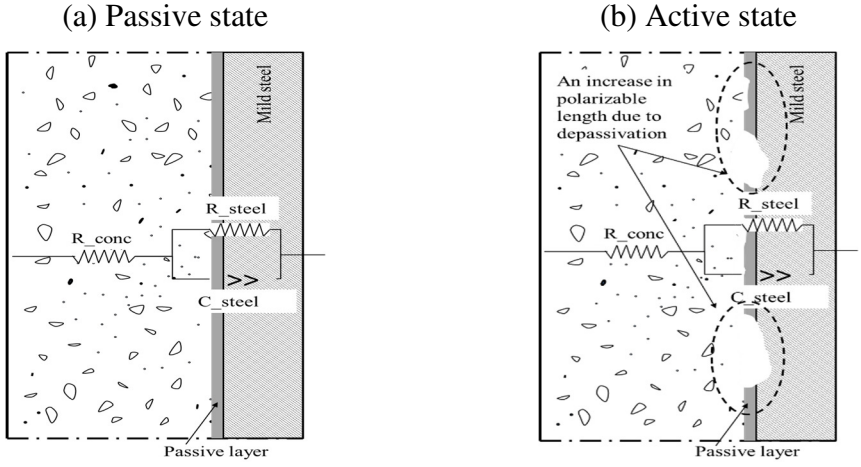

Figure 6.20 Randle circuit in the steel-concrete system (R_conc electrical resistance of concrete, R_steel electrical resistance of steel and C_steel capacitance of steel).

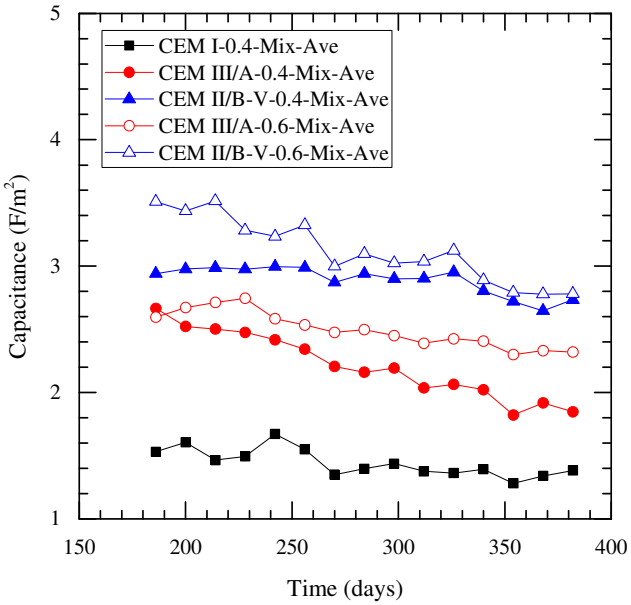

Figure 6.21 Capacitance monitoring for passivated steel using the GP technique.

For CEM I (w/b = 0.6) concretes, it was observed that capacitances increased after depassivation. This indicates that chlorides result in the formation of a pit. An increase in capacitance with time also supports the enhancement of a corrosion pit. However, the capacitance of CEM I-0.6-SS-3 in figure 6.22 is different compared to the others, as the value was stable during the measurement and the corrosion products were distributed uniformly. This is discussed in Section 6.3.5.

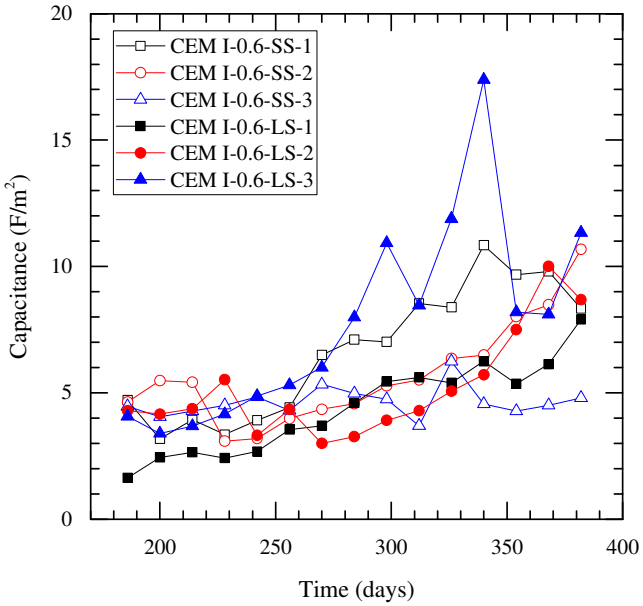

Figure 6.22 Capacitance monitoring for active steel using the GP technique (CEM I concrete, w/b=0.6).

Time-constant

In addition to ohmic resistance and polarisation resistance, several parameters can be obtained which are useful in determining whether corrosion is occurring or not, or to evaluate the condition of the steel. The time constant is the time required to charge a capacitor by ~ 63% of the difference from an initial value, or to discharge a capacitor to ~ 36.8% (Gonzalez *et al.*, 2001); it is an indicator for the electrochemical condition of steel embedded in concrete. If the electrical circuit consists of a resistor in parallel with a capacitor, the time constant, τ, is equal to the product of the resistance and the capacitance ($\tau = RC_p$), and is independent of the testing configuration. The time-constant is given with respect to corrosion potential for all samples in figure 6.23. In the active state, this constant corresponded to < 50s, which was lower than in the passive state corresponding to > 70s and is in agreement with previously reported data (Birbilis and Holloway, 2007). It appears that less adherent/porous corrosion products on the steel surface are conductive to charge/discharge electrons during the polarisation process, leading to rapid response in the time constant (Birbilis *et al.*, 2004). A long time-constant in the passive state can explain why it is difficult to achieve the steady state when using the direct current (DC) polarisation technique and is due to the low capacitance and diffusion process. Clearly, it is beneficial to use the time constant to determine the steel condition, but it appears to be a qualitative indicator instead of a quantitative one.

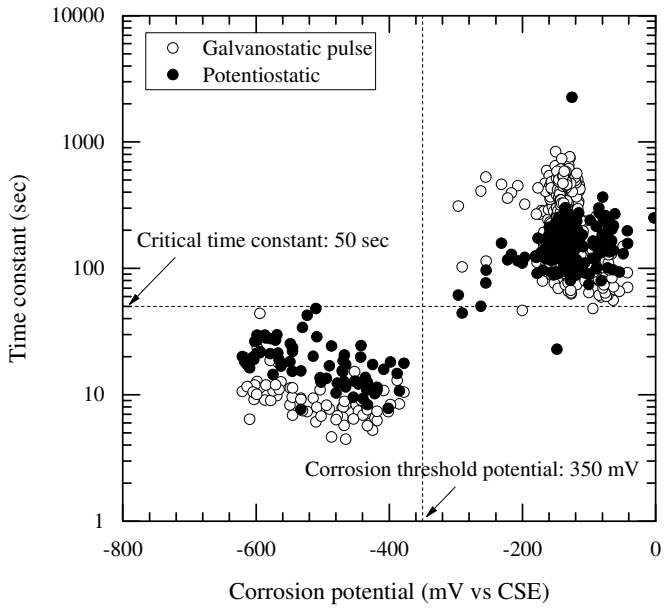

Figure 6.23 Time constant vs corrosion potential.

6.3.4 *Determination of corrosion rate*

To determine the service life of a reinforced concrete structure, the corrosion propagation period is also considered after the initiation of corrosion. In addition to CTL, corrosion rate is an important value for concrete structures subjected to chloride environments. To date, studies have examined corrosion rate but few have tried to obtain the Stern-Geary constant, referred to as B value and normally derived from the Tafel slope. Assumed values, i.e. 26 mV for the active state and 52 mV for passive state are, generally, accepted in the corrosion of steel in concrete (RILEM TC 154-EMC, 2004); however, it is necessary to verify that these values are valid in SCM concretes. B values are generally obtained using the TEP technique; thus, it is impractical to determine them in the field. Therefore, in this section, B values are determined using two methods: a simplified method using the PT technique and a traditional method using the Tafel slopes. The calculated corrosion rates with the values obtained from both methods are compared to the corrosion rate obtained from the gravimetric method.

Determination of B values

Firstly, the present study modifies a simplified method suggested by Poursaee (2010), which is based on Faraday's law and Ohm's law in electrochemistry. The process of calculating the B value is briefly described below.

(i) During the polarisation period, the total charge (q_{total}) shown in Figure 6.24 and the charge by the double layer effect (q_{dl}) are calculated, and then the charge due to the corrosion process (q_{corr}) is extracted from these two values. Hence,

$$q_{corr} = q_{total} - q_{dl} = \int_0^t I(t)dt - C_{dl} \times \mathrm{E}_{in} \tag{6.4}$$

where I is the current (A), C_{dl} is the double layer capacitance (F), and E_{in} is the applied voltage (V).

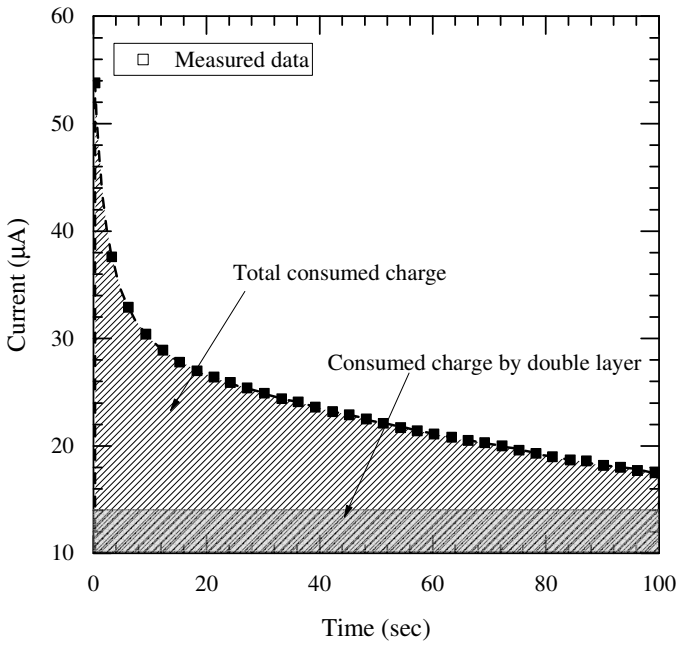

Figure 6.24 Schematic showing total charge and charge by double layer.

(ii) Using Faraday's law, the corrosion rate during the polarisation period is calculated assuming that corrosion by the polarisation effect is uniform,

$$m_{loss} = \frac{q_{corr} \times M}{z \times F} \tag{6.5}$$

$$d_{loss} = \frac{m_{loss}}{\delta_{steel} \times A_{exp} \times t} \times 10 \tag{6.6}$$

$$i_{corr} = \frac{d_{loss}}{11.6} \tag{6.7}$$

where m_{loss} is mass loss during the polarisation time, t (year); M is the atomic weight of steel (≈55.85 g/mol); z is the number of equivalent exchanged electrons ($Fe^{2+} \approx 2$); F is Faraday's constant (≈ 96,487 C/mol); d_{loss} is the penetration depth (mm/year); δ_{steel} is the density of the steel used (≈7.83 g/cm^3); A_{exp} is exposure area (cm^2); and i_{corr} is corrosion rate (mA/cm^2).

(iii) To determine the B value, the calculated corrosion rate is divided by the polarisation resistance:

$$B = i_{corr} \times R_p \quad (6.8)$$

where B is a constant (mV) and R_p is the polarisation resistance ($\Omega \cdot cm^2$).

This process has advantages in determining the B value: the technique is non-destructive and rapid and the analysis is simple. However, as studies using this method are limited, an extensive study needs to be performed to verify the method. The Tafel method, on the other hand, is the traditional method to determine the B value, but the destructive environment and time taken for the technique have limited the number of studies using it. In addition, determining the Tafel region remains controversial (McCafferty, 2005). In the present study, the Tafel slope was determined using the traditional method instead of using new methods proposed in previous studies (Flitt and Schweinsberg, 2005; Mansfeld, 2005; Alfaro, 2014). These new methods are still controversial in their application for reinforced concrete and use complex calculations that are inappropriate for practical purposes.

It is evident that the B value for steel in concrete has not yet been fully studied, and the value could be different from the proposed 26 mV or 52 mV. According to a theoretical analysis by Song (2000), the B value for steel in concrete can range from 8 mV to infinity depending on the test and steel conditions. As shown in the previous section, polarisation resistances are similar regardless of the technique; hence, the B value becomes an additional factor to reduce the difference between the real value and the measured value.

In this study, the B value was calculated using equation (6.4) – (6.8) with data obtained from the PT technique. This is presented in figure 6.25. The values during the passive state are distributed between 6.5 and 8.0 mV and the difference in the values over time is minimal (figure 6.25 (a)). The calculated value is ~7 times lower than the value proposed in RILEM TC 154-EMC (2004). The difference is directly related to the estimated corrosion rate, and the B values vary with the conditions of concrete; thereby, it is difficult to evaluate the corrosion rate accurately. As shown in figure 6.25 (b), the values decrease to ~ 3 mV after depassivation.

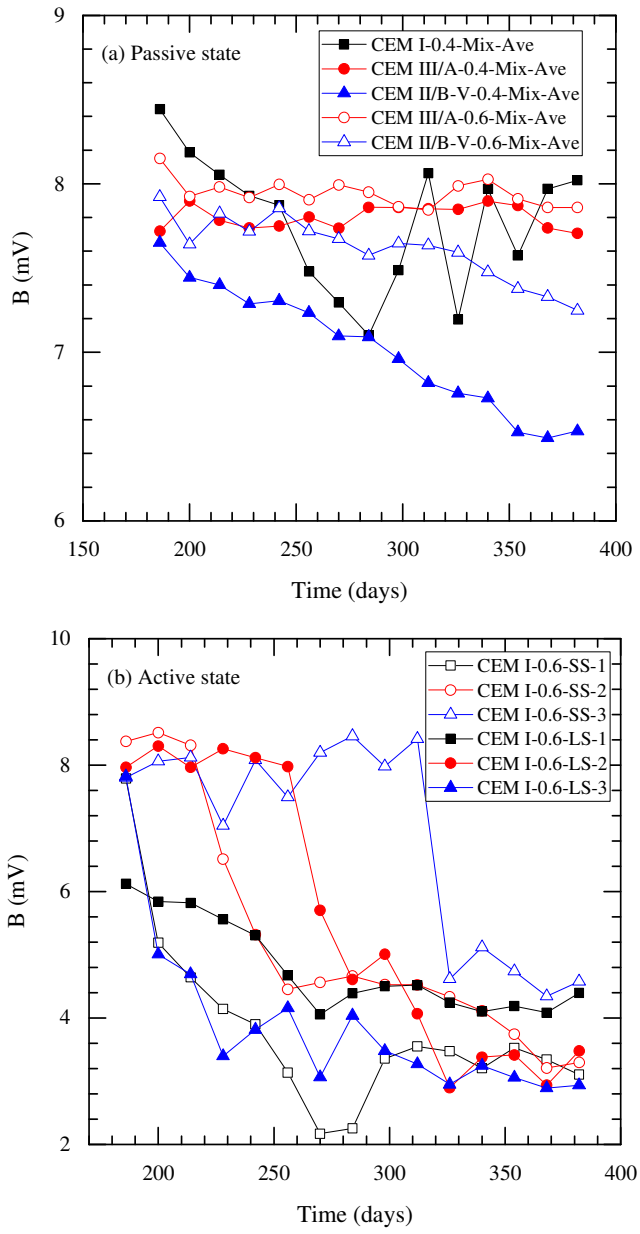

Figure 6.25 *B* values of steel using the PT technique for (a) passive state and (b) active state with time.

The B value from the Tafel slope was calculated at 382 days and table 6.1 presents the Tafel slope and the B value with the mix used in this study. Before discussing the B value, it should be noted that the anodic constant (β_a) is significantly higher for the passive state, so its influence on the B value was first evaluated, as shown in figure 6.26. The B value increases within the β_a range of 1–10,000 mV/dec, and then attains a stable value for β_a > 10,000 mV/dec; β_a is therefore expressed at >10,000 mV/dec using the Tafel extrapolation technique (table 6.1).

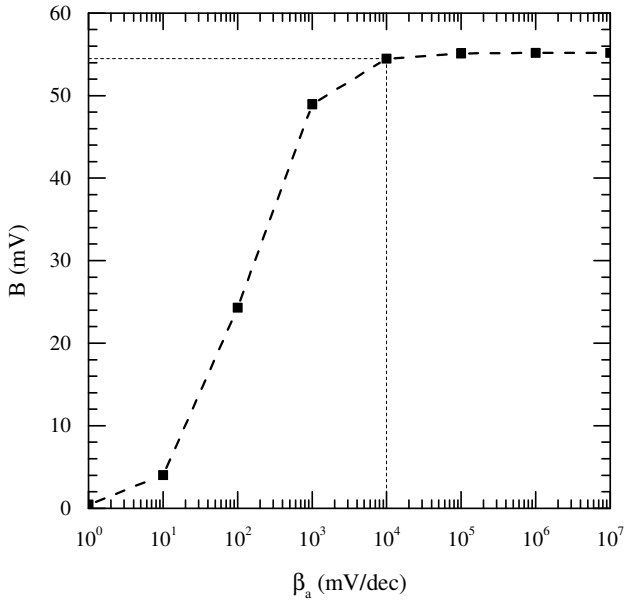

Figure 6.26 Variation in B value with β_a (β_c =127 mV/dec).

For the passive state, except for CEM I (w/b=0.6) concrete, B values range from 23.6 mV to 68.7 mV for all samples. Low B values, ranging from 23.6 mV to 37.9 mV, are caused by fitting error as β_a was calculated from 181.6 to 473.8 mV/dec, which is lower than β_a for the active state. When error values are omitted, B values in the passive state are distributed in the range of 41.2 – 68.7 mV, which is similar to the proposed value of 52 mV for the passive condition. For the active state, the B values calculated using the TEP technique should be compared to the B values proposed in the previous study (RILEM TC 154-EMC, 2004) and the B values calculated using a simplified method in this study. Considering the calculation process, a reduced β_a by vigorous anodic reaction results in a decrease in the B value (see figure 6.26), but the B values increased to 96.0 mV. In the cathodic constant (β_c), the difference between active state and passive state is also evident. β_c lies within the range of 106.6–158.2 mV/dec for the passive state, while the values lie within the range of 303.3–357.1 mV/dec for the active state. The increase in cathodic constant had more influence on the B value than anodic constant in this study. This implies that the consumption of oxygen on the polarised area is higher than the supply leading to an increase in the cathodic slope. There are two reasons for lack of oxygen for cathodic reaction: (i) the concretes were saturated as the measurement was conducted after the end of the wetting phase, and (ii) the electrochemical reaction in the anode was faster than in the cathode due to severe corrosion on the steel surface. After depassivation, the cathodic reaction is a more important factor in the corrosion process.

Table 6.1 Parameters obtained from Tafel extrapolation

Sample notation		β_a(mV/dec)	β_c (mV/dec)	B (mV)	Sample notation		β_a(mV/dec)	β_c (mV/dec)	B (mV)
Mix	Steel type				Mix	Steel type			
CEM I-0.4-	SS-1	2701.4	139.7	57.7	CEM I-0.6-	SS-1	585.9	331.3	91.9
	SS-2	> 10,000	130.9	56.8		SS-2	604.6	348.3	96.0
	SS-3	292.8	94.2	30.9		SS-3	407.6	303.3	75.5
	LS-1	> 10,000	127.1	55.2		LS-1	466.4	357.1	87.9
	LS-2	> 10,000	128.8	55.6		LS-2	411.7	336.3	80.4
	LS-3	181.6	77.5	23.6		LS-3	443.8	342.8	84.1
CEM III/A-0.4-	SS-1	> 10,000	153.2	66.5	CEM III/A-0.6-	SS-1	> 10,000	121.3	52.6
	SS-2	> 10,000	139.6	60.6		SS-2	> 10,000	123.1	53.5
	SS-3	> 10,000	135.6	58.9		SS-3	1745.0	117.1	47.7
	LS-1	> 10,0000	128.5	55.8		LS-1	873.4	106.6	41.2
	LS-2	2599.7	127.3	52.7		LS-2	> 10,000	118.9	51.6
	LS-3	> 10,000	132.0	57.3		LS-3	196.9	78.0	24.3
CEM II/B-V-0.4-	SS-1	> 10,000	128.7	55.9	CEM II/B-V-0.6-	SS-1	3651.7	135.0	56.5
	SS-2	> 10,000	145.4	63.1		SS-2	> 10,000	158.2	68.7
	SS-3	337.4	95.9	32.4		SS-3	473.8	107.1	37.9
	LS-1	> 10,000	145.4	63.1		LS-1	> 10,000	140.0	60.8
	LS-2	> 10,000	152.7	66.3		LS-2	> 10,000	132.0	57.3
	LS-3	616.2	112.4	41.3		LS-3	> 10,000	127.5	55.4

Verification of corrosion rate

The corrosion rate (i.e. corrosion density, mA/m^2) of steel is important in determining the service life of concrete structures subjected to chloride-induced corrosion. The most accurate method to determine the corrosion rate is mass loss of steel. According to González et al. (1995), the corrosion rate measured by mass loss method is up to 10 times higher than the rate measured by polarisation techniques when pitting corrosion occurs on the steel. Nevertheless, it still is necessary to investigate a correction factor between the mass loss technique and the polarisation technique. To compare the corrosion rates obtained by these two techniques, it is necessary to define the corrosion rate.

The corrosion rate by mass loss is the time-averaged value during the whole experimental period, whereas corrosion rates obtained from polarisation techniques represent the instantaneous corrosion rate. For the purpose of comparison, the polarisation resistance obtained from polarisation techniques (i.e. LPR, GP, and PT technique) was averaged with time. In addition, different B values were used to calculate the corrosion rate based on Ohm's law, including (i) the B value from the TEP technique, (ii) the B value from a simplified method, and (iii) a traditional B value. Subsequently, the corrosion rates with different polarisation techniques and B values were compared with the averaged corrosion rate obtained from the mass loss method. Note that corrosion rates were only evaluated for samples in which corrosion occurred, i.e. the CEM I (w/b=0.6) concrete.

The corrosion rate obtained from the mass loss method was calculated using Faraday's law (equation (3.9)). The calculated corrosion rate and mass loss data are presented in table 2.1. The observed corrosion rates are severe except for in CEM I-0.6-SS-3. As noted above, the corrosion rate obtained from the mass loss method is the average value over the whole exposure time, and implies that an instantaneous value at 382 days will be higher than the average value. From visual inspection, cracks were also detected on the exposure surface of concrete. Hence, severe corrosion, i.e. > 10 mA/m^2, can lead to cracking. Cracking is considered in detail in the visual inspection section (Section 6.3.5).

Table 6.2 Corrosion rate of steel in concrete using mass loss method (CEM I, w/b=0.6)

Binder type	CEM I-0.6-					
Steel type	SS-1*	LS-1	SS-2	LS-2	SS-3	LS-3
Mass before corrosion (g)	551.23	551.37	551.25	551.22	551.21	551.32
Mass after treatment (g)	550.31	550.40	550.63	550.33	550.94	549.99
Mass loss considering background loss** (g)	0.84	0.89	0.54	0.81	0.19	1.25
i_{corr} (mA/m^2)	17.50	12.36	11.25	11.25	4.00	17.36

* steel sample notation: 'SS' indicates steel with a small exposure area and 'LS' indicates steel with a large exposure area (see Chapter 4.3), and the number indicates the number of replicates

** Background loss: 0.08g

Table 6.3 Range of corrosion current values (RILEM TC 154-EMC, 2004)

i_{corr} (mA/m^2)	V_{corr} (μm/y)	Corrosion level
≤1.0	≤1.0	Negligible
1.0 – 5.0	1.0 – 5.0	Low
5.0 – 10.0	5.0 – 10.0	Moderate
> 10.0	> 10.0	High

As show in figure 6.27, the shaded part was integrated with time and then divided by the total exposure time to estimate the averaged corrosion rate. To calculate the corrosion rate, polarisation resistances obtained from different techniques were used. Different B values were also used in the calculation; these were estimated from the PT technique, the TEP technique, and a traditional value (i.e. 26 mV for active state). Before corrosion measurement, i.e. 0–185 days, the corrosion rate was set as 0 mA/m^2. During this period, all samples, expect for CEM I-0.6-LS-1, were in the passive state, and the integrated corrosion rate in the passive state is negligible compared to the value in the active state. For CEM I-0.6-LS-1, the range corresponding to 0 mA/m^2 was set based on the corrosion potential measurement.

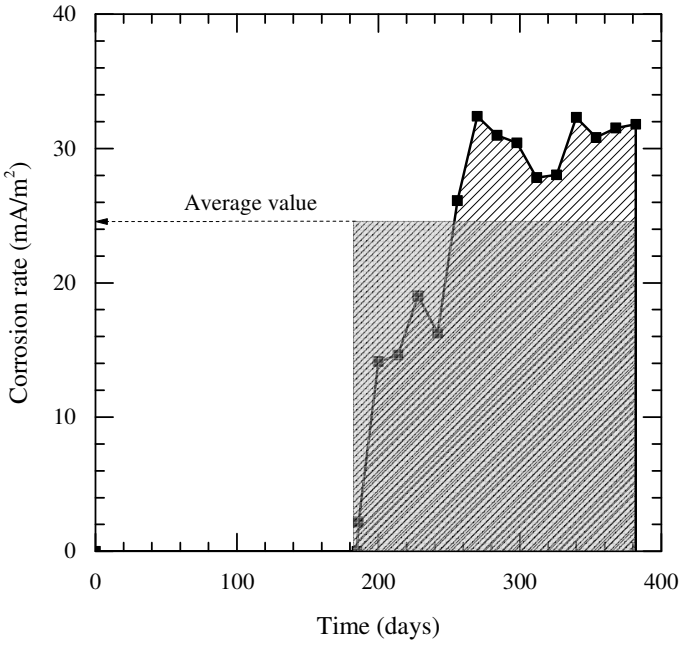

Figure 6.27 Calculating the averaged corrosion rate from monitoring data.

Figure 6.28 presents a comparison of the corrosion rate obtained by mass loss with the averaged corrosion rate using the different polarisation techniques and different B values. Although different polarisation techniques were used, differences in the obtained polarisation resistances were marginal, as described in figure 6.18 and figure 6.19. When the *B* value obtained from the PT technique was used, the corrosion rates were approximately 5.2– 26.5 times lower than when the mass loss method *B* value was used. This is in line with a previous study in which the pitting factor was considered to be 10 (González *et al.*, 1995). Average differences using the Tafel method and traditional value (26 mV) were ~ 53% and ~ 28%, respectively. The differences were dramatically reduced compared to using *B* value obtained from the PT technique. In addition, considering B values were changed by the corrosion process, the error may be lower. After depassivation, the *B* value in the active state increased compared to that in the passive state in the TEP technique, and the *B* values obtained by the TEP technique were calculated at the end of all measurements, i.e. at 382 days. Therefore, it is possible that the corrosion rates calculated using B values from the TEP technique were overestimated compared to the real values.

It is noteworthy that the *B* value was used to determine corrosion rate using the electrochemical techniques and, depending on the value used in the calculation, the error could be significant. Thus, further investigation is required to determine the B value. Although the traditional B values (i.e. 26 mV for active state and 52 mV for passive state) are reasonable to calculate corrosion rate, it would be more useful to determine the

severity of corrosion using the integrated polarisation resistance without the *B* value, or using the monitored *B* value.

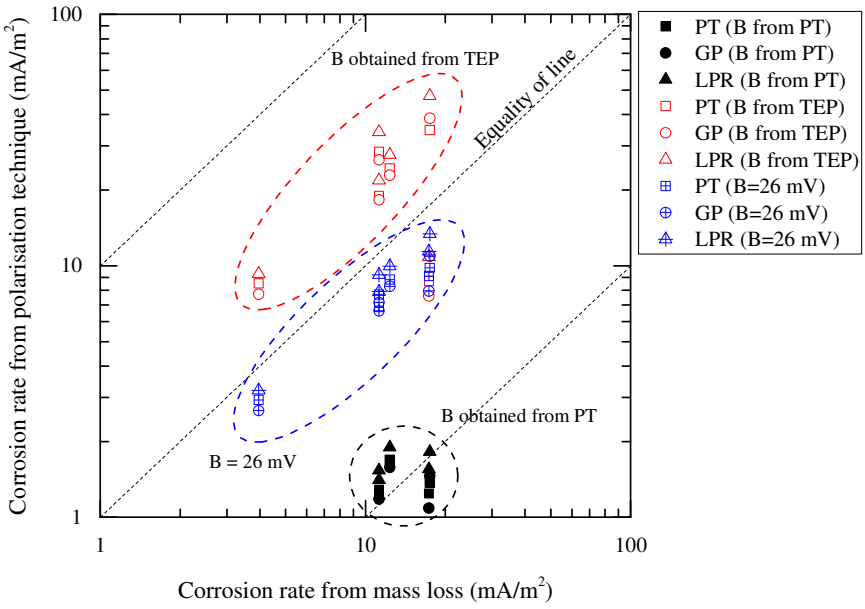

Figure 6.28 Comparison of corrosion rate between polarisation techniques and mass loss.

6.3.5 *Visual inspection for corrosion*

Electrochemical techniques are non-destructive. Hence, to prove the accumulation of corrosion products, or severity of corrosion, it was necessary to conduct a visual inspection. To this end, steels were extracted from the concrete samples and cleaned, and then the mass loss of steel by corrosion and the formation of pit were investigated using a digital microscope.

Before crushing the concrete samples containing corroded steels (CEM I concrete, w/b=0.6), cracks on the exposure surface were detected for the samples. Cracking occurs because of the volume expansion of corrosion products, which vary depending on their type (oxide-type rusts or hydroxide-type rusts) as shown in figure 6.29. Although the chemical compositions of corrosion products were not analysed in this study, the main product can be deduced as $Fe(OH)_3$ because of the sufficient supply of oxygen during the wet/dry cyclic regime.

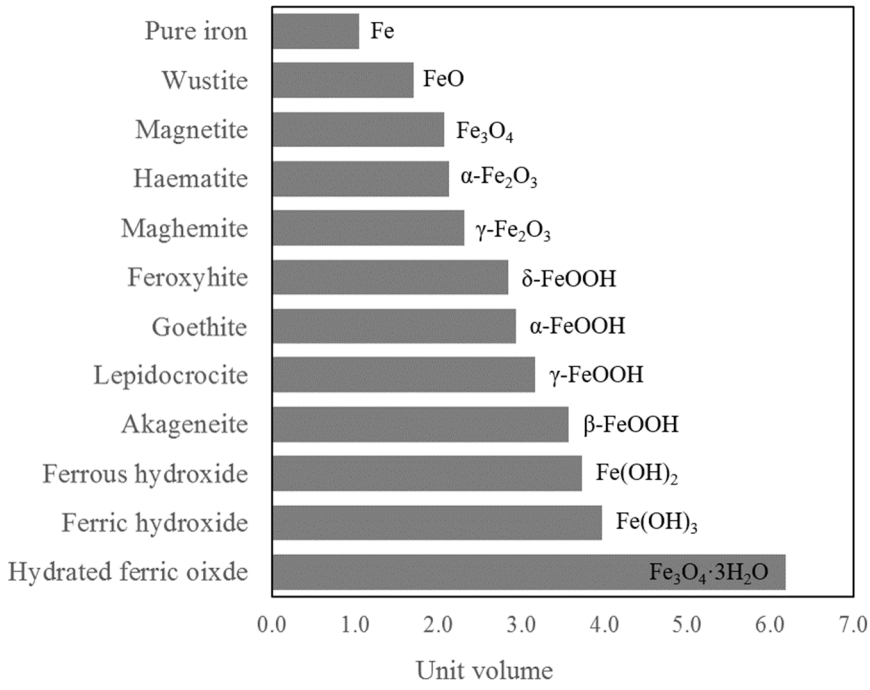

Figure 6.29 Corrosion products of iron (Köliö *et al.* 2015).

As shown in figure 6.30, the position of visual cracking on the surface coincided with the corroded area on the steel, indicating that cracking started from the steel depth and was caused by an expansion of corrosion products. In addition, green rust was found in the corrosion products, in particular for steel in CEM I-0.6-SS/LS-3, and it is known that the green colour in this rust results from chlorides (Koleva *et al.* 2006). No corrosion was detected on the opposite side of the corroded area on the steel; in other words, corrosion was generated at the steel surface close to the exposed concrete surface. The time is shown in table 6.4 when visual cracks on the concrete surface were observed. In summary, the passive film was destroyed when chlorides reached the steel depth, and the corrosion products formed through electrochemical reaction to cause cracking and spalling of the concrete. It was also observed that corrosion distribution was localised instead of uniform, which is indicative of pitting corrosion.

Table 6.4 Time to visual cracks on the surface of CEM I (w/b=0.6) concrete

Concrete type	CEM I-0.6-					
Steel type-replication No.	SS-1	LS-1	SS-2	LS-2	SS-3	LS-3
Time to visual cracking (days)	312	321	369	382	N.D.	327

* N.D. = No detection

(a) CEM I-0.6-LS/SS-1

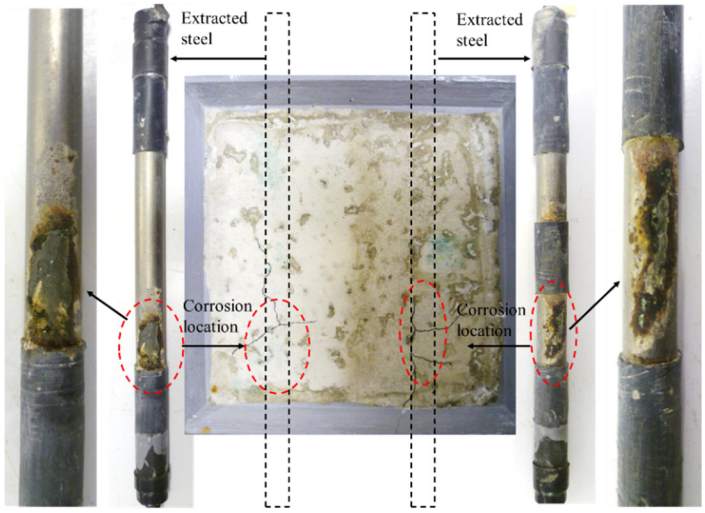

(b) CEM I -0.6-LS/SS-2

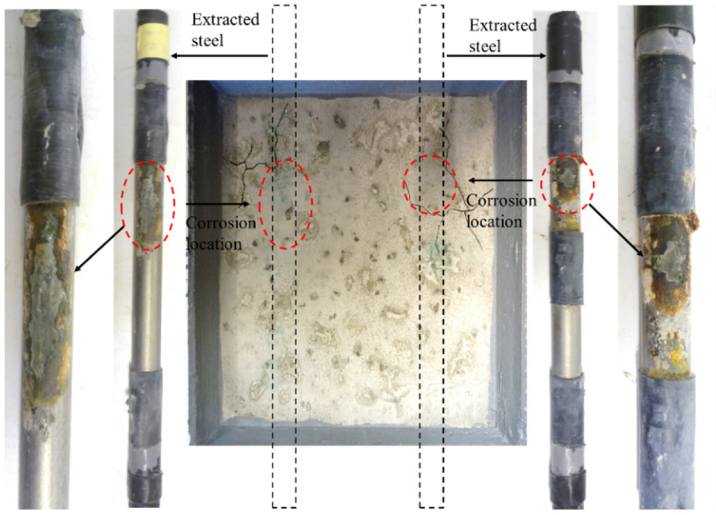

(c) CEM I -0.6-LS/SS-3

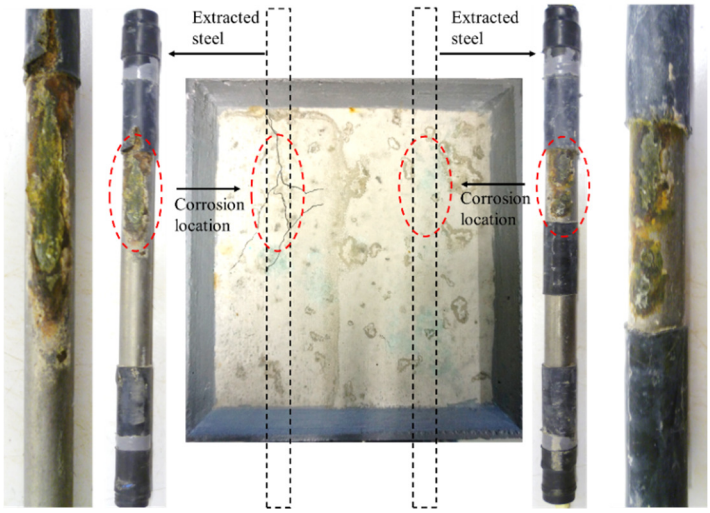

Figure 6.30 Crack patterns on the concrete surface and corroded steels ('LS' on left side and 'SS' on right side) extracted from samples for CEM I (w/b=0.6) concretes.

Sectioned loss of steel (see figure 6.31) was measured using a commercial program: PORTABLECAPTURE PRO software, provided by Veho. The maximum pit depths ranged from 0.227 to 0.946 mm and it was observed that the pit shapes varied across samples. Considering the measurement period from time to corrosion initiation, the corrosion rates in the maximum pit depth were high, from 1,311.7 to 1,554.6 mA/m^2, which is 88 – 393 times higher than those calculated by the mass loss method. However, the corrosion rates in the maximum pit depth indicate a localised corrosion in a very small area; thereby, the corrosion rate obtained from mass loss method could be increased by considering the corroded area, although it was not possible to estimate this area. It should be noted that pit corrosion developed rapidly.

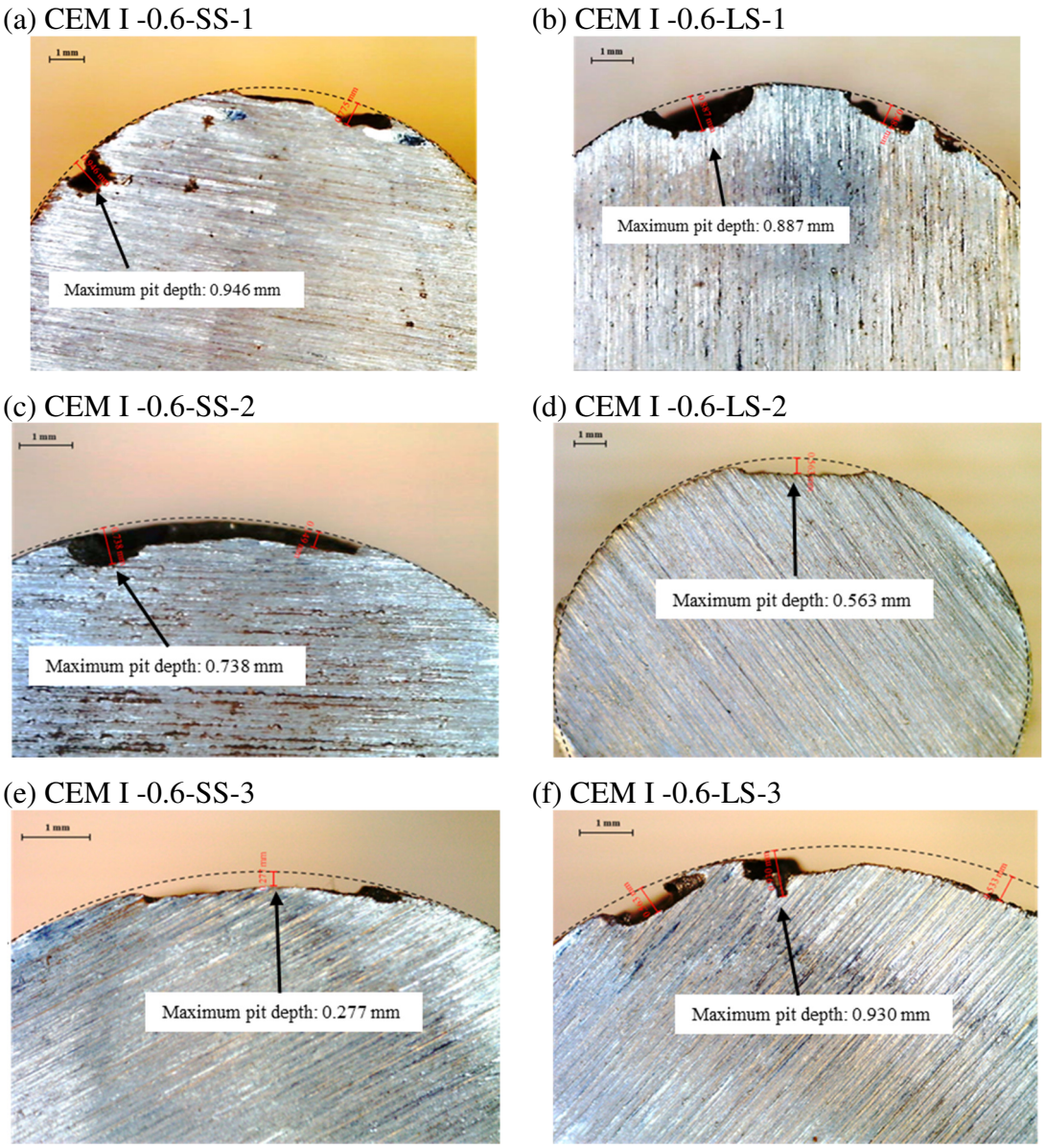

Figure 6.31 Sectioned loss of steel with a small exposure area (SS) and a large exposure area (LS) for CEM I (w/b=0.6) concretes.

6.3.6 *Determination of time to corrosion initiation*

Various corrosion monitoring techniques have been developed, and some have been used commercially (Nygaard 2008). However, as described above, it is difficult to quantify corrosion rate, especially for pitting corrosion. In this section, time to corrosion initiation for CEM I (w/b = 0.6) concretes is briefly evaluated with the techniques used in this study including the half-cell potential, macrocell current and polarisation techniques.

For the half-cell potential measurement, the measured potential is used to determine the corrosion state of the steel. The presence of corrosion is determined when a dramatic decrease in the potential is observed instead of an absolute value. Second, macrocell current is measured directly by a zero-resistance ammeter or multi-meter combined with a specific resistor. The measured current increases abruptly when corrosion is detected. Third, the polarisation resistance obtained using electrochemical techniques is considerably reduced in the active state of steel compared to in the passive state. Finally, in the EIS technique, the presence of two distinct semi-circles in the Nyquist plot indicates corrosion on the steel surface.

The time to corrosion initiation is presented in Table 6.5. Corrosion initiation time using the EIS technique was excluded as the time interval between each measurement was large. Times to corrosion initiation are slightly different. One reason for this difference is the different measurement cycles, i.e. the end of every wet (6-days) /dry (8-days) cycle for the macrocell current and half-cell potential techniques (every ~ 1 week), and the end of every wet cycle for the polarisation technique (every 2 weeks). It is interesting that for CEM I-0.6-SS-1, corrosion potential rebounded after corrosion potential dropped and for CEM I-0.6-SS-1 and CEM I-0.6-SS-2, macrocell currents were opposite. This is considered as the repassivation of the steel (Ann *et al.*, 2010); thereby the interpretation to determine time to corrosion initiation with half-cell potential and macrocell current requires caution. In other words, according to ASTM C876 (ASTM International, 2015), the possibility of corrosion under -350 mV vs CSE is 90%; hence, even though the corrosion potential drops, no corrosion can be detected. Thus, all measurements are adequate to detect corrosion, but the detecting times vary depending on the technique due to influencing factors, including the detecting method and the condition of material. To reduce the error, it is suggested that more than one technique be used to detect corrosion, and continuous monitoring is more effective than a one-off measurement.

Table 6.5 Time to corrosion initiation (in days) for CEM I (w/b = 0.6) concrete using different techniques

Concrete type	CEM I-0.6-					
Steel type-replication No.	SS-1	LS-1	SS-2	LS-2	SS-3	LS-3
Macrocell current technique	194	172	222	270	320	194
Polarisation techniques	200	N.D.*	228	270	326	200
Half-cell potential	191	171	223	269	317	192

* N.D. = not determined due to corrosion presence when measurement was carried out

6.4 Summary

This section evaluated steel corrosion in concrete subjected to a simulated chloride environment. A range of techniques were used, including non-destructive and destructive techniques. During the experimental period, the corrosion of steel was only detected for CEM I (w/b=0.6) concretes. A summary of the findings follows.

- Electrochemical parameters, i.e. ohmic resistance, polarisation resistance, capacitance, corrosion potential and time constant, differed across techniques, type of binder, condition of material and exposure duration. Error with the techniques was marginal, while the B value was sensitive in determining the corrosion rate. To improve the accuracy of evaluation of the corrosion rate, the B value must be set accurately. Hence, this value should be further investigated.

- To determine the corrosion state of steel, the half-cell potential, macrocell current and mass loss techniques are easier than the polarisation techniques, but both half-cell potential and macrocell current techniques are qualitative, and the mass loss technique is destructive. The EIS technique is sophisticated but interpretation requires expert knowledge and the measurement is sensitive to experimental conditions. The TEP technique is destructive and time-consuming, although it can be used to estimate the *B* value. The PT technique is rapid and less destructive than other DC techniques, but during analysis, the capacitance value cannot be extracted directly, leading to an error in estimating the polarisation resistance. Finally, the LPR technique is

convenient, but it cannot evaluate ohmic resistance. Therefore, among the techniques used in this study, the GP technique is the most practical to evaluate corrosion of steel due to its rapid response and easy analysis

- The corrosion rates with different *B* values were compared with the corrosion rate from the mass loss method. According to González *et al.* (1995), for chloride-induced corrosion, the corrosion rate obtained from the mass loss method is 10 times higher than that obtained from the polarisation technique. However, in this study, the difference was sensitive to *B* values. The difference in corrosion rate between non-destructive methods and destructive methods using the *B* value obtained from the TEP technique and a traditional value (=26 mV) were ~ 53% and ~ 28%, respectively. On the other hand, the corrosion rates using the *B* value obtained from the PT technique were 6.3-15.6 times lower than the rates from the mass loss method.

- From the visual inspection, cracking on the concrete surface was observed. This was caused by chloride-induced corrosion. This cracking happened within a short time after depassivation in this study. Hence, it is reasonable to determine the limit state of concrete structures in marine environments with time to corrosion. In addition, it would be more appropriate to set the propagation period as a fixed value, such as LIFE 365 (Ehlen 2012), instead of calculating the value using computational modelling in terms of practical application as corrosion rate is influenced by a wide range of factors that cannot be controlled.

CHAPTER 7
MONITORING THE ELECTRICAL RESISTANCE OF CONCRETE

7.1 Introduction

The service life of reinforced concrete is determined by the performance of the concrete cover-zone as the latter plays an important role in preventing the ingress of aggressive agents. Steel corrosion caused by chloride attack is the main concern in evaluating durability and performance of reinforced concretes. The deterioration rate, including the rate of chloride ingress and the corrosion propagation rate, is influenced by the permeation properties of the cover concrete. Although the laboratory methods for chloride transport and estimating corrosion of steel have been developed, it is difficult to fully use these methods for field concrete due to limitations such as environmental exposure conditions, workmanship and material properties. Chloride profiling and half-cell potential mapping are laborious, and one-off investigations are therefore usually carried out. However, these investigations are limited in covering various influencing factors because of environmental exposure conditions.

To overcome these limitations, it is necessary to monitor the concrete cover-zone (covercrete) to study concrete under a range of exposure conditions over an extended period (McCarter *et al.*, 2001, 2005). For example, Schieβl's ladder system can be used to detect corrosion of steel at discrete points within cover concrete (McCarter and Vennesland, 2004), but water, ionic and moisture movement are not detected with this system. Alternatively, electrical resistance measurements, using embedded electrode arrays (McCarter *et al.*, 2001, 2005) or multi-ring electrodes (Du Plooy *et al.*, 2013), can monitor moisture and ionic movement, but their interpretation requires caution since the measured values contain various effects such as a change in chloride content, a change in degree of saturation and a change in temperature.

This Chapter monitors the electrical resistance of the concrete within the covercrete and on the steel surface to study chloride movement and corrosion propagation.

7.2 Experimental

The sample and electrode details used in this study are presented in Chapter 4. Embedded electrode arrangements can have limitations. The electrode arrangement could cause interference with the natural distribution of the aggregate even though the electrode tip was enough large (> maximum aggregate size). When the aggregate (a non-conductive material) was congested between electrodes, the measured resistance could be significantly larger compared to the original resistivity of concrete. In addition, calibration is required to calculate electrical resistivity when using this method as the electrical field between electrodes is non-uniform. Thus, the resistivity, which is independent of electrode geometry, could not be calculated with equation (2.21) but was, instead, determined using a geometrical factor obtained from an empirical relation (McCarter *et al.*, 2013a) or computation model (Angst *et al.*, 2011c). Nevertheless, this method is attractive. After installation of the electrodes in concrete structures, the measurement can be continuously monitored without considering the service life of the electrode.

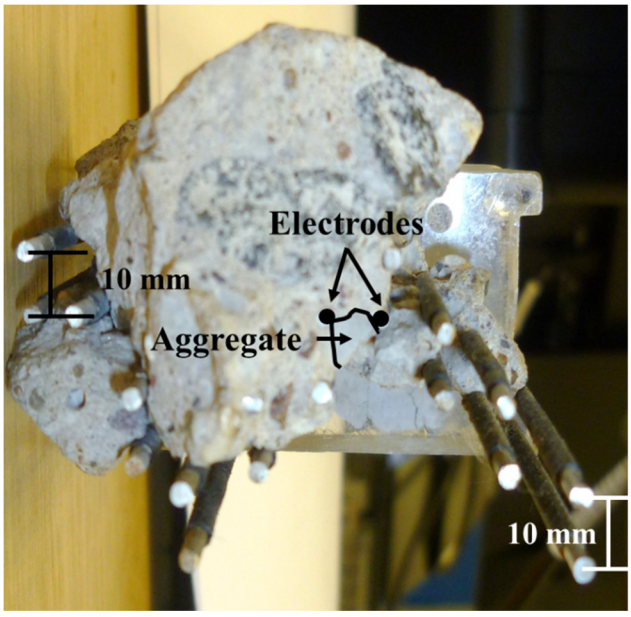

Figure 7.1 Distribution of aggregate around electrodes.

7.2.1 *Experimental set-up*

Electrical resistance measurements were manually taken using an LCR meter (Hewlet Packard 4263B) with a signal amplitude of 350 mV at 1 kHz. These values were used to

minimise the polarisation effect at the electrode-sample interface (McCarter and Brousseau, 1990). At the end of every wet and dry cycle, the electrical resistance was measured to confirm resistance change. Two different types of the electrode array were used, as shown in figure 4.4 and described below:

(i) The first array comprised four pairs of 2-pin electrode, with centre-to-centre spacing of 10 mm. The pairs of 2-pin electrode were embedded at four discrete points, i.e. 5, 15, 25, and 35 mm from the exposure surface for chloride ingress. To avoid measurement noise due to the presence of mild steel and a wall effect, the electrodes were mounted with 50 mm length from the surface and parallel to the mild steel. In addition, to detect the effect of chloride on the 2-pin electrode pairs, the resistance of 2-pin electrode among 4-pin electrodes installed under the 2-pin electrode pairs was measured, as shown in figure 4.4 (a). Thus, it was considered that the measured resistance of the 2-pin electrode in the 4-pin electrode only changed with hydration.

(ii) The second array consisted of three sets of 4-pin electrodes with uniform horizontal spacing of 10mm, which simulated a Wenner electrode arrangement. One of 4-pin electrode was positioned onto the sleeved part of the steel, thereby insulating it from the mild steel bar and avoiding conduction through the steel (figure 4.4 (b)). A second array was installed at the mid-point between the two parallel mild steel bars (figure 4.4 (c)), and a third array was mounted under the 2-pin electrode pairs at 70mm depth from the surface (figure 4.4 (d)), which provided the reference resistance in the progress of normalisation, discussed below.

7.2.2 *Electrical measurement*

Concrete can be regarded as a conductive material comprising non-conductive aggregate particles and ionically conducting hardened cement matrix. By applying an electrical field between the electrodes (see figure 7.2 (a)), the conduction of concrete was determined through connected pores filled with ions (McCarter *et al.*, 2001). The relation can be written as follows:

$$\rho_{bulk} = \rho_p \frac{\xi}{S_r \emptyset} \tag{7.1}$$

where ρ_{bulk} is the resistivity of bulk concrete (Ω·m), ρ_p is the resistivity by ionic concentration in the pore solution (Ω·m), ξ is the tortuosity of the capillary pores between a pair of electrodes, S_r is the saturation degree of the pore and $\emptyset$ is the porosity.

According to the above equation, the resistance of concrete is influenced by pore structure, degree of saturation and chemistry of the pore solution. In other words, the resistance of concrete decreases due to the ingress of ions (chlorides) or an increase in moisture content, while resistance increases due to hydration, a reduction in moisture content due to drying and refinement of the pore by chemical reaction between cement hydrates and ions dissolved in the pore solution, e.g. the formation of Fridel's salt.

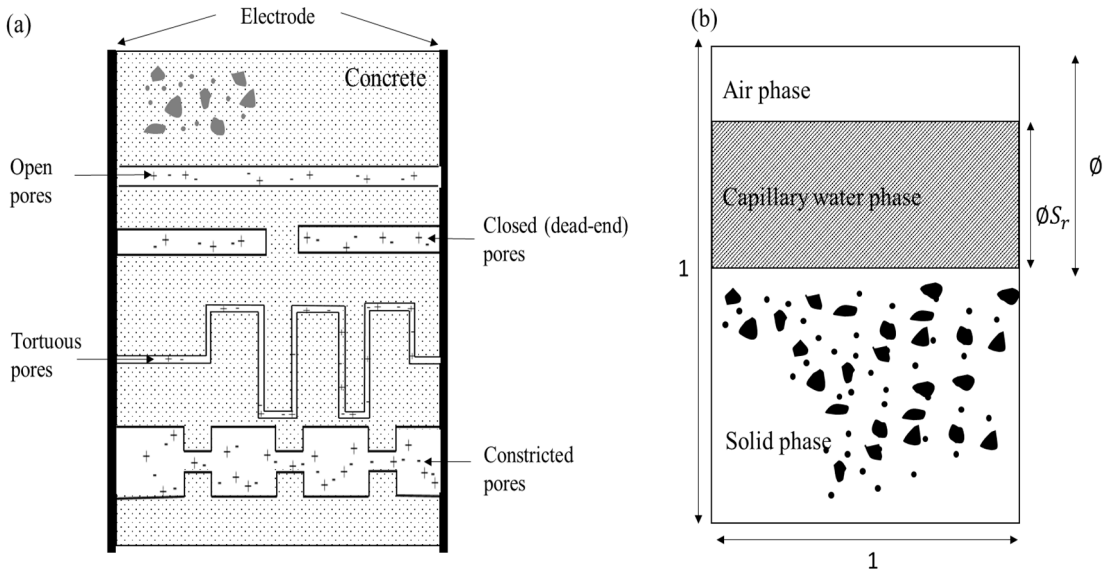

Figure 7.2 (a) Schematic diagram showing conduction in concrete and (b) a three-phase model for concrete (adapted from McCarter *et al.* (2001)).

The electrical resistance is influenced by various factors simultaneously; hence, it is easier to analyse data with the expression of the resistance (or resistivity) with normalisation than the absolute method. This expression can control the measured values with a controlled parameters, but is qualitative. The relative value is expressed by the reference value, as follows:

$$N_R = \frac{\mathrm{R}_t}{\mathrm{R}_{ref}} \tag{7.2}$$

where N_R is the normalised resistance, and R_t and R_r are the measured resistances (Ω) at time, t, and reference time, r.

In this study, the entire process of chloride-induced corrosion in reinforced concrete was investigated with electrical resistance measurement. The resistance monitoring data were analysed with influencing factors including moisture movement, chloride-content and ionic movement caused by corrosion. The results are presented in the following sections.

7.3 Results and discussion

Electrical resistance is sensitive to concrete properties or conditions, as shown in equation 7.1. Under well-controlled conditions (laboratory conditions), electrical resistance is measured with a controlled parameter, but in the field, it is combined with all influencing factors. For practical purposes, it is necessary to investigate the analysis method for the electrical resistance of concrete. This study monitored the electrical resistance of concrete subjected to a simulated chloride environment.

7.3.1 *Electrical resistance monitoring*

Electrical resistance is increasingly garnering interest from engineers and researcher because it is an easy and rapid method. However, the data analysis is still difficult for the following reasons: (i) the value fluctuates with temperature; (ii) the value is sensitive to moisture content, and (iii) the value is affected by hydration or chemical reactions in concrete. Therefore, in this study these factors are considered or offset to improve the analysis.

As-measured electrical resistance

Figure 7.3 and 7.4 present examples of as-measured data for the different electrode arrangements. Figure 7.3 shows that at 5 mm depth, the electrical resistance fluctuated significantly with time compared to other depths. The main reason is the changing moisture content in this region. Differences in the resistance between the end of the wetting phase and the end of the drying phase within a cycle were irregular as, in addition

to moisture-content, influencing factors such as temperature, refinement of the pores and chlorides in the pore solution affected the results.

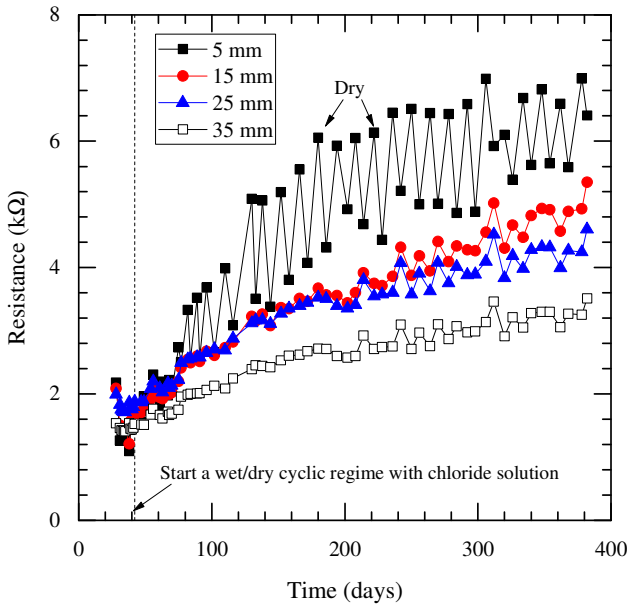

Figure 7.3 Example of monitoring electrical resistance with 2-pin electrode arrangements (for CEM I concrete, w/b=0.4).

This study also included 4-pin electrode measurements. To this end, the equation referred to as a modified Wenner equation (equation (7.3)) can be used to convert the measured resistance into resistivity, which is independent of geometry. However, the theoretical background for the assumption of the equation are not perfectly valid (Angst and Elsener, 2014). Figure 7.4 presents the electrical resistivity using the 4-pin electrode measurement. All values increased continuously with depth, and the *oscillation* of the resistivity resulting from the wet/dry cyclic regime was minimal. This implies that a reduction in moisture content by drying or a sudden inflow of chloride by capillary sorption, especially at steel depth (25 mm depth), is marginal. Note that as-measured resistance is also required to quantify concrete properties.

$$\rho = 4\pi aR \tag{7.3}$$

where ρ is the resistivity (Ω·m), R is the resistance (Ω) and a is the electrode spacing (m).

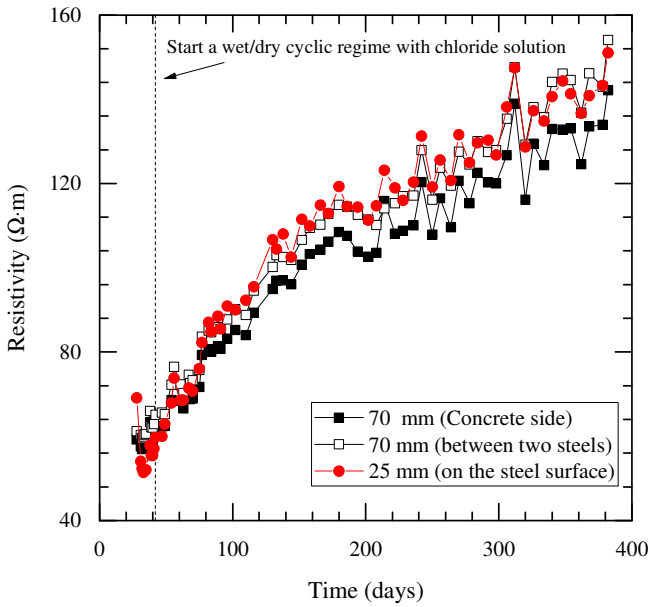

Figure 7.4 Example of monitoring electrical resistance with 4-pin electrode arrangements (for CEM I concrete, w/b=0.4).

Temperature effect

Electrical resistance is affected by ambient temperature. As the electrical conduction in concrete mainly occurs through mobile ions, the measured resistance is dependent on temperature hence it is necessary to 'correct' the electrical resistance to a predefined reference temperature (e.g. 20ºC). It has been found that the electrical resistivity can be related to temperature through the Arrhenius relationship (Chrisp *et al.*, 2001; McCarter *et al.*, 2012).

$$\rho_{ref} = \rho_M e^{\frac{E_a}{R}\left[\frac{1}{T_{K,ref}} - \frac{1}{T_{K,M}}\right]} \tag{7.4}$$

where ρ_{ref} is the corrected resistivity (Ω·m); $T_{K,ref}$ is the reference temperature (=293.15 K in this study) (K); ρ_M is the measured resistivity (Ω·m) at material temperature, $T_{K,M}$ (K); R is the gas constant (8.314 J/mol·K); and E_a is the activation energy for conduction processes in concrete (kJ/mol).Alternatively, the following formula can be used to consider temperature effect on the electrical resistance of concrete, which is applicable to electrolytic solutions. The formula is only valid within a narrow range of temperature (± 5 ºC).

In this study, equation (7.5) was used to reflect the effect of temperature for laboratory samples. The α value (the temperature coefficient) for concrete, irrespective of type of binder and w/b, was taken as 0.035 ºC^{-1} following McCarter *et al.* (2005). This was done because (i) there is a dearth of information on the activation energy for concrete mixes, (ii) the temperature fluctuation is narrow in laboratory conditions, and (iii) the change in the electrical resistance by temperature is marginal compared to other effects.

$$\rho_{ref} = \rho_M\left[1 + \alpha(T_{C,M} - T_{C,ref})\right] \quad (7.5)$$

Where $T_{C,M}$ or $T_{C,ref}$ is the material temperature or the reference temperature (ºC), α is the temperature coefficient (ºC^{-1}).

The values measured by the thermistor were converted into '*Celsius degree*' using equation (7.6), are presented in figure 7.5 (McCarter *et al.*, 2012). The temperature in the laboratory fluctuated within a narrow range (~ 19 – 23ºC). Thus, the influence of temperature on resistance was negligible. However, with larger fluctuations of temperature in field conditions, temperature correction must be considered. As shown in figure 7.5, the trend line for the resistance becomes smoother after correction of the resistance with the temperature coefficient. Note that all electrical resistance presented in this study were corrected to a reference temperature of 20 ºC.

$$T = [\mathrm{a} + \mathrm{b}ln\mathrm{R} + \mathrm{c}(ln\mathrm{R})^3]^{-1} - 273.15 \quad (7.6)$$

where R is the measured resistance by the thermistor (Ω); T is temperature (ºC); and a, b, and c are coefficients depending on the type of thermistor accounting for 1.28×10^{-3}, 2.36×10^{-4}, and 9.31×10^{-8} K^{-1}, respectively.

Convective effect

Under a wet/dry cyclic regime (e.g. tidal action), drying involves moisture movement from inside the concrete to the exposed surface, thereby creating a moisture gradient, while aggressive ions additionally/rapidly penetrate into concrete during wetting. The region influenced by the wet/dry phase has been termed *'the convective zone'*, and it is generally considered that the transport mechanism within this zone is different from that of concrete have a stable moisture condition.

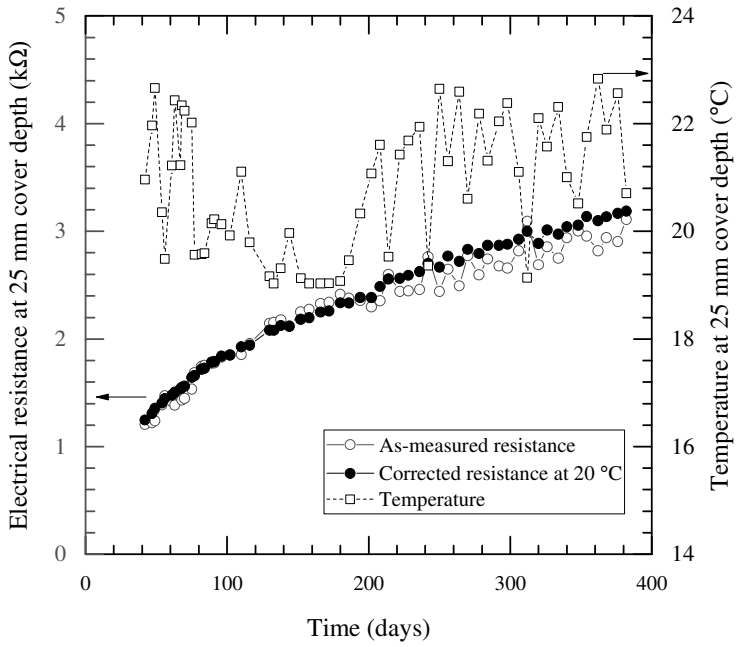

Figure 7.5 Correction of electrical resistance for temperature and monitoring the temperature of concrete using a thermistor embedded in concrete at 25 mm of cover depth (CEM I concrete, w/b=0.4).

For example, in the tidal-zone of marine structures, a successive supply of chlorides by wetting occurs, along with evaporation and salt crystallisation by drying. Seawater absorption within the convective zone leads to rapid chloride ingress. Therefore, it is necessary to confirm the convective zone of concrete subjected to a wet/dry cyclic regime. As both the transport mechanism and the electrical resistance of concrete depend on degree of saturation, this study used a change in electrical resistance to evaluate the convective zone in which absorption dominates as transport mechanism.

The convective zone can be defined as a change in the electrical resistance of concrete subjected to a wet/dry cyclic regime. Within the convective zone, it can be observed that the electrical resistance changes with the wet/dry phase as the degree of saturation changes. This is quantified as:

$$r_e = \frac{\mathrm{R_{wet}}}{\mathrm{R_{dry}}} \tag{7.7}$$

where r_e is the electrical resistance ratio and $\mathrm{R_{wet}}$ and $\mathrm{R_{dry}}$ are the electrical resistance after the end of wetting (6 days) and drying (8 days) within one cycle, respectively.

Figure 7.6 shows *r* with depth. A value close to 1.0 indicates that degree of saturation was stable even though the surface of concrete was subjected to a wet/dry cyclic regime; a value lower than 1.0 occurs within the convective zone as the electrical resistance increased due to drying. Note that some values were measured with more than 1.0. These values are considered to reflect either an increase in resistance due to the hydration process during wetting or a minor error during measurement.

The convective zone was found to be well-formed with an increase in w/b. For example, the *r* at 15 mm was close to 1.0 for concretes with w/b =0.4 regardless of type of binder, while the ratios for CEM III/A (w/b=0.6) concrete and CEM II/B-V (w/b=0.6) concrete were close to 1.0 at 25 mm of cover depth. All values for CEM I (w/b=0.6) concrete were less than 1.0 at all depths. This is because the pore structure in concretes with high w/b have an increased connectivity as well as a high porosity; thereby, an increase in w/b results in a rapid ingress of aggressive ions in concrete.

It was also observed that the convective zone changed with time, especially for CEM II/B-V concrete. This result is similar to that of a previous study (Chrisp *et al.*, 2002). For CEM II/B-V concrete, irrespective of w/b, the convective zone was reduced with increasing wet/dry cycles due to on-going hydration and pozzolanic reaction. For CEM I and CEM III/A concretes, the change in the convective zone with time was relatively small due to rapid hydration compared to CEM II/B-V concrete. Finally, the convective zones for CEM II/B-V (w/b=0.6) concrete and CEM III/A (w/b=0.6) concrete decreased with exposure duration, while the reduction was not observed in CEM I (w/b=0.6) concrete.

The convective zone can be estimated with electrical resistance profiling using small cube samples and chloride profiling (see Sections 5.3.2 and 5.3.3). The estimated convective zones for all samples were within 30 mm using bulk resistance measurements. The convective zones were formed within < 6 mm depth in some samples, corresponding to CEM II/B-V (w/b=0.4 and 0.6) concretes and CEM III/A (w/b=0.6) concrete; however, the convective zones obtained in this study (Section 7.3.1) were < 15 mm for all (w/b=0.4) concretes, < 25 mm for CEM III/A (w/b=0.6) and CEM II/B-V (w/b=0.6) concretes, and > 35 mm for CEM I (w/b=0.6) concrete due to large depths in the cube samples. From the chloride profiling results (Section 5.3.3), it was difficult to determine the convective zone. On the other hand, the presence of the convective zone indicates that different transport mechanisms, i.e. absorption and diffusion, coexist in concrete. Thus, the governing equation for complex transport mechanisms in the computational modelling becomes

complex compared to a governing equation for single transport mechanism. In other words, using a single value for transport rate is easier than using multiple values. In addition, there is no reference (e.g. the critical degree of saturation) to determine the boundary depending on the transport mechanism although this is beyond the scope of the present investigation.

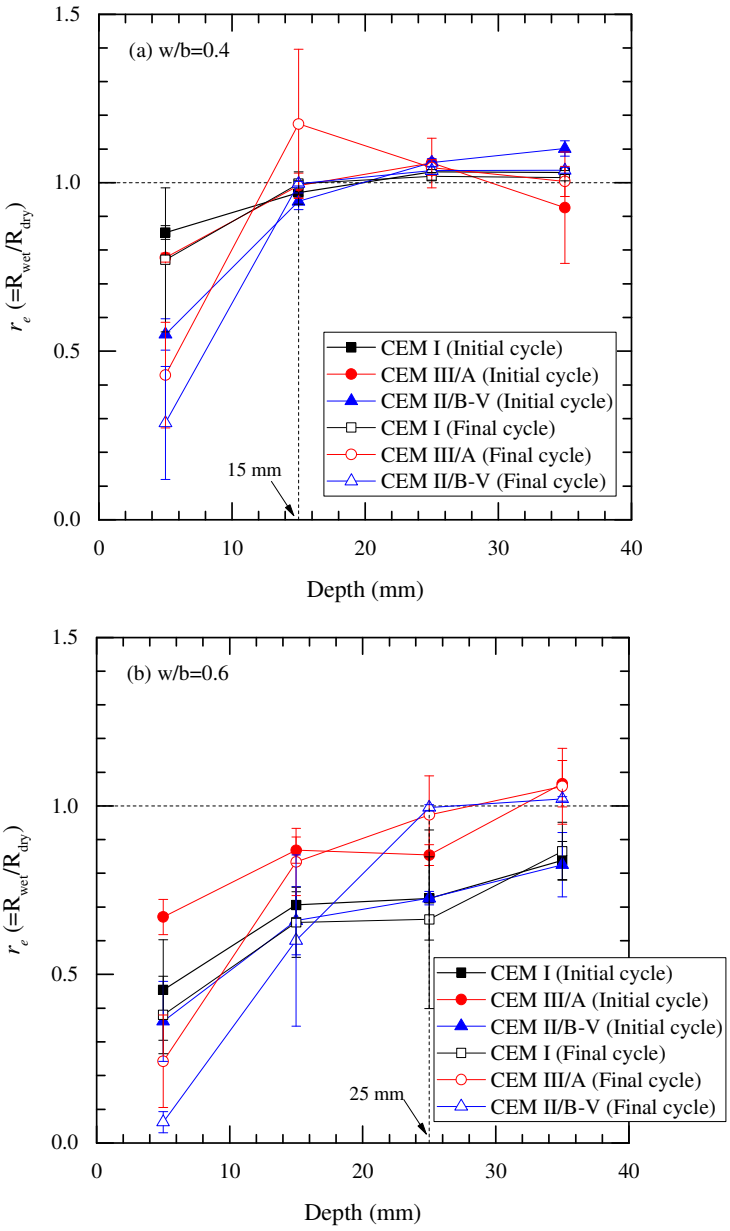

Figure 7.6 Convective effect with concrete having (a) w/b=0.4 and (b) w/b=0.6 at end of initial cycle (49 and 54 days) and at end of final cycle (376and 382 days).

Hydration process

The electrical resistance generally increases with time as the hydration process leads to refined pore structure. The hydration effect on the electrical resistance is high in early age

and for SCMs, the effect has been observed to last for 300 days (McCarter *et al.*, 2013a). To describe the deterioration process (e.g. chloride transport or corrosion) using the electrical resistance, a change of electrical resistance is considered due to hydration. It has been reported that the electrical resistivity continuously increases even though the sample is exposed to a solution of chlorides (Polder and Peelen, 2002; McPolin *et al.*, 2005). Consequently, it is difficult to understand the deterioration of reinforced concrete by chloride ingress without considering the hydration process and its influence on electrical resistivity.

To consider the effect of hydration on electrical resistance, the latter was monitored at 70 mm using a 2-pin electrode measurement. For comparison, the normalised values (N_R) are presented with type of binder and w/b in equation (7.8):

$$N_R = \frac{\mathrm{R_t}}{\mathrm{R_{ref}}} \tag{7.8}$$

where $\mathrm{R_t}$ is the electrical resistance at time (t days) and $\mathrm{R_{ref}}$ is the reference electrical resistance at 42 days.

Figure 7.7 presents N_R at 70 mm depth. It could be observed that the normalised resistances for most samples increased with time, except for CEM I (w/b=0.6) concrete. However, the increments evidently differed with type of binder, in particular for CEM II/B-V concrete. Firstly, the resistances for all CEM II/B-V concretes were up to 15 times higher at 382 days than at 42 days. This large and continuous increase was due to pozzolanic reaction and the hydration was continuous even after 382-days. Although the increments for CEM I and CEM III/A concretes were moderate, the increasing trend was similar to CEM II/B-V concrete; thereby the ongoing hydration could lead to a continuous chloride binding physically, especially at the surface of concrete due to the additional formation of hydrates (e.g. C-S-H gel). In other words, chloride binding is considered to be continuous until completion of hydration rather than an instant chemical reaction. Hence, it can be explained that a build-up of chloride at the surface was caused by ongoing hydration. On the other hand, for CEM I (w/b = 0.6) concrete, the electrical resistance increased until ~ 250 days, and became stable. This indicates that hydration is almost complete after 250 days considering chloride content and moisture movement at 70 mm. Thus, it can be confirmed that the hydration period is significantly influenced by w/b and type of binder.

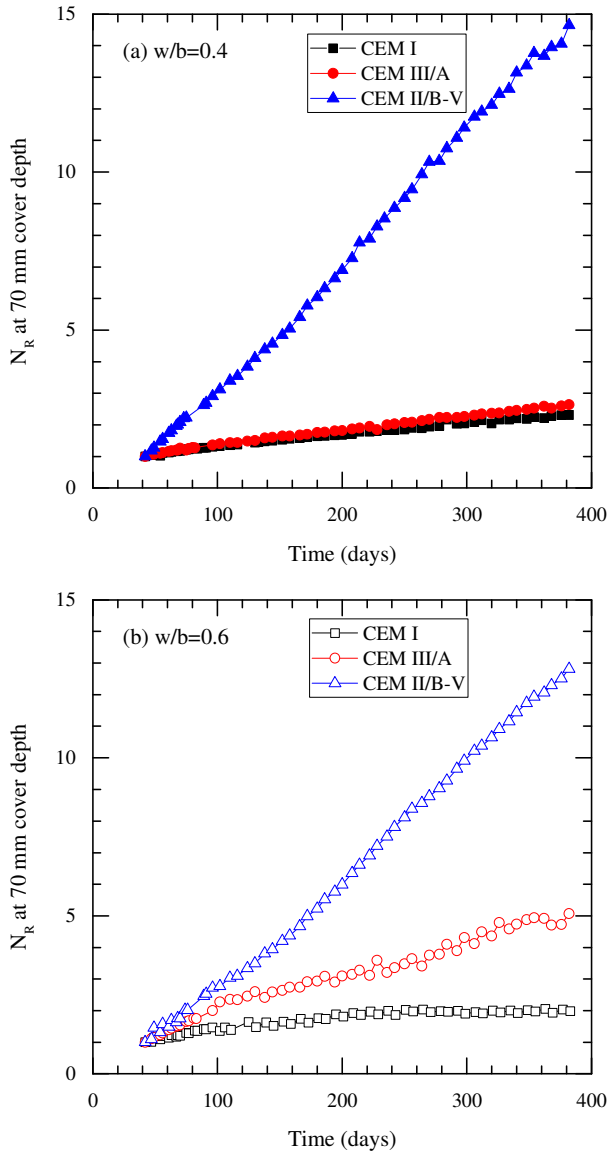

Figure 7.7 Normalised resistance of concrete with (a) w/b = 0.4 and (b) w/b = 0.6 at 70mm cover depth.

7.3.2 *Chloride transport monitoring*

Chloride itself does not deteriorate concrete, but the performance of concrete structures is degraded when free chlorides reach the steel depth. Thus, it is clearly important to detect, or monitor, the movement of chloride to determine the service life of concrete structures. In this sense, many studies have been conducted to determine the CTL on the steel surface (Alonso *et al.*, 2000; Nygaard and Geiker, 2005; Meira *et al.*, 2014) or to quantify the chloride transport rate (Nokken *et al.*, 2006; Safehian and Ramezanianpour, 2015; Kim *et al.*, 2016). Determining chloride content in the field (e.g. chloride profiling) is destructive and time-consuming (Andrade *et al.*, 2014). Laboratory data on chloride

transport has relied on using accelerated methods such as NT Build 492; however, these data are limited in their reflection of realistic environments such as unsaturated conditions or temperature variations. In the present study, chloride movement in concrete was monitored by monitoring changes in electrical resistance.

As presented in equation (7.9), the electrical resistance of concrete is related to the resistance of the pore solution, degree of saturation and pore structure. However, it is difficult to measure the resistance of the pore solution and tortuosity. Therefore, the normalisation method is applied to simplify the interpretation and is beneficial because the geometry factor is not considered.

$$\mathrm{R_t} = \rho_{p,t} \frac{L\xi_t}{A\emptyset_t S_{r,t}} \tag{7.9}$$

where R_t is the electrical resistance of concrete, $\rho_{p,t}$ is the electrical resistivity of the pore solution, A is the electrode area, L is the length between electrodes, $S_{r,t}$ is the degree of saturation, ξ_t is the tortuosity and $\emptyset_t$ is the porosity at the measurement time, t.

The electrical resistance changes depending on the pore-structure, pore solution and moisture-content with time (equation (7.10)). However, the value corresponding to each variable cannot be easily separated from the data in the case of chloride-contaminated concrete, as chlorides dissolved in the pore solution decrease electrical resistance while bound chlorides increase the resistance due to densification of the pore structure (Andrade *et al.*, 2011). On the other hand, considering that main variables affecting the electrical resistance are chloride and hydration and the degree of saturation is stable (N_{S_r} = 1), these variables can be substituted by: hydration (= N_{hyd}) and the chloride effect (= N_{Cl}).

$$N_R = \frac{\mathrm{R_t}}{\mathrm{R_{ref}}} = \frac{\rho_{p,t}}{\rho_{p,ref}} \frac{\emptyset_{ref} S_{r,ref} \xi_t}{\emptyset_t S_{r,t} \xi_{ref}} = N_\rho \cdot N_\phi \cdot \mathrm{N}_{S_r} \cdot \mathrm{N}_\xi \tag{7.10}$$

$$N_R = N_{cl} \cdot N_{hyd} \tag{7.11}$$

where N_ρ is the normalised resistivity for pore solution, N_ϕ is the normalised porosity, N_{S_r} is the normalised degree of saturation and N_ξ is the normalised tortuosity.

Assuming that hydration is uniform over the cover concrete (McCarter *et al.*, 2013b), at no chloride contaminated depth (= at 70 mm depth in this study), N_R can be used as N_{hyd} as N_{cl} is equal to 1; subsequently, N_{cl} is N_R divided by N_{hyd}.

$$N_{hyd} = N_{R\_70mm} \tag{7.12}$$

where N_{R_70mm} is the normalised resistance at 70 mm cover depth in this study.

The normalised resistance relating to chloride effect (N_{cl}) for concretes (w/b = 0.4) is presented with type of binder in figure 7.8 (a) – (c). N_{cl} for all concretes at 35 mm and 25 mm cover depth was distributed around 1.0 over the experimental period. According to the chloride profiling results in Section 5.3.3, chloride contents were distributed with < 0.2% by weight of cement at 25 mm cover depth. This assumes that chlorides have not influenced on the electrical resistance. However, it is noted that the resistance behaviour differed with type of binder at 5 mm cover depth. For CEM I and CEM III/A concretes, the N_{cl} increased with time, while the values decreased for CEM II/B-V concrete and then stabilised. As mentioned above, N_{cl} only considered the effect of chloride on the electrical resistance; in other words, an increase in the N_{cl} indicated densification and refinement of the pore structure, while a decrease in the N_{cl} indicated an increase in chloride content in pore solution. Therefore, assuming that bound chloride increased the resistance due to the refinement of the pore structures and free chloride decreased the resistance due to an increase in chloride content in the pore solution, chlorides at 5 mm cover depth were highly bound in CEM I and CEM III/A, but chlorides present in the pore solution existed predominantly as free chloride in CEM II/B-V concrete. In addition to hydration, the continuous increase of electrical resistance for concretes subjected to chloride environments (McPolin *et al.*, 2005; Polder and Peelen, 2002) could be caused by a chemical or physical reaction between chlorides and the hydration products. On the other hand, considering the lower chloride transport rate and increased porosity from the results regarding CEM II/B-V concrete in the previous sections (Sections 5.3.2 and 5.3.3), it could be deduced that pore connectivity in CEM II/B-V concretes was poor. In summary, the resistance of chloride transport in concrete with SCMs was high, but the mechanisms to reduce chloride transport differed with the SCMs.

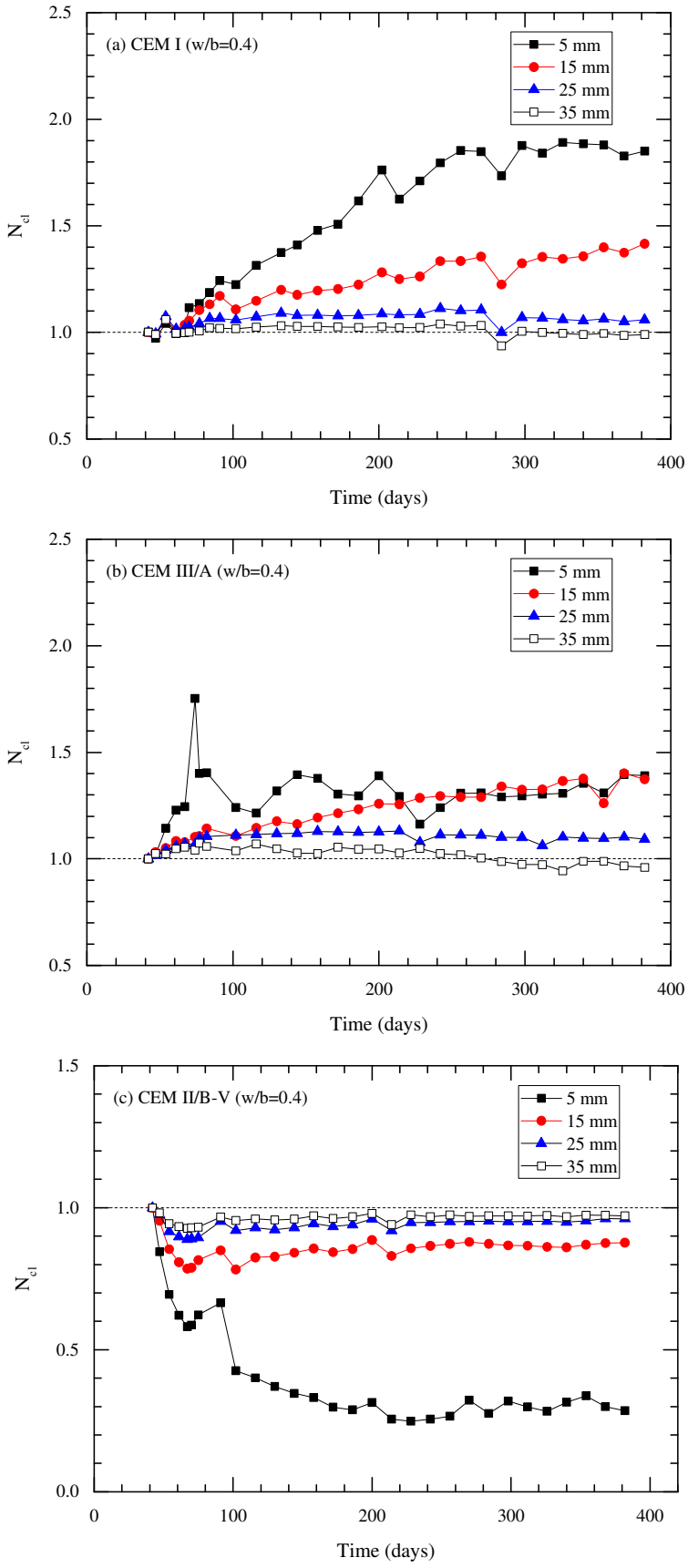

Figure 7.8 Normalised resistance of concrete (w/b=0.4) considering chloride effects for (a) CEM I, (b) CEM III/A, and (c) CEM II/B-V concretes using 2-pin electrode arrangement.

Figure 7.9 shows the normalised resistance (N_{cl}) of concrete with a high w/b (=0.6). First, in CEM I and CEM II/B-V concretes (w/b=0.6), all values were lower than 1.0 irrespective of cover depth. Furthermore, the greater the depth of the measurement, the higher the value of N_{cl}. This is also related to free chloride content. At 25 mm and 35 mm cover depth, chloride in CEM I (w/b = 0.6) concretes was detected after ~70 days, while CEM II/B-V (w/b = 0.6) concretes were influenced by chlorides across all depths from initial exposure time. This is because slower hydration in CEM II/B-V concrete leads to rapid ingress of chloride at an early age. Pozzolanic reaction reduces further penetration or accumulation of chloride at the depth as the N_{cl} became stable after ~ 130 days, i.e. the normalised resistances decreased during the initial period and then stabilised. Considering that surface chloride content increases with exposure time, stabilization can indicate that equilibrium was established between chloride binding rate and chloride ingress from the external source.

For CEM III/A (w/b=0.6) concrete, the value decreased due to free chlorides starting from 256 days at 15 mm depth, while the value at 25 mm depth slightly increased from 242 days. The opposite detection was observed. The electrical resistance measured was an averaged value corresponding to a nominal depth ± 5 mm (Chrisp *et al.*, 2002) and the change in N_{cl} indicated that chloride was detected by both electrodes at 15 mm and 25 mm cover depth. Starting from 256 days, free chloride was dominant at 15 mm, while at 25 mm bound chloride was dominant from 242 days. This explains that chloride binding is dependent on chloride concentration. The value at 35 mm cover depth remained at ~ 1.0 during the measurement due to lack of chloride ingress.

As can be seen in figures 7.8 and 7.9, different behaviour of chlorides were observed in concrete with the influence of the w/b and type of binder. Free chlorides dissolved in the pore solution penetrate into the concrete, leading to a reduction of electrical resistance due to an increase in ionic content of the pore solution. Bound chlorides are not available for conduction and result in an increase in electrical resistance. For chemical binding, chlorides react with calcium aluminate hydrates including monosulfate hydrates (AFm: $C_3A{\cdot}CaSO_4{\cdot}12H_2O$); Friedel's salt is then formed by ionic exchange of SO_4^{2-} with Cl^- (Hirao *et al.* 2005). It is known that the pore structure becomes denser through the process.

$$C_3A{\cdot}CaSO_4{\cdot}12H_2O + 2NaCl \rightarrow C_3A{\cdot}CaCl_2{\cdot}10H_2O \text{ (Friedel's salt)} + 2Na^+ + SO_4^{2-} + 2H_2O \quad (7.13)$$

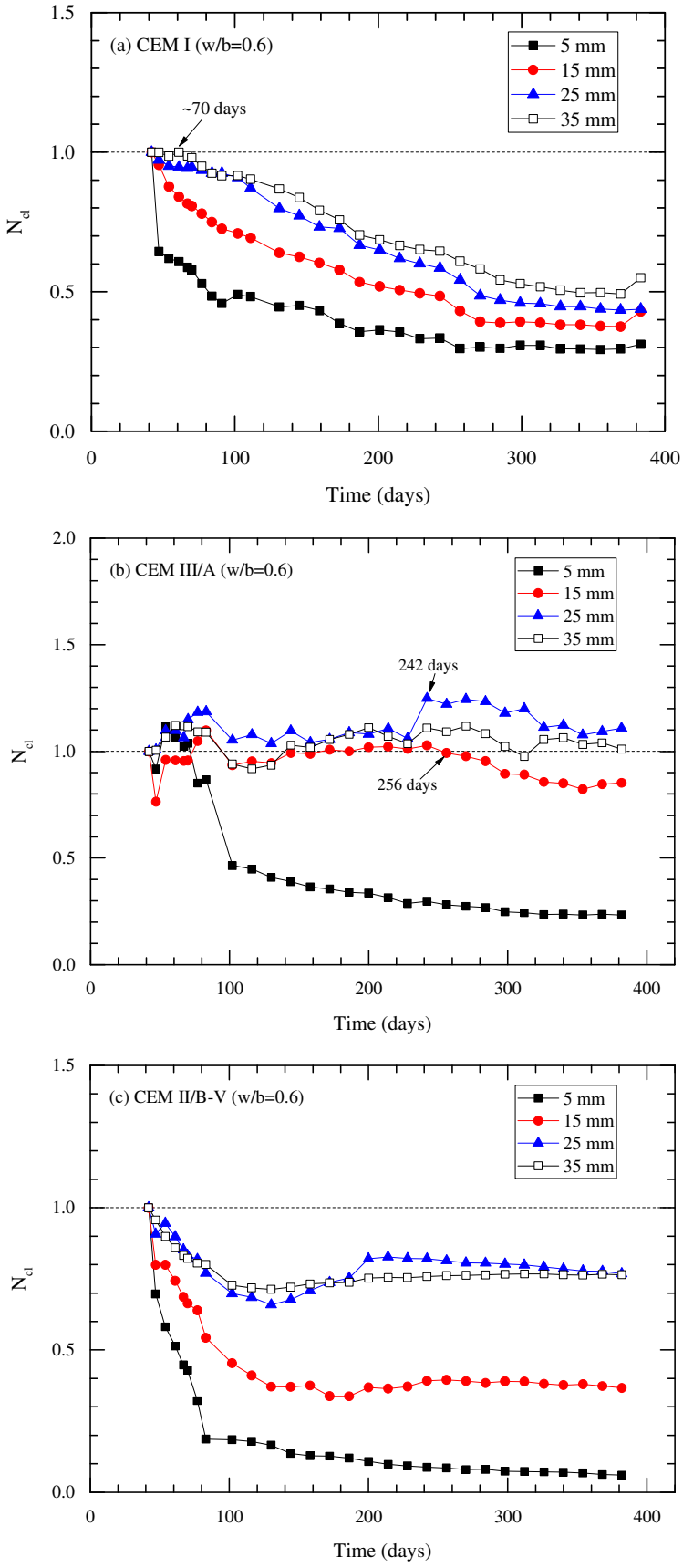

Figure 7.9 Normalised resistance of concrete (w/b=0.6) with time considering chloride effects for (a) CEM I, (b) CEM III/A, and (c) CEM II/B-V concretes using 2-pin electrode arrangement.

However, Hirao et al. (2005), reported that physical binding is more prominent in cementitious materials than chemical binding. Among hydrates in cement, C-S-H ($CaO-SiO_2-nH_2O$) is thought to bind chlorides with its large surface area. The ionic exchange between Cl^- in the pore solution and OH^- in the C-S-H layer is established during the process. It should be noted that the conductivity of the pore solution increases due to the higher conductivity of OH^- caused by the simple ionic exchange by physical chloride binding; however, in this study, the electrical resistance showed an increasing trend for the low w/b at 5 mm cover depth. From the results, it can be deduced that physical binding can also contribute to a densification of pore structures and a reduction in the electrical resistance by OH^- can be cancelled out by leaching. However, additional investigation is required to confirm the mechanism for chloride binding physically and to quantify chloride transport rate using electrical resistance measurement.

7.3.3 *Corrosion monitoring*

The previous section confirmed the changes in electrical resistance by chloride transport, and monitored the electrical resistance for chloride transport. On the other hand, with regard to the electrochemical reaction, the electrical resistance measurement can also detect corrosion of steel caused by chlorides. Theoretically, ionic movement between the cathode and anode is required for propagation of corrosion as the corrosion process is electrochemical. During the corrosion of steel in concrete, ions formed in the cathode area move into the anodic area through the pore network; hence, the movement to sustain corrosion is influenced by the electrical resistance of the concrete. In addition, it has previously been reported that the cathodic area is largely distributed up to a few meters from the anodic site (Elsener, 2002), although concrete resistance is an important factor to determine the anodic/cathodic ratio. Therefore, to investigate the ionic movement through concrete during the corrosion process, electrical resistances were monitored at the steel depth and 70 mm of cover depth, respectively.

Normalizing technique used was also employed here as an analysis method. Although the electrode arrangements are described in Section 4.3 and in figure 4.4, to ensure understanding, the arrangements are briefly summarised below.

(i) 4-pin electrode system at 25 mm cover depth, i.e. steel depth, were positioned above the insulated steel in the transverse direction. The electrical resistance change of concrete was monitored using corrosion on the steel (figure 4.4 (b)).

(ii) 4-pin electrode system at 70 mm cover depth was positioned between two steel bars which were connected electrically to form a large cathode area. The electrical resistance change of concrete was monitored the between anode and cathode areas, corresponding to upper and bottom steel, respectively (figure 4.4(c)).

(iii) 4-pin electrode system at 70 mm of cover depth were installed under the 2-pin electrode system and were used for the detection of chloride transport. The electrical resistance (R_{conc}) obtained by the electrodes was used as a reference value (figure 4.4 (d)).

To evaluate a change in the electrical resistance caused by corrosion process, a variable (= N_{corr}) is added in equation (7.14) and N_{corr} is N_R divided by $N_{hyd} \cdot N_{cl}$

$$N_R = N_{cl} \cdot N_{hyd} \cdot N_{corr} \tag{7.14}$$

N_{hyd} is defined as $N_{R_{conc}}$ (= the normalized resistance for R_{conc}) in this study as the electrical resistance (R_{conc}) is only related to hydration which has not been influenced by chlorides (N_{corr} and N_{cl} = 1). Note that N_{cl} is negligible at 70 mm cover depth, but at 25 mm, the electrical resistance is affected by chlorides, especially in CEM I (w/b=0.6) and CEM II/B-V (w/b=0.6) concrete; thereby N_{cl} should be considered at 25 mm cover depth. In this study, the N_{cl} at 25 mm cover depth from the previous section (Section 7.3.2) is used. Data containing errors due to faulty electrodes were omitted from the calculation (see Appendix C3.2).

Figure 7.10 presents the normalised resistance ($N_{corr} \times N_{cl}$) before correction at 25 mm cover depth. Two trends were observed at 25 mm cover depth as shown in the previous section, one is that the values were >1.0, and the other that the values were <1.0. From the result, the normalised resistance at 25 mm is primarily affected by chlorides; thereby values >1.0 indicates that more bound chlorides are formed, but values <1.0 would indicate increasing chloride content within the pore solution before the correction. The general trend for the 4-pin electrode measurements is similar to that for the 2-pin electrode measurements, but the values for the 4-pin electrode measurements were slightly greater than those for the 2-pin electrode measurement. Especially, for CEM III/A (w/b=0.6) concrete, the normalised resistance using the 4-pin electrodes was < 1.0 at 25 mm cover depth, but the normalised resistance using the 2-pin electrode was ~ 1.0 over the test

period. It appears that the measurement range for the 4-pin electrode arrangement is wider than that for the 2-pin electrode arrangement.

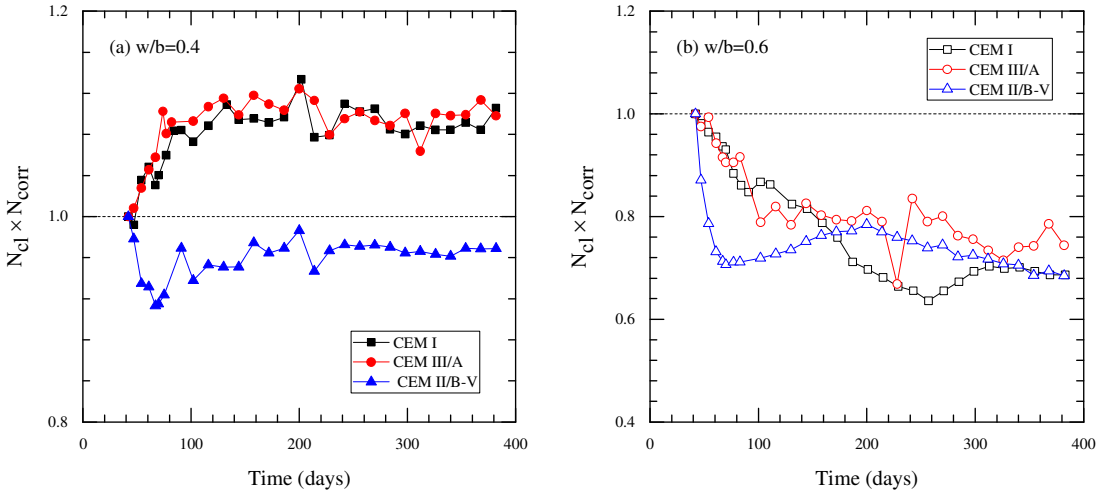

Figure 7.10 The normalised resistance, $N_{corr} \times N_{cl}$, of concrete (a) w/b=0.4 and (b) w/b=0.6 at 25 mm cover depth using 4-pin electrode arrangement.

Except for CEM I (w/b=0.6) concrete, the data in the passive state were averaged from three replicates. The passive state of steel was determined by electrochemical measurements including polarisation techniques, macrocell current measurement, and half-cell potential measurement. For CEM I (w/b=0.6) concrete, the depassivation times for the steel were variable; as a result, data for each steel is presented.

Figure 7.11 presents N_{corr} for steel in the passive state, except for CEM I (w/b=0.6) concrete. The N_{corr} at both 20 mm and 70 mm cover depth remained at ~1.0 for all samples throughout the test period. There appeared to be no influencing factors at that depth other than the hydration process. After correction, it appears that all values at 25 mm cover depth were shifted toward 1.0. It indicates that ionic movement from the cathode to the anode is negligible in the passive state.

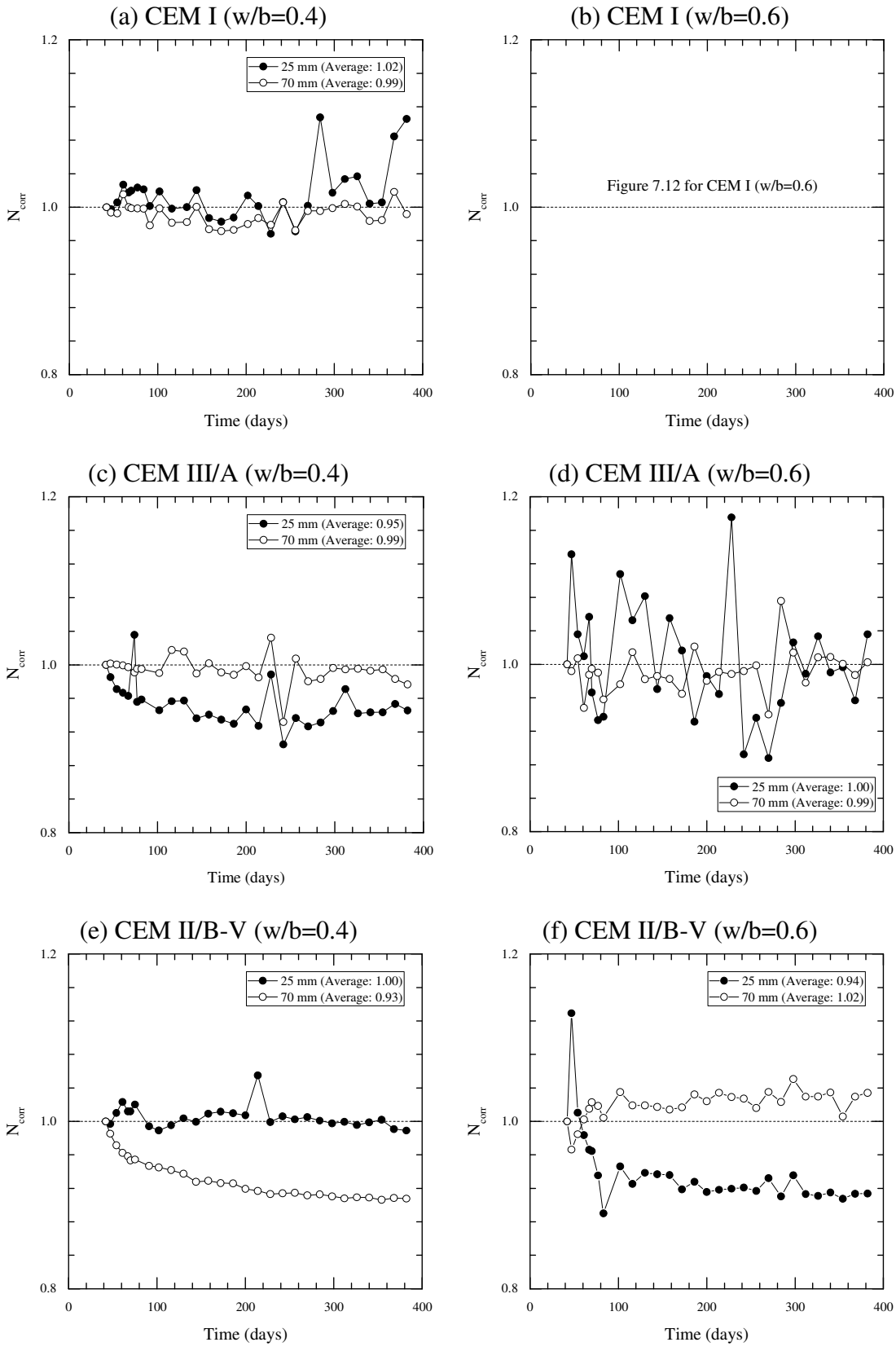

Figure 7.11 The normalised resistance, N_{corr}, of concrete with time for concrete samples using 4-pin electrode arrangement.

The normalised electrical resistance in the active state of steel is shown in figure 7.12. From the results, whether the resistance changed because of the corrosion process remains unclear compared to time to corrosion initiation obtained from half-cell potential measurement. At 25 mm, a decrease in the resistance (N_{corr}× N_{cl}) started from an initial period before the correction of N_{cl} and the values (N_{corr}) were shifted toward 1.0 after correction. The primary factor to change the resistance was chlorides inclusion in the pore solution rather than ionic movement by corrosion process. Also, a change in the resistance (N_{corr}) caused by the ionic movement after corrosion of steel at 70 mm depth was not distinguished from the measured resistance. It is possible that concrete resistance confined ionic movement within a smaller area than expected. In this case, the range of ionic movement would be limited.

From figure 7.12, it is interesting to note that for Sample No.1 among three replicates (CEM I concrete, w/b=0.6), N_{corr} increased after 257 days at 25 mm depth (Figure 7.12 (a)) and after 229 days at 70 mm depth (figure 7.12 (b)). Time to corrosion initiation for each steel, based on the result of corrosion tests (i.e. half-cell potential measurement) was 191 and 171 days, respectively, and cracks on the surface of Sample No.1 were observed at ~320 days. It could be deduced from the results that an increase in the N_{corr} is caused by internal cracking caused by corrosion products on the steel surface.

A decrease in N_{corr} was evident at 70 mm depth in Samples No.2 and 3 at 313 and 243 days, respectively. It is postulated that cracks accelerated the ingress of chloride. Furthermore, it was confirmed that the counter electrode, located at 100 mm from the concrete surface, was also corroded for Sample No. 3. Considering that chloride concentration at 100 mm obtained from the chloride profile (figure 5.9 in Chapter 5) is negligible, corrosion on the counter electrode at 100 mm would be related to a rapid ingress of chloride caused by cracks. From the visual inspection, it is interesting that corrosion products were formed on the upper steel surface, i.e. close to the exposure surface of concrete, but that cracks were formed in both directions, i.e. the upper direction and bottom direction from the result in figure 7.12 (b). In addition, as cracking behaviour is random, it is difficult to predict. This result is incompatible with the cracking by corrosion model in particular (Chen and Leung, 2015).

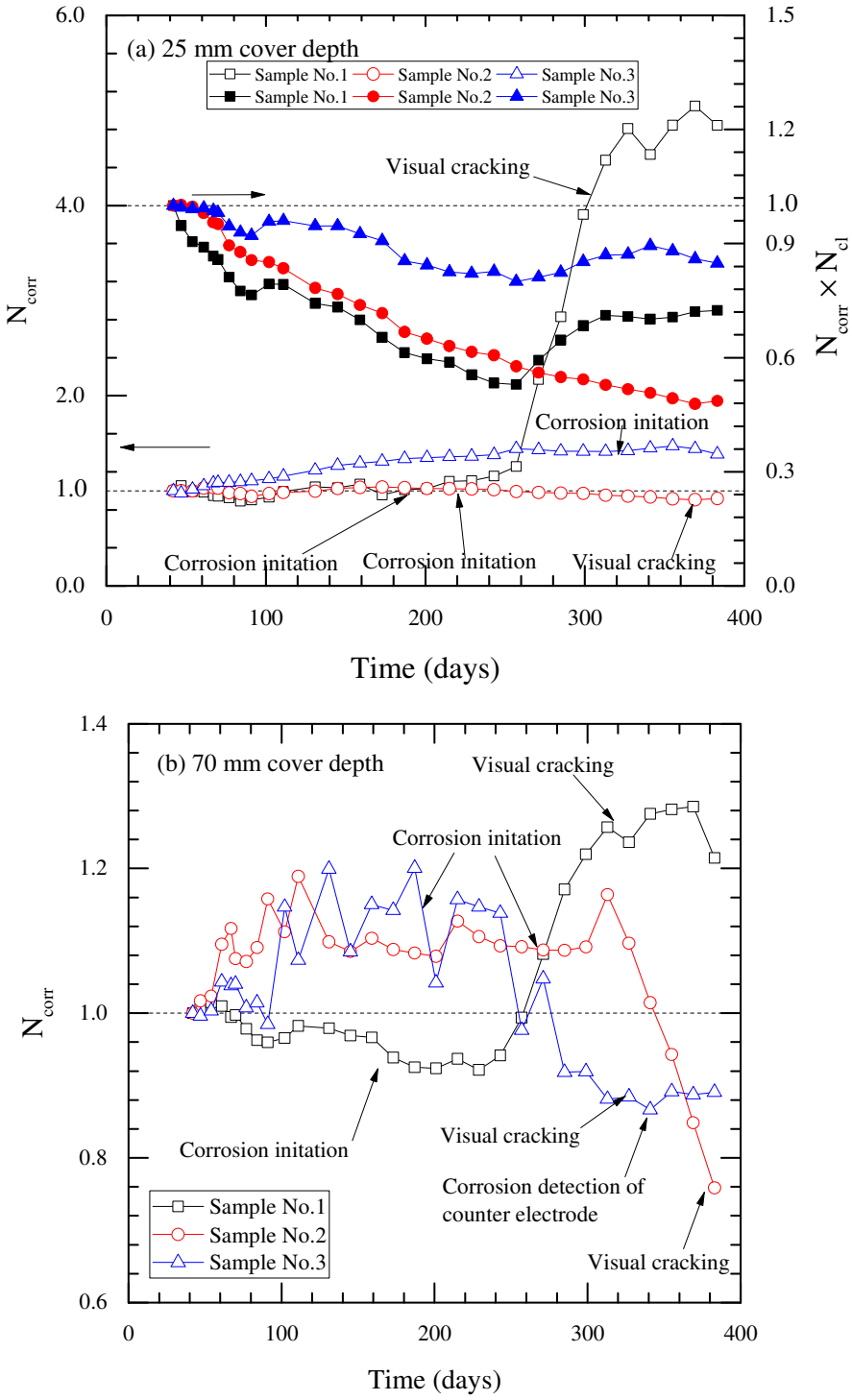

Figure 7.12 Normalised resistance, N_{corr} and $N_{corr} \times N_{cl}$, with time of exposure for CEM I (w/b=0.6) concrete at (a) 25 and (b) 70mm depth using 4-pin electrode arrangement ('open markers' N_{corr}, and 'closed markers' $N_{corr} \times N_{cl}$).

This study used a normalisation technique for electrical resistance in order to evaluate the corrosion behaviour of steel and chloride transport. This method is qualitative but could be used a monitoring technique. However, for computational modelling, the quantified value (e.g. resistivity relating to corrosion) is required as an input parameter. Therefore,

to deepen the understanding of the corrosion mechanism, and to refine the computational model for corrosion propagation, further research is required to identify the resistivity or normalised value relating to corrosion.

(a) Case 1

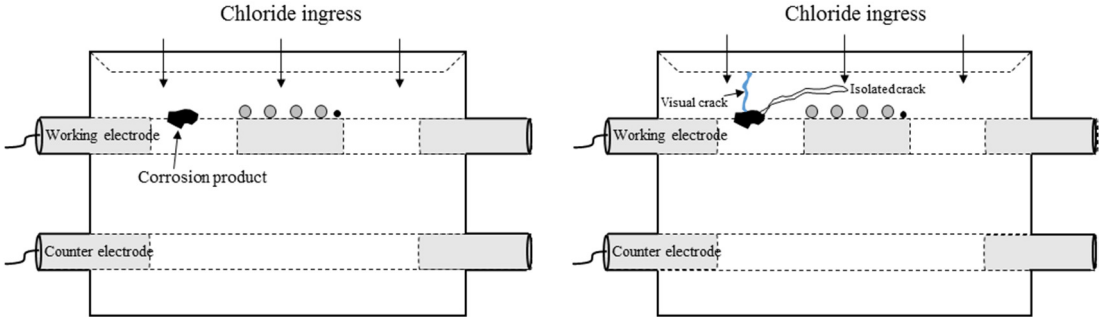

(b) Case 2

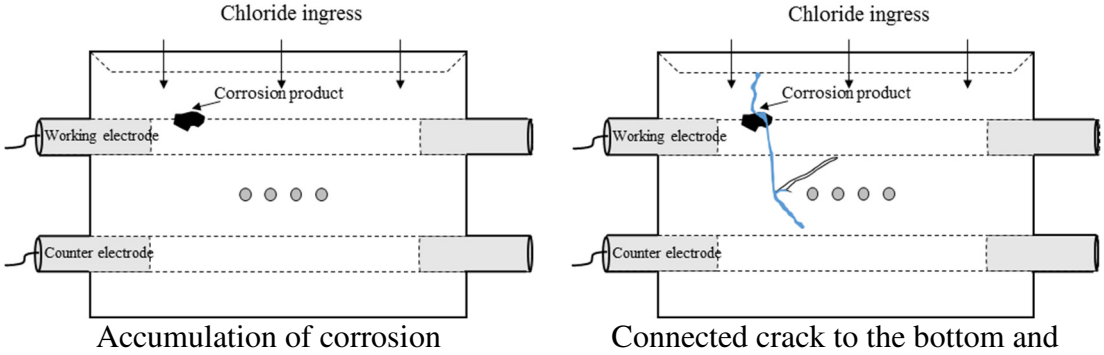

(c) Case 3

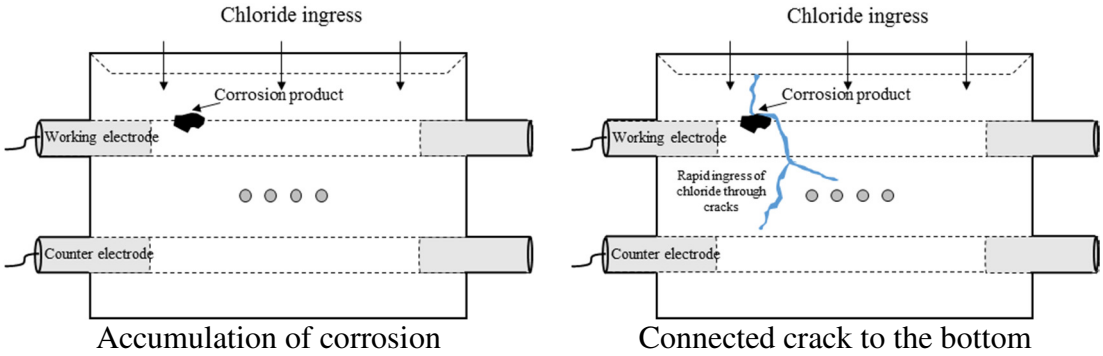

Figure 7.13 Schematics for cracking caused by chloride-induced corrosion; (a) Case 1 corresponding to Sample No. 1 at 25 mm depth, (b) Case 2 corresponding to Sample No. 1 at 70 mm depth and (c) Case 3 corresponding to Sample No. 2 and No. 3 at 70 mm depth.

7.4 Summary

Electrical resistance monitoring was employed to observe the deterioration of concrete subjected to a chloride environment. Tests were conducted up to 382 days. Chloride-induced corrosion of steel was only detected in CEM I (w/b = 0.6) concrete.

The main findings are summarised below.

- The electrical resistance of concrete changed due to chlorides and hydration. w/b is a significant factor to determine the electrical resistance for chloride ingress. For a low w/b, the resistances increased with time except for CEM II/B-V (w/b=0.4) concrete, while the resistances of concrete with a high w/b decreased with time at the chloride-contaminated depth of concrete. Regarding the effect of hydration on the electrical resistance, the normalised resistances for CEM I and CEM III/A concrete moderately increased with time, but the normalised resistance for CEM II/B-V concrete continuously increased with time due to pozzolanic reaction at 70 mm depth.

- After depassivation, a change of electrical resistance was expected due to ionic movement by electrochemical reaction. However, the movement by electrochemical reaction was not distinguished from the measured resistance because a change of electrical resistance caused by chlorides was dominant. Interestingly, the electrical resistance increased or decreased after cracking, but further investigation is required to determine crack patterns, which seemed to be random here.

- To analyse the data regarding the electrical resistance, a normalised value was used instead of the absolute value, i.e. the electrical resistivity. When a sample is influenced by various factors simultaneously, caution is required in the interpretation. This method is useful to control the influencing factors through the analysis process. However, the method is qualitative; therefore, it is difficult to determine a value for computational modelling. On the other hand, it is reasonable for understanding the deterioration behaviour of concrete.

CHAPTER 8
EVALUATING THE SERVICE LIFE OF CONCRETE STRUCTURES

8.1 Introduction

To obtain adequate service life performance, a performance-based approach has been gaining popularity over the prescribed approach. As part of the performance-based approach, predictive models relating to chloride transport or corrosion propagation are attractive. This is because there are limitations to obtaining laboratory/field data about concrete structures with regard to their long-term behaviour, whereas this behaviour is readily predicted through computational simulation (Ožbolt *et al.* 2011).

To improve the accuracy of the predictive model, field data are essential, particularly if the model has been developed based on laboratory studies. Therefore, it is necessary that the differences between field and laboratory conditions are reflected and the model should be refined with data obtained from field tests. This chapter presents a case study of concrete samples exposed to both the field and laboratory environments to update an existing model (ClinConc). Furthermore, the Chapter also discusses a comprehensive suite of tests (including the electrical resistance measurement) undertaken to evaluate the performance of concrete in the field.

8.2 Experimental

8.2.1 *Experiments for chloride transport*

To observe the long-term chloride transport behaviour of concrete exposed to a marine environment, and to obtain input data to update the predictive model, three tests were performed relating to chloride transport: the acid-soluble chloride test (sampling in Section 4.4.1 and measurement in Section 5.2.3), the degree of saturation test (sampling in Section 4.4.1 and measurement in Section 5.2.2) and the electrical resistance test. In addition, sample details and exposure condition are described in Section 4.6.

The electrical resistance of concrete was measured using embedded stainless-steel pin electrodes at discrete distances from the concrete surface. The measurement was

performed with an auto ranging logger using an AC voltage of amplitude 350 mV at a fixed frequency of 1 kHz, as shown in figure 8.1. To verify the applicability of the stainless-steel pin electrodes, the electrical resistivity of small cubes extracted from the electrode-embedded concrete was measured along with the degree of saturation to find input data to update the predictive model. Sampling for small cubes and measurement procedures are also given in Sections 4.4.1 and 5.2.2, respectively. To minimise the moisture loss during the measurement, the samples were kept in a sealed condition, as shown in figure 8.1.

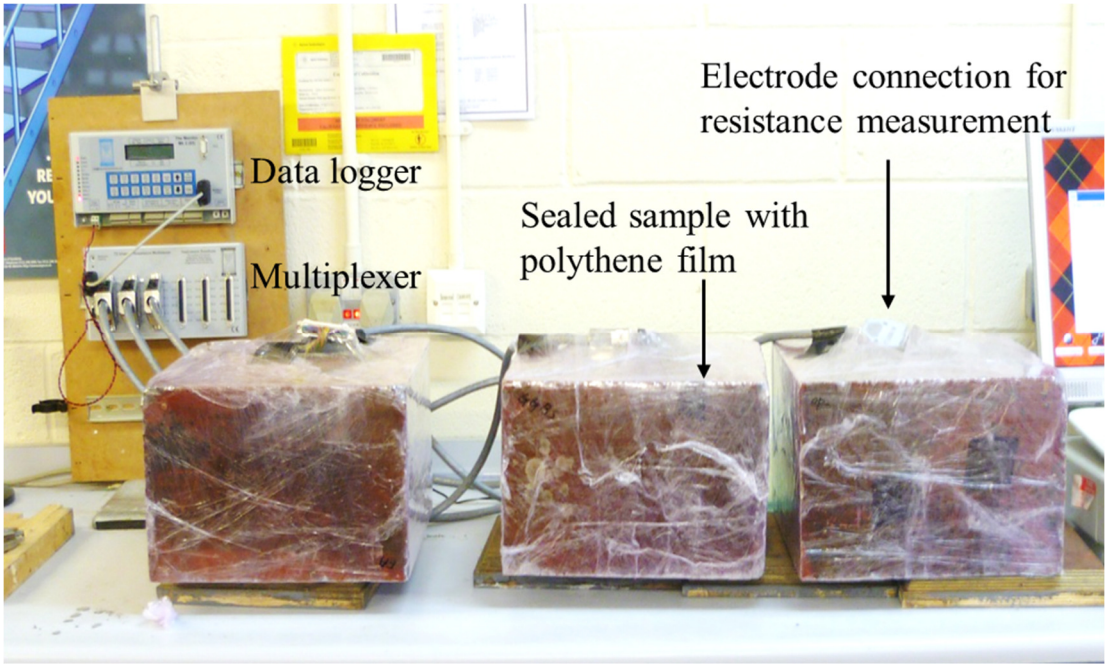

Figure 8.1 Electrical resistance measurement using a multiplexer in conjunction with a data logger.

8.2.2 *Experiments for corrosion*

The main concern regarding the deterioration of concrete structures exposed to chloride environments, especially a marine environment, is chloride-induced corrosion. The condition of steel was investigated using several electrochemical techniques including LPR, GP, EIS, PT and TEP. The experimental set-up and procedures for the techniques are given in Chapter 6.

The measurements were carried out for two steels embedded in each concrete slab as working electrodes. The embedded stainless-steel rod (Ø 6 × 200 mm) was used as

a counter electrode in the polarisation techniques. The exposed area of the working electrode was 100.53 cm^2 (Ø 16 × 200 mm).

8.2.3 *Monitoring electrical resistance using a remote-control system*

Electrical resistances of concrete exposed to a long-term marine environment were directly monitored using a remote interrogated system. Data from the Dornoch field site is received by a modem using a dial-up approach and the uploaded data are recovered in an Excel file using a software utility installed in the office-based computer. To manage the system effectively, the entire system is powered by a rechargeable battery using a solar panel (McCarter *et al.*, 2012). The main purpose of monitoring electrical resistance in this study was to investigate the activation energy of mature concretes with temperature as the hydration of concrete, especially containing SCMs, affects the electrical resistance at an early age (< 300 days), leading to an overestimation of the activation energy of concrete. The time interval between measurement cycles was set to a 6-hour cycle for samples exposed to the XS3 environment. The monitoring period was approximately 1 month (29 September, 2016 – 26 Octorber, 2016).

8.3 Results and discussion

8.3.1 *Evaluating chloride transport*

The main concern regarding the corrosion of steel in concrete is chloride concentration at the steel depth so having an accurate prediction of this content allows for a better estimation of the service life of the concrete structure. To evaluate performance, the following parameters relating to chloride transport were examined: chloride profiling, porosity and degree of saturation. This section investigates the updated parameters for the ClinConc model (Kim *et al.*, 2016), referred to as environmental factors, and modifies them for estimating chloride distribution.

Case studies for transport parameters

Chloride concentrations for the three samples retrieved from the field were measured with depth. The samples had been exposed to the marine environment corresponding to XS3 for 18 years. Figure 8.2 presents the chloride profiles for PC, GGBS/40 and FA/30 concretes. As expected, PC concrete had the highest chloride concentration at all depths. The chloride concentrations at the steel depth (50 mm cover depth) were 0.84, 0.15, and 0.25% by weight of binder for PC, GGBS/40, and FA/30 concrete, respectively. Meanwhile, it is accepted that the CTL for total chloride content in concrete is 0.4% by weight of binder according to BS EN 206 (British Standards Institution, 2014); however, for PC concrete, although the chloride concentration at the steel depth was higher than the accepted threshold level, no corrosion was detected with corrosion testing. However, the threshold value is still controversial due to many influential factors. In a chloride profile, erratic behaviour can be observed when a sample is exposed to wet/dry cyclic regime. The retrieved samples in this study were also exposed to long-term tidal action, but in the chloride profiles, erratic behaviour was not observed in the outer layer. Erratic behaviour is not necessarily observed in sample subjected to wet/dry cyclic regime (Nanukuttan *et al.*, 2008), but, from the result or the shape of the chloride profiles, it could be deduced that the main transport mechanism was diffusion and not absorption.

An analysis was conducted using Fick's second law to calculate the diffusion coefficient and surface chloride concentration. The first point was excluded in the progress of the calculation although there was no erratic behaviour in the outer layer. The diffusion coefficients were evaluated 1.39×10^{-12}, 4.21×10^{-13}, and 4.21×10^{-13} m^2/s for PC, GGBS/40, and FA/30 concrete, respectively and the surface chloride concentrations were 4.54, 4.46, and 5.56% (by weight of binder), respectively. SCM concretes were observed to be beneficial in resisting chloride transport.

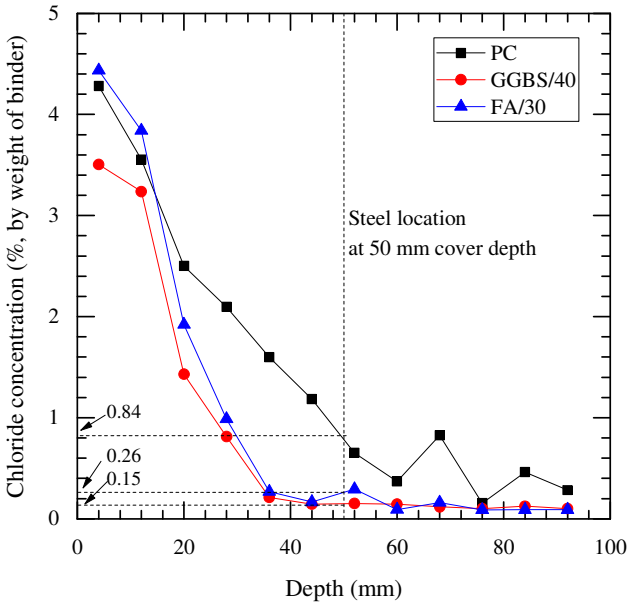

Figure 8.2 Chloride profiling of 18-year-old concrete (retrieved from the field) exposed to the XS3 environment.

For unsaturated concrete, the degree of saturation is one of the main factors in estimating chloride transport. According to Kumar (2010), the diffusion coefficient is influenced by the moisture-content of concrete. Considering only diffusion as a transport mechanism, low moisture-content in the pore leads to a low diffusion rate as ions only move through the pore solution; the tortuosity is also important, as ionic transport occurs through the inter-connected porosity. As shown in figure 8.3, the degree of saturation and the porosity of the field samples were measured with depth. The variation in the degree of saturation was minimal, which is similar to the finding presented in Chapter 5. It can be inferred that the moisture-content was relatively stable over the exposure period. However, the degree of saturation at the nominal depth of 10 mm for all samples was higher than those at other depths. The averaged values for the degree of saturation over the full depth (125 mm) were 78%, 73%, and 63% for PC, GGBS/40, and FA/30 concrete, respectively. The porosity is also similar to the finding presented in Chapter 5. SCMs concretes had higher porosity than PC concrete. However, the porosity itself cannot be represented of performance of concrete in term of chloride transport. At 10 mm cover depth, the lowest porosity was shown, irrespective of type of binder due to a refinement of pore network caused by chloride binding.

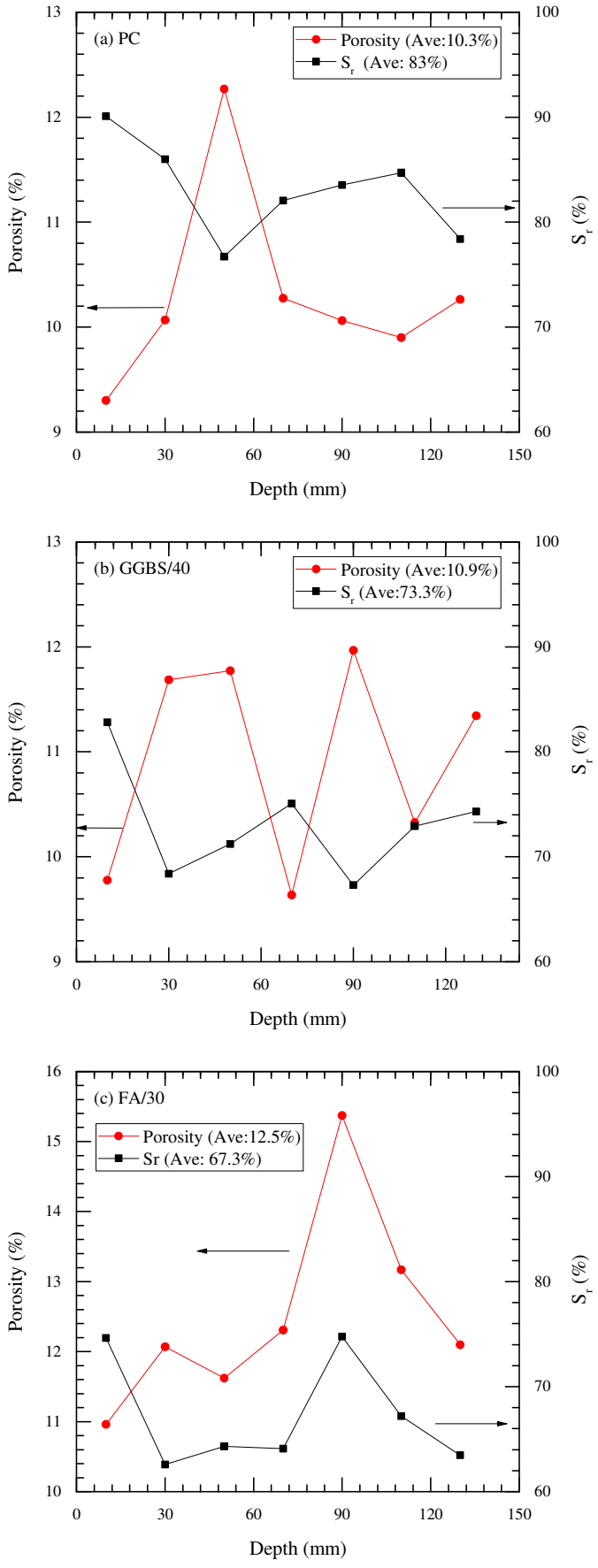

Figure 8.3 Degree of saturation and porosity with depths for (a) PC, (b) GGBS/40, and (c) FA/30 concretes retrieved from the field.

The relation between degree of saturation and resistivity for long-term exposed samples was investigated using Archie's law, as described in figure 8.4. The first two points corresponding to the values at 10 and 30 mm cover depth from the exposure surface ('open' marks on figure 8.4 indicate outliers), were omitted in the fitting due to the high concentration of chloride in the outer layer of concrete, which led to low electrical resistivity. The ratio ($\frac{\rho_{sat}}{\rho_t}$, see equation (5.23)) decreased as the degree of saturation decreased, as shown in figure 8.4 (similar to figure 5.19) and the exponents in Archie's equation were observed to be lower than the values in the early age samples in Chapter 5, corresponding to 1.33, 2.16, and 2.7 for PC, GGBS/40, and FA/30 concrete, respectively. Thus, these exponents are influenced by concrete age, in particular continuous hydration and by type of binder. However, further research is required to determine the exact relationship.

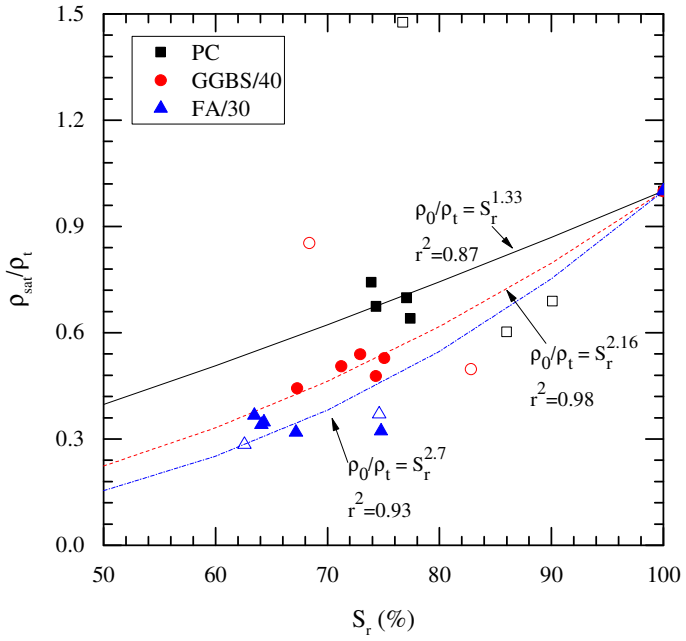

Figure 8.4 Relation between saturation degree and resistivity with binder type (outliners [open markers] are removed from fitting equations).

The Nernst-Einstein equation establishes the relation between the diffusion coefficient of a porous material and electrical resistivity (McCarter *et al.*, 2000) as follows:

$$\frac{D_{eff}}{D_0} \approx \frac{\rho_p}{\rho_{bulk}} \tag{8.1}$$

where D_{eff} is the effective diffusion coefficient in the porous material, D_0 is a diffusion coefficient of the desired ion at infinite dilution, ρ_p is the resistivity of the interstitial pore fluid, and ρ_{bulk} is the bulk resistivity of the saturated material.

The diffusion coefficient decreases with a decrease in moisture content (Kumar, 2010). Furthermore, in this study, the diffusion coefficient for concrete containing SCMs largely decreased with time compared to that for PC concrete. Thus, it can be inferred that a reduction of the exponent is related to an aging factor in the diffusion coefficient. Again, additional research is required due to the narrow range considered in the current analysis.

Determination of environmental factors

A number of chloride transport models have been developed for concrete, and the theoretical background is now well established (see Chapter 3). However, the models are generally only valid for concrete subjected to a certain situation. To overcome this, two environmental factors applied to the ClinConc model, which only considers the saturated condition of concrete. The main purpose of the environmental factors is to consider the unsaturated condition of concrete. Two environmental factors are (i) K_s taking into account the reduction of the diffusion coefficient with the degree of saturation, and (ii) K_{exp} describing the degree of contact of the concrete with aggressive solution, chloride solution. The process used to estimate the factors is briefly described below.

(i) The relation in terms of K_s is formulated from the work of Kumar (2010) (figure 8.5) as follows:

$$K_s = \frac{D_d}{D_{sat}} = S_r^{4.863-3.441\frac{w}{b}} \tag{8.2}$$

where D_{sat} is the diffusion coefficient in saturated concrete; and D_d is the diffusion coefficient in unsaturated concrete including saturation degree, S_r, and water-to-binder ratio, $\frac{w}{b}$.

(ii) To account for the effect of exposure conditions on chloride accumulation, an environmental factor, K_{exp}, is introduced into the ClinConc model. The basic information about the equation used in the ClinConc model has been presented elsewhere (Tang 1996b, 2008). In this study, K_{exp} is added in the function to calculate the total chloride from the free chloride content:

$$C_t = K_{exp} \times \Phi(C_f) \tag{8.3}$$

where C_t is total chloride content, Φ is the functional relationship within the ClinConc model and C_f is free chloride content.

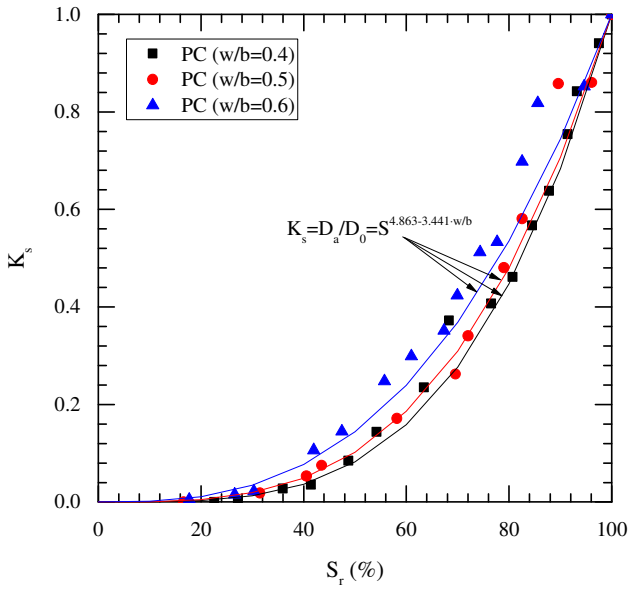

Figure 8.5 The relationship between degree of saturation and relative ratio of diffusion coefficient, K_s (adapted from Kumar (2010)).

To evaluate the $K_{exp.}$ the predicted ClinConc profile is adjusted by incrementally modifying the K_{exp} factor such that it maps onto the actual profile. Figure 8.6 provides an example of the adjusted curve considering K_{exp}. In the calculation process, the main focus is on estimating K_{exp}, as K_s is easily calculated from the degree of saturation measured directly from the sample and less affects the chloride profile. The environmental factors for samples subjected to a cyclic wet/dry regime in the laboratory are also investigated.

As shown in figure 8.7, the variation in temperature in the laboratory and the field are significantly different. The temperature was stable at ~ 20ºC in the well-controlled laboratory, while the concrete located in the field was influenced by seasonal temperature, i.e. ~ 15ºC in the summer and ~ 3ºC in the winter season. To simplify the calculation, the

averaged values for the samples exposed to both conditions were applied when calculating the chloride content with the ClinConc model.

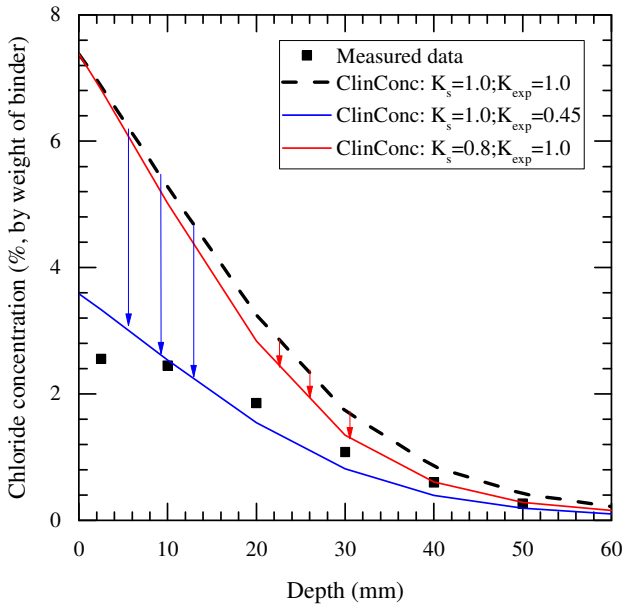

Figure 8.6 Example of the adjustment of a chloride profile (obtained from field specimen) using the modified ClinConc model introducing environmental factors K_s and $K_{exp.}$

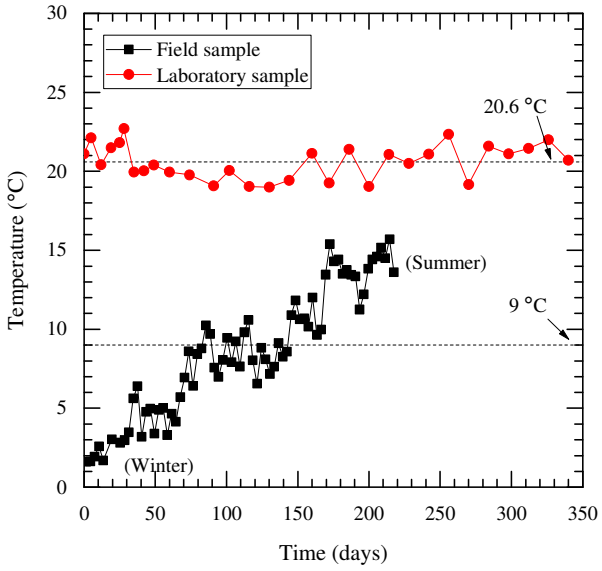

Figure 8.7 Temperature variation in concrete exposed to the field site and the laboratory.

Table 8.1 presents the input parameters used in the ClinConc model containing environmental factors. K_s could be estimated from equation (8.2) while K_{exp} values were found using the least square method between the measured and the predicted value. In addition, K_{exp} is representative of the exposure condition. Therefore, figure 8.8 and 8.9

also present the predicted chloride concentrations using the averaged values of K_{exp} for all samples which were exposed to the same condition.

As shown in figure 8.8 and 8.9, the predicted values are similar to the measured values. In addition, the K_{exp} values evaluated are in good agreement when samples are in the same exposure condition and have the similar w/b. As shown in table 8.2, for samples exposed in the field (w/b = 0.39 – 0.44), K_{exp} ranges from 0.60 to 0.82 (average value = 0.70), while for concretes exposed to the laboratory, K_{exp} is distributed from 0.62 to 0.86 (average value = 0.76) and from 1.93 to 2.09 (average value = 2.01) corresponding to w/b = 0.4 and 0.6, respectively. The main assumption for K_{exp} is that the contact degree of chloride proportionally decreases from the saturated condition (fully immersed condition in chloride solution). Therefore, the value should be lower than 1.0. However, it was estimated from the fitting process that the values for laboratory concretes (w/b = 0.6) were greater than 1.0. From the results, it could be deduced that another transport mechanism, i.e. absorption, which accelerates chloride ingress, affected the chloride transport in addition to diffusion. However, it is difficult to determine absorption behaviour in the chloride profiling. Although the value of K_{exp} >1.0 is invalid based on the assumption, it can indicate that absorption occurs in concrete.

For CEM III/A (w/b = 0.4) concrete, measured chloride content in the outer layer was higher than that predicted by the modified ClinConc model. This is due to high bound chloride by physical absorption or chemical binding. However, the K_{exp} values were lower than 1.0 because the values corresponding to the first two points (up to 6 mm nominal depth) were omitted in the process of fitting. It should be noted that the convective zone for laboratory concretes (w/b = 0.4) was observed within 10 - 15 mm from the electrical resistance measurement, and it is accepted that the convective zone (or wet/dry cyclic region) is subtracted in the fitting process with Fick's second law (Keßler *et al.*, 2014). It can be assumed that diffusion is the only transport mechanism in the regions below the convective zone. However, the results of this study show that the chloride transport mechanism beyond the convective zone is more complex than only diffusion, especially for laboratory concretes with a high w/b. Therefore, environmental factors or complex transport mechanisms should be introduced in the transport model to improve the accuracy of the results. It should also be noted that continuous updating is required in terms of the estimated values for environmental factors, as K_s values are limited in estimating various materials including blended concretes and K_{exp} is only estimated from the fitting process.

Table 8.1 Input parameters for the ClinConc model

Exposure condition	Field			Lab					
Sample designation	PC	GGBS/40	FA/30	CEM I (w/b=0.4)	CEM III/A (w/b=0.4)	CEM II/B-V (w/b=0.4)	CEM I (w/b=0.6)	CEM III/A (w/b=0.6)	CEM II/B-V (w/b=0.6)
Cement content(kg/m^3)	460	270	370	460	270	370	300	180	210
Slag content(kg/m^3) (k value*)	+	180 (0.6)	+	+	180 (0.6)	+	+	120 (0.6)	+
Fly ash content (kg/m^3) (k value*)	+	+	160 (0.4)	+	+	160 (0.4)	+	+	90 (0.4)
Water content (l/m^3)	184	198	206.7	184	180	212	180	180	180
Average saturation degree	0.83	0.73	0.67	0.82	0.84	0.83	0.85	0.87	0.88
Average Temperature	9			20.6					
Concrete age at first exposure (days)	35			42					
Exposure duration (years)	18			1.07					
Chloride concentration applied at the surface (g/l)	19.6			19.6					
Migration coefficient at 6 months (m^2/s)	8.87	3.33	2.92	8.87	3.33	2.92	21.05	6.43	7.46

* an equivalent binder assumption (San Nicolas *et al.*, 2014) replacing the term ‘w/b’ with w/(cement +k×supplementary cementitious materials) defined in BS EN 206 (British Standards Institution, 2014)
Note: Input values for the ClinConc model refer to Appendix D.2

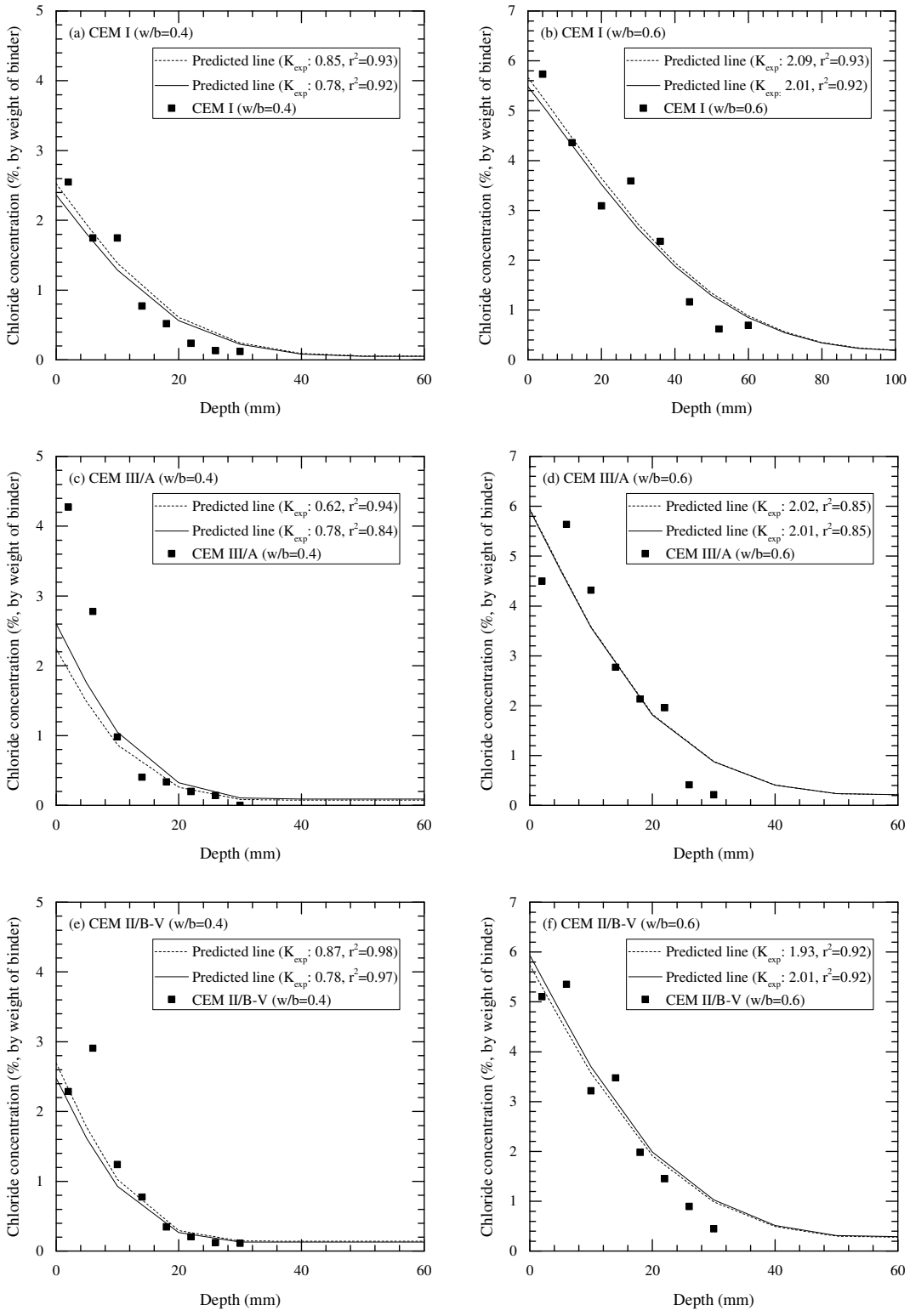

Figure 8.8 Measured profile and predicted profiles from the modified ClinConc model for (a) CEM I, (b) CEM III/A, and (c) CEM II/B-V concrete with w/b=0.4, and (d) CEM I, (e) CEM III/A, and (f) CEM II/B-V with w/b=0.6 subjected to a wet/dry cyclic regime in the laboratory.

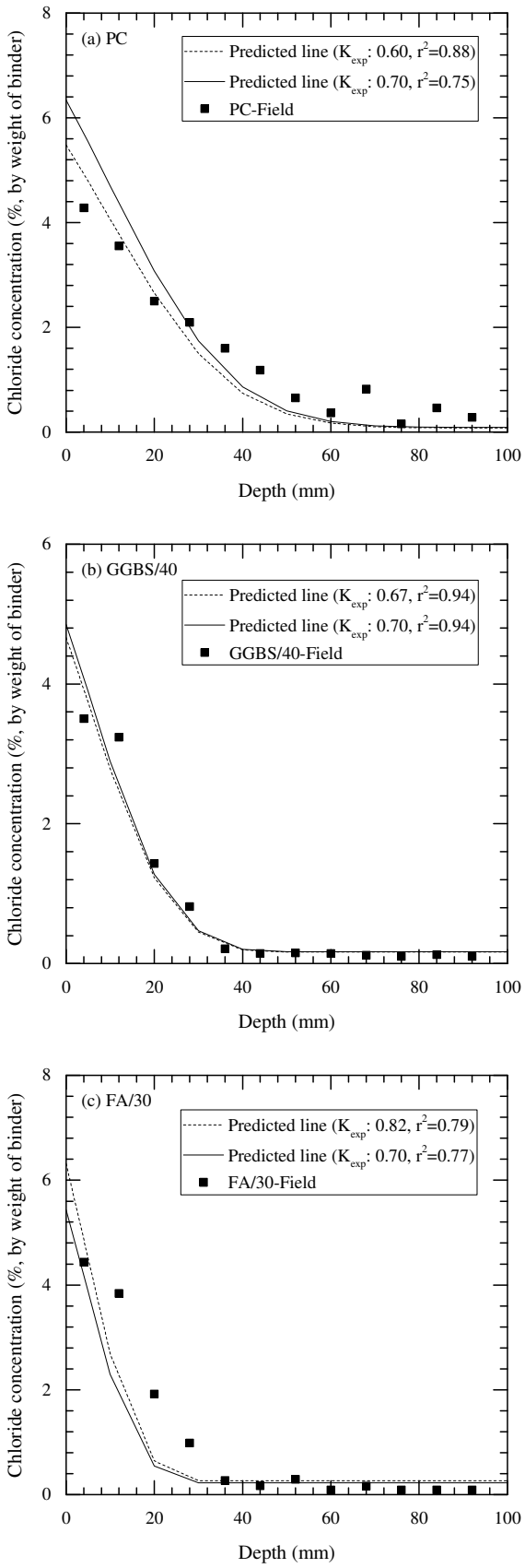

Figure 8.9 Measured profile and predicted profiles from the modified ClinConc model for (a) PC, (b) GGBS/40, and (c) FA/30 concrete subjected to the field site (XS3).

Table 8.2 Environmental factors used in modified ClinConc model

Environmental factors	Field			Laboratory					
	PC (w/b=0.4)	GGBS/40 (w/b=0.44)	FA/30 (w/b=0.39)	CEM I (w/b=0.4)	CEM III/A (w/b=0.4)	CEM II/B-V (w/b=0.4)	CEM I (w/b=0.6)	CEM III/A (w/b=0.6)	CEM II/B-V (w/b=0.6)
K_s	0.42	0.35	0.24	0.50	0.55	0.53	0.64	0.68	0.67
K_{exp}	0.60	0.67	0.82	0.79	0.62	0.86	2.09	2.02	1.93
Average K_{exp}	0.70			0.76			2.01		

Time to corrosion based on chloride threshold level

Experiments and computational modelling of chloride transport are necessary to determine the corrosion initiation of the steel based on CTL. To predict or estimate time to corrosion, information on both the CTL and the chloride transport rate are required, but a number of influencing factors limit an accurate prediction. Empirically based models have sometimes introduced a probabilistic approach to reduce or contain the error. However, a large data-set from the field is required to apply this method (Bertolini and Redaelli 2009) and it is time-consuming. Hence, analytical models are more useful to determine the chloride transport behaviour. As suggested above, the model should be continuously updated and in this study, two analyses were carried out: (i) determining the CTL for CEM I (w/b = 0.6) concrete using a modified ClinConc model with two environmental factors, and (ii) predicting time to corrosion for other concretes with the CTL obtained from CEM I (w/b = 0.6) concrete.

Before estimating the time to corrosion, the CTL was determined. To this end, the environmental factors obtained from the previous section and the time to corrosion initiation from Chapter 6 were used, respectively. The predicted values at 25 mm of cover depth range from 2.0 to 2.8% of total chloride content, and the average and standard deviation are 2.3% and 0.3%, respectively. These values are significantly higher than the accepted value (0.4% by weight of binder) but is similar to a previous study (Angst *et al.*, 2011c). A higher CTL was required in this study because for the PC concrete exposed in the field and for the CEM III/A (w/b = 0.6) and CEM II/B-V (w/b = 0.6) concrete in the laboratory, the chloride contents were also higher than 0.4% at steel depth, and no corrosion on the steel was detected. In addition, as CTLs vary widely due to various steel conditions and materials, in this study the CTLs used to estimate the time to corrosion were set as both 2.32% and 0.4%, for laboratory and fields samples.

Except for the CEM I (w/b=0.6) concrete in the laboratory, table 8.3 presents the predicted initiation times for different mixes and different exposure conditions. Although SCMs are beneficial in increasing the corrosion-free life, their effect on time to corrosion initiation is low compared to other factors. The life for SCM concretes is 1.8 – 5 times longer than that for PC (or CEM I) concrete, but the effect of CTL is moderate when it increases from 0.4% to 2.3%. On the other hand, it was observed that an increase in w/b distinctly led to a reduction in the corrosion-free life, ranging from 12.1 to 23.3 times. When cover depth was doubled (between 25 mm for laboratory samples and 50 mm for field samples), corrosion-free life increased from 16.2 to 37.7 times. This implies that a large difference in the corrosion-free life with cover depth and w/b is closely related to the sorption effect of the wet/dry cyclic regime. Therefore, the best way to increase the service life of concrete structures subjected to a wet/dry cyclic regime is to reduce the convective region using lower w/b or using SCMs, especially GGBS. It is possible that the fully saturated condition is more beneficial in improving the concrete performance than the unsaturated condition. In other words, moisture movement is a key factor to prevent concrete deterioration by chloride attack.

Table 8.3 The predicted time to attain chloride threshold level at the steel depth

Time to reach chloride threshold level (years)									
	Field (cover depth = 50 mm)			Laboratory (cover depth = 25 mm)					
CTL*	PC (w/b=0.4)	GGBS/40 (w/b=0.44)	FA/30 (w/b=0.39)	CEM I (w/b=0.4)	CEM III/A (w/b=0.4)	CEM II/B-V (w/b=0.4)	CEM I (w/b=0.6)	CEM III/A (w/b=0.6)	CEM II/B-V (w/b=0.6)
0.4	22.7	49.4	113.2	1.4	2.5	3	0.2**	0.4	0.4
2.3	78.8	213	391.7	16.3	31.4	36.2	0.7**	2.6	2.2

* Chloride threshold level (%, by weight of binder), ** detection of corrosion

8.3.2 *Evaluating the corrosion of steel*

After depassivation, corrosion products lead to cracking in the concrete. The cracks formed in the concrete accelerate ingress of chlorides, which dramatically reduces the service life of concrete structures. In addition, it is difficult to determine a single CTL, as shown in previous studies (see table 2.5) and the present one. To accurately diagnose the conditions of concrete structures, corrosion detection methods are routinely employed. In this study, parameters relating to steel corrosion were measured using several techniques for the field samples and laboratory samples. Moreover, the corrosion propagation of the

steel with time was investigated for only those laboratory samples (CEM I concrete, w/b=0.6) in which corrosion occurred.

Field studies for corrosion parameters

As mentioned above, a range of electrochemical techniques were undertaken to determine the steel condition regarding field samples. Only the results of the GP and TEP techniques are presented here (table 8.4), while other test results presented in Appendix C.4. The corrosion potential and time constant are useful parameters to rapidly determine corrosion for all steels. In this study, corrosion potentials ranged from -98.85 to -120.40 mV, which indicates that the steels were in the passive state (ASTM International, 2015). The time constants were also high, ranging from 66.80 to 260.25s. All parameters indicate a passive state of the steel. Thus, it is reasonable to consider the steel condition as being in the passive state.

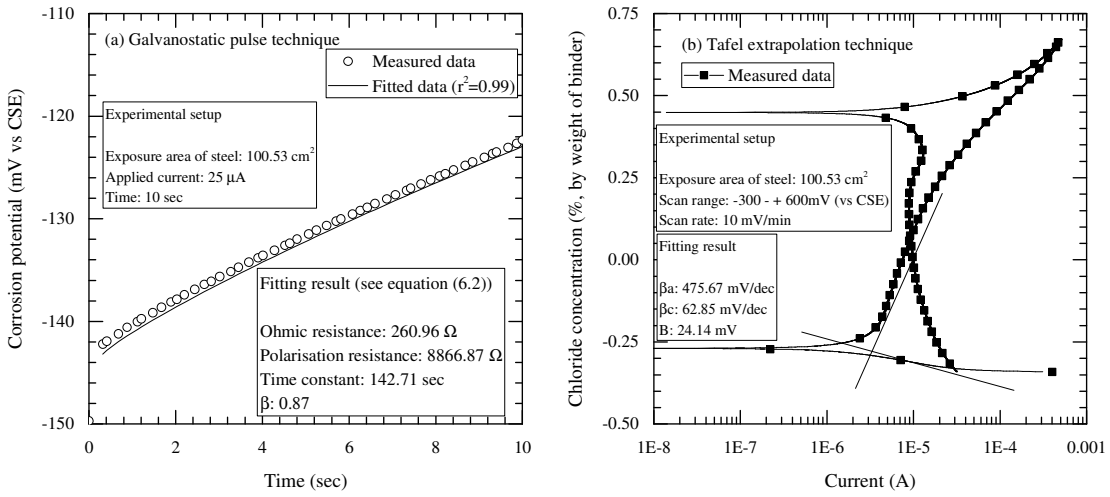

Figure 8.10 Fitting data obtained from the PC concrete using (a) GP technique, and (b) Tafel extrapolartion technique.

Polarisation resistance obtained from the GP technique and Tafel slopes obtained from the TEP technique are necessary to quantify the corrosion rate; the measurement details are given in Section 6.2.3. Overall, the polarisation resistance in the passive state of steel for both field and laboratory samples was high, ranging from 66.25 to 123.70 $\Omega \cdot m^2$ for the former and from 80.76 to 136.20 $\Omega \cdot m^2$ for the latter, respectively, thereby indicating that the corrosion rates were negligible. It is interesting that anodic slopes in the passive state for the field samples were significantly reduced compared to those for the laboratory samples (table 8.5). From the result, it could be deduced that chlorides reaching the steel

could react with the passive film, leading to depassivation. In addition, *B* values from the Tafel slopes were calculated and were distributed around 26 mV, corresponding to the active state in the *B* value which is generally accepted (table 8.4). The B value appeared to be affected by the slope of the cathodic branch, which was determined by availability of oxygen. The availability of oxygen was lower for the laboratory samples than for the field samples, as the TEP test was conducted on the laboratory samples at the end of the wetting cycle (i.e. saturated condition), whereas on the field samples the surface was in a dry condition (transport time from field to laboratory and tide time). This condition led to a more active reaction in the cathodic branch for the field samples. To quantify the corrosion rate, particularly in electrochemical techniques, information on *B* values was required and the values were observed to be sensitive to concrete condition. Therefore, to determine the service life of a concrete structure with corrosion rate, it is first necessary to investigate the *B* value.

Ohmic resistances clearly differed with type of binder. Concretes containing SCMs had a high ohmic resistance compared to PC and CEM I concrete. In addition to type of binder, w/b also affected ohmic resistance and the effect of w/b on the resistance was marginal for CEM III/A concrete compared to other concretes. On the other hand, differences in the ohmic resistances with the exposure duration (between 382 days and 18 years) were small for PC (CEM I) concrete and GGBS/40 (CEM III/A) concrete, but the ohmic resistance of FA/30 concrete (the field sample at 18 years) was 1.7 times higher than that of CEM II/B-V concrete (the laboratory sample at 382 days) due to pozzolanic reaction. Although the effect of ohmic resistance on the corrosion rate was marginal (less than 10 % to determine the polarisation resistance), the value should be considered even if concrete is saturated, as the polarisation resistance decreases dramatically after depassivation.

Table 8.4 Corrosion parameters of steel for field samples at 18 years

	PC		GGBS/40		FA/30	
	AVE	STD	AVE	STD	AVE	STD
Ohmic resistance* ($\Omega \cdot m^2$)	2.45	0.21	3.50	0.00	12.50	0.71
Polarisation resistance*($\Omega \cdot m^2$)	97.40	11.74	66.25	24.82	123.70	15.56
Corrosion potential (mV)	-120.40	29.13	-98.85	5.73	-111.35	21.43
Time constant* (s)	177.40	49.07	66.80	25.31	260.25	47.31
Anodic slope** (mV/dec)	592.05	164.54	519.70	136.75	1,006.59	107.93
Cathodic slope** (mV/dec)	66.55	5.16	75.05	5.73	71.44	1.03
B value (mV)	25.95	2.62	28.45	2.90	28.99	0.18

* Data obtained using the Galvanostatic pulse technique
** Data obtained using the Tafel slope AVE average; STD standard deviation

Table 8.5 Corrosion parameters of steel for laboratory samples at 382 days

	CEM I (w/b=0.4)		CEM III/A (w/b=0.4)		CEM II/B-V (w/b=0.4)		CEM I (w/b=0.6)		CEM III/A (w/b=0.6)		CEM II/B-V (w/b=0.6)	
	AVE	STD	AVE	STD	AVE	STD	AVE	STD	AVE	STD	AVE	STD
Ohmic resistance* ($\Omega \cdot m^2$)	2.17	0.27	3.53	0.14	7.26	0.73	0.93	0.09	3.06	0.23	4.23	0.41
Polarisation resistance*($\Omega \cdot m^2$)	84.53	35.98	80.78	33.86	136.76	42.27	1.56	0.58	136.20	29.30	113.63	38.65
Corrosion potential (mV)	-101.57	43.94	-127.17	3.30	-121.92	12.51	-564.05	48.65	-149.62	6.99	-145.37	14.86
Time constant* (s)	126.75	93.89	158.01	96.25	366.23	126.41	13.54	6.52	311.01	99.06	335.93	181.04
Anodic slope** (mV/dec)	>10,000	+	>10,000	+	>10,000	+	434.03	172.08	>10,000	+	>10,000	+
Cathodic slope** (mV/dec)	116.37	24.61	136.03	9.56	130.08	22.20	279.92	92.51	110.83	17.09	133.30	16.67
B value (mV)	46.63	15.22	58.63	4.71	53.68	13.77	73.43	25.57	45.15	11.17	56.10	10.14

* Data obtained using the Galvanostatic pulse technique
** Data obtained using the Tafel slope
+ Not determined
AVE average; STD standard deviation

Prediction for the propagation of corrosion (laboratory sample)

As shown in the previous section, the B value is sensitive and is difficult to determine the corrosion rate directly. On the other hand, in Chapter 6 polarisation resistances were observed to be similar irrespective of electrochemical technique, especially for steel in the active state. Thus, it is reasonable to estimate the development of polarisation resistance after depassivation to determine corrosion propagation. In this study, as only the corrosion of steel for CEM I (w/b=0.6) concrete in the laboratory was detected regarding corrosion propagation, only changes in the polarisation resistance data on the CEM I (w/b=0.6) concrete were evaluated.

Firstly, time to corrosion initiation was chosen with a half-cell potential measurement. After depassivation, polarisation resistances were plotted with time as shown in Figure 8.11, irrespective of steel replicates in CEM I (w/b=0.6) concrete. The polarisation resistances rapidly decreased in the initial period, i.e. up to ~50 days after depassivation, the values then stablise around 1.5 $\Omega \cdot m^2$ during the remaining period. This implies that the depassivation process and anodic reaction on the steel happened at the same time in the initial period, and then anodic dissolution on the steel only reacted after full depassivation. The corrosion products then accumulated on the steel surface. However, care should be taken in interpreting the polarisation resistance, as the exposure condition was stable for the samples in this study, and the polarisation resistance could thus be stable after full depassivated conditions. If samples were exposed to the field, polarisation resistance could fluctuate with time.

To estimate the trend for the polarisation resistance with time, the regression method using a power-law equation was employed, viz;

$$R_p = a \cdot t^{-b} \tag{8.4}$$

where R_p is the polarisation resistance ($\Omega \cdot m^2$) at time, t (days), and a and b are the constant.

The parameters from each sample were extracted; and presented in Table 8.6. The regression parameters, i.e. a and b, represent the initial corrosion rate after the first depassivation, and the rate for stabilisation.

Table 8.6 Regression parameters for polarisation resistance of laboratory samples

Sample No.	1		2		3		Average
Steel Types	SS*	LS**	SS	LS	SS	LS	
a	4.31	7.39	6.75	3.82	3.74	3.51	4.92
b	-0.29	-0.27	-0.35	-0.24	-0.14	-0.19	-0.25
r^2	0.69	0.63	0.88	0.76	0.14	0.69	+

* Steel with small exposure area (see Chapter 4.3)

** Steel with large exposure area (see Chapter 4.3)

The parameters differed among the steels and the values ranged 3.51 to 7.39 for parameter 'a' and -0.35 to -0.14 for parameter 'b'. To refine the results, further investigation of the steel condition is required.

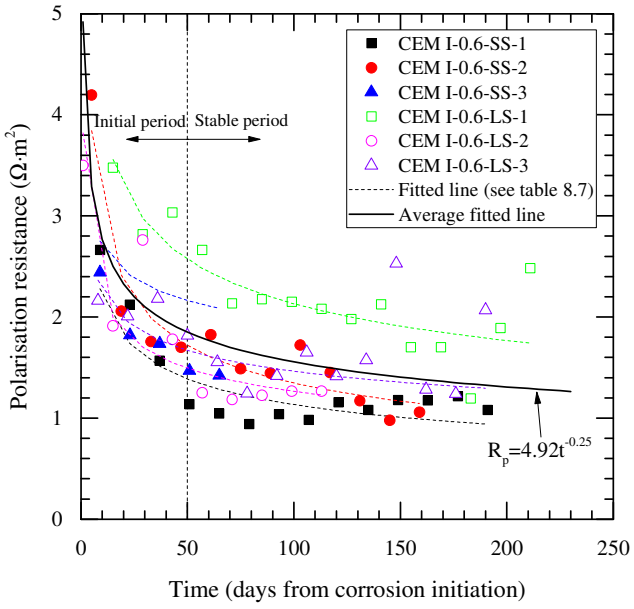

Figure 8.11 Change in polarisation resistance of steel in CEM I (w/b=0.6) concrete in the laboratory after depassivation (large and small area of exposed steel presented)

8.3.3 *Evaluating the electrical resistance of 18-year-old concrete*

In Chapter 7, the electrical resistance using embedded stainless-steel pin electrodes was monitored with exposure duration. This technique is practical for monitoring concrete due to its low cost, ease of installation and rapid response. However, the analysis can be difficult because of a number of influencing factors. Among these, temperature is critical. Electrical resistance/resistivity should consider temperature for analysis purposes and it

is now accepted that the correction of electrical resistivity/resistance can be undertaken using an Arrhenius relationship with activation energy. In this study, the activation energy was estimated for long-term exposure field samples. The change in electrical resistance/resistivity due to hydration will be negligible as the samples were 18 years old.

Because it is independent of electrode geometry, electrical resistivity is more useful for application than electrical resistance. To evaluate electrical resistivity, a geometry factor should be obtained from either computational models or experiments (Lataste, 2010).

In a previous study, the geometry factor for the field samples used in the present study corresponded to 0.0125 m ± 5% (McCarter *et al.*, 2012). To verify this geometry factor, the electrical resistivity from embedded stainless-steel pin electrodes was compared with the resistivity of the prismatic sample (50×50×20 (thickness) mm) directly extracted from the concrete containing the electrodes. For the cube sample, the sampling and measurement methods are the same as in Section 4.5 and Section 5.2.5, respectively. The results are shown in figure 8.12. A slight difference exists between the two measurements, but it was concluded that the geometry factor (0.0125 m) used in this study was appropriate. Subsequently, the electrical resistances monitored by the remote interrogated system were converted to electrical resistivity (described in Section 8.2.4).

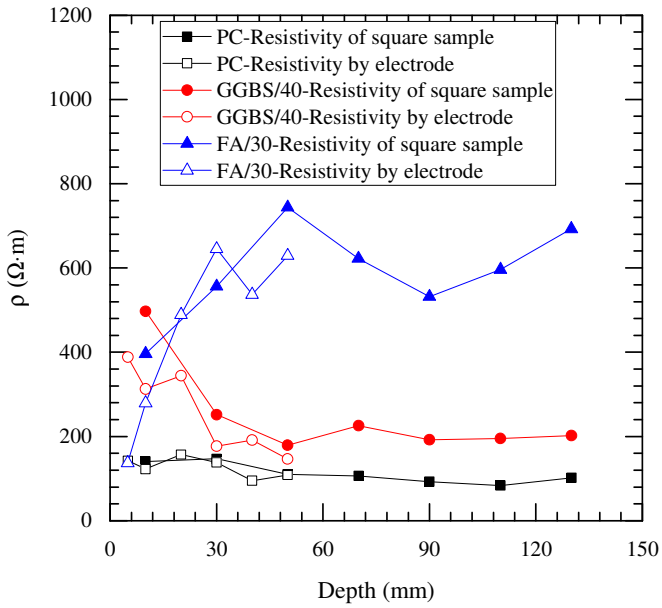

Figure 8.12 Comparison of resistivity obtained from the bulk concrete with resistivity obtained from the embedded electrode.

Figure 8.13 presents as-measured electrical resistivity with type of binder and depth. During monitoring, some of the data were lost due to technical problems which remain

unclear. The electrical resistivity was lowest for PC concrete and highest for FA/30 concrete located in the field. On the other hand, the electrical resistivity at the outer layer, i.e. at 5–10 mm cover depth, was lower than at other depths for PC and FA/30 concrete while for GGBS/40 concrete the values at the outer layers were higher than at other depths. This is because high chloride binding at the outer layer leads to refinement of pore structure and a lower amount of free chloride at the outer layer in GGBS/40 concrete while low electrical resistivity of concrete is due to free chloride in FA/30 concrete. This is in line with the other results in this study (see figure 7.7 and figure 7.8 in Section 7.3.2). On the other hand, unlike CEM I (w/b=0.4) concrete (in figure 7.7(a)), the free chloride at the outer layer in PC concrete mainly affected the electrical resistivity. It seems that the rate of chloride binding significantly decreases or have been exhausted in 18-year-old PC concrete. It is evident that the electrical resistivity for all samples fluctuated with time. To account for this fluctuation, a correction for temperature effects was required.

Determination of activation energy

An Arrhenius relationship between electrical resistivity and temperature can be expressed as follows (McCarter *et al.*, 2012):

$$\rho_T = \rho_0 e^{\frac{E_a}{RT}} \tag{8.5}$$

$$ln\rho_T = ln\rho_0 + \frac{E_a}{RT} \tag{8.6}$$

where ρ_T is the resistivity of concrete (Ω·m) at temperature, T (K) (T=293.15 K in this study), ρ_0 is a constant (Ω·m), R is the gas constant (8.314 J/mol·K) and E_a is the activation energy for conduction processes in concrete (J/mol).

The activation energy can be evaluated using the relationship described in equation (8.5). To illustrate this, figure 8.14 presents the resistivity values in figure 8.13 (a) described against the cover-zone temperature at each depth in the format of equation (8.6) over a period of 27 days.

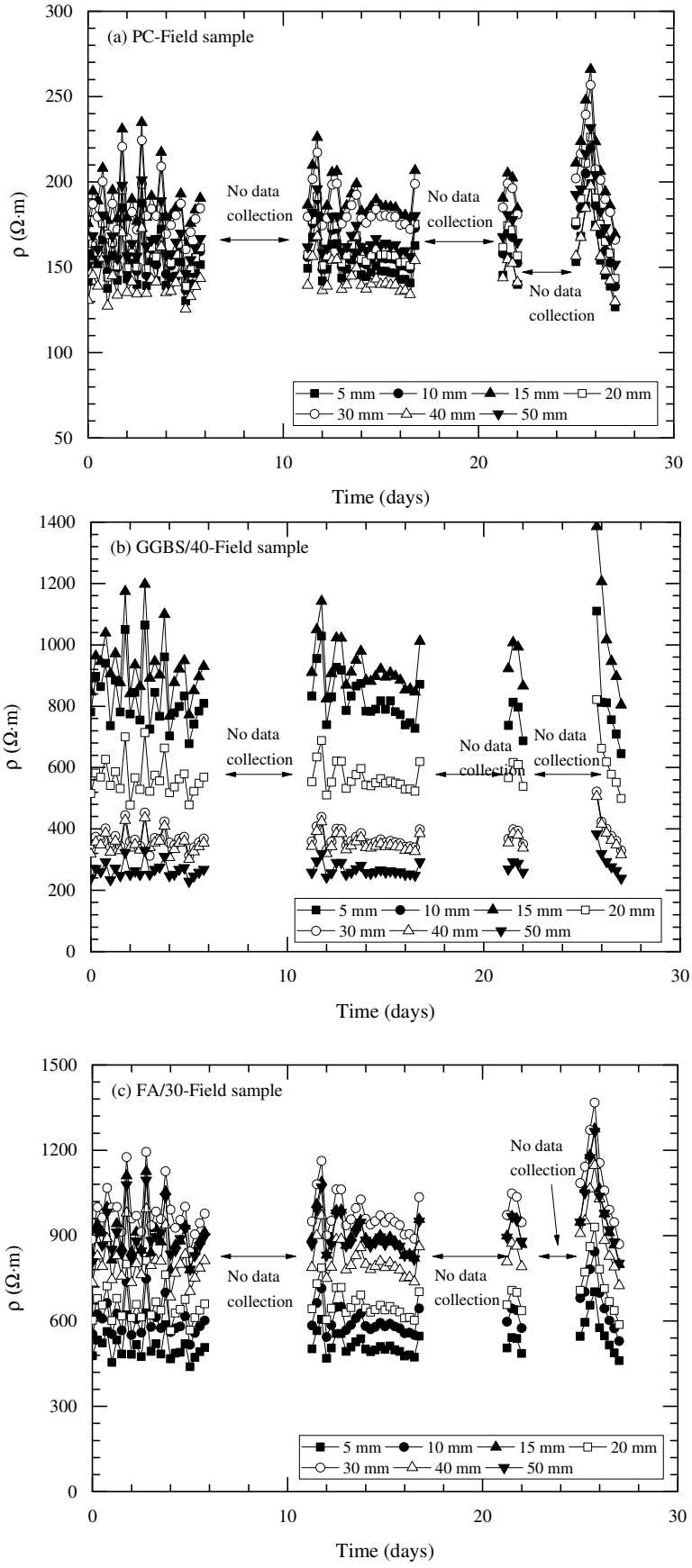

Figure 8.13 Electrical resistivity with depth without temperature correction for (a) PC, (b) GGBS/40, and (c) FA/30 concrete at the Dornoch site.

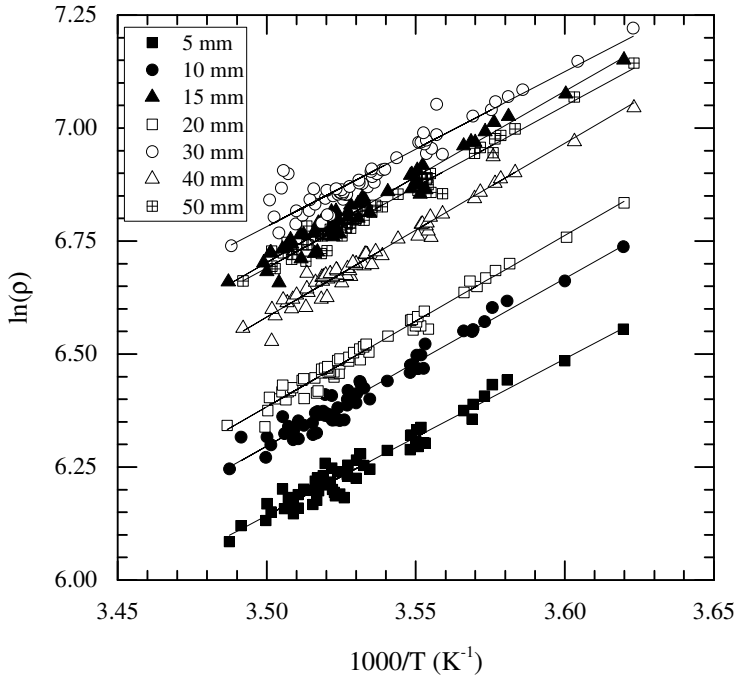

Figure 8.14 Data in figure 8.13 (a) plotted in Arrhenius format.

The activation energies were calculated for,

(i) data based on the whole period; and,

(ii) data based on each part of the period.

For the part-period method, each discontinuous line was considered as one part, consisting of a total of (roughly) three parts. The average values were estimated. Clearly, the Arrhenius relationship using activation energy is important to account for the influence of temperature on electrical resistivity (McCarter *et al.*, 2012). However, it was still necessary to verify whether the activation energy was constant over the whole depth, especially in the convective zone where moisture distribution is unstable.

Figure 8.15 presents the activation energy estimated using the two methods with depth. The activation energies for all samples ranged from 26.1 to 37.9 kJ/mol which are similar to the results in previous study (McCarter *et al.*, 2012). It is interesting that differences in activation energy were marginal below 20 mm of cover depth, whereas larger differences were observed in the outer layers (5 – 15 mm) with different methods. This must indicate that moisture content is also an important factor in estimating the activation energy although it is difficult to evaluate the activation energy with different moisture contents experimentally, and it is reasonable to average the value obtained from monitoring. With the averaged activation energy, the electrical resistivity was corrected to a reference

temperature (at 20ºC); the result is presented in figure 8.16. It can be observed that the fluctuations are removed. Therefore, to accurately analyse the electrical resistivity of concrete, especially in the field, the effect of the temperature must be considered.

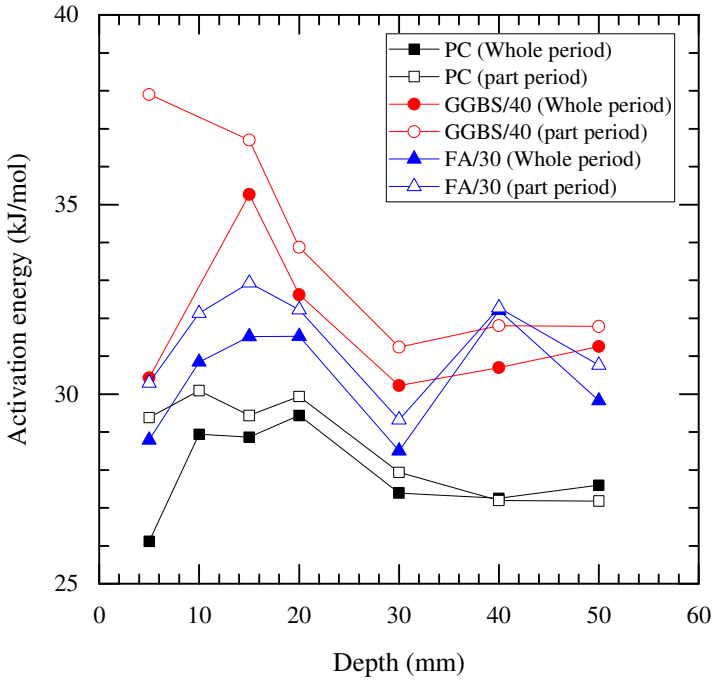

Figure 8.15 Variation of activation energy with depth.

Normalised electrical resistance

Electrical resistance monitoring of concrete subjected to chloride environments could be used to detect ionic movement within the cover-zone, especially the movement of chloride ions present in the pore solution. However, it is difficult to evaluate the effect of chloride on electrical resistivity for concrete at an early age due to hydration. Some investigations, including the present study, have reported that electrical resistivity increases with time even though chloride ingress was observed (Polder and Peelen, 2002; McPolin *et al.*, 2005). In this section, the effect of chloride ingress on electrical resistivity is investigated in samples of long-term exposure, as the hydration effect is negligible in mature samples (~18 years old).

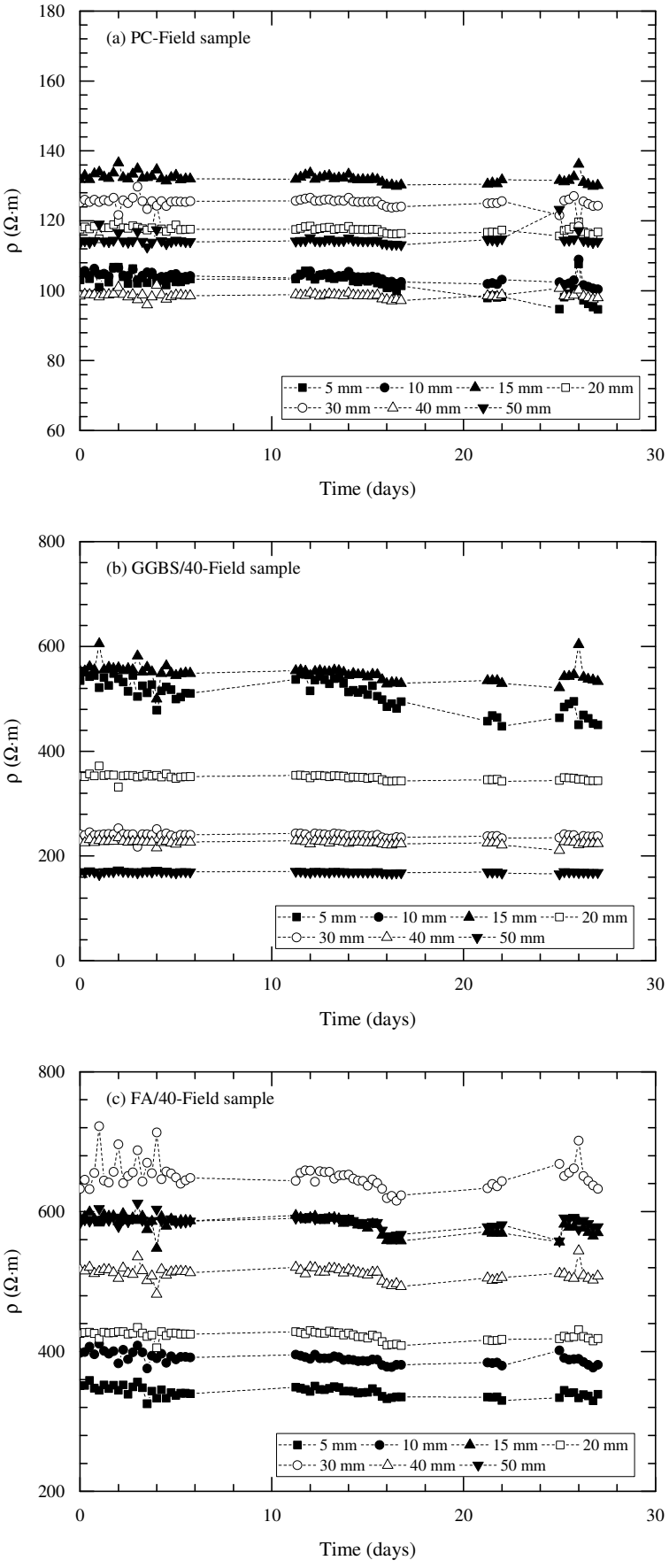

Figure 8.16 Electrical resistivity with depth after temperature correction for (a) PC, (b) GGBS/40, and (c) FA/30 concretes at the Dornoch site.

After applying the activation energy to obtain the equivalent resistivity at a reference temperature, the electrical resistivity was normalised with the resistivity value at the first measurement point (at 0 days), as shown in figure 8.17. The N_ρ ($\frac{\boldsymbol{\rho_t}}{\boldsymbol{\rho_{t=0}}}$) value remained stable with depth and time for all samples, although slight fluctuations were detected and attributed to a wet/dry cyclic regime in the tidal zone. The N_ρ value decreased with time at 5 mm cover depth. This seemed to be caused by chloride ingress; however, considering the entire exposure period (18 years), the reduction for 27 days would be negligible. Long-term data are required to confirm the effect of chloride on electrical resistivity. It is suggested here that an electrical resistivity measurement could be exploited to detect chloride ingress of concrete exposed to a chloride-rich environment. However, regular monitoring is essential in this respect.

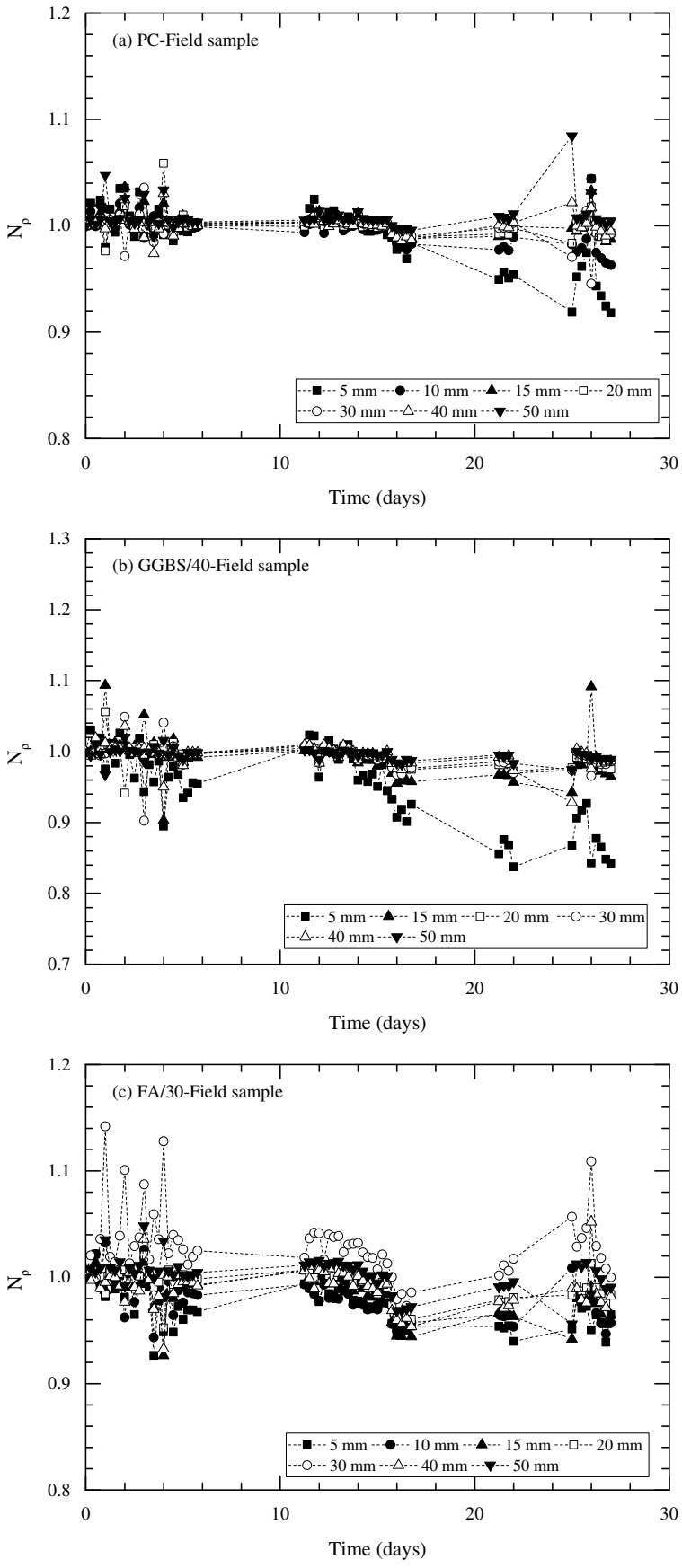

Figure 8.17 Normalised electrical resistivity of concrete at the Dornoch site.

8.4 Summary

This study predicted the chloride transport in concrete using the ClinConc and the corrosion rate of steel embedded in concrete using an empirical model. The data used were obtained from samples exposed to a marine environment for 18 years and from samples exposed to a laboratory environment for 382 days. The main findings are summarised below:

- To update the chloride transport model, two environmental parameters, K_s and K_{exp}, were introduced and determined. Different exposure conditions between the laboratory and the field, i.e. different wet/dry cyclic regime, leads to the different transport behaviour. In the field, the chloride transport was mainly diffusion, and the sorption effect was negligible. In contrast, in the laboratory samples, especially in concrete with a high w/b, this effect was considerable. It was observed that K_{exp} was greater than 1.0 for the high w/b (=0.6) and this is due to the sorption mechanism.

- After depassivation, the polarisation resistance was evaluated as a function of time. As mentioned in Chapter 6, polarisation resistance is less sensitive than corrosion rate. The empirical relation between polarisation resistance and time was expressed using Power's law. Consequently, it was observed that corrosion propagation became stable with time. However, further research is required regarding the parameters used in the empirical equation.

- To consider the effect of temperature on electrical resistivity, the activation energy was evaluated in the field samples connected to the remote-control system. It was observed that the activation energy differed with depth and type of binder, ranging from 26.12 to 37.9 kJ/mol. It was confirmed that the outer layers of the samples were sensitive to the exposed environment namely the wet/dry cycle and the chloride content in the pore solution based on the estimation of the activation energy.

CHAPTER 9
CONCLUSIONS AND RECOMMENDATIONS FOR FUTHER WORK

The work presented evaluated the performance of reinforced concrete subjected to a chloride environment with the chloride-induced corrosion of the embedded steel studied at various stages: chloride ingress, corrosion initiation and corrosion propagation. In addition, the electrical resistance/resistivity of concrete was monitored during chloride ingress. Although many studies have examined chloride transport and the chloride-induced corrosion of steel, their results are scattered due to various influencing factors including type of binder, test techniques, modelling method and exposure conditions. The conclusions of this study are summarised below, along with recommendations further work.

9.1 Electrical resistance and transport properties – laboratory-based studies

Concrete samples with two levels of w/b (=0.4 and 0.6) and OPC, 30% FA and 60% GGBS, were used to establish the relation between transport properties and electrical resistances/resistivity. The electrical resistivity of each sample was measured to establish the relationship between the resistivity and various parameters such as the degree of saturation, migration test and compressive strength. In addition, to accelerate chloride ingress and to estimate chloride concentration, concrete slabs were exposed to a chloride solution under a wet/dry cyclic regime as this represents a more realistic situation than adding chlorides to the mixing water. The conclusions regarding this relationship are:

- Compressive strength is a 'traditional' factor used to determine the performance of concrete. The relationship between electrical resistivity and compressive strength was established although a scatter in the result was observed. Based on the result in this study, whilst compressive strength is important in the quality control of concreting operations, it cannot be used to assess the performance of concrete related to chloride transport.

- The basic parameters including porosity, degree of saturation, migration and diffusion coefficient, and electrical resistivity were investigated with regard to chloride transport. These parameters changed with time, especially in SCM

concretes, and the w/b was observed to be crucial to determine durability and performance of concrete. In terms of migration coefficient/electrical resistivity, CEM II/B-V (w/b=0.4) concrete was superior but the diffusion coefficient of CEM III/A (w/b=0.4) concrete was the lowest. Porosity was beneficial for CEM I (w/b=0.4) concrete. The results suggest that it is necessary to evaluate concrete durability with more than one parameter to assess the resistance of chloride transport as chloride transport in concrete is determined by various factors, e.g. degree of saturation and chloride bindings. In addition, the curing time in CEM II/B-V concrete is crucial to determine the performance to chloride transport.

- The electrical resistivity was highly sensitive to moisture. Archie's law was introduced to show the relationship between electrical resistivity and degree of saturation. The sensitivity of resistivity to degree of saturation was in the order: CEM II/B-V concrete (very sensitive) > CEM III/A concrete > CEM I concrete (less sensitive). On the other hand, comparing the laboratory and field data, the exponent for CEM II/B-V (or FA/30) concrete decreased from 5.61 at 382 days to 2.7 at 18 years, while the value for CEM I (or PC) concrete was stable as 1.61 at 382 days and 1.33 at 18 years; the exponent is highly related to hydration process. In addition, the electrical resistivity was found to be affected by the degree of chloride contamination.

- The electrical resistivity was observed to be in inverse proportion to the migration coefficient, irrespective of type of binder. Based on a simplified Nernst-Planck equation, the constant (chloride concentration in the steady state) was required to convert the electrical resistivity into the migration coefficient directly, and the value for the constant was ~ 0.356 mol/l. However, to refine this value, additional studies are required.

9.2 Electrical resistance and transport properties – Marine Exposure Site

Site-based research is important as the durability/performance of concrete is influenced by its surrounding environment as well as its material properties. Samples exposed to a chloride environment for an extended period of time were extracted from the field and investigated with regard to the transport properties, including porosity/degree of

saturation and diffusion coefficient. The test results were used to evaluate the condition of the concrete and as input parameters in the predictive model (ClinConc model in study). The findings are summarised below:

- When using the 'erf' function to analyse chloride distribution, the diffusion coefficient and surface chloride content were the main input parameters. The diffusion coefficient of PC concrete (1.39×10^{-12} m^2/s) was higher than those of GGBS/40 and FA/30 concrete (4.21×10^{-13} m^2/s), but the surface chloride contents for PC, GGBS/40, and FA/30 concrete (4.54, 4.46, and 5.56% by weight of binder) were similar.

- Although the samples were exposed to the XS3 environment (tidal zone), degrees of saturation were stable across depth except for the outer layer (0 – 20 mm). Averaged degrees of saturation were 0.81, 0.73, and 0.67 corresponding to PC, GGBS/40, and FA/30 concrete, respectively. The unsaturated condition leads to a lower diffusion rate; therefore, the chloride ingress in the XS3 environment could be lower than that in the XS2 environment when sorption is not considered (i.e. convective zone is ignored).

- There is little difference in average porosity over the cover region between CEM I concrete at 390 days and PC concrete at 18 years, corresponding to 10.0% and 10.3%, respectively. On the other hand, porosities from 390 days to 18 years decreased by 0.6% for GGBS/40 (or CEM III/A) concrete and 1.3% for FA/30 (or CEM II/B-V) concrete. On-going hydration in SCMs concrete was observed to be beneficial to improve porosity, but porosity itself cannot be representative of a performance factor regarding chloride transport.

9.3 Electrochemical parameters for the corrosion of steel

To assess the corrosion of embedded steel in concrete, various techniques were applied to the samples: non-destructive methods included linear polarisation, half-cell potential, and macro-cell current; the destructive methods employed was the mass loss test. In spite of the wet/dry cyclic regime only the CEM I (w/b=0.6) concrete showed signs of corrosion activity after 382 days. The electrochemical parameters obtained from the corrosion measurements were investigated to understand corrosion behaviour and B

values for calculating corrosion rate were estimated. The findings are summarised in the following:

- After depassivation, polarisation resistance, corrosion potential, and macro-cell current changed dramatically, but time to corrosion initiation varied with steel. It is evident that all techniques can detect corrosion activity on the steel. The polarisation resistance ranged from 1 to 10 $\Omega \cdot m^2$ for the active state and 75 to 163 $\Omega \cdot m^2$ for the passive state.

- In addition to the polarisation resistance and corrosion potential, the corrosion behaviour was observed using capacitance and time constant. For capacitance, the values increased after depassivation, indicating that the surface of the steel became uneven. On the other hand, the time constant easily indicated the condition of steel. In the results, time constants were < 50s for the active state and > 50s for the passive state.

- The propagation of corrosion was quantified by the corrosion rate, which was estimated using the B value. The B value (active state) obtained from this study (TEP technique) was not a single value but was, instead, distributed across a wide range, i.e. 75.5 – 96.0 mV. The B values varied with steel condition and exposure duration.

- Ohmic resistance is also an important factor in determining corrosion rate. Although the ohmic resistance was marginal in the passive state, the value for the active state accounted for up to 50% of the total resistance (=polarisation resistance and ohmic resistance). The corrosion rate would be underestimated without due consideration of the ohmic resistance.

- The corrosion rates obtained from the galvanostatic pulse technique and the mass loss test were compared. The corrosion rate was affected by the B values (i.e. the traditional value, Tafel extrapolation method and simplified method using a potentiostatic technique), and the difference in the rate obtained by different techniques was minimum when a traditional value was applied, i.e. 26 mV.

9.4 Monitoring electrical resistance

The electrical resistance of the samples was monitored to evaluate a change in concrete properties by chloride ingress. To track chloride transport and detect corrosion behaviour for up to 382 days of concrete age, stainless-steel pins were installed in concrete in discrete depths. The activation energy was determined to account for the effect of temperature on electrical resistivity of concrete in the field. The normalisation resistance was introduced to consider the chloride effect (N_{cl}), hydration effect (N_{hyd}) and corrosion effect (N_{corr}). The findings are summarised as follows:

- Regardless of type of binder, as-measured resistances at the outer layer were sensitive to the surrounding environments, such as the chloride solution, temperature and wet/dry periods. The convective zone was observed in the wet/dry cyclic regime which increased with an increase in w/b due to high porosity.

- For a low w/b, the normalised resistance increased with time, while for a high w/b it decreased after considering the hydration effect on the electrical resistance. This indicates that bound chloride leads to an increase in electrical resistance and free chloride causes a decrease in electrical resistance.

- A change in the electrical resistance caused by the corrosion process of steel, i.e. ionic movement from the cathode to the anode, could not be extracted in this study. From the result, it could be deduced that the change in the electrical resistance by ionic movement is smaller than by chloride ions dissolved in pore solution. However, the normalised resistance (N_{corr}) could detect cracking behaviour in this study. It was observed that N_{corr} increased markedly without any sign of corrosion; an increase in N_{corr} is caused by the formation of cracks.

- The electrical resistivity fluctuated with temperature. It was shown that the electrical resistance/resistivity measurement could be corrected to an equivalent resistance at a reference temperature through the use of an Arrhenius relationship. The activation energy for the field samples ranged from 26.12 to 37.9 kJ/mol and depended on type of binder and moisture content at the time of measurement.

9.5 Mix design – binders and w/b

Six concrete mixes were used in the study: three types of binder and two w/b. The evaluation was carried out from chloride transport to corrosion propagation. For chloride transport, performance factors included porosity/degree of saturation, diffusion/migration coefficients and electrical resistivity; for corrosion propagation, polarisation resistance, ohmic resistance, time constant, capacitance and electrical resistivity were used. The following summarises the durability performance of the mix compositions:

- In the investigation of pore structure relating to transport properties, concrete with SCMs had higher porosity than CEM I (or PC) concrete irrespective of w/b. However, transport rates for concrete with SCMs were lower than those for CEM I (or PC). In particular, the rate is more sensitive to w/b. Therefore, porosity is one of the durability indicators but it cannot fully reflect transport properties.

- Steel corrosion was only detected for CEM I (w/b=0.6) concrete. Therefore, a direct comparison regarding corrosion propagation cannot be made. Nonetheless, SCM, i.e. FA and GGBS, are beneficial as they have a high resistance to chloride-induced corrosion due to their higher resistance to chloride ingress.

- Electrical resistivity as a performance factor was measured with binder and time. At an early age (28 days), the electrical resistivity of CEM II/B-V concrete was lower than that of CEM I and CEM III/A concretes, and CEM III/A concrete had the highest resistivity. On the other hand, the resistivity of CEM II/B-V concrete was the highest at 382 days, followed by that of CEM III/A concrete. Therefore, in the view of long-term durability, SCM concrete is beneficial.

9.6 Predictive models – transport and corrosion model

Predictive modelling is beneficial for describing the deterioration of concrete exposed to a chloride environment. To simulate the deterioration process, two types of models are required: a chloride transport model and a corrosion propagation model. Regarding the transport model, the ClinConc model was updated using two environmental factors, K_{exp} and K_s. These factors were determined for both field and laboratory samples (table 8.2).

An empirical relation for corrosion development was determined using the limited corrosion results as corrosion of steel was only detected in CEM I (w/b=0.6) concrete (laboratory sample). The findings for the models are summarised as follows:

- The environmental factors were determined as input parameters in the ClinConc model. For field samples, K_{exp} is related to the exposure condition and was evaluated as 0.70, irrespective of type of binder, while K_s values, which are related to the degree of saturation, were 0.42, 0.35, and 0.24 for PC, GGBS/40, and FA/30 concretes, respectively. Thus, it can be concluded that FA/30 concrete is the most beneficial for resisting long-term chloride ingress in concrete. Meanwhile, K_s coefficient for laboratory samples, was similar for different binders with the same w/b due to their similar degree of saturation. Therefore, it can be stated that degree of saturation is also an important environmental factor. It is interesting to note that K_{exp} for laboratory concrete with w/b=0.6 is > 1.0 implying a higher w/b leads to more rapid chloride ingress.

- Simulating corrosion behaviour is difficult due to the complex electrochemical reactions in concrete, and it is virtually impossible to reflect all the influencing factors in concrete. In addition, in this study the corrosion rate varied with the B value, therefore an empirical relation using polarisation resistance was introduced. It was observed that the polarisation resistance quickly became stable after depassivation.

9.7 Recommendations for further research

The following are recommendations for further research.

- In this study, the relationship between the migration coefficient and the electrical resistivity was established using the Nernst-Planck relation. However, the assumption of a uniform distribution of chloride content over the sample was not valid for the sample in non-steady state. Instead, it was assumed that the average value for the chloride profile was a constant (0.356 mol/l) (figure 5.20), but this was not confirmed through the experiment. To verify the suggested equation, further test work is required for chloride profiling after migration testing.

- Polarisation resistances were measured using GP, LPR, PT and EIS techniques. It was confirmed that differences in the polarisation resistances obtained from different techniques were small, but the B value was very sensitive to analysis methods. In addition, although a simplified method to estimate the B value was used, the verification for the result was not sufficient due to the limited data on corroding samples. Therefore, further research is recommended regarding the use of the B value to estimate accurate corrosion rates. Furthermore, work of longer duration is also recommended to detect the corrosion of steel embedded in SCM concrete.

- The electrical resistance was monitored with depth to confirm the chloride transport and corrosion behaviour. It was observed that the electrical resistance decreased with chloride contamination, but a change in the resistance due to the corrosion process could not be extracted from the measured resistance. As an analysis method, a normalisation expression for the electrical resistance was used. However, this expression is qualitative hence further work should be undertaken to quantify a change of electrical resistivity caused by chloride content in concrete and to develop an analysis method for monitoring electrical resistance to detect corrosion.

- This study suggested a modified transport model using environmental factors. To verify the model or evaluate the factors, both laboratory and field samples were used. However, the factors must be updated with time and exposure conditions. It is recommended that further studies be conducted on concrete samples in different exposure conditions to refine the model. Furthermore, corrosion behaviour was expressed by the polarisation resistance, but the relation was established with limited data and further research should be carried out in this respect. Finally, a probabilistic method for estimating chloride transport and describing corrosion propagation is recommended to improve the accuracy of the model, as various influencing factors exist simultaneously in the deterioration process.

REFERENCES

Abd elaty, M. abd allah, 2014. Compressive strength prediction of Portland cement concrete with age using a new model. *HBRC Journal*, 10(2), 145–155.

ACI Committee 318, 2014. *Building code requirements for structural concrete (ACI 318-14) and commentary on building code requirements for structural concrete (ACI 318R-14)*. Michigan: American Concrete Institute.

Alexander, M.G., Ballim, Y., and Stanish, K., 2008. A framework for use of durability indexes in performance-based design and specifications for reinforced concrete structures. *Materials and Structures*, 41(5), 921–936.

Alexander, M.G., and Nganga, G., 2016. Introduction: Importance of marine concrete structures and durability design, in M. Alexander (ed.) *Marine concrete structures: design, durability and performance*. *Elsevier Ltd*. [Online]. Available at: http://www.sciencedirect.com/science/article/pii/B9780081000816000015.

Alexander, M.G., and Thomas, M.D.A., 2015. Service life prediction and performance testing - Current developments and practical applications. *Cement and Concrete Research*, 78(A), 155–164.

Alfaro, M., 2014. Modeling of polarization curves not exhibiting a Tafel region using Excel spreadsheets. *Alexandria Engineering Journal*, 53(4), 977–983.

Alonso, C., Andrade, C., Castellote, M., and Castro, P., 2000. Chloride threshold values to depassivate reinforcing bars embedded in a standardized OPC mortar. *Cement and Concrete Research*, 30(7), 1047–1055.

Alonso, C., Andrade, C., and González, J.A., 1988. Relation between resistivity and corrosion rate of reinforcements in carbonated mortar made with several cement types. *Cement and Concrete Research*, 18(5), 687–698.

Alonso, C., Castellote, M., and Andrade, C., 2002. Chloride threshold dependence of pitting potential of reinforcements. *Electrochimica Acta*, 47(21), 3469–3481.

Altmann, F., and Mechtcherine, V., 2013. Durability design strategies for new cementitious materials. *Cement and Concrete Research*, 54(December), 114–125.

Altmann, F., Sickert, J.U., Mechtcherine, V., and Kaliske, M., 2012. A fuzzy-probabilistic durability concept for strain-hardening cement-based composites (SHCCs) exposed to chlorides: Part 1: Concept development. *Cement and Concrete Composites*, 34(6), 754–762.

Amey, S.L., Johnson, D.A., Miltenberger, M.A., and Farzam, H., 1998. Predicting the service life of concrete marine structures: an environmental methodology. *ACI Structural Journal*, 95(2), 205–214.

Andrade, C., and Alonso, C., 2001. On-site measurements of corrosion rate of reinforcements. *Construction and Building Materials*, 15(2–3), 141–145.

Andrade, C., Castellote, M., Alonso, C., and González, C., 1999. Relation between colourimetric chloride penetration depth and charge passed in migration tests of the type of standard ASTM C1202-91. *Cement and Concrete Research*, 29(3), 417–421.

Andrade, C., Castellote, M., and D'Andrea, R., 2011. Measurement of ageing effect on chloride diffusion coefficients in cementitious matrices. *Journal of Nuclear Materials*, 412(1), 209–216.

Andrade, C., D'Andrea, R., and Rebolledo, N., 2014. Chloride ion penetration in concrete: The reaction factor in the electrical resistivity model. *Cement and Concrete Composites*, 47(March), 41–46.

Andrade, C., Diez, J.M., and Alonso, C., 1997. Mathematical modeling of a concrete surface `skin effect' on diffusion in chloride contaminated media. *Advanced Cement Based Materials*, 6(2), 39–44.

Andrade, C., Prieto, M., Tanner, P., Tavares, F., and D'Andrea, R., 2013. Testing and modelling chloride penetration into concrete. *Construction and Building Materials*, 39(February), 9–18.

Angst, U., Elsener, B., Jamali, A., and Adey, B., 2012. Concrete cover cracking owing to reinforcement corrosion - Theoretical considerations and practical experience. *Materials and Corrosion*, 63(12), 1069–1077.

Angst, U., Elsener, B., Larsen, C.K., and Vennesland, Ø., 2011a. Chloride induced reinforcement corrosion: Rate limiting step of early pitting corrosion. *Electrochimica Acta*, 56(17), 5877–5889.

Angst, U., Elsener, B., Larsen, C.K., and Vennesland, Ø., 2009. Critical chloride content in reinforced concrete - A review. *Cement and Concrete Research*, 39(12), 1122–1138.

Angst, U., Rønnquist, A., Elsener, B., Larsen, C.K., and Vennesland, Ø., 2011b. Probabilistic considerations on the effect of specimen size on the critical chloride content in reinforced concrete. *Corrosion Science*, 53(1), 177–187.

Angst, U.M., and Elsener, B., 2014. On the applicability of the wenner method for resistivity measurements of concrete. *ACI Materials Journal*, 111(6), 661–672.

Angst, U.M., Elsener, B., Larsen, C.K., and Vennesland, Ø., 2011c. Chloride induced reinforcement corrosion: Electrochemical monitoring of initiation stage and chloride threshold values. *Corrosion Science*, 53(4), 1451–1464.

Ann, K.Y., Ahn, J.H., and Ryou, J.S., 2009. The importance of chloride content at the concrete surface in assessing the time to corrosion of steel in concrete structures. *Construction and Building Materials*, 23(1), 239–245.

Ann, K.Y., Kim, T.S., Kim, J.H., and Kim, S.H., 2010. The resistance of high alumina cement against corrosion of steel in concrete. *Construction and Building Materials*, 24(8), 1502–1510.

Ann, K.Y., Moon, H.Y., Kim, Y.B., and Ryou, J., 2008. Durability of recycled aggregate concrete using pozzolanic materials. *Waste Management*, 28(6), 993–999.

Ann, K.Y., and Song, H.W., 2007. Chloride threshold level for corrosion of steel in concrete. *Corrosion Science*, 49(11), 4113–4133.

Archie, G.E., 1942. The electrical resistivity log as an aid in determining some reservoir characteristics. *Transactions of the AIME*, 146(1), 54–62.

Arya, C., Buenfeld, N.R., and Newman, J.B., 1990. Factors influencing chloride-binding in concrete. *Cement and Concrete Research*, 20(2), 291–300.

ASTM International, 2015. *ASTM C876 Standard test method for corrosion potentials of uncoated reinforcing steel in concrete*. Pennsylvania: ASTM International.

ASTM International, 2013. *ASTM C642 Standard Test method for density, absorption, and voids in hardened concrete*. Pennsylvania: ASTM International.

ASTM International, 2012. *ASTM C1202 Standard test method for electrical indication of concrete's ability to resist chloride ion penetration*. Pennsylvania: ASTM International.

ASTM International, 2011. *ASTM G1 Standard Practice for Preparing, Cleaning, and Evaluating Corrosion Test Specimens*. Pennsylvania: ASTM International.

ASTM International, 2007. *ASTM G109 Standard test method for determining the effects of chemical admixtures on the corrosion of embedded steel reinforcement in concrete exposed to chloride environments*. Pennsylvania: ASTM International.

Austin, S.A., Lyons, R., and Ing, M.J., 2004. The electrochemical behaviour of steel reinforced concrete during accelerated corrosion testing. *Corrosion*, 60(2), 203–212.

Bamforth, P.B., 1999. The derivation of input data for modelling chloride ingress from eight-year UK coastal exposure trials. *Magazine of Concrete Research*, 51(2), 87–96.

Bamforth, P.B., Price, W.F., and Emerson, M., 1997. *An international review of chloride ingress into structural concrete*. Report 1303S/96/9092. Wokingham: Transport Research Laboratory.

Baroghel-Bouny, V., Thiéry, M., and Wang, X., 2014. Performance-based assessment of durability and prediction of RC structure service life: transport properties as input data for physical models. *Materials and Structures*, 47(10), 1669–1691.

Barsoukov, E., and Macdonald, J.R., 2005. *Impedance spectroscopy theory, experiment, and application*. 2nd ed. [Online]New Jersey: John Wiley & Sons.

Basheer, P.A.., Gilleece, P.R.., Long, A.E., and McCarter, W.J., 2002. Monitoring electrical resistance of concretes containing alternative cementitious materials to assess their resistance to chloride penetration. *Cement and Concrete Composites*, 24(5), 437–449.

Bautista, A., Paredes, E.C., Velasco, F., and Alvarez, S.M., 2015. Corrugated stainless steels embedded in mortar for 9 years: Corrosion results of non-carbonated, chloride-contaminated samples. *Construction and Building Materials*, 93(September), 350–359.

Bentz, D.P., 2007. A virtual rapid chloride permeability test. *Cement and Concrete Composites*, 29(10), 723–731.

Bertolini, L., and Redaelli, E., 2009. Depassivation of steel reinforcement in case of pitting corrosion: detection techniques for laboratory studies. *Materials and Corrosion*, 60(8), 608–616.

Birbilis, N., and Holloway, L.J., 2007. Use of the time constant to detect corrosion speed in reinforced concrete structures. *Cement and Concrete Composites*, 29(4), 330–336.

Birbilis, N., Nairn, K.M., and Forsyth, M., 2004. On the electrochemical response and interfacial properties of steel-Ca(OH)2 and the steel-concrete system measured using galvanostatic pulses. *Electrochimica Acta*, 49(25), 4331–4339.

Bisquert, J., and Compte, A., 2001. Theory of the electrochemical impedance of anomalous diffusion. *Journal of Electroanalytical Chemistry*, 499(1), 112–120.

Bostanci, Ş.C., Limbachiya, M., and Kew, H., 2016. Portland slag and composites cement concretes: Engineering and durability properties. *Journal of Cleaner Production*, 112(1), 542–552.

British Standards Institution, 2016. *BS 8500-1+A1 Concrete-Complementary British Standard to BS EN 206 — Part 1: Method of specifying and guidance for the specifier*. London: British Standards Institution.

British Standards Institution, 2015a. *BS EN 12390-11 Testing hardened concrete Part 11: Determination of the chloride resistance of concrete, unidirectional diffusion*. London: British Standards Institution.

British Standards Institution, 2015b. *BS 1881-124 Testing concrete – Part 124 : Methods for analysis of hardened concrete*. London: British Standards Institution.

British Standards Institution, 2015c. *BS EN 197-1 Cement Part 1 : Composition , specifications and conformity criteria for common cements*. London: British Standards Institution.

British Standards Institution, 2014. *BS EN 206 Concrete — Specification, performanc, production and conformity*. London: British Standards Institution.

British Standards Institution, 2013a. *PD CEN/TR 16563 Principles of the equivalent durability procedure*. London: British Standards Institution.

British Standards Institution, 2013b. *BS 1881-125 Testing concrete — Part 125 : Methods for mixing and sampling fresh concrete in the laboratory*. London: British Standards Institution.

British Standards Institution, 2012a. *BS EN 450-1 Fly ash for concrete — Part 1: Definition, specifications and conformity critera*. London: British Standards Institution.

British Standards Institution, 2012b. *BS EN 934-2+A1 Admixtures for concrete, mortar and grout — Part2: Concrete admixtures-Definations, requirements, conformity, marking and labelling*. London: British Standards Institution.

British Standards Institution, 2009. *BS EN 12390-3 Testing hardened concrete — Part3: Compressive strength of test specimens*. London: British Standards Institution.

British Standards Institution, 2006. *BS EN 15167-1 Ground granulated blast furnace slag for use in concrete , mortar and grout — Part 1: Definations, specifications and conformity criteria*. London: British Standards Institution.

Bu, Y., and Weiss, J., 2014. The influence of alkali content on the electrical resistivity and transport properties of cementitious materials. *Cement and Concrete Composites*, 51(August), 49–58.

Castellote, M., Andrade, C., and Alonso, C., 2001. Measurement of the steady and non-steady-state chloride diffusion coefficients in a migration test by means of monitoring the conductivity in the anolyte chamber. Comparison with natural diffusion tests. *Cement and Concrete Research*, 31(10), 1411–1420.

Chang, Z.T., Cherry, B., and Marosszeky, M., 2008a. Polarisation behaviour of steel bar samples in concrete in seawater. Part 2: A polarisation model for corrosion evaluation of steel in concrete. *Corrosion Science*, 50(11), 3078–3086.

Chang, Z.T., Cherry, B., and Marosszeky, M., 2008b. Polarisation behaviour of steel bar samples in concrete in seawater. Part 1: Experimental measurement of polarisation curves of steel in concrete. *Corrosion Science*, 50(2), 357–364.

Chen, E., and Leung, C.K.Y., 2015. Finite element modeling of concrete cover cracking due to non-uniform steel corrosion. *Engineering Fracture Mechanics*, 134(November), 61–78.

Chen, Y.M., and Orazem, M.E., 2015. Impedance analysis of ASTM A416 tendon steel corrosion in alkaline simulated pore solutions. *Corrosion Science*, 104(March), 26–35.

Choi, Y.S., Kim, J.G., and Lee, K.M., 2006. Corrosion behavior of steel bar embedded in fly ash concrete. *Corrosion Science*, 48(7), 1733–1745.

Chrisp, T.M., McCarter, W.J., Starrs, G., Basheer, P.A.M., and Blewett, J., 2002. Depth-related variation in conductivity to study cover-zone concrete during wetting and drying. *Cement and Concrete Composites*, 24(5), 415–426.

Chrisp, T.M., Starrs, G., McCarter, W.J., Rouchotas, E., and Blewett, J., 2001. Temperature-conductivity relationships for concrete: An activation energy approach. *Journal of Materials Science Letters*, 20(12), 1085–1087.

Christodoulou, C., Sharifi, A., Das, S., and Goodier, C., 2014. Cathodic protection on the UK's Midland Links motorway viaducts. *Proceedings of the Institution of Civil Engineers-Bridge Engineering*, 167(BE1), 43–53.

Costa, A., and Appleton, J., 1999. Chloride penetration into concrete in marine environment - Part II : Prediction of long term chloride penetration. *Materials and Structures*, 32(June), 354–359.

Crank, J., 1975. *The Mathematics of diffusion*. 2nd ed. Oxford: Clarendon Press.

Deus, J.M., Díaz, B., Freire, L., and Nóvoa, X.R., 2014. The electrochemical behaviour of steel rebars in concrete: An Electrochemical Impedance Spectroscopy study of the effect of temperature. *Electrochimica Acta*, 131(June), 106–115.

Dhouibi, L., Triki, E., and Raharinaivo, A., 2002. The application of electrochemical impedance spectroscopy to determine the long-term effectiveness of corrosion inhibitors for steel in concrete. *Cement and Concrete Composites*, 24(1), 35–43.

DuraCrete, 1998. *Modelling of degradation: DuraCrete, probabilistic performance based durability design of concrete structures*. Project BE95-1347. European Union.

Ehlen, M., 2014. *LIFE-365 Service Life Prediction Model, Version 2.2.1 -Users Manual*[online]. Available at: http://www.life-365.org/download/ Life365_v2.2.1_ Users_Manual.pdf, (Accessed 01/1/2014).

Elsener, B., 2005. Corrosion rate of steel in concrete-Measurements beyond the Tafel law. *Corrosion Science*, 47(12), 3019–3033.

Elsener, B., 2002. Macrocell corrosion of steel in concrete - Implications for corrosion monitoring. *Cement and Concrete Composites*, 24(1), 65–72.

Feliu, S., Gonzalez, J.A., Andrade, C., and Feliu, V., 1986. The determination of the corrosion rate of steel in concrete by a non-stationary method. *Corrosion Science*, 26(11), 961–970.

Feliu, V., González, J.A., Andrade, C., and Feliu, S., 1998. Equivalent circuit for modelling the steel-concrete interface. I. Experimental evidence and theoretical predictions. *Corrosion Science*, 40(6), 975–993.

Ferreira, R.M., and Jalali, S., 2010. NDT measurements for the prediction of 28-day compressive strength. *NDT&E International*, 43(2), 55–61.

Flitt, H.J., and Schweinsberg, D.P., 2005. Evaluation of corrosion rate from polarisation curves not exhibiting a Tafel region. *Corrosion Science*, 47(12), 3034–3052.

Florea, M.V.A., and Brouwers, H.J.H., 2012. Chloride binding related to hydration products-Part I: Ordinary Portland cement. *Cement and Concrete Research*, 42(2), 282–290.

Freire, L., Carmezim, M.J., Ferreira, M.G.S., and Montemor, M.F., 2011. The electrochemical behaviour of stainless steel AISI 304 in alkaline solutions with different pH in the presence of chlorides. *Electrochimica Acta*, 56(14), 5280–5289.

Gao, Y. hong, Zhang, J. zhi, Zhang, S., and Zhang, Y. rong, 2017. Probability distribution of convection zone depth of chloride in concrete in a marine tidal environment. *Construction and Building Materials*, 140(June), 485–495.

Garcés, P., Andrade, M.C., Saez, A., and Alonso, M.C., 2005. Corrosion of reinforcing steel in neutral and acid solutions simulating the electrolytic environments in the micropores of concrete in the propagation period. *Corrosion Science*, 47(2), 289–306.

Ghods, P., Isgor, O.B., Carpenter, G.J.C., Li, J., McRae, G.A., and Gu, G.P., 2013. Nano-scale study of passive films and chloride-induced depassivation of carbon steel rebar

in simulated concrete pore solutions using FIB/TEM. *Cement and Concrete Research*, 47(May), 55–68.

Ghods, P., Isgor, O.B., McRae, G.A., and Gu, G.P., 2010. Electrochemical investigation of chloride-induced depassivation of black steel rebar under simulated service conditions. *Corrosion Science*, 52(5), 1649–1659.

Gjørv, O.E., Vennesland, Ø., and El-Busaidy, 1977. Electrical resistivity of concrete in the oceans, *Offshore Technology Conference*, 1977. pp.581–589

Glass, G.K., and Buenfeld, N.R., 2000a. Chloride-induced corrosion of steel in concrete. *Progress in Structural Engineering and Materials*, 2(4), 448–458.

Glass, G.K., and Buenfeld, N.R., 2000b. The influence of chloride binding on the chloride induced corrosion risk in reinforced concrete. *Corrosion Science*, 42(2), 329–344.

Glass, G.K., and Buenfeld, N.R., 1997. The presentation of the chloride threshold level for corrosion of steel in concrete. *Corrosion Science*, 39(5), 1001–1013.

Glass, G.K., Reddy, B., and Buenfeld, N.R., 2000. The participation of bound chloride in passive film breakdown on steel in concrete. *Corrosion Science*, 42(11), 2013–2021.

Glass, G.K., Yang, R., Dickhaus, T., and Buenfeld, N.R., 2001. Backscattered electron imaging of the steel-concrete interface. *Corrosion Science*, 43(4), 605–610.

González, J.A., Andrade, C., Alonso, C., and Feliu, S., 1995. Comparison of rates of general corrosion and maximum pitting penetration on concrete embedded steel reinforcement. *Cement and Concrete Research*, 25(2), 257–264.

Gonzalez, J.A., Cobo, A., Gonzalez, M.N., and Feliu, S., 2001. On-site determination of corrosion rate inreinforced concrete structures by use of galvanostatic pulses. *Corrosion Science*, 43(4), 611–625.

González, J.A., Miranda, J.M., and Feliu, S., 2004. Considerations on reproducibility of potential and corrosion rate measurements in reinforced concrete. *Corrosion Science*, 46(10), 2467–2485.

Hirao, H., Yamada, K., Takahashi, H., and Zibara, H., 2005. Chloride binding of cement estimated by binding isotherms of hydrates. *Journal of Advanced Concrete Technology*, 3(1), 77–84.

Hussain, S.E., and Rasheeduzafar, S., 1994. Corrosion resistance performance of fly ash blended cement concrete. *ACI Materials Journal*, 91(3), 264–272.

Japan Society of Civil Engineers, 2010a. *Standard specifications for concrete structures-2007 'Design'*. Tokyo: Japan Society of Civil Engineers.

Japan Society of Civil Engineers, 2010b. *Standard Specifications for Concrete Structures - 2007 'Materials and construction'*. Tokyo: Japan Society of Civil Engineers.

Ji, Y.S., Zhao, W., Zhou, M., Ma, H.R., and Zeng, P., 2013. Corrosion current distribution of macrocell and microcell of steel bar in concrete exposed to chloride environments. *Construction and Building Materials*, 47(October), 104–110.

Jorcin, J.B., Orazem, M.E., Pébère, N., and Tribollet, B., 2006. CPE analysis by local electrochemical impedance spectroscopy. *Electrochimica Acta*, 51(8–9), 1473–1479.

Kassir, M.K., and Ghosn, M., 2002. Chloride-induced corrosion of reinforced concrete bridge decks. *Cement and Concrete Research*, 32(1), 139–143.

Katwan, M.J., Hodgkiess, T., and Arthur, P.D., 1996. Electrochemical noise technique for the prediction of corrosion rate of steel in concrete. *Materials and Structures*, 29(5), 286–294.

Keßler, S., Fischer, J., Straub, D., and Gehlen, C., 2014. Updating of service-life prediction of reinforced concrete structures with potential mapping. *Cement and Concrete Composites*, 47(March), 47–52.

Kessy, J.G., Alexander, M.G., and Beushausen, H., 2015. Concrete durability standards: International trends and the South African context. *Journal of The South African Institution of Civil Engineering*, 57(1), 47–58.

Kim, J., McCarter, W.J., Suryanto, B., Nanukuttan, S., Basheer, P.A.M., and Chrisp, T.M., 2016. Chloride ingress into marine exposed concrete: A comparison of empirical- and physically- based models. *Cement and Concrete Composites*, 72(September), 133–145.

Koch, G.H., Brongers, M.P.H., Thompson, N.G., Virmani, Y.P., and Payer, J.H., 2002. *Corrosion costs and preventive strategies in the United States*. FHWA-RD-01-156. Texas: NACE Internationals.

Kouřil, M., Novák, P., and Bojko, M., 2006. Limitations of the linear polarization method to determine stainless steel corrosion rate in concrete environment. *Cement and Concrete Composites*, 28(3), 220–225.

Kulkarni, V.R., 2009. Exposure classes for designing durable concrete. *The Indian Concrete Journal*, 83(3), 23–43.

Kumar, A., 2010. *Water flow and transport of chloride in unsaturated concrete*. MSc. University of Saskatchewan.

Kurumisawa, K., and Nawa, T., 2016. Electrical Conductivity and chloride ingress in hardened cement paste. *Journal of Advanced Concrete Technology*, 14(3), 87–94.

Lataste, J.F., 2010. Electrical resistivity for the evaluation of reinforced concrete structures, in C. Maierhofer, H.-W. Reinhardt, and G. Dobmann (eds.) *Non-destructive evaluation of reinforced concrete structures: Volume 2: Non-destructive testing methods*. *Woodhead Publishing*. [Online]. Available at: http://dx.doi.org/10.1533/9781845699604.2.243.

Lataste, J.F., Sirieix, C., Breysse, D., and Frappa, M., 2003. Electrical resistivity measurement applied to cracking assessment on reinforced concrete structures in civil engineering. *NDT&E International*, 36(6), 383–394.

Leng, F., Feng, N., and Lu, X., 2000. An experimental study on the properties of resistance to diffusion of chloride ions of fly ash and blast furnace slag concrete. *Cement and Concrete Research*, 30(6), 989–992.

Li, K., Chen, Z., and Lian, H., 2008. Concepts and requirements of durability design for concrete structures: an extensive review of CCES01. *Materials and Structures*, 41(4), 717–731.

Li, K., Zeng, Q., Luo, M., and Pang, X., 2014. Effect of self-desiccation on the pore structure of paste and mortar incorporating 70% GGBS. *Construction and Building Materials*, 51(January), 329–337.

Li, Q., Xu, S., and Zeng, Q., 2016. The effect of water saturation degree on the electrical properties of cement-based porous material. *Cement and Concrete Composites*, 70(July), 35–47.

Liam, K.C., Roy, S.K., and Northwoodf, D.O., 1992. Chloride ingress measurements and corrosion potential mapping study of a 24-year-old reinforced concrete jetty structure in a tropical marine environment. *Magazine of Concrete Research*, 44(160), 205–215.

Lim, T.Y.D., Teng, S., Bahador, S.D., and GjØrv, O.E., 2016. Durability of very-high-strength concrete with supplementary cementitious materials for marine environments. *ACI Materials Journal*, 113(1), 95–103.

Liu, T., and Weyers, R.., 1998. Modeling the dynamic corrosion process in chloride contaminated concrete structures. *Cement and Concrete Research*, 28(3), 365–379.

Lübeck, A., Gastaldini, A.L.G., Barin, D.S., and Siqueira, H.C., 2012. Compressive strength and electrical properties of concrete with white Portland cement and blast-furnace slag. *Cement and Concrete Composites*, 34(3), 392–399.

Luo, R., Cai, Y., Wang, C., and Huang, X., 2003. Study of chloride binding and diffusion in GGBS concrete. *Cement and Concrete Research*, 33(1), 1–7.

Maage, M., Helland, S., Poulsen, E., Vennesland, O., and Carlsen, J.E., 1996. Service life prediction of existing concrete structures exposed to marine environment. *ACI Materials Journal*, 93(6), 602–608.

Maheswaran, T., and Sanjayan, J.G., 2004. A semi-closed-form solution for chloride diffusion in concrete with time-varying parameters. *Magazine of Concrete Research*, 56(6), 359–366.

Manera, M., Vennesland, Ø., and Bertolini, L., 2008. Chloride threshold for rebar corrosion in concrete with addition of silica fume. *Corrosion Science*, 50(2), 554–560.

Mangat, P.S., and Molloy, B.T., 1994. Prediction of long term chloride concentration in concrete. *Materials and Structures*, 27(6), 338–346.

Mansfeld, F., 2005. Tafel slopes and corrosion rates obtained in the pre-Tafel region of polarization curves. *Corrosion Science*, 47(12), 3178–3186.

Marchand, J., and Samson, E., 2009. Predicting the service-life of concrete structures - Limitations of simplified models. *Cement and Concrete Composites*, 31(8), 515–521.

Martinez, I., Rozas, F., Ramos-Cillan, S., González, M., and Castellote, M., 2015. Chloride Electroremediation in reinforced structures: Preliminary electrochemical tests to detect the steel repassivation during the treatment. *Electrochimica Acta*, 181(November), 288–300.

McCafferty, E., 2005. Validation of corrosion rates measured by the Tafel extrapolation method. *Corrosion Science*, 47(12), 3202–3215.

McCarter, W.J., and Brousseau, R., 1990. The A.C. response of hardened cement paste. *Cement and Concrete Research*, 20(6), 891–900.

McCarter, W.J., Chrisp, T.M., Butler, A., and Basheer, P.A.M., 2001. Near-surface sensors for condition monitoring of cover-zone concrete. *Construction and Building Materials*, 15(2–3), 115–124.

McCarter, W.J., Chrisp, T.M., Starrs, G., Adamson, A., Basheer, P.A.M., Nanukuttan, S., et al., 2013a. Characterization of physio-chemical processes and hydration kinetics in concretes containing supplementary cementitious materials using electrical property measurements. *Cement and Concrete Research*, 50(August), 26–33.

McCarter, W.J., Chrisp, T.M., Starrs, G., Adamson, A., Owens, E., Basheer, P.A.M., et al., 2012. Developments in performance monitoring of concrete exposed to extreme environments. *Journal of Infrastructure Systems*, 18(3), 167–175.

McCarter, W.J., Chrisp, T.M., Starrs, G., Basheer, P.A.M., and Blewett, J., 2005. Field monitoring of electrical conductivity of cover-zone concrete. *Cement and Concrete Composites*, 27(7–8), 809–817.

McCarter, W.J., and Garvin, S., 1989. Dependence of electrical impedance of cement-based materials on their moisture condition. *Journal of Physics D: Applied Physics*, 22(11), 1773–1776.

McCarter, W.J., Linfoot, B.T., Chrisp, T.M., and Starrs, G., 2008. Performance of concrete in XS1, XS2 and XS3 environments. *Magazine of Concrete Research*, 60(4), 261–270.

McCarter, W.J., Starrs, G., Adamson, A., Chrisp, T.M., Basheer, P.A.M., Nanukuttan, S., et al., 2013b. Influence of different european cements on the hydration of cover-Zone concrete during the curing and postcuring periods. *Journal of Materials in Civil Engineering*, 25(9), 1335–1343.

McCarter, W.J., Starrs, G., and Chrisp, T.M., 2000. Electrical conductivity, diffusion, and permeability of Portland cement-based mortars. *Cement and Concrete Research*, 30(9), 1395–1400.

McCarter, W.J., Taha, H.M., Suryanto, B., and Starrs, G., 2015. Two-point concrete resistivity measurements: interfacial phenomena at the electrode–concrete contact zone. *Measurement Science and Technology*, 26(8), 85007.

McCarter, W.J., and Vennesland, Ø., 2004. Sensor systems for use in reinforced concrete structures. *Construction and Building Materials*, 18(6), 351–358.

McPolin, D., Basheer, P.A.M., Long, A.E., Grattan, K.T.V., and Sun, T., 2005. Obtaining progressive chloride profiles in cementitious materials. *Construction and Building Materials*, 19(9), 666–673.

Meira, G.R., Andrade, C., Vilar, E.O., and Nery, K.D., 2014. Analysis of chloride threshold from laboratory and field experiments in marine atmosphere zone. *Construction and Building Materials*, 55(March), 289–298.

Michel, A., Nygaard, P.V., and Geiker, M.R., 2013. Experimental investigation on the short-term impact of temperature and moisture on reinforcement corrosion. *Corrosion Science*, 72(July), 26–34.

Michel, A., Otieno, M., Stang, H., and Geiker, M.R., 2016. Propagation of steel corrosion in concrete: Experimental and numerical investigations. *Cement and Concrete Composites*, 70(July), 171–182.

Midgley, H.G., and Illston, J.M., 1984. The penetration of chlorides into hardened cement pastes. *Cement and Concrete Research*, 14(4), 546–558.

Montemor, M.F., Simoes, A.M.P., and Ferreira, M.G.S., 1998. Analytical characterization of the passive film formed on steel in solutions simulating the concrete interstitial electrolyte. *Corrosion*, 54(5), 347–353.

Montemor, M.F., Simoes, A.M.P., and Salta, M.M., 2000. Effect of fly ash on concrete reinforcement corrosion studied by EIS. *Cement and Concrete Composites*, 22(3), 175–185.

Morozov, Y., Castela, A.S., Dias, A.P.S., and Montemor, M.F., 2013. Chloride-induced corrosion behavior of reinforcing steel in spent fluid cracking catalyst modified mortars. *Cement and Concrete Research*, 47(May), 1–7.

Nanukuttan, S. V., Basheer, L., McCarter, W.J., Robinson, D.J., and Basheer, P.A.M., 2008. Full-scale marine exposure tests on treated and untreated concretes-Initial 7-year results. *ACI Materials Journal*, 105(1), 81–87.

Neville, A.M., 2011. *Properties of Concrete*. 5th ed. London: Pearson.

Newlands, M., Jones, R., Kandasami, S., and Harrison, T., 2007. Sensitivity of electrode contact solutions and contact pressure in assessing electrical resistivity of concrete. *Materials and Structures*, 41(4), 621–632.

Nilsson, L.O., 2000. A numerical model for combined diffusion and convection of chloride in non-saturated concrete, *Second International RILEM Workshop on Testing and Modelling the Chloride Ingress into Concrete*, Bagneux. 2000. Bagneux: RILEM Publications SARL, pp.261–275

Nokken, M., Boddy, A., Hooton, R.D., and Thomas, M.D.A., 2006. Time dependent diffusion in concrete-three laboratory studies. *Cement and Concrete Research*, 36(1), 200–207.

Van Noort, R., Hunger, M., and Spiesz, P., 2016. Long-term chloride migration coefficient in slag cement-based concrete and resistivity as an alternative test method. *Construction and Building Materials*, 115(July), 746–759.

Nordtest, 1999. *NT Build 492 Concrete, mortar and cement-based repair materials: Chloride migration coefficient from non-steady-state migration experiments*. Espoo: Nordtest.

Nordtest, 1995. *NT build 443 Concrete Concrete, hardened: Accelerated chloride penetration*. Espoo: Nordtest.

Nwaubani, S.O., and Katsanos, A., 2014. Effect of alternative de-icers on the corrosion resistance of reinforced concrete bridges and highway structures, in M. Aliofkhazraei (ed.) *Developments in Corrosion Protection*. *InTech*. [Online]. Available at: https://www.intechopen.com/books/developments-in-corrosion-protection/effect-of-alternative-de-icers-on-the-corrosion-resistance-of-reinforced-concrete-bridges-and-highwa.

Nygaard, P. V., Geiker, M.R., and Elsener, B., 2009. Corrosion rate of steel in concrete: evaluation of confinement techniques for on-site corrosion rate measurements. *Materials and Structures*, 42(8), 1059–1076.

Nygaard, P.V., and Geiker, M.R., 2005. A method for measuring the chloride threshold level required to initiate reinforcement corrosion in concrete. *Materials and Structures*, 38(May), 489–494.

Oh, B.H., Cha, S.W., Jang, B.S., and Jang, S.., 2002. Development of high-performance concrete having high resistance to chloride penetration. *Nuclear Engineering and Design*, 212(1–3), 221–231.

Otieno, M., Beushausen, H., and Alexander, M., 2014. Effect of chemical composition of slag on chloride penetration resistance of concrete. *Cement and Concrete Composites*, 46(February), 56–64.

Ožbolt, J., Balabanić, G., and Kušter, M., 2011. 3D Numerical modelling of steel corrosion in concrete structures. *Corrosion Science*, 53(12), 4166–4177.

Pack, S.-W., Jung, M.-S., Song, H.-W., Kim, S.-H., and Ann, K.Y., 2010. Prediction of time dependent chloride transport in concrete structures exposed to a marine environment. *Cement and Concrete Research*, 40(2), 302–312.

Park, Z.T., Choi, Y.S., Kim, J.G., and Chung, L., 2005. Development of a galvanic sensor system for detecting the corrosion damage of the steel embedded in concrete structure: Part 2. Laboratory electrochemical testing of sensors in concrete. *Cement and Concrete Research*, 35(9), 1814–1819.

Pech-Canul, M.A., and Castro, P., 2002. Corrosion measurements of steel reinforcement in concrete exposed to a tropical marine atmosphere. *Cement and Concrete Research*, 32(3), 491–498.

Pereira, E.V., Salta, M.M., and Fonseca, I.T.E., 2015. On the measurement of the polarisation resistance of reinforcing steel with embedded sensors: A comparative study. *Materials and Corrosion*, 66(10), 1029–1038.

Petcherdchoo, A., 2013. Time dependent models of apparent diffusion coefficient and surface chloride for chloride transport in fly ash concrete. *Construction and Building Materials*, 38(January), 497–507.

Du Plooy, R., Palma Lopes, S., Villain, G., and Dérobert, X., 2013. Development of a multi-ring resistivity cell and multi-electrode resistivity probe for investigation of cover concrete condition. *NDT&E International*, 54(March), 27–36.

Polder, R.B., 2001. Test methods for on site measurement of resistivity of concrete - a RILEM TC-154 technical recommendation. *Construction and Building Materials*, 15(2–3), 125–131.

Polder, R.B., and Peelen, W.H.A., 2002. Characterisation of chloride transport and reinforcement corrosion in concrete under cyclic wetting and drying by electrical resistivity. *Cement and Concrete Composites*, 24(5), 427–435.

Polder, R.B., and De Rooij, M.R., 2005. Durability of marine concrete structures - Field investigations and modelling. *Heron*, 50(3), 133–154.

Pour-Ghaz, M., 2007. *A novel approach for practical modelling of steel corrosion in concrete*. MSc. Carleton University.

Pour-Ghaz, M., Burkan Isgor, O., and Ghods, P., 2009. Quantitative interpretation of Half-cell potential measurements in concrete structures. *Journal of Materials in Civil Engineering*, 21(9), 467–475.

Poursaee, A., 2010. Potentiostatic transient technique, a simple approach to estimate the corrosion current density and Stern-Geary constant of reinforcing steel in concrete. *Cement and Concrete Research*, 40(9), 1451–1458.

Powers, R.G., Sagues, A.A., and Virmani, Y.P., 2004. *Corrosion of post-tensioned tendons in Florida Bridges*. FL/DOT/SMO/04-475. Florida Department of Transportation.

Raupach, M., 1996. Chloride-induced macrocell corrosion of steel in concrete - Theoretical background and practical consequences. *Construction and Building Materials*, 10(5), 329–338.

Reou, J.S., and Ann, K.Y., 2009. Electrochemical assessment on the corrosion risk of steel embedment in OPC concrete depending on the corrosion detection techniques. *Materials Chemistry and Physics*, 113(1), 78–84.

RILEM TC 154-EMC, 2004. Test methods for on-site corrosion rate measurement of steel reinforcement in concrete by means of the polarization resistance method. *Materials and Structures*, 37(November), 623–643.

RILEM TC 154-EMC, 2003. Half-cell potential measurements-Potential mapping on reinforced concrete structures. *Materials and Structures*, 36(August), 461–471.

RILEM TC 230-PSC, 2016. *Performance-based specifications and control of concrete durability: State-of-the-art report*. H. Beushausen and L. Fernandez Luco (eds.)[Online]Springer.

Roberge, P.R., 2008. *Corrosion engineering: Principles and practice*. New York: McGraw-Hill.

Saetta, A.V., Scotta, R., and Vitaliani, R.V., 1993. Analysis of chloride diffusion into partially saturated concrete. *ACI Materials Journal*, 90(5), 441–451.

Safehian, M., and Ramezanianpour, A.A., 2015. Prediction of RC structure service life from field long term chloride diffusion. *Computers and Concrete*, 15(4), 589–606.

Samson, E., and Marchand, J., 2007. Modeling the transport of ions in unsaturated cement-based materials. *Computers and Structures*, 85(23–24), 1740–1756.

San Nicolas, R., Cyr, M., and Escadeillas, G., 2014. Performance-based approach to durability of concrete containing flash-calcined metakaolin as cement replacement. *Construction and Building Materials*, 55(March), 313–322.

Sánchez-Moreno, M., Takenouti, H., García-Jareño, J.J., Vicente, F., and Alonso, C., 2009. A theoretical approach of impedance spectroscopy during the passivation of steel in alkaline media. *Electrochimica Acta*, 54(28), 7222–7226.

Sánchez, M., Gregori, J., Alonso, C., García-Jareño, J.J., Takenouti, H., and Vicente, F., 2007. Electrochemical impedance spectroscopy for studying passive layers on steel rebars immersed in alkaline solutions simulating concrete pores. *Electrochimica Acta*, 52(27), 7634–7641.

Sandberg, P., 1999. Studies of chloride binding in concrete exposed in a marine environment. *Cement and Concrete Research*, 29(4), 473–477.

Sengul, O., 2014. Use of electrical resistivity as an indicator for durability. *Construction and Building Materials*, 73(December), 434–441.

Sengul, O., and Gjørv, O.E., 2009. Electrical resistivity measurements for quality control during concrete construction. *ACI Materials Journal*, 105(6), 541–547.

Sleiman, H., Amiri, O., and Aït-Mokhtar, A., 2009. Chloride transport in unsaturated cement-based materials. *European Journal of Environmental and Civil Engineering*, 13(4), 489–499.

Smith, P.E., 2016. Design and specification of marine concrte structures, in M. Alexander (ed.) *Marine concrete structures: design, durability and performance*. *Elsevier Ltd*. [Online]. Available at: http://www.sciencedirect.com/science/article/pii/B9780081000816000039.

Snyder, K.A., Feng, X., Keen, B.D., and Mason, T.O., 2003. Estimating the electrical conductivity of cement paste pore solutions from OH-, K+ and Na+ concentrations. *Cement and Concrete Research*, 33(6), 793–798.

Song, G., 2000. Theoretical analysis of the measurement of polarisation resistance in reinforced concrete. *Cement and Concrete Composites*, 22(6), 407–415.

Song, H.W., Lee, C.H., and Ann, K.Y., 2008a. Factors influencing chloride transport in concrete structures exposed to marine environments. *Cement and Concrete Composites*, 30(2), 113–121.

Song, H.W., Lee, C.H., Jung, M.S., and Ann, K.Y., 2008b. Development of chloride binding capacity in cement pastes and influence of the pH of hydration products. *Canadian Journal of Civil Engineering*, 35(12), 1427–1434.

Spiesz, P., Ballari, M.M., and Brouwers, H.J.H., 2012. RCM: A new model accounting for the non-linear chloride binding isotherm and the non-equilibrium conditions

between the free- and bound-chloride concentrations. *Construction and Building Materials*, 27(1), 293–304.

Spiesz, P., and Brouwers, H.J.H., 2013. The apparent and effective chloride migration coefficients obtained in migration tests. *Cement and Concrete Research*, 48(June), 116–127.

Spiesz, P., and Brouwers, H.J.H., 2012. Influence of the applied voltage on the Rapid Chloride Migration (RCM) test. *Cement and Concrete Research*, 42(8), 1072–1082.

Stanish, K., and Thomas, M., 2003. The use of bulk diffusion tests to establish time-dependent concrete chloride diffusion coefficients. *Cement and Concrete Research*, 33(1), 55–62.

Stanish, K.D., Hooton, R.D., and Thomas, M.D.A., 1997. *Testing the chloride penetration resistance of concrete : A literature review*. DTFH61-97-R-00022. Washington: FHWA.

Stern, M., and Geary, A.L., 1957. Electrochemical polarization I. A theoretical analysis of the shape of polarization curves. *Journal of The Electrochemical Society*, 104(9), 56–63.

Streicher, P.E., and Alexander, M.G., 1995. A chloride conduction test for concrete. *Cement and Concrete Research*, 25(6), 1284–1294.

Tang, L., 2008. Engineering expression of the ClinConc model for prediction of free and total chloride ingress in submerged marine concrete. *Cement and Concrete Research*, 38(8–9), 1092–1097.

Tang, L., 2005. *Resistance of concrete to chloride ingress – From laboratory tests to in-field performance*. EU-Project CHLORTEST(G6RD-CT-2002-00855). Boras: SP Swedish National Testing and Research.

Tang, L., 2003. *Chloride ingress in concrete exposed to marine environment: Field data up to 10 years exposure*. SP Report 2003:16. Boras: SP Swedish National Testing and Resaerch Institute.

Tang, L., 2001. Precision of the Nordic test methods for measuring the chloride diffusion/migration coefficients of concrete. *Materials and Structures*, 34(Octorber), 479–485.

Tang, L., 1996a. *Chloride transport in concrete-measurement and prediction*. PhD. Chalmers University of Technology.

Tang, L., 1996b. Electrically accelerated methods for determining chloride diffusivity in concrete—current development. *Magazine of Concrete Research*, 48(176), 173–179.

Tang, L., and Nilsson, L.-O., 2000. Modeling of chloride penetration into concrete – Tracing five years' field exposure. *Concrete Science and Engineering*, 2(8), 170–175.

Tang, L., and Nilsson, L.-O., 1993. Chloride binding capacity and binding isotherms of OPC pastes and mortars. *Cement and Concrete Research*, 23(2), 247–253.

Tilly, G., 2005. *Performances of concrete repairs in practice*[PowerPoint presentation], Gillford and Partners, UK. Available at: http://projects.bre.co.uk/conrepnet /members/mw5/mw5p3.pdf, (Accessed 15/6/2017).

Thomas, M.D.A., Hooton, R.D., Scott, A., and Zibara, H., 2012. The effect of supplementary cementitious materials on chloride binding in hardened cement paste. *Cement and Concrete Research*, 42(1), 1–7.

Thomas, M.D.A., and Matthews, J.D., 2004. Performance of pfa concrete in a marine environment - 10-year results. *Cement and Concrete Composites*, 26(1), 5–20.

Tuutti, K., 1982. *Corrosion of steel in concrete*. Stockholm: Swedish Cement and Concrete Research Institute.

Val, D.V., and Trapper, P.A., 2008. Probabilistic evaluation of initiation time of chloride-induced corrosion. *Reliability Engineering and System Safety*, 93(3), 364–372.

Vedalakshmi, R., Manoharan, S., Song, H.W., and Palaniswamy, N., 2009a. Application of harmonic analysis in measuring the corrosion rate of rebar in concrete. *Corrosion Science*, 51(11), 2777–2789.

Vedalakshmi, R., Rajagopal, K., and Palaniswamy, N., 2008. Longterm corrosion performance of rebar embedded in blended cement concrete under macro cell corrosion condition. *Construction and Building Materials*, 22(3), 186–199.

Vedalakshmi, R., Saraswathy, V., Song, H.W., and Palaniswamy, N., 2009b. Determination of diffusion coefficient of chloride in concrete using Warburg diffusion coefficient. *Corrosion Science*, 51(6), 1299–1307.

Videm, K., 2007. Electrochemical studies of steel in cement mortar containing chloride and micro-silica. *Corrosion Science*, 49(4), 1702–1717.

Vrouwenvelder, T., and Schießl, P., 1999. Durability aspects of probabilistic ultimate limit state design. *Heron*, 44(1), 19–29.

Vu, K., Stewart, M.G., and Mullard, J., 2005. Corrosion-induced cracking: Experimental data and predictive models. *ACI Structural Journal*, 102(5), 719–726.

Wood, G.M., 1997. Tay Road Bridge: Analysis of Chloride Ingress Variability & Prediction of Long Term Deterioration. *Construction and Building Materials*, 11(8), 249–254.

Xi, Y., and Bažant, Z.P., 1999. Modeling chloride penetration in saturated concrete. *Journal of Materials in Civil Engineering*, 11(1), 58–65.

Xu, Y., Li, K., Liu, L., Yang, L., Wang, X., and Huang, Y., 2016. Experimental study on rebar corrosion using the galvanic sensor combined with the electronic resistance technique. *Sensors*, 16(9), 1–19.

Yalçyn, H., and Ergun, M., 1996. The prediction of corrosion rates of reinforcing steels in concrete. *Cement and Concrete Research*, 26(10), 1593–1599.

Yokozeki, K., Watanabe, K., Hayashi, D., Sakata, N., and Otsuki, N., 2003. Model for estimating ion diffusion coefficients in cementitious materials considering hydration reaction and temperature dependence. *Proceedings of JSCE*, 58(725), 105–119.

Yu, Z., and Ye, G., 2013. New perspective of service life prediction of fly ash concrete. *Construction and Building Materials*, 48(November), 764–771.

Yuan, Q., Shi, C., De Schutter, G., Audenaert, K., and Deng, D., 2009. Chloride binding of cement-based materials subjected to external chloride environment - A review. *Construction and Building Materials*, 23(1), 1–13.

Zou, Y., Wang, J., and Zheng, Y.Y., 2011. Electrochemical techniques for determining corrosion rate of rusted steel in seawater. *Corrosion Science*, 53(1), 208–216.

APPENDIX

APPENDIX A: EQUATIONS USED WITHIN TEXT

A.1 Diffusion coefficient in unsaturated concrete (equation 3.14):

To solve the main function (equation (3.14)) in which diffusion coefficient in unsaturated concrete is influenced by different influencing factors, the sub-functions suggested by Xi & Bažant (1999) are required as follows;

$$f_1\left(\frac{w}{c}, t_0\right) = \frac{28 - t_0}{62500} + \left(\frac{1}{4} + \frac{(28 - t_0)}{300}\right)\left(\frac{w}{c}\right)^{6.55}$$

$$f_2(g_i) = D_{cp}\left(1 + \frac{g_i}{\frac{(1 - g_i)}{3} + \frac{1}{\left(\frac{D_{agg}}{D_{cp}} - 1\right)}}\right)$$

$$D = \frac{2\left(1 - \left(V_p - V_p^c\right)\right)}{S^2}(\emptyset - \emptyset^C)^{4.2}$$

$$f_3(H) = \left(1 + \frac{(1 - H)^4}{(1 - H_c)^4}\right)^{-1}$$

$$f_4(T) = exp\left[\frac{E_a}{R}\left(\frac{1}{T_0} - \frac{1}{T}\right)\right]$$

$$f_5\left(C_f\right) = 1 - k_{ion}\left(C_f\right)^m$$

where t_0 is the curing time (days), w/c is water to cement ratio, g_i is the volume fraction of aggregate in concrete D_{agg} and D_{cp} is the diffusivities of aggregates and cement paste, $\emptyset$ is the porosity, S is the surface area (the monolayer capacity), $\emptyset^C$ is the critical porosity (3% for cement paste), H_c is the critical humidity level (=0.75), E_a is the activation energy of the diffusion process, T_0 is the reference temperature (=296K), k_{ion} is a constant (=8.33) and m is a constant (=0.5)

A.2 Degree of hydration

Degree of hydration was calculated with the following equations. To estimate the resistivity of pore solution, degree of hydration was used as the input parameter.

$$\alpha_t = \alpha_{max} e^{-A_\alpha [ln(t)]^{B\alpha}}$$

$$\alpha_{max} \begin{cases} 1, & {}^{w}/_{b} \geq 0.39 \\ \dfrac{{}^{w}/_{b}}{0.39}, & {}^{w}/_{b} < 0.39 \end{cases}$$

$$A_\alpha = -\frac{ln\left(\frac{\alpha_{1d}}{\alpha_{max}}\right)}{[ln(t_{1d})]^{-B_\alpha}}$$

$$B_\alpha = \frac{ln\left[\frac{ln\left(\frac{\alpha_{2.5y}}{\alpha_{max}}\right)}{ln\left(\frac{\alpha_{1d}}{\alpha_{max}}\right)}\right]}{ln\left[\frac{ln(t_{1d})}{ln(t_{2.5y})}\right]}$$

For OPC, $$\frac{\alpha_{2.5y}}{\alpha_{max}} = \begin{cases} 1, & {}^{w}/_{b} \geq 0.625 \\ 1.265 \times \sqrt{{}^{w}/_{b}}, & {}^{w}/_{b} < 0 \end{cases}$$

$$\alpha_{1d} = 0.48 \times \sqrt{{}^{w}/_{b}} \times e^{\left[-\frac{E_a}{R}\left(\frac{1}{T}-\frac{1}{293}\right)\right]}$$

where α_t is the degree of hydration at time t (hour), α_t is the maximum degree of hydration; α_{1d} is the degree of hydration at 1 day (hour); $\alpha_{2.5y}$ is the degree of hydration at 2.5 years (hour); ${}^{w}/_{b}$ is the effective water to binder ratio; R is gas constant, T is absolute constant (K); and E_a is activation energy ($E_a = 36\ kJ/mol$, $T \geq 293\ K$ or $E_a = 65\ kJ/mol$, $T < 293\ K$).

APPENDIX B: EXPERIMENTAL SET-UPS

B.1 Slab sample fabrication

B1.1 Stainless-steel pin electrodes and steels in plywood mould

For slab samples to monitor the electrical resistance/corrosion rate of steel, plywood mould was fabricated. Plywood plate (trapezoid shape) was additionally attached on the bottom of the mould to make a dyke. To install stainless-steel pin electrodes and the mild steels, holes were directly made on the plywood.

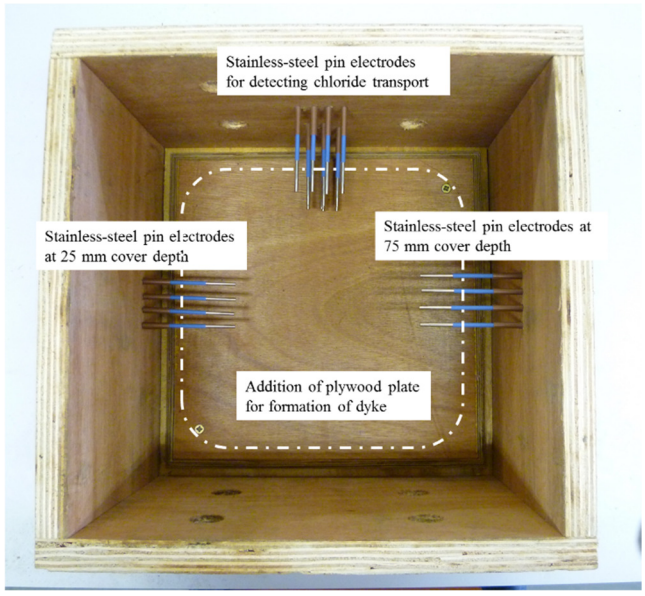

Figure B.1 Installation of stainless-steel pin electrodes in plywood mould

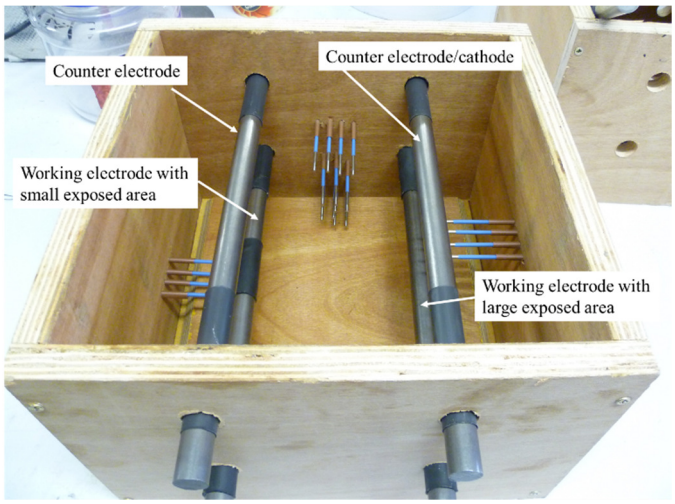

Figure B.2 Installation of four steels in plywood mould

B1.2 Mild-steel

After degreasing, two types of steels using heat-shrinkage sleeving were prepared. The difference between the steels is the exposed area; i) small exposed area (50.27 cm^2) and ii) large exposed area (75.40 cm^2).

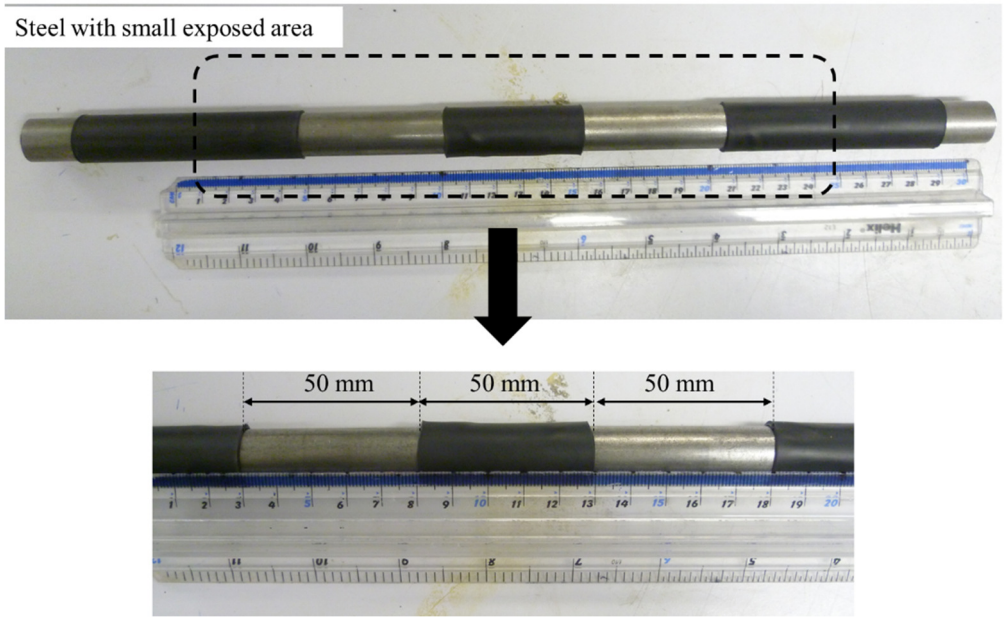

Figure B.3 Steel with small exposure area using heat-shrinkage sleeving

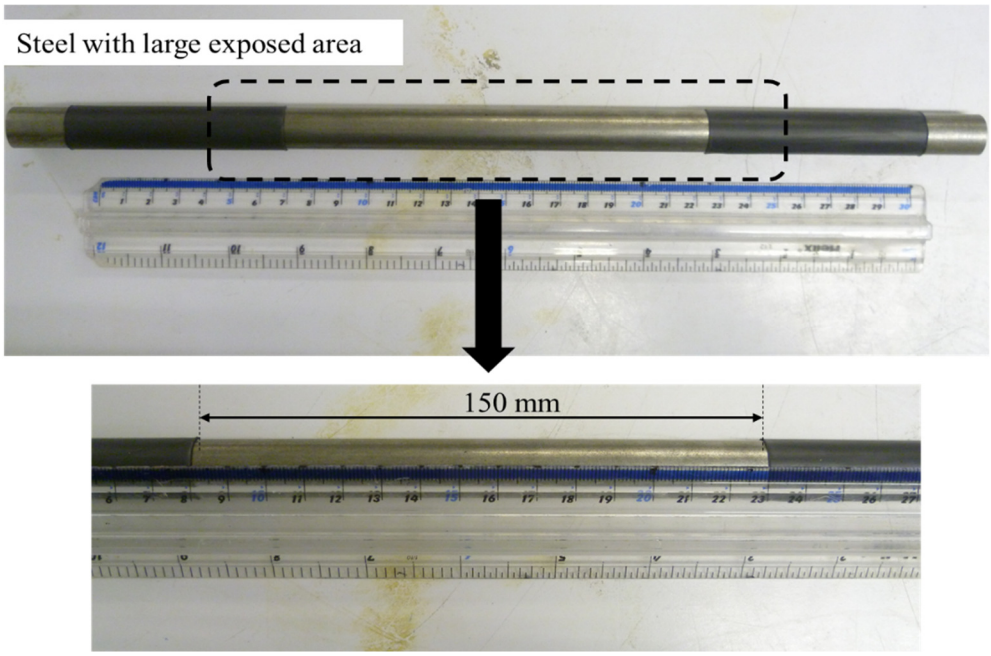

Figure B.4 Steel with large exposure area using heat-shrinkage sleeving

B1.3 Demoulded slabs after air-curing

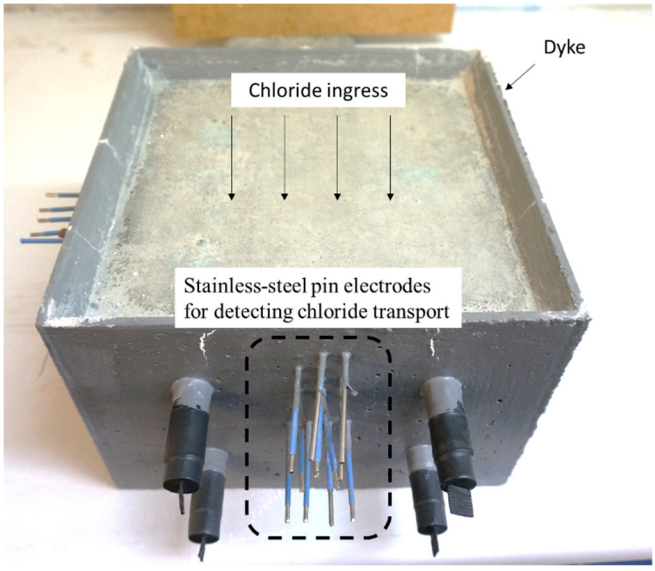

Figure B.5 2-pin electrode arrangements for chloride transport

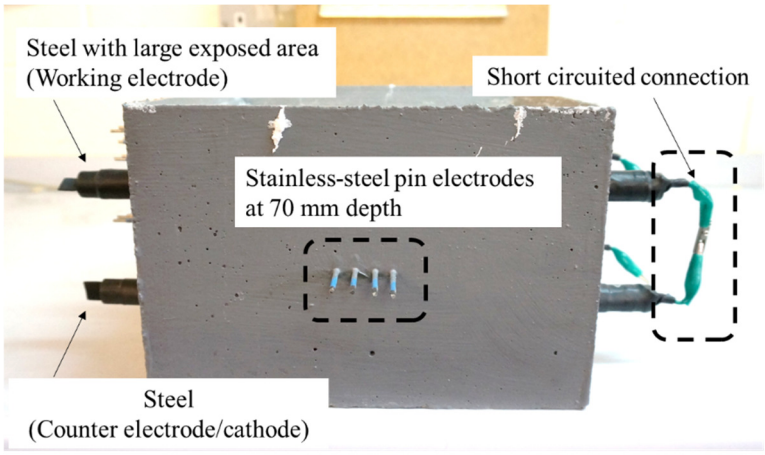

Figure B.6 4-pin electrode arrangements at 70 mm depth for corrosion process

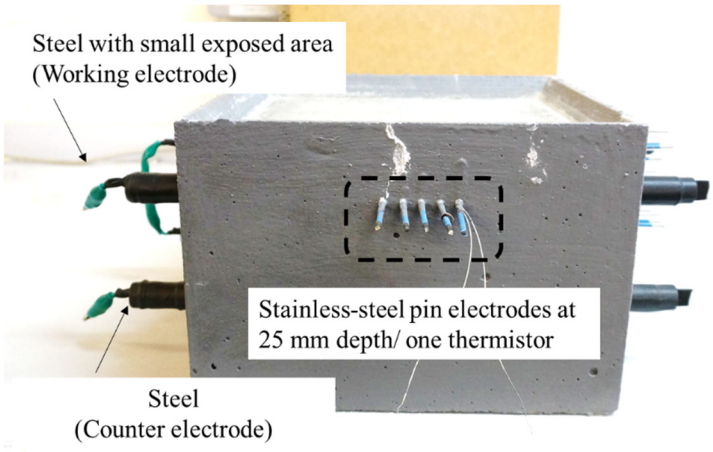

Figure B.7 4-pin electrode arrangements at 25 mm depth for corrosion process

B1.4 Chloride profiling

Measuring chloride content in filtered solution using Chloride QuanTab® strip

Chloride QuanTab® strip was put into the filtered solution. Silver dichromate in the strip reacts with chloride to produce white marks. The white mark represents chloride concentration as ppm unit.

(a)

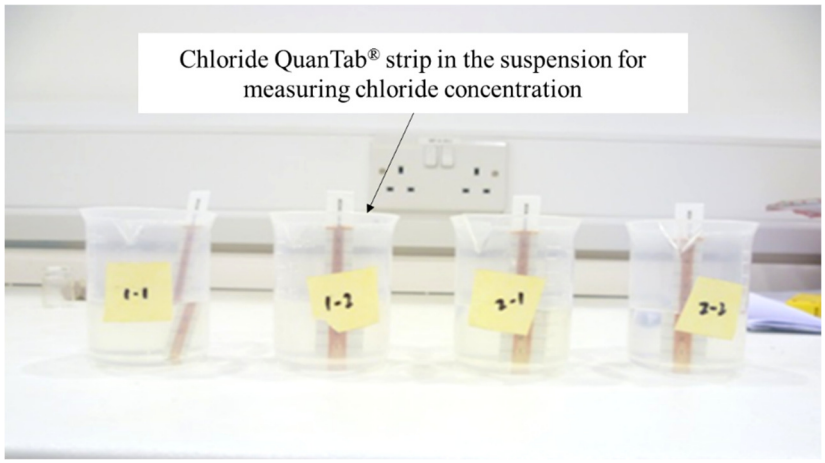

(b)

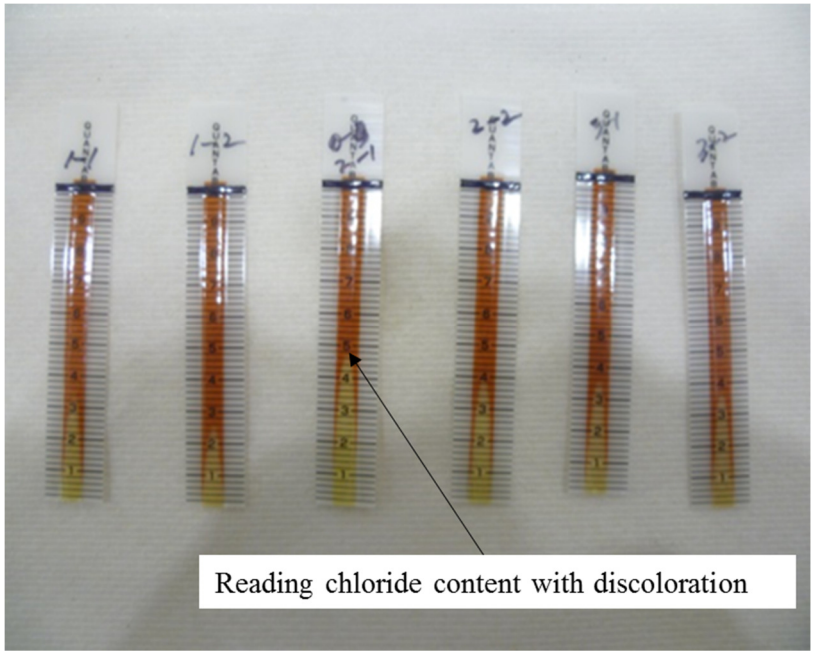

Figure B.8 (a) Measuring chloride concentration in the suspension using QuanTab® strip and (b) reading chloride concentration with discoloration QuanTab® strip

APPENDIX C: TEST RESULTS

C.1 Test results in Chapter 5

C1.1 Compressive strength/electrical resistivity with samples (100 mm cube)

w/b	Binder	Age (days)	Compressive strength (MPa)					Electrical resistivity (Ω·m)				
			No. 1	No. 2	No. 3	AVE	STD	No. 1	No. 2	No. 3	AVE	STD
0.4	CEM I	28	66.31	54.97	73.35	64.88	9.27	79.98	73.14	74.22	75.78	3.68
		90	82.20	75.14	70.20	75.85	6.03	89.83	96.18	98.51	94.84	4.49
		180	85.70	81.70	85.30	84.23	2.20	117.46	117.04	111.83	115.44	3.14
		365	93.20	93.90	92.40	93.17	0.75	135.00	139.37	139.50	137.96	2.57
	CEI III/A	28	53.83	54.81	53.16	53.93	0.83	113.44	108.12	114.63	112.06	3.46
		90	71.85	72.09	63.70	69.21	4.78	199.92	216.03	204.41	206.79	8.31
		180	68.29	72.09	70.04	70.14	1.90	236.81	209.38	246.37	230.85	19.20
		365	78.99	77.37	79.33	78.56	1.05	304.21	302.86	297.38	301.48	3.61
	CEM II/B-V	28	50.51	47.80	48.68	49.00	1.38	63.30	64.12	61.30	62.91	1.45
		90	58.75	66.49	53.53	59.59	6.52	158.56	144.59	154.41	152.52	7.18
		180	72.20	69.84	70.73	70.92	1.19	258.04	237.34	241.00	245.46	11.05
		365	84.00	81.70	82.90	82.87	1.15	479.48	460.50	457.84	465.94	11.80
0.6	CEM I	28	38.81	39.24	36.99	38.35	1.19	49.46	46.43	46.46	47.45	1.74
		90	42.09	42.66	44.41	43.05	1.21	71.18	67.60	66.33	68.37	2.52
		180	45.94	46.51	48.51	46.99	1.35	64.95	70.07	66.20	67.07	2.67
		365	47.77	50.53	50.75	49.68	1.66	75.68	81.52	72.59	76.60	4.54
	CEI III/A	28	36.54	36.49	37.24	36.76	0.42	85.77	89.37	87.70	87.61	1.80
		90	45.23	44.42	47.19	45.61	1.42	175.71	189.24	186.63	183.86	7.18
		180	32.76	50.58	56.73	46.69	12.45	214.12	220.69	226.76	220.52	6.32
		365	49.34	51.05	48.08	49.49	1.49	229.74	234.57	233.53	232.61	2.54
	CEM II/B-V	28	23.13	25.05	24.20	24.13	0.96	60.60	67.36	68.13	65.36	4.15
		90	30.08	32.34	32.87	31.76	1.48	151.15	155.81	164.09	157.02	6.56
		180	36.31	39.94	37.80	38.02	1.82	206.05	178.98	212.39	199.14	17.75
		365	42.03	44.87	43.94	43.61	1.45	363.75	353.95	364.24	360.65	5.81

AVE Average and STD Standard deviation

C1.2 Measuring weight change (Chapter 5.3.2)/electrical resistivity (Chapter 5.3.4) for degree of saturation/porosity test

At 382 days (after the end of wetting phase) and 390 days (after the end of drying phase), to measure degree of saturation and porosity, small cube samples were dried at at 50 ± 2ºC in oven and saturated in a vacuum chamber. The equilibrium state was determined when the change of weight is < 0.1%.

Measuring weigh change

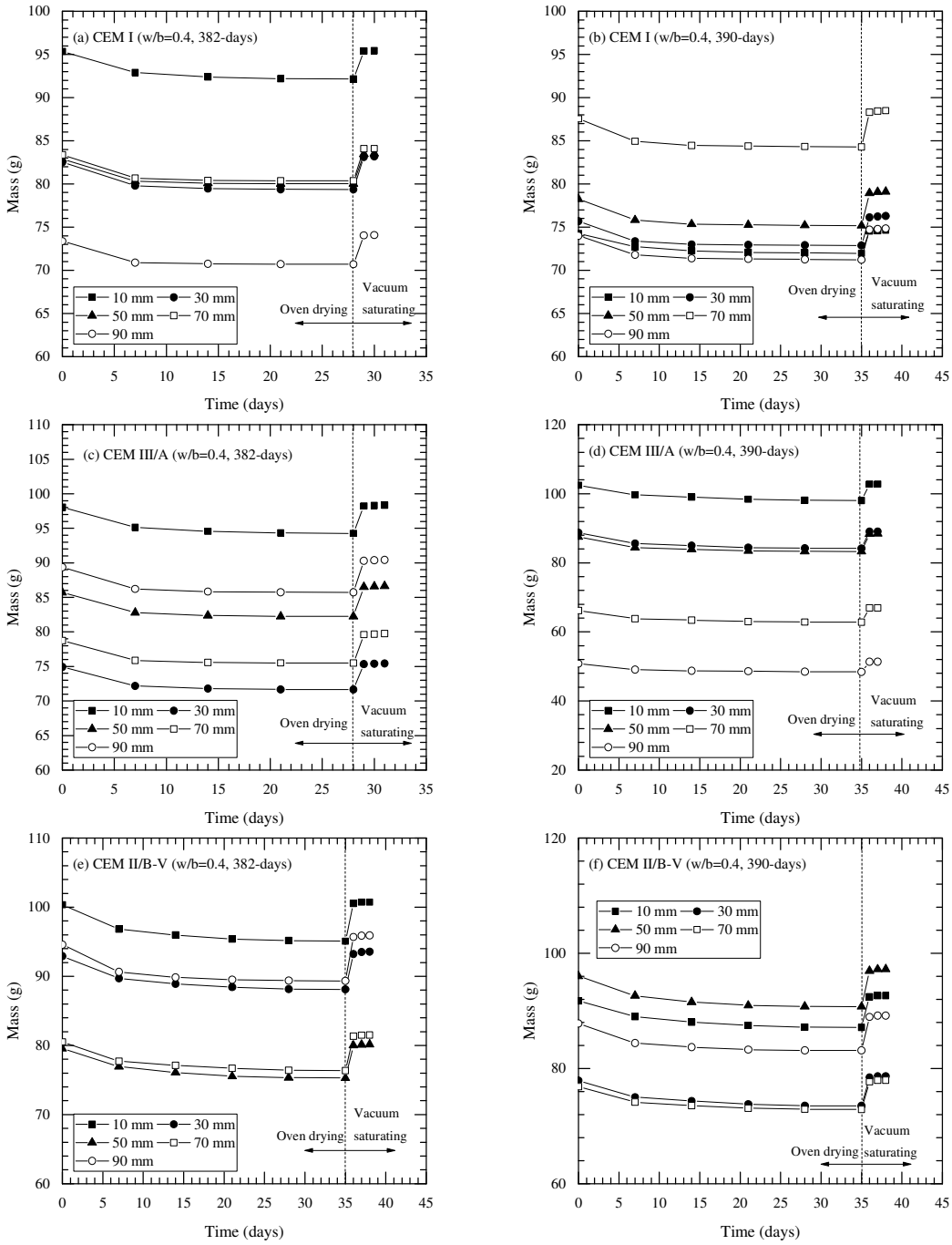

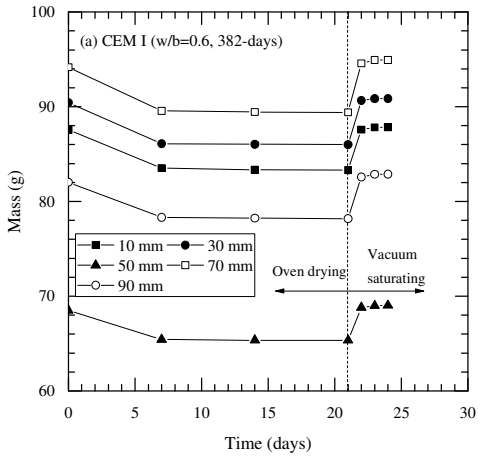

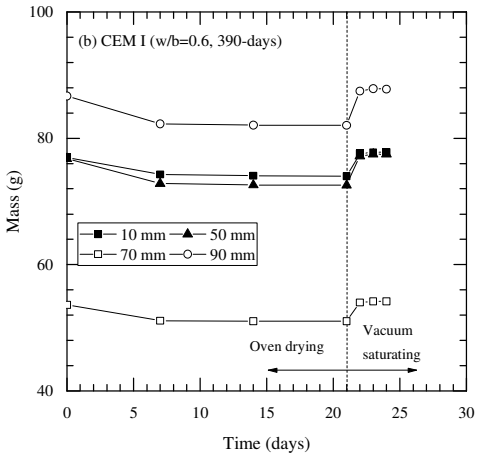

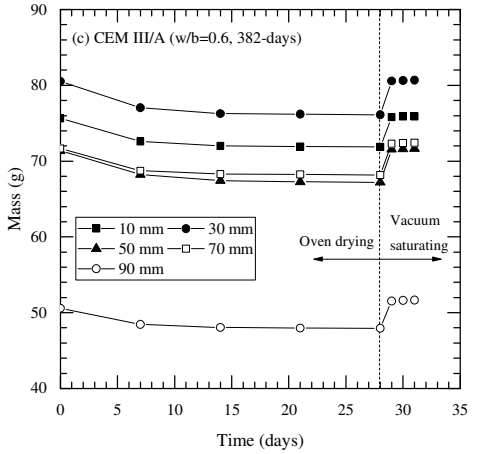

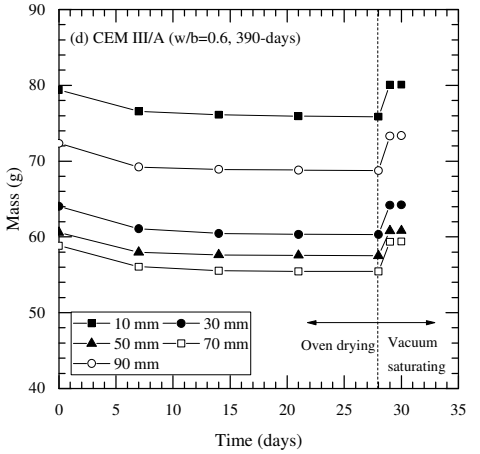

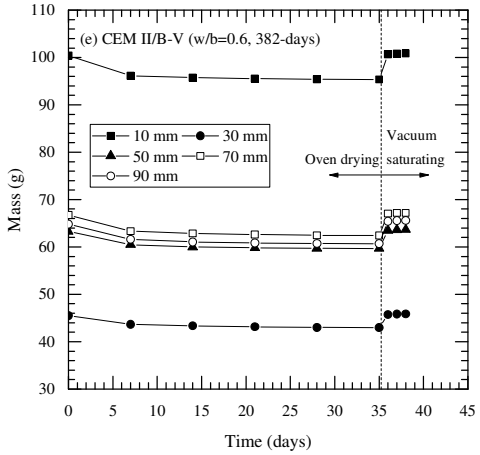

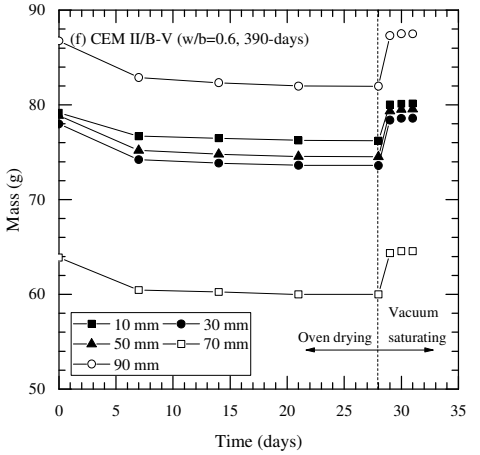

Electrical resistivity profiles at the end of wet/dry cycle

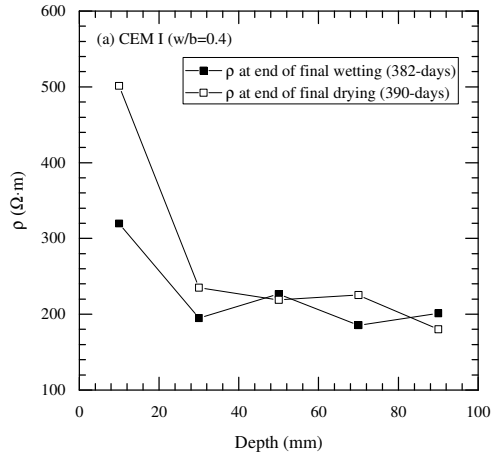

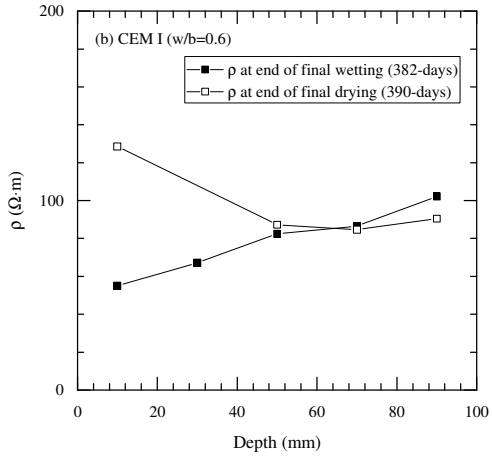

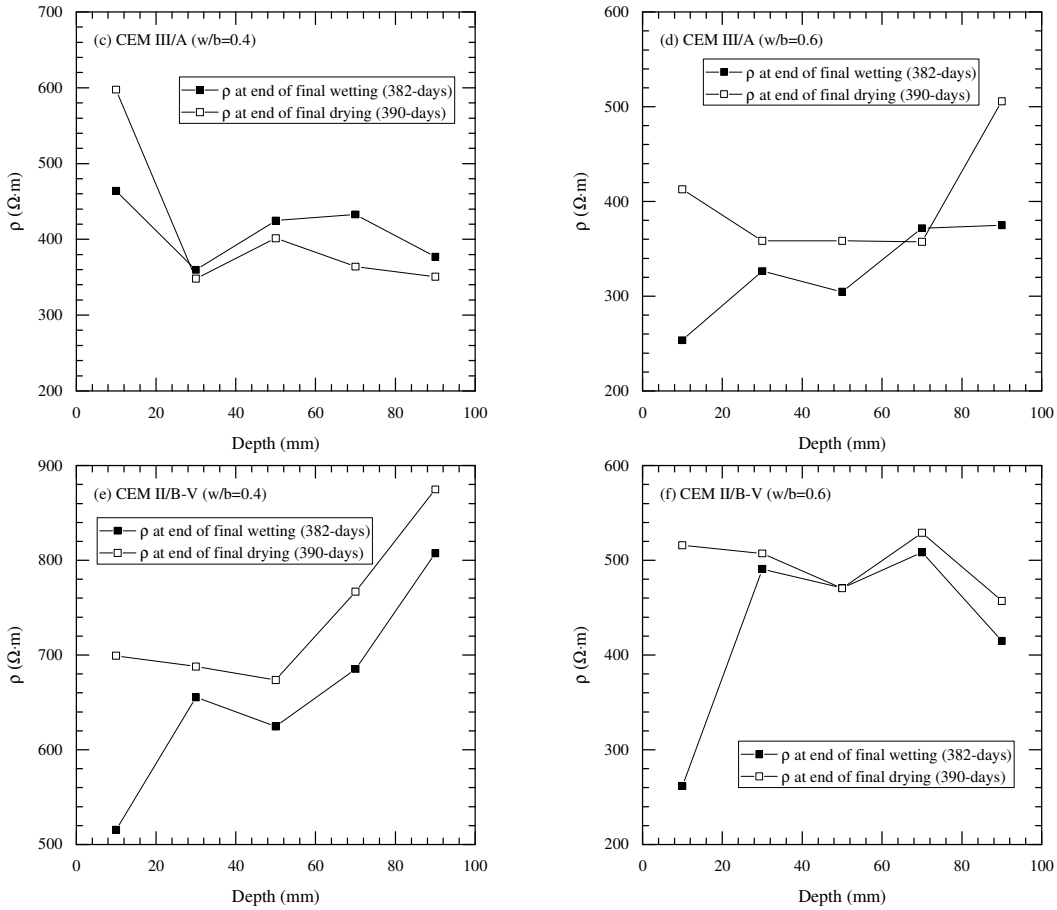

C1.3 Migration coefficient & Resistivity

w/b	Binder	Age (days)	Migration coefficient (x 10^{-12}m^2/s)			Resisvity (Ω·m)		
			No.1	No.2	No.3	No.1	No.2	No.3
0.4	CEM I	180	9.07	8.87	8.68	97.20	99.18	97.67
		270	8.12	6.15	8.12	98.35	92.90	93.78
		365	6.77	7.09	5.00	101.66	108.29	121.04
	CEM III/A	180	3.78	2.80	3.41	183.68	167.24	179.27
		270	3.41	+	3.77	240.04	229.62	232.59
		365	2.10	1.89	2.18	274.33	304.53	268.77
	CEM II/B-V	180	2.52	3.16	3.06	281.82	287.50	271.88
		270	2.55	2.68	+	316.28	312.47	334.84
		365	1.37	0.81	1.52	444.21	395.04	403.45
0.6	CEM I	180	21.91	20.58	20.65	50.27	50.82	48.70
		270	23.04	23.34	21.79	54.23	54.92	57.52
		365	20.66	23.56	18.01	58.33	59.88	48.84
	CEM III/A	180	7.22	5.94	6.13	149.23	154.75	159.55
		270	4.99	5.30	4.47	173.04	173.87	181.11
		365	2.68	3.55	4.44	193.00	183.40	181.22
	CEM II/B-V	180	6.29	7.44	8.65	147.11	146.26	143.98
		270	4.37	5.23	4.44	216.64	220.24	218.33
		365	2.79	3.08	3.53	269.40	276.78	255.19

C1.4 Chloride profiling

w/b= 0.4

	CEM I (%, by weight of binder)			CEM III/A (%, by weight of binder)			CEM II/B-V (%, by weight of binder)		
Depth (mm)	Measured value	Predicted value*	Predicted value**	Measured value	Predicted value*	Predicted value**	Measured value	Predicted value*	Predicted value**
0	+	2.89	2.91		5.38	6.75		3.15	5.60
2	2.55	2.56	2.58	4.27	4.35	5.28	2.29	2.77	4.61
6	1.75	1.92	1.93	2.78	2.52	2.74	2.91	2.04	2.82
10	1.75	1.36	1.36	0.98	1.22	1.12	1.24	1.40	1.48
14	0.77	0.90	0.90	0.40	0.49	0.35	0.77	0.89	0.66
18	0.52	0.56	0.56	0.34	0.16	0.09	0.35	0.53	0.25
22	0.24	0.32	0.32	0.20	0.04	0.02	0.21	0.29	0.08
26	0.13	0.17	0.17	0.14	0.01	0.00	0.12	0.15	0.02
30	0.12	0.09	0.09	0.00	0.00	0.00	0.11	0.07	0.00
40	+	0.01	0.01	+	0.00	0.00	+	0.01	0.00
50	+	0.00	0.00	+	0.00	0.00	+	0.00	0.00

* including first point (at 2 mm cover depth) and ** excluding first point (at 2 mm cover depth)

Diffusion coefficient/Surface chloride

	Fitting result including first point (at 2 mm cover depth)			Fitting result excluding first point (at 2 mm cover depth)		
	C_s	D	r^2	C_s	D	r^2
CEM I (w/b=0.4)	2.89	2.85	0.96	2.91	2.81	0.93
CEM III/A (w/b=0.4)	5.38	1.02	0.99	6.75	0.77	0.98
CEM II/B-V (w/b=0.4)	3.15	2.52	0.87	5.60	1.19	0.98
C_s surface chloride concentration (%, by weight of binder), D diffusion coefficient (m^2/s), r^2 determinant coefficient						

w/b= 0.6

	CEM I (%, by weight of binder)			CEM III/A (%, by weight of binder)			CEM II/B-V (%, by weight of binder)		
Depth (mm)	Measured value	Predicted value*	Predicted value**	Measured value	Predicted value*	Predicted value**	Measured value	Predicted value*	Predicted value**
0	+	6.12	5.89	+	6.09	8.00		6.12	7.02
2	5.73	5.59	5.40	4.50	5.59	7.20	5.10	5.61	6.37
6	4.36	4.58	4.45	5.64	4.61	5.65	5.35	4.61	5.10
10	3.09	3.62	3.55	4.32	3.70	4.24	3.22	3.67	3.93
14	3.59	2.77	2.75	2.77	2.87	3.03	3.48	2.83	2.91
18	2.38	2.05	2.06	2.13	2.16	2.06	1.98	2.11	2.06
22	1.17	1.46	1.49	1.96	1.57	1.33	1.45	1.52	1.40
26	0.62	1.00	1.04	0.41	1.10	0.82	0.90	1.06	0.91
30	0.70	0.66	0.70	0.21	0.75	0.47	0.45	0.71	0.56
40	+	0.37	0.41	+	0.24	0.10	+	0.22	0.14
50	+	0.20	0.22	+	0.06	0.01	+	0.05	0.02

* including first point (at 2 mm cover depth) and ** excluding first point (at 2 mm cover depth)

Diffusion coefficient/Surface chloride

	Fitting result including first point (at 2 mm cover depth)			Fitting result excluding first point (at 2 mm cover depth)		
	C_s	D	r^2	C_s	D	r^2
CEM I (w/b=0.6)	5.89	21.99	0.90	6.12	20.72	0.94
CEM III/A (w/b=0.6)	8.00	3.75	0.97	6.09	5.61	0.87
CEM II/B-V (w/b=0.6)	7.02	4.36	0.95	6.12	5.39	0.94
C_s surface chloride concentration (%, by weight of binder), D diffusion coefficient (m^2/s), r^2 determinant coefficient						

C.2 Test results in Chapter 6

C2.1 Corrosion potential monitoring/macrocell current monitoring

CEM I (w/b=0.4)

Type of measurement	Corrosion potential (mV)						Macrocell current (nA/cm^2)					
Type of steel	SS			LS			SS			LS		
Age (days)	No.1	No.2	No.3	No.1	No.2	No.3	No.1	No.2	No.3	No.1	No.2	No.3
42	-84	-79	-65	-76	-66	-59	1.59	0.40	0.60	-1.33	0.44	0.53
47	-183.7	-167.2	-163.8	-165.6	-150.8	-150.3	1.99	2.88	1.89	1.33	1.33	1.90
49	-183.6	-180.4	-174.2	-174.5	-158.3	-164.7	0.42	1.47	3.24	0.54	1.87	0.90
54	-167.1	-158.2	-165.4	-162.1	-143.2	-151.6	-0.52	0.30	0.46	0.17	-0.40	0.09
56	-168.1	-173.2	-169.7	-160.1	-146.2	-152.9	-0.02	1.59	2.59	-0.03	-0.03	0.01
61	-159.4	-163.1	-151.6	-157.3	-146.1	-140.1	-0.18	-0.10	-0.04	0.16	-0.08	0.12
63	-198.7	-194.7	-180	-191.2	-188.9	-167.6	1.03	-0.40	0.40	0.11	-0.07	-0.03
67	-147.5	-144.3	-154.6	-145.7	-136.6	-143.4	0.22	0.16	0.08	-0.08	-0.05	-0.04
68	-187.5	-175.8	-178.3	-172.1	-170.7	-169.5	0.86	-0.22	0.10	-0.05	-0.07	-0.01
70	-176.1	-175.4	-162.3	-158.9	-148.7	-153.8	1.53	-0.16	0.02	-0.05	-0.05	0.11
75	-187.1	-179.9	-180.4	-180.7	-174.3	-177.9	0.22	-0.22	0.08	-0.08	-0.07	0.01
77	-158.7	-147.1	-157.1	-154.3	-139.2	-147	0.24	-0.42	0.46	-0.25	-0.20	0.01
82	-184.8	-174.4	-174.1	-173.6	-164.4	-172.7	-0.58	-0.12	0.06	-0.07	-0.03	0.01
84	-156	-143.6	-143.1	-150.6	-135.1	-138.5	0.02	-0.54	0.10	-0.08	-0.04	0.01
89	-183.9	-167	-173.4	-172.7	-161.6	-170.1	0.06	-0.18	0.02	-0.27	-0.13	-0.01
91	-169	-151.5	-152.5	-161.8	-142.1	-147	1.03	0.50	0.22	-0.21	-0.08	-0.08
96	-186.2	-169.3	-169	-165.9	-161.5	-165.3	0.84	-0.02	-0.04	-0.05	-0.03	0.03
102	-160.1	-115.9	-105.6	-137	-100	-104.7	1.31	-0.02	0.16	-0.07	0.01	-0.03
110	-172	-159.4	-166.2	-166.1	-154.2	-154.2	0.02	-0.18	0.44	-0.16	-0.07	-0.03
116	-140.1	-121.1	-84.18	-130.2	-102.6	-81.3	0.40	-0.12	0.34	-0.07	0.01	-0.07
130	-162.3	-162.3	-168	-152.4	-152.4	-141.4	0.36	-0.02	1.25	-0.12	-0.04	-0.01
133	-155.2	-148.8	-140.6	-148.7	-131	-127.5	0.36	0.24	0.66	-0.08	0.01	-0.05
138	-179.9	-167.3	-164.4	-167.7	-157.4	-159.8	0.62	-0.08	0.04	-0.16	-0.08	-0.04
144	-136.1	-101.5	-71.5	-127.1	-94.8	-76.5	1.79	-0.66	-0.20	-0.15	-0.01	0.04
152	-161.4	-137.9	-143.8	-161.2	-142.8	-142.5	0.20	-0.14	0.02	-0.08	-0.03	0.01
158	-131.8	-99.9	-71.2	-116.6	-111.2	-80.5	0.32	-0.48	-0.16	-0.08	-0.04	0.01
166	-163.8	-133.1	-120.4	-145.6	-125.1	-119.8	0.62	-1.07	-0.40	-0.15	-0.04	-0.05
172	-126.8	-83.5	-59	-107.8	-73.8	-60.3	0.48	-0.32	0.02	-0.01	0.04	0.03
180	-156.7	-145.7	-168	-162.6	-149.9	-146.3	-0.28	-0.88	0.16	-0.08	-0.03	-0.01
186	-153	-120	-100.2	-146.1	-115.1	-105.9	0.70	-0.99	-0.02	-0.04	0.04	-0.05
194	-172.6	-138.2	-125.3	-129.8	-134.6	-142.1	1.21	-1.11	-0.22	-0.07	-0.01	-0.01
200	-177.9	-169.3	-81.76	-180.2	-133.7	-88.38	-0.26	0.30	-0.06	-0.07	-0.01	-0.04
208	-190	-177.2	-151.6	-190.4	-145.8	-138.1	0.08	-0.24	0.60	-0.05	-0.07	0.07
214	-155.9	-131.4	-63.7	-164.3	-99.57	-66.5	0.24	0.02	0.02	-0.01	-0.05	0.01
222	-184.5	-136.1	-123	-180.1	-139.6	-92	0.40	-0.20	0.20	-0.04	-0.01	0.01
228	-138.8	-125.9	-63.8	-141.8	-110.6	-65.4	1.79	-0.95	-0.16	-0.04	-0.05	-0.03
236	-168.3	-154.6	-158.2	-161.9	-138.7	-135.6	0.46	-0.18	-0.02	-0.25	-0.01	-0.01
242	-130.1	-121.9	-79.8	-137	-106.7	-81.9	0.34	-0.26	-0.06	-0.04	-0.01	-0.03
250	-177.4	-139.6	-161.3	-169.3	-115.3	-150.5	0.30	-0.22	-0.02	-0.11	-0.04	0.01
256	-169.7	-129.6	-84.7	-171.1	-125.5	-89.1	0.38	-0.06	0.46	-0.01	0.27	0.15
264	-177.3	-121	-130.2	-168.8	-99.3	-122.2	0.30	-0.36	0.02	-0.21	-0.05	0.01
270	-152.1	-109.8	-94	-159.8	-98.2	-2.4	0.38	-0.52	-0.08	-0.04	-0.01	-0.01
278	-171.6	-98.5	-117.5	-170.3	-100.2	-111.6	0.16	-0.12	-0.02	-0.04	-0.01	0.01
284	-139.2	-88.3	-74.8	-136.1	-85.1	-79.1	0.50	-0.42	-0.10	-0.07	-0.04	-0.01
292	-164.5	-129.6	-130.8	-158.7	-115.3	-128.1	0.44	-0.32	0.02	-0.05	-0.01	0.01
298	-133.2	-89	-75.9	-129.5	-71.6	-75.4	0.52	-0.42	-0.02	-0.09	-0.05	-0.04
306	-170.5	-131.1	-121.7	-174.6	-112.4	-122.4	0.84	-0.28	0.02	-0.44	-0.12	0.05
312	-127.7	-94.8	-71.8	-127	-85.3	-70.8	-0.54	-1.39	-0.93	-0.53	-0.24	-0.23
320	-158.7	-114.9	-123.8	-153.4	-106.9	-122.7	0.74	-0.48	-0.02	-0.11	-0.05	0.01
326	-123.8	-90.4	-74	-115.3	-78.7	-70.3	0.20	-0.16	-0.02	-0.05	-0.03	-0.03
334	-146.1	-100.9	-110.9	-145.7	-102.1	-108.1	0.26	-0.20	-0.02	-0.04	-0.01	-0.01
340	-126.7	-79.6	-75.6	-137.5	-76.8	-70.2	-0.56	-1.49	-0.95	-0.44	-0.16	-0.21
348	-151.5	-104.9	-111.1	-146.7	-98.2	-109.2	0.66	-0.38	-0.20	-0.08	-0.04	-0.03
354	-131	-65.6	-60.9	-130.8	-63.1	-70.1	-0.20	0.40	-0.02	-0.40	-0.01	-0.27
362	-151.4	-98.4	-120.9	-151.3	-84.6	-117.9	0.24	-0.16	-0.02	-0.11	-0.03	-0.01
368	-119.9	-81.5	-41.8	-118.2	-77.5	-42.3	0.38	-0.30	-0.04	-0.24	-0.16	-0.09
376	-152.1	-110.9	-96.8	-148.5	-104.7	-91.9	0.22	-0.10	-0.02	-0.03	0.01	-0.01
382	-146.1	-118	-54.4	-149.4	-93	-48.5	0.14	-0.06	-0.02	-0.03	-0.03	-0.01

CEM III (w/b=0.4)

Type of measurement	Corrosion potential (mV)						Macrocell current (nA/cm^2)					
Type of steel	SS			LS			SS			LS		
Age (days)	No.1	No.2	No.3	No.1	No.2	No.3	No.1	No.2	No.3	No.1	No.2	No.3
42	-108.1	-100.3	-61.7	-85.1	-103.7	-56.0	-0.30	0.54	0.18	-0.54	0.07	-0.07
47	-131.1	-125.6	-114.9	-125.0	-126.4	-115.2	-0.46	0.20	0.04	-0.24	-0.05	-0.56
49	-159.8	-161.5	-162.9	-158.6	-157.7	-157.7	-1.05	0.42	0.08	-0.24	-0.08	-0.07
54	-150.2	-148.9	-148.3	-148.5	-145.9	-145.7	-0.18	0.06	-0.06	-0.80	-0.32	-0.24
56	-165.7	-161.5	-162.6	-164.9	-155.6	-157.0	-0.54	0.32	-0.06	-0.42	-0.23	-0.20
61	-143.9	-144.2	-143.2	-144.9	-140.2	-140.0	-0.30	0.14	-0.04	-0.27	-0.15	-0.08
63	-172.7	-166.8	-167.8	-167.2	-159.9	-163.3	-0.26	0.04	-0.08	-0.25	-0.15	-0.13
67	-139.8	-141.0	-139.9	-140.9	-138.9	-136.3	-0.28	0.06	-0.06	-0.29	-0.09	-0.11
68	-163.3	-162.8	-164.8	-158.5	-154.4	-159.2	-0.52	0.02	-0.14	-0.53	-0.38	-0.41
70	-137.1	-143.0	-148.5	-139.3	-135.8	-134.5	-0.60	0.46	0.76	-0.32	-0.17	-0.12
75	-167.1	-172.3	-169.5	-166.9	-161.9	-164.7	-0.52	0.50	-0.12	-0.48	-0.24	-0.16
77	-144.4	-144.5	-142.4	-143.5	-140.7	-139.3	-0.50	0.10	-0.10	-0.41	-0.23	-0.12
80	-178.0	-179.2	-187.3	-171.5	-158.0	-163.9	-0.30	0.04	0.60	-0.36	-0.21	-0.15
82	-159.1	-147.1	-145.4	-146.3	-140.8	-144.6	-0.10	0.06	-0.08	-0.34	-0.21	-0.16
96	-183.0	-171.5	-175.6	-170.3	-164.6	-171.2	-0.24	-0.12	0.02	-0.23	-0.15	-0.11
102	-140.8	-141.7	-137.6	-142.4	-138.2	-133.7	-0.16	-0.04	-0.04	-0.20	-0.15	-0.08
110	-168.6	-161.8	-164.3	-168.2	-157.9	-158.3	-0.30	-0.10	0.06	-0.25	-0.16	-0.11
116	-139.5	-133.4	-135.5	-138.5	-126.7	-128.7	-0.28	-0.04	0.18	-0.34	-0.11	-0.05
124	-150.5	-145.1	-154.0	-151.6	-137.3	-145.7	-1.35	0.88	-0.32	-0.13	-0.07	-0.04
130	-135.0	-134.0	-127.8	-134.4	-129.6	-125.7	-0.32	-0.10	-0.22	-0.27	-0.13	-0.05
138	-144.0	-141.2	-142.9	-149.5	-140.1	-141.9	-0.24	-0.06	-0.16	-0.09	-0.11	-0.08
144	-149.4	-156.6	-146.0	-150.5	-149.6	-145.0	-0.14	0.04	-0.16	-0.17	-0.09	-0.05
152	-142.4	-150.8	-148.6	-145.3	-148.0	-150.6	-0.18	0.14	-0.20	-0.11	-0.05	-0.01
158	-150.7	-152.6	-141.5	-149.1	-143.0	-140.4	-0.38	0.70	-0.38	-0.40	-0.15	-0.05
166	-135.3	-124.8	-141.3	-144.2	-143.5	-142.6	-0.60	0.46	-0.56	-0.40	-0.21	-0.11
172	-155.2	-151.6	-140.6	-152.5	-144.3	-136.9	-0.32	0.66	-0.50	-0.24	-0.09	-0.04
180	-174.9	-162.7	-158.4	-170.5	-157.2	-158.7	-0.04	-0.06	-0.10	-0.11	-0.05	-0.03
186	-137.5	-138.3	-153.4	-136.3	-135.7	-154.6	-0.08	-0.10	-0.08	-0.15	-0.08	-0.04
194	-163.1	-155.9	-153.0	-163.4	-154.2	-155.7	-0.10	0.06	-0.18	-0.08	0.01	-0.03
200	-151.7	-131.8	-141.7	-151.8	-143.6	-141.3	-0.10	-0.12	-0.22	-0.11	-0.04	-0.04
208	-170.3	-166.0	-166.4	-165.9	-161.7	-163.9	-0.06	-0.04	-0.06	-0.11	-0.05	-0.03
214	-144.4	-140.8	-140.2	-144.8	-140.9	-135.4	-0.22	-0.20	-0.08	-0.61	-0.33	-0.12
222	-163.5	-160.3	-151.4	-163.5	-157.9	-154.1	-0.08	-0.12	-0.04	-0.12	-0.07	-0.09
228	-143.1	-148.0	-134.9	-143.6	-140.3	-134.1	-0.08	0.30	-0.06	-0.07	-0.01	-0.01
236	-160.8	-160.1	-153.1	-163.1	-155.1	-151.3	-0.10	-0.08	-0.10	-0.58	-0.24	-0.05
242	-146.8	-143.7	-139.5	-151.9	-144.1	-135.8	-0.04	-0.06	-0.06	-0.11	-0.04	-0.01
250	-158.8	-152.8	-146.6	-158.0	-150.9	-144.7	-0.20	0.50	-0.44	-0.24	-0.13	-0.04
256	-143.8	-136.5	-126.7	-144.0	-139.9	-129.9	0.22	-0.34	-0.38	0.13	-0.07	-0.03
264	-159.3	-154.8	-146.8	-159.2	-150.8	-146.4	-0.18	-0.56	-0.40	-0.27	-0.13	-0.03
270	-141.5	-133.8	-129.1	-137.3	-134.3	-127.3	-0.08	-0.14	-0.16	-0.08	-0.09	0.01
278	-153.9	-147.0	-140.2	-153.0	-144.1	-138.7	-0.04	-0.14	-0.14	-0.11	-0.04	0.01
284	-138.0	-132.7	-128.1	-138.5	-132.4	-127.5	-0.04	-0.08	-0.10	-0.08	-0.04	-0.03
292	-148.8	-154.3	-145.0	-159.2	-147.9	-146.1	-0.06	-0.34	-0.26	-0.16	-0.08	-0.05
298	-142.4	-134.4	-131.6	-144.2	-138.5	-130.6	-1.03	-1.57	-0.32	-0.61	-0.15	-0.05
306	-140.9	-146.8	-144.8	-138.5	-147.2	-142.4	-0.06	-0.44	-0.24	-0.77	-0.52	-0.08
312	-141.3	-140.9	-127.3	-136.1	-132.0	-126.1	0.04	-0.12	-0.10	-0.05	-0.03	-0.01
320	-165.2	-162.1	-153.5	-158.7	-153.7	-153.5	0.08	-0.24	-0.10	-0.07	-0.04	-0.03
326	-135.4	-132.8	-124.4	-131.5	-135.1	-122.4	-0.02	-0.26	-0.14	-0.34	-0.17	-0.07
334	-144.8	-134.8	-138.1	-142.2	-133.1	-136.8	-0.02	-0.16	-0.06	-0.29	-0.11	0.04
340	-134.3	-128.7	-121.8	-134.0	-131.9	-122.6	-0.22	-0.32	-0.22	-0.15	-0.11	-0.05
348	-143.0	-144.4	-139.6	-142.0	-142.1	-136.3	-0.50	-0.34	-0.10	0.01	-0.03	-0.33
354	-126.8	-124.8	-123.9	-128.3	-125.1	-121.8	-0.02	-0.06	-0.04	-0.03	-0.01	-0.01
362	-127.5	-126.4	-115.1	-127.9	-125.5	-111.7	-0.04	-0.08	-0.04	-0.03	-0.01	0.01
368	-132.5	-128.6	-122.6	-134.2	-132.0	-121.6	-0.08	-0.12	-0.08	-0.11	-0.07	-0.01
376	-128.1	-121.4	-128.6	-126.8	-123.0	-124.9	0.02	-0.08	-0.04	-0.07	-0.04	-0.01
382	-131.3	-128.0	-124.6	-129.1	-127.9	-122.1	-0.02	-0.08	-0.04	-0.15	-0.08	-0.01

CEM II/B-V (w/b=0.4)

Type of measurement	Corrosion potential (mV)						Macrocell current (nA/cm^2)					
Type of steel	SS			LS			SS			LS		
Age (days)	No.1	No.2	No.3	No.1	No.2	No.3	No.1	No.2	No.3	No.1	No.2	No.3
42	-108.5	-86.3	-109.3	-123.1	-84.8	-110.2	1.77	0.66	3.00	0.60	2.18	1.03
47	-138.4	-125.8	-138.7	-148.2	-129.2	-143.9	0.44	-0.08	1.13	0.23	1.34	0.60
49	-165.2	-164.3	-176.4	-164.5	-171.8	-172.0	0.62	-0.42	1.55	-0.11	0.60	-0.05
54	-167.8	-154.3	-167.2	-156.5	-161.0	-163.1	0.38	-0.92	1.67	-0.17	0.32	-0.03
56	-178.5	-164.1	-176.3	-168.8	-170.7	-170.8	0.12	-0.62	0.54	-0.23	-0.04	-0.16
61	-161.0	-146.0	-157.7	-147.9	-153.9	-154.8	0.04	-1.63	0.92	-0.60	0.32	-0.40
63	-176.6	-165.7	-173.6	-167.4	-173.5	-169.9	0.02	-1.75	0.68	-0.40	0.08	-0.24
67	-157.7	-141.4	-152.8	-143.1	-148.4	-150.5	-0.06	-0.68	0.10	-0.24	0.07	-0.15
68	-176.6	-161.9	-169.5	-160.0	-172.4	-166.5	-0.14	-1.59	0.12	-0.58	0.13	-0.37
70	-158.6	-142.0	-153.1	-145.1	-149.3	-151.3	-0.12	-1.37	0.02	-0.46	0.11	-0.29
73	-181.2	-161.6	-185.6	-161.7	-170.0	-169.2	-0.16	-1.15	-0.06	-0.41	0.04	-0.32
75	-157.4	-143.0	-156.3	-143.1	-152.2	-152.0	-0.16	-1.33	-0.06	-0.37	0.04	-0.34
89	-182.6	-166.7	-175.7	-170.7	-174.1	-175.8	-0.08	-1.21	-0.50	-0.25	-0.03	-0.27
91	-158.0	-141.3	-151.5	-145.0	-148.3	-149.6	-0.06	-0.68	-0.18	-0.19	-0.01	-0.15
96	-175.0	-161.0	-167.7	-163.8	-168.7	-166.4	-0.08	-0.76	-0.24	-0.27	0.01	-0.20
102	-150.6	-136.1	-146.1	-135.5	-140.6	-147.3	-0.06	-0.99	-0.22	-0.17	0.03	-0.13
110	-168.1	-160.4	-162.7	-155.1	-161.3	-163.7	-0.04	-0.36	-0.18	-0.15	-0.01	0.05
116	-143.1	-131.3	-141.9	-144.2	-134.1	-137.4	-0.12	-0.74	-0.30	-0.13	0.03	-0.11
124	-142.6	-134.3	-144.0	-138.5	-147.5	-151.4	-0.50	-2.73	-1.19	-0.27	-0.13	-0.13
130	-137.9	-121.9	-134.8	-118.7	-130.5	-132.5	-0.16	-0.62	-0.32	-0.12	0.01	-0.11
138	-159.1	-144.5	-156.4	-153.8	-157.4	-160.2	-0.14	-0.48	-0.28	-0.11	-0.03	-0.16
144	-150.6	-137.3	-148.3	-142.9	-145.5	-148.2	-0.30	-1.05	-0.62	-0.15	0.01	-0.08
152	-164.8	-154.8	-161.2	-149.1	-159.7	-158.6	-0.12	-0.86	-0.56	-0.17	-0.01	-0.16
158	-148.8	-131.7	-143.4	-133.5	-138.4	-143.1	-0.10	-0.50	-0.36	-0.15	-0.01	-0.11
166	-168.5	-150.7	-161.4	-157.8	-156.0	-163.7	-0.06	-0.82	-0.52	-0.03	0.11	-0.11
172	-137.8	-128.4	-134.1	-125.1	-131.7	-132.7	-0.06	-0.28	-0.20	-0.11	-0.03	-0.11
180	-165.9	-151.5	-160.1	-149.6	-166.9	-158.2	-0.06	-0.40	-0.22	-0.07	0.03	-0.08
186	-140.5	-126.2	-133.9	-125.0	-130.6	-128.6	-0.10	-0.32	-0.28	-0.15	-0.05	-0.11
194	-153.9	-145.8	-149.4	-144.8	-151.9	-150.7	-0.16	-0.54	-0.28	-0.09	-0.01	-0.11
200	-147.7	-129.8	-140.4	-129.6	-134.0	-136.2	0.02	-0.36	-0.14	-0.11	-0.04	-0.12
208	-159.5	-141.6	-151.9	-145.0	-140.9	-145.6	-0.08	-1.15	-0.32	-0.05	-0.01	-0.04
214	-142.8	-128.1	-138.9	-130.7	-135.3	-136.0	-0.10	-0.64	0.62	-0.32	-0.01	-0.33
222	-158.7	-147.7	-160.8	-141.6	-151.3	-152.8	-0.24	-1.05	0.02	-0.53	0.16	-0.62
228	-140.9	-126.9	-136.0	-127.1	-130.7	-130.3	-0.18	-0.50	-0.18	-0.13	-0.03	-0.08
236	-130.3	-125.5	-124.3	-126.1	-132.5	-130.1	-0.60	-0.86	-0.70	-0.07	-0.01	-0.11
242	-137.3	-125.9	-144.6	-125.0	-132.2	-133.7	-0.06	-0.44	-0.32	-0.07	-0.01	-0.07
250	-151.8	-141.0	-146.0	-137.4	-146.0	-146.3	-0.12	-0.44	-0.30	-0.08	-0.01	-0.09
256	-148.0	-123.4	-128.5	-129.2	-127.8	-130.2	-0.10	-0.52	-0.44	-0.08	-0.03	-0.11
264	-145.4	-141.7	-141.2	-132.5	-145.3	-144.2	-0.10	-0.38	-0.36	-0.16	-0.01	-0.19
270	-136.1	-125.0	-125.7	-123.1	-127.8	-126.7	-0.14	-0.93	-0.93	-0.05	0.01	-0.07
278	-146.2	-144.1	-141.5	-135.5	-143.9	-142.6	-0.16	-0.78	-0.95	-0.11	-0.04	-0.11
284	-138.2	-124.9	-127.4	-127.9	-130.5	-131.1	-0.08	-0.30	-0.32	-0.09	-0.82	0.04
292	-142.0	-130.6	-133.9	-129.8	-134.9	-133.7	-0.12	-0.62	-0.66	-0.07	-0.01	-0.08
298	-136.0	-125.1	-128.5	-123.8	-128.1	-128.1	-0.04	-0.24	-0.26	-0.13	0.01	-0.15
306	-118.6	-141.6	-140.6	-111.3	-142.0	-149.7	-0.12	-0.62	-0.76	-0.08	-0.01	-0.08
312	-128.3	-114.2	-116.8	-120.0	-120.2	-120.5	-0.16	-0.54	-0.64	-0.20	-0.01	-0.24
320	-141.9	-127.4	-147.0	-131.7	-133.6	-149.2	-0.06	-0.20	-0.22	-0.09	0.01	-0.12
326	-127.3	-111.4	-115.3	-116.8	-116.4	-116.6	-0.12	-0.64	-0.74	-0.29	-0.04	-0.37
334	-130.2	-121.7	-120.1	-119.3	-124.2	-121.4	-0.02	-0.24	-0.32	-0.03	0.01	-0.04
340	-124.9	-112.2	-120.2	-115.1	-114.6	-119.3	-0.06	-0.44	-0.48	-0.03	0.01	-0.05
348	-134.1	-123.0	-127.5	-120.7	-122.2	-120.9	-0.02	-0.16	-0.14	-0.03	0.01	-0.04
354	-126.3	-113.6	-115.2	-123.1	-119.7	-120.3	-0.18	-0.38	-0.40	-0.11	-0.04	-0.11
362	-132.3	-120.0	-124.1	-127.5	-125.1	-126.0	0.02	-0.38	-0.44	-0.05	0.11	-0.16
368	-131.8	-118.6	-115.8	-121.8	-118.8	-120.6	-0.02	-0.16	-0.20	-0.07	-0.01	-0.11
376	-135.4	-121.2	-123.3	-127.2	-127.8	-133.7	0.02	-0.08	-0.04	0.40	0.40	-0.04
382	-141.2	-108.7	-116.7	-133.1	-113.5	-118.3	0.02	-0.24	-0.40	-0.07	-0.01	-0.20

CEM I (w/b=0.6)

Type of measurement	Corrosion potential (mV)						Macrocell current (nA/cm^2)					
Type of steel	SS			LS			SS			LS		
Age (days)	No.1	No.2	No.3	No.1	No.2	No.3	No.1	No.2	No.3	No.1	No.2	No.3
42	-88.9	-111.1	-91.5	-99.8	-110.7	-83.7	1.99	2.98	1.99	2.79	1.72	2.92
47	-188.5	-196.6	-192	-210.01	-187.5	-185.1	-3.28	1.41	2.51	0.01	3.69	5.23
49	-189.2	-203.7	-191	-197.6	-203.5	-189.6	-1.39	0.08	0.14	0.32	-0.01	0.86
54	-178.8	-178.8	-166	-185.5	-170.9	-164.7	-0.62	0.54	0.20	0.81	0.61	1.22
56	-193	-197.7	-200	-202.6	-189.3	-183.5	-0.99	0.20	1.19	0.40	0.13	0.13
61	-155.2	-138.8	-127	-173	-142.3	-108.18	-0.62	0.18	0.26	0.56	0.33	0.50
63	-175.7	-166	-168	-188.8	-168.3	-152.4	-0.74	0.10	0.30	0.34	0.41	0.92
67	-152.7	-148.4	-142	-165.5	-145.3	-119.6	-0.62	0.18	0.22	0.46	0.31	0.69
68	-162.2	-144.5	-141	-175.3	-149.9	-116.04	-0.66	0.10	0.24	0.37	0.25	0.61
70	-157.1	-144.5	-143	-167.1	-147.7	-133.9	-0.38	0.10	0.24	-0.34	0.23	0.45
75	-166.7	-169.1	-158	-177.9	-166.3	-157	-0.62	0.06	0.16	0.31	0.21	0.41
77	-164.9	-159.5	-147	-157.2	-149.1	-141.2	-0.68	0.06	0.14	0.23	0.12	0.34
82	-168.5	-170.2	-176	-179.7	-167.5	-167.7	-0.48	-0.06	0.18	-0.25	0.15	0.40
84	-154.2	-154.4	-153	-163	-151.3	-148.8	-0.68	0.02	0.30	0.25	0.19	0.40
89	-168.2	-172.8	-166	-176.5	-161.8	-157	-0.46	-0.12	0.06	0.21	0.09	0.34
91	-143.6	-147.4	-147	-155.1	-151.5	-143.7	-0.80	-0.20	0.10	0.31	0.25	0.58
96	-167.3	-173.8	-163	-182.4	-167.8	-166.3	-0.66	-0.28	0.02	0.23	0.24	0.42
102	-119.7	-124.8	-139	-133.3	-146.3	-120	-0.95	-0.30	-0.02	0.20	0.45	0.50
106	-157.9	-162.7	-162	-172.4	-165.6	-156	-1.59	-0.90	-0.30	0.29	0.60	1.01
111	-126.6	-126.5	-128	-142.3	-133.1	-122.5	-0.68	-0.42	-0.10	0.09	0.37	0.36
125	-158.7	-168.6	-169	-176.3	-162.2	-170.7	-0.82	-0.60	-0.22	0.07	0.38	0.33
131	-134.1	-134.3	-140	-145	-136.9	-118.6	-1.11	-0.60	-0.12	0.01	0.17	0.25
138	-175.5	-175.7	-178	-179.3	-170.6	-172.8	-0.54	-0.34	-0.20	0.01	-0.04	0.42
144	-120.9	-125.2	-134	-132.4	-131.4	-120.2	-0.50	-0.66	-0.16	-0.04	0.07	0.34
152	-198.1	-155.3	-153	-190.7	-159	-161.9	0.95	-2.13	-0.36	0.01	-0.66	0.58
158	-207.8	-136.2	-127	-150.1	-144.4	-129.3	4.08	-0.88	-0.36	0.11	0.13	0.31
166	-213.8	-166.6	-161	-170.8	-171.6	-168	3.92	-0.97	-0.52	0.01	0.09	0.24
172	-351.4	-147.2	-142	-379.2	-156.5	-141.5	72.49	-0.66	-0.40	75.45	0.01	0.21
180	-316.6	-179.2	-175	-415.6	-186.3	-173.5	28.70	-0.44	-1.75	100.23	-0.01	0.16
186	-290.6	-163.6	-144	-432.7	-149.9	-141.8	38.77	-1.33	-0.93	129.42	-0.01	0.12
194	-386.7	-175.5	-162	-440.8	-169.9	-443.4	100.88	-1.15	-1.71	129.67	-0.01	129.58
200	-384.7	-296.3	-125	-439.5	-135.3	-401.3	132.13	48.54	-1.71	151.46	-0.05	139.79
208	-398.3	-270.1	-160	-434.8	-170.5	-433.4	110.01	6.35	-0.40	112.98	-0.01	112.03
214	-398.1	-262.2	-128	-433.5	-149.4	-418.3	129.46	13.25	-0.40	132.53	0.03	134.59
222	-423.4	-339.3	-160	-450.6	-238.7	-448.8	135.47	49.47	-1.67	125.93	11.49	140.05
228	-424.8	-388	-136	-453.8	-254.9	-442.3	152.66	98.55	-0.46	141.62	19.34	155.70
236	-453.3	-408.6	-170	-466.4	-276.9	-472.1	170.28	92.24	-0.08	138.59	14.88	150.05
242	-465.3	-421.6	-135	-467.6	-254.4	-467.2	201.23	136.98	-1.11	161.80	13.47	182.36
250	-465.1	-460.9	-160	-480.4	-263	-476	166.94	144.90	-0.64	142.16	7.43	156.42
256	-486.5	-435.8	-138	-489.7	-222.2	-493.9	220.61	157.73	-0.76	180.37	7.00	198.41
264	-476.1	-460.7	-173	-485	-257.8	-494.4	196.58	151.80	-0.34	154.44	9.11	166.45
270	-510	-442.8	-231	-508.6	-377.8	-530.2	252.24	164.31	6.31	194.43	94.32	238.06
278	-500.5	-470.8	-233	-508	-411.7	-529.9	227.01	154.80	3.98	172.41	103.65	206.76
284	-523.1	-465.3	-207	-545.4	-417.9	-545	270.94	165.23	2.63	225.86	124.73	260.61
292	-505.9	-486.9	-221	-529.5	-422.1	-536.4	229.40	170.84	3.28	189.26	117.43	216.05
298	-545	-470.8	-217	-574.5	-408.2	-567.1	288.84	177.96	3.04	250.80	111.30	331.96
306	-521.3	-478.9	-223	-538	-538	-538.9	235.25	161.41	3.12	198.94	98.77	239.26
312	-568.5	-469	-200	-585	-432.6	-570.8	329.82	182.73	2.15	271.22	140.61	334.48
320	-528.5	-486.4	-431	-550.5	-458.3	-549.1	263.58	173.66	144.10	220.16	142.71	263.13
326	-586.9	-503.5	-452	-603	-479.6	-578.6	344.74	197.89	172.49	285.15	171.75	333.42
334	-550.6	-500.8	-457	-575.4	-490.7	-554.1	280.29	176.85	159.86	242.71	161.80	247.35
340	-598.4	-514.1	-450	-620.5	-502.2	-594.3	327.23	212.45	170.50	284.08	192.44	27.32
348	-539.2	-503.7	-428	-574.7	-493.1	-532.8	277.70	192.48	156.20	231.96	181.03	26.74
354	-593.8	-532.5	-446	-609.5	-532.5	-604.4	370.00	241.69	186.49	301.46	229.31	87.35
362	-549.2	-512.8	-464	-583.7	-503.3	-547	279.09	204.50	180.27	240.85	197.75	18.01
368	-602.1	-549	-470	-613.1	-562.5	-598.9	380.55	273.92	208.55	307.43	274.01	111.01
376	-562.6	-542.6	-491	-577.1	-549.1	-562.8	311.32	229.36	205.69	256.37	224.67	16.09
382	-578.1	-548.3	-478	-616.8	-565.5	-597.9	314.90	269.54	218.62	274.80	283.82	140.19

CEM III/A (w/b=0.6)

Type of measurement	Corrosion potential (mV)						Macrocell current (nA/cm^2)					
Type of steel	SS			LS			SS			LS		
Age (days)	No.1	No.2	No.3	No.1	No.2	No.3	No.1	No.2	No.3	No.1	No.2	No.3
42	-135.5	-139	-116.5	-127.4	-120.9	-122.7	-6.52	2.17	2.41	-0.64	-3.74	0.40
47	-171.6	-174	-167.6	-162.6	-160.6	-169.6	-6.19	1.09	1.21	-0.11	-2.32	-0.12
49	-179.7	-171	-174.4	-173.4	-169.2	-179.5	-7.60	1.25	1.33	-0.13	-1.25	-0.17
54	-165.8	-173	-165	-160.9	-158.3	-168.1	-7.94	0.92	1.09	-0.17	-2.04	-0.41
56	-175.6	-183	-174.3	-172.2	-167.3	-178.8	-9.03	1.37	1.23	-0.16	-2.41	-0.38
61	-174.1	-162	-157	-153.2	-166.6	-165.7	-6.35	0.84	0.62	-0.40	-5.00	-0.32
63	-168.3	-178	-169	-166.2	-166.9	-175.1	-8.33	0.93	0.88	-0.42	-4.26	-0.33
67	-152.1	-161	-154.3	-151.2	-155	-157.6	-5.63	0.82	0.99	-0.32	-3.28	-0.44
68	-165	-175	-166.4	-164.5	-165	-171.3	-4.89	0.76	0.60	-0.42	-3.08	-0.23
70	-150	-159	-153.1	-148.9	-152.2	-157.4	-4.58	0.16	0.50	-0.32	-2.88	-0.25
75	-172.1	-181	-174.8	-170.3	-169.6	-179.1	-2.80	0.44	0.12	-0.32	-1.18	-0.41
77	-152.8	-161	-155	-152.4	-151.4	-160.9	-4.08	0.18	0.36	-0.37	-1.10	-0.32
81	-168.7	-179	-163.7	-165.7	-166.9	-176.4	-3.32	-0.18	0.16	-0.44	-0.98	-0.44
83	-160.6	-171	-164.9	-160.7	-158.6	-176.3	-2.94	-0.06	0.04	-0.31	-0.46	-0.12
96	-178	-178	-169.3	-177.2	-168.4	-178.4	-1.01	-0.16	0.06	-0.23	-0.58	-0.13
102	-162.4	-164	-155.8	-164.3	-156.9	-166.7	-0.50	0.22	0.04	-0.01	-0.58	-0.13
110	-171.6	-177	-169.2	-171.3	-174.8	-184.8	-0.26	0.24	0.10	-0.11	-0.44	0.03
116	-153.1	-160	-149.8	-155.4	-142.8	-157.8	-0.48	-0.54	-0.02	-0.11	-1.01	-0.12
124	-149.6	-148	-150.6	-159.4	-146.9	-155	-0.32	1.39	0.02	-0.58	-0.56	-0.17
130	-148.8	-163	-147	-147.8	-142.4	-158.9	-0.48	0.74	0.02	-0.23	-0.46	-0.12
138	-151.3	-177	-156.6	-152.2	-152.9	-167.9	-0.38	0.80	0.02	-0.17	-0.45	-0.07
144	-158	-176	-154.4	-157.6	-151.4	-162.9	-0.22	0.72	0.02	-0.12	-0.12	-0.01
152	-166.5	-182	-160.1	-164	-156	-169.8	-0.24	1.07	0.02	-0.16	-0.17	0.04
158	-162.2	-184	-158.1	-157.1	-156	-167.2	-0.34	1.25	0.08	-0.50	-0.37	-0.01
166	-142.7	-144	-139.4	-139.8	-134.2	-155.7	-0.34	1.01	-0.02	-0.15	-0.15	-0.01
172	-154.6	-168	-151.8	-149.8	-148.7	-159.5	-0.52	1.25	-0.02	-0.16	-0.54	0.11
180	-170.4	-186	-157.8	-169.3	-162.7	-159.5	-0.28	1.55	0.08	-0.15	-0.11	0.01
186	-148.6	-163	-151.2	-132.3	-143.5	-158.3	0.16	-0.74	-0.10	0.05	0.08	-0.04
194	-158.5	-149	-128.5	-161.2	-148.9	-132.1	-0.12	0.32	-0.02	0.03	-0.01	0.11
200	-155.2	-174	-131.3	-157.6	-146.8	-159.6	-0.02	1.17	0.02	-0.03	-0.07	0.03
208	-175.2	-186	-171.4	-177.6	-159.3	-177.9	-0.12	0.74	0.02	0.11	-0.16	0.03
214	-156.2	-168	-151.3	-157.7	-148.7	-161.6	-0.08	0.54	0.02	-0.05	-0.08	0.03
222	-172.1	-185	-169.6	-169.8	-164.9	-174.2	-0.18	0.78	0.02	-0.13	-0.12	0.03
228	-157.1	-196	-156.6	-157.8	-156.3	-166	-0.08	1.13	0.08	-0.09	-0.09	0.16
236	-167.3	-183	-165	-165.9	-166.8	-176.7	-0.10	0.62	0.02	-0.11	-0.07	0.07
242	-153.2	-179	-149.3	-150.2	-147.2	-159	-0.06	0.36	0.04	-0.08	-0.08	0.17
250	-129.5	-163	-148.4	-130.7	-134	-132.1	-0.04	0.92	0.90	-0.12	-0.09	0.04
256	-155.2	-162	-155	-153.8	-148.8	-158.2	-0.04	0.72	0.76	-0.08	-0.08	0.04
264	-167.2	-173	-150.1	-167	-150.6	-153.3	-0.26	1.17	0.40	-0.57	-0.60	0.21
270	-155	-168	-155	-149.8	-146.2	-151.8	-0.04	0.24	0.06	-0.07	-0.07	0.01
278	-157.9	-152	-147.3	-158	-133.4	-147.9	-0.12	0.68	0.18	-0.09	-0.09	0.03
284	-152.6	-159	-150.4	-150.2	-145.3	-154.4	-0.06	0.28	0.06	-0.08	-0.09	0.01
292	-168.4	-178	-164.1	-169.5	-159.4	-171.4	-0.06	0.32	0.04	-0.13	-0.13	0.01
298	-152.7	-166	-152.8	-154.1	-148.6	-157.9	-0.04	0.32	0.02	-0.05	-0.05	0.17
306	-167.4	-170	-161.5	-162.6	-157.1	-167.6	-0.08	0.22	0.02	-0.20	-0.17	-0.01
312	-151.3	-162	-148.3	-150.5	-145.3	-155.8	-0.50	-0.18	-0.44	-0.13	-0.24	-0.12
320	-153.8	-151	-139.8	-151.7	-143.2	-147.9	-0.18	0.90	0.12	-0.07	-0.04	0.03
326	-153.5	-161	-148.3	-147	-142.1	-165.1	-0.46	-0.14	-0.48	-0.07	-0.38	0.07
334	-135	-136	-116.1	-137.7	-121.9	-122.2	-0.04	0.26	0.04	-0.08	-0.05	0.03
340	-148.3	-157	-148.6	-148.6	-141.9	-151.7	-0.08	0.26	0.12	-0.29	-0.20	0.05
348	-162.4	-172	-162.1	-160.9	-159.2	-169.4	-0.06	0.18	0.02	-0.11	-0.08	-0.01
354	-147.1	-156	-143.8	-145.5	-138.3	-152.2	-0.52	-0.26	-0.54	-0.29	-0.27	-0.07
362	-143.5	-155	-144.8	-140.1	-138.7	-148.3	-0.04	0.38	0.02	-0.11	-0.09	0.01
368	-150.8	-158	-148.8	-146.9	-139.7	-154.7	-0.40	0.06	0.04	-0.31	-0.11	-0.09
376	-155.9	-157	-150	-151.6	-146	-156.5	-0.04	0.12	0.02	-0.13	-0.12	0.04
382	-154.7	-158	-147.6	-146.2	-138.4	-153.2	-0.30	-0.36	-0.64	-0.33	-0.42	-0.08

CEM II/B-V (w/b=0.6)

Type of measurement	Corrosion potential (mV)						Macrocell current (nA/cm^2)					
Type of steel	SS			LS			SS			LS		
Age (days)	No.1	No.2	No.3	No.1	No.2	No.3	No.1	No.2	No.3	No.1	No.2	No.3
42	-105.0	-118.0	-120.6	-151.7	-117.7	-263.5	1.05	3.40	3.58	5.09	3.10	5.00
47	-175.3	-188.1	-194.6	-214.2	-187.2	-254.6	0.66	1.83	2.51	3.22	2.19	9.79
49	-178.6	-176.6	-182.6	-182.4	-182.1	-186.9	-1.23	-3.38	-0.34	-1.11	-0.45	-0.08
54	-167.2	-172.8	-180.9	-185.7	-176.4	-181.6	0.44	0.90	2.53	1.76	1.49	1.67
56	-176.7	-173.8	-180.5	-174.8	-177.5	-183.4	-1.05	-1.49	0.18	-0.60	-0.89	0.15
61	-169.5	-174.0	-183.3	-187.1	-175.0	-173.0	0.52	0.84	2.07	1.59	1.27	0.73
63	-169.0	-169.8	-175.9	-173.1	-172.4	-179.4	-0.48	-1.21	0.26	-0.61	-0.12	0.33
67	-159.8	-162.7	-171.3	-177.7	-164.7	-167.2	0.30	0.20	1.77	1.27	0.62	0.66
68	-171.1	-171.3	-182.2	-172.3	-175.2	-182.8	-0.10	-0.44	0.86	-0.31	-0.03	0.52
70	-162.3	-164.7	-174.0	-171.0	-164.0	-168.9	0.38	0.36	1.59	0.66	0.58	0.80
74	-172.5	-173.5	-178.0	-174.4	-173.0	-184.3	-0.58	-1.65	0.28	-1.37	-0.44	0.17
76	-176.0	-169.1	-178.3	-175.8	-182.7	-176.5	-0.12	-0.44	0.26	-0.16	-0.03	0.07
89	-169.8	-169.7	-173.7	-168.0	-174.5	-174.7	-0.26	-0.64	0.02	-0.24	-0.11	-0.01
91	-160.0	-157.8	-161.9	-162.9	-161.9	-163.7	-0.24	-0.52	0.18	-0.25	-0.07	0.07
96	-166.6	-166.9	-171.1	-166.9	-171.7	-171.3	-0.26	-0.44	0.02	-0.21	-0.05	0.01
102	-150.4	-149.4	-150.6	-152.6	-152.1	-155.1	0.16	0.32	-0.08	0.13	0.01	-0.04
110	-163.8	-164.8	-165.9	-164.6	-169.5	-171.0	0.52	-0.66	0.46	-0.41	0.84	-0.29
116	-144.3	-143.1	-143.0	-143.1	-145.1	-150.5	-0.14	-0.44	-0.04	-0.11	-0.04	-0.04
124	-158.1	-157.8	-161.0	-159.4	-162.7	-166.4	-0.36	-0.44	-0.20	-0.25	-0.07	-0.01
130	-140.9	-137.7	-141.6	-142.0	-138.5	-145.9	-0.64	-0.72	-0.22	-0.50	-0.13	0.11
138	-156.3	-153.7	-159.6	-160.1	-156.7	-166.9	-0.30	-1.65	-0.76	-0.69	-0.19	-0.04
144	-153.8	-152.8	-154.9	-154.2	-156.5	-159.4	-0.38	-0.44	0.14	-0.23	-0.08	-0.01
152	-164.1	-165.7	-166.6	-166.9	-170.0	-172.6	-0.56	-0.70	-0.32	-0.17	-0.04	-0.01
158	-150.2	-149.4	-150.0	-149.6	-151.0	-153.0	-0.16	-0.22	-0.10	-0.11	-0.04	-0.03
166	-146.0	-150.1	-149.2	-143.6	-161.5	-155.2	-1.11	-1.41	-0.68	-0.17	-0.04	-0.24
172	-146.5	-145.6	-144.8	-145.5	-144.8	-148.0	-0.32	-0.30	-0.18	-0.11	-0.03	-0.03
180	-153.9	-149.2	-161.5	-152.0	-158.8	-162.7	0.22	0.42	-0.10	-0.20	-0.56	0.28
186	-143.2	-133.1	-143.8	-144.6	-128.8	-147.1	-0.12	-0.20	-0.12	-0.09	-0.08	-0.05
194	-158.4	-154.6	-162.1	-158.4	-160.9	-165.1	-0.22	-0.26	-0.16	-0.09	-0.05	-0.03
200	-148.8	-144.5	-145.8	-147.3	-145.4	-150.3	-0.10	-0.18	-0.12	-0.12	-0.07	-0.05
208	-159.4	-156.9	-163.5	-157.8	-163.0	-163.8	-0.54	-0.74	-0.48	-0.07	-0.04	-0.03
214	-143.6	-143.1	-138.8	-143.2	-137.8	-150.0	-0.14	-0.16	-0.12	-0.08	-0.05	-0.03
222	-159.3	-152.6	-156.6	-160.0	-164.7	-161.2	-0.20	-0.24	-1.99	-0.11	-0.07	-0.05
228	-143.7	-140.8	-142.4	-143.8	-144.7	-148.8	-0.64	-0.76	-0.52	-0.08	-0.07	-0.04
236	-150.5	-146.7	-154.5	-148.8	-154.4	-156.0	-0.20	-0.66	-0.54	-0.03	-0.27	0.01
242	-143.0	-134.3	-135.4	-142.8	-141.1	-140.8	-0.22	0.12	-0.10	-0.08	-0.13	-0.12
250	-158.8	-175.8	-166.1	-159.6	-152.8	-158.2	-0.26	-0.36	-0.30	-0.08	-0.05	-0.05
256	-145.2	-142.9	-140.0	-144.9	-144.8	-146.1	-0.12	-0.06	-0.20	-0.07	-0.08	-0.05
264	-149.7	-140.9	-148.8	-147.7	-145.2	-153.3	-0.12	-0.16	-0.14	-0.05	-0.04	-0.04
270	-137.8	-133.0	-134.3	-137.4	-139.6	-142.4	-0.40	-0.60	-0.48	-0.29	-0.25	-0.15
278	-146.9	-135.0	-141.6	-145.0	-149.0	-143.5	0.86	-0.38	-0.20	-0.21	0.66	-0.03
284	-143.9	-138.5	-140.5	-142.9	-144.7	-147.9	-0.18	-0.22	-0.20	-0.12	-0.09	-0.08
292	-150.1	-147.3	-153.0	-150.3	-151.4	-152.8	-0.14	-0.16	-0.16	-0.05	-0.01	-0.03
298	-141.2	-138.6	-140.7	-142.3	-141.2	-145.0	-1.37	-0.36	-0.04	-0.25	-0.21	-0.15
306	-151.5	-146.4	-165.1	-146.7	-150.5	-154.3	-1.67	-0.58	-0.10	-0.07	-0.11	-0.07
312	-144.9	-146.5	-140.5	-140.8	-139.1	-140.7	-0.86	0.64	-0.04	-0.07	-0.11	-0.05
320	-148.9	-150.7	-147.0	-148.0	-149.9	-150.2	-0.44	-0.04	-0.24	-0.12	-0.13	-0.09
326	-139.2	-142.6	-136.6	-137.9	-137.1	-145.0	0.18	-0.06	-0.26	-0.21	-0.12	-0.11
334	-143.2	-149.1	-148.7	-143.8	-145.3	-145.6	-0.16	0.08	0.10	-0.16	0.36	-0.19
340	-134.9	-158.9	-157.0	-135.3	-136.9	-139.5	-0.02	0.44	0.78	-0.07	-0.08	-0.08
348	-144.2	-145.5	-166.7	-141.2	-143.8	-144.9	-0.12	0.06	0.34	-0.09	-0.05	-0.04
354	-136.0	-142.3	-156.4	-132.8	-133.7	-138.4	-0.10	0.16	0.46	-0.01	-0.03	-0.03
362	-146.2	-129.3	-198.7	-143.5	-125.4	-146.9	-0.10	0.02	2.27	-0.03	-0.01	-0.01
368	-137.5	-167.9	-176.5	-135.2	-134.6	-139.2	-0.10	1.37	0.44	-0.05	-0.05	-0.04
376	-146.3	-173.8	-167.6	-144.8	-148.8	-151.0	-0.06	0.56	0.34	-0.01	-0.04	0.01
382	-148.5	-167.4	-156.8	-129.2	-133.2	-137.1	-0.06	1.39	0.30	-0.01	-0.01	-0.03

C2.2 Parameters from galvanostatic pulse measurement

The following equations is used to obtain the parameters (refer to equation (6.2) in Chapter 6).

$$V_t(t) = I_{app}R_{\Omega} - I_{app}R_p\left[1 - e^{\left(\frac{-t}{\tau}\right)^{\beta}}\right]$$

CEM I (w/b=0.4)

Type of steel	SS																	
Replicate No.	No.1						No.2						No.3					
Age (days)	R_Ω ($\Omega \cdot m^2$)	R_p ($\Omega \cdot m^2$)	τ (sec)	C (F/m^2)	β	r^2	R_Ω ($\Omega \cdot m^2$)	R_p ($\Omega \cdot m^2$)	τ (sec)	C (F/m^2)	β	r^2	R_Ω ($\Omega \cdot m^2$)	R_p ($\Omega \cdot m^2$)	τ (sec)	C (F/m^2)	β	r^2
186	1.14	63.45	94.29	1.49	0.80	1.00	1.39	63.70	113.53	1.78	0.79	1.00	1.41	56.40	64.31	1.14	0.83	1.00
200	1.05	68.47	111.57	1.63	0.79	1.00	1.19	69.77	132.25	1.90	0.79	1.00	1.39	53.34	59.47	1.11	0.84	1.00
214	1.33	62.26	88.34	1.42	0.81	1.00	1.43	58.83	91.34	1.55	0.81	1.00	1.54	63.16	71.39	1.13	0.83	1.00
228	1.26	72.65	112.15	1.54	0.80	1.00	1.75	62.09	96.57	1.56	0.83	1.00	1.54	55.06	56.03	1.02	0.84	1.00
242	1.40	69.99	104.71	1.50	0.80	1.00	1.45	68.98	116.44	1.69	0.80	1.00	1.64	68.62	77.63	1.13	0.83	1.00
256	1.37	59.60	79.29	1.33	0.80	1.00	1.45	74.25	121.48	1.64	0.79	1.00	1.59	61.55	61.51	1.00	0.84	1.00
270	1.60	61.12	76.27	1.25	0.82	1.00	1.82	77.99	123.73	1.59	0.80	1.00	1.79	53.76	47.99	0.89	0.86	1.00
284	1.66	70.05	92.72	1.32	0.81	1.00	1.76	65.33	95.13	1.46	0.81	1.00	1.79	70.57	70.77	1.00	0.84	1.00
298	1.66	66.93	86.63	1.29	0.81	1.00	4.42	126.51	95.13	1.68	0.81	1.00	1.86	70.34	70.72	1.01	0.84	1.00
312	1.87	66.09	78.92	1.19	0.81	1.00	2.08	89.05	140.16	1.57	0.79	1.00	2.16	66.79	60.95	0.91	0.85	1.00
326	1.66	60.38	74.81	1.24	0.82	1.00	1.91	65.26	95.56	1.46	0.80	1.00	1.95	62.13	60.12	0.97	0.84	1.00
340	1.91	54.75	62.98	1.15	0.82	1.00	2.04	69.35	101.29	1.46	0.80	1.00	2.26	66.64	63.96	0.96	0.84	1.00
354	1.84	59.00	65.75	1.11	0.82	1.00	2.06	54.50	66.34	1.22	0.82	1.00	2.11	72.70	67.72	0.93	0.85	1.00
368	1.98	65.04	77.36	1.19	0.81	1.00	2.09	74.57	107.25	1.44	0.80	1.00	2.24	74.56	70.79	0.95	0.84	1.00
382	1.85	60.64	69.62	1.15	0.81	1.00	2.01	58.52	74.36	1.27	0.81	1.00	2.29	71.04	65.81	0.93	0.84	1.00
Type of steel	LS																	
Replicate No.	No.1						No.2						No.3					
Age (days)	R_Ω ($\Omega \cdot m^2$)	R_p ($\Omega \cdot m^2$)	τ (sec)	C (F/m^2)	β	r^2	R_Ω ($\Omega \cdot m^2$)	R_p ($\Omega \cdot m^2$)	τ (sec)	C (F/m^2)	β	r^2	R_Ω ($\Omega \cdot m^2$)	R_p ($\Omega \cdot m^2$)	τ (sec)	C (F/m^2)	β	r^2
186	1.16	65.60	107.64	1.64	0.88	1.00	1.46	64.13	111.08	1.73	0.84	1.00	1.39	57.07	79.88	1.40	0.87	1.00
200	1.14	72.65	124.90	1.72	0.88	1.00	1.38	55.94	95.47	1.71	0.84	1.00	1.47	71.76	112.77	1.57	0.85	1.00
214	1.28	67.16	108.47	1.62	0.87	1.00	1.65	54.88	84.33	1.54	0.85	1.00	1.77	84.28	129.30	1.53	0.86	1.00
228	1.44	89.77	165.94	1.85	0.84	1.00	1.56	62.46	102.20	1.64	0.84	1.00	1.65	61.78	84.24	1.36	0.86	1.00
242	1.52	147.82	318.02	2.15	0.83	1.00	1.74	114.38	236.69	2.07	0.81	1.00	1.69	76.87	115.04	1.50	0.85	1.00
256	1.50	141.41	286.62	2.03	0.83	1.00	1.91	61.09	94.79	1.55	0.83	1.00	1.88	146.93	257.24	1.75	0.83	1.00
270	1.80	67.92	102.36	1.51	0.86	1.00	2.02	66.78	101.15	1.51	0.84	1.00	2.03	57.25	80.06	1.25	0.84	1.00
284	1.62	87.82	146.75	1.67	0.84	1.00	2.28	56.73	80.06	1.41	0.84	1.00	2.05	99.72	151.23	1.52	0.84	1.00
298	1.88	145.13	293.99	2.03	0.82	1.00	7.01	125.04	80.06	0.73	0.84	1.00	2.29	80.79	114.66	1.42	0.84	1.00
312	1.78	143.52	268.25	1.87	0.83	1.00	2.29	59.97	81.65	1.36	0.84	1.00	2.18	82.31	110.76	1.35	0.85	1.00
326	1.66	81.82	133.10	1.63	0.85	1.00	2.05	50.63	69.93	1.38	0.85	1.00	2.03	85.51	127.84	1.50	0.84	1.00
340	1.78	115.38	215.05	1.86	0.82	1.00	2.24	56.35	79.02	1.40	0.84	1.00	2.40	89.33	135.48	1.52	0.83	1.00
354	1.88	131.23	241.67	1.84	0.82	1.00	2.24	55.78	71.60	1.28	0.85	1.00	2.18	75.41	97.65	1.29	0.86	1.00
368	2.11	120.13	217.18	1.81	0.82	1.00	2.39	55.11	74.05	1.34	0.84	1.00	2.27	70.67	92.59	1.31	0.85	1.00
382	1.98	151.27	307.65	2.03	0.80	1.00	2.34	65.77	93.52	1.42	0.83	1.00	2.55	99.97	149.56	1.50	0.83	1.00

CEM III/A (w/b=0.4)

Type of steel	SS																	
Replicate No.	No.1						No.2						No.3					
Age (days)	R_Ω ($\Omega \cdot m^2$)	R_p ($\Omega \cdot m^2$)	τ (sec)	C (F/m^2)	β	r^2	R_Ω ($\Omega \cdot m^2$)	R_p ($\Omega \cdot m^2$)	τ (sec)	C (F/m^2)	β	r^2	R_Ω ($\Omega \cdot m^2$)	R_p ($\Omega \cdot m^2$)	τ (sec)	C (F/m^2)	β	r^2
186	2.40	90.37	242.06	2.68	0.73	1.00	2.46	89.72	224.85	2.51	0.74	1.00	2.46	114.21	268.05	2.35	0.77	1.00
200	2.61	82.22	198.61	2.42	0.73	1.00	2.26	80.62	182.58	2.26	0.75	1.00	2.50	109.23	243.01	2.22	0.76	1.00
214	2.75	87.92	217.43	2.47	0.72	1.00	2.60	96.33	238.10	2.47	0.74	1.00	2.54	95.05	195.28	2.05	0.77	1.00
228	2.72	68.08	144.21	2.12	0.74	1.00	2.45	92.30	218.36	2.37	0.75	1.00	2.66	87.70	170.55	1.94	0.77	1.00
242	3.03	75.05	158.05	2.11	0.74	1.00	2.77	88.36	196.81	2.23	0.75	1.00	2.88	79.09	140.89	1.78	0.77	1.00
256	3.13	85.05	187.13	2.20	0.74	1.00	2.90	97.43	228.79	2.35	0.74	1.00	2.54	80.93	144.35	1.78	0.77	1.00
270	3.26	106.85	254.50	2.38	0.73	1.00	3.08	71.91	135.67	1.89	0.75	1.00	3.02	75.34	124.83	1.66	0.76	1.00
284	3.11	56.80	96.93	1.71	0.74	1.00	3.04	84.63	180.61	2.13	0.74	1.00	2.98	67.43	107.32	1.59	0.76	1.00
298	3.24	58.06	101.81	1.75	0.74	1.00	3.00	66.61	125.05	1.88	0.74	1.00	3.04	67.28	107.52	1.60	0.76	1.00
312	3.31	60.33	105.32	1.75	0.74	1.00	3.31	72.52	136.33	1.88	0.74	1.00	3.08	51.38	67.21	1.31	0.79	1.00
326	3.26	47.72	74.18	1.55	0.74	1.00	2.98	56.39	93.16	1.65	0.76	1.00	3.19	76.42	129.84	1.70	0.75	1.00
340	2.77	56.51	90.08	1.59	0.75	1.00	3.14	65.94	118.43	1.80	0.74	1.00	3.24	71.00	113.81	1.60	0.75	1.00
354	4.00	45.88	64.00	1.39	0.77	1.00	3.49	61.74	98.92	1.60	0.75	1.00	3.41	71.18	104.39	1.47	0.76	1.00
368	3.79	51.40	64.00	1.59	0.77	1.00	3.49	69.99	119.43	1.71	0.74	1.00	3.51	66.22	92.31	1.39	0.76	1.00
382	3.49	52.97	77.09	1.46	0.73	1.00	3.34	68.95	117.21	1.70	0.74	1.00	3.46	64.07	88.12	1.38	0.76	1.00
Type of steel	LS																	
Replicate No.	No.1						No.2						No.3					
Age (days)	R_Ω ($\Omega \cdot m^2$)	R_p ($\Omega \cdot m^2$)	τ (sec)	C (F/m^2)	β	r^2	R_Ω ($\Omega \cdot m^2$)	R_p ($\Omega \cdot m^2$)	τ (sec)	C (F/m^2)	β	r^2	R_Ω ($\Omega \cdot m^2$)	R_p ($\Omega \cdot m^2$)	τ (sec)	C (F/m^2)	β	r^2
186	2.24	128.64	298.47	2.32	0.82	1.00	2.23	109.54	351.05	3.20	0.77	1.00	2.25	128.95	378.63	2.94	0.81	1.00
200	2.69	138.90	328.65	2.37	0.80	1.00	2.23	89.29	260.64	2.92	0.77	1.00	2.65	126.13	370.78	2.94	0.79	1.00
214	2.64	124.27	273.28	2.20	0.81	1.00	2.42	95.61	281.80	2.95	0.76	1.00	2.42	131.01	375.70	2.87	0.80	1.00
228	2.91	141.34	345.15	2.44	0.79	1.00	2.79	95.39	294.31	3.09	0.74	1.00	2.79	120.35	348.41	2.89	0.78	1.00
242	3.34	144.39	348.08	2.41	0.78	1.00	3.06	97.60	299.30	3.07	0.74	1.00	3.80	121.30	352.93	2.91	0.77	1.00
256	3.10	109.71	230.28	2.10	0.79	1.00	3.04	77.09	205.72	2.67	0.75	1.00	3.02	126.81	374.10	2.95	0.78	1.00
270	3.32	147.32	342.08	2.32	0.78	1.00	3.20	61.81	139.44	2.26	0.75	1.00	3.20	116.11	317.03	2.73	0.77	1.00
284	3.39	119.02	253.45	2.13	0.78	1.00	3.19	87.52	234.23	2.68	0.74	1.00	3.14	114.44	311.63	2.72	0.78	1.00
298	3.57	137.33	322.12	2.35	0.77	1.00	3.28	88.90	253.91	2.86	0.73	1.00	3.21	109.11	296.89	2.72	0.77	1.00
312	3.44	118.40	252.53	2.13	0.78	1.00	3.20	68.01	161.33	2.37	0.74	1.00	3.18	116.34	322.54	2.77	0.77	1.00
326	3.29	142.18	331.36	2.33	0.78	1.00	3.15	77.13	199.38	2.58	0.73	1.00	3.34	97.81	250.19	2.56	0.77	1.00
340	3.54	134.10	299.05	2.23	0.77	1.00	3.53	66.34	155.53	2.34	0.73	1.00	3.25	102.61	263.26	2.57	0.77	1.00
354	3.75	99.13	184.37	1.86	0.78	1.00	3.74	64.75	139.23	2.15	0.73	1.00	3.62	100.73	247.62	2.46	0.76	1.00
368	3.96	127.41	261.85	2.06	0.77	1.00	3.83	59.70	119.96	2.01	0.73	1.00	3.77	103.30	250.54	2.43	0.76	1.00
382	3.75	138.66	304.08	2.19	0.76	1.00	3.58	55.62	107.15	1.93	0.74	1.00	3.56	104.38	254.43	2.44	0.76	1.00

CEM II/B-V (w/b=0.4)

Type of steel	SS																	
Replicate No.	No.1						No.2						No.3					
Age (days)	R_Ω ($\Omega \cdot m^2$)	R_p ($\Omega \cdot m^2$)	τ (sec)	C (F/m^2)	β	r^2	R_Ω ($\Omega \cdot m^2$)	R_p ($\Omega \cdot m^2$)	τ (sec)	C (F/m^2)	β	r^2	R_Ω ($\Omega \cdot m^2$)	R_p ($\Omega \cdot m^2$)	τ (sec)	C (F/m^2)	β	r^2
186	3.08	169.68	300.63	1.77	0.80	1.00	3.34	110.15	326.08	2.96	0.76	1.00	2.87	78.14	242.64	3.11	0.80	1.00
200	3.57	172.41	293.50	1.70	0.80	1.00	3.67	110.05	313.73	2.85	0.75	1.00	3.07	129.71	499.26	3.85	0.77	1.00
214	3.81	167.95	288.94	1.72	0.80	1.00	4.05	100.20	272.13	2.72	0.75	1.00	3.33	126.89	487.70	3.84	0.77	1.00
228	4.24	176.45	297.72	1.69	0.80	1.00	4.51	104.02	285.72	2.75	0.74	1.00	3.86	131.55	507.93	3.86	0.76	1.00
242	4.52	179.60	309.83	1.73	0.79	1.00	4.83	105.05	291.00	2.77	0.73	1.00	4.03	126.91	493.84	3.89	0.75	1.00
256	4.92	158.62	255.16	1.61	0.80	1.00	4.91	88.12	222.60	2.53	0.74	1.00	4.25	123.30	475.49	3.86	0.75	1.00
270	5.37	189.11	324.47	1.72	0.78	1.00	5.87	88.08	205.81	2.34	0.75	1.00	4.92	128.35	492.25	3.84	0.74	1.00
284	4.96	179.67	322.92	1.80	0.78	1.00	5.19	94.44	258.98	2.74	0.73	1.00	4.54	82.69	263.80	3.19	0.76	1.00
298	5.60	163.31	269.09	1.65	0.78	1.00	5.71	86.85	213.05	2.45	0.73	1.00	4.90	120.57	464.45	3.85	0.74	1.00
312	5.99	185.33	314.24	1.70	0.78	1.00	6.21	96.57	243.82	2.52	0.72	1.00	5.41	120.59	462.56	3.84	0.73	1.00
326	5.95	174.12	293.87	1.69	0.78	1.00	6.11	93.90	237.73	2.53	0.72	1.00	5.38	116.54	445.29	3.82	0.73	1.00
340	6.26	176.30	295.59	1.68	0.77	1.00	6.53	64.89	128.73	1.98	0.74	1.00	5.59	121.70	462.16	3.80	0.73	1.00
354	7.25	174.80	271.38	1.55	0.77	1.00	7.46	83.57	179.07	2.14	0.72	1.00	6.41	102.50	338.52	3.30	0.72	1.00
368	7.21	168.34	262.19	1.56	0.77	1.00	7.80	55.27	95.78	1.73	0.76	1.00	6.41	97.98	325.74	3.32	0.72	1.00
382	7.04	188.73	311.80	1.65	0.77	1.00	7.20	87.31	196.88	2.25	0.72	1.00	6.21	93.10	297.71	3.20	0.73	1.00
Type of steel	LS																	
Replicate No.	No.1						No.2						No.3					
Age (days)	R_Ω ($\Omega \cdot m^2$)	R_p ($\Omega \cdot m^2$)	τ (sec)	C (F/m^2)	β	r^2	R_Ω ($\Omega \cdot m^2$)	R_p ($\Omega \cdot m^2$)	τ (sec)	C (F/m^2)	β	r^2	R_Ω ($\Omega \cdot m^2$)	R_p ($\Omega \cdot m^2$)	τ (sec)	C (F/m^2)	β	r^2
186	3.08	156.05	566.78	3.63	0.80	1.00	3.79	174.70	489.15	2.80	0.79	1.00	3.10	221.61	745.95	3.37	0.82	1.00
200	3.37	160.78	584.60	3.64	0.79	1.00	4.32	175.19	480.43	2.74	0.79	1.00	3.36	175.37	539.73	3.08	0.82	1.00
214	3.59	156.92	575.62	3.67	0.79	1.00	4.84	175.18	489.22	2.79	0.78	1.00	3.92	185.95	591.85	3.18	0.81	1.00
228	4.47	134.65	470.62	3.50	0.77	1.00	5.47	165.38	452.83	2.74	0.77	1.00	4.36	196.53	653.26	3.32	0.80	1.00
242	4.64	132.42	459.85	3.47	0.77	1.00	5.63	170.02	479.31	2.82	0.76	1.00	4.78	182.69	601.91	3.29	0.80	1.00
256	4.90	141.47	535.79	3.79	0.76	1.00	5.83	161.53	449.25	2.78	0.76	1.00	5.09	182.10	614.93	3.38	0.79	1.00
270	5.48	132.52	464.83	3.51	0.76	1.00	6.63	166.62	447.96	2.69	0.76	1.00	5.55	161.75	509.19	3.15	0.79	1.00
284	5.10	123.70	453.47	3.67	0.76	1.00	5.95	153.49	433.20	2.82	0.76	1.00	5.07	159.69	545.68	3.42	0.78	1.00
298	5.69	131.32	475.45	3.62	0.75	1.00	6.84	148.20	389.59	2.63	0.76	1.00	5.87	146.73	468.77	3.19	0.78	1.00
312	6.16	121.40	416.57	3.43	0.75	1.00	7.20	163.88	439.31	2.68	0.75	1.00	6.29	159.30	516.97	3.25	0.77	1.00
326	6.15	124.74	448.00	3.59	0.74	1.00	7.18	158.91	438.81	2.76	0.75	1.00	6.16	152.39	505.73	3.32	0.77	1.00
340	6.40	118.51	408.35	3.45	0.74	1.00	7.38	166.04	455.91	2.75	0.75	1.00	6.68	149.52	474.49	3.17	0.77	1.00
354	7.41	142.16	525.07	3.69	0.72	1.00	8.74	152.94	383.00	2.50	0.74	1.00	7.52	159.18	497.23	3.12	0.77	1.00
368	7.19	130.55	457.60	3.51	0.73	1.00	8.51	146.38	368.04	2.51	0.74	1.00	7.49	162.09	525.94	3.24	0.76	1.00
382	7.27	120.95	403.51	3.34	0.74	1.00	8.48	162.61	424.25	2.61	0.74	1.00	7.33	167.83	563.22	3.36	0.76	1.00

CEM I (w/b=0.6)

Type of steel	SS																	
Replicate No.	No.1						No.2						No.3					
Age (days)	R_Ω ($\Omega \cdot m^2$)	R_p ($\Omega \cdot m^2$)	τ (sec)	C (F/m^2)	β	r^2	R_Ω ($\Omega \cdot m^2$)	R_p ($\Omega \cdot m^2$)	τ (sec)	C (F/m^2)	β	r^2	R_Ω ($\Omega \cdot m^2$)	R_p ($\Omega \cdot m^2$)	τ (sec)	C (F/m^2)	β	r^2
186	0.84	21.81	102.74	4.71	0.68	1.00	0.72	128.48	595.20	4.63	0.77	1.00	0.73	115.02	513.58	4.47	0.78	1.00
200	0.79	2.66	8.45	3.17	0.70	1.00	0.71	56.73	310.88	5.48	0.73	1.00	0.81	99.89	404.65	4.05	0.79	1.00
214	0.94	2.12	8.35	3.93	0.73	1.00	0.72	75.59	409.75	5.42	0.74	1.00	0.80	109.87	470.29	4.28	0.78	1.00
228	0.86	1.57	5.25	3.35	0.71	1.00	0.76	4.20	12.98	3.09	0.71	1.00	0.75	110.49	498.60	4.51	0.77	1.00
242	0.89	1.14	4.45	3.91	0.78	1.00	0.84	2.06	6.57	3.19	0.74	1.00	0.75	120.55	583.65	4.84	0.76	1.00
256	0.87	1.05	4.63	4.42	0.80	1.00	0.90	1.76	7.00	3.99	0.76	1.00	0.82	109.66	472.18	4.31	0.77	1.00
270	0.85	0.94	6.12	6.50	0.82	1.00	0.85	1.70	7.40	4.35	0.75	1.00	0.85	86.74	463.10	5.34	0.75	1.00
284	0.84	1.04	7.36	7.10	0.75	1.00	0.82	1.82	8.34	4.57	0.73	1.00	0.77	90.42	450.52	4.98	0.75	1.00
298	0.80	0.98	6.89	7.01	0.77	1.00	0.85	1.49	7.86	5.28	0.74	1.00	0.82	83.29	395.63	4.75	0.76	1.00
312	0.80	1.16	9.87	8.53	0.75	1.00	0.82	1.45	7.97	5.51	0.75	1.00	0.78	12.57	46.53	3.70	0.71	1.00
326	0.80	1.08	9.07	8.39	0.73	1.00	0.82	1.72	10.95	6.36	0.72	1.00	0.91	2.44	15.25	6.25	0.71	0.99
340	0.83	1.18	12.76	10.84	0.70	1.00	0.79	1.45	9.42	6.50	0.70	1.00	0.97	1.82	8.31	4.56	0.80	1.00
354	0.79	1.17	11.36	9.68	0.73	1.00	0.80	1.17	9.38	8.02	0.72	1.00	0.86	1.74	7.44	4.28	0.75	1.00
368	0.79	1.22	11.91	9.80	0.69	1.00	0.78	0.98	8.30	8.48	0.72	1.00	0.84	1.47	6.63	4.51	0.77	1.00
382	0.86	1.08	9.01	8.34	0.72	1.00	0.85	1.06	11.31	10.68	0.74	1.00	0.91	1.42	6.83	4.80	0.79	1.00
Type of steel	LS																	
Replicate No.	No.1						No.2						No.3					
Age (days)	R_Ω ($\Omega \cdot m^2$)	R_p ($\Omega \cdot m^2$)	τ (sec)	C (F/m^2)	β	r^2	R_Ω ($\Omega \cdot m^2$)	R_p ($\Omega \cdot m^2$)	τ (sec)	C (F/m^2)	β	r^2	R_Ω ($\Omega \cdot m^2$)	R_p ($\Omega \cdot m^2$)	τ (sec)	C (F/m^2)	β	r^2
186	0.69	3.48	5.69	1.64	0.76	1.00	0.90	121.79	522.22	4.29	0.78	1.00	0.87	136.92	557.61	4.07	0.79	1.00
200	0.89	2.82	6.89	2.44	0.78	1.00	1.01	113.69	473.08	4.16	0.78	1.00	1.04	2.16	7.34	3.39	0.76	1.00
214	0.96	3.03	8.03	2.65	0.77	1.00	1.03	130.24	569.62	4.37	0.78	1.00	1.04	2.01	7.39	3.68	0.75	1.00
228	0.87	2.66	6.43	2.42	0.75	1.00	0.95	95.44	527.30	5.53	0.74	1.00	1.06	2.18	9.08	4.16	0.73	1.00
242	0.99	2.13	5.71	2.68	0.78	1.00	1.07	34.44	114.17	3.31	0.78	1.00	1.06	1.82	8.87	4.88	0.75	1.00
256	1.00	2.17	7.71	3.55	0.76	1.00	1.04	82.67	358.80	4.34	0.77	1.00	1.06	1.56	8.26	5.31	0.79	1.00
270	0.96	2.15	7.96	3.70	0.76	1.00	1.10	3.50	10.49	3.00	0.74	1.00	1.06	1.24	7.48	6.01	0.81	1.00
284	1.01	2.08	9.56	4.59	0.76	1.00	1.12	1.91	6.25	3.27	0.77	1.00	1.05	1.42	11.33	7.99	0.79	1.00
298	0.95	1.98	10.78	5.45	0.72	1.00	1.09	2.76	10.81	3.91	0.73	1.00	1.02	1.65	18.05	10.93	0.71	1.00
312	0.96	2.13	11.93	5.61	0.73	1.00	1.07	1.78	7.63	4.29	0.72	1.00	1.02	1.42	12.00	8.47	0.74	1.00
326	0.97	1.70	9.16	5.39	0.73	1.00	1.09	1.25	6.33	5.06	0.73	1.00	1.01	1.57	18.70	11.88	0.69	1.00
340	1.03	1.70	10.64	6.25	0.76	1.00	1.05	1.18	6.76	5.72	0.72	1.00	0.89	2.53	43.99	17.39	0.59	1.00
354	0.93	1.20	6.40	5.36	0.69	1.00	0.99	1.22	9.19	7.51	0.70	1.00	0.86	1.28	10.52	8.19	0.67	1.00
368	0.99	1.89	11.61	6.14	0.72	1.00	1.03	1.27	12.67	10.00	0.69	1.00	0.88	1.24	10.07	8.11	0.67	1.00
382	1.01	2.48	19.62	7.90	0.68	1.00	1.06	1.27	11.00	8.68	0.74	1.00	0.89	2.07	23.45	11.33	0.63	1.00

CEM III/A(w/b=0.6)

Type of steel	SS																	
Replicate No.	No.1						No.2						No.3					
Age (days)	R_Ω ($\Omega \cdot m^2$)	R_p ($\Omega \cdot m^2$)	τ (sec)	C (F/m^2)	β	r^2	R_Ω ($\Omega \cdot m^2$)	R_p ($\Omega \cdot m^2$)	τ (sec)	C (F/m^2)	β	r^2	R_Ω ($\Omega \cdot m^2$)	R_p ($\Omega \cdot m^2$)	τ (sec)	C (F/m^2)	β	r^2
186	2.02	116.10	347.33	2.99	0.77	1.00	2.12	156.83	278.04	1.77	0.80	1.00	2.13	137.24	374.28	2.73	0.77	1.00
200	2.17	134.35	421.33	3.14	0.76	1.00	2.34	157.56	268.68	1.71	0.79	1.00	2.32	129.82	328.47	2.53	0.77	1.00
214	2.20	127.13	398.71	3.14	0.75	1.00	2.36	166.16	283.36	1.71	0.79	1.00	2.32	129.34	330.68	2.56	0.76	1.00
228	2.10	131.33	422.16	3.21	0.76	1.00	2.23	176.81	321.86	1.82	0.79	1.00	2.30	145.92	406.77	2.79	0.75	1.00
242	2.39	129.39	385.90	2.98	0.76	1.00	2.40	163.60	268.67	1.64	0.79	1.00	2.42	134.47	340.91	2.54	0.75	1.00
256	2.47	120.49	348.06	2.89	0.76	1.00	2.45	151.18	243.03	1.61	0.79	1.00	2.67	127.73	313.94	2.46	0.75	1.00
270	2.32	115.81	319.97	2.76	0.75	1.00	2.64	115.35	155.59	1.35	0.80	1.00	2.68	129.45	307.49	2.38	0.75	1.00
284	2.43	125.64	367.10	2.92	0.75	1.00	2.56	149.18	231.67	1.55	0.79	1.00	2.65	118.13	270.58	2.29	0.75	1.00
298	2.46	113.00	308.37	2.73	0.75	1.00	2.62	125.05	175.04	1.40	0.80	1.00	2.55	122.84	282.74	2.30	0.75	1.00
312	2.62	110.14	287.64	2.61	0.75	1.00	2.71	118.90	156.59	1.32	0.80	1.00	2.69	116.90	250.91	2.15	0.75	1.00
326	2.45	108.68	289.71	2.67	0.75	1.00	2.62	178.23	290.75	1.63	0.78	1.00	2.71	130.51	309.61	2.37	0.74	1.00
340	2.61	111.27	293.10	2.63	0.75	1.00	2.82	153.79	226.57	1.47	0.79	1.00	2.81	130.86	301.33	2.30	0.74	1.00
354	2.75	110.24	273.54	2.48	0.75	1.00	2.89	123.94	159.58	1.29	0.79	1.00	2.94	119.76	248.39	2.07	0.75	1.00
368	2.78	105.70	264.23	2.50	0.74	1.00	2.94	124.90	161.51	1.29	0.79	1.00	2.99	123.27	262.24	2.13	0.74	1.00
382	2.75	120.92	324.40	2.68	0.74	1.00	2.90	117.26	148.33	1.27	0.79	1.00	2.95	121.45	258.22	2.13	0.74	1.00
Type of steel	LS																	
Replicate No.	No.1						No.2						No.3					
Age (days)	R_Ω ($\Omega \cdot m^2$)	R_p ($\Omega \cdot m^2$)	τ (sec)	C (F/m^2)	β	r^2	R_Ω ($\Omega \cdot m^2$)	R_p ($\Omega \cdot m^2$)	τ (sec)	C (F/m^2)	β	r^2	R_Ω ($\Omega \cdot m^2$)	R_p ($\Omega \cdot m^2$)	τ (sec)	C (F/m^2)	β	r^2
186	2.26	121.82	303.21	2.49	0.81	1.00	2.21	144.78	485.25	3.35	0.80	1.00	2.33	162.01	362.08	2.23	0.83	1.00
200	2.35	161.04	451.33	2.80	0.79	1.00	2.59	136.69	457.72	3.35	0.78	1.00	2.52	215.74	363.08	2.50	0.83	1.00
214	2.43	160.47	461.08	2.87	0.78	1.00	2.53	135.61	445.32	3.28	0.78	1.00	2.53	204.20	364.08	2.40	0.83	1.00
228	2.46	151.68	429.36	2.83	0.79	1.00	2.56	133.99	455.82	3.40	0.77	1.00	2.52	195.06	365.08	2.41	0.83	1.00
242	2.70	155.64	435.88	2.80	0.78	1.00	2.65	132.92	428.40	3.22	0.77	1.00	2.66	191.99	366.08	2.32	0.83	1.00
256	2.76	153.08	427.29	2.79	0.77	1.00	3.07	131.32	437.16	3.33	0.76	1.00	2.82	165.28	367.08	2.13	0.83	1.00
270	2.87	152.57	420.43	2.76	0.77	1.00	2.87	140.70	464.76	3.30	0.76	1.00	2.87	202.12	368.08	2.30	0.83	1.00
284	2.80	145.39	397.22	2.73	0.77	1.00	2.78	128.49	404.48	3.15	0.77	1.00	2.84	199.13	369.08	2.33	0.83	1.00
298	2.93	148.69	417.29	2.81	0.76	1.00	2.89	136.50	446.30	3.27	0.76	1.00	3.20	168.51	370.08	2.19	0.83	1.00
312	2.85	153.16	421.87	2.75	0.76	1.00	2.99	130.42	406.87	3.12	0.76	1.00	3.17	197.01	371.08	2.30	0.83	1.00
326	3.26	135.52	353.34	2.61	0.78	1.00	2.99	125.74	382.17	3.04	0.76	1.00	2.90	182.12	372.08	2.23	0.83	1.00
340	3.03	143.47	386.02	2.69	0.76	1.00	3.04	122.26	364.98	2.99	0.76	1.00	3.04	203.81	373.08	2.35	0.83	1.00
354	3.27	140.16	365.73	2.61	0.76	1.00	3.23	132.83	410.11	3.09	0.75	1.00	3.10	202.53	374.08	2.26	0.83	1.00
368	3.18	144.52	391.33	2.71	0.75	1.00	3.21	131.08	413.02	3.15	0.75	1.00	3.23	189.93	375.08	2.21	0.83	1.00
382	3.14	154.06	434.34	2.82	0.75	1.00	3.34	115.14	324.69	2.82	0.76	1.00	3.29	188.34	376.08	2.20	0.83	1.00

CEM II/B-V (w/b=0.6)

Type of steel	SS																	
Replicate No.	No.1						No.2						No.3					
Age (days)	R_Ω ($\Omega \cdot m^2$)	R_p ($\Omega \cdot m^2$)	τ (sec)	C (F/m^2)	β	r^2	R_Ω ($\Omega \cdot m^2$)	R_p ($\Omega \cdot m^2$)	τ (sec)	C (F/m^2)	β	r^2	R_Ω ($\Omega \cdot m^2$)	R_p ($\Omega \cdot m^2$)	τ (sec)	C (F/m^2)	β	r^2
186	1.70	98.19	338.15	3.44	0.78	1.00	1.86	117.69	341.20	2.90	0.79	1.00	2.06	123.42	400.83	3.25	0.81	1.00
200	1.84	109.27	382.00	3.50	0.77	1.00	2.07	108.77	291.40	2.68	0.78	1.00	2.19	136.07	453.99	3.34	0.80	1.00
214	1.89	126.96	471.88	3.72	0.76	1.00	2.15	123.77	352.06	2.84	0.77	1.00	2.30	146.07	498.19	3.41	0.79	1.00
228	2.15	90.18	275.57	3.06	0.77	1.00	2.36	112.11	303.78	2.71	0.77	1.00	2.48	162.06	567.15	3.50	0.79	1.00
242	2.25	87.31	267.17	3.06	0.76	1.00	2.55	87.66	208.64	2.38	0.78	1.00	2.65	144.59	488.01	3.38	0.79	1.00
256	2.00	74.36	366.51	4.93	0.76	1.00	2.63	106.37	265.09	2.49	0.77	1.00	2.74	151.46	514.48	3.40	0.78	1.00
270	2.65	94.54	269.52	2.85	0.75	1.00	2.99	103.19	237.79	2.30	0.77	1.00	3.05	140.50	433.53	3.09	0.79	1.00
284	2.58	76.87	206.60	2.69	0.75	1.00	2.85	88.19	193.00	2.19	0.78	1.00	3.01	150.66	498.76	3.31	0.78	1.00
298	2.89	77.69	214.48	2.76	0.75	1.00	3.16	108.98	256.51	2.35	0.77	1.00	3.37	134.95	411.85	3.05	0.78	1.00
312	2.99	82.32	226.14	2.75	0.74	1.00	3.20	115.96	286.56	2.47	0.76	1.00	3.43	135.41	426.82	3.15	0.78	1.00
326	4.00	63.92	226.14	3.66	0.74	1.00	3.35	114.44	278.27	2.43	0.76	1.00	3.54	145.15	461.00	3.18	0.77	1.00
340	3.13	64.30	146.18	2.27	0.75	1.00	3.52	88.56	184.76	2.09	0.77	1.00	3.68	149.41	476.43	3.19	0.78	1.00
354	3.61	60.49	127.09	2.10	0.75	1.00	3.82	72.40	130.67	1.80	0.77	1.00	3.84	149.95	485.31	3.24	0.76	1.00
368	3.39	51.20	99.56	1.94	0.76	1.00	3.81	91.53	192.75	2.11	0.76	1.00	3.90	138.12	433.01	3.13	0.77	1.00
382	3.61	71.64	163.83	2.29	0.74	1.00	4.04	78.17	147.47	1.89	0.77	1.00	4.11	139.04	433.32	3.12	0.77	1.00
Type of steel	LS																	
Replicate No.	No.1						No.2						No.3					
Age (days)	R_Ω ($\Omega \cdot m^2$)	R_p ($\Omega \cdot m^2$)	τ (sec)	C (F/m^2)	β	r^2	R_Ω ($\Omega \cdot m^2$)	R_p ($\Omega \cdot m^2$)	τ (sec)	C (F/m^2)	β	r^2	R_Ω ($\Omega \cdot m^2$)	R_p ($\Omega \cdot m^2$)	τ (sec)	C (F/m^2)	β	r^2
186	2.12	122.95	460.45	3.74	0.78	1.00	2.09	190.65	763.32	4.00	0.81	1.00	2.17	157.95	587.38	3.72	0.82	1.00
200	2.39	119.47	421.01	3.52	0.78	1.00	2.38	173.28	660.87	3.81	0.81	1.00	2.34	172.16	648.92	3.77	0.81	1.00
214	2.40	118.19	413.78	3.50	0.78	1.00	2.52	145.17	521.00	3.59	0.81	1.00	2.40	208.82	840.66	4.03	0.81	1.00
228	2.73	116.19	385.85	3.32	0.77	1.00	2.75	154.48	556.79	3.60	0.80	1.00	2.66	147.87	519.15	3.51	0.81	1.00
242	2.76	106.54	348.53	3.27	0.77	1.00	2.81	136.52	483.83	3.54	0.79	1.00	2.61	195.60	738.69	3.78	0.81	1.00
256	3.84	116.18	218.94	1.88	0.76	1.00	3.11	160.28	586.73	3.66	0.79	1.00	3.03	155.92	558.79	3.58	0.80	1.00
270	3.18	96.26	268.18	2.79	0.77	1.00	3.39	145.64	490.49	3.37	0.79	1.00	3.27	169.79	610.41	3.60	0.79	1.00
284	3.25	104.18	316.89	3.04	0.76	1.00	3.42	164.11	604.54	3.68	0.78	1.00	3.23	159.35	585.66	3.68	0.79	1.00
298	3.48	113.54	347.20	3.06	0.75	1.00	3.76	154.02	542.25	3.52	0.78	1.00	3.56	143.23	486.57	3.40	0.79	1.00
312	3.57	108.29	327.36	3.02	0.75	1.00	3.85	132.92	444.94	3.35	0.78	1.00	3.57	142.85	496.80	3.48	0.79	1.00
326	3.66	108.20	328.90	3.04	0.75	1.00	4.09	145.45	514.63	3.54	0.77	1.00	3.77	146.63	503.62	3.43	0.79	1.00
340	3.96	94.11	257.99	2.74	0.75	1.00	4.13	145.98	513.55	3.52	0.77	1.00	3.95	152.48	537.68	3.53	0.78	1.00
354	4.12	104.27	293.03	2.81	0.74	1.00	4.53	143.30	482.81	3.37	0.76	1.00	4.17	157.55	539.47	3.42	0.78	1.00
368	4.03	94.69	256.64	2.71	0.75	1.00	4.56	134.18	451.60	3.37	0.76	1.00	4.31	138.59	471.70	3.40	0.77	1.00
382	4.33	89.77	226.87	2.53	0.75	1.00	4.82	138.22	458.53	3.32	0.76	1.00	4.50	164.91	585.59	3.55	0.77	1.00

C2.3 Parameters from potentiostatic measurement

The following equations is used to obtain the parameters (refer to equation (6.3) in Chapter 6).

$$I_t(t) = \frac{E_{app}}{R_\Omega(R_\Omega + R_p)}\left[R_\Omega + R_p e^{\left(\frac{-t}{\frac{C_{dl}R_pR_\Omega}{R_\Omega+R_p}}\right)}\right]$$

CEM I (w/b=0.4)

Type of steel	SS														
Replicate No.	No.1					No.2					No.3				
Age (days)	R_Ω ($\Omega \cdot m^2$)	R_p ($\Omega \cdot m^2$)	τ (sec)	C (F/m^2)	r^2	R_Ω ($\Omega \cdot m^2$)	R_p ($\Omega \cdot m^2$)	τ (sec)	C (F/m^2)	r^2	R_Ω ($\Omega \cdot m^2$)	R_p ($\Omega \cdot m^2$)	τ (sec)	C (F/m^2)	r^2
186	2.50	97.14	2.22	0.91	0.95	2.53	81.46	2.66	1.08	0.95	2.34	95.99	1.77	0.78	0.95
200	2.45	99.32	2.20	0.92	0.95	2.60	88.04	2.77	1.10	0.95	2.67	102.04	2.03	0.78	0.95
214	2.34	99.14	2.15	0.94	0.95	2.43	100.66	2.53	1.07	0.95	2.55	131.91	1.84	0.74	0.95
228	2.92	108.95	2.63	0.92	0.96	2.84	125.55	2.92	1.05	0.96	2.85	191.28	2.05	0.73	0.95
242	2.92	103.77	2.52	0.89	0.95	3.12	150.03	3.01	0.98	0.95	3.10	266.17	2.17	0.71	0.95
256	3.18	91.99	3.52	1.66	0.95	3.25	174.96	3.37	1.06	0.96	3.40	375.19	2.47	0.73	0.96
270	2.87	138.70	2.41	0.85	0.95	3.16	190.02	3.01	0.97	0.96	3.08	231.19	2.16	0.71	0.95
284	2.88	116.66	2.39	0.85	0.95	3.06	162.61	2.86	0.95	0.95	3.33	373.64	2.30	0.70	0.95
298	2.64	116.96	2.17	0.84	0.94	2.86	107.48	2.57	0.92	0.95	3.29	332.42	2.27	0.70	0.95
312	2.81	102.18	2.15	0.79	0.94	3.37	131.55	3.00	0.91	0.96	3.38	154.49	2.16	0.65	0.96
326	2.91	129.57	2.43	0.85	0.95	3.30	120.49	3.19	0.99	0.96	3.36	226.05	2.36	0.71	0.95
340	3.11	115.90	2.53	0.83	0.94	3.32	143.67	3.09	0.95	0.95	3.34	200.88	2.27	0.69	0.95
354	3.31	128.88	2.76	0.85	0.95	3.40	178.64	3.09	0.93	0.95	3.61	401.76	2.40	0.67	0.95
368	3.03	124.51	2.39	0.81	0.94	3.25	192.42	2.89	0.90	0.95	3.51	238.85	2.28	0.66	0.95
382	3.68	109.93	2.96	0.83	0.96	3.63	128.30	3.20	0.91	0.96	3.46	141.14	2.24	0.66	0.96
Type of steel	LS														
Replicate No.	No.1					No.2					No.3				
Age (days)	R_Ω ($\Omega \cdot m^2$)	R_p ($\Omega \cdot m^2$)	τ (sec)	C (F/m^2)	r^2	R_Ω ($\Omega \cdot m^2$)	R_p ($\Omega \cdot m^2$)	τ (sec)	C (F/m^2)	r^2	R_Ω ($\Omega \cdot m^2$)	R_p ($\Omega \cdot m^2$)	τ (sec)	C (F/m^2)	r^2
186	1.81	105.18	2.06	1.16	0.97	2.25	85.54	2.52	1.15	0.96	2.09	91.72	2.05	1.01	0.97
200	1.92	102.61	2.28	1.21	0.98	2.36	81.08	2.74	1.20	0.96	2.35	94.49	2.46	1.07	0.97
214	2.03	106.28	2.36	1.18	0.98	2.42	76.95	2.74	1.17	0.96	2.45	134.33	2.45	1.02	0.97
228	2.20	149.65	2.48	1.14	0.97	2.66	93.11	2.94	1.14	0.97	2.69	207.07	2.61	0.98	0.97
242	2.60	188.50	2.87	1.12	0.97	3.18	99.75	3.40	1.11	0.97	3.19	132.99	3.11	1.00	0.97
256	2.66	115.76	3.02	1.16	0.97	3.42	206.35	3.73	1.09	0.96	3.10	214.89	3.05	1.00	0.97
270	2.64	189.75	2.91	1.12	0.97	3.33	218.89	3.60	1.10	0.96	2.98	256.40	2.88	0.98	0.97
284	2.73	225.43	3.02	1.12	0.97	3.26	272.45	3.56	1.10	0.96	3.04	372.77	2.97	0.98	0.96
298	2.86	199.32	3.16	1.12	0.97	3.23	157.93	3.47	1.10	0.96	3.10	162.25	3.04	1.00	0.97
312	2.43	93.23	2.44	1.03	0.97	3.45	132.48	3.42	1.02	0.96	3.26	158.57	3.03	0.95	0.97
326	2.54	248.74	2.78	1.10	0.97	3.13	232.29	3.35	1.09	0.96	3.08	205.64	3.07	1.01	0.96
340	3.05	166.27	3.36	1.12	0.97	3.35	144.74	3.53	1.08	0.96	3.50	136.98	3.43	1.00	0.97
354	3.75	128.37	4.07	1.11	0.97	3.33	209.54	3.40	1.04	0.96	3.21	253.25	3.00	0.94	0.97
368	3.11	146.02	3.30	1.09	0.97	3.98	148.90	3.98	1.03	0.96	3.22	205.56	3.06	0.96	0.96
382	3.25	133.70	3.37	1.06	0.97	3.53	148.05	3.54	1.03	0.96	3.82	133.44	3.64	0.98	0.97

CEM III/A (w/b=0.4)

Type of steel	SS														
Replicate No.	No.1					No.2					No.3				
Age (days)	R_Ω ($\Omega \cdot m^2$)	R_p ($\Omega \cdot m^2$)	τ (sec)	C (F/m^2)	r^2	R_Ω ($\Omega \cdot m^2$)	R_p ($\Omega \cdot m^2$)	τ (sec)	C (F/m^2)	r^2	R_Ω ($\Omega \cdot m^2$)	R_p ($\Omega \cdot m^2$)	τ (sec)	C (F/m^2)	r^2
186	4.36	92.22	5.69	1.37	0.97	3.97	114.45	5.12	1.34	0.96	4.19	154.58	4.99	1.22	0.97
200	4.44	96.91	5.78	1.36	0.97	4.20	85.78	5.36	1.34	0.97	4.24	140.57	4.99	1.21	0.97
214	4.65	95.60	5.87	1.32	0.97	5.88	109.33	6.36	1.23	0.97	4.16	103.70	4.58	1.14	0.97
228	4.56	129.91	5.59	1.27	0.96	4.30	109.85	7.36	1.26	0.97	4.15	148.50	4.61	1.14	0.96
242	5.00	108.91	6.07	1.27	0.96	4.52	104.39	5.57	1.29	0.96	4.62	125.95	5.01	1.12	0.96
256	4.62	103.08	5.55	1.26	0.96	4.36	117.13	5.27	1.25	0.96	4.51	140.67	5.00	1.14	0.96
270	5.31	108.46	6.12	1.21	0.95	4.88	106.46	5.66	1.21	0.96	5.00	107.06	5.17	1.08	0.96
284	5.04	102.86	5.85	1.22	0.96	4.75	95.95	5.50	1.21	0.96	4.84	115.24	5.06	1.09	0.96
298	5.14	107.30	5.98	1.22	0.96	4.81	100.16	5.54	1.21	0.96	4.98	124.83	5.21	1.09	0.96
312	5.20	101.26	5.89	1.19	0.96	5.01	99.26	5.59	1.17	0.96	4.83	122.56	4.83	1.04	0.96
326	5.26	97.87	6.03	1.21	0.96	5.09	94.32	5.85	1.21	0.96	5.12	119.18	5.27	1.07	0.96
340	7.24	104.70	7.03	1.36	0.96	5.14	89.75	5.83	1.20	0.96	5.00	113.45	5.07	1.06	0.96
354	5.84	106.46	6.15	1.11	0.96	5.54	93.01	5.93	1.13	0.96	5.63	109.81	5.30	0.99	0.96
368	5.88	115.67	6.20	1.11	0.96	5.52	103.07	5.99	1.14	0.96	5.61	151.53	5.46	1.01	0.96
382	6.02	99.96	6.47	1.14	0.96	5.64	103.70	6.08	1.14	0.96	5.59	113.51	5.32	1.00	0.96
Type of steel	LS														
Replicate No.	No.1					No.2					No.3				
Age (days)	R_Ω ($\Omega \cdot m^2$)	R_p ($\Omega \cdot m^2$)	τ (sec)	C (F/m^2)	r^2	R_Ω ($\Omega \cdot m^2$)	R_p ($\Omega \cdot m^2$)	τ (sec)	C (F/m^2)	r^2	R_Ω ($\Omega \cdot m^2$)	R_p ($\Omega \cdot m^2$)	τ (sec)	C (F/m^2)	r^2
186	3.72	128.84	4.90	1.35	0.98	3.77	89.26	6.01	1.66	0.97	3.52	116.93	5.61	1.64	0.98
200	4.07	119.52	5.24	1.33	0.98	4.39	99.48	6.71	1.60	0.98	3.70	113.75	5.78	1.62	0.97
214	4.05	108.36	5.15	1.32	0.97	4.40	88.02	6.84	1.63	0.97	3.80	126.17	5.86	1.59	0.98
228	4.70	167.38	5.79	1.27	0.98	4.21	108.03	6.46	1.60	0.97	4.27	100.44	6.44	1.57	0.98
242	4.57	131.88	5.69	1.29	0.98	4.58	83.34	6.86	1.58	0.97	4.42	109.68	6.52	1.53	0.98
256	4.46	126.58	5.53	1.28	0.97	4.37	99.41	6.56	1.57	0.97	4.09	113.37	6.10	1.55	0.98
270	4.95	129.90	5.87	1.23	0.97	4.94	88.15	6.99	1.49	0.97	4.58	98.67	6.48	1.48	0.98
284	4.83	122.02	5.78	1.24	0.97	4.87	88.28	7.10	1.54	0.97	4.74	100.96	6.83	1.51	0.98
298	4.84	116.64	5.77	1.24	0.97	5.20	92.53	7.62	1.55	0.97	4.64	102.72	6.63	1.49	0.98
312	4.97	115.96	5.84	1.23	0.97	5.13	89.85	7.11	1.46	0.97	4.66	97.07	6.47	1.46	0.98
326	4.73	116.57	5.59	1.23	0.97	4.78	89.65	6.81	1.50	0.96	4.56	97.85	6.35	1.46	0.97
340	4.99	110.60	5.72	1.20	0.97	5.41	82.80	7.63	1.50	0.97	4.66	94.80	6.41	1.44	0.97
354	5.51	111.71	6.23	1.19	0.97	6.00	85.75	7.92	1.41	0.97	5.09	101.33	6.66	1.37	0.97
368	5.69	128.52	6.34	1.16	0.97	5.80	85.35	7.76	1.43	0.97	5.26	103.49	6.95	1.39	0.97
382	5.68	115.74	6.39	1.18	0.97	5.39	87.73	7.09	1.40	0.97	5.26	102.34	6.90	1.38	0.97

CEM II/B-V (w/b=0.4)

Type of steel	SS														
Replicate No.	No.1					No.2					No.3				
Age (days)	R_Ω ($\Omega \cdot m^2$)	R_p ($\Omega \cdot m^2$)	τ (sec)	C (F/m^2)	r^2	R_Ω ($\Omega \cdot m^2$)	R_p ($\Omega \cdot m^2$)	τ (sec)	C (F/m^2)	r^2	R_Ω ($\Omega \cdot m^2$)	R_p ($\Omega \cdot m^2$)	τ (sec)	C (F/m^2)	r^2
186	4.75	165.44	4.54	0.98	0.98	5.06	105.79	7.54	1.56	0.98	3.91	89.49	7.43	1.98	0.98
200	4.93	150.79	4.72	0.99	0.98	5.52	110.41	8.10	1.54	0.98	4.42	93.90	8.36	1.98	0.98
214	5.46	184.83	5.07	0.95	0.98	6.06	97.27	8.52	1.49	0.98	4.82	86.80	8.61	1.89	0.98
228	5.83	210.44	5.42	0.95	0.98	6.39	130.22	9.12	1.50	0.98	5.16	134.36	9.33	1.88	0.98
242	6.23	202.26	5.75	0.95	0.98	6.69	113.68	9.28	1.47	0.98	5.45	112.41	9.70	1.87	0.99
256	6.42	178.50	6.00	0.97	0.97	7.56	113.64	10.39	1.47	0.98	5.69	103.45	10.16	1.88	0.98
270	7.27	175.56	6.42	0.92	0.98	7.79	104.64	10.44	1.44	0.98	6.26	103.52	10.73	1.82	0.99
284	6.75	158.54	6.28	0.97	0.98	7.20	101.62	10.27	1.53	0.98	5.90	91.94	10.61	1.91	0.99
298	7.57	182.11	6.87	0.95	0.98	7.94	103.89	10.91	1.48	0.98	6.56	100.14	11.39	1.85	0.98
312	7.74	169.07	6.95	0.94	0.98	8.51	107.76	11.48	1.45	0.98	7.04	99.40	12.03	1.83	0.99
326	8.02	162.10	7.25	0.95	0.98	8.51	106.37	11.38	1.45	0.98	7.05	98.47	12.01	1.83	0.99
340	8.65	172.79	7.61	0.92	0.98	9.07	104.90	11.90	1.42	0.98	7.49	99.34	12.62	1.81	0.99
354	9.71	197.69	8.18	0.88	0.98	10.30	111.66	12.71	1.35	0.98	8.60	101.13	13.61	1.72	0.99
368	9.46	186.95	8.18	0.91	0.98	9.99	112.92	12.76	1.39	0.98	8.53	98.24	13.63	1.74	0.99
382	9.16	170.70	7.99	0.92	0.98	9.69	105.11	12.53	1.41	0.98	7.95	109.76	12.87	1.74	0.99
Type of steel	LS														
Replicate No.	No.1					No.2					No.3				
Age (days)	R_Ω ($\Omega \cdot m^2$)	R_p ($\Omega \cdot m^2$)	τ (sec)	C (F/m^2)	r^2	R_Ω ($\Omega \cdot m^2$)	R_p ($\Omega \cdot m^2$)	τ (sec)	C (F/m^2)	r^2	R_Ω ($\Omega \cdot m^2$)	R_p ($\Omega \cdot m^2$)	τ (sec)	C (F/m^2)	r^2
186	4.36	132.73	7.92	1.88	0.99	5.35	160.95	7.60	1.47	0.98	4.38	147.49	7.62	1.79	0.98
200	4.84	109.87	8.62	1.86	0.99	6.09	152.13	8.55	1.46	0.98	4.83	153.21	8.19	1.75	0.99
214	5.20	128.69	9.18	1.84	0.99	6.16	213.99	8.45	1.41	0.98	5.16	177.57	8.43	1.68	0.99
228	5.78	135.41	10.18	1.84	0.99	6.79	150.48	9.22	1.42	0.98	5.67	157.19	9.39	1.72	0.99
242	5.95	136.04	10.30	1.81	0.99	7.33	145.33	9.90	1.42	0.98	5.95	159.36	9.75	1.70	0.99
256	6.26	102.21	10.67	1.81	0.99	7.49	140.86	10.15	1.43	0.99	6.28	145.14	10.38	1.72	0.99
270	8.85	128.62	11.67	1.61	0.99	8.53	140.31	11.12	1.38	0.99	6.54	136.76	10.41	1.67	0.99
284	6.37	118.42	11.37	1.88	0.99	7.78	130.13	10.69	1.46	0.99	6.43	120.18	10.73	1.76	0.99
298	7.14	108.33	12.24	1.83	0.99	8.71	129.76	11.57	1.42	0.99	7.21	126.53	11.73	1.72	0.99
312	7.37	112.79	12.40	1.79	0.99	9.27	137.44	12.14	1.40	0.99	7.90	114.65	12.58	1.70	0.99
326	7.95	109.25	13.47	1.82	0.99	9.33	130.52	12.18	1.40	0.99	7.97	117.60	12.68	1.70	0.99
340	8.18	106.40	13.41	1.77	0.99	9.67	134.90	12.35	1.37	0.99	8.05	124.81	12.69	1.68	0.99
354	9.69	102.64	15.04	1.70	0.99	11.18	139.38	13.55	1.31	0.99	9.45	129.76	14.19	1.61	0.99
368	9.23	116.05	14.76	1.73	0.99	11.23	145.82	13.80	1.32	0.99	9.36	130.73	14.23	1.63	0.99
382	9.15	104.99	14.67	1.74	0.99	10.79	132.09	13.51	1.35	0.99	9.10	144.32	14.09	1.65	0.99

CEM I (w/b=0.6)

Type of steel	SS														
Replicate No.	No.1					No.2					No.3				
Age (days)	R_Ω ($\Omega \cdot m^2$)	R_p ($\Omega \cdot m^2$)	τ (sec)	C (F/m^2)	r^2	R_Ω ($\Omega \cdot m^2$)	R_p ($\Omega \cdot m^2$)	τ (sec)	C (F/m^2)	r^2	R_Ω ($\Omega \cdot m^2$)	R_p ($\Omega \cdot m^2$)	τ (sec)	C (F/m^2)	r^2
186	1.83	15.49	4.68	2.86	0.96	1.63	69.74	2.76	1.74	0.97	1.61	74.14	2.94	1.86	0.97
200	1.44	2.06	4.41	5.19	0.96	1.59	29.17	3.17	2.11	0.96	1.54	93.90	2.79	1.84	0.96
214	1.52	2.13	7.53	8.50	0.92	1.61	23.93	3.17	2.10	0.97	1.96	101.87	3.28	1.70	0.96
228	1.39	1.62	8.03	10.71	0.92	1.40	3.70	4.06	3.99	0.97	1.67	114.82	3.08	1.88	0.97
242	1.26	1.34	8.36	12.90	0.92	1.27	1.86	4.12	5.46	0.96	1.63	95.16	2.97	1.85	0.96
256	1.26	1.25	12.22	19.47	0.92	1.33	1.57	6.30	8.73	0.93	1.70	93.93	3.02	1.80	0.96
270	1.23	1.53	21.43	31.50	0.93	1.29	1.82	8.23	10.88	0.91	1.68	74.04	3.51	2.14	0.96
284	1.22	1.40	19.88	30.47	0.92	1.19	1.42	5.25	8.12	0.93	1.64	57.45	3.18	1.99	0.96
298	1.13	1.17	11.57	20.15	0.93	1.24	1.58	6.79	9.79	0.94	1.73	64.02	3.39	2.01	0.96
312	1.08	1.37	13.18	21.81	0.95	1.20	1.65	7.83	11.25	0.92	1.61	54.29	3.17	2.03	0.96
326	1.03	1.30	13.16	22.87	0.94	1.10	1.25	6.38	10.94	0.95	1.27	1.58	5.70	8.09	0.93
340	1.07	1.23	13.86	24.16	0.95	1.15	1.43	8.97	14.11	0.94	1.24	1.84	5.15	6.94	0.93
354	1.02	1.09	10.61	20.12	0.95	1.08	1.04	7.85	14.84	0.94	1.22	1.54	5.37	7.87	0.94
368	1.03	1.15	12.50	23.01	0.95	1.08	0.93	9.80	19.59	0.96	1.22	1.46	6.94	10.46	0.92
382	1.19	1.27	13.45	21.88	0.95	1.08	1.16	12.23	21.85	0.96	1.17	1.41	5.61	8.78	0.95
Type of steel	LS														
Replicate No.	No.1					No.2					No.3				
Age (days)	R_Ω ($\Omega \cdot m^2$)	R_p ($\Omega \cdot m^2$)	τ (sec)	C (F/m^2)	r^2	R_Ω ($\Omega \cdot m^2$)	R_p ($\Omega \cdot m^2$)	τ (sec)	C (F/m^2)	r^2	R_Ω ($\Omega \cdot m^2$)	R_p ($\Omega \cdot m^2$)	τ (sec)	C (F/m^2)	r^2
186	1.53	2.96	2.85	2.82	0.97	1.86	68.80	3.30	1.83	0.97	1.78	82.33	2.84	1.63	0.97
200	1.52	2.69	3.37	3.48	0.93	1.82	75.33	3.28	1.85	0.97	1.41	1.78	3.45	4.39	0.98
214	1.62	2.93	3.89	3.73	0.94	1.94	66.95	3.49	1.85	0.97	1.49	1.82	5.17	6.30	0.95
228	1.46	2.39	3.63	4.00	0.93	1.99	35.79	4.04	2.14	0.97	1.60	1.75	11.67	13.97	0.90
242	1.49	2.38	4.90	5.35	0.93	2.01	43.77	4.25	2.21	0.97	1.52	1.72	9.67	11.96	0.93
256	1.54	2.14	7.10	7.92	0.91	1.98	58.25	3.84	2.01	0.97	1.31	1.40	6.51	9.61	0.96
270	1.59	2.30	11.72	12.46	0.90	1.73	3.54	5.85	5.03	0.95	1.46	1.76	15.40	19.30	0.94
284	1.40	1.68	6.95	9.10	0.94	1.55	1.82	5.00	5.96	0.97	1.39	1.74	9.80	12.66	0.94
298	1.33	1.63	6.50	8.89	0.96	1.65	2.50	6.31	6.34	0.95	1.31	1.35	10.56	15.88	0.96
312	1.47	2.42	10.62	11.62	0.94	1.52	1.53	6.28	8.23	0.95	1.34	1.48	12.81	18.21	0.96
326	1.38	1.73	8.46	11.01	0.95	1.44	0.88	6.41	11.73	0.96	1.29	1.11	11.38	19.03	0.96
340	1.38	1.70	9.00	11.83	0.95	1.38	1.08	7.04	11.65	0.96	1.29	1.22	11.03	17.58	0.97
354	1.33	1.53	7.59	10.65	0.97	1.20	0.82	4.55	9.33	0.99	1.24	1.07	10.64	18.57	0.97
368	1.32	1.49	8.13	11.61	0.96	1.27	0.97	9.55	17.41	0.97	1.28	1.09	11.52	19.61	0.97
382	1.39	1.78	8.00	10.27	0.96	1.31	1.26	9.65	15.05	0.97	1.38	1.36	13.62	19.82	0.96

CEM III/A (w/b=0.6)

Type of steel	SS														
Replicate No.	No.1					No.2					No.3				
Age (days)	R_Ω ($\Omega \cdot m^2$)	R_p ($\Omega \cdot m^2$)	τ (sec)	C (F/m^2)	r^2	R_Ω ($\Omega \cdot m^2$)	R_p ($\Omega \cdot m^2$)	τ (sec)	C (F/m^2)	r^2	R_Ω ($\Omega \cdot m^2$)	R_p ($\Omega \cdot m^2$)	τ (sec)	C (F/m^2)	r^2
186	3.52	98.33	4.99	1.47	0.97	3.45	134.07	3.09	0.92	0.97	5.02	116.14	5.50	1.14	0.98
200	3.55	102.65	4.98	1.45	0.97	3.73	145.71	3.25	0.89	0.97					
214	3.46	100.14	4.87	1.46	0.97	3.94	145.60	3.43	0.89	0.97	4.03	107.82	4.87	1.26	0.97
228	3.63	103.86	5.03	1.43	0.97	3.94	139.03	3.36	0.88	0.97	3.97	115.89	4.73	1.23	0.97
242	3.51	102.66	4.73	1.39	0.97	4.11	141.71	3.43	0.86	0.97	3.98	103.16	4.59	1.20	0.97
256	3.59	106.00	4.88	1.41	0.97	4.12	143.98	3.40	0.85	0.97	4.28	102.74	4.97	1.21	0.97
270	3.81	108.29	5.15	1.40	0.97	4.18	158.22	3.35	0.82	0.97	4.42	110.79	4.91	1.15	0.97
284	3.85	98.48	5.08	1.37	0.97	4.32	141.08	3.49	0.83	0.97	4.31	103.85	4.81	1.16	0.97
298	4.00	100.33	5.32	1.38	0.97	4.40	145.13	3.52	0.83	0.97	4.49	107.29	4.99	1.16	0.97
312	4.03	99.55	5.22	1.35	0.97	4.41	151.60	3.44	0.80	0.97	4.66	110.77	4.99	1.12	0.97
326	3.94	100.32	5.09	1.34	0.97	4.32	146.79	3.38	0.81	0.96	4.45	106.60	4.84	1.13	0.97
340	4.14	104.13	5.30	1.33	0.97	4.49	146.93	3.44	0.79	0.96	4.62	110.33	4.92	1.11	0.97
354	4.39	101.44	5.43	1.29	0.97	4.77	150.40	3.59	0.78	0.97	4.83	112.63	4.97	1.07	0.96
368	4.32	104.22	5.46	1.32	0.97	4.73	149.88	3.63	0.79	0.97	4.89	110.89	5.09	1.09	0.96
382	4.32	104.22	5.46	1.32	0.97	4.73	149.88	3.63	0.79	0.97	4.89	110.89	5.09	1.09	0.96
Type of steel	LS														
Replicate No.	No.1					No.2					No.3				
Age (days)	R_Ω ($\Omega \cdot m^2$)	R_p ($\Omega \cdot m^2$)	τ (sec)	C (F/m^2)	r^2	R_Ω ($\Omega \cdot m^2$)	R_p ($\Omega \cdot m^2$)	τ (sec)	C (F/m^2)	r^2	R_Ω ($\Omega \cdot m^2$)	R_p ($\Omega \cdot m^2$)	τ (sec)	C (F/m^2)	r^2
186	3.47	111.49	4.80	1.43	0.98	3.47	105.84	5.72	1.70	0.98	3.52	130.03	4.42	1.29	0.98
200	3.70	106.31	5.08	1.42	0.98	3.70	96.13	5.97	1.67	0.98	3.75	146.07	4.66	1.27	0.98
214	4.08	119.86	5.62	1.43	0.98	3.82	96.64	6.14	1.67	0.98					
228	3.89	149.26	5.29	1.40	0.97	3.77	99.11	5.99	1.65	0.98	3.94	138.40	4.70	1.23	0.98
242	3.96	122.98	5.26	1.37	0.98	3.89	96.22	6.05	1.62	0.98	3.95	140.23	4.64	1.21	0.98
256	4.06	116.41	5.41	1.38	0.98	4.03	106.72	6.23	1.60	0.98	4.06	138.21	4.81	1.22	0.98
270	4.66	108.93	6.11	1.37	0.98	4.18	109.88	6.31	1.56	0.98	4.30	133.38	4.89	1.17	0.98
284	4.39	117.92	5.75	1.36	0.98	4.20	97.15	6.29	1.56	0.98	4.22	132.44	4.87	1.19	0.98
298	4.38	117.22	5.75	1.36	0.98	4.26	97.84	6.43	1.58	0.98	4.21	132.51	4.79	1.17	0.98
312	4.50	117.33	5.82	1.34	0.98	4.37	98.06	6.36	1.52	0.98	4.30	133.49	4.84	1.16	0.98
326	4.75	105.67	6.27	1.38	0.98	4.36	99.71	6.50	1.56	0.98	4.22	125.07	4.81	1.18	0.98
340	4.36	114.30	5.50	1.31	0.97	4.37	99.38	6.35	1.52	0.98	4.41	134.03	4.91	1.15	0.98
354	4.80	116.27	5.93	1.29	0.97	4.76	104.14	6.72	1.48	0.98	4.63	135.69	5.06	1.13	0.98
368	4.99	113.93	6.33	1.32	0.98	4.79	101.62	6.90	1.51	0.98	4.70	139.52	5.18	1.14	0.98
382	4.99	113.93	6.33	1.32	0.98	4.79	101.62	6.90	1.51	0.98	4.70	139.52	5.18	1.14	0.98

CEM II/B-V (w/b=0.6)

Type of steel	SS														
Replicate No.	No.1					No.2					No.3				
Age (days)	R_Ω ($\Omega \cdot m^2$)	R_p ($\Omega \cdot m^2$)	τ (sec)	C (F/m^2)	r^2	R_Ω ($\Omega \cdot m^2$)	R_p ($\Omega \cdot m^2$)	τ (sec)	C (F/m^2)	r^2	R_Ω ($\Omega \cdot m^2$)	R_p ($\Omega \cdot m^2$)	τ (sec)	C (F/m^2)	r^2
186	2.14	53.58	5.94	2.89	0.98	3.02	86.60	4.35	1.49	0.97	2.89	104.51	4.97	1.77	0.98
200	3.07	81.31	5.09	1.72	0.97	2.98	77.99	4.93	1.72	0.97	3.18	131.32	5.38	1.73	0.98
214	3.26	86.70	5.11	1.63	0.97	3.53	96.98	4.72	1.39	0.97	3.52	112.72	5.70	1.67	0.98
228	3.43	86.59	5.35	1.62	0.97	3.69	101.91	4.88	1.37	0.97	3.58	116.61	5.85	1.69	0.98
242	3.44	85.64	5.38	1.63	0.97	3.81	99.08	5.02	1.37	0.97	3.68	117.02	5.93	1.66	0.98
256	3.73	101.55	5.84	1.63	0.97	4.00	95.62	5.30	1.38	0.97	3.82	108.73	6.15	1.67	0.98
270	4.10	81.95	5.95	1.52	0.97	4.51	97.17	5.62	1.30	0.97	4.26	105.85	6.52	1.59	0.98
284	3.94	76.70	5.96	1.59	0.97	4.25	92.75	5.54	1.36	0.97	4.06	102.46	6.49	1.66	0.98
298	4.27	80.10	6.21	1.53	0.97	4.70	106.42	5.85	1.30	0.97	4.56	107.33	7.03	1.61	0.98
312	4.42	81.61	6.43	1.53	0.97	4.80	92.52	6.00	1.31	0.97	4.57	111.02	7.13	1.62	0.98
326	4.70	80.35	6.75	1.52	0.97	5.05	92.77	6.27	1.31	0.97	4.79	108.97	7.33	1.60	0.98
340	4.92	81.55	6.86	1.48	0.97	5.18	92.77	6.36	1.30	0.97	5.01	103.59	7.69	1.61	0.98
354	5.10	80.94	6.90	1.44	0.97	5.76	98.17	6.83	1.26	0.97	5.37	107.72	8.00	1.56	0.98
368	5.12	82.65	7.08	1.47	0.97	5.70	95.81	6.95	1.29	0.97	5.33	107.54	8.17	1.61	0.98
382	5.60	83.07	7.57	1.44	0.97	5.97	96.67	7.19	1.28	0.97	5.67	108.30	8.49	1.58	0.98
Type of steel	LS														
Replicate No.	No.1					No.2					No.3				
Age (days)	R_Ω ($\Omega \cdot m^2$)	R_p ($\Omega \cdot m^2$)	τ (sec)	C (F/m^2)	r^2	R_Ω ($\Omega \cdot m^2$)	R_p ($\Omega \cdot m^2$)	τ (sec)	C (F/m^2)	r^2	R_Ω ($\Omega \cdot m^2$)	R_p ($\Omega \cdot m^2$)	τ (sec)	C (F/m^2)	r^2
186	4.27	120.77	4.88	1.18	0.97	2.85	85.26	5.36	1.95	0.98	2.88	86.50	5.59	2.00	0.98
200	3.43	76.92	6.02	1.84	0.97	3.35	134.26	6.19	1.89	0.98	3.34	116.25	6.35	1.95	0.99
214	3.80	93.48	6.44	1.76	0.98	3.54	105.12	6.35	1.85	0.98	3.48	99.91	6.40	1.90	0.98
228	3.81	99.25	6.27	1.71	0.98	3.70	117.66	6.62	1.84	0.98	3.60	101.30	6.62	1.90	0.99
242	3.97	99.02	6.44	1.69	0.98	3.99	107.49	7.05	1.83	0.98	3.82	99.65	6.92	1.88	0.98
256	4.09	92.83	6.58	1.68	0.98	4.14	108.54	7.31	1.83	0.98	4.04	99.68	7.39	1.90	0.99
270	4.55	86.40	6.83	1.58	0.98	4.63	107.54	7.78	1.75	0.98	4.41	103.46	7.60	1.79	0.99
284	4.44	81.54	7.03	1.67	0.98	4.35	95.95	7.67	1.84	0.98	3.74	16.29	4.27	1.40	1.00
298	5.03	84.76	7.64	1.61	0.98	4.95	106.84	8.35	1.77	0.98	4.75	101.42	8.21	1.81	0.99
312	5.14	85.82	7.77	1.60	0.98	5.08	110.73	8.59	1.77	0.98	4.63	98.19	8.03	1.82	0.99
326	5.36	86.69	8.04	1.59	0.98	5.42	103.85	9.02	1.75	0.98	5.16	100.92	8.85	1.80	0.99
340	5.53	90.56	8.14	1.56	0.98	5.55	106.15	9.07	1.72	0.98	5.31	100.92	8.95	1.77	0.99
354	5.99	91.58	8.45	1.50	0.98	6.16	109.28	9.83	1.69	0.99	5.63	102.21	9.24	1.73	0.99
368	5.75	94.27	8.34	1.54	0.98	6.16	108.03	9.98	1.71	0.99	5.55	100.99	9.27	1.76	0.99
382	6.16	90.22	8.67	1.50	0.98	6.39	114.66	10.14	1.68	0.99	5.94	106.98	9.72	1.73	0.99

C2.4 Parameters from linear polarisation resistance measurement

Polarisation resistance (R_p, ($\Omega \cdot m^2$))												
w/b	**CEM I (w/b=0.4)**						**CEM I (w/b=0.6)**					
Type of steel	SS			LS			SS			LS		
Age(days)	No.1	No.2	No.3	No.1	No.2	No.3	No.1	No.2	No.3	No.1	No.2	No.3
186	79.74	74.17	89.16	78.80	66.15	73.08	12.91	42.79	60.40	3.64	58.21	65.19
200	84.80	67.29	93.75	80.00	59.13	104.21	2.50	25.56	59.12	3.12	51.85	2.03
214	84.24	72.96	94.38	85.83	68.63	87.50	2.36	23.34	53.26	3.18	55.16	1.70
228	91.32	83.46	97.20	61.58	80.83	76.68	1.90	4.06	64.61	3.04	27.07	1.81
242	83.91	62.63	61.11	50.46	48.31	67.96	1.97	2.00	44.83	2.97	32.81	2.10
256	86.94	86.18	114.83	95.72	76.50	101.89	1.38	1.71	41.75	2.40	35.62	1.37
270	88.05	81.16	103.26	84.02	39.75	80.82	1.17	1.84	40.49	2.12	3.41	1.32
284	89.89	80.86	98.00	90.68	72.66	78.10	1.23	1.90	45.73	1.85	2.15	1.64
298	89.37	35.68	98.22	88.40	61.09	85.12	1.18	1.82	42.11	1.98	2.90	1.49
312	99.09	89.84	117.84	64.69	68.35	90.06	1.22	1.78	17.33	2.17	1.74	1.69
326	97.70	94.21	97.02	83.31	74.62	101.86	1.16	1.45	1.94	1.83	1.10	1.22
340	94.50	88.86	153.06	104.09	88.54	93.57	1.05	1.52	2.10	1.78	1.17	1.47
354	101.05	85.05	108.82	105.59	87.97	96.91	1.07	1.04	1.86	1.83	1.20	1.29
368	96.56	96.28	104.46	105.49	76.54	97.95	1.06	1.07	1.69	1.62	1.12	1.25
382	95.84	92.64	125.58	102.29	96.69	98.52	1.15	1.08	1.53	2.02	1.30	1.55
w/b	**CEM III/A (w/b=0.4)**						**CEM III/A (w/b=0.6)**					
Type of steel	SS			LS			SS			LS		
Age(days)	No.1	No.2	No.3	No.1	No.2	No.3	No.1	No.2	No.3	No.1	No.2	No.3
186	59.50	63.85	81.01	76.84	54.30	68.62	68.41	116.82	77.97	76.74	63.74	99.57
200	59.71	61.68	80.28	77.31	51.34	65.40	69.44	112.67	73.14	76.55	66.33	98.68
214	60.99	63.33	70.76	77.50	51.25	66.54	71.78	112.52	76.34	72.49	66.25	101.36
228	63.60	67.05	82.95	78.98	54.03	61.06	72.40	116.84	78.74	77.36	64.27	100.07
242	66.11	66.32	84.21	79.44	55.89	62.27	71.47	116.99	79.55	76.92	67.01	102.47
256	65.03	67.81	79.18	76.78	54.41	65.81	72.00	121.74	61.49	76.24	64.90	100.24
270	60.92	68.23	79.49	80.93	58.12	52.77	52.67	118.91	78.87	77.44	64.47	101.88
284	64.91	68.40	78.66	63.47	54.21	64.67	71.01	121.68	78.96	74.69	66.18	99.78
298	62.74	66.25	81.71	78.89	51.49	62.61	68.97	121.90	79.76	74.64	64.14	88.57
312	64.73	64.44	42.27	79.29	59.43	65.82	70.85	125.64	82.89	76.24	66.01	103.91
326	9.78	68.19	79.99	78.67	53.71	65.14	71.15	121.15	79.71	67.29	64.42	102.94
340	60.00	64.43	76.90	76.15	51.72	62.68	70.59	126.53	81.70	78.10	66.72	102.06
354	74.70	68.32	80.02	82.78	53.04	63.37	71.67	125.89	82.14	79.79	64.49	103.82
368	64.89	67.07	88.56	81.50	56.15	66.32	68.78	125.26	80.81	57.27	65.57	100.86
382	112.92	69.07	80.85	76.38	55.21	63.56	74.92	124.90	82.15	74.82	67.39	101.30
w/b	**CEM II/B-V (w/b=0.4)**						**CEM II/B-V (w/b=0.6)**					
Type of steel	SS			LS			SS			LS		
Age(days)	No.1	No.2	No.3	No.1	No.2	No.3	No.1	No.2	No.3	No.1	No.2	No.3
186	118.22	57.22	48.08	57.98	71.74	63.90	34.94	67.46	67.81	52.01	63.18	62.20
200	99.85	56.74	49.04	52.70	70.92	64.96	54.79	51.55	68.58	55.83	61.96	58.89
214	118.33	56.35	30.24	57.12	70.33	64.79	57.62	68.49	71.45	54.17	60.54	61.32
228	111.63	56.10	47.42	51.34	69.75	43.63	56.37	67.76	69.76	54.69	65.35	60.67
242	109.78	56.15	47.61	37.89	64.93	58.40	52.64	65.58	69.68	53.64	61.20	60.09
256	107.62	54.58	45.73	46.94	64.67	57.70	51.61	67.88	68.13	51.42	60.65	56.82
270	111.77	52.59	46.38	46.77	46.67	57.64	55.78	67.57	68.58	55.68	59.54	59.93
284	106.91	49.03	43.23	47.96	58.75	55.92	50.73	65.74	63.66	50.92	55.12	56.01
298	104.40	50.69	43.46	45.57	59.59	51.20	39.68	67.24	64.61	52.30	56.84	55.99
312	97.24	51.19	42.81	45.40	59.44	50.61	49.15	63.57	65.33	51.51	57.49	55.50
326	100.18	49.16	42.58	43.86	56.40	48.92	49.64	63.82	65.50	51.67	53.58	53.66
340	102.99	49.00	41.11	41.23	57.00	48.92	50.12	62.97	63.59	51.75	55.78	54.91
354	99.02	51.55	41.18	40.11	56.87	49.48	52.71	64.84	62.95	52.56	52.29	54.95
368	103.69	50.36	42.11	43.37	54.06	47.71	50.40	61.38	57.69	50.77	52.02	53.99
382	104.53	48.91	42.57	42.13	56.15	47.10	48.07	59.90	58.24	51.82	53.89	52.42

C2.5 Electrochemical impedance spectroscopy (Nyquist plot)

CEM I (w/b=0.4)-SS

No.1

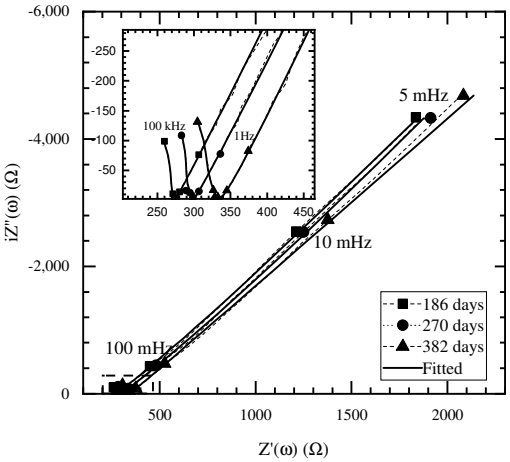

No.2

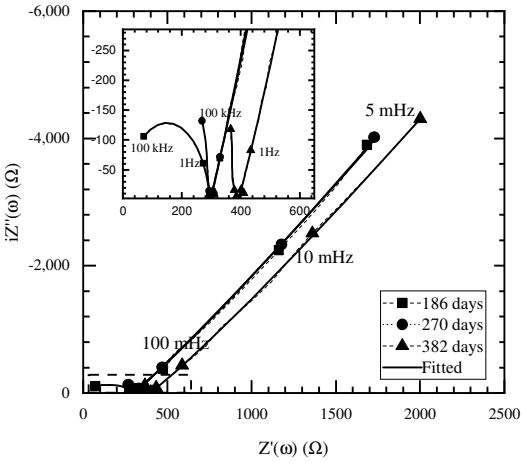

No.3

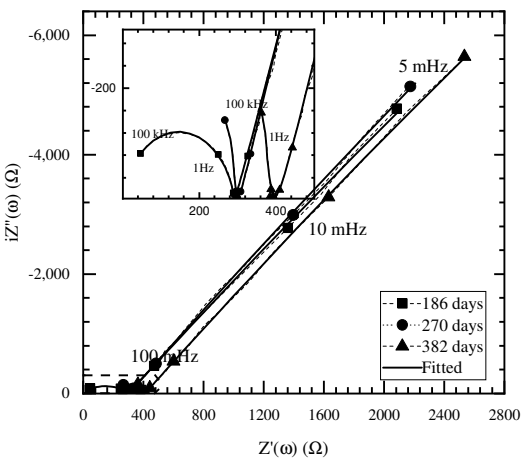

CEM I (w/b=0.4)-LS

No.1

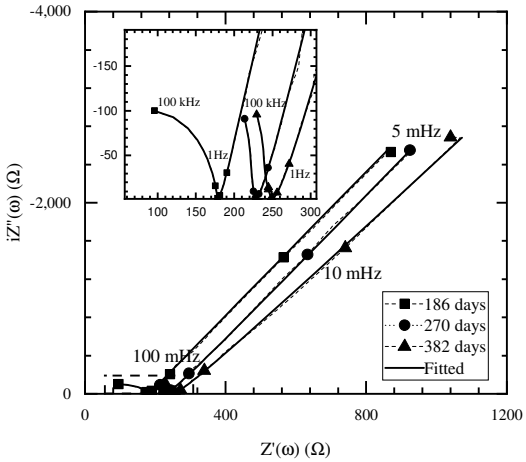

No.2

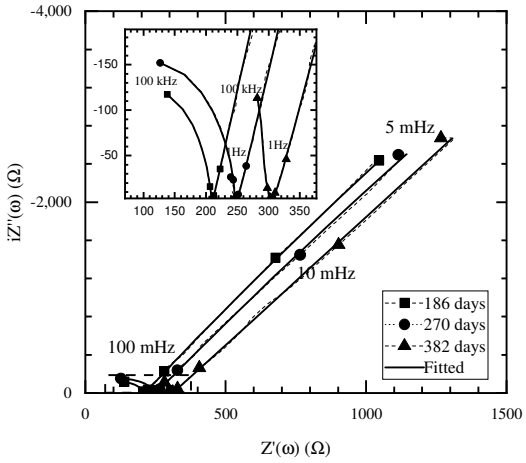

No.3

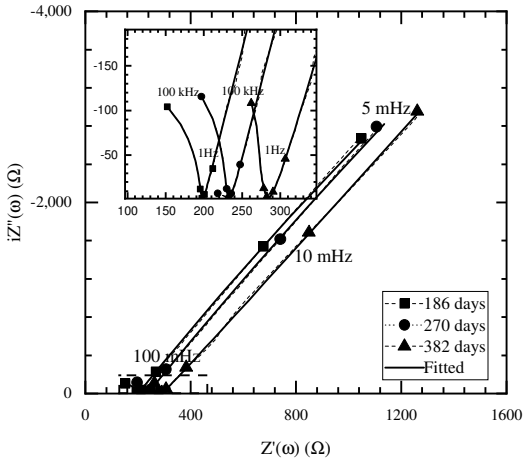

CEM III/A (w/b=0.4)-SS

No.1

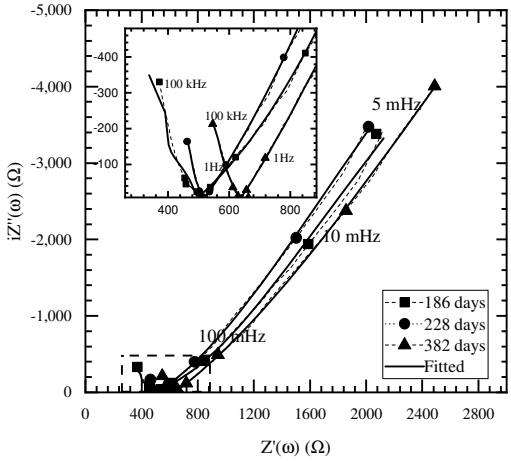

No.2

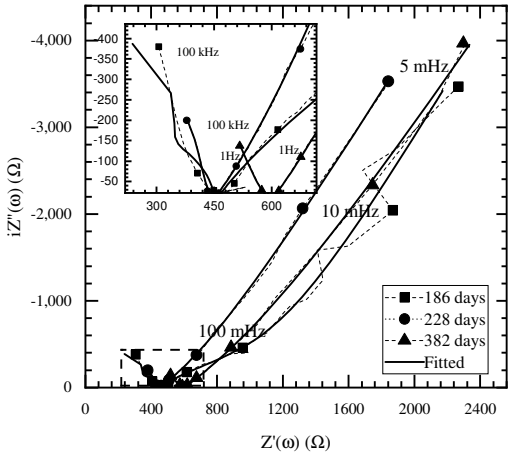

No.3

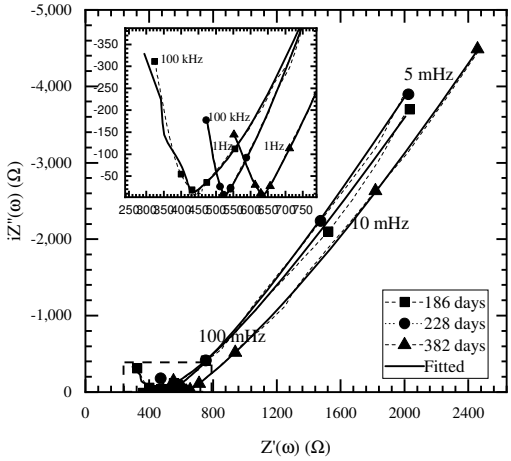

CEM III/A (w/b=0.4)-LS

No.1

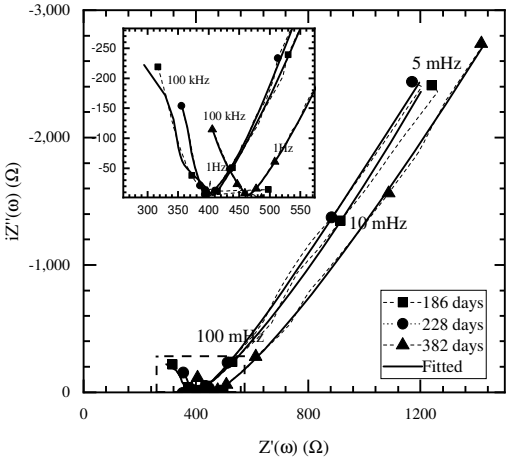

No.2

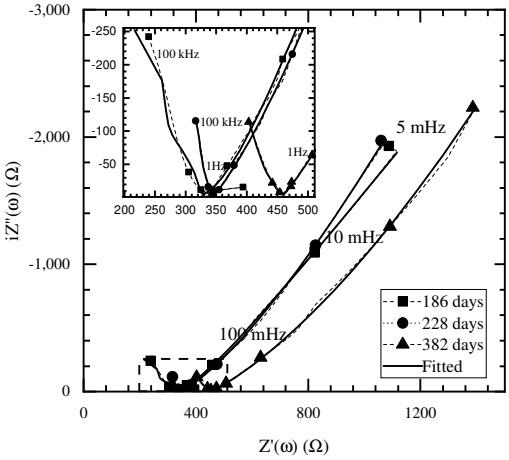

No.3

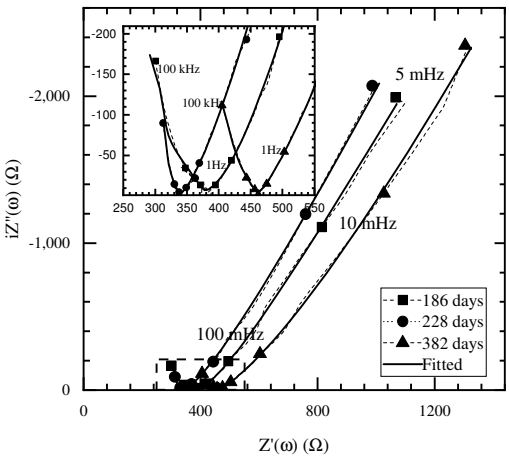

CEM II/B-V (w/b=0.4)-SS

No.1

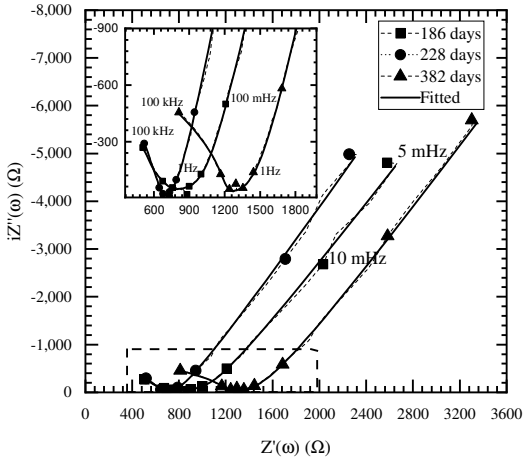

No.2

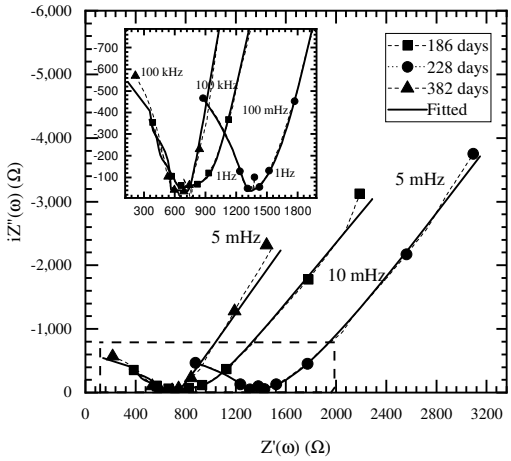

No.3

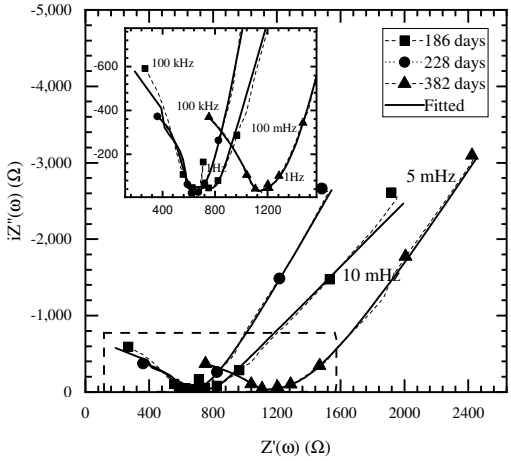

CEM II/B-V (w/b=0.4)-LS

No.1

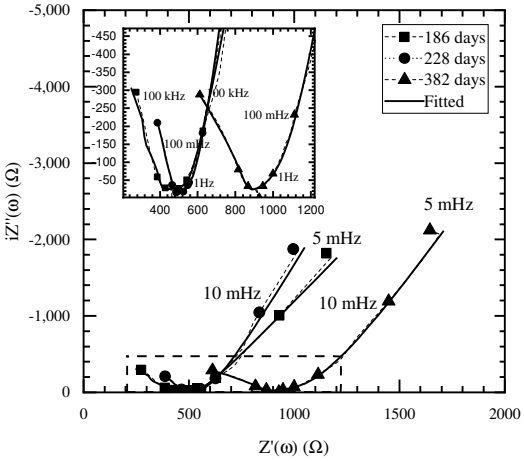

No.2

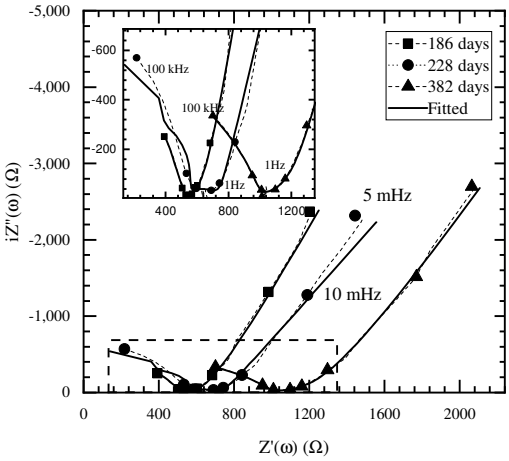

No.3

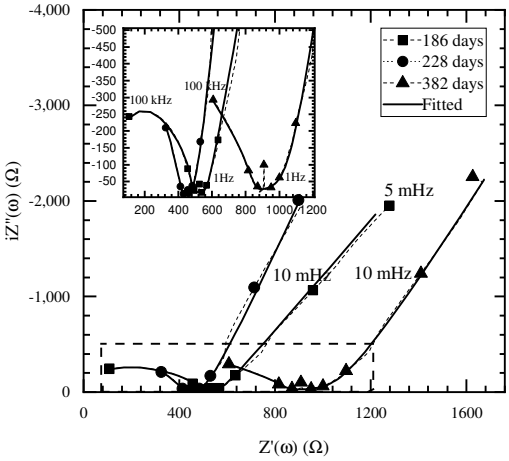

CEM I (w/b=0.6)-SS

No.1

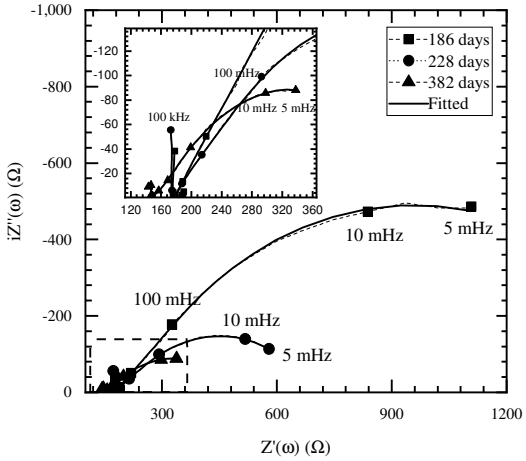

No.2

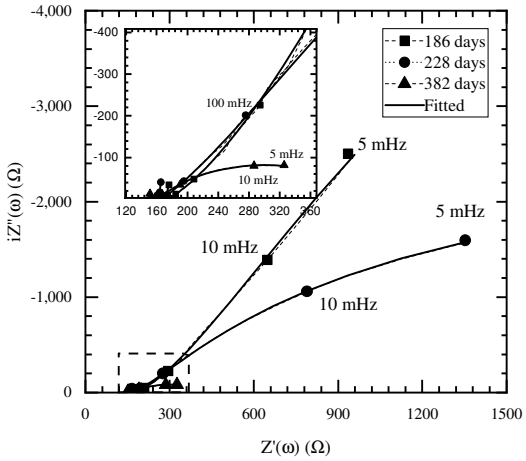

No.3

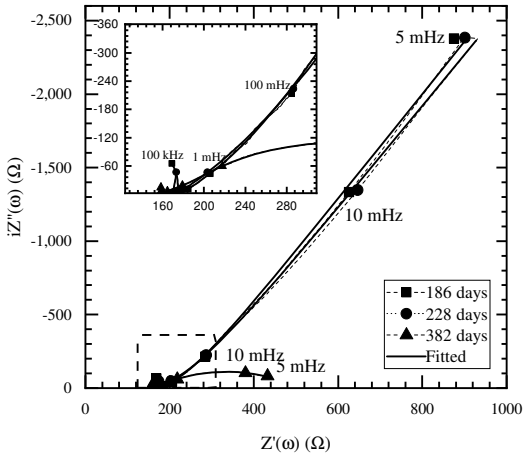

CEM I (w/b=0.6)-LS

No.1

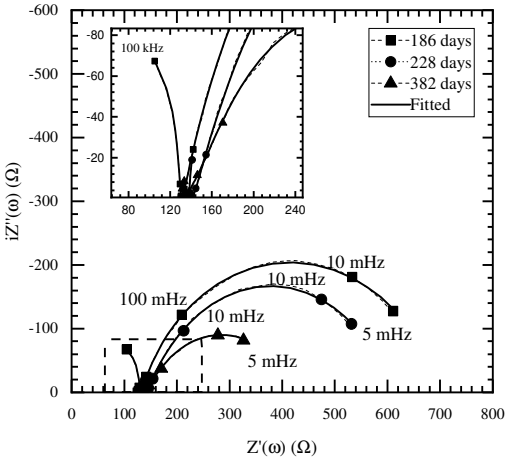

No.2

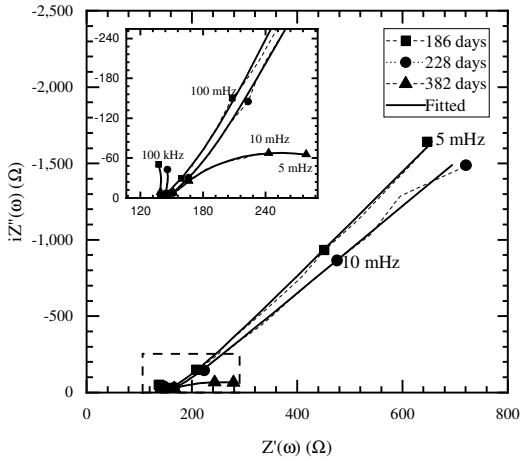

No.3

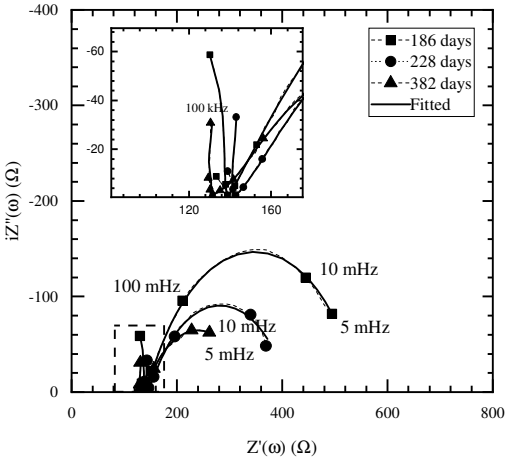

CEM III/A (w/b=0.6)-SS

No.1

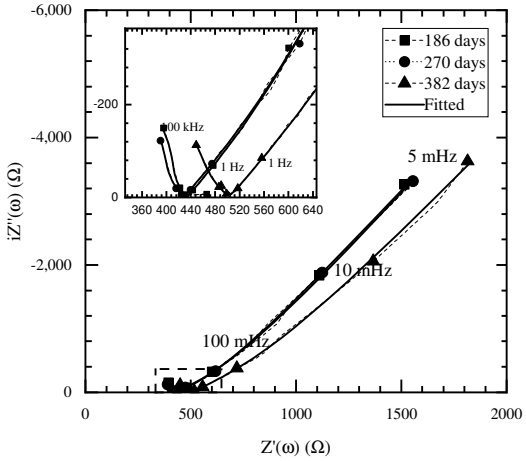

No.2

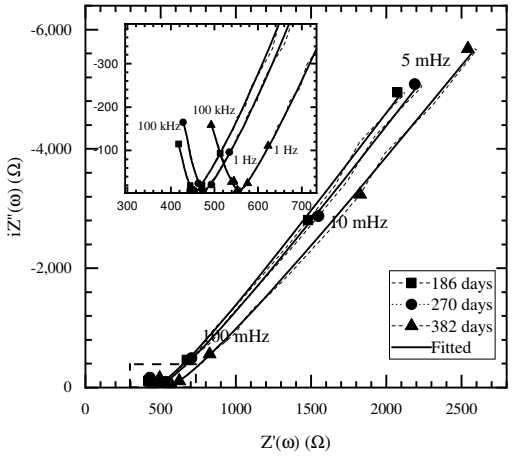

No.3

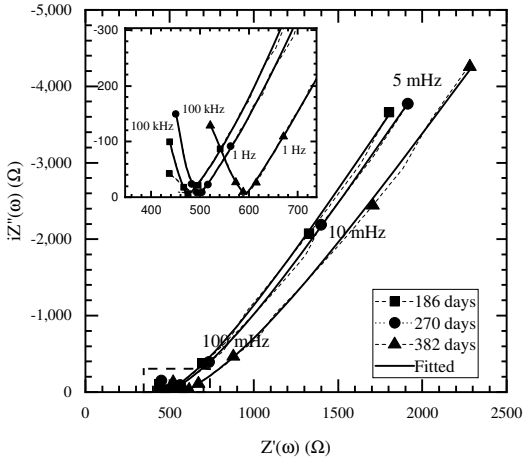

CEM III/A (w/b=0.6)-LS

No.1

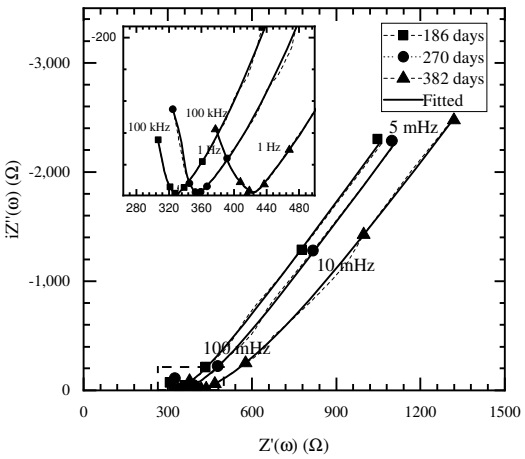

No.2

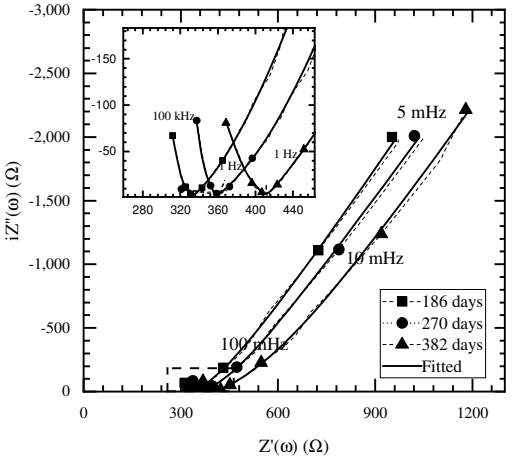

No.3

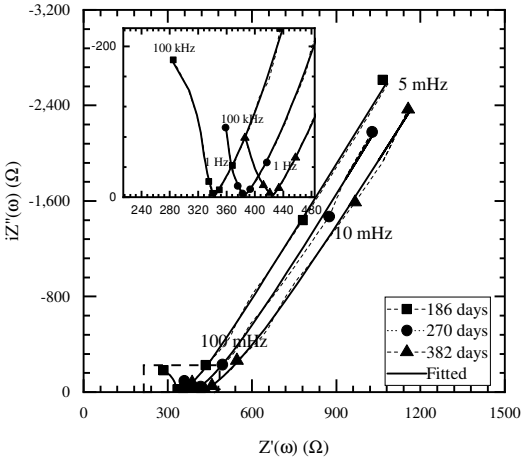

CEM II/B-V (w/b=0.6)-SS

No.1

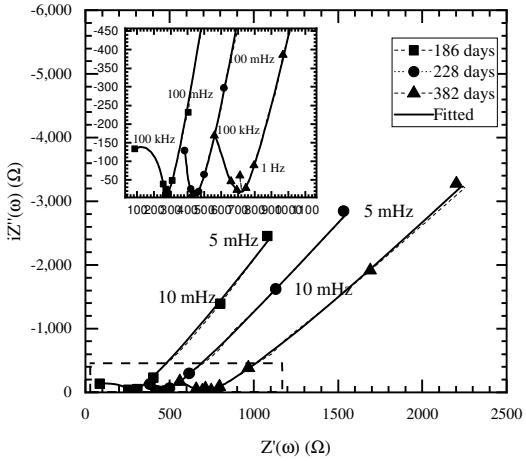

No.2

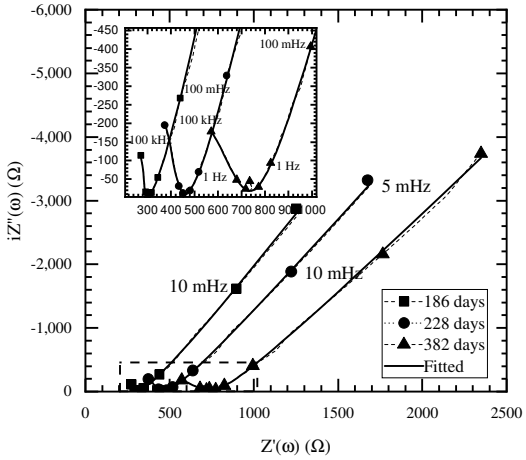

No.3

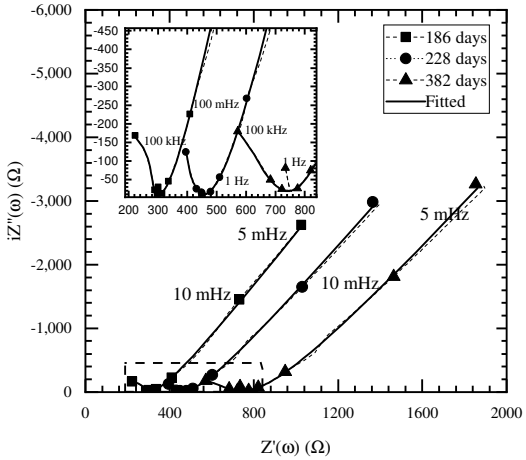

CEM II/B-V (w/b=0.6)-LS

No.1

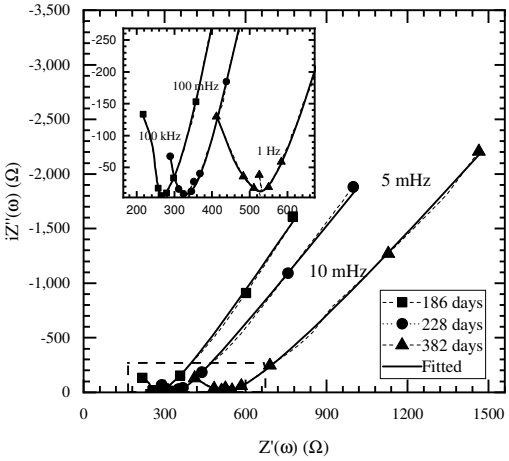

No.2

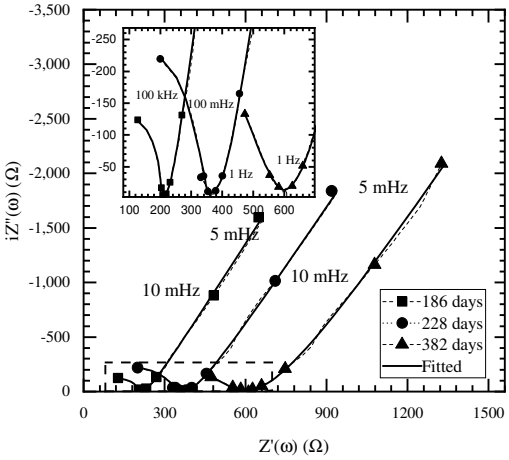

No.3

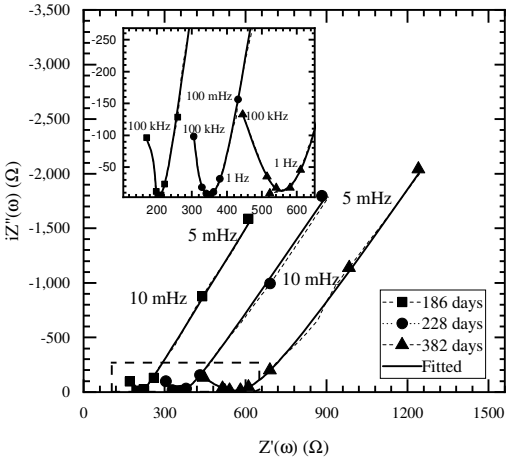

C2.6 Potentiodynamic plot (Tafel's plot)

CEM I (w/b=0.4)-SS

No.1

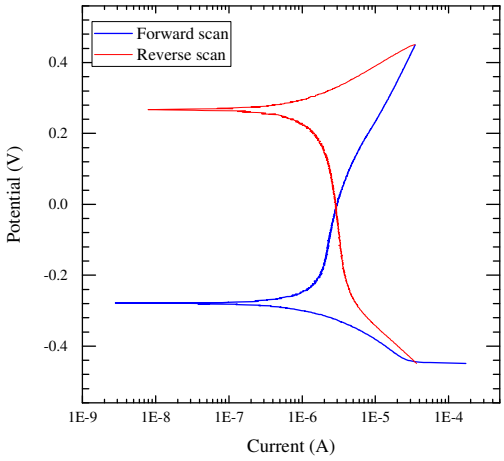

No.2

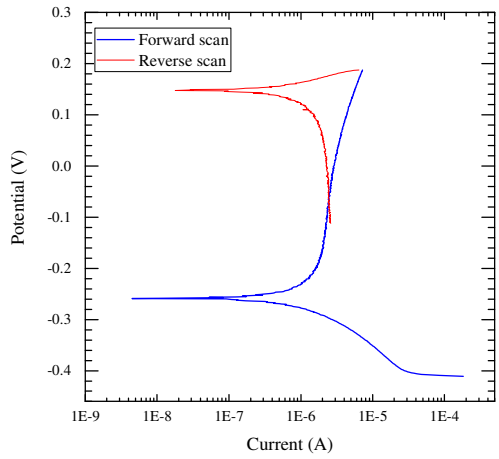

No.3

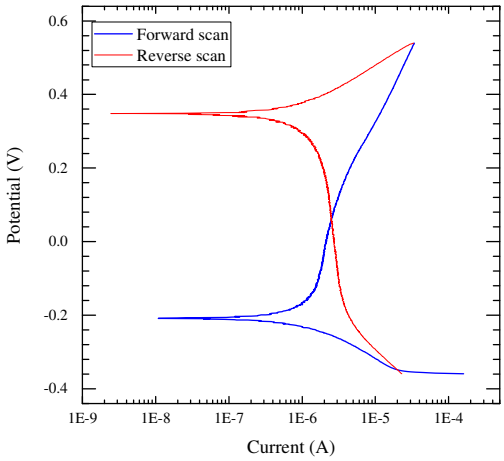

CEM I (w/b=0.4)-LS

No.1

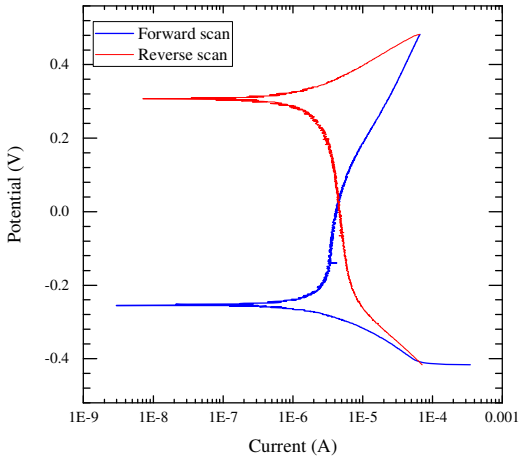

No.2

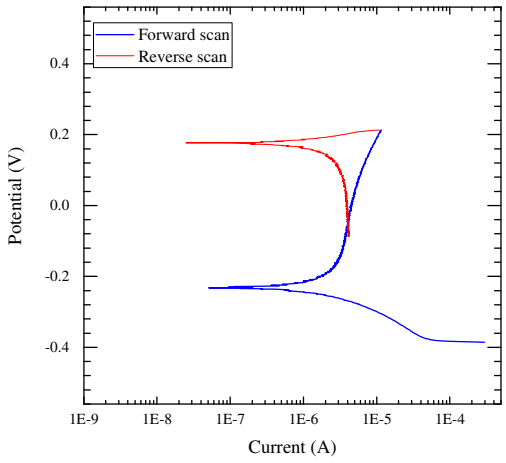

No.3

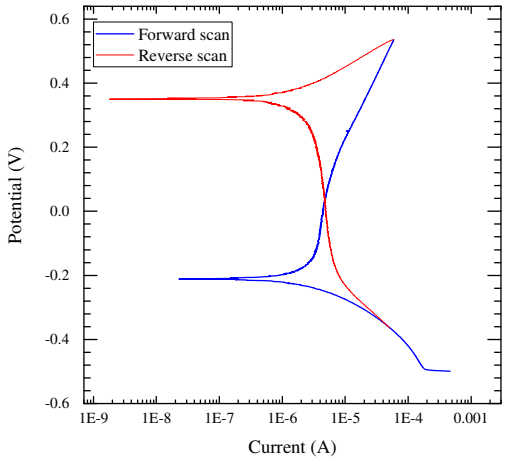

CEM III/A (w/b=0.4)-SS

No.1

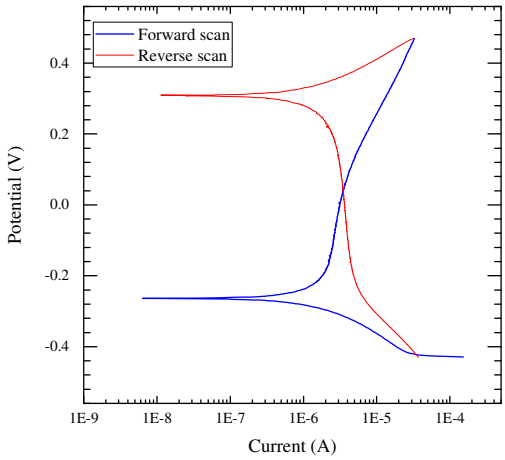

No.2

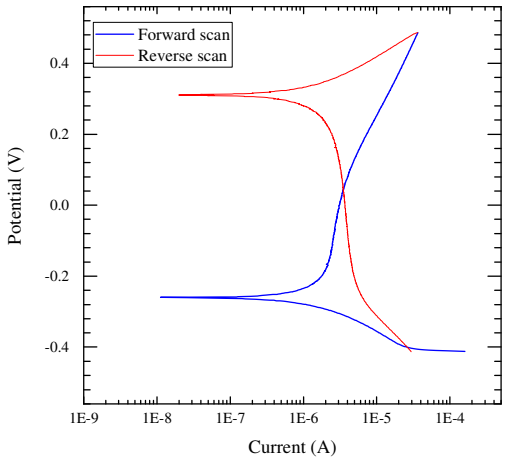

No.3

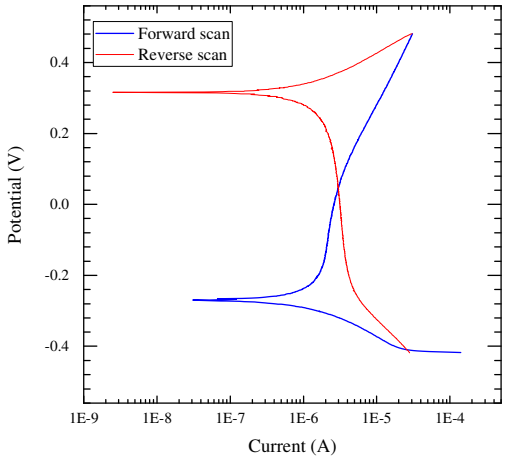

CEM III/A (w/b=0.4)-LS

No.1

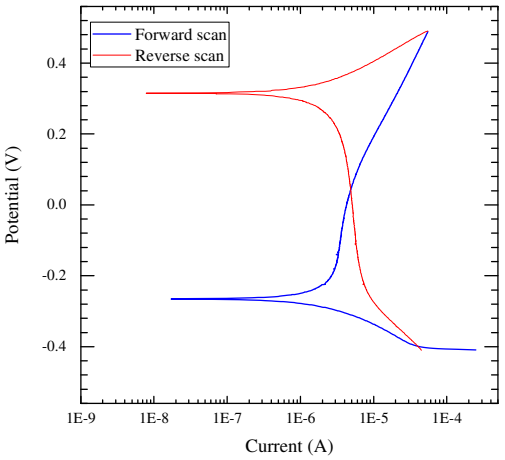

No.2

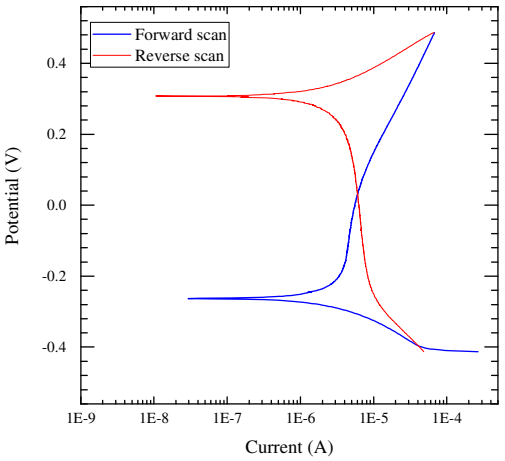

No.3

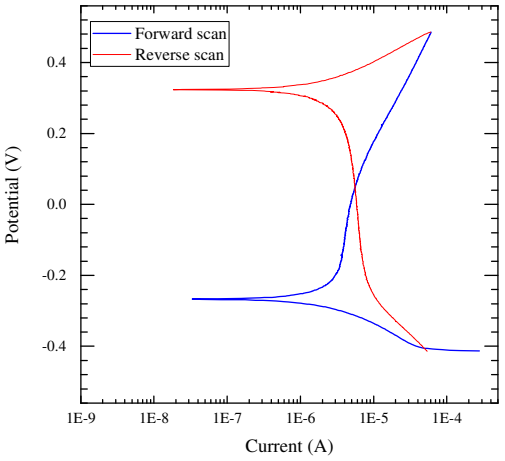

CEM II/B-V (w/b=0.4)-SS

No.1

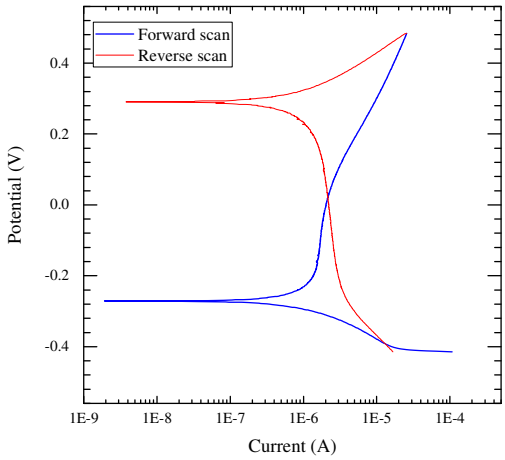

No.2

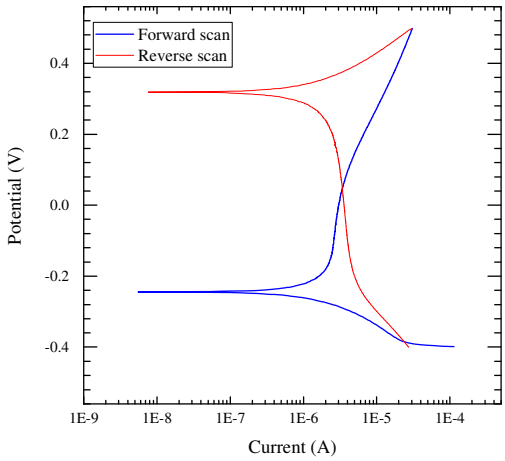

No.3

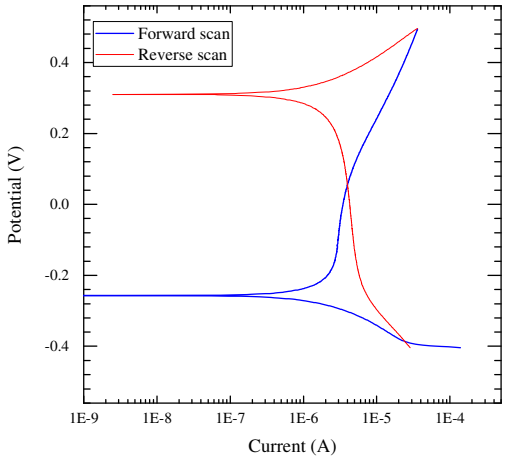

CEM II/B-V (w/b=0.4)-LS

No.1

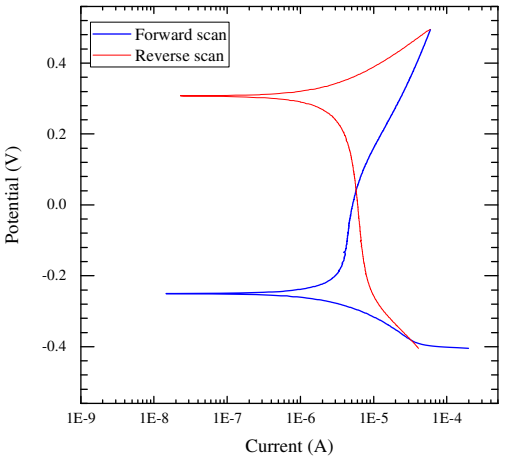

No.2

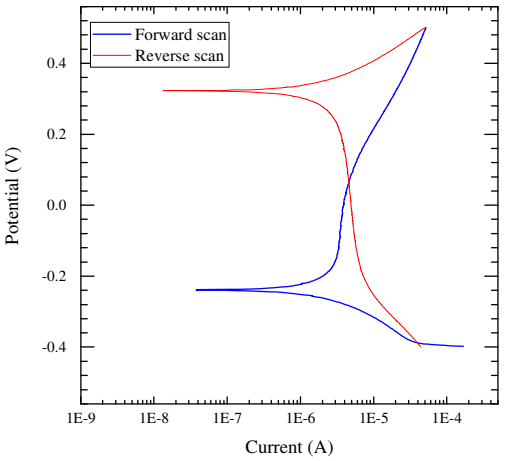

No.3

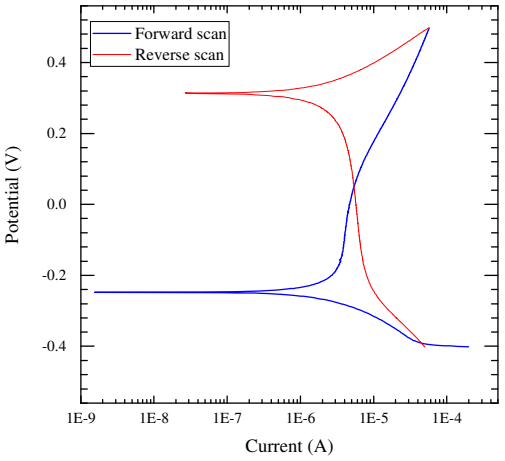

CEM I (w/b=0.6)-SS

No.1

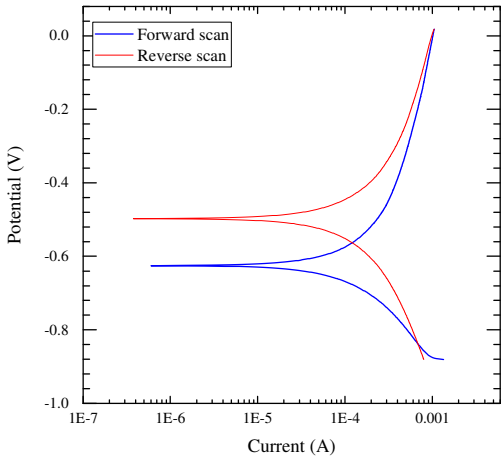

No.2

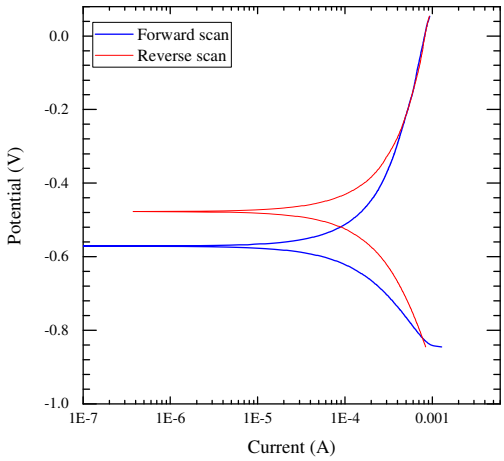

No.3

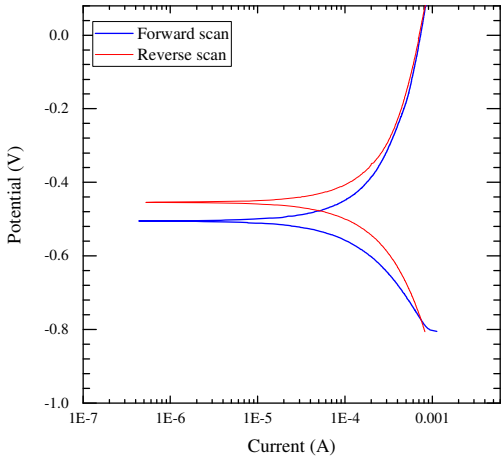

CEM I (w/b=0.6)-LS

No.1

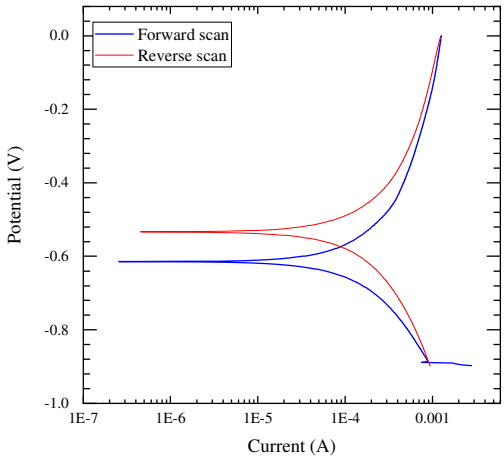

No.2

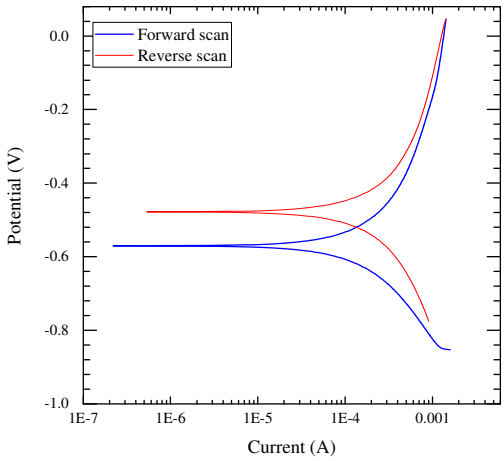

No.3

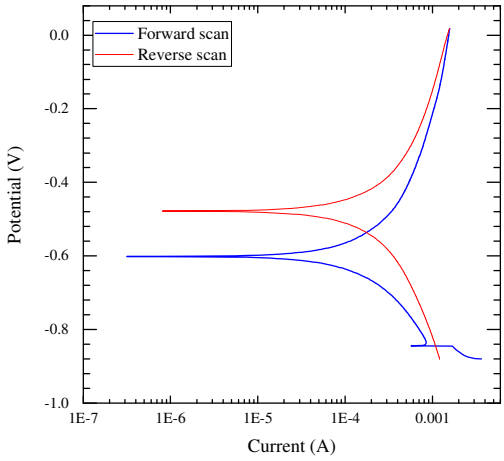

CEM III/A (w/b=0.6)-SS

No.1

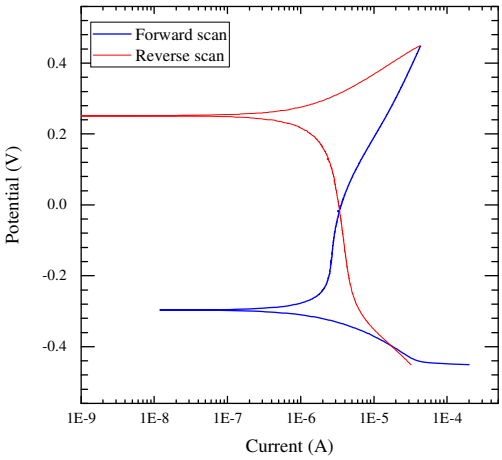

No.2

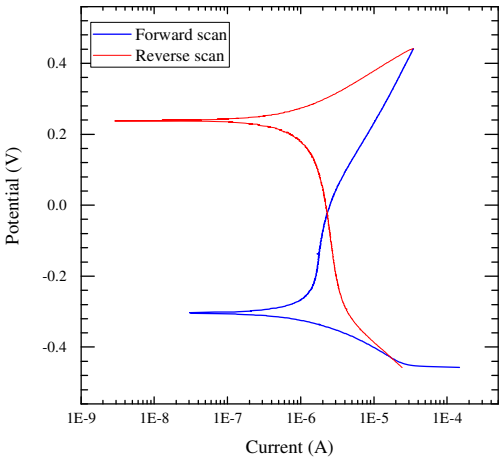

No.3

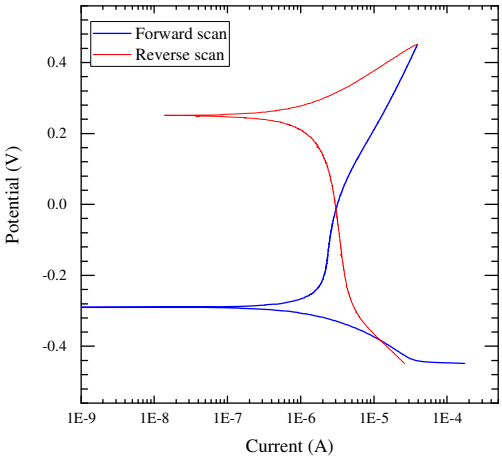

CEM III/A (w/b=0.6)-LS

No.1

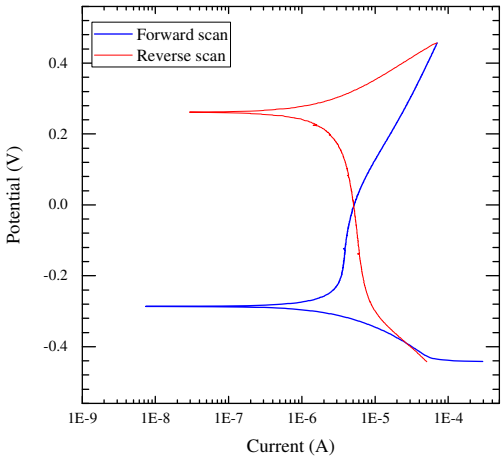

No.2

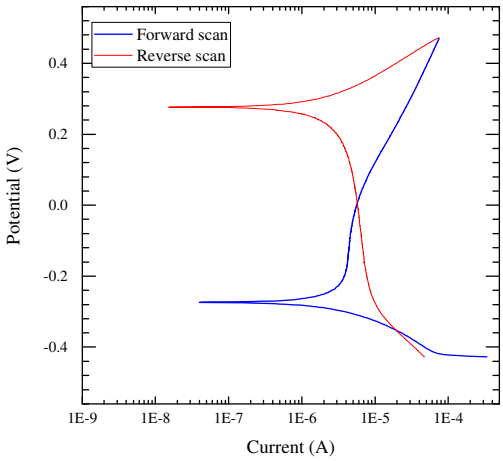

No.3

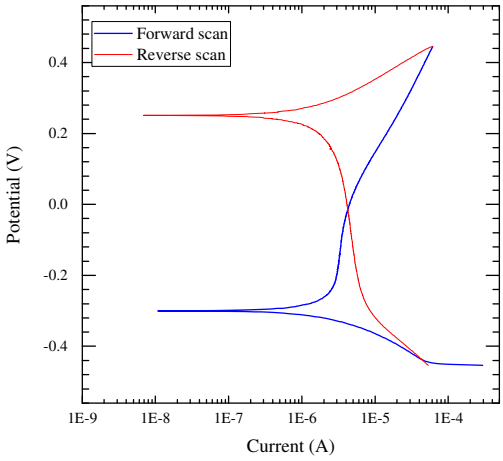

CEM II/B-V (w/b=0.6)-SS

No.1

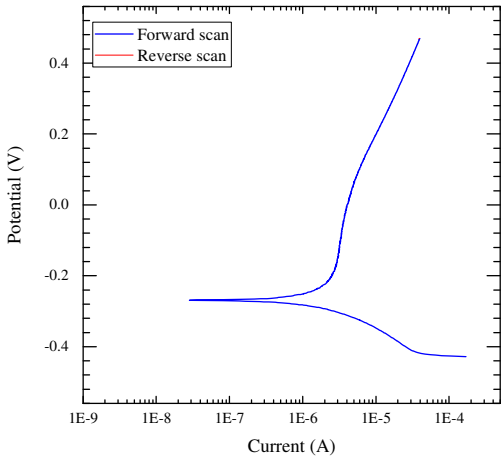

No.2

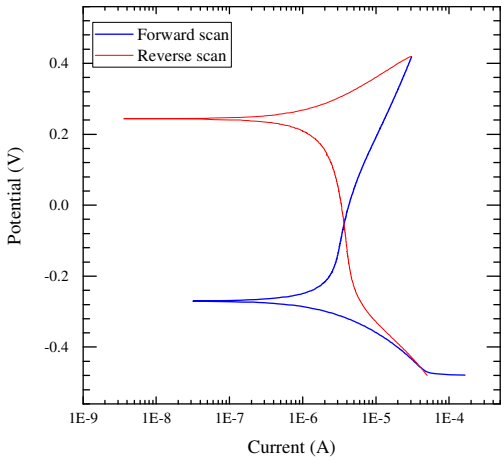

No.3

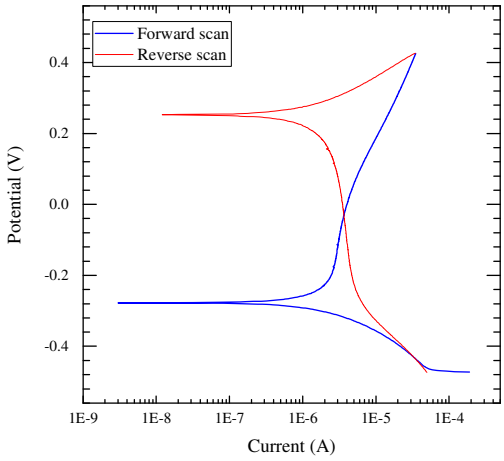

CEM II/B-V (w/b=0.6)-LS

No.1

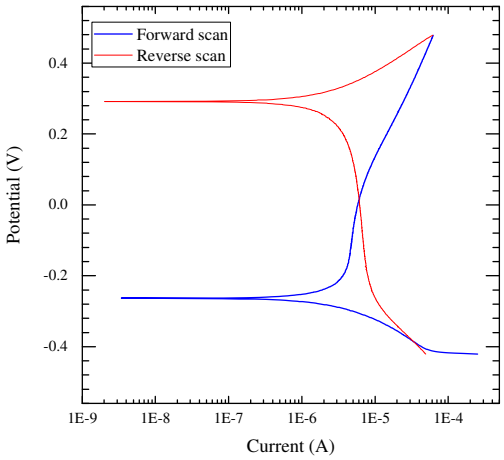

No.2

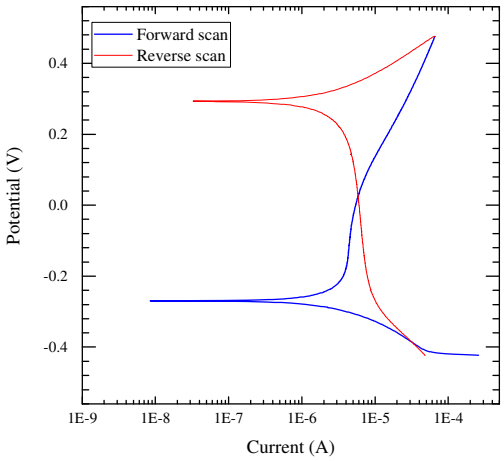

No.3

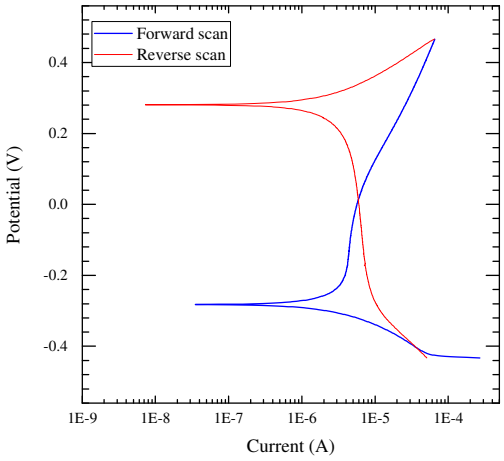

C.3 Teste results in Chapter 7

C3.1 Monitoring electrical resistance using 2-pin electrodes

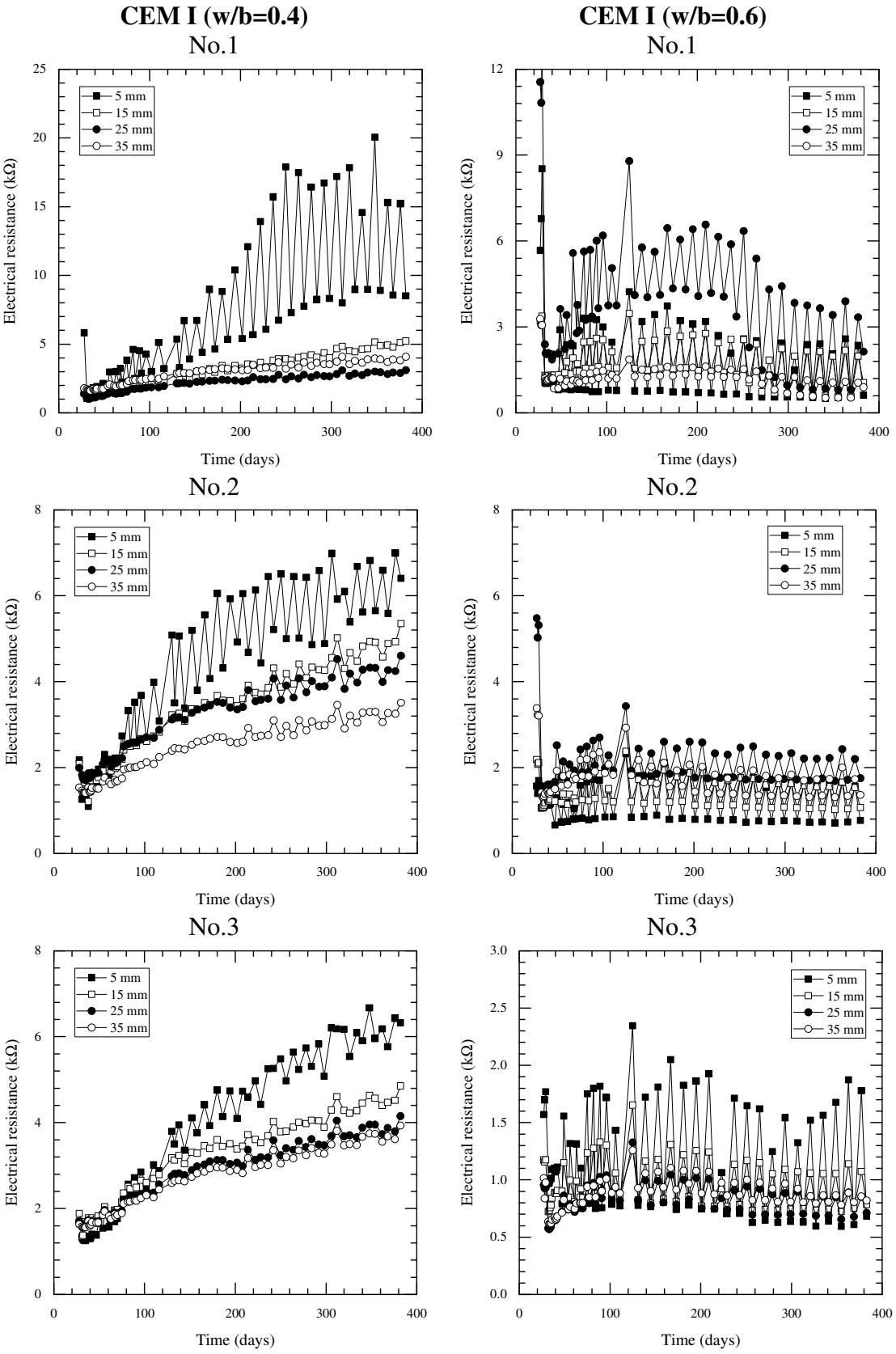

CEM III/A (w/b=0.4)

No.1

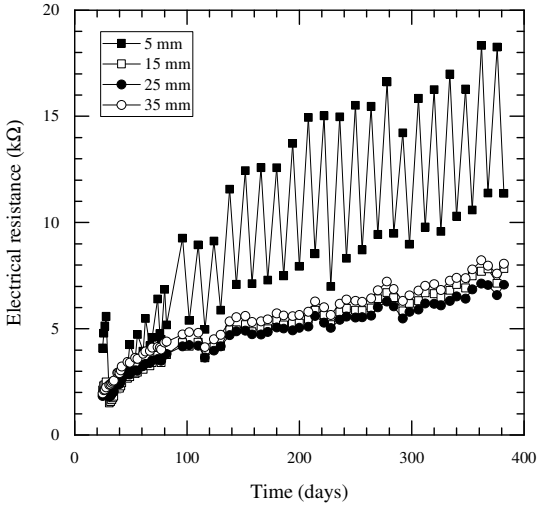

No.2

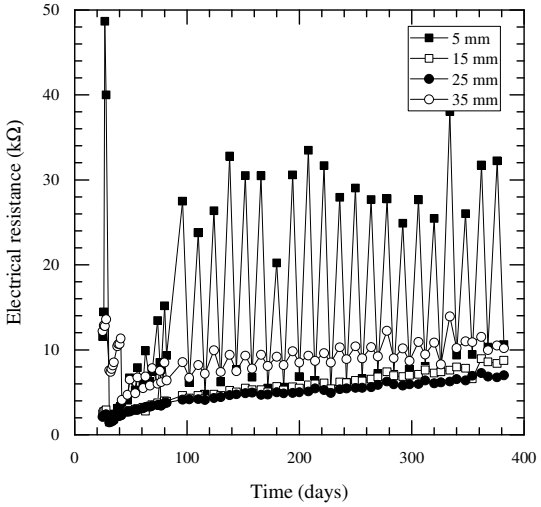

No.3

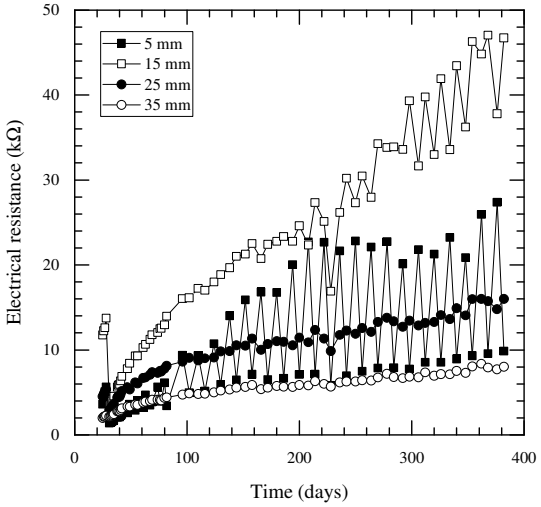

CEM III/A (w/b=0.6)

No.1

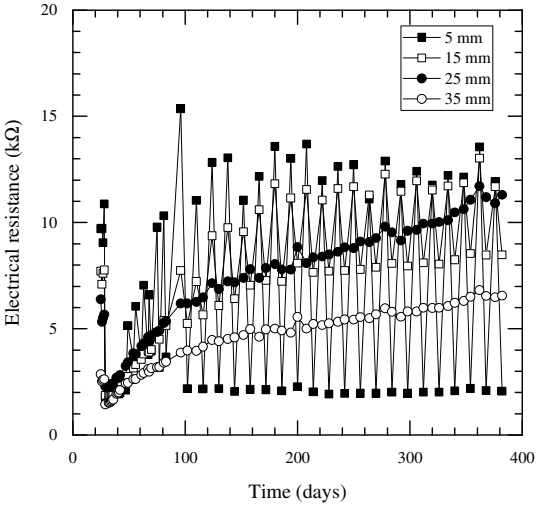

No.2

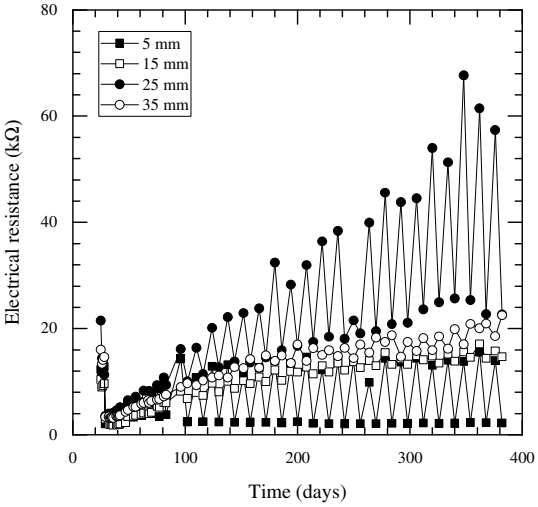

No.3

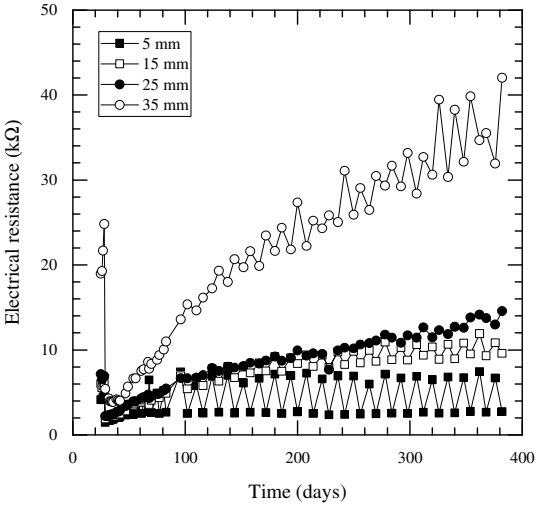

CEM II/B-V (w/b=0.4)

No.1

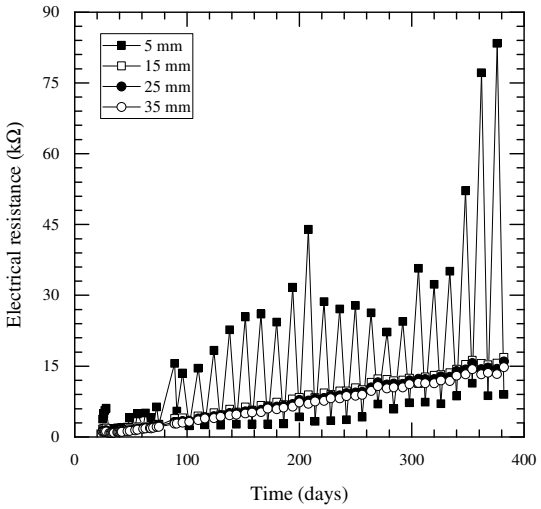

No.2

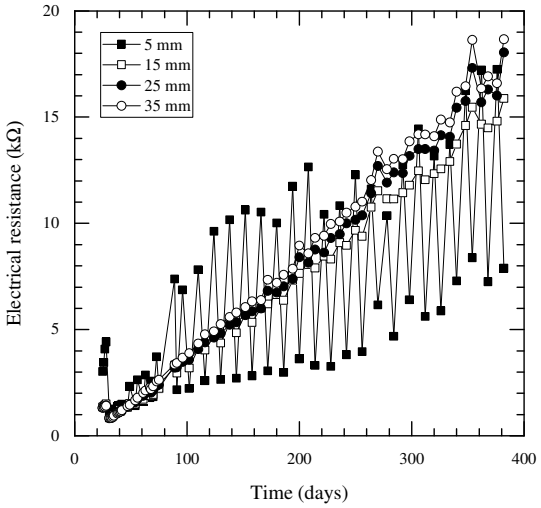

No.3

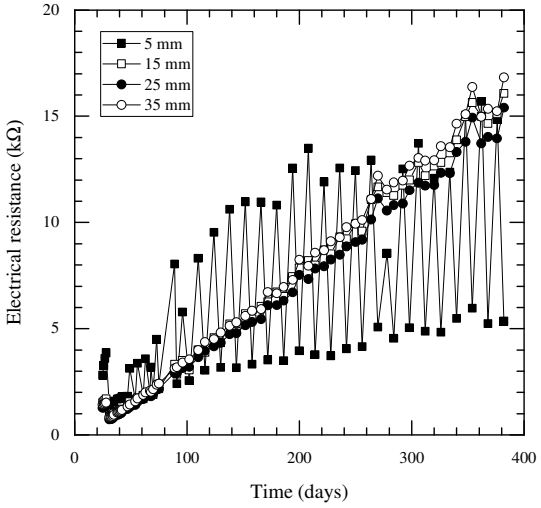

CEM II/B-V (w/b=0.6)

No.1

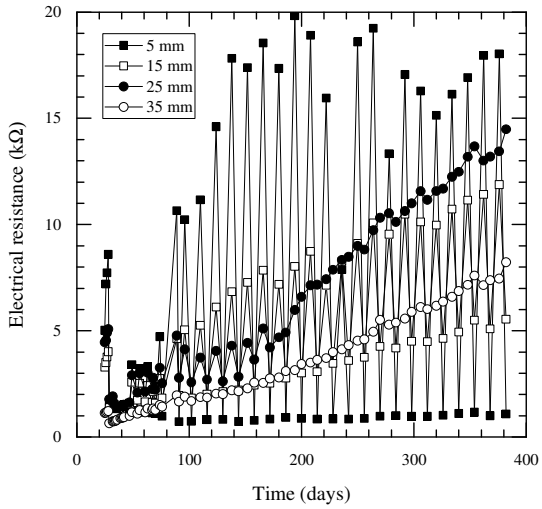

No.2

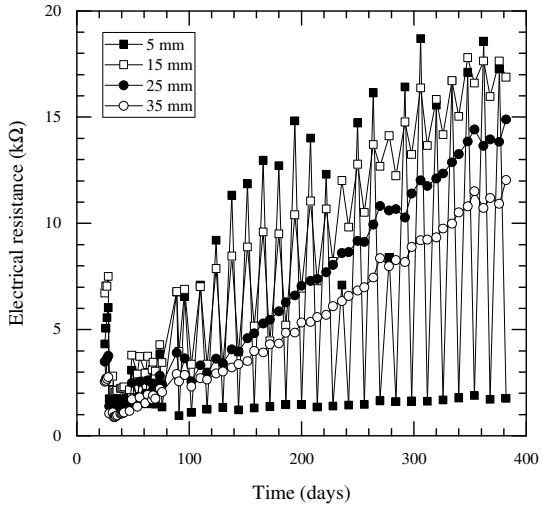

No.3

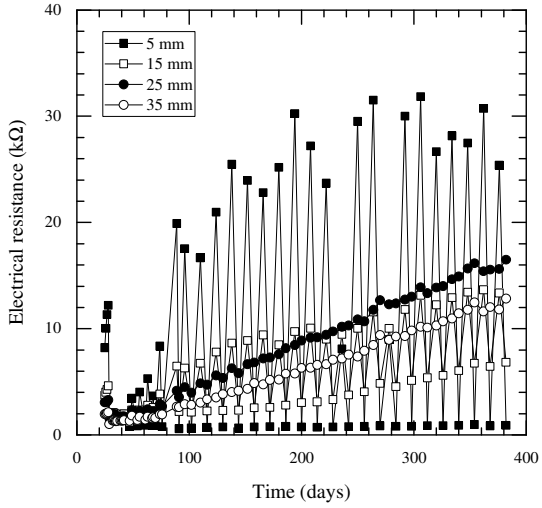

C3.2 Monitoring electrical resistance using 4-pin electrodes

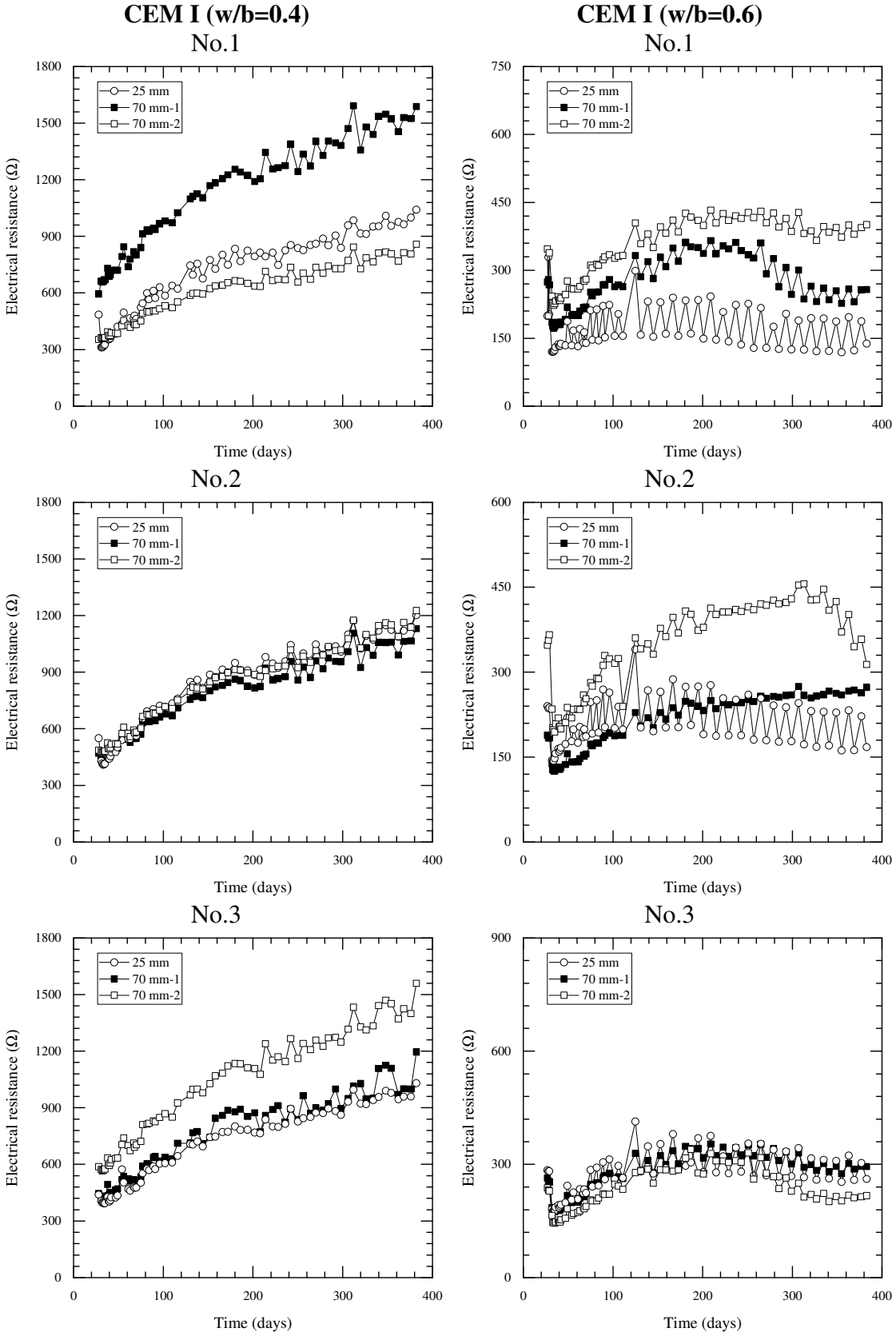

CEM III/A (w/b=0.4)

No.1

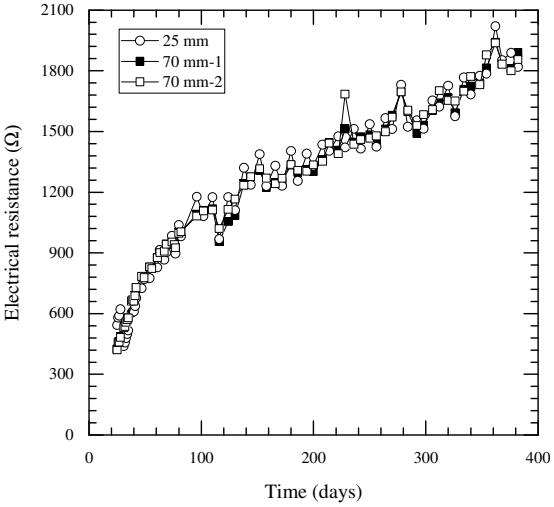

No.2

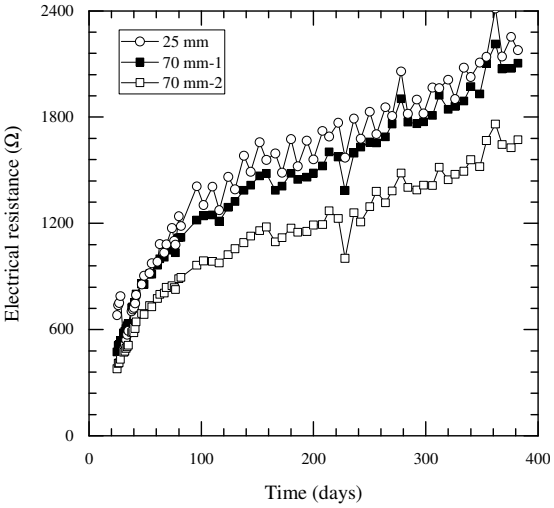

No.3

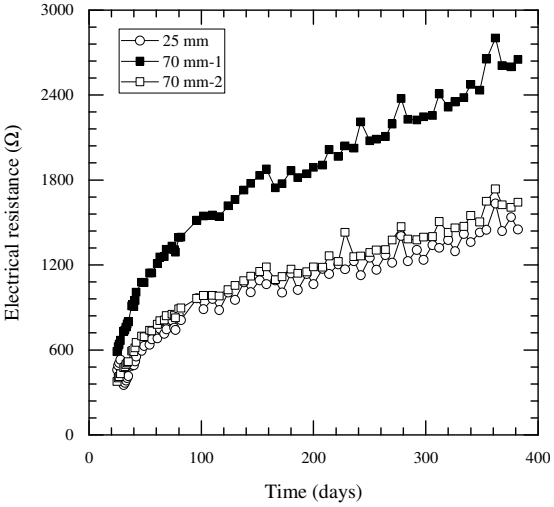

CEM III/A (w/b=0.6)

No.1

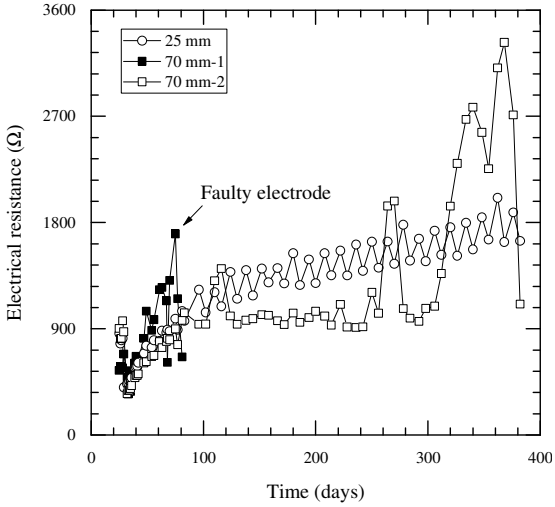

No.2

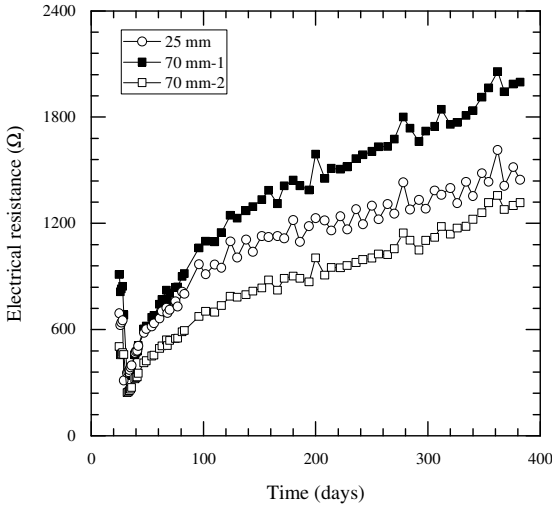

No.3

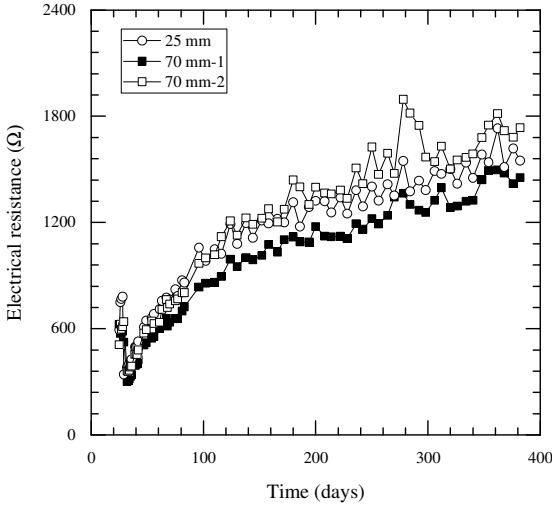

CEM II/B-V (w/b=0.4)

No.1

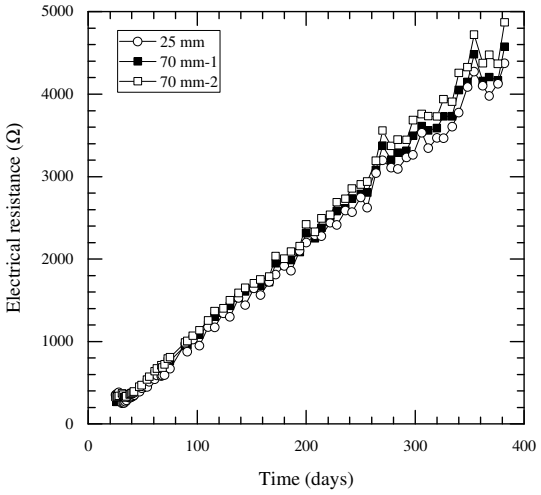

No.2

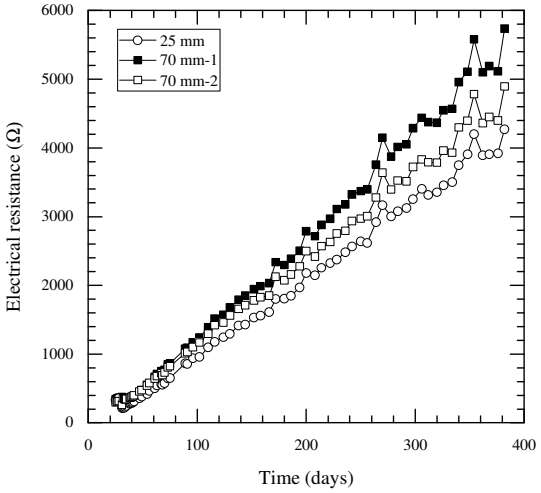

No.3

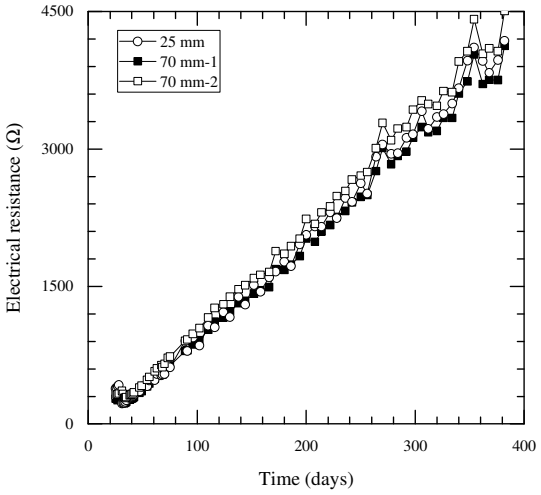

CEM II/B-V (w/b=0.6)

No.1

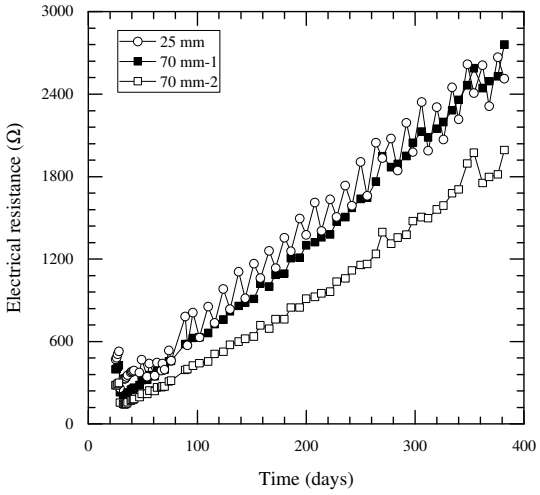

No.2

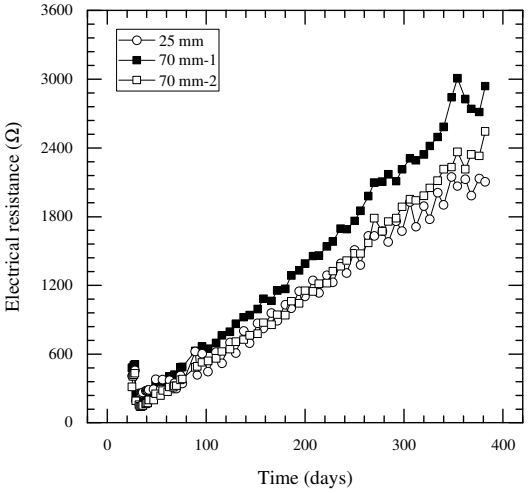

No.3

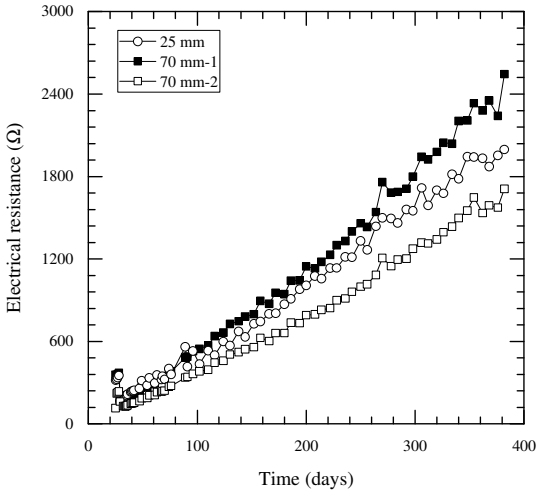

C.4 Test results in Chapter 8

C4.1 Chloride profiles from 18 years-old samples retrieved from Dornoch

Chloride concentration (%, by weight of binder)

	PC	GGBS/40	FA/30
Depth (mm)	Measured value	Measured value	Measured value
4	4.28	3.50	4.43
12	3.55	3.24	3.84
20	2.50	1.43	1.92
28	2.10	0.81	0.99
36	1.80	0.21	0.27
44	1.18	0.15	0.17
52	0.72	0.15	0.29
60	0.37	0.14	0.09
68	0.83	0.12	0.16
76	0.16	0.10	0.09
84	0.46	0.12	0.09
92	0.28	0.10	0.09

C4.2 Measuring weight change of field concrete for degree of saturation/porosity

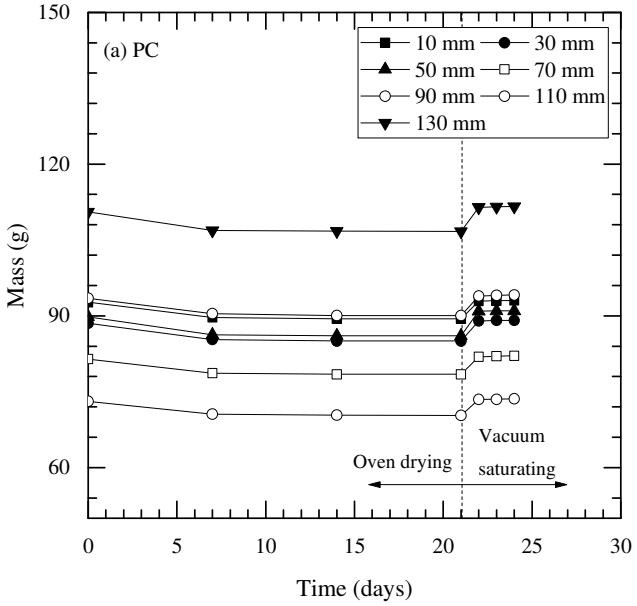

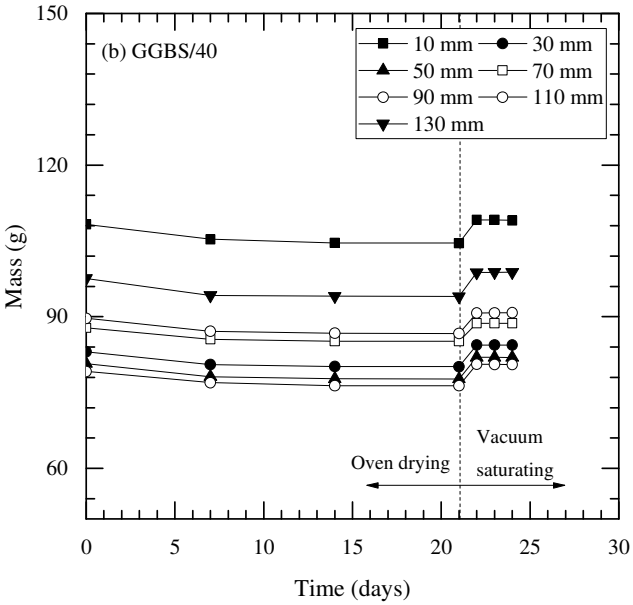
(b) GGBS/40
10 mm
30 mm
50 mm
70 mm
90 mm
110 mm
130 mm
Mass (g)
Time (days)
Oven drying
Vacuum saturating

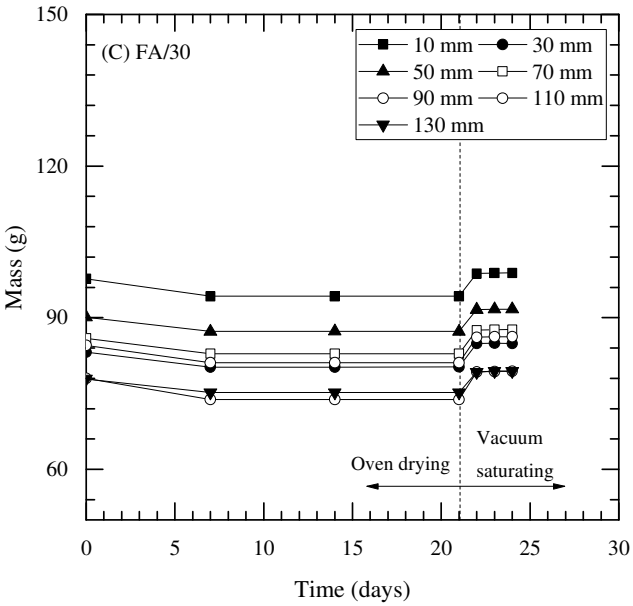
(C) FA/30
10 mm
30 mm
50 mm
70 mm
90 mm
110 mm
130 mm
Mass (g)
Time (days)
Oven drying
Vacuum saturating

C4.3 Monitoring electrical resistance of field concrete in Dornoch

(a) PC

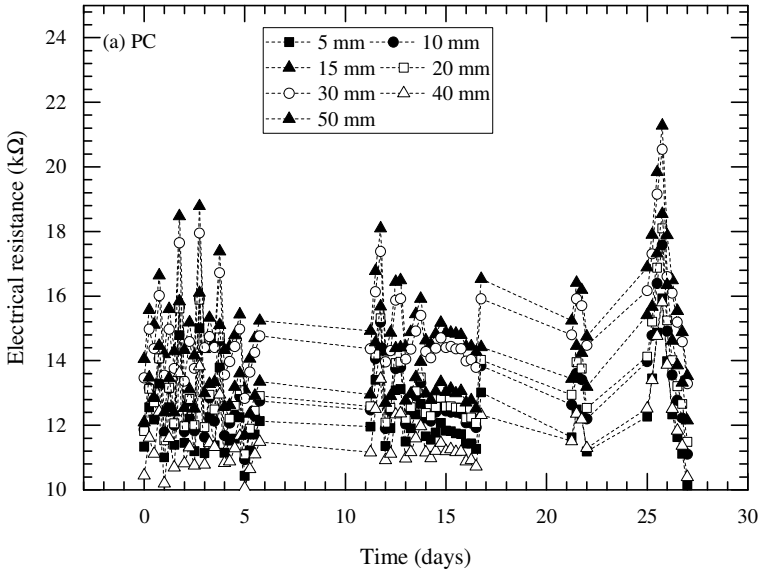

(b) GGBS/40

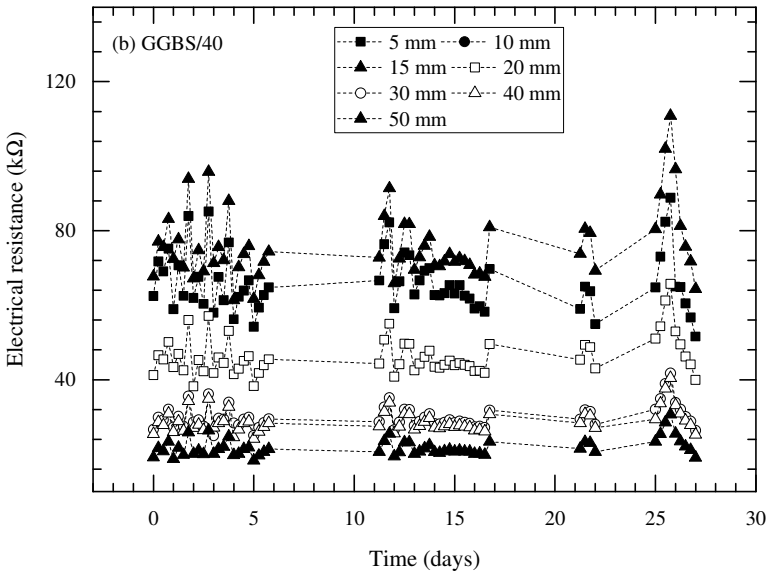

(c) FA/30

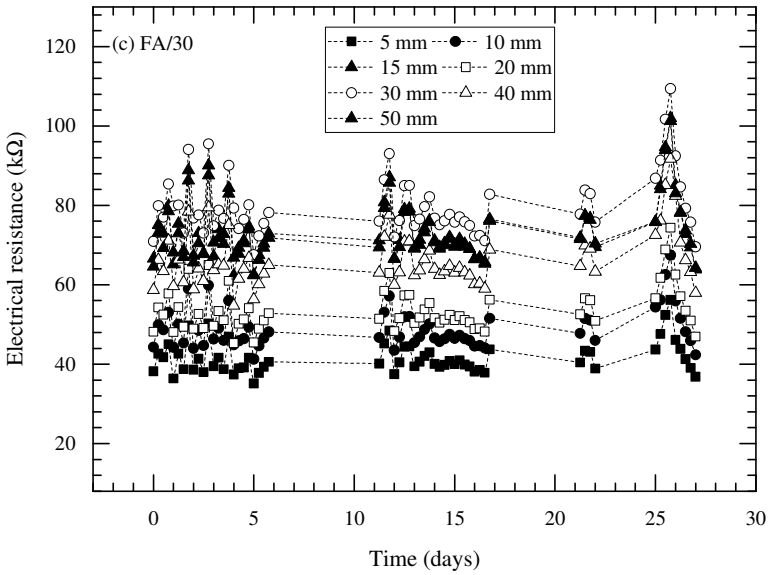

C4.4 Electrochemical parameters of steel in field concrete from polarisation techniques

Measurement	Galvnostatic						Potentiostatic					Linear polarisation resistance	
	R_Ω ($\Omega \cdot m^2$)	R_p ($\Omega \cdot m^2$)	τ (sec)	C (F/m^2)	β	r^2	R_Ω ($\Omega \cdot m^2$)	R_p ($\Omega \cdot m^2$)	τ (sec)	C (F/m^2)	r^2	R_p ($\Omega \cdot m^2$)	r^2
PC-No.1	227.81	10512.44	212.11	0.02	0.86	1.00	312.70	10236.54	4.21	0.01	0.98	6495.74	0.83
PC-No.2	260.96	8866.87	142.71	0.02	0.87	1.00	329.60	11746.09	3.86	0.01	0.98	9258.98	0.96
GGBS/40-No.1	345.81	8337.45	84.68	0.01	0.79	1.00	604.47	11712.91	4.31	0.01	0.96	9567.27	0.96
GGBS/40-No.2	347.71	4840.02	48.86	0.01	0.81	1.00	559.88	8142.56	4.73	0.01	0.95	6530.81	0.96
FA/30-No.1	1188.21	11213.13	226.84	0.02	0.79	1.00	1417.68	14085.98	18.45	0.01	0.99	5356.95	0.92
FA/30-No.2	1289.11	13398.49	293.71	0.02	0.80	1.00	1493.29	15429.34	19.62	0.01	0.99	5073.11	0.92

C4.5 Electrochemical impedance spectroscopy (Nyquist plot) for field samples

PC-No.1

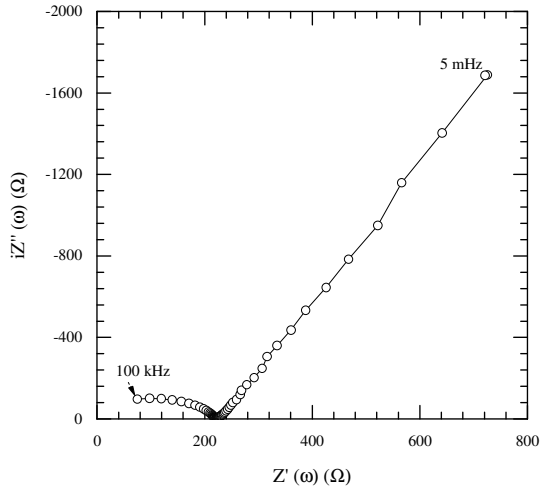

PC-No.2

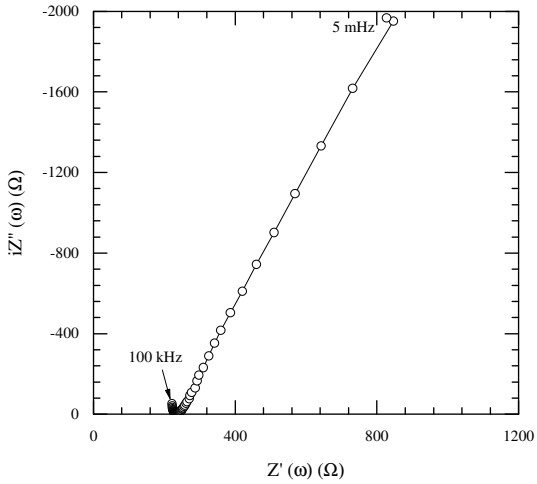

GGBS/40-No.1

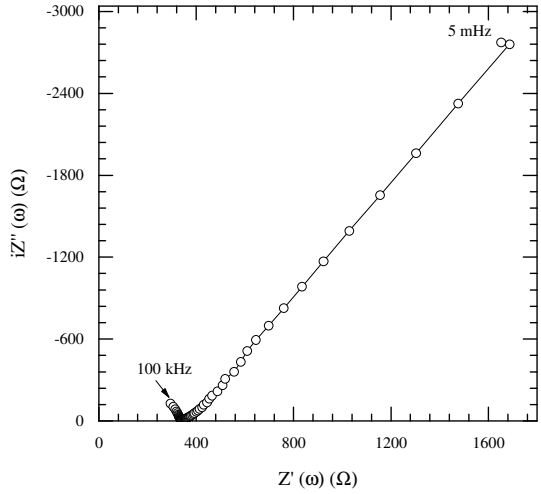

GGBS/40-No.2

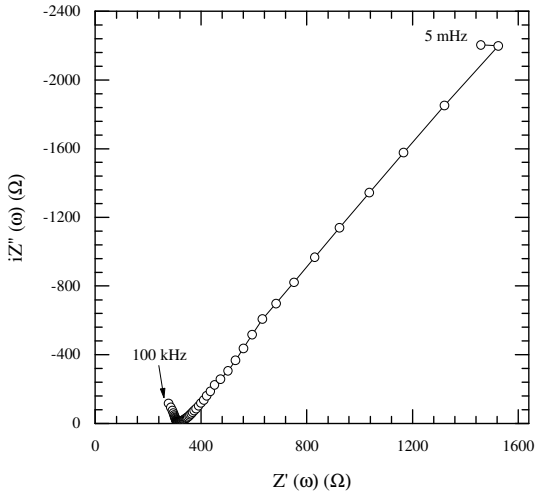

FA/30-No.1

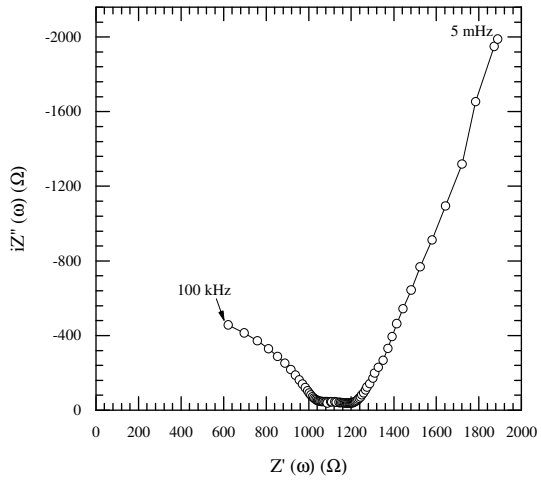

FA/30-No.2

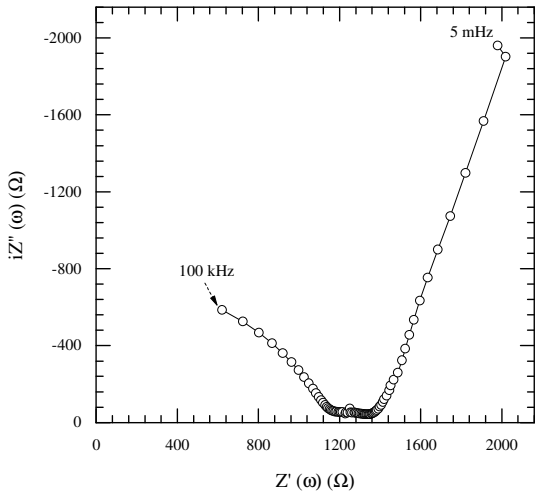

C4.6 Potentiodynamic plot for field samples

PC-No.1

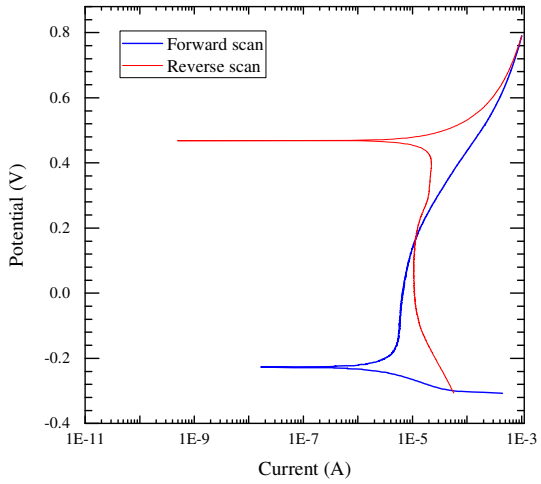

PC-No.2

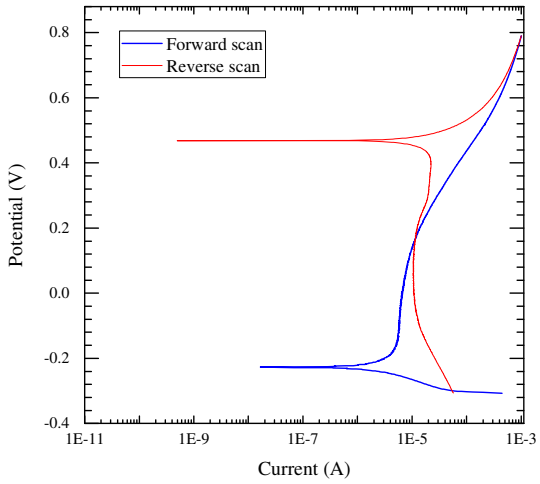

GGBS/40-No.1

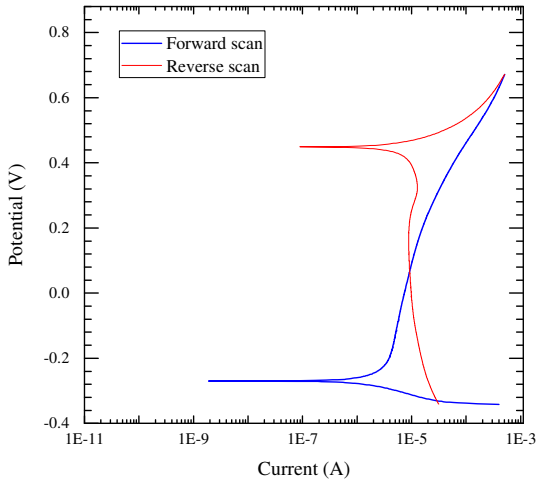

GGBS/40-No.2

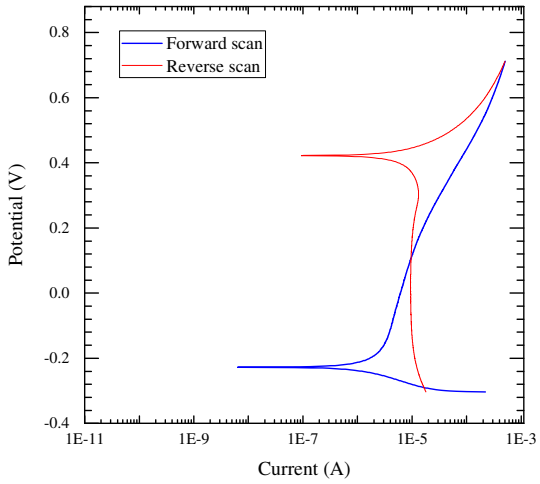

FA/30-No.1

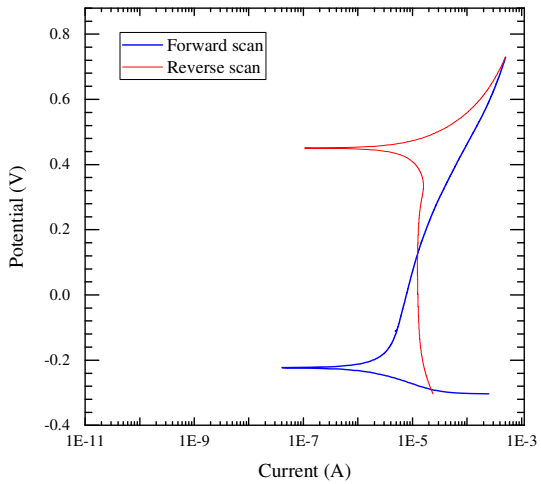

FA/30-No.2

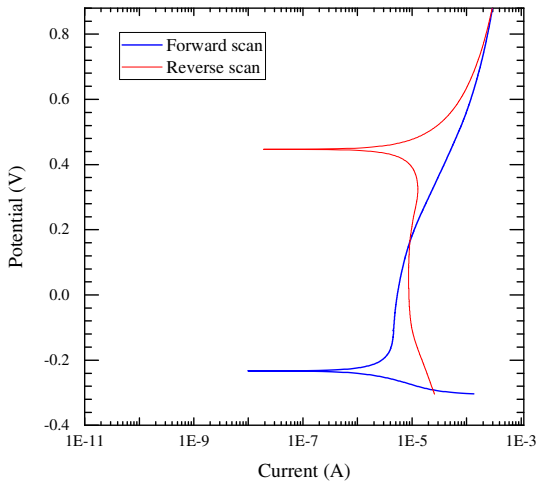

APPENDIX D MODELLING

D.1 Prediction of compressive strength

Input values in equation (5.9) to predict the compressive strength of concrete

w/b	Binder	A	B
0.4	CEM I	8.62	55.11
	CEM III/A	7.98	34.98
	CEM II/B-V	7.58	26.14
0.6	CEM I	6.82	15.25
	CEM III/A	6.69	13.89
	CEM II/B-V	5.39	5.50

D.2 Input values in the ClinConc model (in Excel version)

	A	B	C	D	E	F	G	H
1	**Chloride Ingress**		**Concrete Mix**		**Concrete Hydration**		**Concrete Porosity**	
2	Exposure zone	Tidal zone	Type of cement	CEM II/B-V	Curing temperature T, °C	9	At given age, hr	158520
3	Binder type	CEM II/B-V	Cement, kg/m³	370	Activation energy E_a, J/mol	65000	Hydration degree	0.98
4	Binder, kg/m³	530	Density of cement, kg/m³	3150	a_{max}	1	k_Add 1	0.98
5	D_{6m}	2.92	Type of addition 1	Slag	$a_{1.0}/a_{max}$	0.1169549	k_Add 2	0.5
6	std dev of D_{6m}	0.7	Content of add 1, kg/m³	0	$a_{2.5}/a_{max}$	0.9632189		
7	Binding factor Ab=	5.71	Density of add 1, kg/m³	2900	B_a	3.5328095	Non-evaporable water W_n, kg/m³	90.7
8	Binding exponent Bb=	0.29	Activ coef of add 1	0.6	A_a	127.54487	Gel quantity W_{gel}, kg/m³	501.2
9	Time-dependent binding At =	0.25	Type of addition 2	Flyash	Initial curing age, hr	840	Gel volume V_{gel}, m³/m³concrete	0.2081
10	Dfield/Dlab =	1	Content of add 2, kg/m³	160	Initial hydration degree a_{h_ini}	0.8596409	Pore volume (excl. air pores) V_{pore}, m³/m³concrete	0.0715
11	Age factor n due to At	0.157	Density of add 2, kg/m³	2100			Evaporable water W_e, kg/m³	103.6
12	**At 6 month**		Activ coef of add 2	0.4			**At 6 months age, hr**	4380
13	Gel quantity W_{gel6m}, kg/m³	480.7	Type of aggregate	Granic sand/gravel			Hydration degree	0.933
14	V_{pore6m}	0.0746	Content of aggregate, kg/m³	1675			k_Add 1	0.98
15	ClBindf	36.79	Density of Aggregate, kg/m³	2650			k_Add 2	0.5
16	c[OH]	0.94	Water content, kg/m³	206.7			Non-evaporable water W_n, kg/m³	86.3
17	**At measurement date**		Air content, % vol	3			Gel quantity W_{gel}, kg/m³	480.7
18	Gel quantity W_t, kg/m³	501.2	Na2Oeq_%Binder	0.41			Gel volume V_{gel}, m³/m³concrete	0.1998
19	V_{pore}	0.0715	Ini_Cl_%Binder	0.005			Pore volume (excl. air pores) V_{pore}, m³/m³concrete	0.0746
20	ClBindf	40.03	Total binder, kg/m³	530			Evaporable water W_e, kg/m³	108
21	c[OH]	0.98	Silica fraction *SF*	0				
22	D_0	6.38E-14	Flyash fraction *FA*	0.302				
23	Surface c, g/l	19.6	Slag fraction *BFS*	0				
24	std dev of Surface c, g/l	2	Eqivalent w/c	0.476				
25	Initial c, g/l	0.005	Total volume	1.064				
26	Temp, °C	9						
27	std dev of Temp, °C	5						
28	ClBindf(OH, T)	133.51						
29	Age factor n due to desiccation	0						
30	Effective age-factor n	0.157						
31	Concrete age at exposure, days	35						
32	Exposure duration, yr	18						
33	Environemntal factors							
34	K_e	0.24						
35	K_{mp}	0.82						
36	Moisture content, kg/m³	71.5						

Input page in the ClinConc model (Excel version)

1. Orange color = input values
2. Gray color=calculated values from the ClinConc model

D.3 Determination of K_{exp} with regression method

Field sample

(a) PC

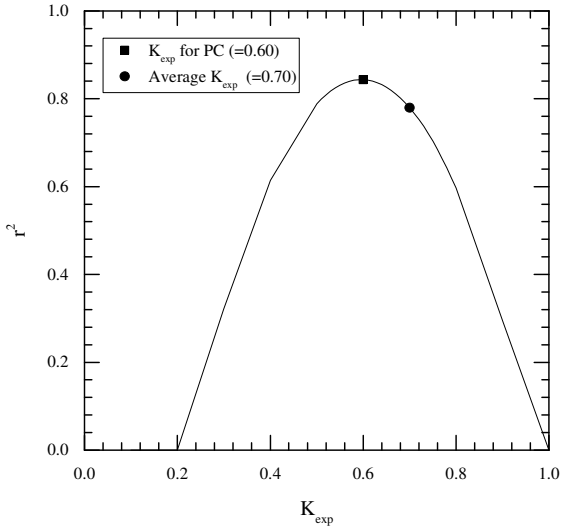

(b) GGBS/40

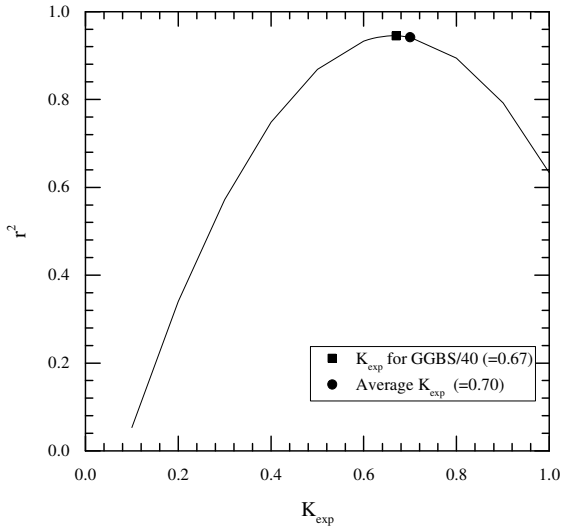

(c) FA/30

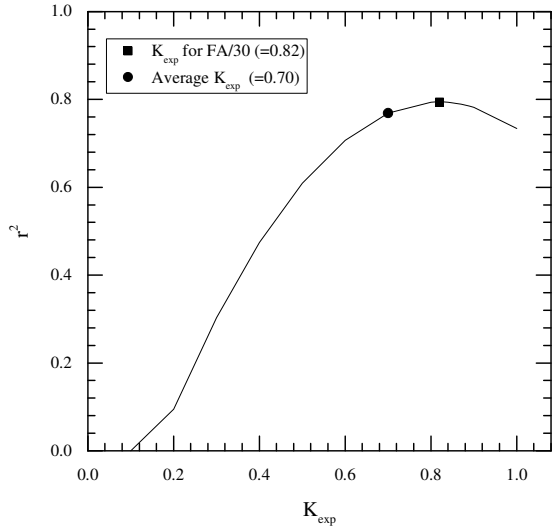

Laboratory sample

(a) CEM I (w/b=0.4)

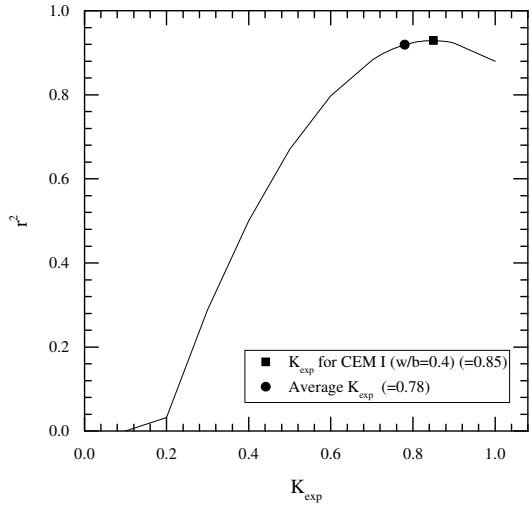

(b) CEM I (w/b=0.6)

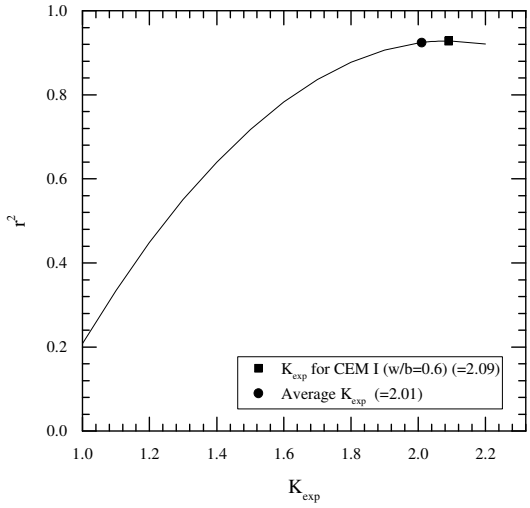

(c) CEM III/A (w/b=0.4)

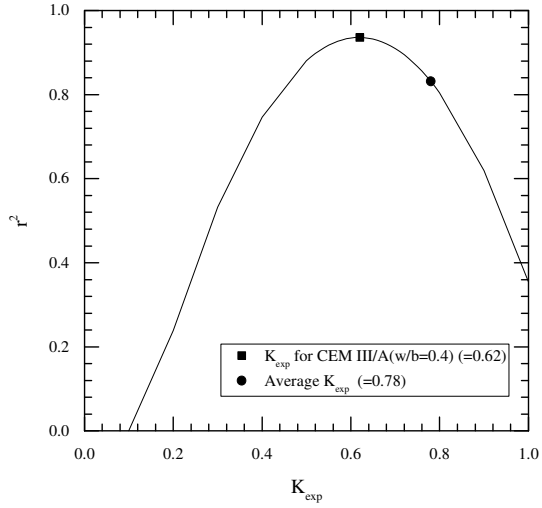

(d) CEM III/A (w/b=0.6)

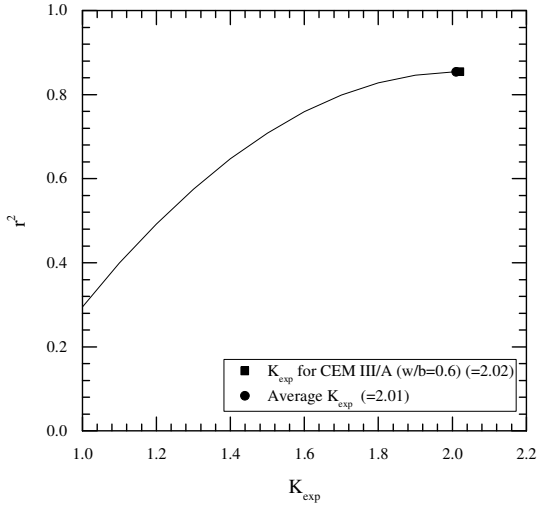

(e) CEM II/B-V (w/b=0.4)

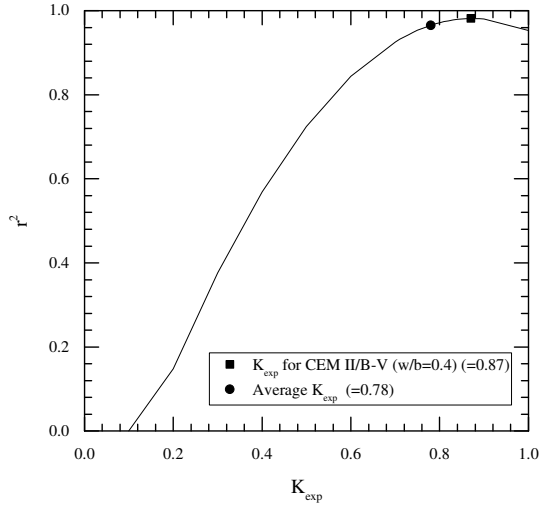

(f) CEM II/B-V (w/b=0.6)